DIGITAL
DIAGNOSTICS

A peer-reviewed scientific medical journal

5 Volume   **4** Issue

ISSN 2712-8490 (Print)
ISSN 2712-8962 (Online)

Digital Diagnostics

Volume 5 | Issue 4 | 2024

QUARTERLY PEER-REVIEWED MEDICAL JOURNAL

EDITOR-IN-CHIEF

Valentin E. Sinitsyn, MD, Dr. Sci. (Med.), Professor (Moscow, Russia)
ORCID: 0000-0002-5649-2193

DEPUTY EDITOR-IN-CHIEF

Yuriy A. Vasilev, MD, Cand. Sci. (Med.) (Moscow, Russia)
ORCID: 0000-0002-5283-5961

SCIENTIFIC EDITOR

Tatiana P. Berezovskaya MD, Dr. Sci. (Med.), Professor (Obninsk, Russia)
ORCID: 0000-0002-3549-4499

RESPONSIBLE SECRETARY

Irina A. Vinogradova, Cand. Sci. (Eng.) (Moscow, Russia)
ORCID: 0000-0001-6465-4132

ECO • VECTOR

16+

© ООО «Эко-Вектор», 2024

ISSN 2712-8490 (Print)
ISSN 2712-8962 (Online)

Digital Diagnostics

Том 5 | Выпуск 4 | 2024
ЕЖЕКВАРТАЛЬНЫЙ РЕЦЕНЗИРУЕМЫЙ НАУЧНЫЙ МЕДИЦИНСКИЙ ЖУРНАЛ

Главный редактор
Синицын Валентин Евгеньевич, д.м.н., профессор (Москва, Россия)
ORCID: 0000-0002-5649-2193

Заместитель главного редактора
Васильев Юрий Александрович, к.м.н., (Москва, Россия)
ORCID: 0000-0002-5283-5961

Научный редактор
Березовская Татьяна Павловна, д.м.н., профессор (Обнинск, Россия)
ORCID: 0000-0002-3549-4499

Ответственный секретарь
Виноградова Ирина Александровна, к.т.н. (Москва, Россия)
ORCID: 0000-0001-6465-4132

ЭКО●ВЕКТОР

CONTENTS

СОДЕРЖАНИЕ

Potential use of cardiac magnetic resonance imaging in differential diagnosis of cardiomyopathies due to light-chain amyloidosis and transthyretin amyloidosis

Zainab M. Magomedova[1,2], Tatyana V. Nikiforova[3], Dmitry Yu. Shchekochikhin[1,2],
Ekaterina S. Pershina[1,2], Konstantin V. Kovalev[1], Khadizhar S. Abdulmazhidova[2],
Daria S. Rassechkina[2], Alexander E. Grachev[4], Irina G. Rekhtina[4], Alexey N. Volovchenko[2],
Susanna D. Sarkisyan[2], Valentin E. Sinitsyn[5], Denis A. Andreev[2]

[1] Pirogov Municipal Clinical Hospital № 1, Moscow, Russia;
[2] Sechenov First Moscow State Medical University, Moscow, Russia;
[3] S.S. Yudin City Clinical Hospital, Moscow, Russia;
[4] National Medical Research Center of Hematology, Moscow, Russia;
[5] Lomonosov Moscow State University, Moscow, Russia

ABSTRACT

BACKGROUND: Cardiac amyloidosis is a serious progressive disease with a high mortality rate. The differential diagnosis of cardiomyopathies due to amyloid light-chain (AL) amyloidosis and transthyretin (ATTR) amyloidosis is important for selecting the optimal treatment strategy.

AIM: The aim of this study was to evaluate the capabilities of cardiac magnetic resonance imaging in the differential diagnosis of cardiomyopathies due to AL and ATTR amyloidosis.

MATERIALS AND METHODS: A retrospective analysis of the medical records of 25 patients with a confirmed diagnosis of amyloid cardiomyopathy was performed. Patients were divided into two groups according to the type of amyloidosis, with group 1 including patients with cardiomyopathy due to AL amyloidosis and group 2 including patients with cardiomyopathy due to ATTR amyloidosis. All patients underwent contrast-enhanced cardiac magnetic resonance imaging. Volumetric and linear cardiac parameters, ventricular function, and late gadolinium enhancement patterns were assessed. Standard statistical methods were used, and differences were considered significant at $p < 0.05$.

RESULTS: Group 2 showed a more significant thickening of the myocardial walls compared to group 1 (interventricular septum: 18 [17; 18] vs. 14.5 mm [12.8; 16.0], $p < 0.01$, posterior wall of the left ventricle: 14 [13; 17] vs. 10.5 mm [10; 12.3], $p < 0.01$). The indexed mass of the left ventricle myocardium was 110 [92; 125] in group 2 and 85 mm [69.3; 91.8] in group 1 ($p < 0.01$). In group 2, late gadolinium enhancement with a transmural left ventricle pattern was more frequently observed in the basal and mid-lower-lateral segments, whereas in group 1, a subendocardial pattern of late gadolinium enhancement was more frequent in the mid-anterior and lower-lateral segments ($p < 0.05$). In addition, frequency of simultaneous contrast enhancement in the subendocardial layers of the interventricular septum on the left ventricle and right ventricle sides was higher in group 2 (100% of cases vs. 50%, $p < 0.01$). Late gadolinium enhancement of the right ventricle was also more common in group 2 (100 vs. 58%, $p < 0.05$), especially in the interventricular septum and inferior wall area ($p < 0.05$). Semi-quantitative assessment of LGE using the Query Amyloid Late Enhancement (QALE) showed greater contrast enhancement in group 2: 13 [12; 14] vs. 10.5 [1.75; 12], $p < 0.01$), and a score greater than 13 differentiated between cardiomyopathy due to AL amyloidosis and ATTR amyloidosis with a sensitivity of 69% and a specificity of 83%.

CONCLUSION: Cardiac MRI identifies typical features of cardiomyopathies due to AL amyloidosis and ATTR amyloidosis for their differential diagnosis. Further research is needed to confirm diagnostic accuracy of the patterns identified.

Keywords: cardiac amyloidosis; systemic amyloidosis; cardiac magnetic resonance imaging; late gadolinium enhancement; QALE; transthyretin amyloidosis; light-chain amyloidosis.

Возможности магнитно-резонансной томографии сердца в дифференциальной диагностике кардиомиопатий вследствие амилоидоза лёгких цепей и транстиретинового амилоидоза

З.М. Магомедова[1,2], Т.В. Никифорова[3], Д.Ю. Щекочихин[1,2], Е.С. Першина[1,2], К.В. Ковалёв[1], Х.С. Абдулмажидова[2], Д.С. Рассечкина[2], А.Е. Грачев[4], И.Г. Рехтина[4], А.Н. Воловченко[2], С.Д. Саркисян[2], В.Е Синицын[5], Д.А. Андреев[2]

[1] Городская клиническая больница № 1 имени Н.И. Пирогова, Москва, Россия;
[2] Первый Московский государственный медицинский университет имени И.М. Сеченова, Москва, Россия;
[3] Городская клиническая больница имени С.С. Юдина, Москва, Россия;
[4] Национальный медицинский исследовательский центр гематологии, Москва, Россия;
[5] Московский государственный университет имени М.В. Ломоносова, Москва, Россия

АННОТАЦИЯ

Обоснование. Амилоидоз сердца — серьёзное прогрессирующее заболевание с высокой смертностью. Дифференциальная диагностика кардиомиопатий вследствие амилоидоза лёгких цепей (AL-амилоидоз) и транстиретинового амилоидоза (ATTR-амилоидоз) важна для выбора оптимальной тактики лечения.

Целью исследования является оценка возможностей магнитно-резонансной томографии сердца в дифференциальной диагностике кардиомиопатий вследствие AL- и ATTR-амилоидоза.

Материалы и методы. Проведён анализ медицинских данных 25 пациентов с подтверждённым диагнозом кардиомиопатия, разделённых на две группы в зависимости от типа амилоидоза. 1-я группа — кардиомиопатия вследствие AL-амилоидоза, 2-я группа — вследствие ATTR-амилоидоза. Всем пациентам проведена магнитно-резонансная томография сердца с контрастированием. Оценивали объёмные и линейные показатели сердца, функцию желудочков и паттерны позднего накопления гадолиния. Использовали стандартные статистические методы, различия считали значимыми при $p <0{,}05$.

Результаты. У пациентов 2-й группы наблюдали более выраженное утолщение стенок миокарда в сравнении с пациентами 1-й группы (межжелудочковая перегородка 18 [17; 18] против 14,5 мм [12,8; 16], $p <0{,}01$, задняя стенка левого желудочка 14 [13; 17] против 10,5 мм [10; 12,3], $p <0{,}01$). Индексированная масса миокарда левого желудочка во 2-й группе — 110 г/м² [92; 125], тогда как в 1-й группе данный показатель составил 85 г/м² [69,3; 91,8], $p <0{,}01$). Среди пациентов 2-й группы чаще отмечали позднее накопление гадолиния с трансмуральным паттерном в базальном и среднем нижне-боковых сегментах левого желудочка, в то время как у пациентов 1-й группы — чаще определяли субэндокардиальный паттерн позднего накопления гадолиния в средних передне- и нижне-боковых сегментах ($p <0{,}05$). Также у пациентов 2-й группы частота случаев одновременного накопления контрастного препарата в субэндокардиальных слоях межжелудочковой перегородки со стороны левого желудочка и правого желудочка оказалась выше (100% случаев против 50%, $p <0{,}01$). Позднее накопление гадолиния в правом желудочке также чаще встречали среди пациентов 2-й группы (100% против 58%, $p <0{,}05$), особенно в области межжелудочковой перегородки и нижней стенки ($p <0{,}05$). Полуколичественная оценка позднего накопления гадолиния с помощью показателя QALE (The query amyloid late enhancement) показала более обширное накопление контраста у пациентов 2-й группы — 13 [12; 14] против 10,5 баллов [1,75; 12], $p <0{,}01$), а количество баллов более 13 предоставило возможность различить кардиомиопатии вследствие AL- и ATTR-амилоидоза с чувствительностью 69% и специфичностью 83%.

Заключение. Магнитно-резонансная томография сердца позволяет выявлять характерные особенности кардиомиопатий вследствие AL- и ATTR-амилоидоза, что может помочь в их дифференциальной диагностике. С целью подтверждения диагностической точности, выявленных паттернов, необходимо продолжение исследований.

Ключевые слова: амилоидоз сердца; системный амилоидоз; магнитно-резонансная томография сердца; отсроченное контрастирование гадолинием; QALE; транстиретиновый амилоидоз; амилоидоз лёгких цепей.

心脏磁共振成像在肺链式淀粉样变性和转甲状腺素淀粉样变性引起的心肌病鉴别诊断中的可能性

Zainab M. Magomedova[1,2], Tatyana V. Nikiforova[3], Dmitry Yu. Shchekochikhin[1,2],
Ekaterina S. Pershina[1,2], Konstantin V. Kovalev[1], Khadizhar S. Abdulmazhidova[2],
Daria S. Rassechkina[2], Alexander E. Grachev[4], Irina G. Rekhtina[4], Alexey N. Volovchenko[2],
Susanna D. Sarkisyan[2], Valentin E. Sinitsyn[5], Denis A. Andreev[2]

[1] Pirogov Municipal Clinical Hospital № 1, Moscow, Russia;
[2] Sechenov First Moscow State Medical University, Moscow, Russia;
[3] S.S. Yudin City Clinical Hospital, Moscow, Russia;
[4] National Medical Research Center of Hematology, Moscow, Russia;
[5] Lomonosov Moscow State University, Moscow, Russia

摘要

论证。心脏淀粉样变性是一种严重的进展性疾病，死亡率很高。肺链淀粉样变性（AL-淀粉样变性）和转甲状腺素淀粉样变性（ATTR-淀粉样变性）引起的心肌病的鉴别诊断，其最佳治疗策略的选择非常重要。

目的。评估心脏磁共振成像鉴别诊断 AL-和ATTR-淀粉样变性引起的心肌病的能力。

材料和方法。对25例确诊为淀粉样变性心肌病的患者的医学数据进行回顾性分析，根据淀粉样变性的类型分为两组。第1组为AL-淀粉样变性引起的心肌病，第2组 为ATTR-淀粉样变性引起的心肌病。所有患者均进行了心脏MRIL造影剂检查。评估了心脏容量和线性指标、心室功能和晚期钆沉积模式。使用标准统计方法，$p < 0.05$时为差异显著。

结果。与第1组患者相比，第2组患者的心肌壁增厚更明显（室间隔18[17；18] vs.14.5mm[12.8；16]，$p < 0.01$，左心室后壁14[13；17]vs.10.5mm[10；12.3]，$p < 0.01$）。第2组的左心室心肌质量指数为110[92；125]，而第1组该指标为85 g/㎡[69.3；91.8]，$p < 0.01$。在第2组患者中，基底和中下外侧段的晚期钆沉积模式更常见于左心室透壁模式，而在第1组患者中，中前部和下外侧段的晚期钆沉积模式更常见于心内膜下模式（$p < 0.05$）。并且在第2组患者中，造影剂同时在左心室和右心室两侧室间隔心内膜下层聚集的频率较高（100 对 50%，$p < 0.01$）。晚期钆沉积模式在第2组患者中的右心室也更为常见（100 vs.58%，$p < 0.05$），尤其是在室间隔和下壁区域（$p < 0.05$）。使用 QALE（淀粉样蛋白晚期增强）指标对晚期钆沉积模式进行半定量评估显示，第2组患者的对比剂聚集更广泛13[12；14] vs.10.5[1.75；12] 分，$p < 0.01$），评分大于13分可以区分AL-和ATTR-淀粉样变性引起的心肌病，敏感性为69%，特异性为83%。

结论。心脏MRI可以识别AL-和ATTR-淀粉样变性引起的心肌病的特征，这可能有助于它们的鉴别诊断。还需要继续研究来确认所查明模式的诊断准确性。

关键词：心脏淀粉样变性；系统性淀粉样变性；心脏磁共振成像；延迟钆造影剂；QALE；转甲状腺素淀粉样变性；肺链淀粉样变性。

BACKGROUND

Cardiac amyloidosis is a serious, progressive disease that causes heart failure and death. It is defined by the extracellular deposition of a specific protein–polysaccharide complex (amyloid) in the myocardium. The most common types of cardiac amyloidosis are amyloid light-chain (AL) amyloidosis and transthyretin (ATTR) amyloidosis, which are caused by immunoglobulin light chain amyloid and transthyretin deposition, respectively. The differential diagnosis of cardiomyopathies due to AL and ATTR amyloidosis is crucial for selecting the optimal treatment strategy [1–3].

Amyloidosis is a rare condition. However, recent findings indicate that amyloid cardiomyopathy is underestimated as a cause of common cardiac disorders. Due to advancements in cardiac imaging and improved diagnosis and treatment strategies, the options for diagnosing and managing cardiac amyloidosis have expanded [4, 5]. Algorithms proposed by the American College of Cardiology [6, 7] and the European Society of Cardiology [8] are currently used for diagnosing this condition.

Cardiac amyloidosis is diagnosed by assessing clonal dyscrasia using an immunochemical analysis of serum and 24-h urine samples. The analysis involved serum and urine protein electrophoresis with immunofixation, as well as a serum-free light chain assay to rule out AL amyloidosis. If the test is positive, a right ventricular (RV) endomyocardial biopsy can be performed to confirm the diagnosis and distinguish between AL and ATTR amyloidosis. In the absence of clonal dyscrasia, ATTR amyloidosis is confirmed using scintigraphy with technetium radiopharmaceuticals (^{99m}Tc-PYP, ^{99m}Tc pyrophosphate; ^{99m}Tc-DPD, ^{99m}Tc-3,3-diphosphono-1,2-propanodicarboxylic acid; ^{99m}Tc-HMDP, ^{99m}Tc-hydroxyl-methylenediphosphonate), with an uptake rate of 2–3; a biopsy is not required. *TTR* genotyping is also possible, particularly for detecting hereditary disease forms, even without family history or signs of polyneuropathy. However, endomyocardial biopsy is the gold standard in cases with inconclusive test results. This method has high specificity and sensitivity for detecting amyloid deposits by Congo red staining [6, 8, 9].

Time-delayed contrast-enhanced magnetic resonance imaging (MRI) is highly effective in diagnosing cardiac amyloidosis and detects contrast uptake patterns in the myocardium characteristic of amyloid deposits and allows the assessment of cardiac functional disorders [10–12]. Moreover, cardiac MRI allows for the differential diagnosis between AL and ATTR amyloidosis-induced cardiomyopathy, considering the pattern of delayed contrast uptake, signs of severe concentric ventricular hypertrophy, and increased myocardial mass [13].

AIM

To assess the potential of cardiac MRI in the differential diagnosis of cardiomyopathy due to AL or ATTR amyloidosis.

METHODS

Study design

We conducted a cross-sectional, observational, single-arm, single-center study to review the medical records of patients with confirmed cardiomyopathy due to AL or ATTR amyloidosis.

Eligibility criteria

We used contrast-enhanced cardiac MRI findings obtained between January 1, 2021, and May 31, 2024.

Inclusion criteria:
- confirmed cardiomyopathy due to AL or ATTR amyloidosis in accordance with the American College of Cardiology guidelines [14, 15], European Society of Cardiology guidelines [8], and Russian guidelines for the diagnosis and treatment of systemic amyloidosis [9];
- available contrast-enhanced cardiac MRI findings; and
- signed informed consent (the study only included data from patients who signed an informed consent form for the use of their data for research purposes, approved by the City Clinical Hospital No. 1 named after N.I. Pirogov).

Study setting

A contrast-enhanced cardiac MRI was performed in the MRI and CT department of the City Clinical Hospital No. 1 named after N.I. Pirogov. We included the medical records of outpatients and inpatients. Amyloid cardiomyopathy could be the principal diagnosis or a complication of another condition.

Study duration

We reviewed the medical records between June 1, 2024, and July 31, 2024.

Intervention

The analysis of medical records included clinical examination, blood test, electrocardiography (ECG), echocardiography, and cardiac MRI findings.

A cardiac MRI was performed using the *Vantage ExelArt TOSHIBA 1.5T* and *Philips Ingenia 1.5-T Evolution* scanners, according to the optimized protocols for diagnosing cardiac amyloidosis. We used a specific sequence of scanning protocols to assess the heart morphology, ventricular function, and signs of amyloid deposits:

1. A series of scans (localizers) in three planes for examination planning.

2. A cine-MRI in the steady-state free precession mode in two-, three-, and four-chamber views and a series of short-axis scans from the base to the apex of the left ventricle (LV).

3. Fat-suppressed T2-weighted imaging.

4. Black blood T2-weighted imaging.

5. TI-scout (look-locker) imaging 8–10 min after contrast injection to determine the optimal myocardial inversion time (TI) or the phase-sensitive inversion recovery sequence.

6. Post-contrast T1-weighted imaging to assess delayed contrast uptake in the myocardium (late gadolinium enhancement, LGE) 10–15 min after contrast injection.

All examinations were ECG-gated, with breath holding, where necessary. The slice thickness and interslice gap were 6–8 and 2 mm, respectively. The total examination time was ~45–60 min.

Main study outcome

The main study outcome was changes in cardiac MRI in patients with cardiomyopathy due to amyloidosis. We assessed the following parameters: LV volumetric and linear measures; LV and RV LGE patterns.

Additional study outcomes

The additional study outcome was a semiquantitative LGE assessment using the Query Amyloid Late Enhancement (QALE) score.

Subgroup analysis

The study included two groups based on the amyloidosis type:
- Group 1: patients with cardiomyopathy due to AL amyloidosis;
- Group 2: patients with cardiomyopathy due to ATTR amyloidosis.

Outcomes registration

Images were processed and analyzed using the specialist *cvi42 software* (Circle Cardiovascular Imaging Inc., Canada). Two qualified radiologists experienced in cardiac imaging independently assessed the cardiac MRI findings. The interobserver variability was additionally assessed. Changes in LV volumetric and linear measures were recorded. Contrast uptake patterns in the myocardium depending on the type of amyloidosis were identified. We used the QALE score developed by Dungu et al. [13] for a semi-quantitative LGE assessment. The analysis involves three LV levels: basal, middle, and apical. The maximum score for each level is four points, depending on the contrast uptake pattern. If the RV is involved, the maximum score for each level increases to six points. Thus, the total QALE score ranged from 0 (no LGE) to 18 (global transmural LV LGE plus RV involvement).

Ethical review

The Local Ethics Committee of I.M. Sechenov First Moscow State Medical University approved this study (Minutes No. 15–24 of June 6, 2024).

Statistical analysis

Sample size calculation: The sample size was not calculated in advance due to the rarity (orphan) of the disease.

Considering the limited number of patients with this condition, all eligible patients were included.

Statistical analysis methods: The qualitative parameters were compared using the χ^2 or Fisher's exact test. The quantitative parameters were compared using the nonparametric Mann–Whitney test. The results were presented as Me [Q25; Q75], where Me is the median and Q25 and Q75 are the 25th and 75th percentiles, respectively. Differences were considered significant at $p < 0.05$.

RESULTS

Participants

The study included 25 patients with confirmed cardiac amyloidosis, with 12 and 13 patients in Groups 1 and 2, respectively. The mean age was 71.7 ± 12 years; 46% of the patients were male.

Table 1 shows the patient characteristics, including demographics and clinical data.

Primary results

MRI: cardiac volumetric and linear measures

Group 2 had more pronounced myocardial wall thickening than Group 1 (interventricular septum, LV involvement, 18 mm [17; 18] vs. 14.5 mm [12.8; 16], $p < 0.01$; LV posterior wall 14 mm [13; 17] vs. 10.5 mm [10.0; 12.3], $p < 0.01$) (Fig. 1). No significant differences were found in LV ejection fraction parameters: 53% [42; 66] vs. 56.5% [51.5; 66.3], $p > 0.05$. However, the LV mass index was higher in Group 2 (110 mm/m² [92; 125] vs. 85.0 mm/m² [69.3; 91.8], $p < 0.01$). Pleural effusion was detected in 67% and 46% of patients in Groups 1 and 2, respectively, but the difference was not significant ($p = 0.530$).

MRI: delayed contrast uptake in the myocardium

LGE was detected in all patients in Group 2 and 11 (85%) patients in Group 1 (Table 2). RV LGE was detected in all patients in Group 2 and 58% of patients in Group 1 ($p < 0.05$). Group 2 had a significantly higher rate of contrast uptake in the interventricular septum and RV inferior wall (62% vs. 8%, $p < 0.05$) (Fig. 2). A simultaneous subendocardial LGE in the LV and RV in the interventricular septum was found Group 2, resulting in the double-line sign (100% vs. 50%, $p < 0.01$) (Fig. 3). Atrial LGE was observed in 69% and 50% of patients in Groups 2 and 1, respectively ($p > 0.05$).

The analysis of contrast uptake distribution by cardiac segments revealed transmural LGE in Group 2 at the basal and middle levels (inferolateral segments, Fig. 4) ($p < 0.05$). Group 1 showed subendocardial LGE at the middle level (antero- and inferolateral segments, Fig. 5) ($p < 0.05$). The other segments showed no specific contrast uptake patterns ($p > 0.05$) (Table 3). The circular contrast uptake rates were not significantly different.

Table 1. Comparison of patient characteristics

Characteristics	Group 1, *n* = 12	Group 2, *n* = 13	*p*-value
Demographics			
Age, years	64.5 [59.3; 71.8]	79 [74; 84]	<0.01
Males, *n* (%)	5 (42)	11 (85)	0.07
Clinical findings			
Chronic heart failure, NYHA class II, *n* (%)	7 (58)	6 (46)	0.83
Chronic heart failure, NYHA class III, *n* (%)	5 (42)	7 (54)	0.83
Hypertension, *n* (%)	4 (33)	4 (31)	1.0
Coronary artery disease, *n* (%)	2 (17)	5 (38)	0.44
Polyneuropathy, *n* (%)	2 (15)	3 (23)	1.0
Spinal stenosis, *n* (%)	0 (0)	1 (8)	1.0
Carpal tunnel syndrome, *n* (%)	0 (0)	1 (8)	1.0
Anamnestic findings			
Pacemaker implantation, *n* (%)	2 (15)	1 (8)	0.94
History of revascularization, *n* (%)	1 (8)	3 (23)	0.65
History of myocardial infarction, *n* (%)	2 (17)	3 (23)	1.00
Electrocardiography			
Low QRS voltage on ECG, *n* (%)	5 (42)	5 (38)	1.00
Pseudo-infarction changes, *n* (%)	6 (50)	2 (15)	0.15
Complete right bundle branch block, *n* (%)	1 (8)	2 (15)	1.00
Grade 1 atrioventricular block, *n* (%)	1 (8)	4 (31)	0.37
Atrial fibrillation, *n* (%)	6 (50)	7 (54)	1.00
Laboratory findings			
NT-proBNP > 300 pg/mL, *n* (%)	12 (100)	13 (100)	0.07
Troponin I > 0.023 ng/mL, *n* (%)	5 (42)	7 (54)	0.83
Proteinuria > 1.0 g/day, *n* (%)	11 (92)	1 (8)	<0.01
Echocardiography			
Left ventricular ejection fraction, %	57 [48; 63]	54 [54; 58]	0.51
Interventricular septum, mm	15 [14; 17]	17 [16; 19]	0.01
Left ventricular posterior wall, mm	13 [12; 15]	16 [14; 17]	0.09

Note. Low voltage on ECG was defined as all QRS amplitudes < 5 mm (standard leads) or < 10 mm (precordial leads). NYHA, New York Heart Association classification; NT-proBNP, N-terminal prohormone of brain natriuretic peptide.
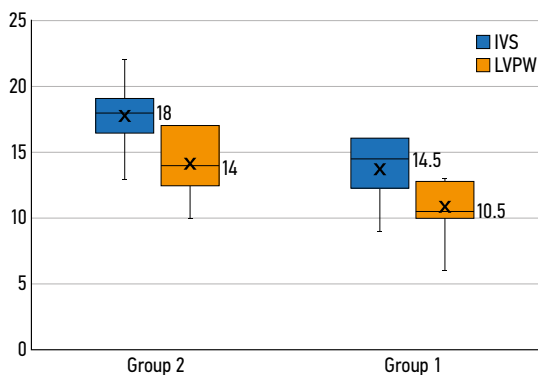
Fig. 1. Box plot of the linear measures of cardiac magnetic resonance imaging in Groups 1 and 2. AL, light-chain amyloidosis (Group 1); ATTR, transthyretin amyloidosis (Group 2); IVS, interventricular septum; LVPW, left ventricular posterior wall.

Secondary results

Semi-quantitative LGE assessment of cardiac amyloidosis

We performed a semiquantitative LGE assessment using the QALE score during the analysis of postcontrast T1-weighted images of the ventricles. Group 2 had larger LGE areas than Group 1: 13 points [12; 14] vs. 10.5 points [1.75; 12], *p* < 0.01 (Fig. 6). We performed a receiver operating characteristic (ROC) analysis to determine a predictive model for the QALE score in patients with cardiomyopathy, depending on the amyloidosis type. The analysis confirmed the QALE score's usefulness in determining the amyloidosis type: the area under the ROC curve (AUC) was 0.83 (sensitivity 69%, specificity 83%, QALE threshold ≥ 13 points).

Table 2. Comparison of late gadolinium enhancement cases depending on the segment on MRI.

	Group 1, *n* = 12				Group 2, *n* = 13			
	0	1	2	3	0	1	2	3
Basal level								
Segment 1 (anterior), *n*	4	2	6	0	3	0	8	2
Segment 2 (anteroseptal), *n*	7	1	3	1	4	3	5	1
Segment 3 (inferoseptal), *n*	6	2	4	0	4	3	5	1
Segment 4 (inferior), *n*	2	2	5	3	1	2	7	3
Segment 5 (inferolateral), *n*	2	1	5	4*	0	1	1	11*
Segment 6 (anterolateral), *n*	3	2	5	2	1	2	5	5
Middle level								
Segment 7 (anterior), *n*	5	1	6	0	4	3	5	1
Segment 8 (anteroseptal), *n*	5	3	4	0	6	1	5	1
Segment 9 (inferoseptal), *n*	6	1	5	0	5	2	5	1
Segment 10 (inferior), *n*	3	1	7	1	6	1	4	2
Segment 11 (inferolateral), *n**	3	0	9*	0*	3	1	1*	8*
Segment 12 (anterolateral), *n**	4	0	8*	0	5	4	2*	2
Apical level								
Segment 13 (anterior), *n*	6	0	6	0	7	0	5	1
Segment 14 (septal), *n*	6	0	6	0	5	1	5	2
Segment 15 (inferior), *n*	6	0	6	0	9	1	3	0
Segment 16 (lateral), *n*	6	0	6	0	8	1	4	0
Total*, *n*	9	5	10	4*	12	9	12	12*
Combination of the segments								
Basal level of the interventricular septum (segments 2 and 3), *n*	6	1	3	0	4	3	5	1
Middle level of the interventricular septum (segments 8 and 9), *n*	5	1	4	0	5	1	5	1
Interventricular septum (segments 2, 3, 8, 9, and 14), *n*	4	0	2	0	2	1	2	0
Basal level, lateral wall (segments 5 and 6), *n*	2	1	3	2	0	1	1	5
Middle level, lateral wall (segments 11 and 12), *n*	3	0	8*	1	3	1	1*	1
Lateral wall (segments 5, 6, 11, 12, and 16), *n*	2	0	3	0	1	0	0	0
Circular distribution with a subendocardial pattern								
Basal level, *n*			2				0	
Middle level, *n*			3				1	
Apical level, *n*			6				2	
Circular distribution with any contrast uptake pattern								
Basal level, *n*			4				7	
Middle level, *n*			6				5	
Apical level, *n*			5				4	

Note. 0, no late gadolinium enhancement areas; 1, intramyocardial late gadolinium enhancement pattern; 2, subendocardial late gadolinium enhancement pattern; 3, transmural late gadolinium enhancement pattern; *, significant intergroup difference (cases of late gadolinium enhancement with the same pattern in the groups).
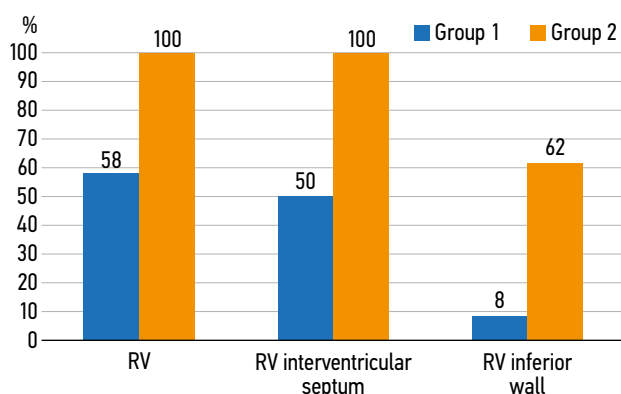
Fig. 2. Distribution of late gadolinium enhancement cases in the right ventricle in the groups. RV, right ventricle; AL, light-chain amyloidosis (Group 1); ATTR, transthyretin amyloidosis (Group 2); LGE, late gadolinium enhancement.

DISCUSSION

Summary of primary results

This retrospective study revealed that cardiac MRI plays a significant role in the differential diagnosis of AL amyloidosis- and ATTR amyloidosis-induced cardiomyopathy. This conclusion is clinically significant because these two conditions require fundamentally different therapeutic approaches [16].

Discussion of primary results

Distinctive signs of amyloid cardiomyopathy include more pronounced myocardial wall thickening (interventricular septum, LV involvement, and LV posterior wall) and an increased LV mass index in ATTR amyloidosis compared with AL amyloidosis, which was consistent with previous findings, indicating that ATTR amyloidosis is associated with more severe myocardial hypertrophy. Based on Dungu et al. [13], AL amyloidosis was characterized by a minimal increase in the LV mass index compared with ATTR amyloidosis. They reported a significant LV wall thickening in ATTR amyloidosis compared with AL amyloidosis: 18 ± 2 vs. 14 ± 3 mm. Kriste et al. reported similar findings: the myocardial mass in ATTR amyloidosis compared with AL amyloidosis was 164 ± 57 vs. 159 ± 61 mg. The maximum LV wall thickness in ATTR amyloidosis was significantly higher than that in AL amyloidosis. These changes are due to an increased amyloid load in ATTR amyloidosis [14, 15].
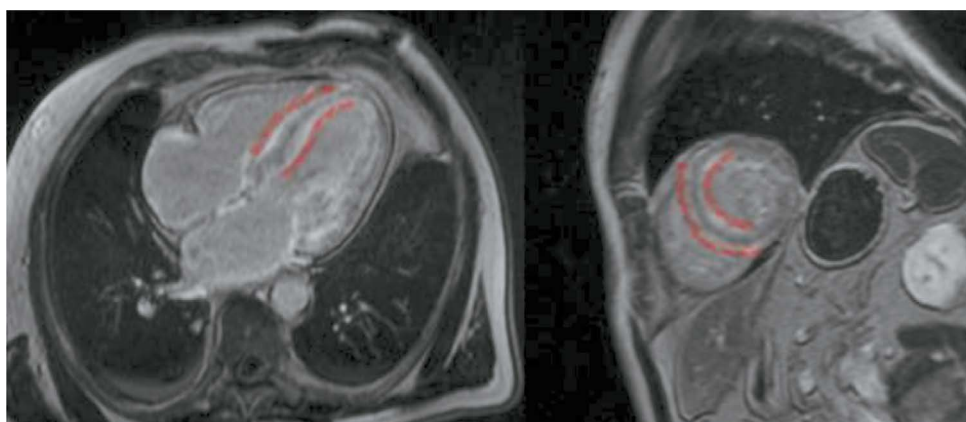
Fig. 3. Time-delayed contrast-enhanced cardiac magnetic resonance imaging scans in transthyretin amyloidosis. Subendocardial contrast uptake in the interventricular septum (right and left ventricular involvement) (red dashed lines).
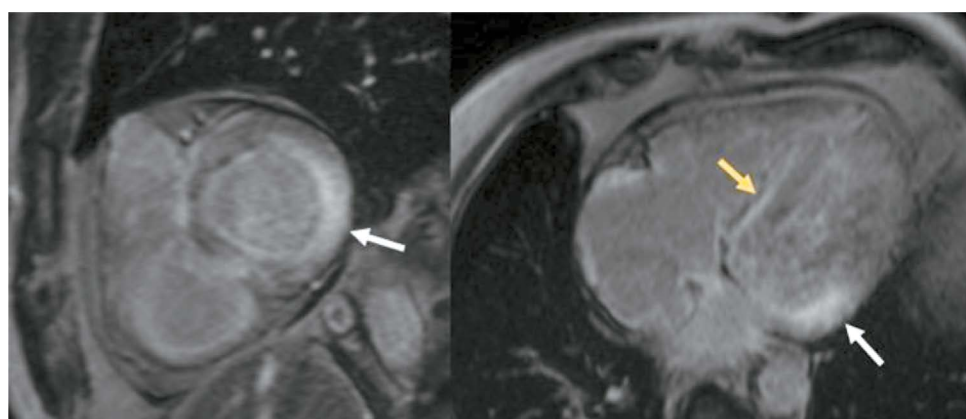
Fig. 4. Time-delayed contrast-enhanced cardiac magnetic resonance imaging scans in transthyretin amyloidosis. Transmural contrast uptake at the basal and middle levels (inferolateral segments), subendocardial contrast uptake at the basal level (anterior, anterolateral, and inferior segments) of the left ventricular myocardium (white arrows), and subendocardial contrast uptake in the interventricular septum (right ventricular involvement) (yellow arrow).
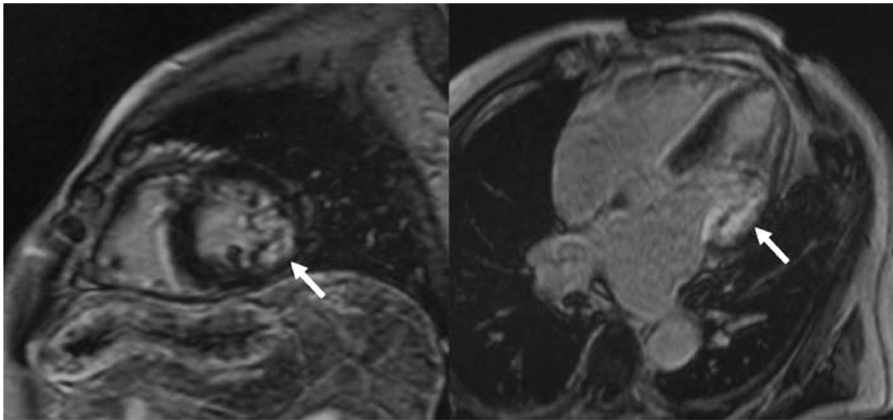
Fig. 5. Time-delayed contrast-enhanced cardiac magnetic resonance imaging scans in light-chain amyloidosis. Subendocardial contrast uptake at the basal and middle levels (inferolateral segments) of the left ventricular myocardium (white arrows).

Table 3. Comparative analysis of late gadolinium enhancement cases in various cardiac structures in the groups.

Characteristics	Group 1, $n = 12$	Group 2, $n = 13$	p-value
Late gadolinium enhancement in the right ventricle, n (%)	7 (58)	13 (100)	<0.05
Late gadolinium enhancement in the right ventricular inferior wall, n (%)	1 (8)	8 (62)	<0.05
Late gadolinium enhancement in the interventricular septum (right ventricular involvement), n (%)	6 (50)	13 (100)	<0.05
Late gadolinium enhancement in the right ventricular wall, n (%)	6 (50)	9 (69)	>0.05
Late gadolinium enhancement in the atria, n (%)	6 (50)	9 (69)	>0.05
Late gadolinium enhancement in the interventricular septum (right and left ventricular involvement), n (%)	6 (50)	13 (100)	<0.05
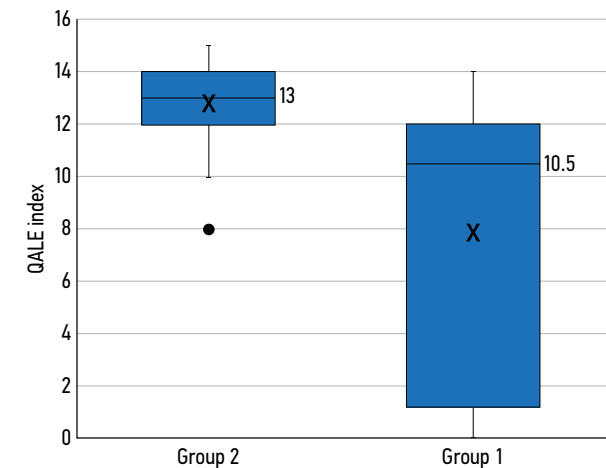
Fig. 6. Box plot of the Query Amyloid Late Enhancement (QALE) score in Groups 1 and 2. AL, light-chain amyloidosis (Group 1); ATTR, transthyretin amyloidosis (Group 2).

Fig. 7. ROC curve for the Query Amyloid Late Enhancement (QALE) score. Solid line: QALE score, area under the curve (AUC) 0.83 (95% confidence interval: 0.64–0.97); sensitivity 69%; specificity 83%.

LGE patterns in these types of cardiac amyloidosis differ, which can be useful in the differential diagnosis. AL amyloidosis is more commonly associated with a global subendocardial contrast uptake, whereas ATTR amyloidosis is characterized by a transmural or focal contrast uptake [13, 17]. Despite these differences, the differential diagnosis between AL amyloidosis- and ATTR amyloidosis-induced cardiomyopathy based on cardiac MRI findings can be challenging due to similar visual patterns. Semiquantitative LGE assessment and additional imaging techniques (scintigraphy with ^{99m}Tc-DPD) have been proposed to improve the diagnostic accuracy [18].

The analysis of LGE characteristics revealed specific patterns for each amyloidosis type, which can be used for the differential diagnosis. The most valuable findings are as follows:
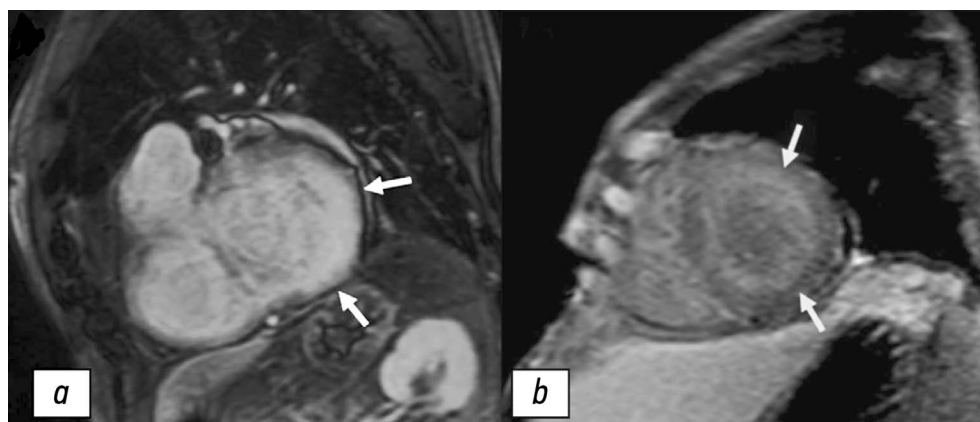
Fig. 8. Time-delayed contrast-enhanced cardiac magnetic resonance imaging scans in transthyretin amyloidosis. a, transmural contrast uptake at the basal level (lateral segments) and intramural contrast uptake at the basal level (inferior segment) of the left ventricular myocardium (white arrows), QALE score: 15 points. b, circular subendocardial contrast uptake at the middle level (all segments) of the left ventricular myocardium (yellow arrows), QALE score: 10 points.

- *ATTR amyloidosis:* more commonly associated with a pronounced transmural LGE at the basal and middle levels, in the inferolateral segments of the LV, with RV involvement, particularly in the interventricular septum (LV involvement) and the RV inferior wall (Fig. 8, *a*).
- *AL amyloidosis:* more commonly associated with a subendocardial LGE, mostly at the middle levels, in the antero- and inferolateral segments (Fig. 8, *b*).

These findings are consistent with those of previous studies [13, 17, 19], which also found specific LGE patterns in AL and ATTR amyloidosis, including a more pronounced contrast uptake in ATTR amyloidosis ($p < 0.001$) [17].

Based on the available data, ATTR amyloidosis can be distinguished from AL amyloidosis with a sensitivity and specificity of 82% and 76%, respectively, based on the QALE score of ≥ 13 points [13]. We found that ATTR amyloidosis was similarly characterized by a more pronounced LGE compared with AL amyloidosis.

The significant amyloid buildup in the myocardium in ATTR amyloidosis is most likely due to a longer disease duration than in AL amyloidosis. In AL amyloidosis, myocardial damage is caused by both amyloid buildup and the direct toxic effect of the immunoglobulin light chains, resulting in lower amyloid levels in the myocardium.

Our study revealed that patients with AL amyloidosis have a higher risk of *pleural effusion* than patients with ATTR amyloidosis. This is a significant finding because it can be associated with more severe systemic involvement in AL amyloidosis, as confirmed by Binder et al. [20].

The double-line sign in the interventricular septum in ATTR amyloidosis is an interesting phenomenon, indicating simultaneous subendocardial LGE in the LV and RV (See Fig. 3). This sign was observed in all patients with ATTR amyloidosis, possibly making it an important diagnostic marker. However, available publications do not describe this contrast uptake pattern, necessitating further studies.

Notably, no significant intergroup differences were observed in the LV ejection fraction and volumetric measures. In this context, myocardial deformation assessment will likely be more useful for assessing the functional aspects of the heart in amyloidosis [21].

Study limitations

This study has the following limitations:
- the sample size was relatively small.
- the study did not assess the effect of concomitant cardiovascular diseases and interventions.

However, we found no significant differences when comparing the clinical and anamnestic signs in the groups (See Table 1). Notably, a significant age difference of 11 years was observed between the groups ($p < 0.01$), which likely affected the result interpretation. However, despite the observed differences, many characteristics of cardiac MRI findings in amyloid cardiomyopathy are nonspecific and can be seen in both amyloidosis types, highlighting the importance of a comprehensive diagnosis, including clinical, laboratory, and imaging examinations.

CONCLUSION

The study findings show that contrast-enhanced cardiac MRI is a highly effective tool for the differential diagnosis of AL amyloidosis- and ATTR amyloidosis-induced cardiomyopathy. Using typical contrast uptake patterns and additional imaging techniques can significantly improve the diagnostic accuracy. Further studies and new diagnostic criteria and tools are required to improve the diagnosis and treatment of this complex condition.

ADDITIONAL INFORMATION

of data for the work, drafting and revising the work, final approval of the version to be published and agree to be accountable for all aspects of the work. Z.M. Magomedova — collection and analysis of patient's data, literature review, statistical analysis, preparation, writing and editing of the article; T.V. Nikiforova, Kh.S. Abdulmazhidova, S.D. Sarkisyan — collection and analysis of

patient's data; D.Yu. Shchekochikhin, V.E. Sinitsyn, D.A. Andreev — editing the text of the article; E.S. Pershina — literature review, collection and analysis of patient's data; K.V. Kovalev — collection and analysis of patient's data; A.E. Grachev, I.G. Rekhtina, A.N. Volovchenko — literature review, collection and analysis of patient's data.

REFERENCES

1. Wechalekar AD, Gillmore JD, Hawkins PN. Systemic amyloidosis. *Lancet.* 2016;387(10038):2641–2654. doi: 10.1016/S0140-6736(15)01274-X

2. Rapezzi C, Lorenzini M, Longhi S, et al. Cardiac amyloidosis: the great pretender. *Heart Fail Rev.* 2015;20(2):117–124. doi: 10.1007/s10741-015-9480-0

3. Myasnikov RP, Andreyenko EYu, Kushunina DV, et al. Cardiac amyloidosis: modern aspects of diagnosis and treatment (clinical observation). *Clinical and experimental surgery.* 2014;(4):72–82. EDN: TRLZYN

4. Maurer MS, Elliott P, Comenzo R, et al. Addressing common questions encountered in the diagnosis and management of cardiac amyloidosis. *Circulation.* 2017;135(14):1357–1377. doi: 10.1161/CIRCULATIONAHA.116.024438

5. Ruberg FL, Grogan M, Hanna M, et al. Transthyretin amyloid cardiomyopathy: JACC state-of-the-art review. *J Am Coll Cardiol.* 2019;73(22):2872–2891. doi: 10.1016/j.jacc.2019.04.003

6. Kittleson MM, Maurer MS, Ambardekar AV, et al.; American Heart Association Heart Failure and Transplantation Committee of the Council on Clinical Cardiology. Cardiac amyloidosis: evolving diagnosis and management: a scientific statement from the American Heart Association. *Circulation.* 2020;142(1):e7–e22. doi: 10.1161/CIR.0000000000000792

7. Maurer MS, Bokhari S, Damy T, et al. Expert consensus recommendations for the suspicion and diagnosis of transthyretin cardiac amyloidosis. *Circ Heart Fail.* 2019;12(9):e006075. doi: 10.1161/CIRCHEARTFAILURE.119.006075

8. Garcia-Pavia P, Rapezzi C, Adler Y, et al. Diagnosis and treatment of cardiac amyloidosis: a position statement of the ESC Working Group on Myocardial and Pericardial Diseases. *Eur Heart J.* 2021;42(16):1554–1568. doi: 10.1093/eurheartj/ehab072

9. Lysenko LV, Rameev VV, Moiseev SV, et al. Clinical guidelines for diagnosis and treatment of systemic amyloidosis. *Clinical pharmacology and therapy.* 2020;29(1):13–24. EDN UCEZAB doi: 10.32756/ 0869-5490-2020-1-13-24

10. Syed IS, Glockner JF, Feng D, et al. Role of cardiac magnetic resonance imaging in the detection of cardiac amyloidosis. *JACC Cardiovasc Imaging.* 2010;3(2):155–164. doi: 10.1016/j.jcmg.2009.09.023

11. Butorova EA, Stukalova OV. Role of cardiac MRI in the diagnosis of cardiac amyloidosis. Clinical cases. *Clinical review for general practice.* 2021;(2):16–20. EDN MUWTXO doi: 10.47407/kr2021.2.2.00037

12. Dorbala S, Ando Y, Bokhari S, et al. ASNC/AHA/ASE/EANM/HFSA/ISA/SCMR/SNMMI expert consensus recommendations for multimodality imaging in cardiac amyloidosis: Part 1 of 2-evidence base and standardized methods of imaging. *J Nucl Cardiol.* 2019;26(6):2065–2123. doi: 10.1007/s12350-019-01760-6

13. Dungu JN, Valencia O, Pinney JH, et al. CMR-based differentiation of AL and ATTR cardiac amyloidosis. *JACC Cardiovasc Imaging.* 2014;7(2):133–142. doi: 10.1016/j.jcmg.2013.08.015

14. Itzhaki Ben Zadok O, Vaturi M, Vaxman I, et al. Differences in the characteristics and contemporary cardiac outcomes of patients with light-chain versus transthyretin cardiac amyloidosis. *PLoS One.* 2021;16(8):e0255487. doi: 10.1371/journal.pone.0255487

15. Quarta CC, Solomon SD, Uraizee I, et al. Left ventricular structure and function in transthyretin-related versus light-chain cardiac amyloidosis. *Circulation.* 2014;129(18):1840–1849. doi: 10.1161/CIRCULATIONAHA.113.006242

16. Stern LK, Patel J. Cardiac Amyloidosis Treatment. *Methodist Debakey Cardiovasc J.* 2022;18(2):59–72. doi: 10.14797/mdcvj.1050

17. Kristen AV., aus dem Siepen F, Scherer K, et al. Comparison of different types of cardiac amyloidosis by cardiac magnetic resonance imaging. *Amyloid.* 2015;22(2):132–141. doi: 10.3109/13506129.2015.1020153

18. Gillmore JD, Maurer MS, Falk RH, et al. Nonbiopsy diagnosis of cardiac transthyretin amyloidosis. *Circulation.* 2016;133(24):2404–2412. doi: 10.1161/CIRCULATIONAHA.116.021612

19. Martinez-Naharro A, Treibel TA, Abdel-Gadir A, et al. Magnetic resonance in transthyretin cardiac amyloidosis. *J Am Coll Cardiol.* 2017;70(4):466–477. doi: 10.1016/j.jacc.2017.05.053

20. Binder C, Duca F, Binder T, et al. Prognostic implications of pericardial and pleural effusion in patients with cardiac amyloidosis. *Clinical Research in Cardiology.* 2021;110(4):532–543. doi: 10.1007/s00392-020-01698-7

21. Reddy A, Singh V, Karthikeyan B, et al. Biventricular strain imaging with cardiac MRI in genotyped and histology validated amyloid cardiomyopathy. *Cardiogenetics.* 2021;11(3):98–110. doi: 10.3390/cardiogenetics11030011

СПИСОК ЛИТЕРАТУРЫ

1. Wechalekar A.D., Gillmore J.D., Hawkins P.N. Systemic amyloidosis // Lancet. 2016. Vol. 387, N 10038. P. 2641–2654. doi: 10.1016/S0140-6736(15)01274-X

2. Rapezzi C., Lorenzini M., Longhi S., et al. Cardiac amyloidosis: the great pretender // Heart Fail Rev. 2015. Vol. 20, N 2. P. 117–124. doi: 10.1007/s10741-015-9480-0

3. Мясников Р.П., Андреенко Е.Ю., Кушунина Д.В., и др. Амилоидоз сердца: современные аспекты диагностики и лечения (клиническое наблюдение) // Клиническая и экспериментальная хирургия. 2014. № 4. С. 72–82. EDN: TRLZYN

4. Maurer M.S., Elliott P., Comenzo R., et al. Addressing common questions encountered in the diagnosis and management of cardiac amyloidosis // Circulation. 2017. Vol. 135, N 14. P. 1357–1377. doi: 10.1161/CIRCULATIONAHA.116.024438

5. Ruberg F.L., Grogan M., Hanna M., et al. Transthyretin amyloid cardiomyopathy: JACC state-of-the-art review // J Am Coll Cardiol. 2019. Vol. 73, N 22. P. 2872–2891. doi: 10.1016/j.jacc.2019.04.003

679

6. Kittleson M.M., Maurer M.S., Ambardekar A.V., et al.; American Heart Association Heart Failure and Transplantation Committee of the Council on Clinical Cardiology. Cardiac amyloidosis: evolving diagnosis and management: a scientific statement from the American Heart Association // Circulation. 2020. Vol. 142, N 1. P. e7–e22. doi: 10.1161/CIR.0000000000000792

7. Maurer M.S., Bokhari S., Damy T., et al. Expert consensus recommendations for the suspicion and diagnosis of transthyretin cardiac amyloidosis // Circ Heart Fail. 2019. Vol. 12, N 9. P. e006075. doi: 10.1161/CIRCHEARTFAILURE.119.006075

8. Garcia-Pavia P., Rapezzi C., Adler Y., et al. Diagnosis and treatment of cardiac amyloidosis: a position statement of the ESC Working Group on Myocardial and Pericardial Diseases // Eur Heart J. 2021. Vol. 42, N 16, P. 1554–1568. doi: 10.1093/eurheartj/ehab072

9. Лысенко Л.В., Рамеев В.В., Моисеев С.В., и др. Клинические рекомендации по диагностике и лечению системного амилоидоза // Клиническая фармакология и терапия. 2020. Т. 29, № 1. С. 13–24. EDN UCEZAB doi: 10.32756/ 0869-5490-2020-1-13-24

10. Syed I.S., Glockner J.F., Feng D., et al. Role of cardiac magnetic resonance imaging in the detection of cardiac amyloidosis // JACC Cardiovasc Imaging. 2010. Vol. 3, N 2, P. 155–164. doi: 10.1016/j.jcmg.2009.09.023

11. Буторова Е.А., Стукалова О.В. Возможности магнитно-резонансной томографии сердца в диагностике амилоидоза сердца. Клинические примеры // Клинический разбор в общей медицине. 2021. № 2. С. 16–20. EDN MUWTXO doi: 10.47407/kr2021.2.2.00037

12. Dorbala S., Ando Y., Bokhari S., et al. ASNC/AHA/ASE/EANM/HFSA/ISA/SCMR/SNMMI expert consensus recommendations for multimodality imaging in cardiac amyloidosis: Part 1 of 2-evidence base and standardized methods of imaging // J Nucl Cardiol. 2019. Vol 26, N 6. P. 2065–2123. doi: 10.1007/s12350-019-01760-6

13. Dungu J.N., Valencia O., Pinney J.H., et al. CMR-based differentiation of AL and ATTR cardiac amyloidosis // JACC Cardiovasc Imaging. 2014. Vol. 7, N 2. P. 133–142. doi: 10.1016/j.jcmg.2013.08.015

14. Itzhaki Ben Zadok O., Vaturi M., Vaxman I., et al. Differences in the characteristics and contemporary cardiac outcomes of patients with light-chain versus transthyretin cardiac amyloidosis // PLoS One. 2021. Vol. 16, N 8. P. e0255487. doi: 10.1371/journal.pone.0255487

15. Quarta C.C., Solomon S.D., Uraizee I., et al. Left ventricular structure and function in transthyretin-related versus light-chain cardiac amyloidosis // Circulation. 2014. Vol. 129, N 18. P. 1840–1849. doi: 10.1161/CIRCULATIONAHA.113.006242

16. Stern L.K., Patel J. Cardiac amyloidosis treatment // Methodist Debakey Cardiovasc J. 2022. Vol. 18, N 2. P. 59–72. doi: 10.14797/mdcvj.1050

17. Kristen A.V., aus dem Siepen F., Scherer K., et al. Comparison of different types of cardiac amyloidosis by cardiac magnetic resonance imaging // Amyloid. 2015. Vol. 22, N 2. P. 132–141. doi: 10.3109/13506129.2015.1020153

18. Gillmore J.D., Maurer M.S., Falk R.H., et al. Nonbiopsy diagnosis of cardiac transthyretin amyloidosis // Circulation. 2016. Vol. 133, N 24. P. 2404–2412. doi: 10.1161/CIRCULATIONAHA.116.021612

19. Martinez-Naharro A., Treibel T.A., Abdel-Gadir A., et al. Magnetic resonance in transthyretin cardiac amyloidosis // J Am Coll Cardiol. 2017. Vol. 70, N 4. P. 466–477. doi: 10.1016/j.jacc.2017.05.053

20. Binder C., Duca F., Binder T., et al. Prognostic implications of pericardial and pleural effusion in patients with cardiac amyloidosis // Clinical Research in Cardiology. 2021. Vol. 110, N 4. P. 532–543. doi: 10.1007/s00392-020-01698-7

21. Reddy A., Singh V., Karthikeyan B., et al. Biventricular strain imaging with cardiac MRI in genotyped and histology validated amyloid cardiomyopathy // Cardiogenetics. 2021. Vol 11, N 3, P. 98–110. doi: 10.3390/cardiogenetics11030011

AUTHORS' INFO

* Zainab M. Magomedova, MD;
address: 4B Verkhnyaya str., village Rumyantsevo, 108811, Moscow, Russia;
ORCID: 0000-0001-6753-1525;
eLibrary SPIN: 5271-4915;
e-mail: magomedova.zainab.97@mail.ru

Tatyana V. Nikiforova, MD;
ORCID: 0000-0003-3072-8951;
eLibrary SPIN: 4997-0330;
e-mail: attrcmp@gmail.com

Dmitry Yu. Shchekochikhin, MD, Cand. Sci. (Medicine), Assistant Professor;
ORCID: 0000-0002-8209-2791;
eLibrary SPIN: 3753-6915;
e-mail: agishm@list.ru

Ekaterina S. Pershina, MD, Cand. Sci. (Medicine);
ORCID: 0000-0002-3952-6865;
eLibrary SPIN: 7311-9276;
e-mail: pershina86@mail.ru

ОБ АВТОРАХ

* Магомедова Зайнаб Магомедовна;
адрес: Россия, 108811, Москва, деревня Румянцево, ул. Верхняя, д. 4Б;
ORCID: 0000-0001-6753-1525;
eLibrary SPIN: 5271-4915;
e-mail: magomedova.zainab.97@mail.ru

Никифорова Татьяна Вячеславовна;
ORCID: 0000-0003-3072-8951;
eLibrary SPIN: 4997-0330;
e-mail: attrcmp@gmail.com

Щекочихин Дмитрий Юрьевич, канд. мед. наук, доцент;
ORCID: 0000-0002-8209-2791;
eLibrary SPIN: 3753-6915;
e-mail: agishm@list.ru

Першина Екатерина Сергеевна, канд. мед. наук;
ORCID: 0000-0002-3952-6865;
eLibrary SPIN: 7311-9276;
e-mail: pershina86@mail.ru

Konstantin V. Kovalev, MD;
ORCID: 0009-0004-4841-041X;
e-mail: radix606@yandex.ru

Khadizhat S. Abdulmazhidova;
ORCID: 0009-0008-5064-7802;
e-mail: abdulmazhidova.kh@mail.ru

Daria S. Rassechkina, MD;
ORCID: 0009-0007-8825-8485;
e-mail: rassechkina@yandex.ru

Alexander E. Grachev, MD, Cand. Sci. (Medicine);
ORCID: 0000-0001-7221-9392;
eLibrary SPIN: 4281-3923;
e-mail: gra4al@yandex.ru

Irina G. Rekhtina, MD, Dr. Sci. (Medicine);
ORCID: 0000-0001-5440-4340;
eLibrary SPIN: 4920-7144;
e-mail: rekhtina.i@blood.ru

Alexey N. Volovchenko, MD, Cand. Sci. (Medicine);
ORCID: 0000-0002-0923-735X;
eLibrary SPIN: 4120-8740;
e-mail: dr.volovchenko@mail.ru

Susanna D. Sarkisyan;
ORCID: 0000-0002-6454-1370;
e-mail: sysanna.sarkisyan.2001@mail.ru

Valentin E. Sinitsyn, MD, Dr. Sci. (Medicine), Professor;
ORCID: 0000-0002-5649-2193;
eLibrary SPIN: 8449-6590;
e-mail: vsini@mail.ru

Denis A. Andreev, MD, Dr. Sci. (Medicine);
ORCID: 0000-0002-0276-7374;
eLibrary SPIN: 8790-8834;
e-mail: dennan@mail.ru

Ковалёв Константин Витальевич;
ORCID: 0009-0004-4841-041X;
e-mail: radix606@yandex.ru

Абдулмажидова Хадижат Салахудиновна;
ORCID: 0009-0008-5064-7802;
e-mail: abdulmazhidova.kh@mail.ru

Рассечкина Дарья Сергеевна;
ORCID: 0009-0007-8825-8485;
e-mail: rassechkina@yandex.ru

Грачев Александр Евгеньевич, канд. мед. наук;
ORCID: 0000-0001-7221-9392;
eLibrary SPIN: 4281-3923;
e-mail: gra4al@yandex.ru

Рехтина Ирина Германовна, д-р мед. наук;
ORCID: 0000-0001-5440-4340;
eLibrary SPIN: 4920-7144;
e-mail: rekhtina.i@blood.ru

Воловченко Алексей Николаевич, канд. мед. наук;
ORCID: 0000-0002-0923-735X;
eLibrary SPIN: 4120-8740;
e-mail: dr.volovchenko@mail.ru

Саркисян Сусанна Давитовна;
ORCID: 0000-0002-6454-1370;
e-mail: sysanna.sarkisyan.2001@mail.ru

Синицын Валентин Евгеньевич, д-р мед. наук, профессор;
ORCID: 0000-0002-5649-2193;
eLibrary SPIN: 8449-6590;
e-mail: vsini@mail.ru

Андреев Денис Анатольевич, д-р мед. наук;
ORCID: 0000-0002-0276-7374;
eLibrary SPIN: 8790-8834;
e-mail: dennan@mail.ru

_____

* Corresponding author / Автор, ответственный за переписку

Potential use of radiomics analysis of cine-mode cardiac MRI to detect post-infarction lesions in the left ventricular myocardium

Aleksandra S. Maksimova[1], Denis S. Samatov[2], Boris S. Merzlikin[2], Tatyana A. Shelkovnikova[1], Artem I. Listratov[3], Konstantin V. Zavadovsky[1]

[1] Tomsk National Research Medical Center of the Russian Academy of Sciences, Tomsk, Russia;
[2] National Research Tomsk Polytechnic University, Tomsk, Russia;
[3] Siberian State Medical University, Tomsk, Russia

ABSTRACT

BACKGROUND: The size and location of an infarct lesion and its clear differentiation from normal tissue are important for clinical diagnosis and precision medicine. This paper is based on the study of radiomic attributes for differentiation of infarct and non-infarct tissue using non-contrast-enhanced cine-mode cardiac magnetic resonance imaging (MRI) data.

AIM: The aim of the study was to evaluate the potential use and informative value of radiomics analysis to identify post-infarction lesions in the left ventricular myocardium in patients with ischemic cardiomyopathy (ICM) using non-contrast-enhanced cine-mode cardiac MRI.

MATERIALS AND METHODS: Results of contrast-enhanced cardiac MRI were evaluated in 33 patients following surgical treatment for ICM. Texture analysis was performed on 66 lesions in cine-mode cardiac MRI images, and 105 texture attributes were determined for each lesion. Cardiac MRI was performed according to a standard technique using a Vantage Titan 1.5 T MRI scanner (Toshiba). For texture analysis, 3D Slicer version 5.2.2 (Pyradiomics) was used.

RESULTS: During the study, attribute collinearity diagrams were plotted, zero-significance attributes were identified, and attribute significance was determined using a gradient boosting algorithm, and the cumulative significance of attributes was estimated as a function of their total number. By identifying low-significance attributes, the least significant parameters that did not affect the overall significance level were determined. When single-valued attributes were extracted, no corresponding attributes were found. Based on the analysis results, an ROC curve was constructed for Lasso logistic regression (Se=57.14%, Sp=71.43%, AUC=0.76). The main result of this study was to determine radiomic attributes that characterized lesions corresponding to post-infarction cardiosclerosis and intact left ventricular wall based on cine-mode cardiac MRI images.

CONCLUSION: This study demonstrated that radiomics analysis of non-contrast-enhanced cine-mode cardiac MRI images is a promising approach to identify lesions corresponding to myocardial infarction and intact wall. This method may potentially be used to identify lesions of post-infarction cardiosclerosis in patients with ICM without contrast enhancement.

Keywords: radiomics; texture analysis; cardiac magnetic resonance imaging; myocardial infarction; ischemic cardiomyopathy.

Возможности радиомического анализа МРТ-изображений сердца в кино-режиме в определении постинфарктных областей миокарда левого желудочка

А.С. Максимова[1], Д.С. Саматов[2], Б.С. Мерзликин[2], Т.А. Шелковникова[1], А.И. Листратов[3], К.В. Завадовский[1]

[1] Научно-исследовательский институт кардиологии, Томский национальный исследовательский медицинский центр Российской академии наук, Томск, Россия;

[2] Национальный исследовательский Томский политехнический университет, Томск, Россия;

[3] Сибирский государственный медицинский университет, Томск, Россия

АННОТАЦИЯ

Обоснование. Размер и локализация, а также чёткая дифференциация между интактной тканью и областью инфаркта важны для клинической диагностики и прецизионной медицины. В основе данной работы лежит исследование радиомических признаков, которые позволяют дифференцировать участки инфарктной и удалённой от области инфаркта ткани по данным бесконтрастных изображений магнитно-резонансной томографии (МРТ) сердца в кино-режиме.

Цель. Оценка возможностей и информативности радиомического анализа в выявлении постинфарктных областей миокарда левого желудочка у пациентов с ишемической кардиомиопатией (ИКМП) по данным бесконтрастных изображений МРТ сердца в кино-режиме.

Материалы и методы. Мы проанализировали результаты МРТ сердца с контрастированием 33 пациентов, которым провели хирургическое лечение по поводу ИКМП. Текстурный анализ выполнили для 66 участков изображений МРТ сердца в кино-режиме, для каждого из них определяли 105 текстурных характеристик. МРТ сердца проводили по стандартной методике на магнитно-резонансном томографе Vantage Titan (Toshiba) 1,5 Тл. Для текстурного анализа использовали программное обеспечение 3D slicer-version 5.2.2, Pyradiomics.

Результаты. В ходе исследования мы построили диаграммы коллинеарности признаков, определили признаки с нулевой важностью и установили важность признаков с помощью алгоритма градиентного бустинга, а также оценили кумулятивную важность признаков в зависимости от их общего количества. С помощью метода выявления признаков с низкой важностью определили параметры с наименьшей значимостью, которые не влияют на указанный общий уровень. Используя метод выявления признаков с единственным значением, мы не нашли соответствующих функций. По результатам анализа сформирована ROC-кривая для логистической регрессии Lasso (Se=57,14%, Sp=71,43%, AUC=0,76). Основным результатом данного исследования является определение радиомических признаков, характеризующих на основе изображений МРТ сердца в кино-режиме участки, соответствующие постинфарктному кардиосклерозу и интактной стенке левого желудочка.

Заключение. Данное исследование показало, что применение радиомического анализа на бесконтрастных изображениях МРТ сердца в кино-режиме — перспективный подход для выявления участков, соответствующих инфаркту миокарда и интактной стенке. Метод потенциально может быть использован для идентификации областей постинфарктного кардиосклероза у пациентов с ИКМП без применения контрастных препаратов.

Ключевые слова: радиомика; текстурный анализ; магнитно-резонансная томография сердца; инфаркт миокарда; ишемическая кардиомиопатия.

在胶片模式下对心脏磁共振图像进行放射组学分析以确定左心室心肌梗死后区域的可能性

Aleksandra S. Maksimova[1], Denis S. Samatov[2], Boris S. Merzlikin[2], Tatyana A. Shelkovnikova[1], Artem I. Listratov[3], Konstantin V. Zavadovsky[1]

[1] Tomsk National Research Medical Center of the Russian Academy of Sciences, Tomsk, Russia;
[2] National Research Tomsk Polytechnic University, Tomsk, Russia;
[3] Siberian State Medical University, Tomsk, Russia

摘要

论证。这项工作的基础是对放射组学特征的研究，通过使用胶片模式下的非对比心脏磁共振成像（MRI）图像，可以区分梗死组织区域和远离梗死区域的组织。尺寸和定位，以及完整组织和梗死区域的明确区分对于临床诊断和精准医疗非常重要。

目的。根据胶片模式下的非对比心脏MRI图像数据，评估放射组学分析在检测缺血性心肌病（ICM）患者左心室心肌梗死后区域方面的能力和信息量。

材料和方法。我们分析了33名接受ICM手术治疗的患者的心脏磁共振成像造影结果。在胶片模式下，对66幅心脏 MRI 图像进行了纹理分析，并确定了每幅图像的 105 个纹理特征。心脏磁共振成像是在Vantage Titan（Toshiba）1.5 Tesla磁共振成像仪上按照标准方法进行的。纹理分析使用的是3D slicer-version 5.2.2, Pyradiomics。

结果。在研究中，我们构建了特征共线性图，识别了重要性为零的特征，并使用梯度提升算法确定了特征的重要性，并根据特征总数估计了特征的累积重要性。使用识别低重要性特征的方法，我们识别出不影响指定总体水平的最低重要性的参数。使用单值特征检测方法，我们没有发现任何相关特征。根据分析结果，生成用于Lasso逻辑回归的ROC曲线（Se=57.14%，Sp=71.43%，AUC=0.76）。该研究的主要成果是在胶片模式的心脏磁共振成像基础上，确定心肌梗塞后心肌梗死和左心室壁完整区域的放射组学特征。

结论。该研究表明，在胶片模式下非对比心脏磁共振图像进行放射组学分析是一种很有前途的方法，可用于识别心肌梗死和完整壁的相应区域。这种方法可用于识别 ICM 患者梗死后心脏硬化的区域，而无需使用造影剂。

关键词：放射组学；纹理分析；心脏磁共振成像；心肌梗死；缺血性心肌病。

BACKGROUND

The incidence of cardiovascular diseases continues to rise each year. Coronary artery disease is the most prevalent cardiovascular complication and the leading cause of death and disability in adults globally [1]. Myocardial infarction (MI), the most common form of coronary artery disease, is characterized by irreversible cardiac muscle necrosis caused by an acute disruption of coronary circulation [2, 3]. The size and location of the lesion, along with its distinction from normal tissue, are critical for accurate clinical diagnosis and treatment planning [4]. MI is often followed by left ventricular (LV) remodeling, a progressive condition that involves changes in LV size and function within hours after the coronary circulation disturbance [5]. Post-ischemic LV remodeling has a complex pathophysiology, involving various ultrastructural, metabolic, and neurotransmitter processes in the affected and surrounding myocardial tissue. Cardiac remodeling is thought to influence the clinical progression of heart failure [6].

Contrast-enhanced cardiac MRI is widely used and is an important tool for assessing the presence, prevalence, and severity of post-infarction changes in the myocardium. It is also employed to assess myocardial viability and LV remodeling. This technique provides a qualitative assessment of MI and detects microvascular obstruction and hyperemia, which are key factors for determining unfavorable remodeling and predicting adverse cardiovascular outcomes [7–9]. However, this technique has several limitations, including a high dependency on subjective physician judgment and intraoperator variability. Additionally, gadolinium-based contrast agents can lead to nephrogenic systemic fibrosis in patients with renal insufficiency [10], a significant concern given the high prevalence of concurrent renal disorders in patients with cardiovascular diseases [11].

To address these challenges, emerging techniques such as radiomics and texture analysis offer promising alternatives for extracting quantitative data from digital medical images. Radiomics enables a reliable assessment of abnormal changes detected in medical imaging by transforming image data into quantitative measures. Previous studies have explored the potential of texture analysis in cardiac MRI images to differentiate between conditionally normal and nonviable myocardial segments [12]. Some investigations have focused on detecting cicatricial changes in the LV myocardium using non-contrast-enhanced cardiac cine-MRI [13]. Given the morphological differences between affected and healthy myocardium, the corresponding texture features of these areas will also differ [14]. It was assumed that subtle differences between nonviable and conditionally normal segments could be detected on cardiac cine-MRI images using radiomics analysis, based on variations in gray level nonuniformity. However, few studies have confirmed this hypothesis [15, 16]. This theory suggests that post-infarction cardiosclerosis areas could be identified using only non-contrast-enhanced cardiac cine-MRI images, reducing the risks associated with gadolinium-based contrast agents and significantly lowering both the cost and time of analysis. Currently, no such studies have been conducted in patients with ischemic cardiomyopathy (ICM).

AIM

To assess the potential and diagnostic value of radiomics analysis in detecting post-infarction lesions in the LV myocardium in patients with ICM using non-contrast-enhanced cardiac cine-MRI.

MATERIALS AND METHODS

Study design

This observational, single-center, retrospective, cross-sectional, single-arm study involved male and female patients aged 52–65 years who underwent surgical treatment for ICM. All patients received a contrast-enhanced cardiac MRI either as part of their clinical care or according to the study protocol.

Eligibility criteria

The study included patients who met the established criteria for ICM [17]:

1) A history of MI

2) Multivessel coronary artery disease, confirmed by invasive coronary angiography

3) Left ventricular ejection fraction (LVEF) of <40%

4) Increased end-systolic volume (ESV) >60 mL/m^2

5) Heart failure classified as New York Heart Association (NYHA) class II–IV

Patients with infectious and rheumatic heart diseases, stroke, acute MI, and right ventricular failure were extracted from the study.

The study used contrast-enhanced cardiac MRI images from patients who underwent surgical treatment for ICM between 2019 and 2023.

Study setting

Patients were enrolled at the Research Institute of Cardiology, Tomsk National Research Medical Center, Russian Academy of Sciences.

The study included patients who underwent cardiac MRI with paramagnetic contrast to assess myocardial viability.

Main study outcome

The primary outcome was the difference in radiomic features between intact myocardium and post-infarction cardiosclerosis (PICS) areas on cardiac cine-MRI images.

Outcomes registration

Contrast-enhanced cardiac MRI

The study reviewed patients' medical records to gather data from cardiac MRIs with paramagnetic contrast agents, performed to assess myocardial viability. ECG- and respiratory-gated MRI scans were conducted according to standard procedures using a *Vantage Titan 1.5-T scanner* (Toshiba). Short- and long-axis myocardial images were acquired before and after gadolinium-based contrast injection (gadobutrol 0.1–0.15 mmol/kg body weight). The slice thickness was 7–8 mm, and images were acquired using a 256 × 256 matrix. The MRI protocol included T1- and T2-weighted images, fat-suppressed images to assess the myocardium, dynamic SSFP sequences for LV volume and function assessment, and gradient inversion-recovery (GR-IR) sequences to identify areas of abnormal contrast uptake. The inversion time was selected individually for each case (mean TI, 300 ± 10 ms). Abnormal myocardial changes were assessed using a standardized 17-segment system for LV myocardium segmentation. The primary LV parameters were calculated using segment post-processing software (version 2.2, Medviso AB).

Radiomics analysis

Texture analysis was performed using non-contrast-enhanced cardiac cine-MRI images. All images were segmented using *3D slicer software* (version 5.2.2), and radiomic features were automatically extracted using the *SlicerRadiomics extension* (version aa418a5).

The radiomic features of intact myocardium were compared with those of the PICS areas on non-contrast-enhanced cine-MRI images.

Regions of interest (ROIs) were manually selected to assess differences in radiomic features between intact myocardium and PICS areas. The size and position of the ROIs corresponded to the PICS areas and intact myocardium

regions based on time-delayed contrast-enhanced MRI images. Initially, ROIs were manually selected on MRI slices along the short axis (in SSFP mode) that matched the PICS areas on post-contrast MRI images. Texture features were then extracted using the PyRadiomics library. The ROI selection process is illustrated in Fig. 1.

Texture analysis was performed on 66 areas from the cardiac cine-MRI images, with 105 texture features calculated for each area. These texture features were categorized as follows:
- First-order features (Energy, Entropy, Range, Kurtosis, etc.)
- 3D shape features (Mesh Volume, Voxel Volume, Sphericity, etc.)
- 2D shape features (Perimeter, Pixel Surface, Elongation, etc.)
- Gray Level Co-occurrence Matrix
- Gray Level Run Length Matrix
- Gray Level Size Zone Matrix
- Neighboring Gray Tone Difference Matrix
- Gray Level Dependence Matrix

Ethical review

The study was conducted in accordance with Good Clinical Practice and the Declaration of Helsinki. All patients provided written informed consent. The study received approval from the Institutional Review Board of the Research Institute of Cardiology, Tomsk National Research Medical Center (Minutes No. 210, dated February 18, 2021).

Statistical analysis

Statistical processing included the following steps: selection of significant texture features, plotting of feature collinearity diagrams, feature selection based on significance, and application of Lasso regression. Features selection was performed using the following *Python* functions: *identify_collinear*, *identify_zero_importance*, *identify_low_importance*, *identify_single_unique*, and *identify_all*. The sample size was not predetermined.
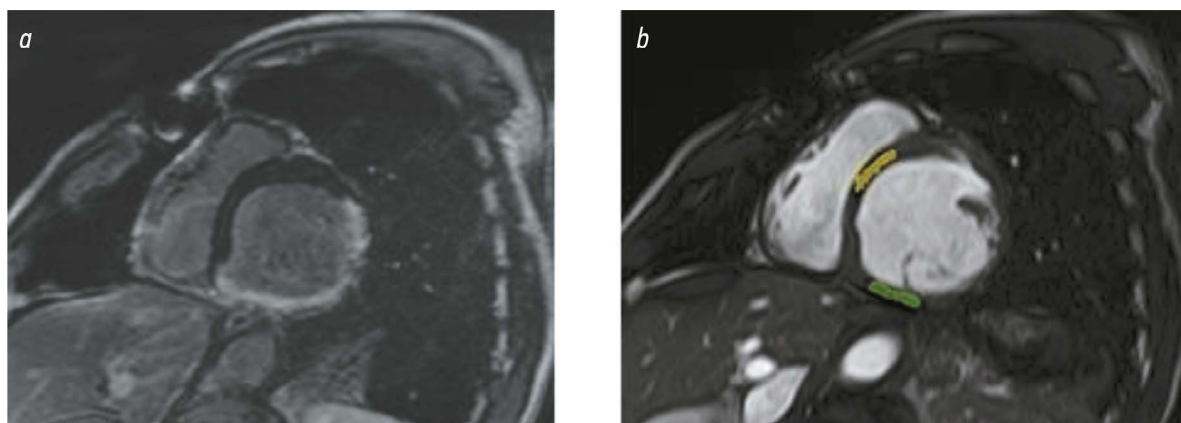
Fig. 1. Selection of regions of interest in post-contrast and non-contrast-enhanced cardiac MRI images, short axis view. *a*: time-delayed contrast-enhanced MRI showing transmural contrast uptake along the LV inferior wall with no signs of damage in the interventricular septum. *b*: cardiac cine-MRI showing regions of interest in the posterior wall (green), corresponding to a PICS area in the inferior segment at the middle LV level, and in the anteroseptal segment at the middle level (yellow), corresponding to an intact interventricular septum.

RESULTS

Participants

Study sample characteristics

The study included 33 patients with ICM. The mean age was 58.3 ± 5.7 years, and 94% of the patients were male. All patients had angina pectoris and heart failure, with NYHA class III being the most prevalent (67% and 61%, respectively). Hypertension was present in 85% of the patients, dyslipidemia in 73%, and diabetes mellitus in 24%. The clinical characteristics of these patients are shown in Table 1.

Contrast-enhanced cardiac MRI

Table 1. Clinical characteristics of the patients

Parameter	Value
Age, years	58.3 ± 5.7
Male, n (%)	31 (94%)
BMI, kg/m^2	27.5 ± 3.9
History of hypertension, n (%)	28 (85%)
Heart failure NYHA class, n (%):	
• I	0 (0%)
• II	12 (39%)
• III	20 (61%)
• IV	0 (0%)
Angina pectoris NYHA class, n (%):	
• I	1 (3%)
• II	10 (30%)
• III	22 (67%)
• IV	0 (0%)
Diabetes mellitus, n (%)	8 (24%)
Dyslipidemia, n (%)	24 (73%)

Note. BMI, body mass index; NYHA, New York Heart Association classification.

Table 2. Findings from contrast-enhanced cardiac magnetic resonance imaging

Parameter	Value
LVEF, %	31.5 ± 7.5
ESV, mL/m^2	79.7 ± 16.7
LVMM, g	190.8 ± 2.1
VMM, g	140.8 ± 30.05
Number of segments with transmurality >50%	4.4 ± 2.6
Ratio of myocardial mass with contrast uptake to LVMM, %	27.1 ± 6.9
Thrombosis, n (%)	5 (15)

Note. LVEF, left ventricular ejection fraction; LVMM, left ventricular myocardial mass; VMM, viable myocardial mass.

All patients had a LVEF <40% on contrast-enhanced cardiac MRI. The myocardial mass and LV ESV were elevated. Time-delayed contrast-enhanced MRI identified areas of abnormal contrast uptake corresponding to PICS in all patients. Five (15%) patients had thrombotic masses in a thinned LV wall, and 31 (94%) showed evidence of LV spherical remodeling. The contrast-enhanced cardiac MRI findings are provided in Table 2.

Primary results

Data preprocessing

We removed columns and rows with a missing value rate >0.75. For the remaining data, missing values were imputed using the feature means.

Feature collinearity diagrams

The identify_collinear function was used to detect collinear predictors. For each pair of highly correlated features, the function identified which one to remove. In machine learning, strong correlations between features can increase variance and reduce model interpretability. We identified 33 radiomic features with a correlation coefficient of >0.98. Heat maps were used to visually represent feature collinearity, with columns indicating correlated features and rows indicating the features marked for removal (Fig. 2, 3).

Features with zero importance

The identify_zero_importance function was used to identify features with zero importance. Removing these features does not impact diagnostic performance. Additionally, we applied the FeatureSelector function and a gradient boosting algorithm to assess feature importance. To minimize variance, the importance value was averaged over 10 training iterations. Early stopping with a control dataset was used to prevent overtraining. Fig. 4 shows the normalized importance of the most significant features, with the X-axis representing the normalized importance of each feature.

We also assessed the cumulative importance of the features based on their total number. We found that 27 features contributed to the overall variation (Fig. 5).

Features with low importance

The identification of features with low importance was based on the same approach used previously. *The identify_low_importance function* was used to identify features with minimal importance that do not affect the overall outcome. We found that 27 features were needed to achieve a total importance of 0.98, whereas 78 features contributed no additional value to the total importance.

Features with a single value

To identify features with a single value, we selected columns containing only one distinct value. These features exhibit zero variance and are not informative for machine
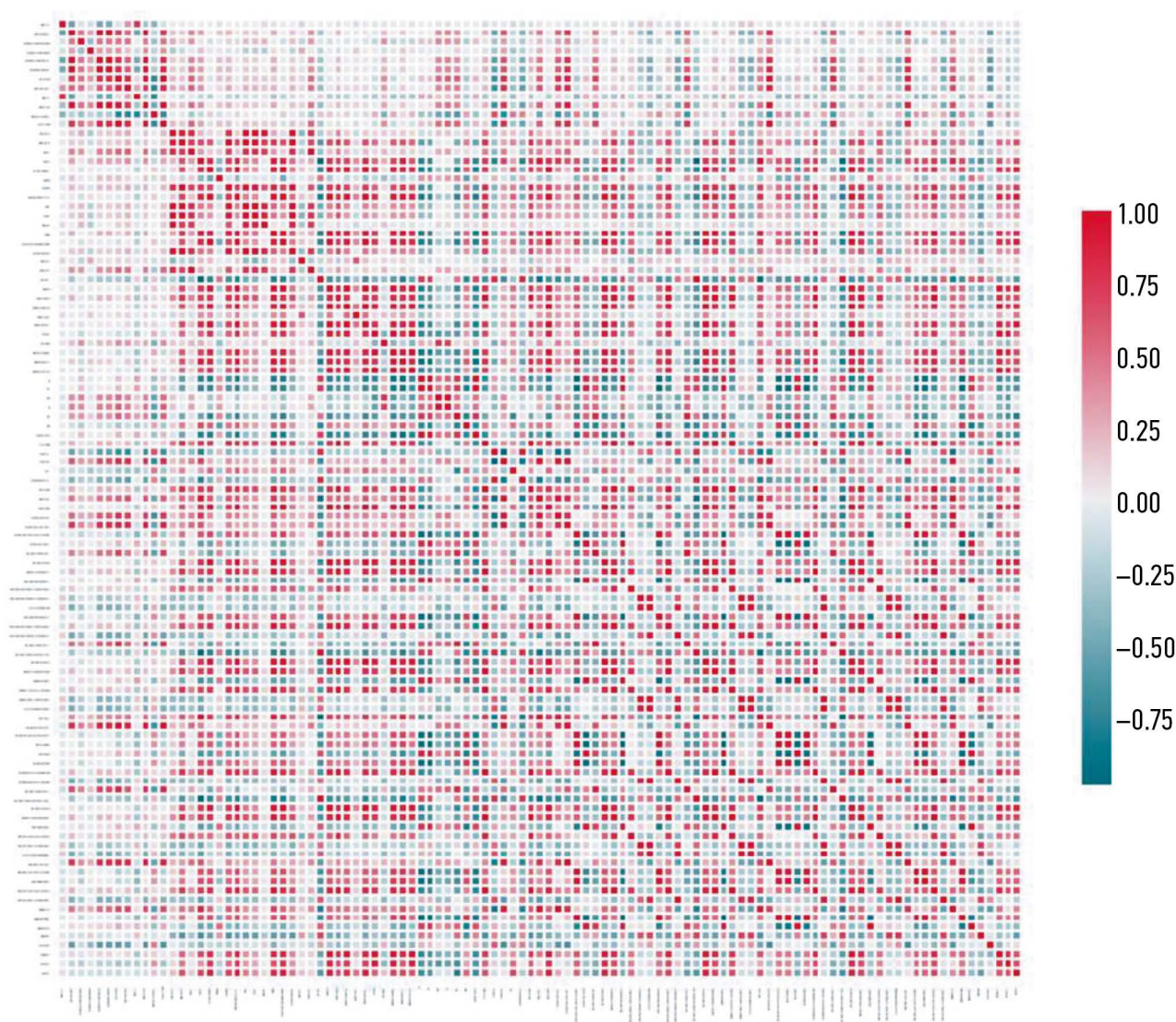
Fig. 2. Heat map showing correlations across the dataset.

learning. Using this method, we found no features with a single unique value (Fig. 6).

We applied Lasso logistic regression to select features and generate a receiver operating characteristic (ROC) curve (Fig. 7). The training accuracy and test accuracy were 0.77 and 0.64, respectively (sensitivity, 57.14%; specificity, 71.43%).

DISCUSSION

Main study outcome

This study assessed the potential of radiomics analysis of non-contrast-enhanced cardiac cine-MRI images for detecting areas corresponding to PICS and intact myocardial tissue in patients with ICM. Using Lasso regression, the method achieved a specificity and sensitivity of 57.14% and 71.43%, respectively. The findings support the ability to differentiate between cicatricial changes in the myocardium and conditionally normal tissue. The relatively low sensitivity and specificity are likely attributable to the small sample size.

Discussion of primary results

The study findings suggest that radiomic features extracted from cine-MRI images can help in identifying post-infarction lesions, thereby potentially improving MI detection and reducing the risks associated with gadolinium-based contrast agents. Few studies have focused on texture analysis of non-contrast-enhanced cardiac cine-MRI images, and none were found in patients with ICM.

These findings align with the study by Smith et al., which showed the significance of machine learning-based radiomic features from non-contrast-enhanced cardiac MRI images for distinguishing between MI and normal myocardial tissue, providing new avenues for clinical diagnosis (AUC 0.88) [16]. Similarly, another study showed that radiomics analysis of non-contrast-enhanced cardiac MRI images in patients with ST-elevation MI (STEMI) helps to assess unfavorable LV remodeling, enhancing diagnostic accuracy and prognosis (AUC 0.82) [18]. Additionally, combining native T1 mapping and extracellular volume mapping in cardiac MRI with radiomics analysis improves the prediction of cardiac function recovery
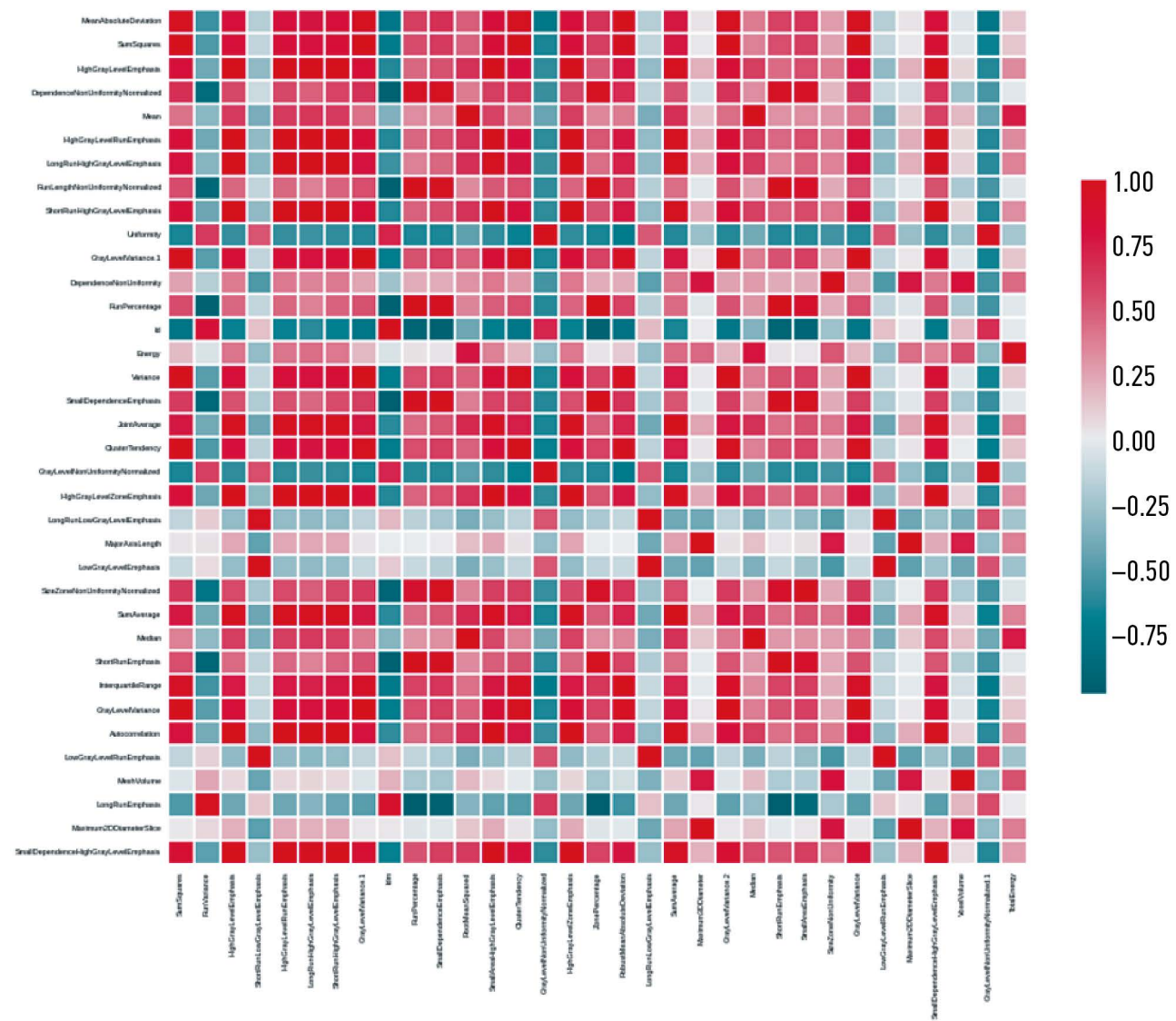
Fig. 3. Correlation heat map for 33 features with a correlation coefficient >0.98.
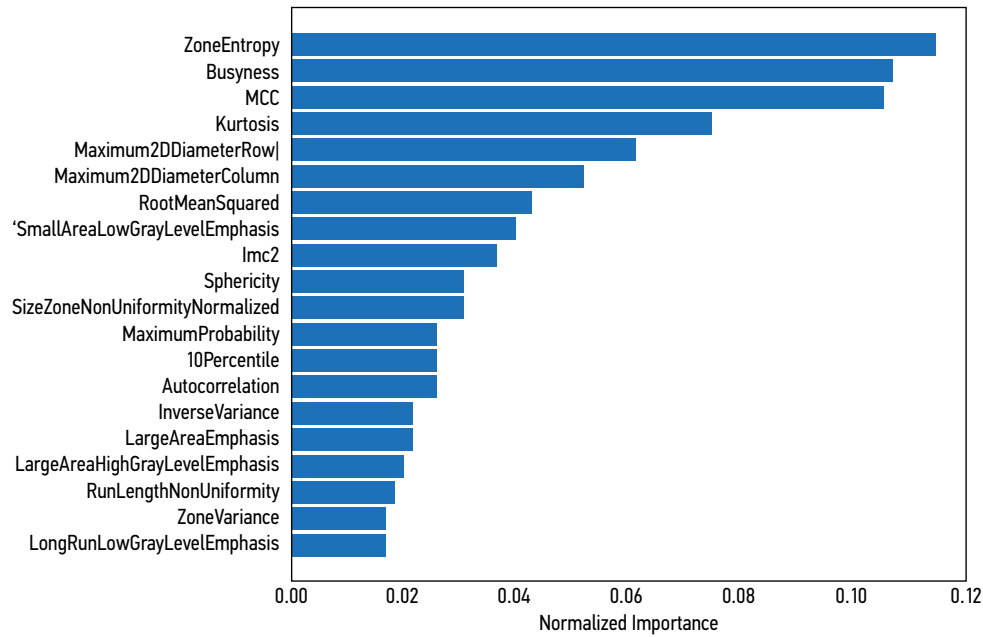
Fig. 4. Normalized importance values.
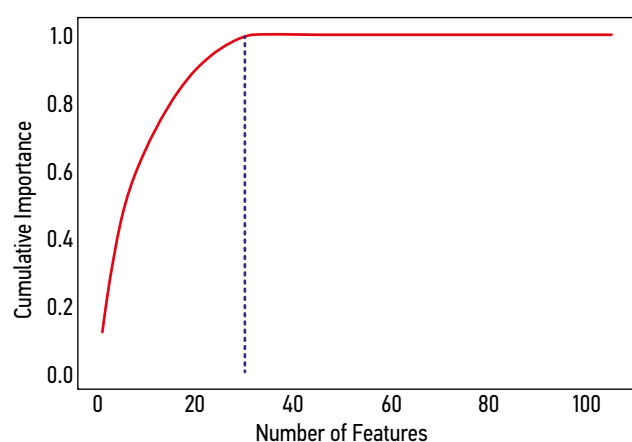
Fig. 5. Changes in cumulative feature importance.
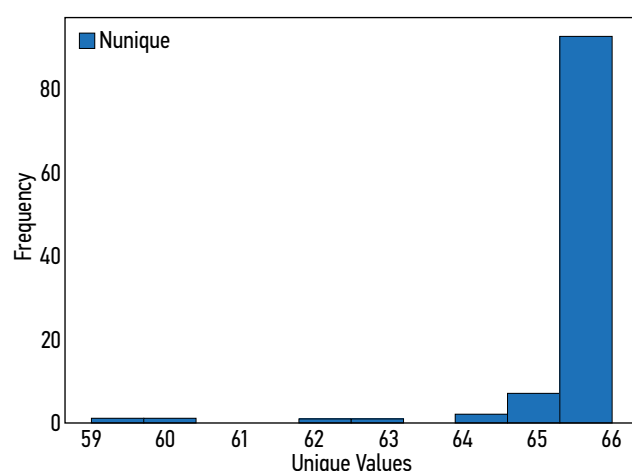
Fig. 6. Number of unique values for each feature.

and microvascular damage. Ma et al. demonstrated that radiomics analysis of non-contrast-enhanced T1 mapping images aids in diagnosing acute MI and predicting myocardial function recovery [19]. This approach improves the accuracy of detecting microvascular obstruction and enhances the long-term prognosis of myocardial contractility. Additionally, native T1 mapping-based radiomics can predict major adverse cardiovascular events in patients with STEMI, aiding in risk stratification [20]. Chen et al. found that extracellular volume mapping-based texture analysis can differentiate between reversible and irreversible myocardial damage in STEMI patients, helping to predict unfavorable LV remodeling, which has clinical significance (AUC 0.91) [21]. Another study showed that native T1 mapping-based radiomic features can predict the risk of unfavorable LV remodeling in patients with non-ischemic dilated cardiomyopathy (AUC 0.81) [22]. Modern mapping techniques can effectively detect various myocardial disorders, but their availability is currently limited. We propose an alternative method using non-contrast-enhanced cardiac cine-MRI images, without the need for mapping or contrast enhancement, which provides sufficient accuracy (AUC 0.77).
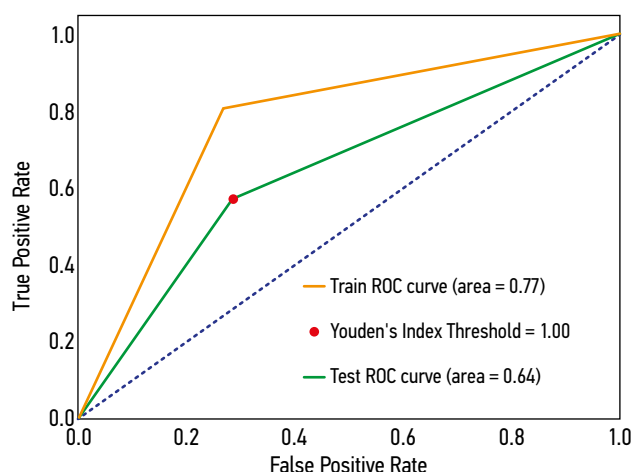
Fig. 7. ROC curves for training accuracy (AUC 0.77) and test accuracy (AUC 0.64).

In recent years, MRI has become the gold standard for noninvasive diagnosis and comprehensive assessment of structural changes in the myocardium [23]. In addition to the well-established diagnostic value of dynamic SSFP sequences for assessing LV volume and function, time-delayed contrast-enhanced MRI is a unique tool for detecting and quantifying PICS areas. The lesion area derived from time-delayed contrast-enhanced MRI findings plays a crucial role in predicting LV remodeling [24]. However, the use of contrast agents is limited to specific patient groups. Many post-infarction patients are clinically unstable during the examination and cannot undergo lengthy procedures. Additionally, gadolinium-based contrast agents may cause side effects, such as renal function impairment, in patients with renal insufficiency.

Study limitations

This study has several limitations, including its retrospective design and small sample size. The sample size required to achieve sufficient statistical power was not determined prior to or during the study. As a result, the sample may not be fully representative, limiting the ability to generalize the findings to the broader population of patients with this condition. Moreover, the study did not include a validation sample to assess the diagnostic value of the model. However, despite the small sample, the study successfully identified significant differences between intact tissue and PICS areas using radiomics analysis of cine-MRI images.

CONCLUSION

Radiomics analysis of non-contrast-enhanced cardiac cine-MRI images can differentiate between PICS areas and viable myocardium. Therefore, this technique could serve as an alternative to time-delayed contrast-enhanced MRI in patients with MI. However, further studies with larger sample sizes and models with stronger prognostic value are needed to identify patients with ICM and support clinical decision-making in their management.

ADDITIONAL INFORMATION

REFERENCES

1. Shalnova SA, Drapkina OM, Kutsenko VA, et al. Myocardial infarction in the population of some Russian regions and its prognostic value. *Russian Journal of Cardiology.* 2022;27(6):4952. EDN: OCPROJ doi: 10.15829/1560-4071-2022-4952

2. Desai R, Mishra V, Chhina AK, et al. Cardiovascular disease risk factors and outcomes of acute myocardial infarction in young adults: evidence from 2 nationwide cohorts in the United States a decade apart. *Curr Probl Cardiol.* 2023;48(9):101747. doi: 10.1016/j.cpcardiol.2023.101747

3. Martins-Marques T, Hausenloy DJ, Sluijter JP, et al. Girao Intercellular communication in the heart: therapeutic opportunities for cardiac ischemia. *Trends Mol Med.* 2021;27:248–262. doi: 10.1016/j.molmed.2020.10.002

4. Schuleri KH, Centola M, Evers KS, et al. Cardiovascular magnetic resonance characterization of peri-infarct zone remodeling following myocardial infarction. *J Cardiovasc Magn Reson.* 2012;14:24. doi: 10.1186/1532-429X-14-24

5. Bodi V, Monmeneu JV, Ortiz-Perez JT, et al. Prediction of Reverse Remodeling at Cardiac MR Imaging Soon after First ST-Segment-Elevation Myocardial Infarction: Results of a Large Prospective Registry. *Radiology.* 2016;278:54–63. doi: 10.1148/radiol.2015142674

6. Del Buono MG, Garmendia CM, Seropian IM, et al. Heart Failure After ST-Elevation Myocardial Infarction: Beyond Left Ventricular Adverse Remodeling. *Curr Probl Cardiol.* 2022;48(8):101215. doi: 10.1016/j.cpcardiol.2022.101215

7. Ibanez B, Aletras AH, Arai AE, et al. Cardiac MRI Endpoints in Myocardial Infarction Experimental and Clinical Trials: JACC Scientific Expert Panel. *J Am Coll Cardiol.* 2019;74(2):238–256. doi: 10.1016/j.jacc.2019.05.024

8. Ussov WYu, Babokin VE, Mochula OV, et al. Contrast-enhanced magnetic resonance tomography in patients with myocardial infarction and supraventricular tachyarrhythmias. *Siberian Journal of Clinical and Experimental Medicine.* 2014;29(4):33–38. EDN: TBFGPX doi: 10.29001/2073-8552-2014-29-4-33-38

9. Usov VYu, Vyshlov EV, Mochula OV, et al. Contrast-ehanced MRI in time-structure analysis of myocardial damage in acute infarction and early prehospital thrombolytic therapy. *Medical Visualization.* 2018;(2):56–69. EDN: XMLLXN doi: 10.24835/1607-0763-2018-2-56-69

10. Kuo PH, Kanal E, Abu-Alfa AK, Cowper SE Gadolinium-based MR contrast agents and nephrogenic systemic fibrosis. *Radiology.* 2007;242(3):647–649. doi: 10.1148/radiol.2423061640

11. Kim RJ, Wu E, Rafael A, et al. The use of contrast-enhanced magnetic resonance imaging to identify reversible myocardial dysfunction. *N Engl J Med.* 2000;343(20):1445–1453. doi: 10.1056/NEJM200011163432003

12. Kotu LP, Engan K, Eftestol T, et al. Segmentation of scarred and non-scarred myocardium in LG enhanced CMR images using intensity-based textural analysis. *Annu Int Conf IEEE Eng Med Biol Soc.* 2011:5698–5701. doi: 10.1109/IEMBS.2011.6091379

13. Larroza A, Lopez-Lereu MP, Monmeneu JV, et al. Texture analysis of cardiac cine magnetic resonance imaging to detect nonviable segments in patients with chronic myocardial infarction. *Med Phys.* 2018;45(4):1471–1480. doi: 10.1002/mp.12783

14. Maksimova AS, Ussov WYu, Shelkovnikova TA, et al. Cardiac MRI Radiomics: review. *Siberian Journal of Clinical and Experimental Medicine.* 2023;38(3):13–22. EDN: RUADYI doi: 10.29001/2073-8552-2023-39-3-13-22

15. Larroza A, Materka A, Lopez-Lereu MP, et al. Differentiation between acute and chronic myocardial infarction by means of texture analysis of late gadolinium enhancement and cine cardiac magnetic resonance imaging. *Eur J Radiol.* 2017;92:78–83. doi: 10.1016/j.ejrad.2017.04.024

16. Avard E, Shiri I, Hajianfar G, et al. Non-contrast Cine Cardiac Magnetic Resonance image radiomics features and machine learning algorithms for myocardial infarction detection. *Comput Biol Med.* 2022;141:105145. doi: 10.1016/j.compbiomed

17. Felker GM, Shaw LK, O'Connor CM A standardized definition of ischemic cardiomyopathy for use in clinical research. *J Am Coll Cardiol.* 2002;39(2):210–218. doi: 10.1016/s0735-1097(01)01738-7

18. Liu M, Xin A, Chen T, et al. Non-contrast cine cardiac magnetic resonance derived-radiomics for the prediction of left ventricular adverse remodeling in patients with ST-segment elevation myocardial infarction. *Korean J Radiol.* 2023;24(9):827–837. doi: 10.3348/kjr.2023.0061

19. Ma Q, Ma Y, Yu T, et al. Radiomics of non-contrast-enhanced T1 mapping: diagnostic and predictive performance for myocardial injury in acute ST-segment-elevation myocardial infarction. *Korean J Radiol.* 2021;22(4):535–46. doi: 10.3348/kjr.2019.0969

20. Ma Q, Ma Y, Wang X, et al. A radiomic nomogram for prediction of major adverse cardiac events in ST-segment elevation myocardial infarction. *Eur Radiol.* 2021;31(2):1140–1150. doi: 10.1007/s00330-020-07176-y

21. Chen BH, An DA, He J, et al. Myocardial extracellular volume fraction radiomics analysis for differentiation of reversible versus irreversible myocardial damage and prediction of left ventricular adverse remodeling after ST-elevation myocardial infarction. *Eur Radiol.* 2021;31(1):504–514. doi: 10.1007/s00330-020-07117-9

22. Chang S, Han K, Kwon Y, et al. T1 Map-based radiomics for prediction of left ventricular reverse remodeling in patients with non-ischemic dilated cardiomyopathy. *Korean J Radiol.* 2023;24:395–405. doi: 10.3348/kjr.2023.0065

23. Frederiksen H, Iorgoveanu C, Mahi A. State of the Art and New Advances: Cardiac MRI. New Advances in Magnetic Resonance Imaging. 2023. Available from: http://dx.doi.org/10.5772/intechopen.112413. doi: 10.5772/intechopen.112413

24. Bodi V, Monmeneu JV, Ortiz-Perez JT, et al. Prediction of Reverse Remodeling at Cardiac MR Imaging Soon after First ST-Segment-Elevation Myocardial Infarction: Results of a Large Prospective Registry. *Radiology.* 2016;278(1):54–63. doi: 10.1148/radiol.2015142674

СПИСОК ЛИТЕРАТУРЫ

1. Шальнова С.А., Драпкина О.М., Куценко В.А., и др. Инфаркт миокарда в популяции некоторых регионов России и его прогностическое значение // Российский кардиологический журнал. 2022. Т. 27, № 6. С. 4952. EDN: OCPROJ doi: 10.15829/1560-4071-2022-4952

2. Desai R., Mishra V., Chhina A.K., et al. Cardiovascular disease risk factors and outcomes of acute myocardial infarction in young adults: evidence from 2 nationwide cohorts in the United States a decade apart // Curr Probl Cardiol. 2023. Vol. 48, N 9. P. 101747. doi: 10.1016/j.cpcardiol.2023.101747

3. Martins-Marques T., Hausenloy D.J., Sluijter J.P., et al. Girao Intercellular communication in the heart: therapeutic opportunities for cardiac ischemia // Trends Mol. Med. 2021. Vol. 27, P. 248–262. doi: 10.1016/j.molmed.2020.10.002

4. Schuleri K.H., Centola M., Evers K.S., et al. Cardiovascular magnetic resonance characterization of peri-infarct zone remodeling following myocardial infarction // J Cardiovasc Magn Reson. 2012. Vol. 14, P. 24. doi: 10.1186/1532-429X-14-24

5. Bodi V., Monmeneu J.V., Ortiz-Perez J.T., et al. Prediction of Reverse Remodeling at Cardiac MR Imaging Soon after First ST-Segment-Elevation Myocardial Infarction: Results of a Large Prospective Registry // Radiology. 2016. Vol. 278, P. 54–63. doi: 10.1148/radiol.2015142674

6. Del Buono M.G., Garmendia C.M., Seropian I.M., et al. Heart Failure After ST-Elevation Myocardial Infarction: Beyond Left Ventricular Adverse Remodeling // Curr Probl Cardiol. 2022. Vol. 48, N 8. P. 101215. doi: 10.1016/j.cpcardiol.2022.101215

7. Ibanez B., Aletras A.H., Arai A.E., et al. Cardiac MRI Endpoints in Myocardial Infarction Experimental and Clinical Trials: JACC Scientific Expert Panel // J Am Coll Cardiol. 2019. Vol. 74, N 2. P. 238–256. doi: 10.1016/j.jacc.2019.05.024

8. Усов В.Ю., Бабокин В.Е., Мочула О.В., и др. Контрастированная магнитно-резонансная томография у пациентов с перенесенным инфарктом миокарда и предсердными тахиаритмиями // Сибирский журнал клинической и экспериментальной медицины. 2014. Т. 29, № 4. С. 33–38. EDN: TBFGPX doi: 10.29001/2073-8552-2014-29-4-33-38

9. Усов В.Ю., Вышлов Е.В., Мочула О.В., и др. МРТ с парамагнитным контрастным усилением в структурно-временной оценке повреждения миокарда при остром инфаркте и догоспитальной тромболитической терапии // Медицинская визуализация. 2018. Т. 22, № 2. С. 56–69. EDN: XMLLXN doi: 10.24835/1607-0763-2018-2-56-69

10. Kuo P.H., Kanal E., Abu-Alfa A.K., et al. Gadolinium-based MR contrast agents and nephrogenic systemic fibrosis // Radiology. 2007. Vol. 242, N 3. P. 647–649. doi: 10.1148/radiol.2423061640

11. Kim R.J., Wu E., Rafael A., et al. The use of contrast-enhanced magnetic resonance imaging to identify reversible myocardial dysfunction // N Engl J Med. 2000. Vol. 343, N 20. P. 1445–1453. doi: 10.1056/NEJM200011163432003

12. Kotu L.P., Engan K., Eftestol T., et al. Segmentation of scarred and non-scarred myocardium in LG enhanced CMR images using intensity-based textural analysis // Annu Int Conf IEEE Eng Med Biol Soc. 2011. P. 5698–5701. doi: 10.1109/IEMBS.2011.6091379

13. Larroza A., Lopez-Lereu M.P., Monmeneu J.V., et al. Texture analysis of cardiac cine magnetic resonance imaging to detect nonviable segments in patients with chronic myocardial infarction // Med Phys. 2018. Vol. 45, N 4. P. 1471–1480. doi: 10.1002/mp.12783

14. Максимова А.С., Усов В.Ю., Шелковникова Т.А., и др. Радиомический анализ магнитно-резонансных изображений сердца: обзор литературы // Сибирский журнал клинической и экспериментальной медицины. 2023. Т. 39, № 3. С. 13–22. EDN: RUADYI doi: 10.29001/2073-8552-2023-39-3-13-22

15. Larroza A., Materka A., Lopez-Lereu M.P., et al. Differentiation between acute and chronic myocardial infarction by means of texture analysis of late gadolinium enhancement and cine cardiac magnetic resonance imaging // Eur J Radiol. 2017. Vol. 92, P. 78–83. doi: 10.1016/j.ejrad.2017.04.024

16. Avard E., Shiri I., Hajianfar G., et al. Non-contrast Cine Cardiac Magnetic Resonance image radiomics features and machine learning algorithms for myocardial infarction detection // Comput Biol Med. 2022. Vol. 141, P. 105145. doi: 10.1016/j.compbiomed

17. Felker G.M., Shaw L.K., O'Connor C.M. A standardized definition of ischemic cardiomyopathy for use in clinical research // J Am Coll Cardiol. 2002. Vol. 39, N 2. P. 210–208. doi: 10.1016/s0735-1097(01)01738-7

18. Liu M., Xin A., Chen T., et al. Non-contrast cine cardiac magnetic resonance derived-radiomics for the prediction of left ventricular adverse remodeling in patients with ST-segment elevation myocardial infarction // Korean J Radiol. 2023. Vol. 24, N 9. P. 827–837. doi: 10.3348/kjr.2023.0061

19. Ma Q., Ma Y., Yu T., et al. Radiomics of non-contrast-enhanced T1 mapping: diagnostic and predictive performance for myocardial injury in acute ST-segment-elevation myocardial infarction // Korean J Radiol. 2021. Vol. 22, N 4. P. 535–546. doi: 10.3348/kjr.2019.0969

20. Ma Q., Ma Y., Wang X., et al. A radiomic nomogram for prediction of major adverse cardiac events in ST-segment elevation myocardial infarction // Eur Radiol. 2021. Vol. 31, N 2. P. 1140–1150. doi: 10.1007/s00330-020-07176-y

21. Chen B.H., An D.A., He J., et al. Myocardial extracellular volume fraction radiomics analysis for differentiation of reversible versus irreversible myocardial damage and prediction of left ventricular adverse remodeling after ST-elevation myocardial infarction // Eur Radiol. 2021. Vol. 31, N 1. P. 504–514. doi: 10.1007/s00330-020-07117-9

22. Chang S., Han K., Kwon Y., et al. T1 Map-based radiomics for prediction of left ventricular reverse remodeling in patients with non-ischemic dilated cardiomyopathy // Korean J Radiol 2023. Vol. 24, P. 395–405. doi: 10.3348/kjr.2023.0065

23. Frederiksen H., Iorgoveanu C., Mahi A. State of the Art and New Advances: Cardiac MRI. New Advances in Magnetic Resonance Imaging. 2023. Available from: http://dx.doi.org/10.5772/intechopen.112413. Accessed: Apr 2, 2024. doi: 10.5772/intechopen.112413

24. Bodi V., Monmeneu J.V., Ortiz-Perez J.T., et al. Prediction of Reverse Remodeling at Cardiac MR Imaging Soon after First ST-Segment-Elevation Myocardial Infarction: Results of a Large Prospective Registry // Radiology. 2016. Vol. 278, N 1. P. 54–63. doi: 10.1148/radiol.2015142674

AUTHORS' INFO

* Aleksandra S. Maksimova, MD, Cand. Sci. (Medicine);
address: 111a Kievskaya str., 634012, Tomsk, Russia;
ORCID: 0000-0002-4871-3283;
eLibrary SPIN: 2879-9550;
e-mail: asmaximova@yandex.ru

Denis S. Samatov;
ORCID: 0009-0000-1821-323X;
e-mail: denissamatov470@gmail.com

Boris S. Merzlikin, Cand. Sci. (Physics and Mathematics);
ORCID: 0000-0001-8545-9491;
eLibrary SPIN: 4815-6169;
e-mail: merzlikin@tpu.ru

Tatyana A. Shelkovnikova, MD, Cand. Sci. (Medicine);
ORCID: 0000-0003-1367-5309;
eLibrary SPIN: 1826-7850;
e-mail: fflly@mail.ru

Artem I. Listratov;
ORCID: 0009-0004-3202-8179;
e-mail: listrat312@gmail.com

Konstantin V. Zavadovsky, MD, Dr. Sci. (Medicine);
ORCID: 0000-0002-1513-8614;
eLibrary SPIN: 5081-3495;
e-mail: konstz@cardio-tomsk.ru

_____
* Corresponding author / Автор, ответственный за переписку

ОБ АВТОРАХ

* Максимова Александра Сергеевна, канд. мед. наук;
адрес: Россия, 634012, Томск, ул. Киевская, д. 111а;
ORCID: 0000-0002-4871-3283;
eLibrary SPIN: 2879-9550;
e-mail: asmaximova@yandex.ru

Саматов Денис Сергеевич;
ORCID: 0009-0000-1821-323X;
e-mail: denissamatov470@gmail.com

Мерзликин Борис Сергеевич, канд. физ.-матем. наук;
ORCID: 0000-0001-8545-9491;
eLibrary SPIN: 4815-6169;
e-mail: merzlikin@tpu.ru

Шелковникова Татьяна Александровна, канд. мед. наук;
ORCID: 0000-0003-1367-5309;
eLibrary SPIN: 1826-7850;
e-mail: fflly@mail.ru

Листратов Артём Игоревич;
ORCID: 0009-0004-3202-8179;
e-mail: listrat312@gmail.com

Завадовский Константин Валерьевич, д-р мед. наук;
ORCID: 0000-0002-1513-8614;
eLibrary SPIN: 5081-3495;
e-mail: konstz@cardio-tomsk.ru

Evaluating the performance of artificial intelligence-based software for digital mammography characterization

Yuri A. Vasilev[1,2], Alexander V. Kolsanov[3], Kirill M. Arzamasov[1], Anton V. Vladzymyrskyy[1,4], Olga V. Omelyanskaya[1], Serafim S. Semenov[1], Lubov E. Axenova[1]

[1] Research and Practical Clinical Center for Diagnostics and Telemedicine Technologies, Moscow, Russia;

[2] National Medical and Surgical Center named after N.I. Pirogov, Moscow, Russia;

[3] Samara State Medical University, Samara, Russia;

[4] Sechenov First Moscow State Medical University, Moscow, Russia

ABSTRACT

BACKGROUND: Digital screening mammography is a key modality for early detection of breast cancer, reducing mortality by 20–40%. Many artificial intelligence (AI)-based services have been developed to automate the analysis of imaging data.

AIM: The aim of the study was to compare mammography assessments using three types of AI services in multiple versions with radiologists' conclusions.

MATERIALS AND METHODS: Binary mammography scoring scales were compared with several types and versions of AI services regarding diagnostic accuracy, Matthews correlation coefficient, and maximum Youden's index.

RESULTS: A comparative analysis showed that the use of a binary scale for evaluating digital mammography affects the number of detected abnormalities and accuracy of AI results. In addition, diagnostic accuracy was found to be threshold dependent. AI Service 1 in version 3 had the best performance, as confirmed by most diagnostic accuracy parameters.

CONCLUSION: Our results can be used to select AI services for interpreting mammography screening data. Using Youden's index maximization to set up an AI service provides a balance of sensitivity and specificity that is not always clinically relevant.

Keywords: malignant tumors of breast; digital mammography; artificial intelligence services; diagnostic accuracy; Youden's index.

Оценка производительности программного обеспечения на основе технологии искусственного интеллекта при описании цифровых маммографических исследований

Ю.А. Васильев[1,2], А.В. Колсанов[3], К.М. Арзамасов[1], А.В. Владзимирский[1,4], О.В. Омелянская[1], С.С. Семёнов[1], Л.Е. Аксёнова[1]

[1] Научно-практический клинический центр диагностики и телемедицинских технологий, Москва, Россия;

[2] Национальный медико-хирургический Центр имени Н.И. Пирогова, Москва, Россия;

[3] Самарский государственный медицинский университет, Самара, Россия;

[4] Первый Московский государственный медицинский университет имени И.М. Сеченова, Москва, Россия

АННОТАЦИЯ

Обоснование. Цифровая скрининговая маммография — это основной инструмент для раннего выявления злокачественных новообразований молочной железы, позволяющий снизить смертность на 20–40%. На сегодняшний день разработано множество сервисов на основе искусственного интеллекта (ИИ), позволяющих автоматизировать анализ таких исследований.

Цель — сравнить результаты оценки цифровых маммографических исследований, выполненной тремя типами ИИ-сервисов в нескольких версиях, с заключениями врачей-рентгенологов.

Материалы и методы. Проведено сравнение бинарных шкал оценки маммографических исследований и нескольких типов и версий ИИ-сервисов по показателям диагностической точности, коэффициенту Мэтьюса и максимальному индексу Юдена.

Результаты. Сравнительный анализ показал, что выбор бинарной шкалы для оценки цифрового маммографического исследования влияет на количество выявляемых случаев патологии и точность результатов ИИ-сервисов. Кроме того, обнаружена зависимость показателей диагностической точности от порогового значения. Наилучшей производительностью обладает ИИ-сервис 1 в версии 3, что подтверждается большинством показателей диагностической точности.

Заключение. Полученные нами результаты могут быть полезны при выборе ИИ-сервисов для интерпретации данных скрининговой маммографии. Настройка ИИ-сервиса методом максимизации индекса Юдена позволяет получать сбалансированные значения чувствительности и специфичности, что не всегда целесообразно с клинической точки зрения.

Ключевые слова: злокачественные новообразования молочной железы; цифровая маммография; сервисы искусственного интеллекта; показатели диагностической точности; индекс Юдена.

基于人工智能技术的软件在描述数字乳房造影检查中的性能评估

Yuri A. Vasilev[1,2], Alexander V. Kolsanov[3], Kirill M. Arzamasov[1], Anton V. Vladzymyrskyy[1,4], Olga V. Omelyanskaya[1], Serafim S. Semenov[1], Lubov E. Axenova[1]

[1] Research and Practical Clinical Center for Diagnostics and Telemedicine Technologies, Moscow, Russia;

[2] National Medical and Surgical Center named after N.I. Pirogov, Moscow, Russia;

[3] Samara State Medical University, Samara, Russia;

[4] Sechenov First Moscow State Medical University, Moscow, Russia

摘要

论证。数字乳房造影筛查是早期发现乳腺恶性肿瘤的主要工具，可将死亡率降低20~40%。目前，已开发出许多基于人工智能（AI）的服务来自动分析此类检查。

目的 — 比较三种人工智能服务在不同版本中进行的乳房造影检查评估结果与放射科医生的意见。

材料和方法。比较了乳房造影检查二元评估量表与多种类型和版本的AI服务在诊断准确性指标、马修斯系数和最大尤登指数等方面的差异。

结果。比较分析表明，评估数字乳房造影检查的二元评估量表的选择会影响检测到的病理病例数量和AI服务结果的准确性。此外，还发现了诊断准确性指标对阈值的依赖性。版本3中的AI服务1实现了最佳性能，大多数诊断准确性指标都证实了这一点。

结论。我们的研究结果可能有助于选择AI服务来解读乳房造影筛查数据。通过最大化尤登指数来设置AI服务，可以获得灵敏度和特异性的平衡值，但从临床角度来说，并不总是合理的。

关键词：乳腺恶性肿瘤；数字乳房造影；人工智能服务；诊断准确性指标；尤登指数。

BACKGROUND

In X-ray radiography, digital mammography is the primary diagnostic tool and the sole method of breast cancer screening. Screening lowers cancer mortality by 20%–40% by enabling much earlier diagnosis of cancer-associated abnormal mammary gland changes [1]. As artificial intelligence (AI) evolves, novel AI-based systems and services are being introduced for the automated analysis of digital mammography images [2–4]. Certain studies indicate that AI services facilitate reliable diagnosis and can even outperform radiologists. This has especially been demonstrated in the detection of breast cancer signs at early stages and/or when fibroglandular breast tissue is the predominant site of abnormality. Other studies, however, indicate that radiologists are still able to interpret mammograms more accurately than AI systems[5]. Machine learning models constitute the core functional elements of AI services that are responsible for the detection and segmentation of areas of interest with anomalous changes, data processing and classification, and generating predictions or solutions based on these data. To compare machine learning models, diagnostic accuracy parameters such as sensitivity (Sens) and specificity (Spec) are computed, and the area under the curve (AUC) is analyzed [6, 7].

A true value must be chosen and contrasted with the outcomes of the AI service in order to evaluate the AI performance. Calculations are typically performed relative to the model's output and the gold standard, which is based on the findings of additional studies [8, 9]. Moreover, AI outcomes can be evaluated by comparing them with a physician's opinion [10, 11]. The ability to fine-tune AI systems is their primary benefit. However, the accuracy testing of software that produces probabilistic data instead of conventional binary data is critical for the deployment and use of AI services in medicine.

A threshold that differentiates the probabilities deemed "abnormal" from those considered "normal" must be established in order to interpret the probabilistic data. The optimal probability threshold depends on the purpose and intended application of the AI service. Since probability distributions for imbalanced data tend to shift toward the "normal" category [12], setting a threshold at 0.5 may not be the optimal option. Effective cancer detection and a reduction in false positives require a balance between a machine learning model's sensitivity and specificity. Using Youden's index to maximize the sum of the Sens and Spec values is a commonly employed technique [7]. Additionally, Chen et al. proposed a technique for comparing the maximum Youden's index values for several diagnostic tests [13]. Given that the subpar performance of AI systems in medical diagnosis can be linked to serious risks, a comprehensive assessment of the capabilities and operational constraints of such AI systems is required.

AIM

This study aimed to evaluate how various AI service versions interpret digital mammography findings in comparison to the conclusions of radiologists.

MATERIALS AND METHODS

Study design

This was a multicenter, observational, cross-sectional study. Fig. 1 illustrates the dataset production chart for the analysis as well as the study design.
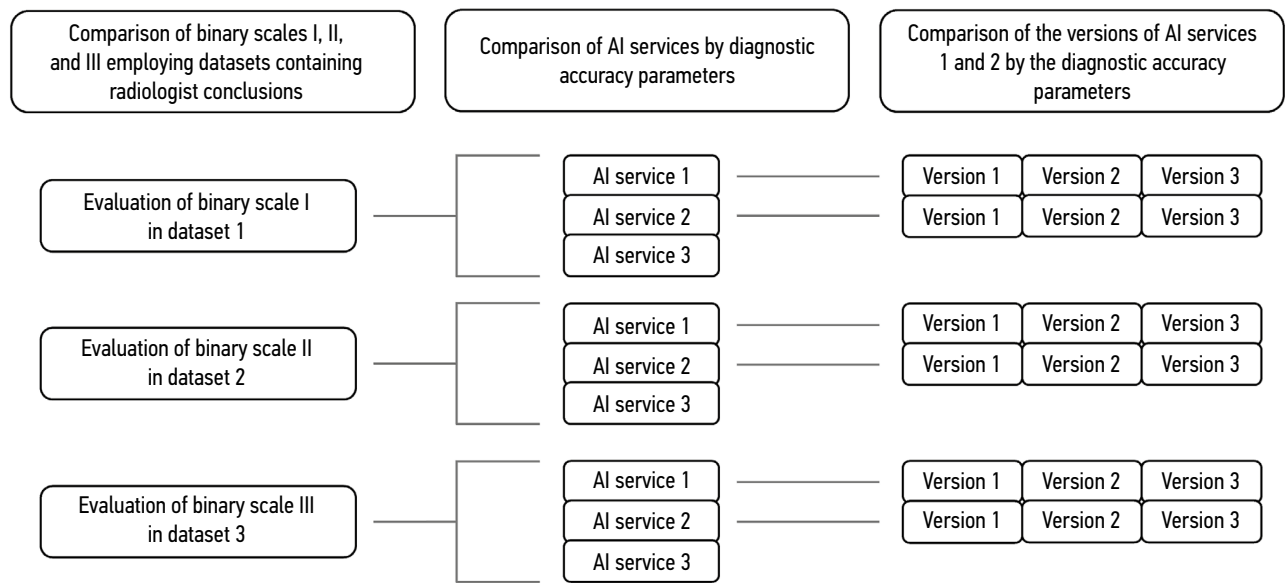
Fig. 1. Study design and generation of datasets for analysis. AI service, artificial intelligence service.

Eligibility criteria

Inclusion criteria. Female patients (independent of age or comorbidities) who received digital mammograms performed between July 22, 2020, and December 29, 2022, with DICOM pictures and other data available for analysis using an AI service, were included in the study.

Exclusion criteria:

1. Insufficient data in the medical records for at least one evaluated AI service to process;

2. Technically flawed images that impede correct interpretation (e.g., artifacts, partially missing data);

3. Incompleteness of the metadata essential for the analysis.

Additional information. Examinations in patients with breast implants and those who had received radiotherapy were not categorized into separate subgroups, and their numbers in the sample were not reported.

Study setting

The study sample included examination results from 123 outpatient healthcare facilities of the Moscow Healthcare Department. The study comprised 531 radiologists who specialized in mammography. All participating radiologists analyzed the examinations performed at the healthcare facilities of the Moscow Healthcare Department. The results of the AI service were compared to the true value obtained from a radiologist's conclusion for each examination. Each radiologist reported an average of 1,250 examinations during the study period.

Data generation and analysis

The accuracy of the AI service results was evaluated using radiologist opinions from medical records as reference values. The conclusions were presented in accordance with categories 1–6 of the Breast Imaging Reporting and Data System (BI-RADS), independently for each mammary gland. Three binary diagnostic scales were utilized based on the probability of cancer according to BI-RADS: Scale I classified BI-RADS categories 1–2 as "normal" and categories 3–6 as "abnormal"; Scale II classified BI-RADS categories 1–3 as "normal" and categories 4–6 as "abnormal"; and Scale III classified BI-RADS categories 1–2 as "normal" and categories 4–6 as "abnormal" (BI-RADS category 3 was not considered in this case).

The study assessed three AI services: TrioDM-MT® (Medical Technologies Ltd., Russia) (AUC 0.90; specificity 0.85; sensitivity 0.83; accuracy 0.84); Celsus® (Medical Screening Systems LLC, Russia) (AUC 0.96); and Lunit INSIGHT MMG® (Lunit Inc., Republic of Korea) (AUC 0.96; sensitivity 0.89 when assessed together with a radiologist) [2–4]. The AI service results for every mammography test were displayed as probabilities, with 0% denoting a low likelihood of cancer and 100% denoting a high probability of cancer. The trade names of the AI services are anonymized and randomized further in the text.

During data preprocessing, lines lacking radiologist descriptions and/or AI service results were excluded. Moreover, test results from male patients, female patients aged <40 years or >100 years, and examinations in which the radiologist's conclusion did not correspond to BI-RADS categories 1–6 or any AI service mentioned above were excluded from the dataset.

After performing data preprocessing for each mammography examination, diagnostic accuracy parameters were determined, including AUC, sensitivity (Sens), specificity (Spec), accuracy (Acc), positive predictive value (PPV), false negative rate (FNR), case detection rate (CDR), abnormal interpretation rate (AIR), Matthews correlation coefficient (MCC), and Youden's index (J). Table 1 presents a description of each parameter, along with diagnostic scales where the maximum values of these parameters were observed.

Table 1. Descriptions of diagnostic accuracy parameters and diagnostic scales with the highest values of these parameters

Parameter	Description	Diagnostic scale
AUC	Area Under the Curve: represents the ability to differentiate between classes; is not sensitive to class imbalance	II and III
Sens	Sensitivity: represents the ability to detect the "abnormal" class	III
Spec	Specificity: represents the ability to detect the "normal" class	II
Acc	Accuracy: represents the proportion of correctly classified objects in the total number of objects in the sample; sensitive to class imbalance	II
PPV	Positive Predictive Value: represents the consistency of the detected "abnormal" class with a true abnormality	I
AIR	Abnormal Interpretation Rate: the proportion of examinations classified as "abnormal" and requiring additional diagnostic procedures; represents the highest number of false positives	I
CDR	Case Detection Rate: represents the detection of abnormalities irrespective of the total number of false positives	I
FNR	False Negative Rate: represents the number of "abnormal" cases not detected by an AI service	I
MCC	Matthews Correlation Coefficient: evaluates the quality of classification, considering all four elements of the error matrix; not sensitive to class imbalance	I
J	Youden's index	–

AI services were updated during the study, including fine-tuning and other modifications. Every update matched a change in the version of the AI service. The study only addressed the modifications made to the AI service core that influenced the diagnostic accuracy parameters. Consequently, three iterations of AI service 1 and AI service 2 were identified, each of which represented a subsequent model modification and was used during different periods. Since AI service 3 had not undergone any major changes, different versions were not considered.

The optimal probability threshold was ascertained using the AUC and the maximum Youden's index value. The calculations were performed employing a web tool developed by the Center for Diagnostics and Telemedicine (Moscow)[1]. Youden's index was calculated using the following formula:

$$J = Sens - Spec - 1 \qquad (1)$$

where Sens = sensitivity; Spec = specificity.

The binary AI service results were calculated using the threshold. The outcomes of the AI service were then compared with the radiologist's judgments using the following parameters:

- TP, the number of true positives;
- TN, the number of true negatives;
- FP, the number of false positives;
- FN, the number of false negatives.

The resulting TP, TN, FP, and FN values were utilized to calculate the following AI service accuracy parameters (Table 1) [14]:

$$AUC = \frac{1}{2}\sum_{i=1}^{n-1}(x_{i+1} - x_i)*(y_i + y_{i+1}) \qquad (2)$$

where x = X-axis values (e.g., false positives); y = Y-axis values (e.g., true positives); n = total number of points on a curve; and i = current point index.

$$Sens = \frac{TP}{TP + FN} \qquad (3)$$

$$Sens = \frac{TP}{TP + FN} \qquad (4)$$

$$Acc = \frac{TP + TN}{FP + FN + TP + TN} \qquad (5)$$

$$PPV = \frac{TP}{TP + FP} \qquad (6)$$

$$AIR = \frac{TP + FP}{TP + TN + FP + FN} \times 1000 \qquad (7)$$

$$CDR = \frac{TP}{TP + TN + FP + FN} \times 1000 \qquad (8)$$

$$FNR = \frac{FN}{FN + TP} \qquad (9)$$

$$MCC = \frac{TP \times TN + FP + FN}{\sqrt{(TP + FP)(TP + FN)(TN + FP)(TN + FN)}} \qquad (10)$$

To model the ratios calculated in datasets 1–3, 100 data samples (1,000 samples each) with a category 0 ("normal") to category 1 ("abnormal") ratio of 9:1 (Scale I), 33:1 (Scale II), and 31:1 (Scale III) were created, and the accuracy parameters and confidence intervals were calculated using bootstrapping.

Ethical review

This srudy was part of the Experiment on the Use of Innovative Computer Vision Technologies for Analysis of Medical Images in the Moscow Healthcare System (Moscow Experiment) (Protocol No. NCT04489992 of February 21, 2020) previously approved by the local ethics committee.

Statistical analysis

The study compared the accuracy of breast cancer detection for three binary scales based on radiologist's conclusions and three AI services. The nonparametric Kolmogorov-Smirnov test was used to determine if the resulting datasets were normally distributed.

The significance of the differences between the maximum Youden's index values for various types and versions of AI services was assessed in accordance with the method outlined by Chen et al. [13]. The variance (Var) of the difference

between two independent Youden's index values was ascertained using the following formula:

$$Var\left(J_1 - J_2\right) = Var\left(J_1\right) + Var\left(J_2\right) \qquad (11)$$

where J = Youden's index; Var is calculated using the following formula:

$$Var\left(J\right) = Spec^2 \times Var\left(Sens\right) + Sens^2 \times Var\left(Spec\right) \quad (12)$$

where Spec = specificity; Sens = sensitivity.

Thus, the formula is as follows:

$$Var\left(J_1 - J_2\right) = Spec_1^2 \times Var\left(Sens_1\right) + Sens_1^2 \times \\ \times Var\left(Spec_1\right) + Spec_2^2 \times Var\left(Sens_2\right) + Sens_2^2 \times \\ \times Var\left(Spec_2\right) \qquad (13)$$

The statistical test and two-sided confidence interval for the difference between two independent Youden's index (J) values were computed based on the central limit theorem:

$$Z = \frac{J_1 - J_2}{\sigma_{D_J}} = \frac{J_1 - J_2}{\sqrt{Var\left(J_1 - J_2\right)}} \qquad (14)$$

$$d \pm Z_{\alpha/2} \times \sigma_{D_J} = d \pm Z_{\alpha/2} \times \sqrt{Var\left(J_1 - J_2\right)} \quad (15)$$

where Z = standard normal random value that represents the variation of the difference from zero, in standard deviations; Var = variance; d = difference between two Youden's index values; σ_{D_J} = standard deviation of the difference between Youden's index values.

P-values < 0.05 were considered statistically significant. The confidence interval was determined to be 95%. Calculations were performed using the Python libraries Pandas, Matplotlib, Seaborn, Scikit-learn, NumPy, and Statistics (stats) (Python Software Foundation, version 3.11.0).

RESULTS

Comparison of binary diagnostic scales based on radiologist conclusions

Based on a radiologist's evaluation of the normal distribution of BI-RADS categories 1–6, the distribution of these parameters was considered to be nonnormal. The distribution histograms for the BI-RADS categories are illustrated in Fig. 2. Peaks in the graph correspond to the most probable categories. In this case, the greatest peak corresponds to BI-RADS category 2 (benign), indicating that most examinations included in the sample did not reveal any aberrant cancer-associated changes.

Datasets 1 and 2 included 663,606 examinations, while dataset 3 comprised 618,947 examinations. The number of "normal" cases in datasets 1, 2, and 3 was 64,100, 19,441, and 19,441, respectively, while the number of "abnormal" cases was 599,506, 644,165, and 599,506, respectively. Thus, the incidence of cancer in the evaluated data sample was 9.66% for binary scale I and 2.9% for binary scales II and III (Fig. 3). Comprehensive details about the datasets are presented in Table 2 and Table 3.

To evaluate the agreement between radiologist decisions and AI service outcomes, diagnostic accuracy measures were calculated (Table 1 and Table 4). AUC for Scale I significantly
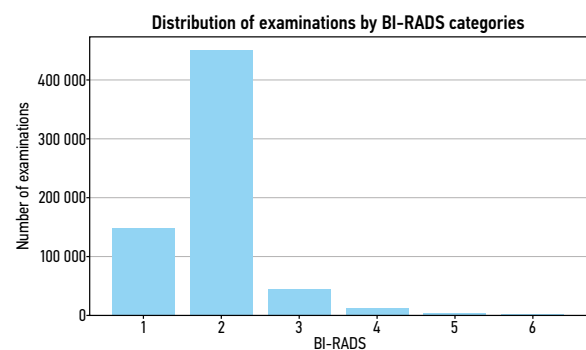
Fig. 2. Distribution of BI-RADS categories 1–6 allocated by a radiologist when analyzing digital mammography findings for the assessed datasets: X-axis values = BI-RADS categories 1–6; Y-axis values = number of examinations.
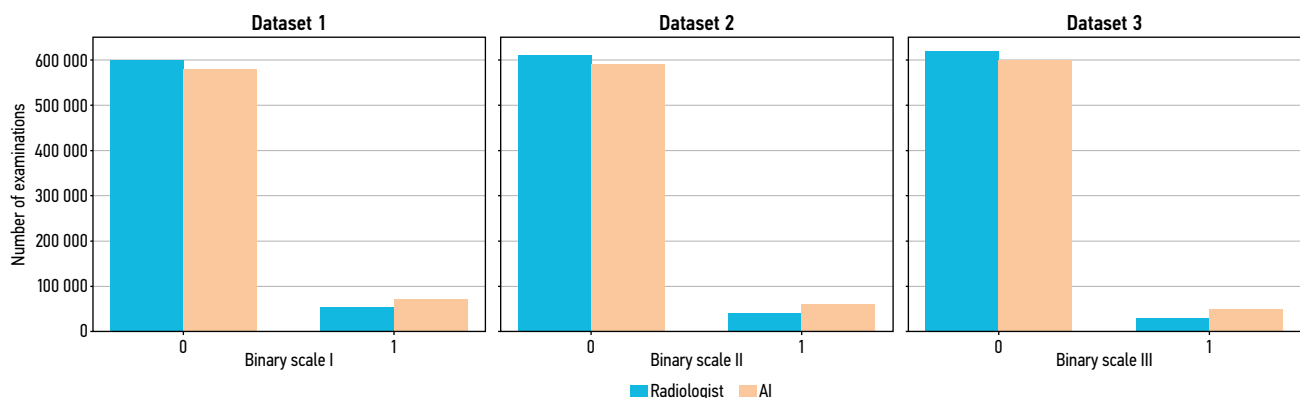
Fig. 3. Comparison of the distribution of categories 0–1 allocated by radiologists and an artificial intelligence service for three binary scales: X-axis values = binary scales I–III; Y-axis values = number of examinations.

Table 2. Number of normal and abnormal cases in datasets 1–3

	"Normal"	"Abnormal"	All examinations	Amount of "normal" per "abnormal" case
Scale I	599,506	64,100	663,606	9
Scale II	644,165	19,441	663,606	33
Scale III	599,506	19,441	618,947	31

Table 3. Number of examinations in the datasets (2020–2022)

Scales	I–II						III					
Number of examinations	663,606						618,947					
Services	1		2		3		1			2		
Number of examinations	545,362		108,763		9481		508,929			101,654		
Versions	1	2	3	1	2	3	–	1	2	3	1	2	3
Number of examinations	90,949	212,968	241,445	4922	46,851	56,990	–	83,828	198,231	226,870	4711	43,687	53,256

Table 4. Artificial intelligence services and their versions with the highest accuracy parameters compared to diagnostic scales

Parameter	Scale	AI service	AI service 1 version number	AI service 2 version number
AUC	I	1	3	1 and 3
	II	1	3	1 and 2
	III	1	3	1 and 2
Sens	I	1 and 2	2 and 3	2 and 3
	II	1 and 2	3	2
	III	1 and 2	3	2
Spec	I	1	3	1
	II	1	1 and 3	1
	III	1	1	1
Acc	I	1	3	1
	II	1	3	1
	III	1	1	1
PPV	I	1	3	1
	II	1	3	1
	III	1	2 and 3	1
AIR	I	3	1	2
	II	3	2	2
	III	3	3	2
CDR	I	1 and 2	2 and 3	2 and 3
	II	1 and 3	3	2
	III	1 and 3	3	2
FNR	I	3	1	1
	II	2	1	1 and 3
	III	2	1	1 and 3
MCC	I	1	3	1
	II	1	3	1
	III	1	3	1
Youden's index	I	1	3	1
	II	1	3	2
	III	1	3	2

Note. AI service, artificial intelligence service.

differed from that for Scales II and III (there were no differences in AUC between the latter). Moreover, Scale III had a higher sensitivity (Sens), whereas Scale II demonstrated a higher specificity (Spec). Scale I displayed the highest abnormal interpretation rate (AIR) and false negative rate (FNR), whereas Scale II exhibited the lowest AIR and FNR. Scale I demonstrated the highest consistency level measured using MCC, as well as the highest PPV and CDR (Table 5).

Comparison of AI services with each other and with scales based on radiologist conclusions

Fig. 4 displays the probability distributions of anomalous changes for AI services 1–3. Scales II and III exhibited the most comparable distribution of the AI service probabilities. The distribution for the "normal" category demonstrated a right shift, particularly for AI services 2 and 3. The distribution for the "abnormal" category exhibited a left shift for AI services 1, 2, and 3.

The performance of AI services 1, 2, and 3 was evaluated and compared using the same diagnostic accuracy metrics. AI service 1 was the most consistent with the radiologist's conclusions in determining the "normal" and "abnormal" categories, whereas the highest abnormal interpretation rate (AIR) and false negative rate (FNR) were noted for AI services 2 and 3 (Table 6).

Comparison of AI service versions with each other

Additionally, diagnostic accuracy metrics were measured to evaluate the different versions of AI services 1 and 2 (Table 7 and Table 8). The majority of the diagnostic accuracy parameters varied depending on the scale; however, some of these variations were nonsignificant. Consequently, the optimal version of AI services cannot be identified.

Table 5. Diagnostic accuracy parameters evaluated for the artificial intelligence service results (AI service 1)

Parameter	Binary diagnostic scale		
	I	II	III
Threshold	62	74	68
AUC	0.659 [0.654; 0.663]	0.726 [0.717; 0.735] *	0.738 [0.730; 0.745] *
Sens	0.569 [0.560; 0.578]	0.626 [0.609; 0.644]	0.679 [0.664; 0.694] *
Spec	0.748 [0.746; 0.751]	0.826 [0.823; 0.828] *	0.796 [0.793; 0.798]
Acc	0.730 [0.728; 0.733]	0.820 [0.817; 0.822] *	0.792 [0.790; 0.795]
PPV	0.201 [0.198; 0.204] *	0.100 [0.098; 0.103]	0.099 [0.097; 0.101]
AIR	283.280 [280.57; 285.988] *	187.810 [185.199; 190.421]	219.24 [216.787; 221.693]
CDR	56.870 [55.960; 57.780] *	18.790 [18.273; 19.307]	21.730 [21.252; 22.208]
FNR	0.431 [0.422; 0.440] *	0.374 [0.356; 0.391]	0.321 [0.306; 0.336]
MCC	0.211 [0.205; 0.217] *	0.198 [0.190; 0.205]	0.202 [0.196; 0.209]

Note. The data are presented as means [95% CI]; *, significant differences between Scales I and II, I and III, and II and III (CIs do not overlap).
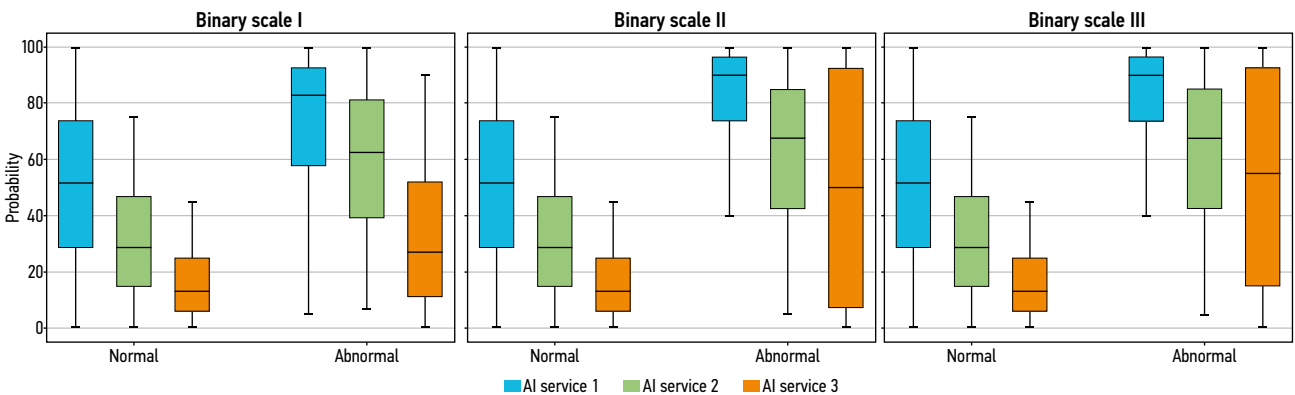
Fig. 4. Distribution of the outcomes of three artificial intelligence services when analyzing the three datasets: X-axis values = artificial intelligence services; Y-axis values = probability; the data are presented as follows: central line = median; edges of the "box" = first (Q1) and third (Q3) quartiles; "whiskers" = minimum and maximum.

Table 2 presents the assessment results for the scales, services, and versions with the highest diagnostic accuracy parameters.

In addition to the diagnostic accuracy parameters, the maximum Youden's index value was employed to contrast the performance of different AI service types and versions. This parameter assesses how well an AI service balances sensitivity and specificity. When assessed using the highest Youden's index value, AI service 1 performed best (see Table 2). When comparing the versions of AI service 1, version 3 exhibited the best diagnostic accuracy parameters. However, in terms of Youden's index, version 1 of AI service 1 had the best results for Scale I, whereas version 2 performed best for Scales II and III. Significant differences were observed for all results.

DISCUSSION

The study examined the binary diagnostic scales for digital mammography, three AI services, and three versions of AI services 1 and 2. The standard diagnostic accuracy parameters and Youden's index were ascertained.

The ratio of detected cancer cases to the total number of examinations performed was 0.10, 0.03, and 0.03 for Scales I, II, and III, respectively. Because the risk of undiagnosed abnormalities must be taken into account, variations in diagnostic scales are essential for screening. For example, BI-RADS category 3 necessitates an additional examination; based on it, certain individuals may be placed in categories with a higher level of malignancy. Thus, employing Scale II, which classifies BI-RADS category 3 as class 1 ("abnormal"), lowers the probability of undetected abnormalities.

Notably, when using Scale I, the incidence of abnormalities was neither influenced by the presence of BI-RADS category 3 in the "abnormal" group nor its complete absence from the dataset. However, including this category in the "normal" group significantly elevated the estimated cancer incidence in the screened population. Moreover, in BI-RADS category 3, Scale I exhibits a similar pattern for AUC, with Scales II and III exhibiting no significant variations.

When comparing the three AI services on the basis of diagnostic accuracy parameters, it was discovered that AUC, specificity, sensitivity, accuracy, PPV, CDR, and MCC

Table 6. Diagnostic accuracy parameters evaluated for the results of three artificial intelligence services compared to radiologist conclusions

Parameter	Binary scale	AI service 1	AI service 2	AI service 3
Threshold	I	64	32	10
	II	75	44	20
	III	74	44	20
AUC	I	0.671 [0.666; 0.676] *	0.647 [0.641; 0.652]	0.597 [0.592; 0.602]
	II	0.750 [0.740; 0.759] *	0.698 [0.689; 0.708]	0.713 [0.704; 0.722]
	III	0.755 [0.746; 0.763] *	0.708 [0.699; 0.717]	0.720 [0.713; 0.728]
Sens	I	0.610 [0.600; 0.620] *	0.602 [0.591; 0.613] *	0.578 [0.569; 0.587]
	II	0.687 [0.669; 0.706] *	0.609 [0.591; 0.627]	0.676 [0.658; 0.693] *
	III	0.689 [0.672; 0.705] *	0.616 [0.598; 0.633]	0.679 [0.664; 0.693] *
Spec	I	0.731 [0.728; 0.734] *	0.691 [0.688; 0.694]	0.616 [0.613; 0.619]
	II	0.812 [0.810; 0.815] *	0.788 [0.785; 0.790]	0.749 [0.746; 0.752]
	III	0.821 [0.819; 0.824] *	0.800 [0.798; 0.803]	0.762 [0.759; 0.765]
Acc	I	0.719 [0.717; 0.722] *	0.682 [0.679; 0.685]	0.612 [0.609; 0.615]
	II	0.809 [0.806; 0.811] *	0.782 [0.779; 0.785]	0.747 [0.744; 0.750]
	III	0.817 [0.815; 0.819] *	0.794 [0.792; 0.797]	0.760 [0.757; 0.762]
PPV	I	0.202 [0.199; 0.205] *	0.178 [0.175; 0.181]	0.143 [0.141; 0.145]
	II	0.102 [0.099; 0.105] *	0.082 [0.079; 0.084]	0.077 [0.075; 0.079]
	III	0.113 [0.110; 0.116] *	0.093 [0.090; 0.095]	0.086 [0.084; 0.088]
AIR	I	302.800 [299.851; 305.749]	338.140 [335.251; 341.029]	403.640 [400.720; 406.560] *
	II	202.600 [200.315; 204.885]	224.330 [221.624; 227.036]	263.320 [260.371; 266.269] *
	III	195.130 [192.823; 197.437]	212.940 [210.594; 215.286]	251.890 [249.124; 254.656] *
CDR	I	61.040 [60.041; 62.039] *	60.210 [59.113; 61.307] *	57.780 [56.889; 58.671]
	II	20.620 [20.062; 21.178] *	18.280 [17.735; 18.825]	20.270 [19.750; 20.790] *
	III	22.040 [21.507; 22.573] *	19.700 [19.131; 20.269]	21.720 [21.260; 22.180] *
FNR	I	0.390 [0.380; 0.400]	0.398 [0.387; 0.409]	0.422 [0.413; 0.431] *
	II	0.313 [0.294; 0.331]	0.391 [0.373; 0.409] *	0.324 [0.307; 0.342]
	III	0.311 [0.295; 0.328]	0.384 [0.367; 0.402] *	0.321 [0.307; 0.336]
MCC	I	0.223 [0.217; 0.230] *	0.186 [0.179; 0.193]	0.118 [0.113; 0.124]
	II	0.212 [0.204; 0.220] *	0.163 [0.155; 0.170]	0.165 [0.158; 0.172]
	III	0.227 [0.219; 0.234] *	0.179 [0.171; 0.187]	0.179 [0.173; 0.185]

Note. AI service, artificial intelligence service; the data are presented as means [95% CI]; *, significant differences between services 1 and 2, 1 and 3, and 2 and 3 (CIs do not overlap).

were greater for AI service 1 than for all diagnostic scales. AI service 3 demonstrated the highest AIR, whereas AI services 2 and 3 exhibited the highest FNR, depending on the binary scale. In general, these results indicate the superior performance of AI service 1. When comparing the maximum Youden's index values, AI service 1 demonstrated superior accuracy to all the diagnostic scales. However, while the assessment using Youden's index revealed significant differences between all scales and services, the assessment using bootstrap confidence intervals exhibited no significant differences in CDR and sensitivity between certain services.

Similar to binary scales, when selecting AI services and their versions, it is crucial to consider their intended use. For example, when the early detection of radiological signs of cancer is required, sensitivity (Sens) will be the primary diagnostic accuracy parameter because an AI service needs to identify as many true positive (abnormal) cases as feasible. Another crucial parameter is the FNR, which should be minimized to lower the possibility of undetected abnormalities. This study indicates that AI services 1 and 2 are the most sensitive. However, AI service 2 displayed the highest FNR for Scales II and III. Versions 3 and 2 of AI services 1 and 2, respectively, performed best in this study.

Table 7. Diagnostic accuracy parameters assessed for the results of three versions of artificial intelligence service 1 compared to radiologist conclusions

Scale	AI service	AI service version	Threshold	AUC	Sens	Spec	Acc
I	1	1	29	0.633 [0.627; 0.638]	0.617 [0.607; 0.627]	0.648 [0.645; 0.652]	0.645 [0.642; 0.648]
		2	68	0.674 [0.669; 0.679]	0.643 [0.634; 0.653] *	0.705 [0.702; 0.708]	0.699 [0.696; 0.702]
		3	66	0.702 [0.697; 0.706] *	0.647 [0.638; 0.656] *	0.757 [0.754; 0.760] *	0.746 [0.743; 0.748] *
II	1	1	57	0.684 [0.674; 0.693]	0.525 [0.506; 0.545]	0.842 [0.840; 0.844] *	0.833 [0.830; 0.835]
		2	78	0.750 [0.741; 0.760]	0.683 [0.664; 0.702]	0.817 [0.815; 0.819]	0.813 [0.811; 0.815]
		3	79	0.782 [0.774; 0.791] *	0.725 [0.708; 0.742] *	0.840 [0.837; 0.842] *	0.836 [0.834; 0.839] *
III	1	1	57	0.701 [0.692; 0.711]	0.548 [0.530; 0.566]	0.855 [0.853; 0.857] *	0.845 [0.843; 0.847] *
		2	78	0.756 [0.746; 0.766]	0.678 [0.659; 0.698]	0.833 [0.831; 0.836]	0.828 [0.826; 0.831]
		3	75	0.789 [0.783; 0.796] *	0.758 [0.745; 0.770] *	0.821 [0.819; 0.823]	0.819 [0.817; 0.821]

Scale	AI service	AI service version	PPV (95% CI)	AIR (95% CI)	CDR (95% CI)	FNR (95% CI)	MCC (95% CI)
I	1	1	0.163 [0.161; 0.166]	378.070 [375.137; 381.003] *	61.690 [60.650; 62.730]	0.383 [0.373; 0.393] *	0.164 [0.157; 0.171]
		2	0.195 [0.193; 0.198]	329.660 [326.815; 332.505]	64.340 [63.384; 65.296] *	0.357 [0.347; 0.366]	0.223 [0.216; 0.229]
		3	0.228 [0.225; 0.231] *	283.71 [280.851; 286.569]	64.670 [63.768; 65.572] *	0.353 [0.344; 0.362]	0.269 [0.263; 0.275] *
II	1	1	0.093 [0.090; 0.097]	169.010 [166.841; 171.179]	15.760 [15.175; 16.345]	0.475 [0.455; 0.494] *	0.167 [0.158; 0.176]
		2	0.104 [0.101; 0.106]	198.140 [195.926; 200.354] *	20.500 [19.931; 21.069]	0.317 [0.298; 0.336]	0.214 [0.206; 0.222]
		3	0.123 [0.120; 0.126] *	177.240 [174.831; 179.649]	21.750 [21.234; 22.266] *	0.275 [0.258; 0.292]	0.253 [0.245; 0.260] *
III	1	1	0.111 [0.108; 0.115]	158.040 [155.998; 160.082]	17.540 [16.969; 18.111]	0.452 [0.434; 0.470] *	0.195 [0.186; 0.203]
		2	0.119 [0.115; 0.122] *	183.040 [180.595; 185.485]	21.710 [21.078; 22.342]	0.322 [0.302; 0.341]	0.233 [0.224; 0.242]
		3	0.123 [0.121; 0.125] *	197.480 [195.148; 199.812] *	24.240 [23.826; 24.654] *	0.242 [0.230; 0.255]	0.256 [0.250; 0.262] *

Note. AI service, artificial intelligence service; the data are presented as means [95% confidence interval]; *, confidence intervals do not overlap, indicating significant differences.

Table 8. Diagnostic accuracy parameters assessed for the results of three versions of artificial intelligence service 2 compared to radiologist conclusions

Scale	AI service	AI service version	Threshold	AUC	Sens	Spec	Acc
I	2	1	32	0.660 [0.655; 0.665] *	0.592 [0.581; 0.602]	0.728 [0.725; 0.731] *	0.714 [0.712; 0.71] *
		2	30	0.647 [0.642; 0.652]	0.621 [0.611; 0.631] *	0.673 [0.670; 0.676]	0.668 [0.665; 0.671]
		3	32	0.654 [0.649; 0.660] *	0.619 [0.609; 0.629] *	0.690 [0.687; 0.693]	0.683 [0.68; 0.685]
II	2	1	44	0.712 [0.702; 0.721] *	0.587 [0.568; 0.606]	0.837 [0.834; 0.839]*	0.829 [0.827; 0.832] *
		2	42	0.708 [0.700; 0.716] *	0.653 [0.637; 0.669] *	0.763 [0.760; 0.765]	0.759 [0.757; 0.762]
		3	44	0.688 [0.679; 0.696]	0.582 [0.566; 0.598]	0.793 [0.790; 0.795]	0.786 [0.784; 0.789]
III	2	1	44	0.709 [0.701; 0.718] *	0.576 [0.560; 0.593]	0.843 [0.841; 0.845] *	0.834 [0.832; 0.836] *
		2	39	0.722 [0.714; 0.731] *	0.688 [0.672; 0.705] *	0.756 [0.753; 0.759]	0.754 [0.751; 0.756]
		3	44	0.698 [0.689; 0.706]	0.587 [0.570; 0.604]	0.808 [0.806; 0.810]	0.801 [0.799; 0.803]

Scale	AI service	AI service version	PPV	AIR	CDR	FNR	MCC
I	2	1	0.195 [0.192; 0.198] *	304.02 [301.225; 306.815]	59.190 [58.143; 60.237]	0.408 [0.398; 0.419] *	0.209 [0.202; 0.216] *
		2	0.174 [0.172; 0.177]	356.470 [353.548; 359.392] *	62.110 [61.135; 63.085] *	0.379 [0.369; 0.389]	0.184 [0.178; 0.191]
		3	0.182 [0.179; 0.184]	341.050 [338.332; 343.768]	61.880 [60.877; 62.883]*	0.381 [0.371; 0.391]	0.195 [0.189; 0.202]
II	2	1	0.100 [0.097; 0.104] *	175.920 [173.412; 178.428]	17.600 [17.029; 18.171]	0.413 [0.394; 0.432] *	0.190 [0.181; 0.199] *
		2	0.079 [0.077; 0.080]	249.890 [247.158; 252.622] *	19.590 [19.115; 20.065] *	0.347 [0.331; 0.363]	0.164 [0.158; 0.170]
		3	0.080 [0.078; 0.082]	218.500 [216.045; 220.955]	17.470 [16.991; 17.949]	0.418 [0.402; 0.434] *	0.155 [0.148; 0.162]
III	2	1	0.108 [0.105; 0.111] *	170.700 [168.638; 172.762]	18.440 [17.907; 18.973]	0.424 [0.407; 0.440] *	0.196 [0.188; 0.204] *
		2	0.085 [0.083; 0.088]	258.390 [255.703; 261.077] *	22.030 [21.511; 22.549] *	0.312 [0.295; 0.328]	0.179 [0.172; 0.186]
		3	0.092 [0.089; 0.095]	204.570 [202.244; 206.896]	18.790 [18.255; 19.325]	0.413 [0.396; 0.430] *	0.173 [0.165; 0.180]

Note. AI service, artificial intelligence service; the data are presented as means [95% confidence interval]; *, confidence intervals do not overlap, indicating significant differences.

Both PPV, which verifies that the majority of positive findings are actual abnormalities, and specificity are essential for minimizing false positives and achieving the maximum possible interpretation accuracy. AI service 1 was the most effective in these cases. Differences in the specificity and PPV were found between various AI service 1 versions for different scales.

A decrease in AIR cuts down the time spent by radiologists on additional data interpretation, as long as the AI service classification is unambiguous and reliable. In this study, AI service 1 exhibited the lowest AIR for all scales.

Two parameters must be considered to examine the accuracy of "normal" and "abnormal" case classification for AI services and their versions. These include the accuracy (Acc) parameter, where a high value denotes the degree to which both groups can be classified correctly, and the Matthews correlation coefficient, which examines the overall performance of a classifier, considering all components of the error matrix. The study found that version 3 of AI service 1 achieved the highest overall categorization accuracy. Notably, the AI service results were compared with radiologists' conclusions allocated to a specific class, resulting in certain limitations because it is vital to understand the diagnostic accuracy parameters used by a radiologist. A reference dataset, where the correct value is established based on histology findings, can be used to evaluate the diagnostic accuracy of radiologists' conclusions. Such a study has already been conducted and verified the high diagnostic accuracy of radiologist conclusions (AUC 0.928) [15]. Lower AUC values for the evaluated AI services were found in our study, indicating the necessity of updating, which was subsequently completed between 2020 and 2022. Furthermore, it is important to consider the sensitivity and specificity, which are inferior to those of radiologist conclusions [15]. The optimization of a particular parameter's settings was not covered in this study. Importantly, the sensitivity settings in the AI services can vary for the same AUC value. For example, a sensitivity of approximately 100% removes the risk of undetected abnormalities but raises the number of false positives. We intend to perform a thorough examination of the AI service fine-tuning in the future to enhance the sensitivity and specificity.

The primary usage of AI services in mammography is for the initial reading, which will augment the accuracy of breast cancer diagnosis [16] by improving the sensitivity. Alternatively, AI services can be used for image sorting when the sensitivity is close to 100%. In this scenario, radiologists will submit the examinations as electronic medical records right away and won't need to explain the ones that an AI service has deemed "normal." A recent study exhibited promising results for this approach in the autonomous sorting of fluorography findings [17]. Numerous benign changes that may potentially necessitate attention and additional testing may make this scenario less effective in mammography.

Study limitations

This paper covers the data collected during the first three years of the large-scale Experiment on the Use of Innovative Computer Vision Technologies for Analysis of Medical Images in the Moscow Healthcare System [18]. It does not address the optimal settings of AI services. One limitation of this study is that AUC may be inadequate for evaluating the performance of AI services in a clinical setting because specific thresholds are not always applicable in real-world practice. Moreover, the sensitivity (Sens) and specificity (Spec) do not account for the population-wide prevalence of the disease. Thus, in future research, we plan to employ various techniques of assessing AI service efficacy in a clinical setting, as well as to use histological verification findings as true values. Furthermore, this study only included mammography examinations with AI service results; mammograms where an AI service failed to produce results were not evaluated. Moreover, this study did not ascertain AI service performance in patients with a foreign body in the breast (breast implants) or those with radiotherapy-induced changes. However, such cases are highly relevant to practice, and additional research is warranted.

CONCLUSION

This study discovered that the method for developing a "normal/abnormal" binary scale affects the diagnostic accuracy parameters of various types and versions of AI services. Significant discrepancies between the accuracy parameters of AI services and diagnostic scales were identified by Youden's index, and the clinical setting determines which parameters should be utilized in the comparative evaluation of AI services. Using Youden's index maximization to set up an AI service provides a balance of sensitivity and specificity that is not necessarily clinically significant.

ADDITIONAL INFORMATION

REFERENCES

1. Seely JM, Alhassan T. Screening for breast cancer in 2018-what should we be doing today? *Curr Oncol.* 2018;25(suppl 1):S115–S124. doi: 10.3747/co.25.3770

2. Artificial intelligence in mammography screening. *Clinical applications, issues and directions for development* [Internet; cited 20 August 2023]. Available from: https://www.itmportal.ru/upload/iblock/69e/7q981uhfaxjhcntal0exngxtq43xeth2/2.2.3.-Kandoba-ITM_AI-2022.pdf (in Russ.)

3. Celsus — *AI-software for analysis of X-ray and CT studies.* Mammography [Internet; cited 20 Aug 2023]. Available from: https://celsus.ai/products-mammography/

4. Kim HE, Kim HH, Han BK, et al. Changes in cancer detection and false-positive recall in mammography using artificial intelligence: a retrospective, multireader study. *Lancet Digit Health.* 2020;2(3):e138–e148. doi: 10.1016/S2589-7500(20)30003-0

5. Yoon JH, Strand F, Baltzer PAT, et al. Standalone AI for Breast Cancer Detection at Screening Digital Mammography and Digital Breast Tomosynthesis: A Systematic Review and Meta-Analysis. *Radiology.* 2023;307(5):e222639. doi: 10.1148/radiol.222639

6. Zhou X-H, Obuchowski NA, McClish DK. *Statistical Methods in Diagnostic Medicine.* NJ: John Wiley & Sons, Inc.; 2011. doi: 10.1002/9780470906514

7. Habibzadeh F, Habibzadeh P, Yadollahie M. On determining the most appropriate test cut-off value: the case of tests with continuous results. *Biochem Med (Zagreb).* 2016;26(3):297–307. doi: 10.11613/BM.2016.034

8. Schaffter T, Buist DSM, Lee CI, et al. Evaluation of Combined Artificial Intelligence and Radiologist Assessment to Interpret Screening Mammograms. *JAMA Netw Open.* 2020;3(3):e200265. doi: 10.1001/jamanetworkopen.2020.0265

9. McKinney SM, Sieniek M, Godbole V, et al. International evaluation of an AI system for breast cancer screening. *Nature.* 2020;577(7788):89–94. doi: 10.1038/s41586-019-1799-6

10. Nam JG, Kim M, Park J, et al. Development and validation of a deep learning algorithm detecting 10 common abnormalities on chest radiographs. *Eur Respir J.* 2021;57(5):2003061. doi: 10.1183/13993003.03061-2020

11. Sakhnov SN, Axenov KD, Axenova LE, et al. Development of a cataract screening model using an open dataset and deep machine learning algorithms. *Fyodorov Journal of Ophthalmic Surgery.* 2022;(S4):13–20. EDN: VEGPAW doi: 10.25276/0235-4160-2022-4S-13-20

12. King G, Zeng L. Logistic Regression in Rare Events Data. *Political Analysis.* 2001;9(2):137–163. doi: 10.1093/oxfordjournals.pan.a004868

13. Chen F, Xue Y, Tan MT, Chen P. Efficient statistical tests to compare Youden index: accounting for contingency correlation. *Stat Med.* 2015;34(9):1560–1576. doi: 10.1002/sim.6432

14. Vasiliev YuA, Vladzimirsky AV, Sharova DE, et al. *Clinical trials of artificial intelligence systems (radiation diagnostics).* Moscow: State budgetary healthcare institution of the city of Moscow «Scientific and Practical Clinical Center for Diagnostics and Telemedicine Technologies of the Moscow Health Department». 2023. 40 p. (In Russ.) EDN: PUIJLD

15. Arzamasov KM, Vasilev YuA, Vladzymirskyy AV, et al. The use of computer vision for the mammography preventive research. *The Russian Journal of Preventive Medicine.* 2023;26(6):117–123. EDN: YBKHPS doi: 10.17116/profmed202326061117

16. Vasilev YuA, Tyrov IA, Vladzymirskyy AV, et al. Double-reading mammograms using artificial intelligence technologies: A new model of mass preventive examination organization. *Digital Diagnostics.* 2023;4(2):93–104. EDN: VRIEOH doi: 10.17816/DD321423

17. Vasilev YuA, Tyrov IA, Vladzymirskyy AV, et al. A New Model of Organizing Mass Screening Based on Stand-Alone Artificial Intelligence Used for Fluorography Image Triage. *Public Health and Life Environment — PH&LE.* 2023;31(11):23-32. EDN: SYIQBX doi: 10.35627/2219-5238/2023-31-11-23-32

18. Vladzimirskyy AV, Vasilev YuA, Arzamasov KM, et al. *Computer vision in radiology: the first stage of the Moscow experiment.* Moscow: Izdatel'skie resheniya; 2022. (In Russ.) EDN: FOYLXK

СПИСОК ЛИТЕРАТУРЫ

1. Seely J.M., Alhassan T. Screening for breast cancer in 2018-what should we be doing today? // Curr Oncol. 2018. Vol. 25, Suppl. 1. P. S115–S124. doi: 10.3747/co.25.3770

2. Кандоба В.И. Искусственный интеллект в скрининговой маммографии. Клиническое использование, проблемы и направления развития [интернет]. Режим доступа: https://www.itmportal.ru/upload/iblock/69e/7q981uhfaxjhcntal0exngxtq43xeth2/2.2.3.-Kandoba-ITM_AI-2022.pdf Дата обращения: 20.08.2023

3. Цельс. Система поддержки принятия врачебных решений на базе технологий искусственного интеллекта для анализа цифровых медицинских изображений. Маммография [интернет]. Режим доступа: https://celsus.ai/products-mammography/ Дата обращения: 20.08.2023

4. Kim H.E., Kim H.H., Han B.K., et al. Changes in cancer detection and false-positive recall in mammography using artificial intelligence: a retrospective, multireader study // Lancet Digit Health. 2020. Vol. 2, N 3. P. e138–e148. doi: 10.1016/S2589-7500(20)30003-0

5. Yoon J.H., Strand F., Baltzer P.A.T., et al. Standalone AI for Breast Cancer Detection at Screening Digital Mammography and Digital Breast Tomosynthesis: A Systematic Review and Meta-Analysis // Radiology. 2023. Vol. 307, N 5. ID: e222639. doi: 10.1148/radiol.222639

6. Zhou X.-H., Obuchowski N.A., McClish D.K. Statistical Methods in Diagnostic Medicine. NJ: John Wiley & Sons, Inc.; 2011. doi: 10.1002/9780470906514

7. Habibzadeh F., Habibzadeh P,, Yadollahie M. On determining the most appropriate test cut-off value: the case of tests with continuous results // Biochem Med (Zagreb). 2016. Vol. 26, N 3. P. 297–307. doi: 10.11613/BM.2016.034

8. Schaffter T., Buist D.S.M., Lee C.I., et al. Evaluation of Combined Artificial Intelligence and Radiologist Assessment to Interpret Screening Mammograms // JAMA Netw Open. 2020. Vol. 3, N 3. ID: e200265. doi: 10.1001/jamanetworkopen.2020.0265

9. McKinney S.M., Sieniek M., Godbole V., et al. International evaluation of an AI system for breast cancer screening // Nature. 2020. Vol. 577, N 7788. P. 89–94. doi: 10.1038/s41586-019-1799-6

10. Nam J.G., Kim M., Park J., et al. Development and validation of a deep learning algorithm detecting 10 common abnormalities on chest radiographs // Eur Respir J. 2021. Vol. 57, N 5. ID: 2003061. doi: 10.1183/13993003.03061-2020

11. Сахнов С.Н., Аксенов К.Д., Аксенова Л.Е., и др. Разработка модели скрининга катаракты с использованием открытого набора данных и алгоритмов глубокого машинного обучения. Офтальмохирургия. 2022. № S4. С. 13–20. EDN: VEGPAW doi: 10.25276/0235-4160-2022-4S-13-20

12. King G., Zeng L. Logistic Regression in Rare Events Data // Political Analysis. 2001. Vol. 9, N 2. P. 137–163. doi: 10.1093/oxfordjournals.pan.a004868

13. Chen F., Xue Y., Tan M.T., Chen P. Efficient statistical tests to compare Youden index: accounting for contingency correlation // Stat Med. 2015. Vol. 34, N 9. P. 1560–1576. doi: 10.1002/sim.6432

14. Васильев Ю.А., Владзимирский А.В., Шарова Д.Е., и др. Клинические испытания систем искусственного интеллекта (лучевая диагностика). Москва: Государственное бюджетное учреждение здравоохранения города Москвы «Научно-практический клинический центр диагностики и телемедицинских технологий Департамента здравоохранения города Москвы», 2023. 40 с. EDN: PUIJLD

15. Арзамасов К.М., Васильев Ю.А., Владзимирский А.В., и др. Применение компьютерного зрения для профилактических исследований на примере маммографии // Профилактическая медицина. 2023. Т. 26, № 6. С. 117–123. EDN: YBKHPS doi: 10.17116/profmed202326061117

16. Васильев Ю.А., Тыров И.А., Владзимирский А.В., и др. Двойной просмотр результатов маммографии с применением технологий искусственного интеллекта: новая модель организации массовых профилактических исследований // Digital Diagnostics. 2023. Т. 4, № 2. С. 93–104. EDN: VRIEOH doi: 10.17816/DD321423

17. Васильев Ю.А., Тыров И.А., Владзимирский А.В., и др. Новая модель организации массовых профилактических исследований, основанная на автономном искусственном интеллекте для сортировки результатов флюорографии // Здоровье населения и среда обитания — ЗНиСО. 2023. Т. 31, № 11. С. 23–32. EDN: SYIQBX doi: 10.35627/2219-5238/2023-31-11-23-32

18. Владзимирский А.В., Васильев Ю.А., Арзамасов К.М., и др. Компьютерное зрение в лучевой диагностике: первый этап Московского эксперимента. Москва: Издательские решения, 2022. EDN: FOYLXK

AUTHORS' INFO

* Kirill M. Arzamasov, MD, Cand. Sci. (Medicine);
address: 24 bldg. 1 Petrovka str., 127051, Moscow, Russia;
ORCID: 0000-0001-7786-0349;
eLibrary SPIN: 3160-8062;
e-mail: ArzamasovKM@zdrav.mos.ru

Yuriy A. Vasilev, MD, Cand. Sci. (Medicine);
ORCID: 0000-0002-5283-5961;
eLibrary SPIN: 4458-5608;
e-mail: VasilevYA1@zdrav.mos.ru

Alexander V. Kolsanov, MD, Dr. Sci. (Medicine), Professor;
ORCID: 0000-0002-4144-7090;
eLibrary SPIN: 2028-6609;
e-mail: a.v.kolsanov@samsmu.ru

Anton V. Vladzymyrskyy, MD, Dr. Sci. (Medicine), Professor;
ORCID: 0000-0002-2990-7736;
eLibrary SPIN: 3602-7120;
e-mail: VladzimirskijAV@zdrav.mos.ru

Olga V. Omelyanskaya;
ORCID: 0000-0002-0245-4431;
eLibrary SPIN: 8948-6152;
e-mail: OmelyanskayaOV@zdrav.mos.ru

Serafim S. Semenov;
ORCID: 0000-0003-2585-0864;
eLibrary SPIN: 4790-0416;
e-mail: SemenovSS3@zdrav.mos.ru

Lubov E. Axenova;
ORCID: 0000-0003-0885-1355;
eLibrary SPIN: 7705-6293;
e-mail: AksenovaLE@zdrav.mos.ru

ОБ АВТОРАХ

* Арзамасов Кирилл Михайлович, канд. мед. наук;
адрес: Россия, 127051, Москва, ул. Петровка, д. 24, стр. 1;
ORCID: 0000-0001-7786-0349;
eLibrary SPIN: 3160-8062;
e-mail: ArzamasovKM@zdrav.mos.ru

Васильев Юрий Александрович, канд. мед. наук;
ORCID: 0000-0002-5283-5961;
eLibrary SPIN: 4458-5608;
e-mail: VasilevYA1@zdrav.mos.ru

Колсанов Александр Владимирович, д-р мед. наук, профессор;
ORCID: 0000-0002-4144-7090;
eLibrary SPIN: 2028-6609;
e-mail: a.v.kolsanov@samsmu.ru

Владзимирский Антон Вячеславович, д-р мед. наук, профессор;
ORCID: 0000-0002-2990-7736;
eLibrary SPIN: 3602-7120;
e-mail: VladzimirskijAV@zdrav.mos.ru

Омелянская Ольга Васильевна;
ORCID: 0000-0002-0245-4431;
eLibrary SPIN: 8948-6152;
e-mail: OmelyanskayaOV@zdrav.mos.ru

Семёнов Серафим Сергеевич;
ORCID: 0000-0003-2585-0864;
eLibrary SPIN: 4790-0416;
e-mail: SemenovSS3@zdrav.mos.ru

Аксёнова Любовь Евгеньевна;
ORCID: 0000-0003-0885-1355;
eLibrary SPIN: 7705-6293;
e-mail: AksenovaLE@zdrav.mos.ru

* Corresponding author / Автор, ответственный за переписку

Neuroendocrine tumors of stomach and pancreas: diagnostic potential of radiomics, issues, and solutions

Nikolay V. Nudnov[1,2,3], Elina S.-A. Shakhvalieva[1], David G. Karelidze[1], Aleksandr A. Borisov[1], Mikhail E. Ivannikov[1]

[1] Russian Research Center of Roentgenology and Radiology, Moscow, Russia;
[2] Russian Medical Academy of Continuing Professional Education, Moscow, Russia;
[3] RUDN University, Moscow, Russia

ABSTRACT

BACKGROUND: Radiomics is currently a promising and prospective tool for diagnosing and treating neuroendocrine neoplasms at various sites. This method is often used for differential diagnosis of gastrointestinal neuroendocrine tumors with other neoplasms at this site.

AIM: The aim of the study was to evaluate the potential of radiomics for differential diagnosis of neuroendocrine tumors of stomach and pancreas.

MATERIALS AND METHODS: The study included data of 12 patients with morphologically proven neoplasms of the stomach (6 with neuroendocrine tumors and 6 with adenocarcinomas) and data of 22 patients with morphologically proven neoplasms of the pancreas (11 with neuroendocrine tumors and 11 with adenocarcinomas). All patients underwent abdominal computed tomography (CT) with intravenous contrast enhancement prior to treatment at the Russian Scientific Center of Roentgenology and Radiology. Radiomics parameters were calculated for the area of gastric and pancreatic tumor manually segmented in the native phase of the CT scan. The results were processed and statistically analyzed using Microsoft Office Excel and R-Studio, a free, open-source software development environment for the R programming language.

RESULTS: CT scan examples demonstrate typical and atypical visual signs of neuroendocrine tumors of stomach and pancreas, contrast enhancement characteristics, location and structure of neoplasms. Fifteen radiomics parameters were identified that were statistically significantly different between gastric neuroendocrine tumor and gastric adenocarcinoma. In pancreas, neuroendocrine tumors differed significantly from adenocarcinomas in 14 radiomics parameters.

CONCLUSION: Neuroendocrine tumors of stomach and pancreas are rare neoplasms that are mostly asymptomatic and difficult to visualize due to their small size and contrast enhancement characteristics. Texture analysis may be a promising approach to differentiate gastrointestinal neuroendocrine tumors from other neoplasms at these sites, especially in the view of the difficulty in obtaining a biopsy.

Keywords: neuroendocrine tumor; neuroendocrine tumor of stomach; neuroendocrine tumor of pancreas; neuroendocrine neoplasia; radiology.

Нейроэндокринные опухоли желудка и поджелудочной железы: диагностические возможности радиомики, проблемы и пути их решения

Н.В. Нуднов[1,2,3], Э.С.-А. Шахвалиева[1], Д.Г. Карелидзе[1], А.А. Борисов[1], М.Е. Иванников[1]

[1] Российский научный центр рентгенорадиологии, Москва, Россия;
[2] Российская медицинская академия непрерывного профессионального образования, Москва, Россия;
[3] Российский университет дружбы народов имени Патриса Лумумбы, Москва, Россия

АННОТАЦИЯ

Обоснование. В настоящее время радиомика является многообещающим и перспективным инструментом в диагностике и лечении нейроэндокринных новообразований различной локализации. Этот метод часто используют для дифференциальной диагностики нейроэндокринных опухолей желудочно-кишечного тракта с другими новообразованиями данной локализации.

Цель — оценить возможности применения радиомики для дифференциальной диагностики нейроэндокринных опухолей желудка и поджелудочной железы.

Материалы и методы. В исследование включены данные 12 пациентов с морфологически верифицированными новообразованиями желудка (6 — с нейроэндокринной опухолью и 6 — с аденокарциномой) и данные 22 пациентов с морфологически верифицированными новообразованиями поджелудочной железы (11 — с нейроэндокринной опухолью и 11 — с аденокарциномой). Всем пациентам до лечения в Российском научном центре рентгенорадиологии выполнено компьютерно-томографическое (КТ) исследование органов брюшной полости с внутривенным контрастированием. Показатели радиомики рассчитаны в области опухоли желудка и поджелудочной железы, которую сегментировали вручную в нативную фазу КТ-исследования. Обработку результатов и статистический анализ проводили с использованием Microsoft Office Excel и свободной среды разработки программного обеспечения с открытым исходным кодом для языка программирования R — R-Studio.

Результаты. На примерах КТ-исследований продемонстрированы типичные и нетипичные визуальные признаки нейроэндокринных опухолей желудка и поджелудочной железы, особенности контрастирования, локализации и структуры новообразований. Выявлено 15 показателей радиомики, которые статистически значимо различаются между нейроэндокринной опухолью желудка и аденокарциномой желудка. В случае поджелудочной железы нейроэндокринные опухоли статистически значимо отличались от аденокарцином по 14 показателям радиомики.

Заключение. Нейроэндокринные опухоли желудка и поджелудочной железы — редкие новообразования, которые в большинстве случаев не проявляют себя клинически и трудно визуализируются из-за малых размеров и особенностей контрастирования. Текстурный анализ может стать перспективным подходом для дифференциальной диагностики нейроэндокринных опухолей желудочно-кишечного тракта с другими новообразованями данной локализации, особенно с учётом сложности взятия биопсии.

Ключевые слова: нейроэндокринная опухоль; нейроэндокринная опухоль желудка; нейроэндокринная опухоль поджелудочной железы; нейроэндокринная неоплазия; лучевая диагностика.

胃和胰腺神经内分泌肿瘤：放射组学的诊断能力、问题及其解决方法

Nikolay V. Nudnov[1,2,3], Elina S.-A. Shakhvalieva[1], David G. Karelidze[1], Aleksandr A. Borisov[1], Mikhail E. Ivannikov[1]

[1] Russian Research Center of Roentgenology and Radiology, Moscow, Russia;
[2] Russian Medical Academy of Continuing Professional Education, Moscow, Russia;
[3] RUDN University, Moscow, Russia

摘要

论证。目前，放射组学是诊断和治疗各种局部化神经内分泌肿瘤的一种前景广阔的工具。这种方法常用于胃肠道神经内分泌肿瘤与该部位的其他肿瘤的鉴别诊断。

目的 — 评估放射组学在胃和胰腺神经内分泌肿瘤鉴别诊断中的应用可能性。

材料和方法。研究中，包括12名经形态学验证的胃肿瘤患者（6名神经内分泌肿瘤患者和6名腺癌患者）的数据和 22名经形态学验证的胰腺肿瘤患者（11名神经内分泌肿瘤患者和11名腺癌患者）的数据。所有患者在治疗前都在俄罗斯放射学科学中心接受了静脉注射造影剂的腹腔器官计算机断层扫描（CT）检查。计算了胃和胰腺肿瘤区域的放射组学指数，该区域在CT检查的原生相进行了手动分割。使用Microsoft Office Excel和R — R-Studio编程语言的免费开源软件开发环境进行结果处理和统计分析。

结果。通过CT研究实例，展示了胃和胰腺神经内分泌肿瘤的典型和非典型视觉征象、肿瘤的对比度、定位和结构的特征。研究发现，胃神经内分泌瘤和胃腺癌的15项放射组学指标在统计学上存在显著差异。就胰腺而言，神经内分泌肿瘤与腺癌在14项放射组学指标上有明显统计学差异。

结论。胃和胰腺的神经内分泌肿瘤是一种罕见的肿瘤，在大多数情况下临床上并无症状，且由于其体积小、对比度特征而难以成像。纹理分析可能是鉴别胃肠道神经内分泌肿瘤与该部位其他肿瘤的一种很有前途的方法，特别是考虑到活检取样的复杂性。

关键词：神经内分泌肿瘤；胃神经内分泌肿瘤；胰腺神经内分泌肿瘤；神经内分泌瘤；放射诊断。

BACKGROUND

Neuroendocrine neoplasms (NENs) represent a heterogeneous group of tumors derived from neuroendocrine cells. These tumors encompass a broad spectrum, with the most common types arising in the gastrointestinal tract, lungs, bronchi, thymus, and pancreas [1]. The term *neuroendocrine* refers to cells that exhibit both neural and endocrine characteristics [2]. Under the standardized classification system, all neuroendocrine neoplasms are categorized as *neuroendocrine tumors* (NETs), which include both low-grade NETs and high-grade neuroendocrine carcinomas. Some tumors contain a combination of low- and high-grade histological features and are classified as mixed neuroendocrine–non-neuroendocrine neoplasms, in which the neuroendocrine component constitutes at least 30% of the tumor [1].

Accurate staging of NETs is essential for determining prognosis and guiding treatment decisions [3]. Gastrointestinal and pancreatic NETs are currently graded into three categories: G1 (low grade), G2 (intermediate grade), and G3 (high grade). According to the 2019 World Health Organization classification and the 2016 guidelines from the European Neuroendocrine Tumor Society (ENETS), grading is based on the mitotic count and the Ki-67 proliferation index (Table 1). These grading criteria are similar for both gastrointestinal and pancreatic NETs [4].

Tumor grade significantly influences survival outcomes. Data from 64,971 patients with NETs in the Surveillance, Epidemiology, and End Results (SEER) database showed median survival times of 16.2 years for G1, 8.3 years for G2, and 10 months for G3 NETs. Survival also varies markedly with disease stage: patients with localized disease had a median survival of over 30 years, those with regional spread had a median of 10 years, and those with distant metastases had a median of 1 year [5].

Gastric NETs represent approximately 11%–12% of newly diagnosed NETs [3]. Pancreatic NETs account for about one-third of gastrointestinal NETs. Among pancreatic NETs, 45%–60% are non-functioning, while 40%–55% are hormone-secreting [6].

In Russia, data on the incidence of NENs are currently unavailable [4]. In contrast, the incidence in the USA was reported at 6.98 cases per 100,000 population in 2012. An independent analysis of the SEER database also indicated an increase in the incidence of gastrointestinal NENs between 1975 and 2008. Although the exact cause of this rise is unclear, improvements in diagnostic techniques and classification may have contributed [1].

To determine the tumor grade, tissue sections were stained using antibodies against pancytokeratin; cytokeratins 7, 14, 18, and 20; as well as synaptophysin (Syn) and chromogranin A (CgA). If one of the neuroendocrine differentiation markers is not expressed, staining with anti-CD56 antibodies is performed, and the expression of somatostatin receptors 2 and 5 (SSTR2 and SSTR5) is assessed as additional markers [4].

The clinical presentation of NETs varies based on the location of the primary tumor, and all NET types are characterized by a high potential for metastasis. A study by Halfdanarson et al. analyzing NET cases in the USA from 1973 to 2000 found that over 60% of patients had distant metastases and more than 20% had regional metastases at the time of diagnosis [7]. Similar results were reported by Loosen et al. in a European cohort, where 84.6% of patients were found to have distant metastases at diagnosis [8].

Diagnosis of gastric and pancreatic neuroendocrine tumors

The clinical symptoms and NENs can vary widely depending on the tumor location. In functioning tumors, symptoms may result from the secretion of biologically active substances.

Most pancreatic NETs are non-functioning, meaning they do not produce clinical signs of hormone overproduction, which makes diagnosis more difficult. In some instances, these tumors are discovered incidentally during evaluations for unrelated conditions [9]. Non-functioning tumors may remain asymptomatic for extended periods or present with nonspecific symptoms. Typical manifestations include diarrhea, hot flashes, and skin flushing, while bronchospasm is observed less frequently. Other symptoms such as intestinal cramping, telangiectasia, edema, cyanosis, joint involvement, muscle pain, and myopathy are rare [4].

Upper endoscopy with biopsy is commonly used for diagnosis, as NETs require confirmation by immunohistochemistry [10]. Abdominal CT is recommended for G1 and G2 NETs larger than 2 cm, as well as for all G3 NETs. In certain cases, abdominal magnetic resonance imaging (MRI), octreotide scintigraphy, and positron emission tomography combined with CT (PET/CT) may also be useful [11].

Table 1. Classification of gastrointestinal and pancreatic neuroendocrine tumors

Grade	Mitotic index (10HPF)	Proliferation index Ki67, %
G1 neuroendocrine tumors	<2	<3
G2 neuroendocrine tumors	2–20	3–20
G3 neuroendocrine tumors	>20	>20
Neuroendocrine carcinomas	>20	>20

Note. G, neuroendocrine tumor grade; HPF, high-power field.

Pancreatic NETs exhibit the greatest contrast enhancement during the early arterial phase (25–35 s), rather than the late arterial phase (35–45 s), which is typically used for pancreatic imaging. This distinction is important because small tumors may be missed during the late arterial phase when the lesion becomes isodense with the surrounding pancreatic tissue [12]. Fig. 1 illustrates characteristic imaging features of pancreatic NETs. Abdominal CT with intravenous contrast revealed a hypervascular lesion in the head of the pancreas, measuring 13 × 9 mm, located near the pancreatic duct and common bile duct, without clear signs of duct compression on CT. The tumor demonstrated marked contrast enhancement during the early arterial phase (10 s) but was poorly visualized in the subsequent contrast phases.

Some pancreatic NETs may appear hypovascular, requiring differentiation from other lesions such as serous cystadenomas, intrapancreatic accessory spleens, renal cell carcinoma metastases, and both cystic and solid masses, including hypovascular adenocarcinomas [13]. Fig. 2 presents a CT image of a pancreatic NET with these features. The lesion, located in the pancreatic body, is round with irregular margins, measuring approximately 2.3 × 2.1 cm, and contains a centrally hypodense area suggestive of necrosis [14]. It appears isodense relative to the pancreatic parenchyma in the venous phase and shows only mild enhancement during the arterial phase. There is no evidence of tumor infiltration into the surrounding fat or vascular structures. In this case, the tumor was identified based on indirect signs, including dilatation of the pancreatic duct, compression of the splenic vein, and moderate enlargement of the pancreatic body. This presentation is atypical for pancreatic NETs. Rare cases have been described in which venous phase enhancement is more pronounced [15].

Gastric NETs are generally hypervascular and typically show increased contrast enhancement during the early arterial phase [16]. G1 and G2 gastric NETs are usually small (<1 cm) and are most often located in the gastric fundus or body [10, 17]. Fig. 3 illustrates typical imaging features of gastric NETs. An exophytic, hypervascular lesion measuring 10 × 9 mm is visible along the greater curvature of the gastric body, with strong arterial phase enhancement.

As with pancreatic NETs, gastric NETs can also show variable contrast enhancement. Fig. 4 illustrates a NET located in the upper wall of the gastric cardia, which displayed increased enhancement during the venous phase and minimal enhancement during the arterial phase.

These cases highlight the diagnostic complexity and variability in imaging features of gastric and pancreatic
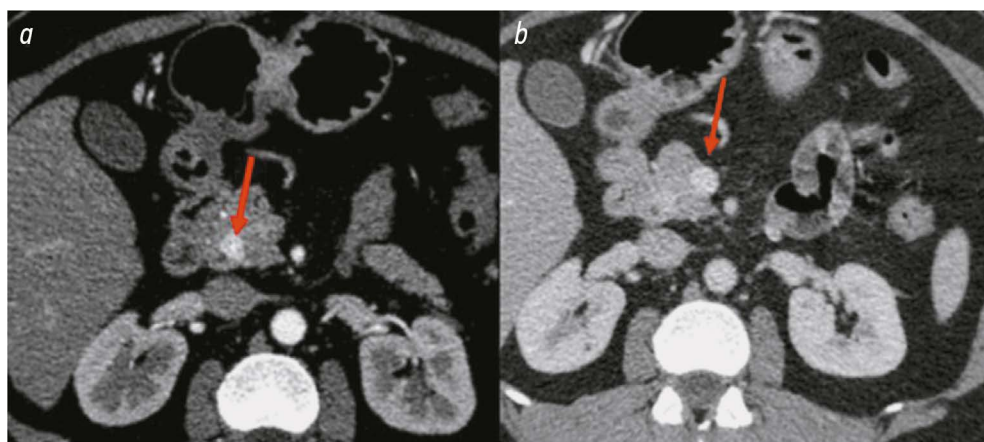
Fig. 1. Abdominal computed tomography with intravenous contrast: *a*, a hypervascular lesion near the common bile duct during the arterial phase (10th second); *b*, venous phase image.

Fig. 2. Computed tomography of a hypovascular pancreatic neuroendocrine tumor: *a*, a moderately hypervascular lesion in the pancreatic body with a hypodense central area and dilatation of the pancreatic duct, arterial phase (10th second); *b*, moderate compression of the splenic vein, venous phase.
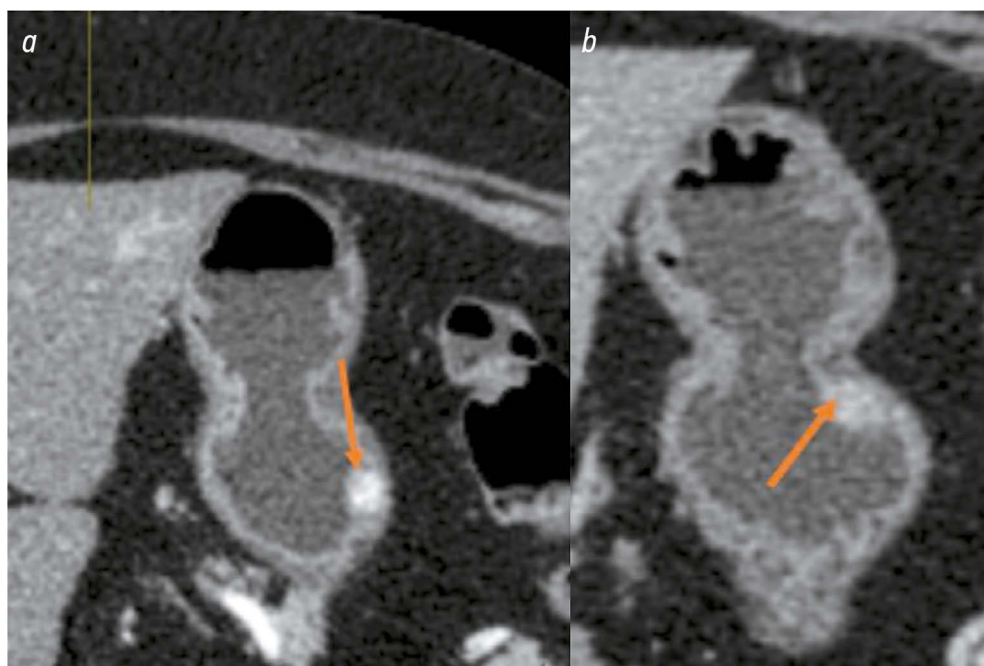
Fig. 3. Gastric neuroendocrine tumor: *a*, tumor tissue showing high contrast uptake, arterial phase; *b*, tumor tissue showing moderate contrast uptake, venous phase.
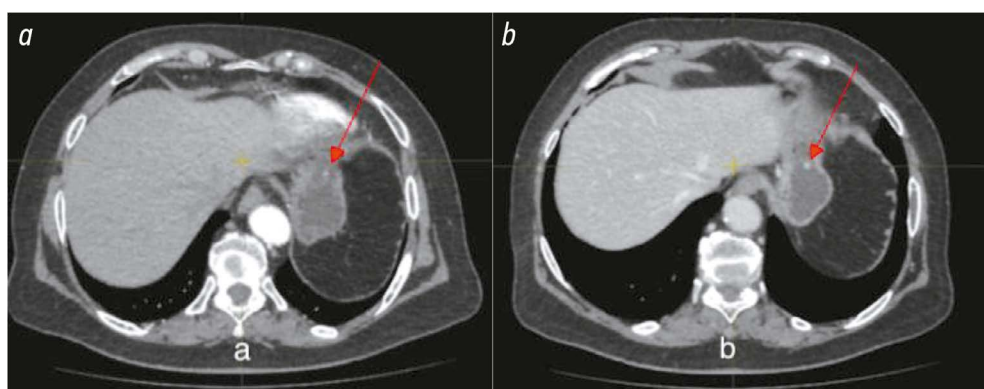
Fig. 4. Gastric neuroendocrine tumor: *a*, low contrast uptake by tumor tissue, arterial phase; *b*, a hyperintense lesion in the upper wall of the gastric cardia (up to 6 mm), venous phase.

NETs. According to recommendations from the European Society for Medical Oncology and the National Comprehensive Cancer Network, pancreatic biopsy is advised only when the tumor is not clearly visualized on three-phase MRI or CT. The sensitivity of cytological and histological evaluation for diagnosing pancreatic cancer does not exceed 90%. In cases where imaging does not provide morphological confirmation of pancreatic cancer, most patients still undergo radical surgical treatment. However, biopsy carries risks, including potential complications and the possibility of tumor cell spread [18].

Therefore, research into the potential for achieving morphological confirmation of malignancy through imaging studies is of particular relevance.

Radiomics is currently regarded as a promising approach for the diagnosis and management of NENs at various anatomical sites [19]. It involves the extraction and analysis of numerous quantitative features from medical imaging data, including parameters related to shape, size, texture, intensity, and voxel relationships [20].

Radiomics is applied in research to solve specific clinical tasks. In gastrointestinal NENs, its most common application is in predicting tumor grade [21–23]. Texture analysis has also been used to differentiate gastrointestinal NETs from other gastrointestinal neoplasms. Most studies indicate that models combining radiomics features with clinical and additional diagnostic data yield the highest accuracy. Texture analysis is used less frequently to evaluate treatment response in gastrointestinal NETs. Additionally, some studies have explored the role of radiomics in predicting disease progression and recurrence.

AIM

To assess the potential of radiomics for the differential diagnosis of gastric and pancreatic NETs.

MATERIALS AND METHODS

Study design

This study is an observational, single-center, cross-sectional investigation.

Eligibility criteria

Inclusion criteria: morphologically confirmed gastric or pancreatic neoplasm; abdominal CT with intravenous contrast performed before the initiation of treatment; and documented voluntary informed consent allowing the use of the participant's medical data for research purposes

Non-inclusion criteria: CT scans conducted outside the Russian Scientific Center of Roentgenology and Radiology

Exclusion criteria: absence of CT images of the tumor

Study setting

Data that met the inclusion criteria were collected at the Russian Scientific Center of Roentgenology and Radiology.

Study duration

The study was conducted from December 1, 2023, to March 22, 2024.

Intervention

All participants underwent contrast-enhanced abdominal CT using various scanners, with a slice thickness of 1 mm. CT scans were acquired during the early arterial phase, which is not typically included in standard imaging protocols.

Main study outcome

The primary outcomes were radiomics parameters in patients diagnosed with NETs and adenocarcinoma.

Outcomes registration

CT data from all patients were uploaded into the open-source software 3D Slicer (https://www.slicer.org/), which allows extraction of radiomics parameters from defined regions of interest.

Radiomics features were calculated within the gastric or pancreatic tumor regions. For each patient, the tumor was manually segmented in either the arterial or venous phase, and the resulting contour was aligned with the precontrast phase. Image processing in the precontrast phase is challenging due to the tumor appearing isodense with the surrounding parenchyma. Segmentation in contrast-enhanced phases also presents difficulties, as anatomical mismatches can occur between slices across different CT phases. These factors necessitate an evaluation of segmentation reproducibility, which is a limitation of the study.

A total of 93 radiomics features were extracted for both gastric NETs and adenocarcinomas and for pancreatic NETs and adenocarcinomas. These included first-order statistics and features derived from adjacency and uniformity matrices. Parameters related to the geometry of the region of interest were not analyzed due to challenges in reliably differentiating between healthy and tumor tissues.

The comparison results, including the median, first and third quartiles, and statistical significance of the differences, are presented in the tables.

Subgroup analysis

The study participants' data were categorized into four groups based on tumor site and histologic type:
- Gastric neuroendocrine tumor
- Gastric adenocarcinoma
- Pancreatic neuroendocrine tumor
- Pancreatic adenocarcinoma

Ethics approval

The study was approved by the Independent Ethics Committee of the Russian Scientific Center of Roentgenology and Radiology (Meeting Minutes No. 2, March 1, 2023).

Statistical analysis

The data were processed and analyzed using Microsoft Office Excel and R-Studio, an open-source software development environment for the R programming language. To assess significant differences between medical imaging biomarkers, pairwise intergroup comparisons for each radiomics parameter were conducted using the Mann–Whitney U test. Differences were considered significant if $p < 0.05$.

RESULTS

Participants

The study analyzed data from 12 patients with morphologically confirmed gastric neoplasms (6 with NETs and 6 with adenocarcinomas) and 22 patients with morphologically confirmed pancreatic neoplasms (11 with NETs and 11 with adenocarcinomas). Abdominal CT with intravenous contrast was performed on all patients prior to treatment at the Russian Scientific Center of Roentgenology and Radiology. The neoplasms examined in the study were small (2–3 cm) and varied in grade (G1–G3) and contrast enhancement. Most of the neoplasms included in the study were not initially classified as NETs in prospective CT analysis due to challenges with visual differentiation, requiring further assessment of the CT scans.

Primary results

The study identified 15 radiomics parameters that showed significant differences between patients with gastric NETs and adenocarcinomas. The comparison results, including the median, first and third quartiles, and the significance of the differences (Mann–Whitney U test), are shown in Table 2.

Table 2. Comparison of radiomics parameters between the two groups of patients with gastric neoplasms

Parameters	Gastric neuroendocrine tumor, Me [Q1; Q3]	Gastric adenocarcinoma, Me [Q1; Q3]	p-value
First order Entropy	2.01 [1.88; 2.23]	1.83 [1.62; 1.86]	0.041
First order Interquartile Range	31.50 [27.56; 38.94]	23.50 [19.25; 26.94]	0.026
First order Mean Absolute Deviation	19.19 [17.25; 21.53]	15.54 [12.92; 16.41]	0.041
First order Robust Mean Absolute Deviation	13.36 [12.07; 15.23]	10.04 [8.38; 11.57]	0.026
First order Skewness	-0.25 [-0.43; -0.10]	0.05 [-0.13; 0.24]	0.026
First order Uniformity	0.29 [0.26; 0.31]	0.34 [0.32; 0.40]	0.041
First order Variance	562.42 [479.32; 803.18]	414.40 [311.13; 429.14]	0.041
GLCM Cluster Tendency	2.41 [1.90; 4.08]	1.92 [1.36; 2.02]	0.041
GLCM Joint Entropy	3.83 [3.47; 4.02]	3.48 [2.99; 3.60]	0.041
GLCM Sum Entropy	2.63 [2.44; 2.98]	2.48 [2.22; 2.52]	0.041
GLCM Sum Squares	0.92 [0.78; 1.32]	0.72 [0.57; 0.78]	0.041
GLDM Dependence Non Uniformity Normalized	0.07 [0.06; 0.09]	0.06 [0.06; 0.06]	0.015
GLDM Gray Level Variance	0.97 [0.84; 1.38]	0.76 [0.59; 0.79]	0.041
GLRLM Gray Level Non Uniformity Normalized	0.27 [0.24; 0.29]	0.30 [0.30; 0.35]	0.041
GLRLM Gray Level Variance	1.09 [0.91; 1.56]	0.87 [0.73; 0.98]	0.041

Note. Me, median; Q1, first quartile; Q3, third quartile; GLCM, Gray Level Co-occurrence Matrix; GLDM, Gray Level Dependence Matrix; GLRLM, Gray Level Run Length Matrix.

Table 3. Comparison of radiomics parameters between the two groups of patients with pancreatic neoplasms

Parameters	Pancreatic neuroendocrine tumor, Me [Q1; Q3]	Pancreatic adenocarcinoma, Me [Q1; Q3]	p-value
First order Energy	691,524 [580,555; 1,727,135]	2,953,926 [2,318,229; 6,503,888]	0.007
First order Total Energy	1,425,223.71 [284,018.65; 3,100,864.22]	5,091,794.59 [1,502,766.76; 8,727,525.25]	0.047
GLDM Dependence Non Uniformity	28.01 [18.41; 44.78]	116.43 [88.79; 194.84]	0.007
GLDM Gray Level Non Uniformity	219.75 [132.80; 431.55]	868.90 [494.56; 1919.16]	0.001
GLRLM Gray Level Non Uniformity	119.69 [79.75; 161.57]	512.56 [308.03; 731.74]	0.002
GLRLM Run Length Non Uniformity	122.55 [71.16; 271.96]	702.16 [426.47; 1297.70]	0.001
GLSZM Gray Level Non Uniformity	10.52 [4.69; 32.08]	29.51 [19.39; 45.98]	0.034
GLSZM Large Area Emphasis	2826.63 [2243.10; 6732.92]	18,275.14 [7206.26; 42,549.14]	0.007
GLSZM Large Area High Gray Level Emphasis	38 429.22 [20,178.45; 62 109.69]	156,116.40 [102,536.10; 367,510.22]	0.001
GLSZM Low Gray Level Zone Emphasis	0.21 [0.17; 0.27]	0.17 [0.10; 0.23]	0.028
GLSZM Zone Variance	2632.37 [1928.10; 5957.51]	17 305.27 [7058.35; 41,998.41]	0.005
NGTDM Busyness	3.26 [2.01; 5.02]	10.23 [9.13; 26.37]	0.0001
NGTDM Coarseness	0.02 [0.01; 0.03]	0 [0; 0.01]	0.002
NGTDM Strength	0.13 [0.08; 0.26]	0.04 [0.01; 0.06]	0.001

Note. Me, median; Q1, first quartile; Q3, third quartile; GLDM, Gray Level Dependence Matrix; GLRLM, Gray Level Run Length Matrix; GLSZM, Gray Level Size Zone Matrix; NGTDM, Neighboring Gray Tone Difference Matrix.

According to Table 2, patients with gastric NETs exhibited significantly higher entropy (indicating greater heterogeneity of gray levels in an image) and variance (representing the distribution of gray level intensity relative to the mean). The GLDM Dependence Non-Uniformity Normalized, where lower values suggest higher tissue uniformity, was also higher in patients with NETs. These results may suggest that NET tissues are more heterogeneous compared to adenocarcinomas.

In patients with pancreatic NETs and adenocarcinomas, 14 radiomics parameters showed significant differences. The results of these comparisons, including the median, first

and third quartiles, and the significance of the differences (Mann–Whitney U test), are presented in Table 3.

The findings in Table 3 show that nearly all parameters were significantly higher in patients with pancreatic adenocarcinoma. The Energy and Total Energy parameters were 76% and 72% higher, respectively, in these patients. The GLSZM Gray Level Non-Uniformity, where lower values indicate higher uniformity in gray level intensity, was also higher in the adenocarcinoma group. Additionally, NGTDM Busyness (reflecting pixel value changes relative to neighboring pixels) was 68% higher in this group, indicating a more heterogeneous texture with sharper intensity variations in pancreatic adenocarcinoma tissues. Therefore, pancreatic adenocarcinoma tissue appears more heterogeneous and denser than NET tissue.

DISCUSSION

The results of this study and the potential application of radiomics in diagnosing gastrointestinal and pancreatic neoplasms are supported by international research. Chiti et al. used texture parameters in the arterial CT phase to differentiate between high-grade (G3) and low-grade (G1/G2) pancreatic NETs, achieving an area under the curve (AUC) of 0.82 [24]. Liang et al. developed a model for distinguishing between carcinoids (G1) and intermediate-to high-grade (G2/G3) pancreatic NETs. This model, which incorporates both radiomics parameters and clinical data, demonstrated a high prognostic value with an AUC of 0.89 [25].

Wang et al. created a prognostic model for differentiating gastric NETs from adenocarcinomas. The best results were obtained by combining radiomics parameters with data on metastasis and tumor margins, yielding an AUC of 0.821 [0.725; 0.895] [26]. Han et al. developed a model using radiomics parameters to distinguish between cystadenomas and pancreatic NETs. Combining machine learning models at various stages of the study produced excellent classification parameters: AUC 0.99, sensitivity 0.98, and specificity 1.0 [27]. Additionally, other studies have addressed the differential diagnosis between NETs and other gastrointestinal malignancies [28–30].

An et al. developed a model to predict relapses of gastrointestinal and pancreatic NETs by combining radiomics parameters with clinical and laboratory data. This model had an AUC of 0.824 [0,751; 0.883], demonstrating strong prognostic value [31]. Similarly, Song et al. predicted tumor relapse in patients with pancreatic NETs following radical resection. The model, which combined radiomics parameters and clinical data, showed the best results with an AUC of 0.83 [32].

Caruso et al. predicted the response to everolimus treatment in patients with NETs from various sites. The prognostic model achieved an AUC of 0.87 [33].

These published studies suggest that radiomics is a promising and effective tool for analyzing medical images of gastrointestinal NETs at different stages of diagnosis and treatment.

CONCLUSION

The clinical cases presented highlight the challenges in diagnosing gastric and pancreatic NETs. Similar density values between NETs and surrounding tissues, small tumor size, and variable contrast uptake can lead to underdiagnosis of these neoplasms. However, texture analysis shows promise as a tool for differentiating gastrointestinal NETs from other gastrointestinal tumors, particularly in the early stages when biopsy is challenging.

We identified biomarkers that significantly differed between NETs and adenocarcinomas of the same location: 15 biomarkers for gastric NETs and 14 biomarkers for pancreatic NETs. These findings suggest that further research is needed, particularly in developing models that combine image texture features with clinical data.

ADDITIONAL INFORMATION

REFERENCES

1. Shah MH, Goldner WS, Benson AB, et al. Neuroendocrine and Adrenal Tumors, Version 2.2021, NCCN Clinical Practice Guidelines in Oncology. *J Natl Compr Canc Netw.* 2021;19(7):839–868. doi: 10.6004/jnccn.2021.0032

2. Menshikov KV, Sultanbaev AV, Musin ShI, et al. Neuroendocrine Tumours: a Literature Review. *Creative surgery and oncology.* 2021;11(2):174–182. EDN: RTJQRK doi: 10.24060/2076-3093-2021-11-2-174-182

3. Alekberzade AV, Krylov NN, Lipnitskiy EM, et al. Gastric neuroendocrine tumors. *Pirogov Russian Journal of Surgery.* 2019;(12):111–120. EDN: RIRQGH doi: 10.17116/hirurgia2019121111

4. Ministry of Health of the Russian Federation. Clinical guidelines «Neuroendocrine tumors» [Internet]. 2020. Available from: https://cr.minzdrav.gov.ru/schema/610_1 (In Russ.) Accessed 2024 Mar 4.

5. Dasari A, Shen C, Halperin D, et al. Trends in the Incidence, Prevalence, and Survival Outcomes in Patients With Neuroendocrine Tumors in the United States. *JAMA Oncol.* 2017;3(10):1335–1342. doi: 10.1001/jamaoncol.2017.0589

6. Department of Health of the City of Moscow. Guidelines «Neuroendocrine tumors of the pancreas» [Internet]. 2019. Available from: https://niioz.ru/upload/iblock/4ee/4ee9895614aa276f538069c aee698fce.pdf (In Russ.) Accessed 2024 Mar 4.

7. Halfdanarson TR, Rabe KG, Rubin J, Petersen GM. Pancreatic neuroendocrine tumors (PNETs): incidence, prognosis and recent trend toward improved survival. *Ann Oncol.* 2008;19(10):1727–1733. doi: 10.1093/annonc/mdn351

8. Loosen SH, Kostev K, Jann H, et al. Distribution of gastrointestinal neuroendocrine tumors in Europe: results from a retrospective cross-sectional study. *J Cancer Res Clin Oncol.* 2023;149(4):1411–1416. doi: 10.1007/s00432-022-04003-3

9. Chernousov AF, Egorov AV, Musaev GKh, et al. Neuroendocrine tumors of a pancreas: 30 year's experience of clinic of faculty surgery of N.N. Burdenko. *Pirogov Russian Journal of Surgery.* 2013;(7):13–19. EDN: QYSJLV

10. Dias AR, Azevedo BC, Alban LBV., et al. Gastric neuroendocrine tumor: review and update. *Arq Bras Cir Dig.* 2017;30(2):150–154. doi: 10.1590/0102-6720201700020016

11. Sundin A, Vullierme MP, Kaltsas G, Plöckinger U. ENETS Consensus Guidelines for the Standards of Care in Neuroendocrine Tumors: radiological examinations. *Neuroendocrinology.* 2009;90(2):167–183. doi: 10.1159/000184855

12. Radiographia.info [Internet]. Pancreatic endocrine tumors. Available from: https://radiographia.info/article/endokrinnye-opuholi-podzheludochnoy-zhelezy (In Russ.) Accessed: 04.03.2024

13. Gruzdev IS. *Application of texture analysis for differential diagnosis and prognosis in the surgical treatment of hypervascular pancreatic masses* [dissertation]. Moscow; 2022. Available from: https://www.rncrr.ru/nauka/dissertatsionnyy-sovet/obyavleniya-o-zashchitakh/upload%202023/Груздев_диссертация.pdf (In Russ.) EDN: BKPRVN

14. Lewis RB, Lattin Jr GE, Paal E. Pancreatic endocrine tumors: radiologic-clinicopathologic correlation. *Radiographics.* 2010;30(6):1445–1464. doi: 10.1148/rg.306105523

15. Raman SP, Hruban RH, Cameron JL, et al. Pancreatic imaging mimics: part 2, pancreatic neuroendocrine tumors and their mimics. *AJR Am J Roentgenol.* 2012;199(2):309–318. doi: 10.2214/AJR.12.8627

16. Sahani DV, Bonaffini PA, Fernández-Del Castillo C, Blake MA. Gastroenteropancreatic neuroendocrine tumors: role of imaging in diagnosis and management. *Radiology.* 2013;266(1):38–61. doi: 10.1148/radiol.12112512

17. Ganeshan D, Bhosale P, Yang T, Kundra V. Imaging features of carcinoid tumors of the gastrointestinal tract. *AJR Am J Roentgenol.* 2013;201(4):773–786. doi: 10.2214/AJR.12.9758

18. Mikhailov IV, Beliakouski VN, Kudrashou VA, et al. Biopsy of pancreatic tumors prior to resection: for and against. *Health and Ecology Issues.* 2021;18(1):62–69. EDN: ECTEZT doi: 10.51523/2708-6011.2021-18-1-9

19. Staal FCR, Aalbersberg EA, van der Velden D, et al. GEP-NET radiomics: a systematic review and radiomics quality score assessment. *Eur Radiol.* 2022;32(10):7278–7294. doi: 10.1007/s00330-022-08996-w

20. van Griethuysen JJM, Fedorov A, Parmar C, et al. Computational Radiomics System to Decode the Radiographic Phenotype. *Cancer Res.* 2017;77(21):e104–e107. doi: 10.1158/0008-5472.CAN-17-0339

21. Wang X, Qiu JJ, Tan CL, et al. Development and Validation of a Novel Radiomics-Based Nomogram With Machine Learning to Preoperatively Predict Histologic Grade in Pancreatic Neuroendocrine Tumors. *Front Oncol.* 2022;12:843376. doi: 10.3389/fonc.2022.843376

22. Dong Y, Yang DH, Tian XF, et al. Pancreatic neuroendocrine tumor: prediction of tumor grades by radiomics models based on ultrasound images. *Br J Radiol.* 2023;96(1149):20220783. doi: 10.1259/bjr.20220783

23. Ye JY, Fang P, Peng ZP, et al. A radiomics-based interpretable model to predict the pathological grade of pancreatic neuroendocrine tumors. *Eur Radiol.* 2024;34(3):1994–2005. doi: 10.1007/s00330-023-10186-1

24. Chiti G, Grazzini G, Cozzi D, et al. Imaging of Pancreatic Neuroendocrine Neoplasms. *Int J Environ Res Public Health.* 2021;18(17):8895. doi: 10.3390/ijerph18178895

25. Liang W, Yang P, Huang R, et al. A Combined Nomogram Model to Preoperatively Predict Histologic Grade in Pancreatic Neuroendocrine Tumors. *Clin Cancer Res.* 2019;25(2):584–594. doi: 10.1158/1078-0432.CCR-18-1305

26. Wang R, Liu H, Liang P, et al. Radiomics analysis of CT imaging for differentiating gastric neuroendocrine carcinomas from gastric adenocarcinomas. *Eur J Radiol.* 2021;138:109662. doi: 10.1016/j.ejrad.2021.109662

27. Han X, Yang J, Luo J, et al. Application of CT-Based Radiomics in Discriminating Pancreatic Cystadenomas From Pancreatic Neuroendocrine Tumors Using Machine Learning Methods. *Front Oncol.* 2021;11:606677. doi: 10.3389/fonc.2021.606677

28. Shi YJ, Zhu HT, Liu YL, et al. Radiomics Analysis Based on Diffusion Kurtosis Imaging and T2 Weighted Imaging for Differentiation of Pancreatic Neuroendocrine Tumors From Solid Pseudopapillary Tumors. *Front Oncol.* 2020;10:1624. doi: 10.3389/fonc.2020.01624

29. Li X, Zhu H, Qian X, et al. MRI Texture Analysis for Differentiating Nonfunctional Pancreatic Neuroendocrine Neoplasms From Solid Pseudopapillary Neoplasms of the Pancreas. *Acad Radiol.* 2020;27(6):815–823. doi: 10.1016/j.acra.2019.07.012

30. He M, Liu Z, Lin Y, et al. Differentiation of atypical non-functional pancreatic neuroendocrine tumor and pancreatic ductal adenocarcinoma using CT based radiomics. *Eur J Radiol.* 2019;117:102–111. doi: 10.1016/j.ejrad.2019.05.024

31. An P, Zhang J, Li M, et al. Clinical Data-CT Radiomics-Based Model for Predicting Prognosis of Patients with Gastrointestinal Pancreatic Neuroendocrine Neoplasms (GP-NENs). *Comput Math Methods Med.* 2022;2022:4186305. doi: 10.1155/2022/4186305

32. Song C, Wang M, Luo Y, et al. Predicting the recurrence risk of pancreatic neuroendocrine neoplasms after radical resection using deep learning radiomics with preoperative computed tomography images. *Ann Transl Med.* 2021;9(10):833. doi: 10.21037/atm-21-25

33. Caruso D, Polici M, Rinzivillo M, et al. CT-based radiomics for prediction of therapeutic response to Everolimus in metastatic neuroendocrine tumors. *Radiol Med.* 2022;127(7):691–701. doi: 10.1007/s11547-022-01506-4

СПИСОК ЛИТЕРАТУРЫ

1. Shah M.H., Goldner W.S., Benson A.B., et al. Neuroendocrine and Adrenal Tumors, Version 2.2021, NCCN Clinical Practice Guidelines in Oncology // J Natl Compr Canc Netw. 2021. Vol. 19, N 7. P. 839–868. doi: 10.6004/jnccn.2021.0032

2. Меньшиков К.В., Султанбаев А.В., Мусин Ш.И., и др. Нейроэндокринные опухоли. Обзор литературы // Креативная хирургия и онкология. 2021. Т. 11, № 2. С. 174–182. EDN: RTJQRK doi: 10.24060/2076-3093-2021-11-2-174-182

3. Алекберзаде А.В., Крылов Н.Н., Липницкий Е.М., и др. Нейроэндокринные опухоли желудка // Хирургия. Журнал им. Н.И. Пирогова. 2019. № 12. С. 111–120. EDN: RIRQGH doi: 10.17116/hirurgia2019121111

4. Клинические рекомендации «Нейроэндокринные опухоли» [интернет]. Министерство здравоохранения Российской Федерации. 2020– Режим доступа: https://cr.minzdrav.gov.ru/schema/610_1 Дата обращения: 04.03.2024.

5. Dasari A., Shen C., Halperin D., et al. Trends in the Incidence, Prevalence, and Survival Outcomes in Patients With Neuroendocrine Tumors in the United States // JAMA Oncol. 2017. Vol. 3, N. 10. P. 1335–1342. doi: 10.1001/jamaoncol.2017.0589

6. Методические рекомендации «Нейроэндокринные опухоли поджелудочной железы» [интернет]. Департамент здравоохранения города Москвы. 2019– Режим доступа: https://niioz.ru/upload/iblock/4ee/4ee9895614aa276f538069caee698fce.pdf Дата обращения: 04.03.2024

7. Halfdanarson T.R., Rabe K.G., Rubin J., Petersen G.M. Pancreatic neuroendocrine tumors (PNETs): incidence, prognosis and recent trend toward improved survival // Ann Oncol. 2008. Vol. 19, N. 10. P. 1727–1733. doi: 10.1093/annonc/mdn351

8. Loosen S.H., Kostev K., Jann H., et al. Distribution of gastrointestinal neuroendocrine tumors in Europe: results from a retrospective cross-sectional study // J Cancer Res Clin Oncol. 2023. Vol. 149, N. 4. P. 1411–1416. doi: 10.1007/s00432-022-04003-3

9. Черноусов А.Ф., Егоров А.В., Мусаев Г.Х., и др. Нейроэндокринные опухоли поджелудочной железы: 30-летний опыт клиники факультетской хирургии им. Н.Н. Бурденко // Хирургия. Журнал им. Н.И. Пирогова. 2013. № 7. С. 13–19. EDN: QYSJLV

10. Dias A.R., Azevedo B.C., Alban L.B.V., et al. Gastric neuroendocrine tumor: review and update // Arq Bras Cir Dig. 2017. Vol. 30, N. 2. P. 150–154. doi: 10.1590/0102-6720201700020016

11. Sundin A., Vullierme M.P., Kaltsas G., Plöckinger U. ENETS Consensus Guidelines for the Standards of Care in Neuroendocrine Tumors: radiological examinations // Neuroendocrinology. 2009. Vol. 90, N. 2. P. 167–183. doi: 10.1159/000184855

12. Radiographia.info [интернет]. Эндокринные опухоли поджелудочной железы Режим доступа: https://radiographia.info/article/endokrinnye-opuholi-podzheludochnoy-zhelezy Дата обращения: 04.03.2024

13. Груздев И.С. Применение текстурного анализа в дифференциальном диагнозе и прогнозе при хирургическом лечении гиперваскулярных образований поджелудочной железы: диссертация на соискание учёной степени кандидата медицинских наук. Москва, 2022. Режим доступа: https://www.rncrr.ru/nauka/dissertatsionnyy-sovet/obyavleniya-o-zashchitakh/upload%202023/Груздев_диссертация.pdf Дата обращения: 04.03.2024 EDN: BKPRVN

14. Lewis R.B., Lattin Jr G.E., Paal E. Pancreatic endocrine tumors: radiologic-clinicopathologic correlation. Radiographics. 2010. Vol. 30, N. 6. P. 1445–1464. doi: 10.1148/rg.306105523

15. Raman S.P., Hruban R.H., Cameron J.L., et al. Pancreatic imaging mimics: part 2, pancreatic neuroendocrine tumors and their mimics // AJR Am J Roentgenol. 2012. Vol. 199, N. 2. P. 309–318. doi: 10.2214/AJR.12.8627

16. Sahani D.V., Bonaffini P.A., Fernández-Del Castillo C., Blake M.A. Gastroenteropancreatic neuroendocrine tumors: role of imaging in diagnosis and management // Radiology. 2013. Vol. 266, N 1. P. 38–61. doi: 10.1148/radiol.12112512

17. Ganeshan D., Bhosale P., Yang T., Kundra V. Imaging features of carcinoid tumors of the gastrointestinal tract // AJR Am J Roentgenol. 2013. Vol. 201, N. 4. P. 773–786. doi: 10.2214/AJR.12.9758

18. Михайлов И.В., Беляковский В.Н., Кудряшов В.А., и др. Биопсия опухолей поджелудочной железы перед резекцией: за и против // Проблемы здоровья и экологии. 2021. Т. 18, № 1. С. 62–69. EDN: ECTEZT doi: 10.51523/2708-6011.2021-18-1-9

19. Staal F.C.R., Aalbersberg E.A., van der Velden D., et al. GEP-NET radiomics: a systematic review and radiomics quality score assessment // Eur Radiol. 2022. Vol. 32, N. 10. P. 7278–7294. doi: 10.1007/s00330-022-08996-w

20. van Griethuysen J.J.M., Fedorov A., Parmar C., et al. Computational Radiomics System to Decode the Radiographic Phenotype // Cancer Res. 2017. Vol. 77, N. 21. P. e104–e107. doi: 10.1158/0008-5472.CAN-17-0339

21. Wang X., Qiu J.J., Tan C.L., et al. Development and Validation of a Novel Radiomics-Based Nomogram With Machine Learning to Preoperatively Predict Histologic Grade in Pancreatic Neuroendocrine Tumors // Front Oncol. 2022. Vol. 1. ID: 843376. doi: 10.3389/fonc.2022.843376

22. Dong Y., Yang D.H., Tian X.F., et al. Pancreatic neuroendocrine tumor: prediction of tumor grades by radiomics models based on ultrasound images // Br J Radiol. 2023. Vol. 96, N. 1149. ID: 20220783. doi: 10.1259/bjr.20220783

23. Ye J.Y., Fang P., Peng Z.P., et al. A radiomics-based interpretable model to predict the pathological grade of pancreatic neuroendocrine tumors. // Eur Radiol. 2024. Vol 34, N 3. P. 1994–2005. doi: 10.1007/s00330-023-10186-1

24. Chiti G., Grazzini G., Cozzi D., et al. Imaging of Pancreatic Neuroendocrine Neoplasms // Int J Environ Res Public Health. 2021. Vol. 18, N. 17. ID: 8895. doi: 10.3390/ijerph18178895

25. Liang W., Yang P., Huang R., et al. A Combined Nomogram Model to Preoperatively Predict Histologic Grade in Pancreatic Neuroendocrine Tumors // Clin Cancer Res. 2019. Vol. 25, N. 2. P. 584–594. doi: 10.1158/1078-0432.CCR-18-1305

26. Wang R., Liu H., Liang P., et al. Radiomics analysis of CT imaging for differentiating gastric neuroendocrine carcinomas from gastric adenocarcinomas // Eur J Radiol. 2021. Vol. 138. ID: 109662. doi: 10.1016/j.ejrad.2021.109662

27. Han X., Yang J., Luo J., et al. Application of CT-Based Radiomics in Discriminating Pancreatic Cystadenomas From Pancreatic Neuroendocrine Tumors Using Machine Learning Methods // Front Oncol. 2021. Vol. 11. ID: 606677. doi: 10.3389/fonc.2021.606677

28. Shi Y.J., Zhu H.T., Liu Y.L., et al. Radiomics Analysis Based on Diffusion Kurtosis Imaging and T2 Weighted Imaging for Differentiation of Pancreatic Neuroendocrine Tumors From Solid Pseudopapillary Tumors // Front Oncol. 2020. Vol. 10. ID: 1624. doi: 10.3389/fonc.2020.01624

29. Li X., Zhu H., Qian X., et al. MRI Texture Analysis for Differentiating Nonfunctional Pancreatic Neuroendocrine Neoplasms From Solid Pseudopapillary Neoplasms of the Pancreas // Acad Radiol. 2020. Vol. 27, N. 6. P. 815–823. doi: 10.1016/j.acra.2019.07.012

30. He M., Liu Z., Lin Y., et al. Differentiation of atypical non-functional pancreatic neuroendocrine tumor and pancreatic ductal adenocarcinoma using CT based radiomics // Eur J Radiol. 2019. Vol.117. P. 102–111. doi: 10.1016/j.ejrad.2019.05.024

31. An P., Zhang J., Li M., et al. Clinical Data-CT Radiomics-Based Model for Predicting Prognosis of Patients with Gastrointestinal Pancreatic Neuroendocrine Neoplasms (GP-NENs) // Comput Math Methods Med. 2022. Vol. 2022. ID: 4186305. doi: 10.1155/2022/4186305

32. Song C., Wang M., Luo Y., et al. Predicting the recurrence risk of pancreatic neuroendocrine neoplasms after radical resection using deep learning radiomics with preoperative computed tomography images // Ann Transl Med. 2021. Vol. 9, N. 10. ID: 833. doi: 10.21037/atm-21-25

33. Caruso D., Polici M., Rinzivillo M., et al. CT-based radiomics for prediction of therapeutic response to Everolimus in metastatic neuroendocrine tumors // Radiol Med. 2022. Vol. 127, N. 7. P. 691–701. doi: 10.1007/s11547-022-01506-4

AUTHORS' INFO

* Elina S.-A. Shakhvalieva;
address: 86 Profsoyuznaya str., 117997, Moscow, Russia;
ORCID: 0009-0000-7535-8523;
e-mail: shelina9558@gmail.com

Nikolay V. Nudnov, MD, Dr. Sci. (Medicine), Professor;
ORCID: 0000-0001-5994-0468;
eLibrary SPIN: 3018-2527;
e-mail: nudnov@rncrr.ru

David G. Karelidze;
ORCID: 0009-0002-0375-1291;
e-mail: david_ka@mail.ru

Aleksandr A. Borisov;
ORCID: 0000-0003-4036-5883;
eLibrary SPIN: 4294-4736;
e-mail: aleksandrborisov10650@gmail.com

Mikhail E. Ivannikov;
ORCID: 0009-0007-0407-0953;
eLibrary SPIN: 3419-2977;
e-mail: ivannikovmichail@gmail.com

ОБ АВТОРАХ

* Шахвалиева Элина Саид-Аминовна;
адрес: Россия, 117997, Москва, ул. Профсоюзная, д. 86;
ORCID: 0009-0000-7535-8523;
e-mail: shelina9558@gmail.com

Нуднов Николай Васильевич, д-р мед. наук, профессор;
ORCID: 0000-0001-5994-0468;
eLibrary SPIN: 3018-2527;
e-mail: nudnov@rncrr.ru

Карелидзе Давид Георгиевич;
ORCID: 0009-0002-0375-1291;
e-mail: david_ka@mail.ru

Борисов Александр Александрович;
ORCID: 0000-0003-4036-5883;
eLibrary SPIN: 4294-4736;
e-mail: aleksandrborisov10650@gmail.com

Иванников Михаил Евгеньевич;
ORCID: 0009-0007-0407-0953;
eLibrary SPIN: 3419-2977;
e-mail: ivannikovmichail@gmail.com

_____

* Corresponding author / Автор, ответственный за переписку

Detecting new lung cancer cases using artificial intelligence: clinical and economic evaluation of a retrospective analysis of computed tomography scans 2 years after the COVID-19 pandemic

Ruslan A. Zukov[1,2], Ivan P. Safontsev[1,2], Marina P. Klimenok[2], Tatyana E. Zabrodskaya[2], Natalya A. Merkulova[2], Valeria Yu. Chernina[3], Mikhail G. Belyaev[3], Mikhail Yu. Goncharov[3,4,5], Vitaly V. Omelyanovskiy[6,7,8], Ksenia A. Ulianova[9], Evgenia A. Soboleva[3,5], Maria E. Blokhina[11], Elena A. Nalivkina[11], Victor A. Gombolevskiy[3,4,10,12]

[1] Professor V.F. Voino-Yasenetsky Krasnoyarsk State Medical University, Krasnoyarsk, Russia;
[2] Krasnoyarsk Regional Clinical Oncological Dispensary named after A.I. Kryzhanovskogo, Krasnoyarsk, Russia;
[3] «IRA Labs», Moscow, Russia;
[4] Artificial Intelligence Research Institute AIRI, Moscow, Russia;
[5] Skolkovo Institute of Science and Technology, Moscow, Russia;
[6] Center for Expertise and Quality Control of Medical Care, Moscow, Russia;
[7] Russian Medical Academy of Continuous Professional Education, Moscow, Russia;
[8] Financial Research Institute, Moscow, Russia;
[9] Ministry of Health of the Russian Federation, Moscow, Russia;
[10] World-Class Research Center «Digital biodesign and personalized healthcare», Moscow, Russia;
[11] AstraZeneca Pharmaceuticals LLC, Moscow, Russia;
[12] Sechenov First Moscow State Medical University, Moscow, Russia

ABSTRACT

BACKGROUND: Chest computed tomography (CT) is the main modality used to diagnose lung lesions caused by COVID-19 infection. Since 2020, the use of this modality in the Krasnoyarsk krai has increased. However, the incidence of lung cancer decreased by 5.2%. The current situation has raised concerns about missing radiographic signs typical of lung cancer and has stimulated the search for new diagnostic modalities using artificial intelligence (AI) for data analysis.

AIM: The aim of the study was to evaluate the feasibility of using an AI algorithm to search for lung nodules based on chest CT data obtained during the COVID-19 pandemic to identify lung cancer.

MATERIALS AND METHODS: The retrospective study included chest CT scans of patients from Krasnoyarsk krai diagnosed with COVID-19 reported in the PACS base between 1 November 2020 and 28 February 2021. The interval between chest CT and AI analysis ranged from two years and one month to two years and five months. Chest-IRA algorithm was used. AI detected lung nodules with a volume greater than 100 mm^3. The radiologists divided the results into three groups based on the potential for lung cancer. The assessment of the economic benefits of using the AI algorithm considered the cost of wages and savings in the treatment of early-stage lung cancer, which affects gross regional product.

RESULTS: The AI algorithm identified nodules in 484 out of 10,500 CT scans. A total of 192 patients with a high potential for lung cancer, 103 with no signs and 60 with inconclusive signs were identified, and 112 patients with a high and moderate potential for lung cancer did not seek medical care. AI confirmed 100 (28.2%) histologically proven cases of lung cancer, with stages I–II detected in 35%.

Using AI instead of radiologists would save 25 months and 4 days of work, which is equal to 2 million 430 thousand rubles. Expected budget savings due to early detection of lung cancer vary from 10 million 600 thousand to 12 million 500 thousand rubles for each 10,500 CTs. The total economic effect for a five-year period would be from 259 million 400 thousand rubles to 305 million 100 thousand rubles.

CONCLUSION: The use of AI to evaluate chest CT scans demonstrates high performance in identifying lung nodules, including those in patients with COVID-19, confirming its potential use for early detection of incidental lung nodules that might otherwise be missed.

Keywords: lung cancer; computed tomography; artificial intelligence; chest; health economics; performance evaluation.

Выявление новых случаев рака лёгкого с помощью искусственного интеллекта: клиническая и экономическая оценка ретроспективного анализа результатов компьютерной томографии через 2 года после пандемии COVID-19

Р.А. Зуков[1,2], И.П. Сафонцев[1,2], М.П. Клименок[2], Т.Е. Забродская[2], Н.А. Меркулова[2], В.Ю. Чернина[3], М.Г. Беляев[3], М.Ю. Гончаров[3,4,5], В.В. Омельяновский[6,7,8], К.А. Ульянова[9], Е.А. Соболева[3,5], М.Е. Блохина[11], Е.А. Наливкина[11], В.А. Гомболевский[3,4,10,12]

[1] Красноярский государственный медицинский университет имени профессора В.Ф. Войно-Ясенецкого, Красноярск, Россия;
[2] Красноярский краевой клинический онкологический диспансер имени А.И. Крыжановского, Красноярск, Россия;
[3] «АЙРА Лабс», Москва, Россия;
[4] Институт искусственного интеллекта AIRI, Москва, Россия;
[5] Сколковский институт науки и технологий, Москва, Россия;
[6] Центр экспертизы и контроля качества медицинской помощи, Москва, Россия;
[7] Российская медицинская академия непрерывного профессионального образования, Москва, Россия;
[8] Научно-исследовательский финансовый институт, Москва, Россия;
[9] Министерство здравоохранения Российской Федерации, Москва, Россия;
[10] Научный центр мирового уровня «Цифровой биодизайн и персонализированное здравоохранение», Москва, Россия;
[11] «АстраЗенека Фармасьютикалз», Москва, Россия;
[12] Первый Московский государственный медицинский университет имени И.М. Сеченова, Москва, Россия

АННОТАЦИЯ

Обоснование. Компьютерная томография органов грудной клетки — основной метод диагностики изменений лёгочной ткани, вызванных инфекцией COVID-19. Так, с 2020 года в Красноярском крае увеличилась частота применения данного исследования. Тем не менее заболеваемость раком лёгкого снизилась на 5,2%. Сложившаяся ситуация вызвала опасения в отношении пропуска рентгенологических изменений, характерных для рака лёгкого, и стимулировала поиск новых диагностических методов, включая искусственный интеллект для анализа данных.

Цель — оценка возможности использования алгоритма искусственного интеллекта, направленного на поиск лёгочных узлов по данным компьютерной томографии органов грудной клетки, полученным в период пандемии COVID-19, для выявления рака лёгкого.

Материалы и методы. В ретроспективное исследование вошли результаты компьютерной томографии органов грудной клетки пациентов из Красноярского края с диагнозом COVID-19 из PACS-архива, выполненные в период с 01.11.2020 по 28.02.2021. Интервал времени между проведёнными компьютерными томографиями и применением алгоритма искусственного интеллекта составил от двух лет и одного месяца до двух лет и пяти месяцев. Использовали алгоритм искусственного интеллекта Chest-IRA. Он выявлял лёгочные узлы объёмом более 100 мм³. Рентгенологи разделили результаты на три группы в зависимости от вероятности рака лёгкого. Оценка экономической выгоды применения алгоритма учитывала затраты на заработную плату и экономию на лечении ранних стадий рака лёгкого, влияющую на валовой региональный продукт.

Результаты. Из 10 500 результатов компьютерной томографии, алгоритм искусственного интеллекта выявил узловые образования в 484 случаях. Определены 192 пациента с высокой вероятностью рака лёгкого, 103 — без признаков и 60 — с неубедительными признаками. 112 пациентов с высокой и средней вероятностью рака лёгкого не обращались за медицинской помощью. Применение искусственного интеллекта позволило подтвердить 100 (28,2%) гистологически верифицированных случаев рака лёгкого, при этом I–II стадия выявлена в 35%.

Использование искусственного интеллекта вместо рентгенологов сэкономило бы 25 мес. и 4 дня работы — 2 430 тыс. рублей. Ожидаемая экономия бюджета в связи с выявлением рака лёгкого на ранней стадии варьирует от 10 600 тыс. до 12 500 тыс. рублей на каждые 10 500 компьютерных томографий. Общий экономический эффект за пять лет — от 259 400 тыс. до 305 100 тыс. рублей.

Заключение. Использование искусственного интеллекта для анализа результатов компьютерной томографии органов грудной клетки демонстрирует высокую эффективность в отношении выявления узловых образований лёгких, в том числе на фоне COVID-19, что подтверждает перспективы его применения для раннего обнаружения случайных лёгочных узлов, которые могли бы быть пропущены.

Ключевые слова: рак лёгкого; компьютерная томография; искусственный интеллект; грудная клетка; экономика здравоохранения; оценка эффективности.

利用人工智能检测肺癌新病例：COVID-19大流行2年后计算机断层扫描结果回顾性分析的临床和经济评估

Ruslan A. Zukov[1,2], Ivan P. Safontsev[1,2], Marina P. Klimenok[2], Tatyana E. Zabrodskaya[2], Natalya A. Merkulova[2], Valeria Yu. Chernina[3], Mikhail G. Belyaev[3], Mikhail Yu. Goncharov[3,4,5], Vitaly V. Omelyanovskiy[6,7,8], Ksenia A. Ulianova[9], Evgenia A. Soboleva[3,5], Maria E. Blokhina[11], Elena A. Nalivkina[11], Victor A. Gombolevskiy[3,4,10,12]

[1] Professor V.F. Voino-Yasenetsky Krasnoyarsk State Medical University, Krasnoyarsk, Russia;
[2] Krasnoyarsk Regional Clinical Oncological Dispensary named after A.I. Kryzhanovskogo, Krasnoyarsk, Russia;
[3] «IRA Labs», Moscow, Russia;
[4] Artificial Intelligence Research Institute AIRI, Moscow, Russia;
[5] Skolkovo Institute of Science and Technology, Moscow, Russia;
[6] Center for Expertise and Quality Control of Medical Care, Moscow, Russia;
[7] Russian Medical Academy of Continuous Professional Education, Moscow, Russia;
[8] Financial Research Institute, Moscow, Russia;
[9] Ministry of Health of the Russian Federation, Moscow, Russia;
[10] World-Class Research Center «Digital biodesign and personalized healthcare», Moscow, Russia;
[11] AstraZeneca Pharmaceuticals LLC, Moscow, Russia;
[12] Sechenov First Moscow State Medical University, Moscow, Russia

摘要

论证。胸腔器官计算机断层扫描是COVID-19感染引起的肺组织变化的主要诊断方法。因此，自2020年以来，这项研究在克拉斯诺亚尔斯克边疆区的应用频率有所增加。然而，肺癌的发病率却下降了5.2%。这种情况引起了人们对肺癌漏检特征性放射学变化的担忧，并促使人们寻找新的诊断技术，包括用于数据分析的人工智能（AI）。

目的 — 评估使用人工智能算法从COVID-19大流行期间获得的胸腔器官计算机断层扫描数据中，搜索肺结节发现肺癌的可行性。

材料和方法。这项回顾性研究，包括从2020年1月11日至 2021年2月28日期间，克拉斯诺亚尔斯克地区 从PACS档案中诊断为COVID-19的患者的胸腔器官计算机断层扫描结果。进行胸腔器官计算机断层扫描与应用人工智能算法之间的时间间隔从两年零一个月到两年零五个月。使用了Chest-IRA AI算法。AI检测到体积大于$100mm^3$的肺部结节。放射科医生根据肺癌的概率将结果分为三组。使用该算法的经济效益评估，考虑到了工资成本和早期治疗肺癌所节省的费用，这些也会影响地区生产总值。

结果。在10500个计算机断层扫描结果中，人工智能算法检查出484例结节性肿块。确定了192名患肺癌高概率的患者，103名无体征，60名体征根据不足。112名肺癌高概率和中概率的患者没有就医。 通过使用人工智能，100例（28.2%）经组织学验证的肺癌患者得到了确诊，其中35%的患者处于I-II期。

使用人工智能代替放射科医生可以节省25个月零4 天的工作时间，也就是243万卢布。每进行10500次计算机断层扫描，因早期发现肺癌而节省的预算预计从1060万卢布到1250万卢布。五年的总经济效益为2.594亿卢布至3.051亿卢布。

结论。使用人工智能分析胸腔器官计算机断层扫描结果显示肺结节检测的高效率，包括在COVID-19的背景下，这证实其用于早期发现那些可能被遗漏的随机肺结节的前景。

关键词：肺癌；计算机断层扫描；人工智能；胸腔；卫生经济学；效能评估。

BACKGROUND

Lung cancer is one of the cancers with the highest global prevalence and mortality rates. An estimated 2.2 million cases of lung cancer and 1.8 million deaths from this condition are reported each year [1]. The standardized lung cancer incidence in Russia is 20.8 cases per 100,000 population, with a 2.7% increase since 2020 [2]. Lung cancer rates across several Russian regions, notably the Krasnoyarsk Krai, are concerning. It ranks third among all malignancies reported in the Krasnoyarsk Krai, with breast and skin cancer being the most prevalent.

The number of chest computed tomography (CTs) in the Krasnoyarsk Krai has increased significantly since 2020 due to the COVID-19 pandemic (36,577 in 2019 vs. 236,234 in 2021). However, the lung cancer prevalence in this region declined by a mere 5.2% in comparison to 2019.

One potential reason is undiagnosed pulmonary nodular lesions brought on by alterations typical of COVID-19-associated pneumonia. This necessitates the search for novel diagnostic tools to enhance the effectiveness of lung cancer detection. Artificial intelligence (AI) is one such instrument that can serve as the primary component of hybrid diagnostics in lung cancer. During the first stage, the AI systems execute the initial screening of the CT findings; during the second stage, the AI-selected images are reviewed by specialist physicians to reach a final decision. Thus, in 2022, the population of Krasnoyarsk Krai participated in the pilot project "Retrospective Analysis of Chest CT Findings Using the Chest-IRA AI Algorithm by IRA-Labs."

AIM: To evaluate the effectiveness of an AI algorithm for lung nodule detection based on chest CT findings acquired during the COVID-19 pandemic to detect lung cancer.

MATERIALS AND METHODS

Study design

This was an observational, single-center, retrospective, cross-sectional, single-arm study. The study design is illustrated in Fig. 1.

Eligibility criteria

The study sample was established based on the inclusion and exclusion criteria.

Inclusion criteria:
- Chest CT findings for patients from the Krasnoyarsk Krai PACS, both male and female;
- Chest CT performed without intravenous contrast for COVID-19, with the findings being interpreted by radiologists between November 1, 2020, and February 28, 2021;
- Age of patients >18 years;
- Chest CT scans are available in the DICOM file format.

Exclusion criteria:
- Available chest CT scans are in the non-DICOM file format;
- False-positive AI findings;
- CT slice thickness >1.5 mm;
- Incomplete chest CT findings;
- Significant motion artifacts;
- Recovery of anonymized patient data are unfeasible.

Study setting

Chest CT scans were conducted at the Krasnoyarsk Regional Clinical Oncological Dispensary (named after A.I. Kryzhanovsky).

Study duration

The study employed chest CT results collected between November 1, 2020, and February 28, 2021. The interval between chest CT and AI analysis varied from two years and one month to two years and five months. The specialists evaluated the results between December 5, 2022, and January 9, 2023.

Intervention

The Toshiba Aquilion 64, GE Revolution EVO, and GE Healthcare Revolution Discovery CT scanners were used for conducting chest CT scans in accordance with the standard
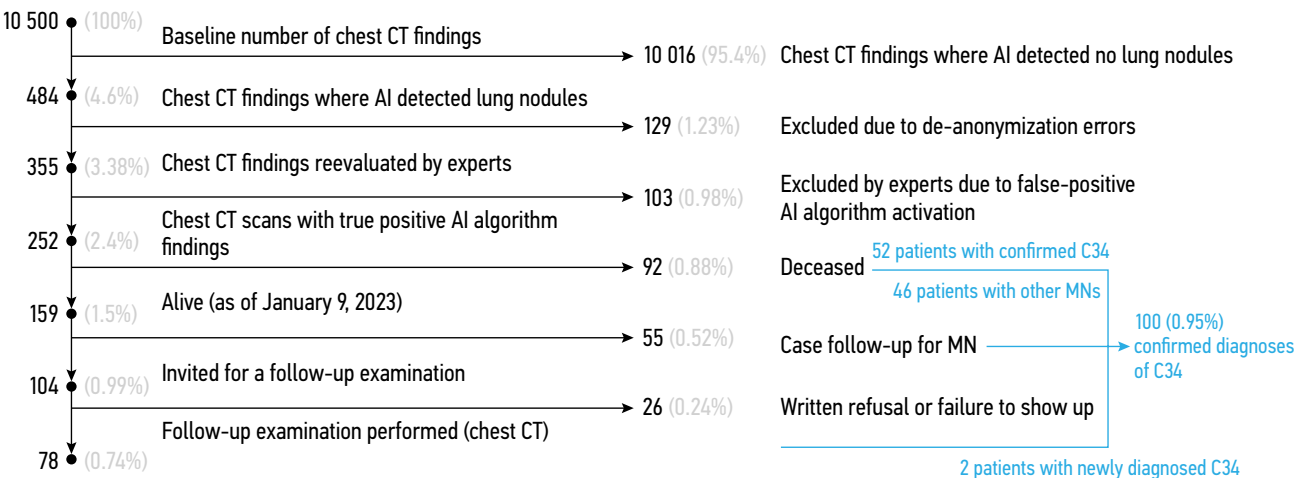
Fig. 1. Study design. CT, computed tomography; AI, artificial intelligence; MN, malignant neoplasm; C34, malignant neoplasm of the bronchus and lung according to the International Classification of Diseases, 10th revision.

protocol: X-ray tube voltage 120 kV with automated tube voltage selection; rotation time 0.50 s; pitch 0.938; slice thickness 1 mm.

All CT findings included in the study were processed using the Chest-IRA AI algorithm (LungNodules-IRA, v4.0). This algorithm was validated using a dedicated calibration dataset obtained in the Moscow Experiment [3]. The Chest-IRA algorithm was approved for use in compliance with the rules for clinical trials involving AI-based software because it exceeded the accuracy threshold of at least an ROC AUC of 0.81 [4]. The parameters of the Chest-IRA algorithm are as follows: ROC AUC 0.96; sensitivity 0.94; specificity 0.94; and accuracy 0.94 [3].

The Chest-IRA algorithm is based on two neural networks. The semantic segmentation of lung lesions and nodules is carried out by the first neural network (N1). N1 was trained using the publicly available LIDC-IDRI dataset [5], which includes chest CT findings for 1,018 patients, with lung nodule labeling using binary masks. N1 creates a binary mask for an input image. The mask is divided into connected components; some correspond to lung nodules and lesions, while others are false positives. The second neural network (N2) classifies the connected components as true positives or false positives to lower the false-positive rate. N2 was trained using a dataset of 2,351 chest CT findings. Open data were labeled based on the coordinates of various N1 findings and classification labels.

The IRA-Labs algorithm is the first differential diagnosis algorithm based on medical sorting of chest CT results. It uses the following classification: histologically confirmed lung cancer, bacterial pneumonia, COVID-19-associated pneumonia, or no abnormalities [6].

The Chest-IRA algorithm (LungNodules-IRA, v4.0) examined the obtained images; when lung nodules of >100 mm^3 were detected, the algorithm provided their location, size, and volume. Calcifications were eliminated from the algorithm's classification of nodular lesions. The algorithm had the following limitations:
- Chest CT findings had to include at least one series of lung images with axial slices;
- The spacing between slices in a series had to be consistent (for >95% of slices) and not exceed 3 mm;
- A series had to cover an area greater than 192 × 192 × 96 mm.

Main study outcome

The study's null hypothesis was that the AI algorithm does not substantially enhance early lung cancer detection when compared to the conventional interpretation of CT findings by radiologists.

The effectiveness of the AI algorithm in detecting lung cancer was the study's endpoint. The efficacy of the algorithm was determined employing the following parameters:
- Number of lung cancer cases detected using the AI algorithm;
- Proportion of early-stage (I–II) lung cancer cases detected;

- Sensitivity and specificity of the AI algorithm in identifying lung nodules;
- False-positive rate of the AI algorithm;
- Comparative analysis of the interpretation of CT findings by the AI algorithm and radiologists.

These parameters might be regarded as surrogate endpoints since they indirectly represent the potential impact of AI on the main objective: lowered lung cancer mortality. The true endpoint in this case was lung cancer mortality; however, its assessment necessitates long-term monitoring.

Additional study outcomes

To calculate the AI algorithm's economic impact, labor expenses were evaluated while accounting for the average income of radiologists in the Krasnoyarsk Krai. Moreover, the cost-effectiveness of treating patients with early-stage versus advanced lung cancer was assessed [7, 8]. The economic impact was also analyzed in terms of the life years gained and their potential contribution to the gross regional product.

Outcomes registration

Chest CT findings deemed abnormal according to the AI algorithm were reviewed once by one of the four radiologists at the Krasnoyarsk Regional Clinical Oncological Dispensary (named after A.I. Kryzhanovsky) with over ten years of experience in thoracic radiology.

Subgroup analysis

During the analysis of the CT scans, the patients were divided into three groups:
- Group 1 included patients with a high probability of lung cancer (images with signs of lung tumors);
- Group 2 included patients with no signs of lung cancer (false-positive algorithm activation);
- Group 3 included patients with inconclusive signs of lung cancer.

Patients in group 1 exhibited solid lung nodules with a diameter of ≥6 mm and >5 nodules with benign signs [7]. Benign tumor indicators included areas of ground-glass opacity with a diameter of <6 mm, perifissural nodules, and benign calcification. Patients whose examination findings did not meet these criteria were placed in group 3.

Each patient's medical records were reviewed to determine the accuracy of the AI algorithm and the need for further examinations in patients with aberrant findings.

Ethical review

The study was approved by the local ethics committee of the Krasnoyarsk Regional Clinical Oncological Dispensary (named after A.I. Kryzhanovsky) (source: Meeting Minutes No. 48/1 of February 9, 2023). Since the study employed anonymized patient data, it was in accordance with all applicable legal standards for personal data and medical

privacy. Each study group was allocated a unique encryption key, allowing for the subsequent identification of patients requiring additional examinations (patients with lung cancer signs) in a cancer center. Data were anonymized and forwarded to the IRA-Labs platform.

Statistical analysis

Sample calculation principles. A sensitivity evaluation with the lower bound of the 95% CI of at least 85% and an expected sensitivity of 95% required approximately 93 positive cases. A specificity assessment with the same accuracy and an expected sensitivity of 95% required approximately 93 negative cases. Given that the incidence of suspicious cases is 4.6%, a sample size of approximately 2,022 CT examinations was shown to be adequate for identifying 93 positive cases (93/0.046). Thus, the minimal recommended sample size in this study was determined to be 2,022 CT examinations. However, the study employed a substantially larger sample of 10,500 CT examinations, which enhances the statistical power and accuracy of the results.

Statistical analysis methods. Descriptive statistics (calculating absolute and relative frequencies for categorical variables) were used to assess the primary study data. For continuous data, ranges were computed; for time intervals, the median and ranges were ascertained. The economic analysis included the following: man-hours and labor expenses in rubles, treatment cost savings, potential contribution to the gross regional product, and a comparative analysis of early lung cancer detection rates in the Krasnoyarsk Krai and Russia. Thus, the study mostly employed descriptive statistics and economic analytical techniques.

RESULTS

Participants

The study analyzed 10,500 chest CT data from patients residing in the Krasnoyarsk Krai PACS (56% male, 44% female; ages 28–91 years) (Fig. 1).

Primary results

The AI algorithm identified lung cancer signs in 484 images (4.6% of cases). The results of 129 CT examinations (26.6%) were excluded from the study due to de-anonymization errors.

Radiologists categorized the 355 AI-selected photos into three groups (Fig. 2):
- Group 1 comprised patients with a high probability of lung cancer (192 images; 39.7% of the images selected by AI [1.83% of all examinations]);
- Group 2 consisted of patients with no signs of lung cancer (103 images; 21.3% of the images selected by AI [0.98% of all examinations]);
- Group 3 included patients with inconclusive signs of lung cancer (60 images; 12.4% of the images selected by AI [0.57% of all examinations]).

Fig. 3 and Fig. 4 illustrate the AI algorithm findings.

As of September 1, 2023, among the 252 patients in groups 1 and 3:
- 93 patients had succumbed by the time of the analysis:
  – 52 patients were being monitored for malignant neoplasms at the time of the study (lungs, bronchi, and other locations with lung metastases);
  – 11 patients with no lung metastases were being followed up for other malignant neoplasms;
  – 30 patients were not being monitored for cancer;
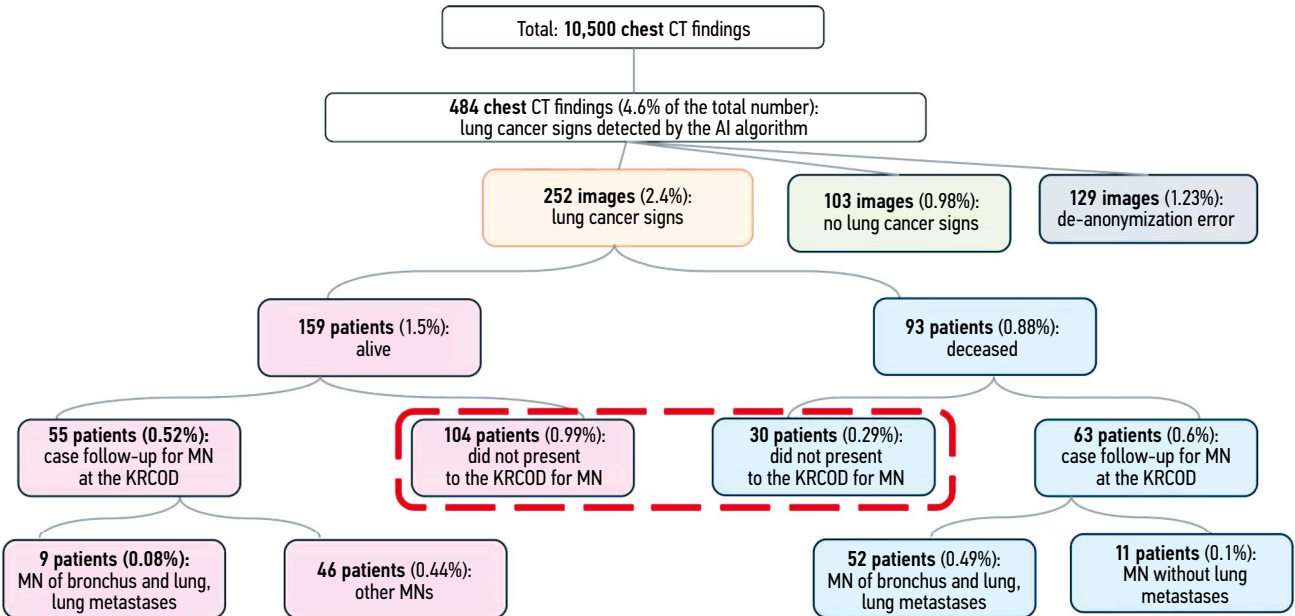
Fig. 2. Analysis of chest computed tomography findings employing artificial intelligence CT, computed tomography; AI, artificial intelligence; KRCOD, Krasnoyarsk Regional Clinical Oncological Dispensary (named after A.I. Kryzhanovsky); MN, malignant neoplasm. The red dashed line indicates that 134 people did not seek medical attention for malignant neoplasms.

- 159 patients were alive:
  - 46 patients were being followed up for malignant neoplasms at the time of the study (lungs, bronchi, and other locations with lung metastases);
  - 9 patients were being observed for other malignant neoplasms without lung metastases;
  - 10 patients experienced stage I–II lung cancer, while seven patients exhibited stage III–IV lung cancer.
- A total of 104 patients who had not sought medical care for malignant neoplasms were invited for a follow-up chest CT:
  - Nine patients submitted a formal refusal of further testing and treatment;
  - 17 patients did not show up for a follow-up examination;
  - A total of 78 patients were examined, and the diagnosis was histologically verified: two patients exhibited

stage Ia and Ib lung cancer (Fig. 5), while 76 patients experienced other pulmonary diseases (Table 1).

Thus, lung cancer was confirmed in 100 out of 355 patients (28.2%) selected using the AI algorithm.

Thirty-five percent of lung cancer cases were detected at stages I–II, while 65% were identified at stages III–IV. The lung cancer lesions in all the identified patients were histologically confirmed and analyzed based on the diagnostic date. During the seven years of follow-up prior to the use of AI, 90 lung cancer cases (90%) were identified; the remaining patients underwent a chest CT to assess treatment efficacy. In 50% of patients ($n = 50$), lung cancer was detected in the interval between the CT examination performed in this study and the use of AI, provided that this period was 762–881 days. Newly diagnosed lung cancer cases were identified in this study as those found following the application of AI.

The analysis of the CT findings, based on which the patients were included in group 2, revealed that the AI algorithm identified the following (Fig. 6):
- Fibrotic changes in the lung tissue in most cases (71 patients; 68.9%);
- Infiltration regions (14 patients; 13.6%);
- Hamartomas (11 patients; 10.7%);
- Lung tissue vessels (3 images).

Radiologists identified intrapulmonary lymph nodes (1.0%) and tuberculomas (1.0%) in a few isolated cases based on the results of the AI system.

The AI algorithm also detected other lung diseases.

Secondary results

Economic efficiency assessment

It is crucial to evaluate both the clinical efficacy of the experiment and the economic impact of the AI algorithm.
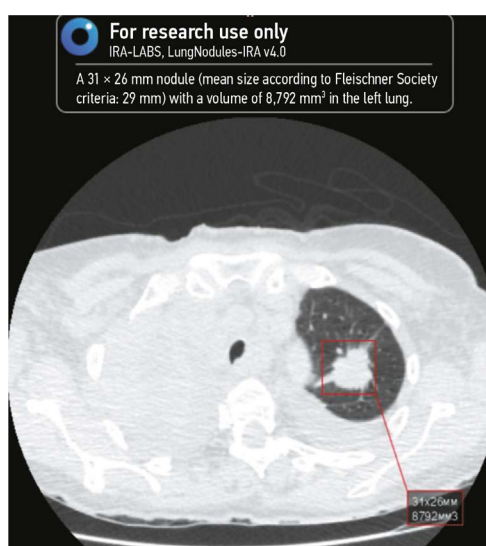
Fig. 3. Left lung nodule detected by artificial intelligence. The detected nodule is marked by the red square. Image with a high probability of lung cancer.
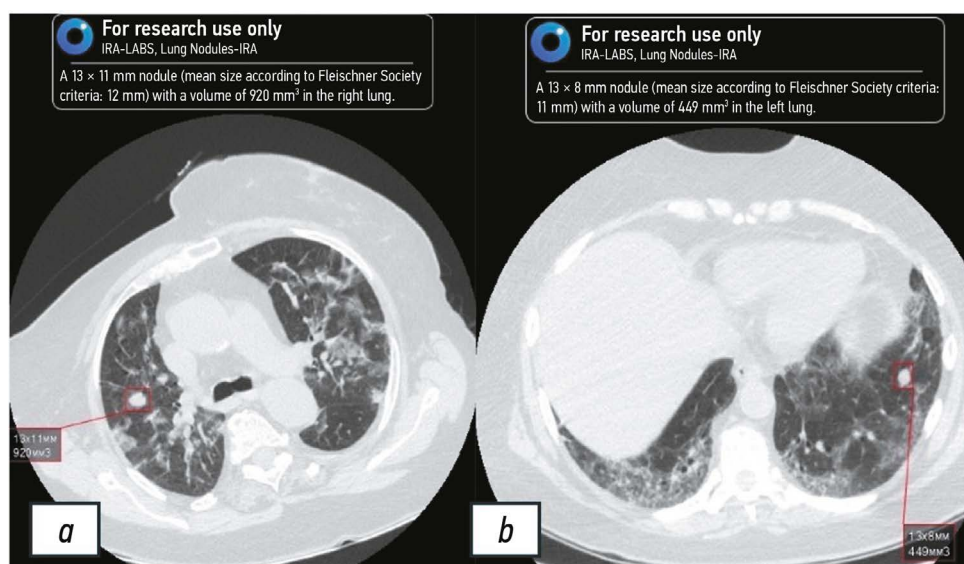
Fig. 4. Nodules in the right (*a*) and left (*b*) lungs detected by artificial intelligence. The detected nodules are marked by the red square. Images with inconclusive signs of lung cancer.
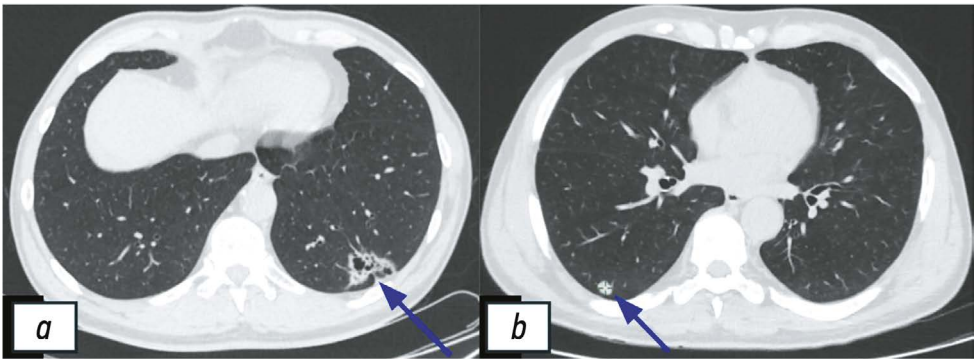
Fig. 5. Chest computed tomography findings in patients with confirmed lung cancer (blue arrows). *a*, cystic and solid mass in the left lung (stage Ia); *b*, solid mass in the right lung (stage Ib).

Table 1. Distribution of the lung lesions identified during a follow-up examination

Abnormal	Number of patients
Pulmonary hamartoma	17
Lung nodules	13
Post-inflammatory changes in the lungs	12
Tuberculoma	7
Benign neoplasm of the bronchus and lung	4
Sarcoidosis	3
Post-operative changes in the lungs	2
Pulmonary cyst	2
Fibrotic changes in the lungs	1
Chronic obstructive pulmonary disease	1
Pneumosclerosis	1
Other interstitial lung diseases with mention of fibrosis	1
Normal	12

Note. Patients diagnosed with benign neoplasm of the bronchus and lung: surgical treatment (2 patients) and consultation (2 patients) at the Krasnoyarsk Regional Clinical Oncological Dispensary named after A.I. Kryzhanovsky; a patient diagnosed with other interstitial lung disease with mention of fibrosis: surgical treatment in a cancer center (St. Petersburg).
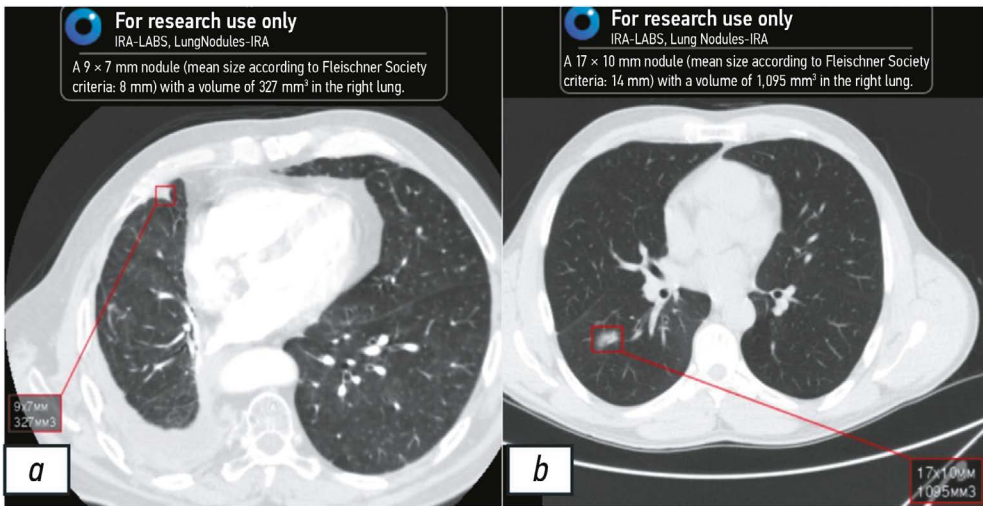
Fig. 6. Examples of the most common cases of false-positive artificial intelligence algorithm activation. *a*, fibrotic changes classified as a lung nodule; *b*, lung tissue infiltration area classified as a lung nodule.

The average pay of 96,900 rubles for radiologists in the Krasnoyarsk Krai was used to calculate potential labor costs (Table 2). A radiologist processes approximately 400 CT results per month (20 examinations per day). An initial sample of 10,500 images would therefore take a radiologist 26 months and 25 days to analyze, whereas the AI algorithm independently assessed 10,016 examinations, saving 25 months and 4 days of work. For this scope of work, a healthcare facility would need to spend 2,430 thousand rubles (which is equivalent to $27,421 or ¥196,830) on salary, excluding taxes and other payments.

Another method for assessing the effectiveness of the AI algorithms is based on the cancer treatment cost savings. Based on data from the Krasnoyarsk Regional Clinical Oncological Dispensary [named after A.I. Kryzhanovsky], at 2023 prices, the average cost of treating stage I–II lung cancer is 352 thousand rubles ($3,872 or ¥28,512) per patient. This means that the total cost of treatment for 35 patients in the early stages of the disease will be 12,350 thousand rubles ($135,811 or ¥1,066,000) (Table 3). Assuming an average treatment cost of 587 thousand rubles ($6,465 or ¥47,606), patients with advanced lung cancer will incur treatment costs of 20,570 thousand rubles ($226,278 or ¥1,666,229). Thus, the anticipated direct regional budget savings resulting from the detection of patients with early lung cancer will be 8,220,000 rubles ($90,466 or ¥666,162) per 10,500 patients undergoing a chest CT.

Another commonly used method for assessing the economic impact is based on the life years gained and their potential contribution to the gross regional product. Patients with early-stage lung cancer who receive timely detection have a 90% 5-year survival rate. Thus, 157 years and 5 days of life can be saved for 35 patients. According to data from the Federal State Statistics Service for the Krasnoyarsk Krai, the financial equivalent of the life years saved can be estimated at 173,250 thousand rubles ($1,905,750 or ¥14,033,250) if the gross regional product is calculated to be 1,100 thousand rubles (Table 4).

Furthermore, as the implications of early cancer detection with AI algorithms are noted concurrently, calculated effects can be summed together. These include healthcare professional time and salary savings, reduced treatment costs, and a potential contribution to the gross regional product owing to enhanced five-year survival rates. Thus, the overall cost can be expected to be 183,009 thousand rubles ($2,022,907 or ¥14,895,949) for 35 identified patients with early lung cancer per 10,500 chest CT examinations over 5 years.

Table 2. Comparison of the financial effects on two analysis models for chest computed tomography scan results

Parameters	Model 1	Model 2
Baseline number of chest computed tomography findings	10,500	
Number of chest computed tomography findings excluded from reassessment by a radiologist	0	10,016
Number of chest computed tomography findings reassessed by a radiologist	10,500	484
Time required to reassess chest computed tomography findings (400 computed tomography scans per month)	26 months and 25 days	1 month and 21 days
Cost of reassessment by a physician (monthly salary: 96,900 rubles)	2,543,625 rubles ($27,980 or ¥206,033)	117,249 rubles ($1,290 or ¥9,497)
Physician time savings	0 months	25 months and 4 days
Financial savings (employing artificial intelligence without payment)	0 rubles	2,426,376 rubles ($26,690 or ¥196,536)

Note. Model 1: all computed tomography findings were evaluated by a radiologist. Model 2 (two-stage analysis): all computed tomography findings were assessed by the artificial intelligence algorithm; subsequently, a radiologist reassessed images with lung cancer signs.

Table 3. Estimated financial effect of lowered treatment costs in patients with advanced lung cancer attained by implementing the artificial intelligence algorithm

Parameters	Treatment costs per patient	Treatment costs in all patients identified at early stages (*n* = 35)
Treatment costs in patients with stage III–IV lung cancer (combination therapy: surgical treatment + chemoradiotherapy, excluding immunotherapy costs)	587,735 rubles ($6,465 or ¥47,606)	20,570,725 rubles ($226,278 or ¥1,666,229)
Treatment costs in patients with stage I–II lung cancer	352,757 rubles ($3,880 or ¥28,573)	12,346,495 rubles ($135,811 or ¥908,659)
Economic efficiency of mitigated treatment costs in patients with advanced lung cancer (excluding immunotherapy costs)	234,978 rubles ($2,585 or ¥19,033)	8,224,230 rubles ($90,466 or ¥666,162)

Table 4. Cumulative financial effect of artificial intelligence in reassessing computed tomography results to detect lung cancer signs

Parameters	Project savings
Radiologist salary savings	2,426,376 rubles ($26,690 or ¥196,536)
Reduced treatment costs in patients with advanced lung cancer (35 patients with early stages)	8,224,230 rubles ($90,466 or ¥666,162)
Economic impact over five years, taking into account the estimated gross regional product per life years saved	173,250,000 rubles ($1,905,750 or ¥14,033,250)
Cumulative economic impact over one year	10,650,606 rubles ($11,157 or ¥862,699)
Cumulative economic impact over five years, considering the life years saved	183,900,606 rubles ($2,022,907 or ¥14,895,949)

DISCUSSION

Summary of the primary results

During a retrospective analysis of chest CT findings using the AI algorithm, 355 cases were selected from 10,500 processed images for reanalysis by experts of the Krasnoyarsk Regional Clinical Oncological Dispensary (named after A.I. Kryzhanovsky). Based on the chest CT changes, 252 patients (2.4%) were included in groups 1 and 3. There were 35 patients with stage I–II lung cancer and 65 patients with stage III–IV lung cancer. The expected direct regional budget savings resulting from the detection of patients with early lung cancer was estimated to be 8,220,000 rubles ($90,466 or ¥666,162) per 10,500 patients undergoing a CT scan.

Discussion of the primary results

In most patients, the Chest-IRA AI algorithm reliably diagnosed lung nodules with a high or moderate probability of lung cancer secondary to COVID-19-associated inflammatory alterations. These data support the efficacy of the hybrid retrospective assessment of chest CT findings. Notably, the average proportion of detected early lung cancer cases (stages I–II) in Russia does not exceed 30% [9]. This is partly due to the inadequate efficacy of photofluorography conducted during medical check-ups in adults in terms of early lung cancer diagnosis. Detecting neoplasms larger than 1 cm, even with modern X-ray technologies, demands skilled radiologists and patient-specific examination of risk factors, such as family history, occupational factors, and infectious or chronic diseases. Thus, X-ray tests typically detect advanced lung cancer, where curative therapy is not feasible, and the prognosis is generally unfavorable [10].

High-quality, timely screening for lung cancer is a potential solution to this issue. Low-dose computed tomography (LDCT) is the most effective technique; it detects twice as many small foci and three to four times as many focal lesions as X-ray imaging. The National Lung Screening Trial, the most extensive study on the subject conducted in the USA, demonstrated that LDCT as a screening tool lowered lung cancer mortality by 16% compared to chest X-ray [10]. In selected adult populations, LDCT has been recommended as a lung cancer screening method during physical examinations since 2015 as part of a pilot project in Krasnoyarsk[1]. *n*LDCT was performed in high-risk patients who met all the following criteria: males aged 50–64 years residing in Krasnoyarsk with a smoking index ⩾30. Between 2015 and 2017, when LDCT was incorporated into the lung cancer screening protocols, the lung cancer detection rate was 17.1 per 1,000 examined high-risk patients, which was 30 times higher than that of photofluorography or X-ray imaging (0.57 per 1,000 examined patients) [11]. This strategy has been used across Krasnoyarsk Krai since 2018. It was included in the medical check-up standards for selected adult populations in 2019, along with an expansion of the high-risk criteria (Fig. 7).

The use of LDCT as a lung cancer screening tool between 2015 and 2021 improved the early lung cancer detection rate; in the Krasnoyarsk Krai, the detection rates became higher than the Russian average. In the Krasnoyarsk Krai, the early lung cancer detection rate improved from 22.1 per 100,000 population in 2015–34.2 per 100,000 population in 2021 (a 54.8% increase). From 27.3 per 100,000 people in 2015 to 29.6 per 100,000 population in 2021 (an 8.4% rise), the average early lung cancer detection rate in Russia improved. Moreover, between 2015 and 2021, the Krasnoyarsk Krai experienced a decline in lung cancer mortality by 7.0% (from 48.7 to 45.3 per 100,000 population), in contrast to the Russian average, which increased by 13.2% (from 34.1 to 38.6 per 100,000 population) during the same period [2].

Recent research indicates that AI is as accurate as radiologists in predicting the risk of lung cancer. Complex lung cancer screening using AI algorithms demonstrates high efficacy (ROC AUC 94.4%) and improves the accuracy of radiologist conclusions, with an absolute reduction in the false-positive and false-negative rates by 11% and 5%, respectively [11]. A recent systematic review that evaluated the effectiveness of AI in diagnosing and predicting lung cancer

---

[1] Letter of the Ministry of Health of the Krasnoyarsk Krai No. 71/08-26/9923 of May 15, 2015. On Lung Cancer Screening in Medical Check-up Programs for Selected Adult Populations
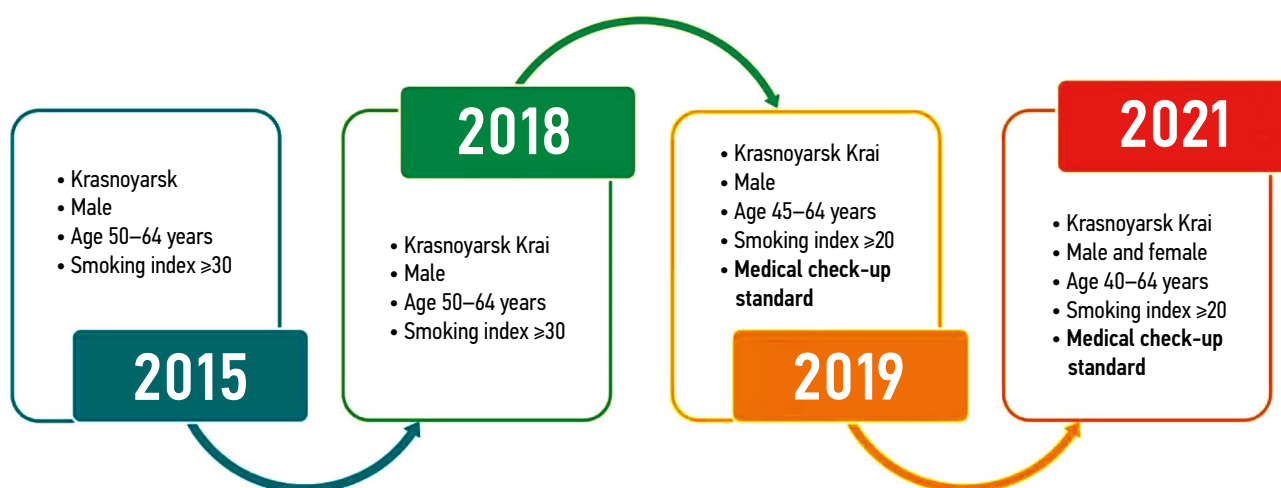
Fig. 7. Evolution of lung cancer screening in the Krasnoyarsk Krai.

found that radiologists utilizing AI algorithms were more accurate in their examination of CT scan results. AI algorithms predict tumor grade reliably and accurately, as indicated by the method's high sensitivity and specificity [12].

Goncalves et al. [13] employed SWOT analysis to ascertain the advantages, disadvantages, opportunities, and risks of using AI algorithms to detect lung cancer. The advantages included the high accuracy of modern algorithms, reduced workload, and a lowered risk of errors in lung cancer diagnosis. The main disadvantage, as per the authors, is the need for real-world validation studies before implementation in clinical practice. The risks included confidentiality and data security concerns, as well as the use of biased samples for algorithm training. In 21.3% of all CT scans in which the AI system identified lung nodules (103 images), experts observed false-positive AI algorithm activation. In most cases (71 images; 68.9%), the AI algorithm incorrectly classified areas of lung tissue scarring as signs of lung cancer. The absolute number was within the permissible range for review, even though the false-positive AI algorithm activation rate was comparatively high. Moreover, the project primarily aimed to detect the maximum number of patients with suspected lung cancer based on chest CT findings obtained during the COVID-19 pandemic. For this purpose, a low AI algorithm activation threshold was employed. However, a reduction in the target parameters may occur when specificity is prioritized over sensitivity when establishing the AI activation threshold. As specificity increases, the rate of false-positive AI findings (and workload) and the number of findings also increase, contributing to the risk of undetected lung cancer.

Ziegelmayer et al. [14] used the Markov model to determine the economic efficiency of an AI algorithm during the first stage of lung cancer screening. The authors concluded that utilizing AI during primary screening saves $1,240 per patient, with a willingness to pay $100,000 for quality-adjusted life years, confirming the economic efficiency of this approach. Both during the study and five years later, our method of reanalysis of chest CT findings using AI for the detection of lung cancer signs can also be considered economically feasible. Life years gained, lower treatment costs for patients with advanced disease, and a notable reduction in the need for doctors to reevaluate chest CT results—all of which take into account the patients' potential future economic contribution to the area—are indicators of cost savings. The cumulative effect (salary savings, reduced treatment costs, and potential contribution to the gross regional product) over five years is estimated at 183,900 thousand rubles ($2,022,907 or ¥14,895,949). However, since the following two patient groups were left out of our estimates, the overall economic benefits might be greater:
- Patients with de-anonymization errors;
- Patients who received a postmortem cancer diagnosis between the time of the chest CT scan and the commencement of the retrospective study.

If the data of all 484 patients were analyzed, with no de-anonymization errors and an early-stage distribution comparable to that of the 355 patients included in the analysis, the number of patients with early lung cancer identified using AI would be 43. Thus, the cumulative economic impact (2,430 thousand rubles + 10,105 thousand rubles + 236,005 thousand rubles from reassessment, lowered treatment costs, and life years saved, respectively) was 249,080 thousand rubles ($2,739,880 or ¥20,175,480) over five years.

Study limitations

This study has several limitations. First, there is its retrospective design; nevertheless, the design aligned with the study aim. Second, only the results where the AI algorithm identified lung nodules greater than 100 mm³ were reevaluated by a radiologist. This was done to preserve resources and time when reevaluating large datasets. The economic efficiency assessment did not consider lowered immunotherapy costs in patients with advanced

disease, as well as indirect costs. Another limitation is that the AI algorithm was developed to detect lung nodules rather than lung cancer. Thus, the AI algorithm findings encompassed diverse conditions, which necessitated additional studies to confirm lung cancer.

CONCLUSION

The use of AI technology to analyze large sets of chest CT scans conducted for various indications may contribute to ancillary lung nodule detection. This includes CT findings from screening programs or examinations for lung diseases other than lung cancer, such as COVID-19. The Chest-IRA AI algorithm has demonstrated encouraging results. However, additional research is required to determine the efficacy and safety of this algorithm in real-world practice. Further information is needed on how AI technology affects lung cancer detection rates and the feasibility of incorporating it into current diagnostic processes. It is crucial to continue research and clinical trials in this promising but inadequately studied area.

ADDITIONAL INFORMATION

REFERENCES

1. Siegel RL, Miller KD, Jemal A. Cancer statistics, 2020. CA Cancer J Clin. 2020;70(1):7–30. doi: 10.3322/caac.21590
2. Kaprin AD, Starinsky VV, Shakhzadova AO, editors. Malignant neoplasms in Russia in 2021 (morbidity and mortality). Moscow: P. Herzen MORI – the branch of the FSBI NMRRC of the Ministry of Health of the Russian Federation, 2022. (In Russ).
3. Chest-IRA [Internet]; 2020. [cited 2024 May 16]. Available from: https://mosmed.ai/service_catalog/chestira/
4. Morozov SP, Vladzimirsky AV, Klyashtorny VG, et al. Clinical trials of software based on intelligent technologies (Radiology). Series «Best Practices of Radiology and Instrumental Diagnostics». N 56. Moscow: SBHI «SPCC for DTT of MHD», 2019. (In Russ).
5. Armato SG 3rd, McLennan G, Bidaut L, et al. The lung image database consortium (LIDC) and image database resource initiative (IDRI): a completed reference database of lung nodules on CT scans. Med Phys. 2011;38(2):915–931. doi: 10.1118/1.3528204
6. Goncharov M, Pisov M, Shevtsov A, et al. CT-Based COVID-19 triage: dep multitask learning improves joint identification and severity quantification. Med Image Anal. 2021;71:102054. doi: 10.1016/j.media.2021.102054
7. MacMahon H, Naidich DP, Goo JM, et al. Guidelines for management of incidental pulmonary nodules detected on CT images: from the Fleischner Society 2017. Radiology. 2017;284(1):228–243. doi: 10.1148/radiol.2017161659
8. Rate agreement of the compulsory medical system of Krasnoyarsk Territory. In: territorial fund of compulsory medical insurance; 2012– [cited 2024 May 16]. Available from: https://www.krasmed.ru/content/18137/page.html

9. Kaprin AD, Starinsky VV, Shakhzadova AO. State of oncological care for the Russian population in 2021. Moscow: P. Herzen MORI — the branch of the FSBI NMRRC of the Ministry of Health of the Russian Federation, 2022. (In Russ).
10. National Lung Screening Trial Research Team. Reduced lung-cancer mortality with low-dose computed tomographic screening. N Engl J Med. 2011;365(5):395–409. doi: 10.1056/NEJMoa1102873
11. Gusamova NV, Komleva MI, Saphontsev IP, et al. Lung cancer screening by LDCT. Results for 2015–2017 years RSBHCI «Krasnoyarsk Regional Clinical Oncological Dispensary named after A.I. Kryzhanovsky». In: Modern achievements of oncology in clinical practice. Proceedings of the All-Russian scientific and practical conference. Krasnoyarsk, 2018. P. 54–57. (In Russ).
12. Ardila D, Kiraly AP, Bharadwaj S, et al. End-to-end lung cancer screening with three-dimensional deep learning on low-dose chest computed tomography. Nat Med. 2019;25(6):954–961. doi: 10.1038/s41591-019-0447-x
13. Goncalves S, Fong PC, Blokhina M. Artificial intelligence for early diagnosis of lung cancer through incidental nodule detection in low- and middle-income countries-acceleration during the COVID-19 pandemic but here to stay. Am J Cancer Res. 2022;12(1):1–16.
14. Graf M, Makowski M, Gawlitza J, Gassert F. Cost–effectiveness of artificial intelligence support in computed tomography–based lung cancer screening. Cancers (Basel). 2022;14(7):1729. doi: 10.3390/cancers14071729

СПИСОК ЛИТЕРАТУРЫ

1. Siegel R.L., Miller K.D., Jemal A. Cancer statistics, 2020 // CA Cancer J Clin. 2020. Vol. 70, N 1. P. 7–30. doi: 10.3322/caac.21590

2. Злокачественные новообразования в России в 2021 году (заболеваемость и смертность) / под ред. А.Д. Каприна, В.В. Старинского, А.О. Шахзадовой. Москва: МНИОИ им. П.А. Герцена — филиал ФГБУ «НМИЦ радиологии Минздрава России, 2022.

3. Chest-IRA [Internet]; 2020. Режим доступа: https://mosmed.ai/service_catalog/chestira/ Дата обращения: 28.10.2024.

4. Морозов С.П., Владзимирский А.В., Кляшторный В.Г., и др. Клинические испытания программного обеспечения на основе интеллектуальных технологий (лучевая диагностика). Серия «Лучшие практики лучевой и инструментальной диагностики». Вып. 57. Москва: ГБУЗ «НПКЦ ДиТ ДЗМ», 2019.

5. Armato S.G. 3rd, McLennan G., Bidaut L., et al. The lung image database consortium (LIDC) and image database resource initiative (IDRI): a completed reference database of lung nodules on CT scans // Med Phys. 2011. Vol. 38, N 2. P. 915–931. doi: 10.1118/1.3528204

6. Goncharov M., Pisov M., Shevtsov A., et al. CT-Based COVID-19 triage: deep multitask learning improves joint identification and severity quantification // Med Image Anal. 2021. Vol. 71. P. 102054. doi: 10.1016/j.media.2021.102054

7. MacMahon H., Naidich D.P., Goo J.M., et al. Guidelines for management of incidental pulmonary nodules detected on CT images: from the Fleischner Society 2017 // Radiology. 2017. Vol. 284, N 1. P. 228–243. doi: 10.1148/radiol.2017161659

8. Тарифное соглашение системы обязательного медицинского соглашения Красноярского края. В: территориальный фонд обязательного медицинского страхования [Internet], 2012– .

Режим доступа: https://www.krasmed.ru/content/18137/page.html Дата обращения: 16.05.2024.

9. Состояние онкологической помощи населению России в 2021 году / под ред. А.Д. Каприна, В.В. Старинского, А.О. Шахзадовой. Москва: МНИОИ им. П.А. Герцена — филиал ФГБУ «НМИЦ радиологии Минздрава России, 2022.

10. National Lung Screening Trial Research Team. Reduced lung-cancer mortality with low-dose computed tomographic screening // N Engl J Med. 2011. Vol. 365. P. 395–409. doi: 10.1056/NEJMoa1102873

11. Гусамова Н.В., Комлева М.И., Сафонцев И.П., и др. Скрининг рака лёгкого методом НДКТ. Результаты за 2015–2017 годы КГБУЗ «Красноярский краевой клинический онкологический диспансер им. А.И. Крыжановского». В кн.: Современные достижения онкологии в клинической практике. Материалы Всероссийской научно-практической конференции. Красноярск, 2018. С. 54–57.

12. Ardila D., Kiraly A.P., Bharadwaj S., et al. End-to-end lung cancer screening with three-dimensional deep learning on low-dose chest computed tomography // Nat Med. 2019. Vol. 25, N 6. P. 954–961. doi: 10.1038/s41591-019-0447-x

13. Goncalves S., Fong P.C., Blokhina M. Artificial intelligence for early diagnosis of lung cancer through incidental nodule detection in low-and middle-income countries-acceleration during the COVID-19 pandemic but here to stay // Am J Cancer Res. 2022. Vol. 12, N 1. P. 1–16.

14. Graf M., Makowski M., Gawlitza J., Gassert F. Cost–effectiveness of artificial intelligence support in computed tomography–dased lung cancer screening // Cancers (Basel). 2022. Vol. 14, N 7. P. 1729. doi: 10.3390/cancers14071729

AUTHORS' INFO

* Valeria Yu. Chernina, MD;
address: 30 Bolshoy Boulevard, Skolkovo Innovation Center, 121205, Moscow, Russia;
ORCID: 0000-0002-0302-293X;
eLibrary SPIN: 8896-8051;
e-mail: v.chernina@ira-labs.com

Ruslan A. Zukov, MD, Dr. Sci. (Medicine), Professor;
ORCID: 0000-0002-7210-3020;
eLibrary SPIN: 3632-8415;
e-mail: zukov_rus@mail.ru

Ivan P. Safontsev, MD, Cand. Sci. (Medicine);
ORCID: 0000-0002-8177-6788;
eLibrary SPIN: 1548-5565;
e-mail: sip@onkolog24.ru

Marina P. Klimenok, MD;
ORCID: 0009-0001-7849-0770;
eLibrary SPIN: 7179-8793;
e-mail: klimenokmp@onkolog24.ru

Tatyana E. Zabrodskaya, MD;
ORCID: 0000-0003-4987-5222;
eLibrary SPIN: 8365-3582;
e-mail: ZabrodskayaTE@onkolog24.ru

ОБ АВТОРАХ

* Чернина Валерия Юрьевна;
адрес: Россия, 121205, Москва, тер. Сколково инновационного центра, Большой б-р, д. 30 стр. 1;
ORCID: 0000-0002-0302-293X;
eLibrary SPIN: 8896-8051;
e-mail: v.chernina@ira-labs.com

Зуков Руслан Александрович, д-р мед. наук, профессор;
ORCID: 0000-0002-7210-3020;
eLibrary SPIN: 3632-8415;
e-mail: zukov_rus@mail.ru

Сафонцев Иван Петрович, канд. мед. наук;
ORCID: 0000-0002-8177-6788;
eLibrary SPIN: 1548-5565;
e-mail: sip@onkolog24.ru

Клименок Марина Петровна;
ORCID: 0009-0001-7849-0770;
eLibrary SPIN: 7179-8793;
e-mail: klimenokmp@onkolog24.ru

Забродская Татьяна Евгеньевна;
ORCID: 0000-0003-4987-5222;
eLibrary SPIN: 8365-3582;
e-mail: ZabrodskayaTE@onkolog24.ru

Natalya A. Merkulova, MD;
ORCID: 0009-0006-9254-1331;
e-mail: MerkulovaNA@onkolog24.ru
Mikhail G. Belyaev, Cand. Sci. (Physics and Mathematics);
ORCID: 0000-0001-9906-6453;
eLibrary SPIN: 2406-1772;
e-mail: belyaevmichel@gmail.com
Mikhail Yu. Goncharov;
ORCID: 0009-0009-8417-0878;
e-mail: mig0nch@yandex.ru
Vitaly V. Omelyanovskiy, MD, Dr. Sci. (Medicine),
Professor;
ORCID: 0000-0003-1581-0703;
eLibrary SPIN: 1776-4270;
e-mail: vvo@rosmedex.ru
Ksenia A. Ulianova, MD;
ORCID: 0000-0002-3462-0123;
eLibrary SPIN: 6491-6072;
e-mail: UlyanovaKA@minzdrav.gov.ru
Evgenia A. Soboleva;
ORCID: 0009-0009-4037-6911;
e-mail: e.soboleva@ira-labs.com
Maria E. Blokhina, MD;
ORCID: 0009-0002-9008-9485;
e-mail: mariya.blokhina@astrazeneca.com
Elena A. Nalivkina;
ORCID: 0009-0003-5412-9643;
e-mail: elena.nalivkina@astrazeneca.com
Victor A. Gombolevskiy, MD, Cand. Sci. (Medicine);
ORCID: 0000-0003-1816-1315;
eLibrary SPIN: 6810-3279;
e-mail: v.gombolevskiy@ira-labs.com

Меркулова Наталья Алексеевна;
ORCID: 0009-0006-9254-1331;
e-mail: MerkulovaNA@onkolog24.ru
Беляев Михаил Геннадьевич, канд. физ.-мат. наук;
ORCID: 0000-0001-9906-6453;
eLibrary SPIN: 2406-1772;
e-mail: belyaevmichel@gmail.com
Гончаров Михаил Юрьевич;
ORCID: 0009-0009-8417-0878;
e-mail: mig0nch@yandex.ru
Омельяновский Виталий Владимирович, д-р мед. наук,
профессор;
ORCID: 0000-0003-1581-0703;
eLibrary SPIN: 1776-4270;
e-mail: vvo@rosmedex.ru
Ульянова Ксения Александровна;
ORCID: 0000-0002-3462-0123;
eLibrary SPIN: 6491-6072;
e-mail: UlyanovaKA@minzdrav.gov.ru
Соболева Евгения Александровна;
ORCID: 0009-0009-4037-6911;
e-mail: e.soboleva@ira-labs.com
Блохина Мария Евгеньевна;
ORCID: 0009-0002-9008-9485;
e-mail: mariya.blokhina@astrazeneca.com
Наливкина Елена Александровна;
ORCID: 0009-0003-5412-9643;
e-mail: elena.nalivkina@astrazeneca.com
Гомболевский Виктор Александрович, канд. мед. наук;
ORCID: 0000-0003-1816-1315;
eLibrary SPIN: 6810-3279;
e-mail: v.gombolevskiy@ira-labs.com

* Corresponding author / Автор, ответственный за переписку

Remote monitoring of patients with rheumatoid arthritis using a personal messenger

Yuliya A. Prokofeva, Yuri N. Belenkov, Maria V. Kozhevnikova, Elena A. Zheleznykh, Zarina V. Alborova, Irina V. Menshikova

Sechenov First Moscow State Medical University, Moscow, Russia

ABSTRACT

BACKGROUND: Remote medical technologies are a promising way to monitor patients during disease diagnosis, treatment, and subsequent rehabilitation. This paper reviews the clinical implementation and effectiveness of digital tools for remote monitoring and treatment control in patients with rheumatoid arthritis.

AIM: The aim of the study was to evaluate safety, efficacy and technological features of monitoring patients with rheumatoid arthritis using a remote monitoring platform.

MATERIALS AND METHODS: The prospective, non-randomized, controlled study included patients over 18 years of age with moderately to severely active rheumatoid arthritis who were discharged from the hospital for outpatient monitoring. Patients were divided into two groups for remote and in-person monitoring. Data for remote patient monitoring was collected through questionnaires using a Telemedbot Personal Messenger. The authors also used the Health Assessment Questionnaire (HAQ) to assess daily life functioning in patients with rheumatoid arthritis; the European Quality of Life Questionnaire EQ-5D questions to assess patient adherence, duration of morning stiffness, number of painful and swollen joints; and a visual analog scale to assess the overall condition. After 6 months, efficacy of rheumatoid arthritis treatment was assessed in both groups using the DAS28 index.

RESULTS: The remote monitoring program involved 30 patients for 6 months. The in-person monitoring group also included 30 people. After 6 months, patients using the Telemedbot Personal Messenger achieved low rheumatoid arthritis activity and remission more often than the second group (p=0.049). In the remote monitoring group, 9 (30.0%) and 11 (36.7%) patients achieved remission and low disease activity, compared to 3 (10.0%) and 8 (26.7%) patients in the in-person monitoring group. Therefore, 20 (66.7%) people in the remote monitoring group were able to control the disease, while only 11 (36.7%) patients in the in-person monitoring group were able to do so.

CONCLUSION: Remote monitoring using the Telemedbot Personal Messenger can be considered a potential way to increase the availability of medical care and efficacy of treatment for rheumatoid arthritis.

Keywords: rheumatoid arthritis; activity monitoring; mobile health; mHealth; telemedicine; digital medicine; remote monitoring.

Удалённое наблюдение за пациентами с ревматоидным артритом с применением платформы на базе персонального мессенджера

Ю.А. Прокофьева, Ю.Н. Беленков, М.В. Кожевникова, Е.А. Железных, З.В. Алборова, И.В. Меньшикова

Первый Московский государственный медицинский университет имени И.М. Сеченова, Москва, Россия

АННОТАЦИЯ

Обоснование. Дистанционные медицинские технологии — перспективный способ наблюдения за пациентами в ходе диагностики заболевания, лечения и последующей реабилитации. В настоящей статье авторы рассматривают интеграцию в клиническую практику и эффективность цифрового инструмента для осуществления удалённого наблюдения и контроля лечения пациентов с ревматоидным артритом.

Цель — оценка безопасности, эффективности и технологических особенностей наблюдения за пациентами с ревматоидным артритом с помощью платформы для удалённого мониторинга.

Материалы и методы. В проспективное нерандомизированное контролируемое исследование включены пациенты старше 18 лет с ревматоидным артритом с высокой и умеренной степенью активности, выписанные из стационара для амбулаторного наблюдения. Пациенты разделены на две группы: удалённого и очного наблюдения. Данные для удалённой оценки состояния пациентов получены путём анкетирования при помощи программного комплекса для наблюдения за пациентами на основе персонального мессенджера «Телемедбот». Также авторы использовали опросник HAQ для оценки функциональной способности в повседневной жизни у пациентов с ревматоидным артритом; европейский опросник качества жизни EQ-5D; вопросы для оценки приверженности пациентов рекомендациям, длительности утренней скованности, числа болезненных и припухших суставов; визуальную аналоговую шкалу для общей оценки заболевания. Через 6 мес. в обеих группах проведена оценка эффективности лечения ревматоидного артрита по индексу DAS28.

Результаты. 30 пациентов использовали программу дистанционного наблюдения 6 мес. Группа очного наблюдения также состояла из 30 человек. Через 6 мес. среди пациентов, использующих персональный мессенджер «Телемедбот», низкая активность ревматоидного артрита и ремиссия достигались чаще, чем во второй группе (p=0,049). В группе удалённого наблюдения ремиссии и низкой активности заболевания достигли 9 (30,0%) и 11 (36,7%) пациентов против 3 (10,0%) и 8 (26,7%) в группе очного контроля. Таким образом, в группе дистанционного наблюдения у 20 (66,7%) человек удаётся контролировать заболевание, в то время как в группе очного наблюдения это удаётся сделать лишь у 11 (36,7%).

Заключение. Удалённое наблюдение с помощью мессенджера «Телемедбот» можно считать потенциальным инструментом повышения доступности медицинской помощи и эффективности лечения ревматоидного артрита.

Ключевые слова: ревматоидный артрит; контроль активности; мобильное здравоохранение; mHealth; телемедицина; цифровая медицина; удалённое наблюдение.

利用个人聊天软件平台对类风湿性关节炎患者进行远程监测

Yuliya A. Prokofeva, Yuri N. Belenkov, Maria V. Kozhevnikova, Elena A. Zheleznykh,
Zarina V. Alborova, Irina V. Menshikova

Sechenov First Moscow State Medical University, Moscow, Russia

摘要

论证。远程医疗技术是在疾病诊断、治疗和后续康复过程中，监测患者的一种很有前景的方法。在本文中，作者对类风湿关节炎患者的远程监测和治疗控制的数字工具有效性与临床实践的融合进行了研究。

目的 — 评估使用远程监控平台对类风湿性关节炎患者进行监测的安全性、有效性和技术特点。

材料和方法。这项前瞻性非随机对照研究，纳入了出院接受门诊随访的18岁以上，患有严重和中度活动性类风湿关节炎患者。患者分为两组：远程监测和面对面监测。远程评估患者病情的数据是通过个人聊天软件平台 "Telemedbot"的患者监测软件包进行问卷调查获得的。同时，作者还使用了HAQ问卷来评估类风湿关节炎患者的日常生活能力；欧洲生活质量问卷EQ-5D；评估患者对建议的遵守情况、晨僵持续时间、疼痛和肿胀关节数量的问题；用于整体疾病评估的视觉模拟量表。6个月后，使用DAS28指数对两组患者的类风湿关节炎疗效进行评估。

结果。30名患者参加了为期6个月的远程监测计划。　　面对面监测组也有30名患者。6个月后，使用个人聊天软件平台"Telemedbot"的患者中，类风湿关节炎的低活动度和病情缓解高于第二组（p=0.049）。在远程监测组中，分别有9名(30.0%)和11名(36.7%) 患者获得缓解，且疾病活动度较低，而面对面对照组中分别有 3名(10.0%)和8名(26.7%) 患者获得缓解。因此，在远程监测组中，有20人（66.7%）成功控制了疾病，而在面对面监测组中，只有11人（36.7%）能够控制病情。

结论。使用个人聊天软件平台"Telemedbot"进行远程监控可以被认为是提高医疗服务的可用性和类风湿性关节炎治疗有效性的潜在工具。

关键词：类风湿性关节炎；活跃性监控；移动医疗；mHealth；远程医疗；数字医学；远程监测。

BACKGROUND

Optimizing medical care in the setting of overwhelming healthcare system burdens as well as staffing and time constraints requires innovative, flexible solutions. Modifications are being made to the medical institutions' workflow management, patient routing systems, and continuing medical education programs. With a greater number of software being available every year, modern technology breakthroughs offer an array of possibilities.

These devices and software have been employed in diverse medical fields, especially by rheumatologists. Rheumatic and musculoskeletal disorders require long-term (sometimes lifelong) monitoring by specialists. Without appropriate monitoring, these disorders exert permanent effects on patients' physical and mental health, as well as their social lives [1]. To enhance treatment outcomes, rheumatologists use electronic medical records, artificial intelligence, machine learning, clinical decision support systems, and wearable technology with data transfer capabilities, including mobile devices [2]. This software facilitates patient data classification and rapid, long-distance data transfer. Moreover, it allows delegation of certain routine tasks to digital assistants, streamlines diagnostic search, and minimizes time expenditures for healthcare personnel [3].

The most diverse set of digital tools in rheumatology are available to patients with rheumatoid arthritis (RA), the most prevalent autoimmune inflammatory disease [4, 5]. In recent years, RA incidence in Russia has risen by 17.5%. The prevalence of RA-related disability is rising along with the number of RA patients [6]. A comprehensive understanding of RA mechanisms and treatment approaches, skilled rheumatologists, and advancements in drug therapy and rehabilitation programs enable effective treatment of RA, resulting in remission or minimal disease activity [7–10]. However, maintaining treatment outcomes over the long term remains a challenge in real-world clinical settings. Furthermore, for certain patients, the mitigation in baseline disease activity during treatment was inadequate. This may result from less stringent monitoring of treatment efficacy following therapy initiation at the onset, during relapses, and after treatment [11, 12].

Remote monitoring solutions for patients with RA exhibit substantial clinical promise. Current guidelines indicate that regular monitoring by a rheumatologist during outpatient follow-up enhances the likelihood of achieving and maintaining remission or low-level disease activity, which is the primary objective of RA treatment [4, 13]. Several studies and systematic reviews on remote medical care have been published in the past five years. In 2022, the European League Against Rheumatism (EULAR) published the first guidelines for remote medical care in patients with rheumatic and musculoskeletal disorders [14]. In most publications, patients who use specialized remote monitoring programs typically have better or equivalent treatment outcomes than those who use traditional patient care techniques. However, recent systematic reviews have highlighted several challenges in the development, implementation, funding, and safety and efficacy assessment of remote monitoring software [15].

AIM

To evaluate the safety, efficacy, and technological features of remote monitoring in RA utilizing a personal messenger developed by the Department of Hospital Therapy of the Sechenov University and to examine patient satisfaction parameters.

MATERIALS AND METHODS

Study design

This was a prospective, non-randomized, controlled, open-label, experimental, single-center study (Fig. 1).

Eligibility criteria

The study included male and female patients over 18 years old with moderate to high disease activity who were discharged for outpatient-based follow-up and had signed a voluntary informed consent form. The Russian and EULAR recommendations were followed in making the diagnosis [3, 8, 12]. The exclusion criteria were as follows:
- Patients who developed RA before the age of 16;
- Patients with malignancies or mental disorders;
- Patients with a history of stroke or a transient ischemic attack during the previous six months;
- Patients with injuries or other conditions that exacerbate pain and restrict joint mobility;
- Patients who were pregnant or lactating; those without smartphones; and those who were not proficient in the joint self-assessment procedure (for the remote monitoring group).

Patients were omitted from the study if they met the exclusion criteria or declined to participate further.

Study setting

Every patient was followed up at the Rheumatology Department of the Sechenov University Clinical Hospital No. 1.

Subgroup analysis

The study included two groups. Group 1 patients received the standard of care with in-person consultations and used remote monitoring software. Group 2 patients only received in-person consultations.

Intervention

Questionnaires were employed to collect data for the remote patient status evaluation. The study used questionnaires
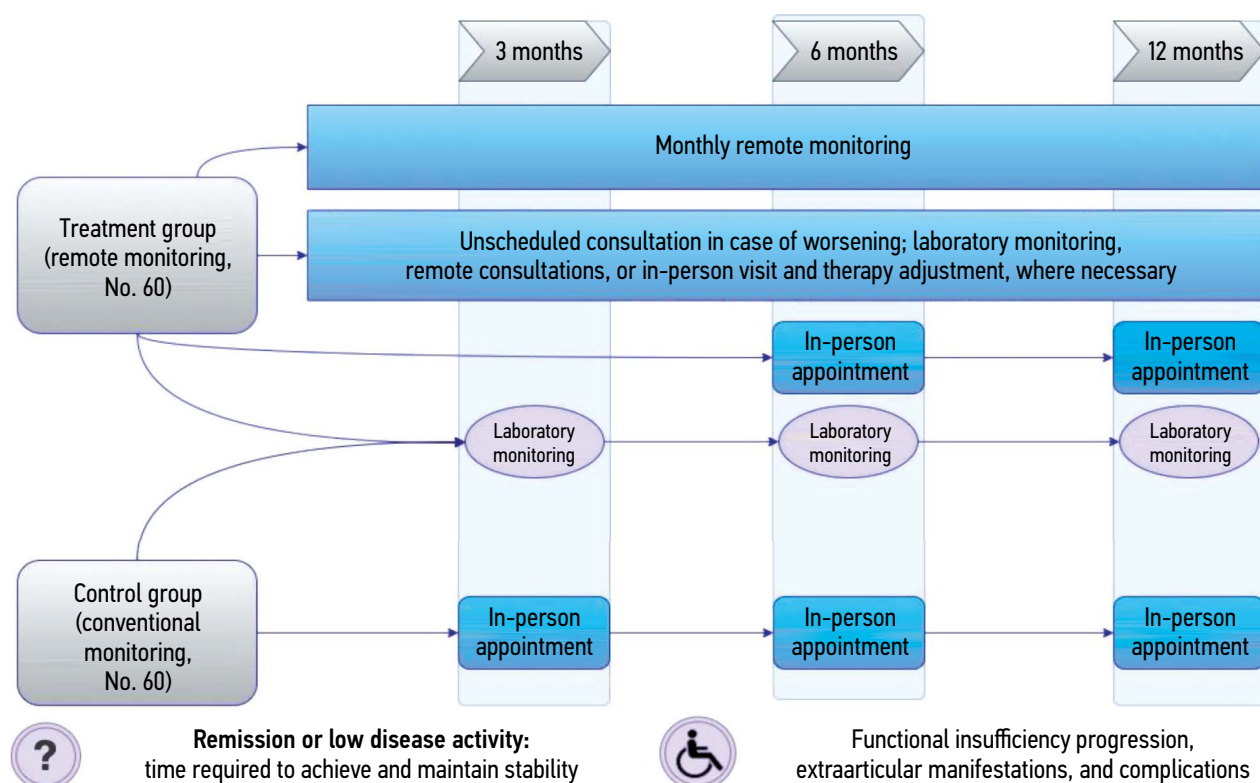
Fig. 1. Study design.

validated for clinical studies as well as recommended for treating and monitoring patients with RA and validated for clinical studies. These included the Health Assessment Questionnaire (HAQ) to assess daily life functioning in patients with rheumatoid arthritis; the European Quality of Life Questionnaire (EQ-5D) questions to ascertain patient adherence, duration of morning stiffness, and the number of tender and swollen joints; and a visual analog scale to assess the overall condition [3]. Moreover, the questionnaires were employed to gauge alterations in the condition of the RA patients.

Remote monitoring

Patients in the remote monitoring group received monthly reminders to complete a questionnaire in the software (mobile application). Patients could request an unannounced consultation and complete an unscheduled survey if their condition deteriorated. The questionnaire responses were immediately reported to the attending physician. The physician contacted the patients by phone in the following scenarios:

• When the responses in the questionnaire indicated adverse developments;
• At the patient's request and on unscheduled questionnaire completion;
• Insufficient decrease in RA activity.

Where necessary, these patients were referred for a follow-up examination to assess RA activity using DAS28 and CDAI. Additionally, the patients were consulted over the phone or in person.

Personal messenger-based software

The personal messenger-based remote monitoring software Telemedbot consists of interface subsystems, an internal software interface (Application Programming Interface, API), a backup subsystem, and PostgreSQL and Redis database management systems (DBMS) for short-term and long-term data storage.

The interface subsystem is responsible for the application logic, interactions with personal messenger APIs (specifically the use of the Telethon V2 library for the Telegram API), and data presentation in the personal messenger for both patients and physicians. An illustration of how patient data is displayed on the Telegram mobile app is provided in Fig. 2.

The internal API subsystem effectively regulates data management in the DBMS (standard operations of record generation, updating, and removal). Redis is used for caching, and PostgreSQL secures the long-term storage of patient data, questionnaires, and outcomes. Patient data are stored anonymously, with a unique code (nickname) assigned to each patient when creating a new patient account. Consequently, only the physician who created the account can identify the patient.

The backup subsystem ensures that data are regularly uploaded and saved to an external independent object storage service called S3 (Simple Storage Service).

All subsystems run in independent Docker containers and are managed using Docker Compose. All Telemedbot messenger components are located on a virtual server in Russia.
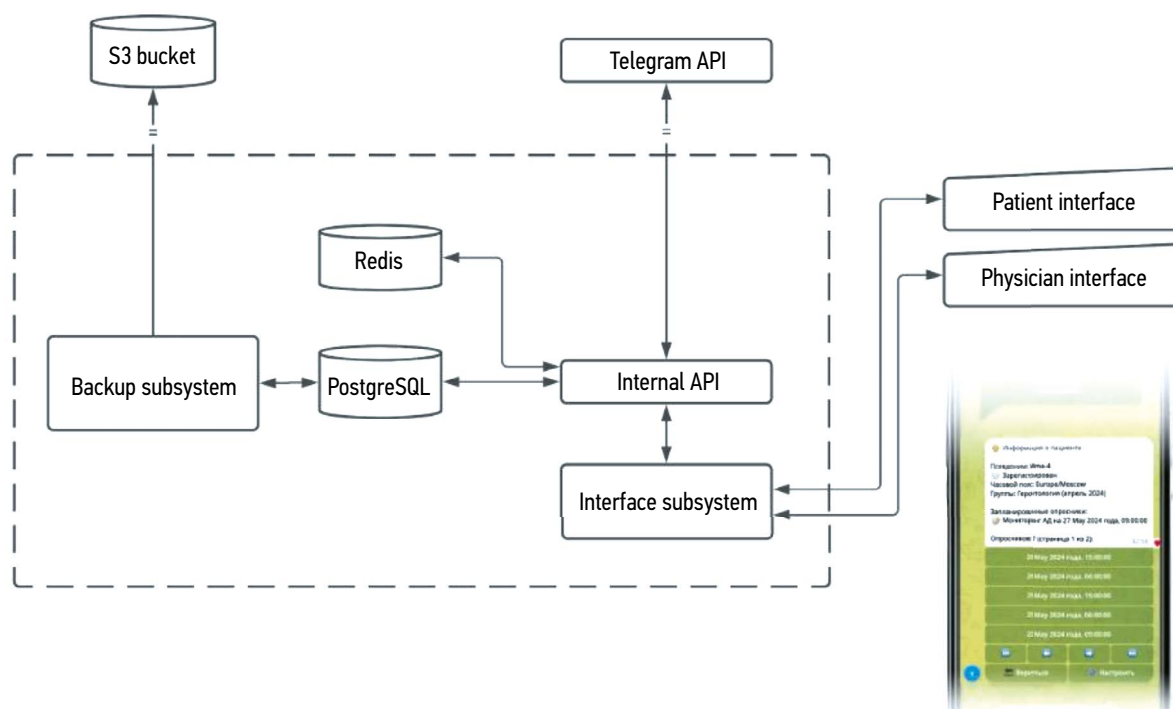
Fig. 2. Layout of the personal messenger-based software for remote monitoring.

To use Telemedbot, patients and physicians only need an IOS or Android smartphone installed with a personal messenger.

The patient interface communicates with Telemedbot by sending and receiving messages using a dedicated account in a personal messenger. Depending on the physician's treatment strategy, the patient was reminded to complete a questionnaire on a regular basis (e.g., once a month). Once the patient agreed to complete the questionnaire, the Telemedbot would send successive messages with various questions (single- or multiple-choice, free- or semifree-form responses; in the latter case, the response was checked for conformity with the set regular expression). The questionnaire results, including the partially completed questionnaires, were immediately reported to the physician.

The physician interface also interacts via a personal messenger. Physicians can create and update new accounts as well as review patient data and questionnaire results.

Main study outcomes

The following parameters were assessed during an in-person visit after six months:
- Clinical treatment outcomes;
- Level of patient satisfaction with software-based remote monitoring;
- Time spent by healthcare personnel on remote monitoring.

Additional study outcomes

Assessments were conducted on the self-monitoring skills during treatment, technical difficulties, and willingness to continue monitoring.

Outcomes registration

Treatment efficacy (clinical outcome) was assessed based on RA activity changes from baseline using DAS28.

After six months, to assess overall satisfaction with the messenger-based medical care, patients were asked to rate the technique using the following parameters:
- Convenience and user-friendliness of the software;
- Time needed per month to utilize the software;
- Physician's time to respond;
- Convenience of format;
- Satisfaction with treatment outcomes over six months.

Each parameter was assessed on a five-point scale, where 1 = very bad, 2 = rather bad than good, 3 = satisfactory, 4 = rather good than bad, and 5 = excellent.

Ethical review

The study was approved by the local ethics committee of the Sechenov First State Medical University (Minutes No. 22-22 of November 3, 2022).

Statistical analysis

Statistical analysis was performed using the StatTech v. 4.2.6 software (StatTech LLC, Russia). Based on the effect size determined in previous studies, an expected minimal significance level of 5%, and a statistical power of 90%, the sample size was estimated to be a minimum of 30 patients in each group. The descriptive statistics for the quantitative parameters are presented as median (Me) and interquartile range [Q1; Q3]. The Pearson's chi-square test was used for intergroup comparisons of the categorical variables. Differences were considered significant at a *p-value* <0.05.

RESULTS

The two study groups were matched based on sex, age, serological parameters (rheumatoid factor [RF] and anti-cyclic citrullinated peptide antibody [anti-CCP] levels), and RA activity parameters at baseline (Table 1).

After six months, RA activity was assessed in both groups using DAS28 (Table 2). To achieve optimal RA control, disease activity must be minimal, or the patient should be in remission. By the end of the follow-up, Group 1 patients who used Telemedbot attained a state of low disease activity or remission more frequently than those in Group 2 (see Table 2, Fig. 3). In the remote monitoring group, 9 (30.0%) and 11 (36.7%) patients achieved remission and low disease activity, respectively, compared to 3 (10.0%) and 8 (26.7%) patients in the in-person monitoring group (see Table 2). Thus, the disease was effectively controlled in 20 (66.7%) patients in Group 1, compared to 11 (36.7%) patients in Group 2 (see Fig. 3).

Table 1. Clinical characteristics of the patients

Parameter	Remote monitoring	In-person monitoring
Number of patients, *n*	30	30
Male, *n* (%)	6 (20.0)	4 (13.3)
Female, *n* (%)	24 (80.0)	26 (86.7)
Age, years, M ± SD	52.20 ± 15.23	54.10 ± 12.62
DAS28, Me [Q1–Q3]	4.46 [3.76–5.62]	4.70 [4.12–5.59]
Moderate RA activity* (%)	20 (66.7)	17 (56.7)
High RA activity (%)	10 (33.3)	13 (43.3)
RF*+, *n* (%)	25 (83.3)	22 (73.3)
anti-CCP*+, *n* (%)	10 (33.3)	10 (33.3)

Note. RA, rheumatoid arthritis; RF, rheumatoid factor; anti-CCP, anticyclic citrullinated peptide antibody.

Table 2. Rheumatoid arthritis activity in the different group patients after six months

Activity by DAS28	Remote monitoring, *n* (%)	In-person monitoring, *n* (%)	*p-value*
Remission	9 (30.0)	3 (10.0)	
Low activity	11 (36.7)	8 (26.7)	0.049
Moderate activity	10 (33.3)	16 (53.3)	
High activity	0 (0.0)	3 (10.0)	

Note. DAS28 (Disease Activity Score), rheumatoid arthritis activity score in 28 joints.
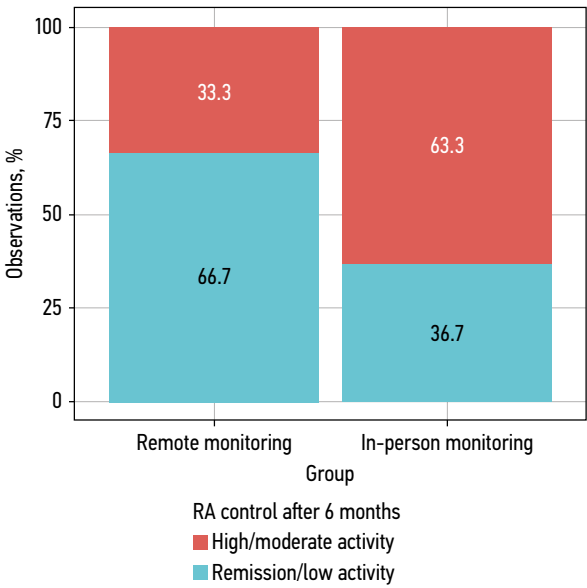
Fig. 3. RA control in the groups after six months.

Observed intergroup differences were likely due to earlier detection of worsening and absence of on-treatment improvements in the remote monitoring group, which enabled timely treatment modifications. During the follow-up period, 11 (36.6%) patients in the remote monitoring group had unfavorable changes, such as increasing pain and tender/swollen joint counts, which required an unscheduled consultation. One (3.3%) patient required previous prescriptions to be explained once more. Four patients (13.3%) received remote treatment adjustments, whereas six (20%) patients were recommended an unscheduled in-person appointment, follow-up examination, and inpatient treatment adjustment.

The analysis of patient satisfaction with medical care utilizing remote monitoring software indicated that most Group 1 (20 patients, 66.7%) patients were completely satisfied with treatment outcomes, comparable to the proportion of patients who achieved RA activity control. Most patients (27 patients, 90.0%) reported that the physician responded immediately. The convenience of the chatbot was rated excellent by 24 (80.0%) patients and good by five (16.7%) patients. One (3.3%) patient encountered difficulties in using the software and considered it inconvenient. One patient (3.3%) considered the time required to complete the questionnaires to be excessive, while another patient (3.3%) deemed it satisfactory. The remaining patients rated the application as good (3 patients, 10.0%) or excellent (25 patients, 83.3%) (Fig. 4). Three (10.0%) patients encountered technical issues (temporary switch-off during the software update process, patient mobile device issues) (Fig. 5).

A greater understanding of self-monitoring and self-assessment while undergoing RA treatment was reported by patients (25 patients, 83.3%) who utilized the remote monitoring program. In total, 24 (80.0%) patients consented to use the chatbot for continued monitoring (see Fig. 5).
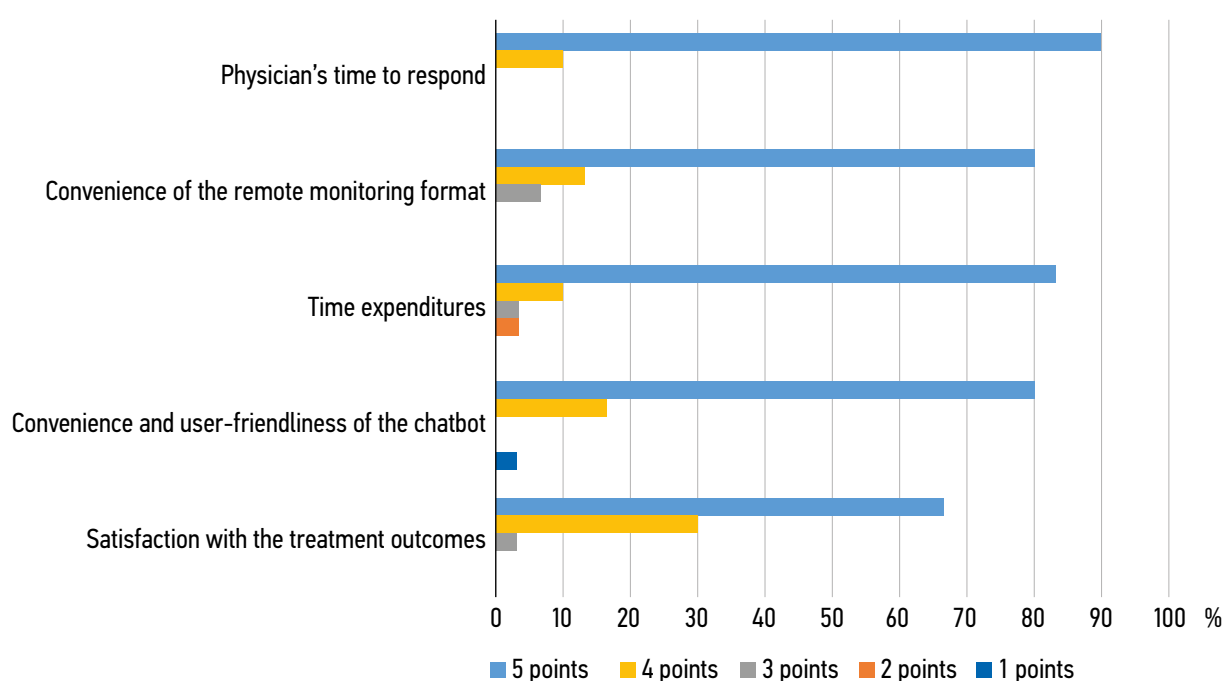
Fig. 4. Subjective patient assessment of the remote monitoring software: 1 = very bad, 2 = rather bad than good, 3 = satisfactory, 4 = rather good than bad, and 5 = excellent.
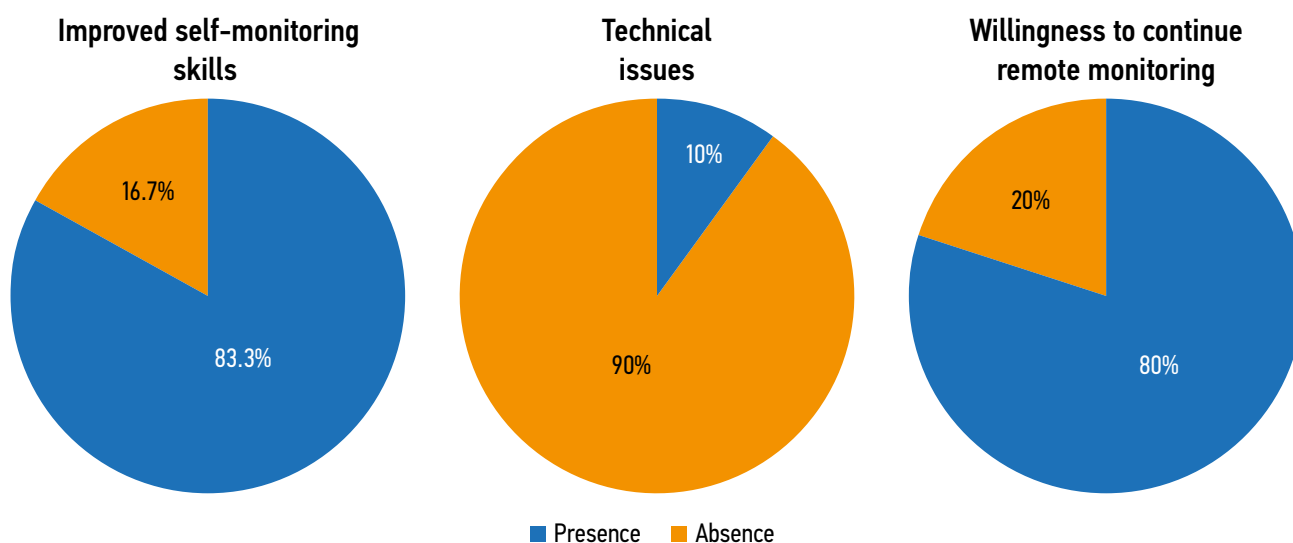
Fig. 5. Subjective patient assessment of the remote monitoring software (2).

DISCUSSION

In recent years, remote monitoring in RA patients has become a convenient and accessible tool for enhancing treatment outcomes. Although the number of available monitoring applications and software is rapidly expanding, only a few of them have been scientifically proven to be effective and safe. A systematic review of mobile applications for RA patients by Luo et al. revealed that only seven of the 20 assessed applications were designed in consultation with healthcare professionals [16]. Very few applications are assessed in clinical studies prior to release, and software proven to be effective in clinical studies is not widely available. The lack of information on data transfer and storage makes it challenging to evaluate the confidentiality of the available mobile applications. There have been few studies on technical solutions for the remote diagnosis of relapses [17]. According to most studies in a systematic review by Marques et al., the management of RA patients employing dedicated applications provides comparable or superior outcomes compared to conventional in-person appointments in terms of efficacy, safety, compliance, and user experience. Publication bias cannot be excluded in more than half of the analyzed randomized clinical studies, as positive outcomes are more likely to be published than negative ones [15]. Remote monitoring applications can boost patient engagement in therapy. Greater awareness of the disease and treatment modalities,

confidence in the outcome from following physician advice, and improved self-assessment skills contribute to favorable treatment outcomes [18]. Notably, all remote monitoring studies in RA patients focused on clinical safety. However, the lack of knowledge on the storage and transfer of patient data makes it nearly impractical to evaluate cybersecurity, especially personal data security.

Our study demonstrates that monitoring RA patients with moderate or high disease activity using the Telemedbot personal messenger facilitates the timely accomplishment of treatment goals: remission or minimal disease activity. The treatment efficacy after six months, as determined by evaluating RA activity using DAS28, was significantly greater in the remote monitoring group than in the conventional in-person monitoring group. One significant advantage of telemonitoring is the possibility to maintain the obtained results via regular monitoring of patients for deterioration and inadequate improvements while on treatment. The method has demonstrated high patient satisfaction with treatment outcomes, increased patient engagement in therapy, and boosted the user-friendliness of the messenger.

Study limitations

Despite the reliability of the findings, the study exhibits several limitations. Although the study sample can be considered representative, the sample size precludes a multivariate analysis of the impact of individual patient characteristics, such as drug therapy variations, on treatment efficacy. The study findings can serve as a basis for future, more extensive randomized controlled studies of remote digital monitoring in RA patients.

CONCLUSION

This study confirms the efficacy of the RA treatment monitoring program developed at Sechenov University. Telemedbot exhibits the potential to enhance access to medical care by facilitating direct communication with physicians and providing patients with information support. The software promotes more frequent monitoring of changes in the condition, early detection of elevated RA activity, and timely treatment. Moreover, remote monitoring mitigates the need for in-person appointments, which is especially crucial for patients with mobility issues and those residing in remote areas.

ADDITIONAL INFORMATION

REFERENCES

1. Erdes ShF. Definition of the term «Rheumatology»: do we need this and how do the eular and the acr look at this? *Rheumatology Science and Practice.* 2018;56(3):389–390. (In Russ.) doi: 10.14412/1995-4484-2018-389-390

2. Solomon DH, Rudin RS. Digital health technologies: opportunities and challenges in rheumatology. *Nature Reviews Rheumatology.* 2020;16:525–535. doi: 10.1038/s41584-020-0461-x

3. Kim OT, Dadaeva VA, Telkhigova AA, Drapkina OM. Mobile medical applications: opportunities, challenges and prospects. *Russian Journal of Preventive Medicine.* 2021;24(7):96–102. (In Russ.) doi: 10.17116/profmed20212407196

4. Clinical guidelines — Rheumatoid arthritis. ID: KR250. Approved by the Ministry of Health of the Russian Federation. 2021. Available from: https://www.garant.ru/products/ipo/prime/doc/402775973/ (In Russ.)

5. Venuturupalli RS, Sufka P, Bhana S. Digital Medicine in Rheumatology. *Rheumatic Disease Clinics of North America.* 2019;45(1):113–126. doi: 10.1016/j.rdc.2018.09.010

6. Black RJ, Cross M, Haile LM, et al. Global, regional, and national burden of rheumatoid arthritis, 1990–2020, and projections to 2050: a systematic analysis of the Global Burden of Disease Study 2021. *The Lancet Rheumatology.* 2023;5(10):e594–e610. doi: 10.1016/S2665-9913(23)00211-4

7. Karateev AE, Polishchuk EY, Makhmudov HR, et al. How Russian patients with rheumatoid arthritis assess their condition: initial data from the OPTIMA (Patient Assessment of Severity, Outcomes and Medical Care in Arthritis) pilot study. *Modern Rheumatology Journal.* 2023;17(6):65–71. (In Russ.) doi: 10.14412/1996-7012-2023-6-65-71

8. Smolen JS, Aletaha D, Bijlsma JW, et al. Treating rheumatoid arthritis to target: recommendations of an international task force. *Annals of the Rheumatic Diseases.* 2010;69(4):631–637. doi: 10.1136/ard.2009.123919

9. Combe B, Landewe R, Daien CI, et al. 2016 update of the EULAR recommendations for the management of early arthritis. *Annals of the Rheumatic Diseases.* 2017;76(6):948–959. doi: 10.1136/annrheumdis-2016-210602

10. Stoffer MA, Schoels MM, Smolen JS, et al. Evidence for treating rheumatoid arthritis to target: results of a systematic literature search update. *Annals of the Rheumatic Diseases.* 2016;75(5):16–22. doi: 10.1136/annrheumdis-2015-207526corr1

11. Schett G, Emery P, Tanaka Y, et al. Tapering biologic and conventional DMARD therapy in rheumatoid arthritis: current evidence and future directions. *Annals of the Rheumatic Diseases.* 2016;75(8):1428–1437. doi: 10.1136/annrheumdis-2016-209201

12. Nasonov EL, Olyunin YuA, Lila AM. Rheumatoid Arthritis: the Problems of Remission and Therapy Resistance. *Rheumatology Science and Practice.* 2018;56(3):263–271. (In Russ.) doi: 10.14412/1995-4484-2018-263-271

13. Smolen JS, Landewé RBM, Bergstra SA, et al. EULAR recommendations for the management of rheumatoid arthritis with synthetic and biological disease-modifying antirheumatic drugs: 2022 update. *Annals of the Rheumatic Diseases.* 2023;82(3):3–18. doi: 10.1136/ard-2022-223356corr1

14. De Thurah A, Bosch P, Marques A, et al. 2022 EULAR points to consider for remote care in rheumatic and musculoskeletal diseases. *Annals of the Rheumatic Diseases.* 2022;81(8):1065–1071. doi: 10.1136/annrheumdis-2022-222341

15. Marques A, Bosch P, de Thurah A, et al. Effectiveness of remote care interventions: a systematic review informing the 2022 EULAR Points to Consider for remote care in rheumatic and musculoskeletal diseases. *RMD Open.* 2022;8(1):e002290. doi: 10.1136/rmdopen-2022-002290

16. Luo D, Wang P, Lu F, et al. Mobile Apps for Individuals With Rheumatoid Arthritis: A Systematic Review. *JCR: Journal of Clinical Rheumatology.* 2019;25(3):133–141. doi: 10.1097/RHU.0000000000000800

17. Gandrup J, Ali SM, McBeth J, et al. Remote symptom monitoring integrated into electronic health records: A systematic review. *Journal of the American Medical Informatics Association.* 2020;27(11):1752–1763. doi: 10.1093/jamia/ocaa177

18. Nikiphorou E, Santos EJF, Marques A, et al. 2021 EULAR recommendations for the implementation of self-management strategies in patients with inflammatory arthritis. *Annals of the Rheumatic Diseases.* 2021;80(10):1278–1285. doi: 10.1136/annrheumdis-2021-220249

СПИСОК ЛИТЕРАТУРЫ

1. Эрдес Ш.Ф. Определение термина «ревматология»: нужно ли это нам и как на это смотрят EULAR и ACR? // Научно-практическая ревматология. 2018. Т. 56, № 3. С. 389–390. doi: 10.14412/1995-4484-2018-389-390

2. Solomon D.H., Rudin R.S. Digital health technologies: opportunities and challenges in rheumatology // Nature Reviews Rheumatology. 2020. Vol. 16. P. 525–535. doi: 10.1038/s41584-020-0461-x

3. Ким О.Т., Дадаева В.А., Тельхигова А.А., Драпкина О.М. Мобильные медицинские приложения: возможности, проблемы и перспективы // Профилактическая Медицина. 2021. Т. 24, № 7. С. 96–102. doi: 10.17116/profmed20212407196

4. Клинические рекомендации — Ревматоидный артрит. ID: КР250. Утверждены Министерством здравоохранения РФ. 2021. Режим доступа: https://www.garant.ru/products/ipo/prime/doc/402775973/

5. Venuturupalli R.S., Sufka P., Bhana S. Digital Medicine in Rheumatology: Challenges and Opportunities // Rheumatic Disease Clinics of North America. 2019. Vol. 45, N 1. P. 113–126. doi: 10.1016/j.rdc.2018.09.010

6. Black R.J., Cross M., Haile L.M., et al. Global, regional, and national burden of rheumatoid arthritis, 1990–2020, and projections to 2050: a systematic analysis of the Global Burden of Disease Study 2021 // The Lancet Rheumatology. 2023. Vol. 5, N 10. P. e594–e610. doi: 10.1016/S2665-9913(23)00211-4

7. Каратеев А.Е., Полищук Е.Ю., Махмудов Х.Р., и др. Как российские пациенты с ревматоидным артритом оценивают свое состояние: первые данные пилотного исследования ОПТИМА (Оценка Пациентами Тяжести, Исходов и Медицинской помощи при Артрите) // Современная Ревматология. 2023. Т. 17, № 6. С. 65–71. doi: 10.14412/1996-7012-2023-6-65-71

8. Smolen J.S., Aletaha D., Bijlsma J.W., et al. Treating rheumatoid arthritis to target: recommendations of an international task force // Annals of the Rheumatic Diseases. 2010. Vol. 69, N 4. P. 631–637. doi: 10.1136/ard.2009.123919

9. Combe B., Landewe R., Daien C.I., et al. 2016 update of the EULAR recommendations for the management of early arthritis // Annals of the Rheumatic Diseases. 2017. Vol. 76, N 6. P. 948–959. doi: 10.1136/annrheumdis-2016-210602

10. Stoffer M.A., Schoels M.M., Smolen J.S., et al. Evidence for treating rheumatoid arthritis to target: results of a systematic literature search update // Annals of the Rheumatic Diseases. 2016. Vol. 75, N 5. P. 16–22. doi: 10.1136/annrheumdis-2015-207526corr1

11. Schett G., Emery P., Tanaka Y., et al. Tapering biologic and conventional DMARD therapy in rheumatoid arthritis: current evidence and future directions // Annals of the Rheumatic Diseases. 2016. Vol. 75, N 8. P. 1428–1437. doi: 10.1136/annrheumdis-2016-209201

12. Насонов Е.Л., Олюнин Ю.А., Лила А.М. Ревматоидный артрит: проблемы ремиссии и резистентности к терапии // Научно-практическая ревматология. 2018. Т. 56, № 3. С. 263–271. doi: 10.14412/1995-4484-2018-263-271

13. Smolen J.S., Landewé R.B.M., Bergstra S.A., et al. EULAR recommendations for the management of rheumatoid arthritis with synthetic and biological disease-modifying antirheumatic drugs: 2022 update // Annals of the Rheumatic Diseases. 2023. Vol. 82, N 3. P. 3–18. doi: 10.1136/ard-2022-223356corr1

14. De Thurah A., Bosch P., Marques A., et al. 2022 EULAR points to consider for remote care in rheumatic and musculoskeletal diseases // Annals of the Rheumatic Diseases. 2022. Vol. 81, N 8. P. 1065–1071. doi: 10.1136/annrheumdis-2022-222341

15. Marques A., Bosch P., de Thurah A., et al. Effectiveness of remote care interventions: a systematic review informing the 2022 EULAR Points to Consider for remote care in rheumatic and musculoskeletal diseases // RMD Open. 2022. Vol. 8, N 1. P. e002290. doi: 10.1136/rmdopen-2022-002290

16. Luo D., Wang P., Lu F., et al. Mobile Apps for Individuals With Rheumatoid Arthritis: A Systematic Review // JCR: Journal of Clinical Rheumatology. 2019. Vol. 25, N 3. P. 133–141. doi: 10.1097/RHU.0000000000000800

17. Gandrup J., Ali S.M., McBeth J., et al. Remote symptom monitoring integrated into electronic health records: A systematic review // Journal of the American Medical Informatics Association. 2020. Vol. 27, N 11. P. 1752–1763. doi: 10.1093/jamia/ocaa177

18. Nikiphorou E., Santos E.J.F., Marques A., et al. 2021 EULAR recommendations for the implementation of self-management strategies in patients with inflammatory arthritis // Annals of the Rheumatic Diseases. 2021. Vol. 80, N 10. P. 1278–1285. doi: 10.1136/annrheumdis-2021-220249

AUTHORS' INFO

* Yuliya A. Prokofeva;
address: 8 bldg. 2 Trubetskaya str., 119048, Moscow, Russia;
ORCID: 0000-0001-8658-3435;
eLibrary SPIN: 3545-2640;
e-mail: ulyaprokofeva@gmail.com

Yuri N. Belenkov, MD, Dr. Sci. (Medicine), academician member
of the Russian Academy of Sciences;
ORCID: 0000-0002-3014-6129;
eLibrary SPIN: 5661-4691;
e-mail: belenkov_yu_n@staff.sechenov.ru

Maria V. Kozhevnikova;
ORCID: 0000-0003-4778-7755;
eLibrary SPIN: 8501-9812;
e-mail: kozhevnikova_m_v@staff.sechenov.ru

Elena A. Zheleznykh, MD, Cand. Sci. (Medicine);
ORCID: 0000-0002-2596-192X;
eLibrary SPIN: 2941-4875;
e-mail: zheleznykh_e_a@staff.sechenov.ru

Zarina B. Alborova;
ORCID: 0009-0004-6090-4922;
e-mail: Zari.Alborova2002@yandex.ru

Irina V. Menshikova, MD, Dr. Sci. (Medicine), Professor;
ORCID: 0000-0003-3181-5272;
eLibrary SPIN: 5373-7486;
e-mail: menshikova_i_v@staff.sechenov.ru

———————————

* Corresponding author / Автор, ответственный за переписку

ОБ АВТОРАХ

* Прокофьева Юлия Артуровна;
адрес: Россия, 119048, Москва, ул. Трубецкая, д. 8, стр. 2;
ORCID: 0000-0001-8658-3435;
eLibrary SPIN: 3545-2640;
e-mail: ulyaprokofeva@gmail.com

Беленков Юрий Никитич, д-р мед. наук,
академик РАН;
ORCID: 0000-0002-3014-6129;
eLibrary SPIN: 5661-4691;
e-mail: belenkov_yu_n@staff.sechenov.ru

Кожевникова Мария Владимировна;
ORCID: 0000-0003-4778-7755;
eLibrary SPIN: 8501-9812;
e-mail: kozhevnikova_m_v@staff.sechenov.ru

Железных Елена Анатольевна, канд. мед. наук;
ORCID: 0000-0002-2596-192X;
eLibrary SPIN: 2941-4875;
e-mail: zheleznykh_e_a@staff.sechenov.ru

Алборова Зарина Вадимовна;
ORCID: 0009-0004-6090-4922;
e-mail: Zari.Alborova2002@yandex.ru

Меньшикова Ирина Вадимовна, д-р мед. наук, профессор;
ORCID: 0000-0003-3181-5272;
eLibrary SPIN: 5373-7486;
e-mail: menshikova_i_v@staff.sechenov.ru

Use of radiomics and dosiomics to identify predictors of radiation-induced lung injury

Nikolay V. Nudnov[1,2,3], Vladimir M. Sotnikov[1], Mikhail E. Ivannikov[1], Elina S-A. Shakhvalieva[1], Aleksandr A. Borisov[1], Vasiliy V. Ledenev[4], Aleksei Yu. Smyslov[1], Alina V. Ananina[1]

[1] Russian Scientific Center of Roentgenoradiology, Moscow, Russia;
[2] Russian Medical Academy of Continuous Professional Education, Moscow, Russia;
[3] Peoples' Friendship University of Russia, Moscow, Russia;
[4] Central Clinical Military Hospital, Moscow, Russia

ABSTRACT

BACKGROUND: Radiomics is a machine learning-based technology that extracts, analyzes, and interprets quantitative features from digital medical images. In recent years, dosiomics has become an increasingly common term in the literature to describe a new radiomics method. Dosiomics is a texture analysis method for evaluating radiotherapy dose distribution patterns. Most of the published research in dosiomics evaluates its use in predicting radiation-induced lung injury.

AIM: The aim of the study was to identify predictors (biomarkers) of radiation-induced lung injury using texture analysis of computed tomography (CT) images of lungs and chest soft tissues using radiomics and dosiomics.

MATERIALS AND METHODS: The study used data from 36 women with breast cancer who received postoperative conformal radiation therapy. Retrospectively, the patients were divided into two groups according to the severity of post-radiation lung lesions. 3D Slicer was used to evaluate CT results of all patients obtained during radiation treatment planning and radiation dose distribution patterns. The software was able to unload radiomic and dosiomic features from regions of interest. The regions of interest included chest soft tissue and lung areas on the irradiated side where the dose burden exceeded 3 and 10 Gy.

RESULTS: The first group included 13 patients with minimal radiation-induced lung lesions, and the second group included 23 patients with post-radiation pneumofibrosis. In the lung area on the side irradiated with more than 3 Gy, statistically significant differences between the patient groups were obtained for three radiomic features and one dosiomic feature. In the lung area on the side irradiated with more than 10 Gy, statistically significant differences were obtained for 12 radiomic features and 1 dosiomic feature. In the area of chest soft tissues on the irradiated side, significant differences were obtained for 18 radiomic features and 4 dosiomic features.

CONCLUSION: As a result, a number of radiomic and dosiomic features were identified which were statistically different in patients with minimal lesions and pulmonary pneumofibrosis following radiation therapy for breast cancer. Based on texture analysis, predictors (biomarkers) were identified to predict post-radiation lung injury and identify higher-risk patients.

Keywords: dosiomics; radiomics; radiation therapy; texture analysis; post-radiation pneumonitis.

Опыт применения методов радиомики и дозиомики для нахождения предикторов лучевых повреждений лёгких

Н.В. Нуднов[1,2,3], В.М. Сотников[1], М.Е. Иванников[1], Э.С-А. Шахвалиева[1], А.А. Борисов[1], В.В. Леденёв[4], А.Ю. Смыслов[1], А.В. Ананьина[1]

[1] Российский научный центр рентгенорадиологии, Москва, Россия;
[2] Российская медицинская академия непрерывного профессионального образования, Москва, Россия;
[3] Российский университет дружбы народов имени Патриса Лумумбы, Москва, Россия;
[4] Центральный клинический военный госпиталь, Москва, Россия

АННОТАЦИЯ

Обоснование. Радиомика — это технология извлечения, анализа и интерпретации количественных характеристик из цифровых медицинских изображений, основанная на машинном обучении. В последние годы в литературе всё чаще встречается термин «дозиомика», обозначающий новое направление в радиомике. Дозиомика — это метод текстурного анализа планов распределения дозы облучения при лучевой терапии. Бо́льшая часть опубликованных исследований в области дозиомики посвящена её применению в прогнозировании лучевого повреждения лёгких.

Цель — выявление предикторов (биомаркёров) лучевых повреждений лёгких с помощью текстурного анализа (методами радиомики и дозиомики) изображений лёгких, а также мягких тканей грудной клетки, полученных с помощью компьютерной томографии.

Материалы и методы. В исследовании использовали данные 36 женщин с раком молочной железы, прошедших послеоперационный курс конформной лучевой терапии. Ретроспективно пациенток разделили на две группы по степени постлучевых изменений лёгких. Результаты компьютерной томографии всех пациенток, полученные на этапе планирования лучевой терапии, и планы распределения доз облучения анализировали с помощью программного обеспечения 3D Slicer с функцией выгрузки показателей радиомики и дозиомики из областей интереса. В качестве областей интереса выбирали область мягких тканей грудной клетки и области лёгкого на стороне облучения, дозовая нагрузка на которые превышала 3 и 10 Гр.

Результаты. В первую группу включили 13 пациенток с минимальными постлучевыми изменениями в лёгких, во вторую группу — 23 пациентки с постлучевым пневмофиброзом. В области лёгкого на стороне облучения с дозовой нагрузкой более 3 Гр статистически значимые различия между группами пациенток получены по трём показателям радиомики и одному показателю дозиомики. В области лёгкого на стороне облучения с дозовой нагрузкой более 10 Гр статистически значимые различия получены по 12 показателям радиомики и 1 показателю дозиомики. В области мягких тканей грудной клетки на стороне облучения значимые различия получены по 18 показателям радиомики и 4 показателям дозиомики.

Заключение. В результате выполненного исследования получен ряд показателей радиомики и дозиомики, статистически различающихся у пациенток с минимальными постлучевыми изменениями и постлучевым пневмофиброзом лёгких после проведения лучевой терапии по поводу рака молочной железы. Предикторы (биомаркёры), выявленные нами на основе текстурного анализа, можно использовать для прогнозирования постлучевых повреждений лёгких и выявления пациентов с более высоким риском их развития.

Ключевые слова: дозиомика; радиомика; лучевая терапия; текстурный анализ; постлучевой пневмонит.

放射组学和剂量组学在寻找肺辐射损伤预测因数方面的应用经验

Nikolay V. Nudnov[1,2,3], Vladimir M. Sotnikov[1], Mikhail E. Ivannikov[1], Elina S-A. Shakhvalieva[1], Aleksandr A. Borisov[1], Vasiliy V. Ledenev[4], Aleksei Yu. Smyslov[1], Alina V. Ananina[1]

[1] Russian Scientific Center of Roentgenoradiology, Moscow, Russia;
[2] Russian Medical Academy of Continuous Professional Education, Moscow, Russia;
[3] Peoples' Friendship University of Russia, Moscow, Russia;
[4] Central Clinical Military Hospital, Moscow, Russia

摘要

论证。 放射组学是一种基于机器学习从数字医学影像中提取、分析和解释定量特征的技术。近年来，"剂量组学"一词在文献中越来越常见，标志着放射组学的新方向。剂量组学是一种对放射治疗过程中辐射剂量分布计划进行纹理分析的方法。剂量组学领域已发表的大多数研究都致力于其在预测辐射引起的肺损伤中的应用。

目的 — 利用放射组学的纹理方法和肺部图像的剂量组学分析，以及计算机断层扫描获得的胸部软组织，从而确定肺部辐射损伤的预测因数（生物标志物）。

材料和方法。 研究中，使用了36名接受术后适形放射治疗的乳腺癌妇女的数据。根据放疗后肺部变化的程度回顾性地将患者分为两组。使用3D Slicer软件对所有患者在放疗计划阶段获得的CT扫描结果和辐射剂量分布计划进行分析，该软件具有上传研究区域的放射组学和剂量组学指标的功能。选择照射一侧的胸部软组织和肺部区域作为研究区域，剂量负荷分别超过3 Gy和10 Gy。

结果。 第一组包括13名放疗后肺部变化最小的患者，第二组包括23名放疗后肺纤维化的患者。在剂量负荷超过3 Gy的照射侧肺区，三项放射组学指标和一项剂量组学指标在患者组间存在显著统计学差异。在剂量负荷超过10 Gy的照射侧肺区，12项放射组学指标和1项剂量组学指标存在显著统计学差异。在照射一侧的胸部软组织区域，18项放射组学指标和4项剂量组学指标存在显著差异。

结论。 研究结果表明，在乳腺癌放疗后、肺部放疗后微小变化和放疗后肺纤维化的患者中，一系列的放射组学和剂量组学指标存在统计学差异。我们根据纹理分析确定的预测因数（生物标志物）可用于预测放射后肺损伤，并确定发生肺损伤的发展风险较高的患者。

关键词： 剂量组学；放射组学；放疗；纹理分析；放疗后肺炎。

BACKGROUND

Radiation therapy is a widely used method in cancer treatment [1]. However, it carries the risk of radiation-induced lung injury, particularly in patients with thoracic tumors. To mitigate this complication, various studies have explored the development of prognostic models using clinical, radiomic, and other relevant parameters [2].

Radiomics is an emerging technique based on texture analysis that evaluates quantitative image features to support the interpretation of medical images. It extracts image biomarkers that reflect abnormal changes from DICOM-format medical images. In this study, radiomic features were extracted using the open-source PyRadiomics library (AIM, USA). Radiomic features are generally categorized into two groups: first-order statistics and texture matrices related to co-occurrence and uniformity. These texture matrices include the following:

- Gray Level Co-occurrence Matrix (GLCM)
- Gray Level Run Length Matrix (GLRLM)
- Gray Level Size Zone Matrix (GLSZM)
- Neighboring Gray Tone Difference Matrix (NGTDM)
- Gray Level Dependence Matrix (GLDM) [3, 4].

A comprehensive explanation of these parameters and the formulas used for their calculation is available at pyradiomics.readthedocs.io [4].

Current evidence supports the utility of radiomics in predicting disease progression and treatment-related complications [5].

The term *dosiomics*, introduced by Gabryś et al. [6], is now widely used to describe a subfield within radiomics. Dosiomics applies texture analysis techniques to assess patterns in radiotherapy dose distributions. Similar to radiomic features, dosiomic features include co-occurrence and uniformity matrices that represent spatial relationships among pixels and voxels within an image. Most international studies on dosiomics have concentrated on its application in predicting radiation-induced lung injury [7].

The reported incidence of radiation-induced lung injury varies between 5% and 58% [8]. Risk factors for this condition can be categorized into two main groups. The first group comprises treatment-related factors, such as total radiation dose, dose fractionation, the volume of lung tissue exposed, the irradiation technique used, and the administration of chemotherapy or immunotherapy. The second group includes patient-related factors, such as age, smoking status, preexisting interstitial lung disease or chronic obstructive pulmonary disease, the location of the irradiated tumor, and individual, genetically determined radiosensitivity [9].

Radiation-induced lung injury progresses in two stages [10]. The first stage, known as postradiation pneumonitis or pulmonitis, is characterized by acute interstitial inflammation of lung tissue and typically occurs within 3–6 weeks after radiation therapy [11]. The second stage develops over the following 6 months, during which the acute changes may completely resolve or, especially at doses ≥30 Gy, evolve into chronic changes of varying severity. In such cases, edema and infiltration may lead to irreversible postradiation pneumofibrosis [12, 13]. The diagnosis of postradiation pneumonitis is based on three key criteria: a prior history of radiation therapy; the presence of symptoms such as fever, cough with mucoid sputum, and dyspnea; and characteristic findings on computed tomography (CT) scans [14]. Typical CT features include initial ground-glass opacities, followed by areas of consolidation, fibrous bands, and in some cases, aerial bronchograms and traction bronchiectasis [12, 15]. Postradiation pneumonitis negatively impacts both quality of life and survival in cancer patients [9]. Enhancing radiation therapy techniques to achieve effective local tumor control while minimizing radiation exposure to surrounding lung tissue can reduce the risk of radiation-induced lung injury [16].

AIM

To identify predictors of radiation-induced lung injury by performing texture analysis of CT images of the lungs and chest soft tissues obtained prior to radiation therapy, using radiomic and dosiomic methods.

MATERIALS AND METHODS

Study design

This was a single-center, retrospective study involving the analysis of chest CT scans from patients with breast cancer.

Eligibility criteria

The study included patients with breast cancer who underwent postoperative conformal radiotherapy at the Russian Scientific Center of Roentgenology and Radiology between 2022 and 2023. The inclusion criterion was the availability of follow-up chest CT data obtained at least 6 months after radiation therapy, recorded in the Radiology Information System of the same center. These CT scans were used to assess the extent of postradiation lung changes. Participants were grouped based on the severity of these changes, as determined by the conclusions of an independent radiologist.

Intervention

Pre-radiation preparation included a chest CT scan performed on a SOMATOM Definition AS scanner (Siemens, Germany), followed by volumetric dosimetric planning for radiation therapy. Irradiation of the chest wall and tumor bed was carried out using the TrueBeam system (Varian MS, USA) with a total equivalent radiation dose ranging from 50 to 60 Gy. A follow-up chest CT scan was conducted no earlier than 6 months after the completion of radiation therapy.

Main study outcome

The study's null hypothesis assumed no statistically significant differences between groups in any of the 107 evaluated radiomic and dosiomic features.

Outcomes registration

CT images acquired during radiation therapy planning, along with corresponding dose distribution data, were processed using 3D Slicer software (3D Slicer Community). This software enabled the extraction of radiomic and dosiomic features from defined regions of interest [17]. Features were calculated for chest soft tissues within the irradiation zone along the anterior surface, as well as for lung regions that received radiation doses exceeding 3 Gy and 10 Gy. Regions of interest were identified semi-automatically using Varian software (Varian, USA). For each region, 107 radiomic and dosiomic features were extracted, including first-order statistics, shape descriptors, and texture matrices related to co-occurrence and uniformity.

Subgroup analysis

Participants were retrospectively divided into two groups based on follow-up chest CT findings obtained 6 months after radiation therapy. Group 1 consisted of patients with minimal postradiation changes, while Group 2 included those with pronounced postradiation pneumofibrosis.

Ethics approval

The study protocol was reviewed and approved by the Independent Ethics Committee of the Russian Scientific Center of Roentgenology and Radiology on March 1, 2024 (Meeting Minutes No. 2).

Statistical analysis

The sample size was not predetermined. Data processing and statistical analysis were performed using Microsoft Office Excel and R-Studio, an open-source development environment for the R programming language (Posit, USA). The Mann–Whitney U test and Fisher's exact test were used to evaluate differences in quantitative and qualitative variables, respectively. Data are reported as the median along with the 25th and 75th percentiles (first and third quartiles). A p-value of <0.05 was considered statistically significant.

RESULTS

Participants

The study analyzed pre-radiation therapy CT scans of the lungs and chest soft tissues from 36 patients with breast cancer.

Group 1 consisted of 13 patients who exhibited minimal postradiation changes (Fig. 1a), while Group 2 included 23 patients with severe postradiation pneumofibrosis (Fig. 1b).

Quantitative and qualitative parameter comparisons between the two groups are shown in Tables 1 and 2.

The results support the validity of the intergroup comparisons.

Primary results

For the calculation of radiomic and dosiomic features, regions of interest on CT scans were selected based on a radiomic dose threshold of 3 Gy. This threshold was chosen based on previous studies showing that doses between 0 and 3 Gy do not lead to radiation-induced lung injury [13]. Additionally, some international studies consider a 3 Gy dose as a potential predictor of pneumonitis [18]. In texture analysis involving large tissue volumes, radiomic features are averaged, which can obscure significant differences and occasionally lead to missing relevant texture parameters in small regions of interest. Therefore, an additional threshold dose of 10 Gy was used to improve accuracy.

In the lung regions exposed to radiation doses greater than 3 Gy, significant differences were observed in three radiomic features and one dosiomic feature. The comparisons of these parameters—including median values, first and third quartiles, and statistical significance levels—are presented in Table 3.

The GLSZM Size Zone Nonuniformity values suggest that patients in Group 2 (with postradiation pneumofibrosis) exhibited more uniform gray level zone volumes. This is in line with findings for NGTDM Busyness, which measures
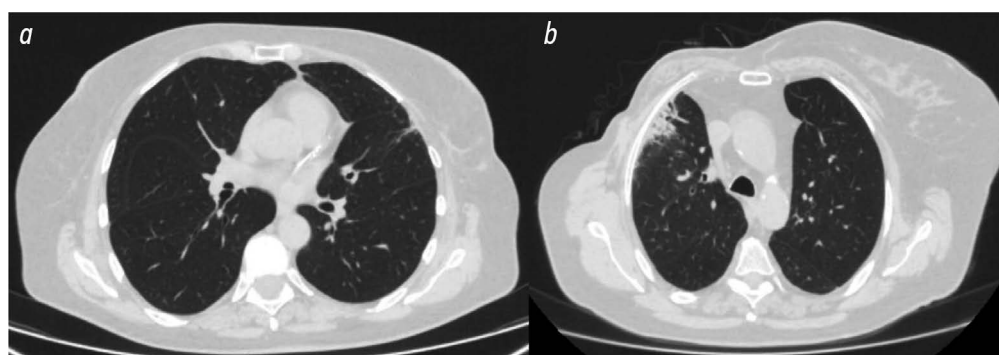
Fig. 1. Chest computed tomography at 6 months postradiation therapy: *a*, minimal postradiation changes in the left lung; *b*, severe postradiation pneumofibrosis in the right lung.

Table 1. Comparison of study groups by quantitative parameters

Parameter		Group 1 (minimal postradiation changes)	Group 2 (postradiation pneumofibrosis)	p-value
Age, years		61 [54; 67]	65 [55; 72]	0.179
Irradiated lung volume, cm³, radiation exposure	>3 Gy	945.94 [781.81; 1175.68]	828.67 [668.27; 1032.38]	0.190
	>10 Gy	613.88 [420.02; 694.52]	527.27 [403.10; 611.62]	0.344
	>30 Gy	330.36 [239.15; 449.71]	354.03 [248.07;447.64]	0.771

Note. Data are presented as Me [Q1; Q3], where Me is the median, Q1 is the first quartile, and Q3 is the third quartile.

Table 2. Comparison of study groups by qualitative parameters

Parameter		Number of patients (% of the total number of patients in the group)		p-value
		Group 1 (minimal postradiation changes)	Group 2 (postradiation pneumofibrosis)	
Smoking status		0	0	–
Concomitant lung diseases		1 (7,7)	0	0.361
Concomitant heart disease		5 (38,5)	10 (43.5)	0.526
History of chemotherapy		8 (61,5)	15 (65.2)	0.821
Affected mammary gland	Left	6 (46.1)	12 (52.2)	0.5
	Right	7 (53.8)	11 (47.8)	
Disease stage	T1–4N1–3M0	10 (76.9)	12 (52.2)	0.175
	T1–3N0M0	3 (23.1)	11 (47.8)	
Surgery type	Radical mastectomy	7 (53.8)	15 (65.2)	0.480
	Partial mastectomy	6 (46.1)	7 (30.4)	

Note. Disease stage is indicated according to the TNM staging system, where T0–4 (tumor) represents the size of the primary tumor, N0–3 (nodes) refers to the degree of spread to regional lymph nodes, and M0–1 (metastasis) indicates the presence of distant metastasis.

Table 3. Comparison of the two patient groups by radiomic and dosiomic features in lung fields with radiation exposure exceeding 3 Gy

Parameter	Group 1 (minimal postradiation changes)	Group 2 (postradiation pneumofibrosis)	p-value
Radiomic features			
GLRLM Gray Level Nonuniformity	17 464.52 [12199.53; 26481.37]	11 904.86 [7059.69; 20646.00]	0.05
GLSZM Size Zone Nonuniformity	19 096.83 [15693.52; 23905.24]	13 307.97 [11842.68; 19368.63]	0.043
NGTDM Busyness	74.81 [55.15; 102.73]	56.56 [34.50; 78.11]	0.047
Dosiomic features			
GLCM Maximum Probability	0.60 [0.55; 0.68]	0.55 [0.53; 0.61]	0.05

Note. Data are presented as Me [Q1; Q3], where Me is the median, Q1 is the first quartile, and Q3 is the third quartile. GLRLM, Gray Level Run Length Matrix; GLSZM, Gray Level Size Zone Matrix; NGTDM, Neighboring Gray Tone Difference Matrix; GLCM, Gray Level Co-occurrence Matrix.

the heterogeneity of adjacent pixels and was higher in Group 1 (patients with minimal postradiation changes). These results may indicate that lung tissue in Group 1, which demonstrates better recovery from radiation injury, has more distinct gray level variations and is less likely to form large homogeneous areas. Early postradiation pneumonitis on CT is typically characterized by local interstitial inflammation and damage to the microvascular endothelium [19, 20]. The baseline condition of the pulmonary microvasculature may influence the tissue's ability to recover from radiation injury, and the observed texture features may reflect the degree of vascular development.

In the lung regions receiving more than 10 Gy of radiation, significant differences were identified in 12 radiomic features and 1 dosiomic feature. The comparisons for these parameters are summarized in Table 4.

For instance, the GLCM Cluster Shade, which reflects the heterogeneity of gray level cluster distribution, was approximately 44% higher in patients with postradiation pneumofibrosis. This is further supported by the GLCM Cluster Prominence values, which indicate that in Group 1 (patients with minimal radiation-induced injury), the gray levels within clusters are closer to the overall average for lung tissue. In contrast, Group 2 (patients with postradiation

Table 4. Comparison of the two patient groups by radiomic and dosiomic features in lung fields with radiation exposure exceeding 10 Gy

Parameter	Group 1 (minimal postradiation changes)	Group 2 (postradiation pneumofibrosis)	*p*-value
Radiomic features			
Flatness	0.23 [0.22; 0.25]	0.26 [0.24; 0.29]	0.040
First-order Mean Absolute Deviation	112.38 [97.82; 152.24]	129.81 [118.67; 153.71]	0.048
GLCM Cluster Prominence	186 230.89 [148727.18; 306231.09]	321 625.90 [230877.79; 417140.54]	0.028
GLCM Cluster Shade	3366.36 [2860.31; 5779.96]	5998.08 [4269.97; 6497.98]	0.037
GLCM Cluster Tendency	105.53 [84.37; 171.43]	156.66 [122.25; 179.47]	0.048
GLCM Correlation	0.55 [0.49; 0.60]	0.59 [0.55; 0.63]	0.048
GLCM Sum Squares	34.48 [27.65; 54.08]	46.15 [37.78; 55.89]	0.044
GLDM Dependence Entropy	7.10 [6.95; 7.21]	7.19 [7.03; 7.34]	0.056
GLRLM High Gray Level Run Emphasis	149.91 [129.33; 200.75]	176.32 [159.08; 199.05]	0.044
GLRLM Run Entropy	4.85 [4..70; 5.00]	5.01 [4.85; 5.08]	0.024
GLRLM Short Run High Gray Level Emphasis	143.26 [121.04; 193.03]	168.49 [152.61; 191.58]	0.048
GLSZM Zone Entropy	6.63 [6.55; 6.73]	6.75 [6.67; 6.81]	0.031
Dosiomic features			
NGTDM Flatness	0.23 [0.22; 0.25]	0.26 [0.24; 0.30]	0.040

Note. Data are presented as Me [Q1; Q3], where Me is the median, Q1 is the first quartile, and Q3 is the third quartile. GLCM, Gray Level Co-occurrence Matrix; GLDM, Gray Level Dependence Matrix; GLRLM, Gray Level Run Length Matrix; GLSZM, Gray Level Size Zone Matrix; NGTDM, Neighboring Gray Tone Difference Matrix.

pneumofibrosis) showed over 40% greater variability in gray level distribution within individual clusters. These results suggest that, at baseline, patients in Group 2 had more areas of increased density and heterogeneity compared to the more uniform lung tissue in Group 1. The GLRLM High Gray Level Run Emphasis shows that Group 2 had 15% more regions with high gray levels, suggesting denser lung tissue at baseline in patients who later developed significant postradiation changes. This observation aligns with previous studies [13]. Morphologically, this could be associated with a greater presence of fibrotic lung areas before treatment.

In the irradiated chest soft tissues, significant differences between groups were found in 18 radiomic features (Table 5) and 4 dosiomic features (Table 6).

As shown in Table 5, significant intergroup differences were observed in the texture parameters. For instance, GLSM autocorrelation, which measures texture fineness or coarseness, was 42% higher in Group 2. GLSZM Large Area Emphasis, which indicates coarser texture in large areas, was 46% higher in Group 1. NGTDM Busyness, which reflects intensity changes between neighboring pixels, was 31% higher in Group 1. The latter two parameters suggest that Group 1 has a less uniform texture with sharper intensity changes.

Table 6 shows that Group 2 had higher total GLCM Entropy, indicating more significant intensity variations

in the image. The GLRLM Long Run Low Gray Level Emphasis, which reflects the distribution of low gray level values, was higher in Group 1, suggesting a greater number of low gray level values in the image. The larger number of parameters with intergroup differences (Tables 5 and 6) suggests that the condition of chest soft tissues and mammary glands could serve as predictors of lung tissue recovery following radiation therapy. However, the underlying mechanisms and nature of this association require further study.

DISCUSSION

The variety of risk factors for radiation-induced lung injury allows for the use of different quantitative and qualitative parameters to predict this complication. For instance, Zhao et al. [21] found that elevated levels of transforming growth factor beta (TGF-β) in the blood within the first 4 weeks of radiation therapy could predict the risk of lung injury with 66.7% sensitivity and 95.0% specificity. Chen et al. [22] developed a model based on an artificial neutral network to predict the risk of postradiation pneumonitis using factors such as the volume of lung tissue exposed to >16 Gy, cumulative equivalent uniform dose, forced expiratory volume in 1 s, diffusing capacity for carbon monoxide, and chemotherapy history. Additionally, many researchers have applied radiobiological models to predict the risk of radiation-induced damage to healthy tissues [23].

Table 5. Comparison of the two patient groups by radiomic features in irradiated chest soft tissues

Parameter	Group 1 (minimal postradiation changes)	Group 2 (postradiation pneumofibrosis)	*p*-value
GLCM Autocorrelation	327.37 [26.23; 716.81]	778.92 [250.21; 1299.00]	0.04
GLCM Joint Average	17.92 [5.00; 26.57]	27.83 [15.66; 36.00]	0.04
GLCM SumAverage	35.85 [10.00; 53.15]	55.67 [31.32; 72.01]	0.04
GLDM High Gray Level Emphasis	330.75 [26.84; 722.33]	785.17 [252.23; 1301.19]	0.04
GLDM Large Dependence High Gray Level Emphasis	34,520.55 [4229.63; 90 474.35]	94,735.42 [34,425.42; 178,891.14]	0.031
GLDM Small Dependence Emphasis	0.04 [0.04; 0.05]	0.06 [0.04; 0.06]	0.031
GLDM Small Dependence High Gray Level Emphasis	15.94 [1.32; 36.06]	40.80 [14.16; 69.29]	0.034
GLRLM High Gray Level Run Emphasis	337.14 [29.46; 731.67]	786.90 [257.09; 1312.39]	0.044
GLRLM Long Run High Gray Level Emphasis	1047.96 [132.06; 2600.37]	2816.82 [992.76; 5222.59]	0.028
GLRLM Short Run High Gray Level Emphasis	259.01 [20.99; 561.86]	573.11 [186.60; 970.35]	0.048
GLSZM Gray Level NonUniformity Normalized	0.13 [0.09; 0.20]	0.10 [0.07; 0.11]	0.031
GLSZM Large Area Emphasis	1,738,981.12 [415,642.22; 3,268,243.47]	815,272.55 [212,074.04; 1,207,397.63]	0.048
GLSZM Large Area Low Gray Level Emphasis	8843.95 [1392.9; 148,364.17]	1025.44 [474.68; 4267.21]	0.011
GLSZM Small Area High Gray Level Emphasis	232.12 [27.48; 493.15]	517.89 [205.88; 828.21]	0.044
GLSZM Zone Percentage	0.03 [0.03; 0.04]	0.04 [0.03; 0.05]	0.044
GLSZM Zone Variance	1,737,696.14 [414,536.61; 3,266,421.34]	814,359.34 [211,603.3; 1,206,631.61]	0.048
NGTDM Busyness	25.52 [9.61; 135.47]	8.10 [4.51; 17.92]	0.012
NGTDM Strength	0.09 [0.05; 0.25]	0.28 [0.15; 0.54]	0.037

Note. Data are presented as Me [Q1; Q3], where Me is the median, Q1 is the first quartile, and Q3 is the third quartile. GLCM, Gray Level Co-occurrence Matrix; GLDM, Gray Level Dependence Matrix; GLRLM, Gray Level Run Length Matrix; GLSZM, Gray Level Size Zone Matrix; NGTDM, Neighboring Gray Tone Difference Matrix.

Table 6. Comparison of the two patient groups by dosiomic features in irradiated chest soft tissues

Parameter	Group 1 (minimal postradiation changes)	Group 2 (postradiation pneumofibrosis)	*p*-value
GLCM SumEntropy	1.10 [0.55; 1.23]	1.26 [0.65; 1.31]	0.05
GLRLM Long Run Low Gray Level Emphasis	64.07 [39.55; 120.07]	38.78 [25.75; 55.68]	0.028
GLRLM Short Run High Gray Level Emphasis	0.40 [0.25; 0.49]	0.47 [0.42; 0.94]	0.026
NGTDM Complexity	0.06 [0.04; 0.07]	0.08 [0.06; 0.25]	0.05

Note. Data are presented as Me [Q1; Q3], where Me is the median, Q1 is the first quartile, and Q3 is the third quartile. GLCM, Gray Level Co-occurrence Matrix; GLRLM, Gray Level Run Length Matrix; NGTDM, Neighboring Gray Tone Difference Matrix.

Radiomics may enhance the prognostic value of predictive models. For example, Wang et al. [24] developed a radiomics nomogram with a concordance index of 0.921. Several studies on predicting the risk of radiation-induced lung injury have shown that models incorporating radiomic and dosiomic features are highly effective [7]. A key study by Huang et al. [18] reported a prognostic model that combined dosiomic and radiomic features with a high prognostic value (AUC 0.9). Importantly, including clinical findings in prognostic models further improves their performance [25]. Comparative studies examining

the effectiveness of dosimetry parameters (which describe the radiation therapy received) versus dosiomic features suggest that dosiomics can be integrated into prognostic models [26–28]. Adachi et al. [29] found that combining dosimetry parameters with dosiomic features enhanced the prognostic value of models. Based on international research, combined models using dosiomics, radiomics, clinical findings, and dosimetry can be a powerful prognostic tool [25, 30].

The studies mentioned above support our results, showing significant differences in radiomic and dosiomic features between patients with minimal postradiation changes and those with postradiation pneumofibrosis. These differences, identified before radiation therapy, were predictive of the risk of postradiation pneumofibrosis.

Study limitations

This study has several notable limitations. First, the sample size is small, and we plan to address this in future research. Second, the study utilized images from a single CT scanner. This limitation could be overcome by conducting a multicenter study or using external datasets, though this would require additional standardization of image generation and processing. The third limitation is the lack of universally accepted criteria for differentiating between minimal postradiation changes and postradiation pneumofibrosis. This could be addressed by employing computer vision techniques to measure the volume of affected and unaffected lung tissue. While this is an experimental, pilot study, it provides promising results for future development.

CONCLUSION

The study identified several radiomic and dosiomic features that significantly differed between patients with minimal postradiation changes and those with postradiation pneumofibrosis after radiation therapy for breast cancer. These differences were observed in both lung tissue and irradiated chest soft tissues. The findings suggest that the risk of radiation-induced lung injury may be influenced by individual patient characteristics, including lung tissue structure and the status of chest soft tissues. The texture parameters identified in this study can help predict the risk of radiation-induced lung injury and identify high-risk patients. International research indicates that predicting the risk of radiation-induced lung injury should involve not only the texture parameters of CT images but also dosimetry, laboratory, and other clinical parameters. This approach will enable the most comprehensive, patient-specific assessment and lead to highly accurate prognostic models.

ADDITIONAL INFORMATION

REFERENCES

1. Khmelevsky EV, Kaprin AD. The state of a radiotherapy service in Russia: Comparative analysis and prospects for development. *P.A. Herzen Journal of Oncology.* 2017;6(4):38–41. EDN: ZFCHGJ doi: 10.17116/onkolog20176438-41

2. Kuipers ME, van Doorn-Wink KCJ, Hiemstra PS, Slats AM. Predicting radiation-induced lung injury in lung cancer patients — challenges and opportunities: Predicting radiation-induced lung injury. *Int J Radiat Oncol Biol Phys.* 2023;118(3):639–649. doi: 10.1016/j.ijrobp.2023.10.044

3. Mayerhoefer ME, Materka A, Langs G, et al. Introduction to Radiomics. *J Nucl Med.* 2020;61(4):488–495. doi: 10.2967/jnumed.118.222893

4. Radiomic Features: pyradiomics v3.0.1.post15+g2791e23 documentation [Internet]. [cited 25 Nov 2023]. Available from: https://pyradiomics.readthedocs.io/en/latest/features.html#.

5. Avanzo M, Stancanello J, Pirrone G, Sartor G. Radiomics and deep learning in lung cancer. *Strahlenther Onkol.* 2020;196(10):879–887. doi: 10.1007/s00066-020-01625-9

6. Gabryś HS, Buettner F, Sterzing F, et al. Design and selection of machine learning methods using radiomics and dosiomics for normal tissue complication probability modeling of xerostomia. *Front Oncol.* 2018;8:35. doi: 10.3389/fonc.2018.00035

7. Solodkiy VA, Nudnov NV, Ivannikov ME, et al. Dosiomics in the analysis of medical images and prospects for its use in clinical practice. *Digital Diagnostics.* 2023;4(3):340–355. EDN: EQRWGJ doi: 10.17816/DD420053

8. Arroyo-Hernández M, Maldonado F, Lozano-Ruiz F, et al. Radiation-induced lung injury: Current evidence. *BMC Pulm Med.* 2021;21(1):9. doi: 10.1186/s12890-020-01376-4

9. Rahi MS, Parekh J, Pednekar P, et al. Radiation-Induced Lung Injury — Current Perspectives and Management. *Clin Pract.* 2021;11(3):410–429. doi: 10.3390/clinpract11030056

10. Yan Y, Fu J, Kowalchuk RO, et al. Exploration of radiation-induced lung injury, from mechanism to treatment: a narrative review. *Transl Lung Cancer Res.* 2022;11(2):307–322. doi: 10.21037/tlcr-22-108

11. Gladilina IA, Shabanov MA, Kravets OA, et al. Radiation-Induced Lung Injury. *Journal of oncology: diagnostic radiology and radiotherapy.* 2020;3(2):9–18. EDN: SKOAAY doi: 10.37174/2587-7593-2020-3-2-9-18

12. Nudnov NV, Sotnikov VM, Ledenev VV, Baryshnikova DV. Features a Qualitative Assessment of Radiation-Induced Lung Damage by CT. *Medical Visualization.* 2016;(1):39–46. EDN: VWOIIB

13. Ledenev VV. *Methodology for quantitative assessment of radiation damage to lungs in cancer patients using CT* [dissertation]. Moscow, 2023. Available from: https://www.rncrr.ru/nauka/dissertatsionnyy-sovet/obyavleniya-o-zashchitakh/upload%202023/Леденев_Диссертация.pdf (In Russ.) EDN: YBWROM

14. Zhou C, Yu J. Chinese expert consensus on diagnosis and treatment of radiation pneumonitis. *Prec Radiat Oncol.* 2022;6(3):262–271. doi: 10.1002/pro6.1169

15. Konkol M, Śniatała P, Milecki P. Radiation-induced lung injury — what do we know in the era of modern radiotherapy? *Rep Pract Oncol Radiother.* 2022;27(3):552–565. doi: 10.5603/RPOR.a2022.0046

16. Shaymuratov RI. Radiation-induced lung injury. A review. *The Bulletin of Contemporary Clinical Medicine.* 2020;13(3):63–73. EDN: BIZZHU doi: 10.20969/VSKM.2020.13(3).63-73

17. 3D Slicer image computing platform [Internet]. [cited 25 Nov 2023]. Available from: https://www.slicer.org/

18. Wang L, Gao Z, Li C, et al. Computed Tomography-Based Delta-Radiomics Analysis for Discriminating Radiation Pneumonitis in Patients With Esophageal Cancer After Radiation Therapy. *Int J Radiat Oncol Biol Phys.* 2021;111(2):443–455. doi: 10.1016/j.ijrobp.2021.04.047

19. Begosh-Mayne D, Kumar SS, Toffel S, et al. The dose-response characteristics of four NTCP models: using a novel CT-based radiomic method to quantify radiation-induced lung density changes. *Sci Rep.* 2020;10(1):10559. doi: 10.1038/s41598-020-67499-0

20. Korpela E, Liu SK. Endothelial perturbations and therapeutic strategies in normal tissue radiation damage. *Radiat Oncol.* 2014;9:266. doi: 10.1186/s13014-014-0266-7

21. Zhao L, Sheldon K, Chen M, et al. The predictive role of plasma TGF-beta1 during radiation therapy for radiation-induced lung toxicity deserves further study in patients with non-small cell lung cancer. *Lung Cancer.* 2008;59(2):232–239. doi: 10.1016/j.lungcan.2007.08.010

22. Chen S, Zhou S, Zhang J, et al. A neural network model to predict lung radiation-induced pneumonitis. *Med Phys.* 2007;34(9):3420–3427. doi: 10.1118/1.2759601

23. Jain V, Berman AT. Radiation Pneumonitis: Old Problem, New Tricks. *Cancers (Basel).* 2018;10(7):222. doi: 10.3390/cancers10070222

24. Huang Y, Feng A, Lin Y, et al. Radiation pneumonitis prediction after stereotactic body radiation therapy based on 3D dose distribution: Dosiomics and/or deep learning-based radiomics features. *Radiat Oncol.* 2022;17(1):188. doi: 10.1186/s13014-022-02154-8

25. Zhang Z, Wang Z, Yan M, et al. Radiomics and dosiomics signature from whole lung predicts radiation pneumonitis: A model development study with prospective external validation and decision-curve analysis. *Int J Radiat Oncol Biol Phys.* 2023;115(3):746–758. doi: 10.1016/j.ijrobp.2022.08.047

26. Puttanawarut C, Sirirutbunkajorn N, Khachonkham S, et al. Biological dosiomic features for the prediction of radiation pneumonitis in esophageal cancer patients. *Radiat Oncol.* 2021;16(1):220. doi: 10.1186/s13014-021-01950-y

27. Liang B, Yan H, Tian Y, et al. Dosiomics: Extracting 3D spatial features from dose distribution to predict incidence of radiation pneumonitis. *Front Oncol.* 2019;(9):269.doi: 10.3389/fonc.2019.00269

28. Liang B, Tian Y, Chen X, et al. Prediction of radiation pneumonitis with dose distribution: A convolutional neural network (CNN) based model. *Front Oncol.* 2020;9:1500. doi: 10.3389/fonc.2019.01500

29. Adachi T, Nakamura M, Shintani T, et al. Multi-institutional dose-segmented dosiomic analysis for predicting radiation pneumonitis after lung stereotactic body radiation therapy. *Med Phys.* 2021;48(4):1781–1791. doi: 10.1002/mp.14769

30. Zheng X, Guo W, Wang Y, et al. Multi-omics to predict acute radiation esophagitis in patients with lung cancer treated with intensity-modulated radiation therapy. *Eur J Med Res.* 2023;28(1):126. doi: 10.1186/s40001-023-01041-6

СПИСОК ЛИТЕРАТУРЫ

1. Хмелевский Е.В., Каприн А.Д. Состояние радиотерапевтической службы России: сравнительный анализ и перспективы развития // Онкология. Журнал им. П.А. Герцена. 2017. Т. 6, № 4. С. 38–41. EDN: ZFCHGJ doi: 10.17116/onkolog20176438-41

2. Kuipers M.E., van Doorn-Wink K.C.J., Hiemstra P.S., Slats A.M. Predicting radiation-induced lung injury in lung cancer patients — challenges and opportunities: Predicting radiation-induced lung injury // Int J Radiat Oncol Biol Phys. 2023. Vol. 118, N 3. P. 639–649. doi: 10.1016/j.ijrobp.2023.10.044

3. Mayerhoefer M.E., Materka A., Langs G., et al. Introduction to Radiomics // J Nucl Med. 2020. Vol. 61, N 4. P. 488–495. doi: 10.2967/jnumed.118.222893

4. Radiomic Features: pyradiomics v3.0.1.post15+g2791e23 documentation [Internet]. [дата обращения: 25.11.2023]. Режим доступа: https://pyradiomics.readthedocs.io/en/latest/features.html#

5. Avanzo M., Stancanello J., Pirrone G., et al. Radiomics and deep learning in lung cancer // Strahlenther Onkol. 2020. Vol. 196, N 10. P. 879–887. doi: 10.1007/s00066-020-01625-9

6. Gabryś H.S., Buettner F., Sterzing F., et al. Design and selection of machine learning methods using radiomics and dosiomics for normal tissue complication probability modeling of xerostomia // Front Oncol. 2018. Vol. 8. ID 35. doi: 10.3389/fonc.2018.00035

7. Солодкий В.А., Нуднов Н.В., Иванников М.Е., и др. Дозиомика в анализе медицинских изображений и перспективы её использования в клинической практике // Digital Diagnostics. 2023. Т. 4, № 3. С. 340–355. EDN: EQRWGJ doi: 10.17816/DD420053

8. Arroyo-Hernández M., Maldonado F., Lozano-Ruiz F., et al. Radiation-induced lung injury: Current evidence // BMC Pulm Med. 2021. Vol. 21, N 1. ID 9. doi: 10.1186/s12890-020-01376-4

9. Rahi M.S., Parekh J., Pednekar P., et al. Radiation-Induced Lung Injury — Current Perspectives and Management // Clin Pract. 2021. Vol. 11, N 3. P. 410–429. doi: 10.3390/clinpract11030056

10. Yan Y., Fu J., Kowalchuk R.O., et al. Exploration of radiation-induced lung injury, from mechanism to treatment: a narrative review // Transl Lung Cancer Res. 2022. Vol. 11, N 2. P. 307–322. doi: 10.21037/tlcr-22-108

11. Гладилина И.А., Шабанов М.А., Кравец О.А., и др. Постлучевые повреждения лёгких // Онкологический журнал: лучевая диагностика, лучевая терапия. 2020. Т. 3, № 2. С. 9–18. EDN: SKOAAY doi: 10.37174/2587-7593-2020-3-2-9-18

12. Нуднов Н.В., Сотников В.М., Леденёв В.В., Барышникова Д.В. Возможности качественной оценки лучевых повреждений лёгких методом компьютерной томографии // Медицинская визуализация. 2016. № 1. С. 39–46. EDN: VWOIIB

13. Леденёв В.В. Методика количественной оценки лучевых повреждений лёгких у онкологических пациентов по данным рентгеновской компьютерной томографии: диссертация на соискание учёной степени канд. мед. наук. Москва, 2023. 133 с. Режим доступа: https://www.rncrr.ru/nauka/dissertatsionnyy-sovet/obyavleniya-o-zashchitakh/upload%202023/Леденев_Диссертация.pdf Дата обращения: 25.11.2023. EDN: YBWROM

14. Zhou C., Yu J. Chinese expert consensus on diagnosis and treatment of radiation pneumonitis // Prec Radiat Oncol. 2022. Vol. 6, N 3. P. 262–271. doi: 10.1002/pro6.1169

15. Konkol M., Śniatała P., Milecki P. Radiation-induced lung injury — what do we know in the era of modern radiotherapy? // Rep Pract Oncol Radiother. 2022. Vol. 27, N 3. P. 552–565. doi: 10.5603/RPOR.a2022.0046

16. Шаймуратов Р.И. Радиационно-индуцированные поражения лёгких. Современное состояние проблемы // Вестник современной клинической медицины. 2020. Т. 13, № 3. С. 63–73. EDN: BIZZHU doi: 10.20969/VSKM.2020.13(3).63-73

17. 3D Slicer image computing platform [Internet]. [дата обращения: 25.11.2023]. Режим доступа: https://www.slicer.org/

18. Wang L., Gao Z., Li C., et al. Computed Tomography-Based Delta-Radiomics Analysis for Discriminating Radiation Pneumonitis in Patients With Esophageal Cancer After Radiation Therapy // Int J Radiat Oncol Biol Phys. 2021. Vol. 111, N 2. P. 443–455. doi: 10.1016/j.ijrobp.2021.04.047

19. Begosh-Mayne D., Kumar S.S., Toffel S., et al. The dose-response characteristics of four NTCP models: using a novel CT-based radiomic method to quantify radiation-induced lung density changes // Sci Rep. 2020. Vol. 10, N 1. ID 10559. doi: 10.1038/s41598-020-67499-0

20. Korpela E., Liu S.K. Endothelial perturbations and therapeutic strategies in normal tissue radiation damage // Radiat Oncol. 2014. Vol. 9. ID 266. doi: 10.1186/s13014-014-0266-7

21. Zhao L., Sheldon K., Chen M., et al. The predictive role of plasma TGF-beta1 during radiation therapy for radiation-induced lung toxicity deserves further study in patients with non-small cell lung cancer // Lung Cancer. 2008. Vol. 59, N 2. P. 232–239. doi: 10.1016/j.lungcan.2007.08.010

22. Chen S., Zhou S., Zhang J., et al. A neural network model to predict lung radiation-induced pneumonitis // Med Phys. 2007. Vol. 34, N 9. P. 3420–3427. doi: 10.1118/1.2759601

23. Jain V., Berman A.T. Radiation Pneumonitis: Old Problem, New Tricks // Cancers (Basel). 2018. Vol. 10, N 7. ID 222. doi: 10.3390/cancers10070222

24. Huang Y., Feng A., Lin Y., et al. Radiation pneumonitis prediction after stereotactic body radiation therapy based on 3D dose distribution: Dosiomics and/or deep learning-based radiomics features // Radiat Oncol. 2022. Vol. 17, N 1. ID 188. doi: 10.1186/s13014-022-02154-8

25. Zhang Z., Wang Z., Yan M., et al. Radiomics and dosiomics signature from whole lung predicts radiation pneumonitis: A model development study with prospective external validation and decision-curve analysis // Int J Radiat Oncol Biol Phys. 2023. Vol. 115, N 3. P. 746–758. doi: 10.1016/j.ijrobp.2022.08.047

26. Puttanawarut C., Sirirutbunkajorn N., Khachonkham S., et al. Biological dosiomic features for the prediction of radiation pneumonitis in esophageal cancer patients // Radiat Oncol. 2021. Vol. 16, N 1. ID 220. doi: 10.1186/s13014-021-01950-y

27. Liang B., Yan H., Tian Y., et al. Dosiomics: Extracting 3D spatial features from dose distribution to predict incidence of radiation pneumonitis // Front Oncol. 2019. Vol. 9. ID 269. doi: 10.3389/fonc.2019.00269

28. Liang B., Tian Y., Chen X., et al. Prediction of radiation pneumonitis with dose distribution: A convolutional neural network (CNN) based model // Front Oncol. 2020. Vol. 9. ID 1500. doi: 10.3389/fonc.2019.01500

29. Adachi T., Nakamura M., Shintani T., et al. Multi-institutional dose-segmented dosiomic analysis for predicting radiation pneumonitis after lung stereotactic body radiation therapy // Med Phys. 2021. Vol. 48, N 4. P. 1781–1791. doi: 10.1002/mp.14769

30. Zheng X., Guo W., Wang Y., et al. Multi-omics to predict acute radiation esophagitis in patients with lung cancer treated with intensity-modulated radiation therapy // Eur J Med Res. 2023. Vol. 28, N 1. ID 126. doi: 10.1186/s40001-023-01041-6

AUTHORS' INFO

* Mikhail E. Ivannikov, MD;
address: 86 Profsoyuznaya str., 117997, Moscow, Russia;
ORCID: 0009-0007-0407-0953;
eLibrary SPIN: 3419-2977;
e-mail: ivannikovmichail@gmail.com

Nikolay V. Nudnov, MD, Dr. Sci. (Medicine), Professor;
ORCID: 0000-0001-5994-0468;
eLibrary SPIN: 3018-2527;
e-mail: nudnov@rncrr.ru

Vladimir M. Sotnikov, MD, Dr. Sci. (Medicine), Professor;
ORCID: 0000-0003-0498-314X;
eLibrary SPIN: 3845-0154;
e-mail: vmsotnikov@mail.ru

Elina S-A. Shakhvalieva, MD;
ORCID: 0009-0000-7535-8523;
e-mail: shelina9558@gmail.com

ОБ АВТОРАХ

* Иванников Михаил Евгеньевич;
адрес: Россия, 117997, Москва, ул. Профсоюзная, д. 86;
ORCID: 0009-0007-0407-0953;
eLibrary SPIN: 3419-2977;
e-mail: ivannikovmichail@gmail.com

Нуднов Николай Васильевич, д-р мед. наук, профессор;
ORCID: 0000-0001-5994-0468;
eLibrary SPIN: 3018-2527;
e-mail: nudnov@rncrr.ru

Сотников Владимир Михайлович, д-р мед. наук, профессор;
ORCID: 0000-0003-0498-314X;
eLibrary SPIN: 3845-0154;
e-mail: vmsotnikov@mail.ru

Шахвалиева Элина Саид-Аминовна;
ORCID: 0009-0000-7535-8523;
e-mail: shelina9558@gmail.com

Aleksandr A. Borisov, MD;
ORCID: 0000-0003-4036-5883;
eLibrary SPIN: 4294-4736;
e-mail: aleksandrborisov10650@gmail.com
Vasiliy V. Ledenev, MD, Cand. Sci. (Medicine);
ORCID: 0000-0002-2856-2107;
eLibrary SPIN: 2791-0329;
e-mail: Ledenevvv007@gmail.com
Aleksei Yu. Smyslov, Cand. Sci. (Engineering);
ORCID: 0000-0002-6409-6756;
eLibrary SPIN: 9341-0037;
e-mail: smyslov.ay@gmail.com
Alina V. Ananina;
ORCID: 0009-0002-4562-9729;
eLibrary SPIN: 9699-7690;
e-mail: vastruhina.a.v@yandex.ru

Борисов Александр Александрович;
ORCID: 0000-0003-4036-5883;
eLibrary SPIN: 4294-4736;
e-mail: aleksandrborisov10650@gmail.com
Леденёв Василий Владимирович, канд. мед. наук;
ORCID: 0000-0002-2856-2107;
eLibrary SPIN: 2791-0329;
e-mail: Ledenevvv007@gmail.com
Смыслов Алексей Юрьевич, канд. техн. наук;
ORCID: 0000-0002-6409-6756;
eLibrary SPIN: 9341-0037;
e-mail: smyslov.ay@gmail.com
Ананьина Алина Валентиновна;
ORCID: 0009-0002-4562-9729;
eLibrary SPIN: 9699-7690;
e-mail: vastruhina.a.v@yandex.ru

* Corresponding author / Автор, ответственный за переписку

Assessing the probability of metastatic mediastinal lymph node involvement in patients with non–small cell lung cancer using convolutional neural networks on chest computed tomography

Alexey E. Shevtsov[1], Iaroslav D. Tominin[1], Vladislav D. Tominin[1], Vsevolod M. Malevanniy[1], Yury S. Esakov[2], Zurab G. Tukvadze[2], Andrey O. Nefedov[3], Piotr K. Yablonskii[3], Pavel V. Gavrilov[3], Vadim V. Kozlov[4], Mariya E. Blokhina[5], Elena A. Nalivkina[5], Victor A. Gombolevskiy[1,7], Yuriy A. Vasilev[6], Mariya N. Dugova[1], Valeria Yu. Chernina[1], Olga V. Omelyanskaya[6], Roman V. Reshetnikov[6], Ivan A. Blokhin[6], Mikhail G. Belyaev[1]

[1] IRA Labs, Moscow, Russia;
[2] Moscow City Clinical Oncological Hospital № 1, Moscow, Russia;
[3] Saint-Petersburg State Research Institute of Phthisiopulmonology, Saint-Petersburg, Russia;
[4] Novosibirsk Regional Clinical Oncology Dispensary, Novosibirsk, Russia;
[5] AstraZeneca Pharmaceuticals LLC, Moscow, Russia;
[6] Research and Practical Clinical Center for Diagnostics and Telemedicine Technologies, Moscow, Russia;
[7] Sechenov First Moscow State Medical University, Moscow, Russia

ABSTRACT

BACKGROUND: Lung cancer is the second most common cancer worldwide, accounting for approximately 20% of all cancer-related deaths and having a <10% 5-year survival rate for very late-stage cases. For the prevalent non-small cell lung cancer (NSCLC), recent guidelines advise staging based on the 8th edition of the TNM classification, highlighting the importance of mediastinal lymph node involvement. While noninvasive methods are generally accurate, they often lack sensitivity, and invasive methods may not be suitable for all patients. Advances in deep learning present potential in solving such problems. However, most research focuses on algorithm development more than clinical relevance. Moreover, none of them addressed individual lymph node malignancies, limiting comprehensive analysis and interpretability and leaving clinicians without sufficient means to validate the results effectively.

AIM: To develop a local data-trained and validated algorithm for segmenting each mediastinal lymph node in chest computed tomography (CT) and assessing the probability of its involvement in metastasis.

MATERIALS AND METHODS: Initially, IASLC lymph node stations are segmented, providing a bounding box of the mediastinum for further processing. Next, the image is cropped to this box and passed through a second network to identify and mask all visible lymph nodes. Finally, each detected lymph node is extracted, stacked with its mask, and evaluated by a feed-forward network to determine malignancy probabilities.

RESULTS: The pipeline achieved an average recall and object Dice Score of 0.74±0.01 and 0.53±0.26 for the clinically relevant lymph node segmentation task. Further, it recorded a 0.73 ROC AUC for predicting a patient's N-stage, outperforming traditional size-based criteria.

CONCLUSION: The proposed algorithm enables new research algorithms to optimize the management of patients with nonenlarged intrathoracic lymph nodes, thus improving the quality of medical care for patients with cancer.

Keywords: lung cancer; lymph nodes; medical imaging; deep learning.

Оценка вероятности метастатического поражения лимфатических узлов средостения у пациентов с немелкоклеточным раком лёгкого при использовании свёрточных нейронных сетей для интерпретации данных компьютерной томографии органов грудной клетки

А.Е. Шевцов[1], Я.Д. Томинин[1], В.Д. Томинин[1], В.М. Малеванный[1], Ю.С. Есаков[2], З.Г. Туквадзе[2], А.О. Нефёдов[3], П.К. Яблонский[3], П.В. Гаврилов[3], В.В. Козлов[4], М.Е. Блохина[5], Е.А. Наливкина[5], В.А. Гомболевский[1,7], Ю.А. Васильев[6], М.Н. Дугова[1], В.Ю. Чернина[1], О.В. Омелянская[6], Р.В. Решетников[6], И.А. Блохин[6], М.Г. Беляев[1]

[1] «АЙРА Лабс», Москва, Россия;
[2] Городская клиническая онкологическая больница № 1, Москва, Россия;
[3] Санкт-Петербургский научно-исследовательский институт фтизиопульмонологии, Санкт-Петербург, Россия;
[4] Новосибирский государственный медицинский университет, Новосибирск, Россия;
[5] «АстраЗенека Фармасьютикалз», Москва, Россия;
[6] Научно-практический клинический центр диагностики и телемедицинских технологий, Москва, Россия;
[7] Первый Московский государственный медицинский университет имени И.М. Сеченова, Москва, Россия

АННОТАЦИЯ

Обоснование. Рак лёгкого — второй по распространённости тип рака во всём мире. На данное заболевание приходится приблизительно 20% всех случаев смерти от рака, а пятилетняя выживаемостью на поздних стадиях — менее 10%. Для стадирования немелкоклеточного рака лёгкого, характеризующегося высокой распространённостью, в новейших клинических рекомендациях предлагают использовать классификацию TNM (8-е издание). Это подчёркивает значимость оценки поражения лимфатических узлов средостения. Неинвазивные методы обследования в целом обеспечивают точную оценку, однако часто обладают недостаточной чувствительностью, в то время как инвазивные — могут быть противопоказаны отдельным пациентам. Благодаря совершенствованию технологий глубокого обучения появилась возможность преодолеть эти сложности. Тем не менее в большинстве исследований по данному вопросу основное внимание уделяют разработке алгоритмов, а не клинической значимости результатов. Кроме того, ни в одном из таких исследований не оценивают поражение отдельных лимфатических узлов, что ограничивает возможности комплексного анализа и интерпретацию результатов, а также препятствует их эффективной валидации в клинической практике.

Цель — разработать валидированный алгоритм, обученный на внутренних данных, для сегментации отдельных лимфатических узлов средостения по данным компьютерной томографии органов грудной клетки, а также оценить вероятность их метастатического поражения.

Материалы и методы. Выполнение сегментации групп лимфатических узлов в соответствии с рекомендациями Международной ассоциации по изучению рака лёгкого, чтобы получить ограничивающий прямоугольник для области средостения с целью последующей обработки данных. Затем изображение кадрируют при использовании этого ограничивающего прямоугольника и обрабатывают с помощью второй сети для выявления всех визуализируемых лимфатических узлов и генерации масок. На заключительном этапе выделяют каждый визуализируемый лимфатический узел, применяют соответствующую маску и оценивают с использованием сети прямого распространения, чтобы определить вероятность метастатического поражения.

Результаты. В данной последовательности действий средний отклик и значение Dice Score объекта составили 0,74±0,01 и 0,53±0,26 соответственно для задачи клинически значимой сегментации лимфатических узлов. Кроме того, значение площади под ROC-кривой для прогнозирования степени поражения регионарных лимфатических узлов составило 0,73, что превосходит традиционные критерии, основанные на размере.

Заключение. Предложенный алгоритм обеспечивает оптимизацию лечения пациентов без увеличения внутригрудных лимфатических узлов за счёт новых алгоритмов исследований, что повышает качество медицинского обслуживания пациентов с онкологическими заболеваниями.

Ключевые слова: рак лёгкого; лимфатические узлы; медицинская визуализация; глубокое обучение.

使用卷积神经网络评估非小细胞肺癌患者纵隔淋巴结转移可能性的研究

Alexey E. Shevtsov[1], Iaroslav D. Tominin[1], Vladislav D. Tominin[1], Vsevolod M. Malevanniy[1], Yury S. Esakov[2], Zurab G. Tukvadze[2], Andrey O. Nefedov[3], Piotr K. Yablonskii[3], Pavel V. Gavrilov[3], Vadim V. Kozlov[4], Mariya E. Blokhina[5], Elena A. Nalivkina[5], Victor A. Gombolevskiy[1,7], Yuriy A. Vasilev[6], Mariya N. Dugova[1], Valeria Yu. Chernina[1], Olga V. Omelyanskaya[6], Roman V. Reshetnikov[6], Ivan A. Blokhin[6], Mikhail G. Belyaev[1]

[1] IRA Labs, Moscow, Russia;
[2] Moscow City Clinical Oncological Hospital № 1, Moscow, Russia;
[3] Saint-Petersburg State Research Institute of Phthisiopulmonology, Saint-Petersburg, Russia;
[4] Novosibirsk Regional Clinical Oncology Dispensary, Novosibirsk, Russia;
[5] AstraZeneca Pharmaceuticals LLC, Moscow, Russia;
[6] Research and Practical Clinical Center for Diagnostics and Telemedicine Technologies, Moscow, Russia;
[7] Sechenov First Moscow State Medical University, Moscow, Russia

摘要

背景。肺癌是全球第二大常见癌症，约占所有癌症死亡病例的 20%。其中晚期肺癌的五年生存率不足 10%。对于高发的 非小细胞肺癌（NSCLC），最新临床指南（TNM分类第8版）强调 纵隔淋巴结受累 的评估在分期中的重要性。非侵入性检查方法： 敏感性不足；侵入性检查方法： 某些患者可能存在禁忌；深度学习技术 的发展为克服上述挑战提供了新途径。然而，现有研究大多集中于 算法开发，忽略了 单个淋巴结受累评估的临床意义，限制了其在临床应用中的综合性和有效性。

目的。开发并验证一个基于内部数据训练的算法，通过 胸部CT图像 分割单个纵隔淋巴结，并评估其转移的可能性。

材料与方法。数据分割与处理：按照国际肺癌研究协会建议，对 淋巴结组 进行分割；获取纵隔区域的限制性矩形框，用于后续数据处理。深度学习技术应用：使用第一个神经网络对图像裁剪；使用第二个神经网络识别所有可视淋巴结并生成掩膜；在最后阶段，分离每个可视淋巴结，应用掩膜并利用前馈网络评估其转移的可能性。

结果。分割任务性能：平均响应值为 0.74±0.01；Dice Score 为 0.53±0.26。预测淋巴结转移性能：ROC曲线下面积（AUC）为 0.73；该结果优于基于传统 大小标准 的评估方法。

结论。所提出的算法通过深度学习技术实现了对纵隔淋巴结转移可能性的自动评估，在无显著肿大的淋巴结患者中优化了治疗方案。该方法提升了 肿瘤患者医疗服务的质量，并为淋巴结评估提供了一种有效的非侵入性选择。

关键词：肺癌；淋巴结；医学影像；深度学习。

BACKGROUND

Lung cancer is the second most prevalent cancer globally. In 2018, 2.1 million new lung cancer cases were reported, with 1.8 million deaths, representing approximately 20% of all cancer-related deaths [1]. The 5-year survival rate for early-stage lung cancer is 68%–92%. However, in advanced disease, it drops to <10%, accounting for 42% of lung cancer cases [2]. Thus, an early diagnosis and timely treatment are crucial for improving survival and lowering treatment costs.

Screening examinations are crucial for detecting early-stage lung cancer because they can identify the disease in asymptomatic high-risk patients. These examinations are recommended in patients aged over 50 years who are currently smoking or who have quit smoking within the last 15 years (smoking index ≥20) [3]. Low-dose *computed tomography* (CT) is used to screen for lung pathology because it has been proven effective in multiple randomized prospective studies [6–11]. However, this noninvasive technique, while associated with minimal risks, provides insufficient information.

It is recommended to utilize minimally invasive biopsies or noninvasive positron emission tomography with CT (PET/CT) to acquire initial results [4, 5]. For patients with confirmed lung cancer, staging is crucial for determining the degree of metastasis and selecting the best treatment strategy based on the cancer type.

Recent guidelines recommend using the TNM staging system (8th edition, 2017) for staging non-small cell lung cancer (NSCLC), the most prevalent lung cancer, where *T* indicates the primary tumor size and invasiveness, *N* the degree of spread to thoracic lymph nodes, and *M* represents distant metastasis [12]. This system enables the determination of disease stage based on clinical examination findings (typically prior to surgery, using noninvasive methods), histopathological findings, and repeated staging following treatment.

Since thoracic lymph node involvement is frequent in lung cancer, evaluating regional lymph node involvement is essential for staging the disease and selecting appropriate treatment approaches. Whether aggressive surgery or adjuvant therapy is employed in NSCLC patients depends on the extent of mediastinal lymph node involvement [4, 5]. There are currently two main types of treatment strategies for NSCLC patients:
- Perform PET/CT followed by diagnostic surgery [5, 13, 14];
- Perform diagnostic surgery irrespective of the PET/CT findings [4].

The *National Comprehensive Cancer Network* guidelines recommend *radical surgery* as a preferable therapeutic option in patients with early NSCLC, while *radiotherapy* or *chemotherapy* is considered appropriate for patients with advanced NSCLC [15].

Despite the wide range of approaches for detecting mediastinal lymph node involvement, it can be challenging to confirm or rule out the presence of metastases. Studies performed by Roberts et al. [6] and Kanzaki et al. [17] reveal that compared to histological examination, which is considered the gold standard, the misdiagnosis and false-negative rates are higher when PET/CT is used for detecting lymph node involvement compared with histological examinations. Moreover, PET/CT is not accessible to most patients in remote areas [18]. Diagnostic surgeries, even minimally invasive ones, require anesthesia, which may be contraindicated in some patients. This necessitates the use of noninvasive, cost-effective techniques for predicting mediastinal lymph node involvement in patients with primary NSCLC.

Advancements in *deep learning* technologies make it possible to address these challenges [19]. Published studies have demonstrated encouraging outcomes for single or group lymph node segmentation [20–22]. However, most studies focus on algorithm development rather than on the clinical relevance of the findings. Moreover, to the best of our knowledge, no studies have assessed individual lymph node involvement, which limits the possibilities of integrating and independently validating the findings in clinical practice [23–25].

Determining the extent of lymph node involvement is crucial for administering effective treatment in patients with NSCLC. Clinicians employ two main groups of methods:
- Noninvasive: techniques that do not physically affect the patient's body;
- Invasive: diagnostic surgeries.

Despite their high sensitivity and low rates of post-operative tumor grade changes, invasive techniques necessitate anesthesia and surgical intervention [14, 26]. This calls for more affordable and accessible noninvasive techniques.

Several studies have revealed that this technique has limitations when the short axis diameter is the only parameter for determining the histological status of lymph nodes based on CT or *magnetic resonance imaging* (MRI) findings [27–29]. For example, Brown et al. [27] reported that mesorectal MRI findings do not differentiate between histologically benign (2–10 mm) and malignant (3–15 mm) lymph nodes. The same problem arises in MRI of the head and neck, where the standard threshold of 10 mm yields a sensitivity and specificity of 0.88 and 0.39, respectively [28, 29]. However, additional morphological criteria such as irregular boundaries or mixed signal intensity raise the sensitivity to 0.85 (95% confidence interval [CI]: 0.74–0.92) and specificity to 0.97 (95% CI: 0.95–0.99). Although a recent study identified the classification accuracy for various combinations of criteria, it did not propose a standardized approach [30]. To address this issue, Elsholtz et al. [31] developed the *Node-RADS lymph node assessment system*. It assesses the visible lymph nodes based on their short axis diameter, texture, border, and shape, using five categories. Moreover, it considers other factors such as the anatomical site.

When used with PET, CT with contrast yields precise results. Significant differences ($p < 0.05$) in sensitivity and specificity were observed when ascertaining the degree of lymph node involvement using PET/CT compared to CT with contrast (0.78 and 0.92 vs. 0.56 and 0.73, respectively) [32]. However, this technique is expensive and not available to patients in remote areas [18].

Algorithmic Approach

Mediastinal lymph node segmentation and classification remain unexplored because of the lack of publicly available high-quality datasets. However, several studies have explored the algorithm components proposed in this paper.

Lymph Node Segmentation

Over the last 5–10 years, several approaches to volumetric medical image segmentation have emerged. Some architectures, such as *DeepMedic3D U-Net or V-Net*, provide credible results when assessing publicly available medical image sets [33–37]. The proposed pyramid convolutional neural networks are optimal for lymph node segmentation. Employing fourfold cross-validation, Iuga et al. [21] discovered that the detection rate for large lymph nodes was 0.77; however, the false positive rate was 10.3 per case [21]. Furthermore, this approach has low sensitivity (0.34) for lymph nodes measuring 5–10 mm, with a total Dice Score of 0.44.

Identification of Lymph Node Groups

Iuga et al. [21, 22] used a multiclass classification to analyze the distribution of mediastinal lymph nodes by group, building on their earlier work. Tops-1, -2, and -3 classifications demonstrated high accuracy values of 0.86, 0.94, and 0.96, respectively. Despite these findings, the proposed algorithm lacks sensitivity for critical lymph node groups and only partially meets the recommendations of Goldstraw et al. [2]. In contrast, Guo et al. [20] reported effective segmentation with a Dice score of 0.81 ± 0.06. However, the authors did not ascertain the accuracy of the lymph node distribution and its influence on the extent of regional lymph node involvement.

Classification of lymph node involvement

Previous studies have proposed algorithms for the indirect analysis of mediastinal lymph node involvement using primary tumor image features, without indicating specific groups or individual lymph nodes [23–25]. This is partially due to the difficulties in acquiring precise reference labels. Determining the location of each lymph node on CT images after receiving the biomaterial can be challenging. In this scenario, the simplest solution was to assign labels to each lymph node, similar to the method employed for grading pulmonary nodules. Simple patch-based convolutional neural networks exhibit an area under the ROC curve (AUC) of 0.928 ± 0.027 for classification. Pretraining a convolutional autoencoder for picture fragment reconstruction and employing an encoder as a basis for metastatic classification improves outcomes, with an AUC of 0.936 ± 0.009 [38]. However, using weak supervision, it is possible to establish a shared histological label for many lymph nodes from the same group. Dubost et al. [39] proposed the innovative concept of using a single label for training, with a prognostic map generation when receiving outputs. However, max-pooling can result in the loss of significant information for small targets, such as lymph nodes, limiting the efficacy of their histological status assessment.

AIM

To develop and validate a CT-based algorithm trained on internal data for individual mediastinal lymph node segmentation and to predict the probability of metastasis for each lymph node.

MATERIALS AND METHODS

Study Design

This was an observational, single-center, retrospective study.

Eligibility Criteria

Inclusion criteria:
- Histologically confirmed NSCLC;
- Availability of data acquired using contrast enhanced-chest CT (venous phase), slice thickness ⩽1 mm;
- Presence of a two-month interval between the CT and surgery.

Non-inclusion criteria:
- Lack of data obtained through chest CT with contrast (venous phase) or lymph node biopsy;
- More than two months between the CT and surgery.

Exclusion criteria:
- CT artifacts preventing reliable assessment;
- Low diagnostic value of the biopsy findings.

Study Site

Patients who had undergone chest CT with contrast and thoracic lymph node biopsy were enrolled at the City Clinical Oncology Hospital No. 1 (Moscow).

Intervention

The proposed algorithm for lymph node segmentation and metastasis classification involves a three-stage process:

First stage: identification of lymph node groups and mediastinum segmentation in the region of interest are essential for determining the extent of regional lymph node involvement [12];

Second stage: cropping the input image and segmentation of all visible lymph nodes using a bounding box for the mediastinum;

Third stage: analyzing all identified lymph nodes using a feedforward network to determine the probability of metastasis.

The results provide information on lymph node involvement in specific groups, enabling evaluation of the degree of involvement based on the tumor site. *Subsection 3.1* addresses the segmentation of lymph node groups; *subsection 3.2* examines the segmentation of individual lymph nodes; and *subsection 3.3* discusses the classification of lymph node involvement.

Segmentation of the lymph node groups

In patients with NSCLC, the affected lymph nodes are located in a narrow range (mediastinal area). The anatomical and primary tumor sites dictate the extent of regional lymph node involvement [12]. The *International Association for the Study of Lung Cancer* (IASLC) guidelines recognize ten lymph node groups in the mediastinum [40]. Lymph node groups near the trachea and bronchi are divided into left and right groups. No additional specialized classification system is used for the subcarinal lymph nodes. During diagnostic procedures, biopsies are not typically performed for Groups 1, 8, and 9 lymph nodes. Therefore, they were excluded from this study.

This study used a two-component *U-Net model* for the 3D segmentation of lymph node groups (Fig. 1) [41]. While the first component distinguished between the mediastinum and the background, the second component classified each voxel within the mediastinal mask to a specific lymph node group. Advanced deep learning technologies, such as *ResBlocks*, batch normalization, and *the ReLU activation function*, were used after each convolution, except for the data output [42–44].
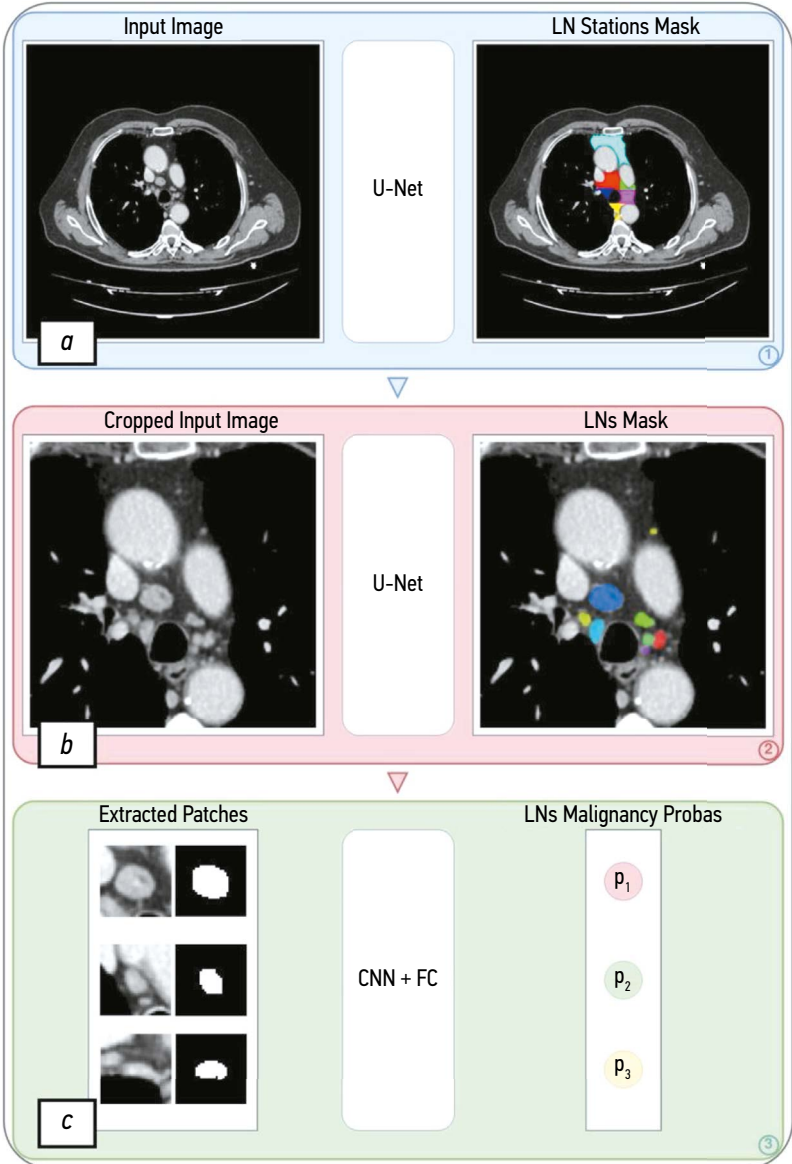
Fig. 1. Three-stage algorithm for lymph node segmentation and metastasis classification: *a*, segmentation of lymph node groups; *b*, image coding based on the bounding box and processing using a second network; *c*, marking each identified lymph node, applying the respective mask, and assessment through a feedforward network. LN, lymph node.

Lymph node segmentation

To preserve computing resources during the second stage, the region of interest should be marked employing the bounding box for the mediastinum obtained in the first stage. If the size in the axial view exceeds 128 pixels, filling is used to achieve the minimal size of 128 pixels.

During this stage, the architecture was comparable to the one used for the segmentation of the lymph node groups. However, it offers a pooled binary data output for a lymph node segmentation prognostic map with more channels and fewer levels (see Fig. 1). This design is adapted to individual lymph nodes that are substantially smaller than the groups; thus, a large receptive field is not required. The design provides for additional characteristics that boost segmentation accuracy.

Classification of lymph node involvement

In weak supervision, a metastasis label is assigned to a lymph node group, and the probability of metastasis for each lymph node is predicted. Lymph nodes are marked on 32×32 image fragments for study purposes. They are merged with respective masks to combine all identified objects in a single dataset. Data is processed using convolutional neural networks with a five-level *ResNet architecture*, followed by max-pooling to minimize spatial dimensions [42]. During the final stage, data is analyzed using the sigmoid and fully connected layers to assess the probability of metastasis for each lymph node.

This is further complicated by the fact that in contrast to benign lymph nodes, metastases might be present or absent in malignant lymph node groups. Thus, a benign lymph node group has no affected lymph nodes, whereas a malignant group must have at least one. To satisfy this requirement, a unique loss function is used. The binary cross-entropy loss function was used for training to assess the probability of metastasis in all benign group lymph nodes. For lymph nodes with metastasis, training is only performed if the prognostic data indicates that is all lymph nodes in this region are benign (see Fig. 1). This method has both advantages and disadvantages.

EXPERIMENT

Data

The publicly available dataset exhibited several limitations [45]:
- It contains inadequate information on the diagnosis and histological status of the mediastinal lymph nodes;
- The groups are not specified, and the annotation only includes lymph nodes with a short axis diameter of >10 mm;
- Contrast-enhanced CT images were likely obtained during the arterial rather than the venous phase.

Thus, a private dataset for 60 patients with confirmed NSCLC who underwent diagnostic surgery to assess specific lymph node groups was used.

The following inclusion criteria were applied to the dataset:
- presence of CT images acquired during the venous contrast phase, which allows the most effective differentiation between the lymph nodes and surrounding structures (particularly blood vessels);
- diagnostic surgery performed within two months after the previous examination, which included the venous phase contrast-enhanced CT images;
- contrast-enhanced CT slice thickness of <1 mm, with eight image series selected for annotation.

Lymph node groups

The same radiologist annotated the lymph node groups, meticulously adhering to the IASLC guidelines for generating prognostic maps for the mediastinum [40]. The annotation protocol required that large blood vessels, such as the aorta, pulmonary trunk, and azygos vein, as well as the esophagus, be differentiated from the lymph node groups (Fig. 2).

Lymph nodes

Two radiologists annotated the mediastinal lymph nodes and assigned binary masks to all the identifiable lymph nodes. If the boundaries between several lymph nodes were uncertain, a single mask was assigned.

Degree of lymph node involvement

Lymph node group involvement was determined based on the outcomes of *video-assisted mediastinoscopic lymphadenectomy* (VAMLA) [14]. A biopsy of the dissected lymph nodes was performed to establish their status. During the final stage, each group was assigned one of the three labels based on the histological examination findings:
- *No data* for lymph node groups that were not resected;
- *benign*;
- *malignant*.

The statistics for the training dataset are presented in Table 1.

Training

All experiments were performed using a standard pre-processing method, with input images amplified to a fixed voxel spacing (1, 1, 1). The CT images were scaled at 0–1 HU for intensity and set to the soft tissue window level (160–240 HU) for window level. Goncharov et al. [46] used a pretrained neural network to crop the input image to match the lung area, then adjusted it to fit the mediastinal area. Given the small dataset, high amplification was used during training, including 10° and 90° rotation, random shifts, and vertical and horizontal flip (Fig. 3).

Segmentation of lymph node groups

The first stage involved training with 30,000 iterations using the *Adam optimizer*, including mixed precision and gradient scaling. The first component was binary cross-entropy with adaptive foreground voxel reweighting. For the second
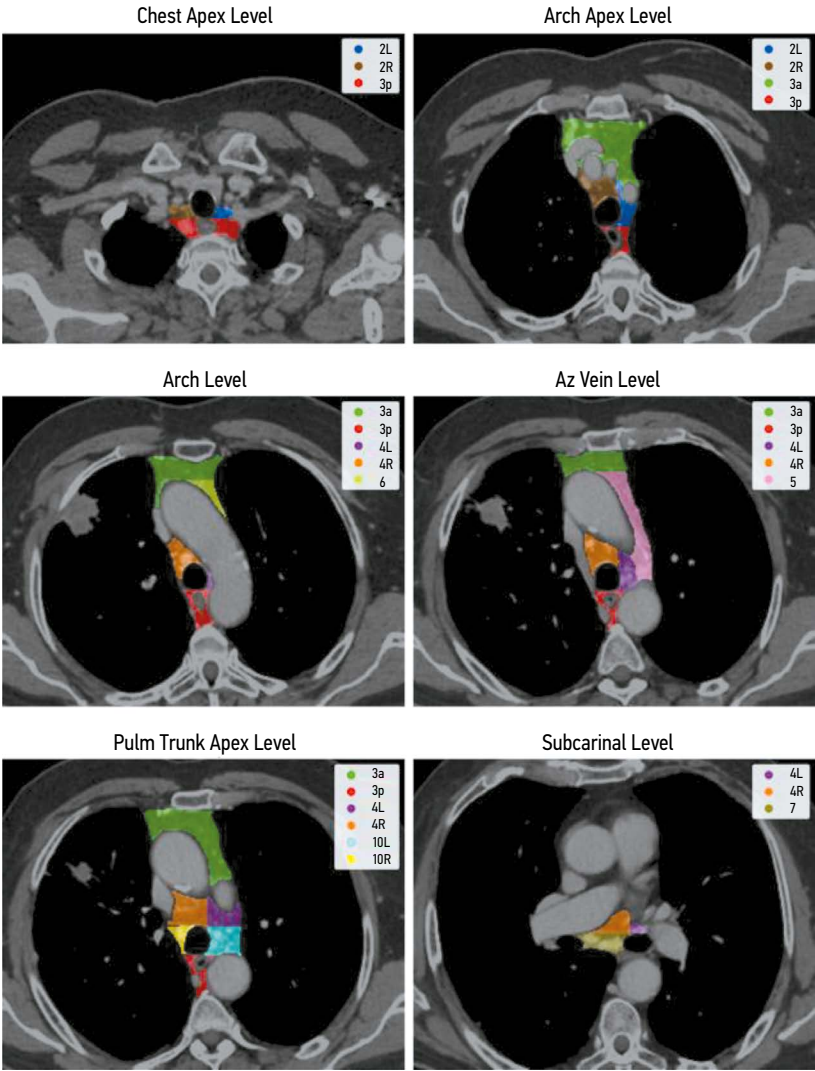
Fig. 2. Example of lymph node group annotation at different mediastinal levels.

Table 1. Training dataset: biopsy findings for the lymph node groups

Lymph node groups	Benign	Malignant	No data
Right low cervical, supraclavicular, and sternal notch nodes	0	0	8
Left low cervical, supraclavicular, and sternal notch nodes	0	0	8
Right upper paratracheal nodes	5	2	1
Left upper paratracheal nodes	3	0	5
Prevascular nodes	0	0	8
Prevertebral (retrotracheal) nodes	0	0	8
Right lower paratracheal nodes	6	2	0
Left lower paratracheal nodes	8	0	0
Subaortic nodes	0	1	7
Paraaortic nodes	0	1	7
Subcarinal nodes	6	1	1
Paraesophageal nodes	0	0	8
Pulmonary ligament nodes	1	0	7
Right hilar nodes	2	2	4
Left hilar nodes	2	1	5

Note. Regional lymph node classification according to the *International Association for the Study of Lung Cancer* (IASLC) guidelines.
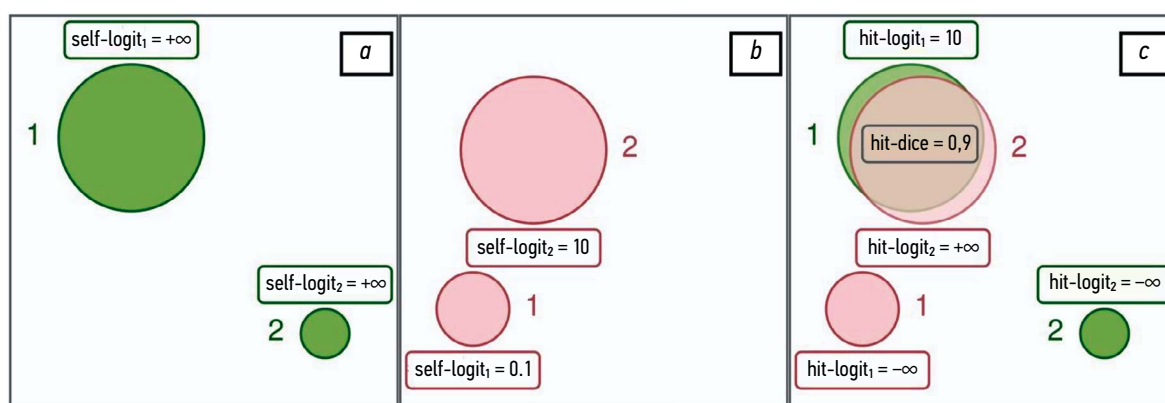
Fig. 3. Example of assigning the assessed statistical parameters to different connected components of the sample mask (*a*) and the respective logit mask (*b*); self-logit and hit-logit, personal statistics for each connected component; hit-dice, shared parameters for a pair of connected components with a positive value (*c*).

component, cross-entropy was employed. Throughout the training, the learning rate remained consistent at 0.003.

Lymph node segmentation

In the second stage, training was performed with 70,000 iterations using the *Adam optimizer*, incorporating mixed precision and gradient scaling. Like the first stage, the second stage was aimed at minimizing the binary cross-entropy and adaptive foreground voxel reweighting. The learning rate was 10^{-3} at the beginning of training and gradually decreased by 3, 3, 2, and 2 times during 5,000, 15,000, 50,000, and 60,000 iterations, respectively.

Classification of lymph node involvement

The classification network was trained with 40,000 iterations using the *Adam optimizer*, with loss minimization using positive class example reweighting (coefficient 100). The learning rate was 3×10^{-5} at the beginning of the training and remained constant throughout the training.

Parameters

To assess the first stage, the accuracy of assigning lymph nodes to respective groups was ascertained, as conventional segmentation parameters were of little relevance in this case. Moreover, prognoses based on the final outcome were assessed for the third stage. Patients with and without metastases had their regional lymph node involvement levels evaluated using the AUC.

FROC method

The *FROC method* developed by Van Ginneken et al. [36] was used to assess the quality of lymph node detection. The FROC curve represents the relationship between the model response to the object (*Y-axis*) and the average false positive rate in the image (*X-axis*).

The FROC curves were plotted employing a sample mask for the entire image (Fig. 3*a*) and the respective logit map, which was converted to binary form using the threshold of 0 to obtain a logit mask (Fig. 3*b*). Both masks were then divided into interconnected components. Each connected component was assigned three statistical parameters:

- *self-logit*: maximum logit value within the connected component; is set to infinity if the connected component is within the sample mask;
- *hit-dice*: maximum Dice score between the selected connected component and another mask (Fig. 3*c*);
- *hit-logit*: the same statistical parameter as *self-logit*; however, it is derived from a connected component within another mask that matches the first mask in terms of the *hit-dice* value; is set to negative infinity if *hit-dice* = 0.

These statistical parameters enable the *hit-logit* value to be used plot an FROC curve by selecting different *l* thresholds. Moreover, the *hit-dice* value was considered when the curve points were obtained to check the hit condition. The hit condition for two connected components was considered to be met if the *hit-dice* value was positive. Thus, for the selected *l* threshold:

- *The false positive value* was defined as the number of connected components within a logit mask with a *self-logit* > *l* threshold, but with *hit-dice* = 0;
- *The true positive value* was defined as the number of connected components within a sample mask with *hit-logit* > *l* threshold and *hit-dice* > 0;
- *The false negative value* was defined as the number of connected components within a sample mask with a *self-logit* ≤ *l* threshold or *hit-dice* = 0.

In experiments, we used *l* thresholds in the range of 0.1 to *max-logit*, where the *max-logit* value is the maximum logit value for the control sample of the predictions.

In contrast to traditional approaches for plotting such curves, this approach ensures uniformity because each connected component within a prognostic mask appears in full or does not appear at all, preventing the separation or merging of the connected components. Given the limited accuracy of the floating point calculations, we used a logit value search instead of using a classical probability search. It allows plotting curves for the whole range, because large logit values can be found with greater accuracy than large probabilities, which are usually rounded to 1.

Table 2. Lymph node detection rates for groups based on the short axis diameter

Group	Mean response	Dice score
d > 0 mm	0.48 ± 0.01	0.53 ± 0.24
d > 5 mm	0.74 ± 0.01	0.53 ± 0.26
d > 10 mm	0.95 ± 0.01	0.56 ± 0.26

Note. d, short axis diameter.

Mean response

The FROC method yields comprehensive analysis results; however, their interpretation can be challenging. We used an additional parameter to simplify and integrate the data derived from the FROC curves. This paper presents the mean values for false positive points in the range of 0 to 5, with an increment of 0.01. Because it identifies a crucial clinical characteristic—the number of detected lesions per case—this method establishes the detection efficacy and functions as the primary quality criterion in this investigation.

Dice Score of an object

The *Dice* score is the most frequently employed approach for analyzing segmentation [37]. However, applying its average value for multiple objects in several images may cause small objects to be obscured by large ones, which is a significant drawback. This paper reveals the average Dice score for an object:

$$objDSC = \sum_{i=1}^{N} \left(\frac{1}{M} \sum_{j=1}^{M} \frac{2 \cdot \left| Y_j \cap \hat{Y}_j \right|}{\left| Y_j \right| + \left| \hat{Y}_j \right|} \right) \quad (1)$$

where N is the number of images in the control sample; M is the number of lesions within the sample mask; Y_j is the set

Table 3. Patient status by the degree of regional lymph node involvement for the maximum short axis diameter; predicted probability of metastasis

Patient	Lymph node involvement	Maximum d, mm	Maximum *p*-value
0	0	11	0.29
1	0	14	0.41
2	+	38	1.00
3	+	14	0.54
4	+	14	0.54
5	0	21	0.83
6	+	15	0.61
7	+	11	0.96

Note. Lymph nodes selected by diameter can differ from the lymph nodes with the highest probability of metastasis. d, short axis diameter.

of voxels associated with the j-th connected component within this mask; and $\hat{Y}_j$ is the respective connected component for the prognostic mask with the greatest hit rate for the Dice Score (DSC).

RESULTS

Lymph Node Segmentation

In the second stage, the parameters for different size ranges are presented:
- All lymph nodes;
- Lymph nodes >5 mm in size: clinically significant according to the guidelines;
- Lymph nodes >10 mm in size: are used as a baseline parameter of potential metastasis [31].

The results are presented in Table 2 and Table 3.

Despite the low detection rate in the first group, the convolutional neural networks demonstrated optimal sensitivity for the highest risk (last) group, as evidenced by a low false positive rate (three per case) (Fig. 4, 5).

Classification of Lymph Node Involvement

The metastasis classification outcomes are consistent with those obtained using a simplified approach, where
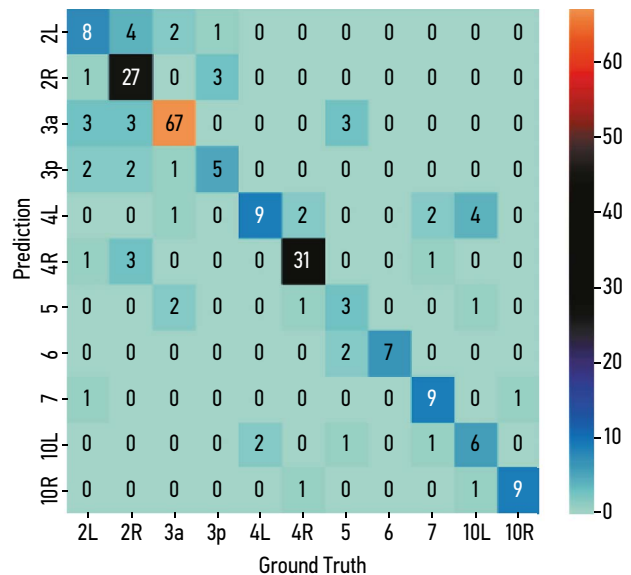
Fig. 4. Accuracy of assigning lymph nodes to groups in accordance with the International Association for the Study of Lung Cancer (IASLC) guidelines.
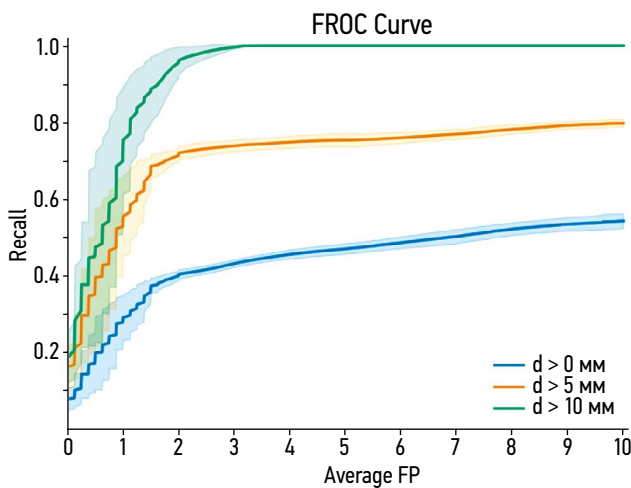
Fig. 5. Detection results during lymph node segmentation. FP, false positive; d, short axis diameter.

a lymph node with the greatest short axis diameter was considered a marker of metastasis. Using a threshold of 10 mm, this straightforward criterion produced three false positive findings. However, the proposed algorithm is more effective than this approach (Fig. 6) because it provided a larger AUC compared to the simplified approach (0.73 vs. 0.53). The Node-RADS classification indicates that lymph nodes with a short axis diameter of >30 mm be definitely considered as lymph nodes with metastasis. The only error was detected in *patient 5*: the selected lymph node had a very high probability of metastasis (Fig. 7).

DISCUSSION

The proposed *loss function* exhibits both advantages and disadvantages. It allows a convolutional neural network to independently determine the relationship between lymph nodes classified as malignant groups, using prior experience
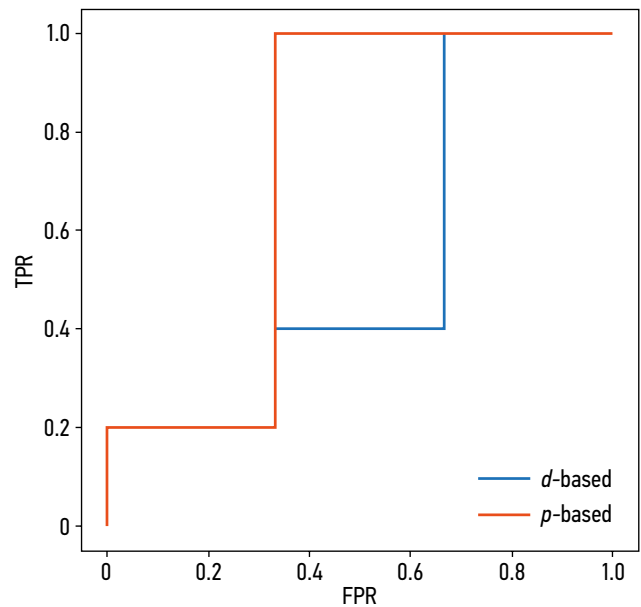
Fig. 6. Comparison of baseline criteria derived from the short axis diameter for predicting patient status regarding the degree of regional lymph node involvement and the proposed algorithm. TPR, true positive rate; FPR, false posi-tive rate; SAD, short axis diameter.

to make modifications. Conversely, it is limited in its capacity to assign respective probabilities to positive class examples because specific information for each lymph node in the malignant group is unavailable. This training method can improve sensitivity but can also increase the false positive rate.

The clinical classification of lymph node locations places stringent requirements on the method. However, its main disadvantage is the *small dataset*, which lacks examples of different lymph nodes with and without metastasis. This is primarily due to the labor- and time-intensive process of establishing the boundaries of the lymph node groups
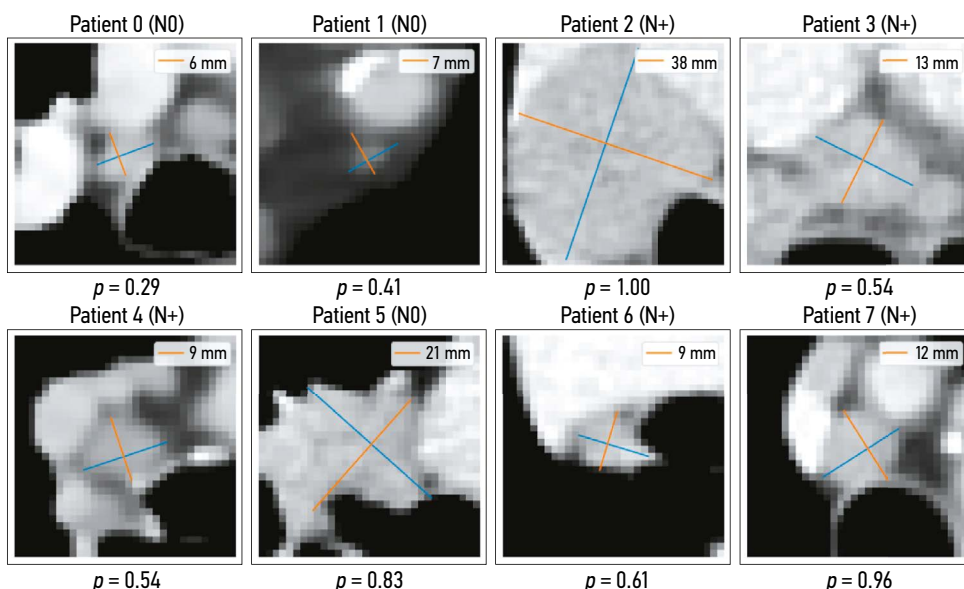
Fig. 7. Lymph nodes with the highest probability of metastasis for each patient. N0, no metastasis; N+, metastasis.

and individual lymph nodes from scratch. For one patient, mapping lymph node groups and individual lymph nodes takes approximately 1 hour and 2–3 hours, respectively. Ambiguous human anatomy criteria further complicate the process, making it unfeasible to establish broad guidelines. Thus, it is essential to augment the efficacy of the algorithm parameters by expanding the training dataset by including new cases of lymph node involvement without enlargement and enlarged lymph nodes without metastasis for each group of thoracic lymph nodes.

Multiphase CT images can significantly boost the capability to determine the degree of lymph node involvement by providing detailed information on each lymph node with and without intravenous contrast enhancement. The venous contrast phase is especially valuable [25]. However, the potential benefits of multiphase CT, including the native (without contrast), arterial, venous, and delayed intravenous contrast phases, are poorly understood. Their assessment can provide further insight into the mechanism of contrast uptake and distribution in the lymph nodes.

CONCLUSION

This paper presents a three-stage algorithm for lymph node segmentation and metastasis classification in patients with NSCLC. Training was conducted using the histological confirmation results for the lymph node groups. The proposed algorithm has an overall response of 0.74 ± 0.01 and a Dice score of 0.53 ± 0.26 for the segmentation of clinically significant lymph nodes (with a short axis diameter of 5 mm). It also has an AUC of 0.73 for predicting patient status regarding the degree of regional lymph node involvement. Thus, the proposed three-stage algorithm is superior to the conventional size-based methods. In enlarged lymph nodes (with a short axis diameter of 10 mm), segmentation was more effective, with an overall response of 0.95 and a Dice score of 0.56. This provides an opportunity for future studies to improve the quality of cancer therapy and the treatment of patients without thoracic lymph node enlargement.

Moreover, the proposed algorithm can be incorporated into the current management protocol for patients with confirmed NSCLC as a transitional step between the initial diagnosis and PET/CT. This algorithm has several potential applications. If the algorithm predicts a low probability of mediastinal lymph node involvement, radical surgery can be considered immediately, eliminating the need for PET/CT and diagnostic surgery. In contrast, if there is a high chance of metastasis, radical surgery is not recommended. In this case, neoadjuvant chemotherapy can be considered without the need for PET/CT and diagnostic surgery. It is anticipated that this algorithm will be more affordable and accessible to patients, even if its accuracy is on par with PET/CT.

ADDITIONAL INFORMATION

REFERENCES

1. Thandra KCh, Barsouk A, Saginala K, et al. Epidemiology of lung cancer. *Contemporary Oncology.* 2021;25(1):45–52. doi: 10.5114/wo.2021.103829

2. Goldstraw P, Chansky K, Crowley J, et al. The IASLC lung cancer staging project: Proposals for revision of the TNM stage groupings in the forthcoming (Eighth) edition of the TNM classification for lung cancer. *J Thorac Oncol.* 2016;11(1):39–51. doi: 10.1016/j.jtho.2015.09.009

3. Tanoue LT, Tanner NT, Gould MK, Silvestri GA. Lung cancer screening. *Am J Respir Crit Care Med.* 2015;191(1):19–33. doi: 10.1164/rccm.201410-1777CI

4. Ettinger DS, Wood DE, Aggarwal C, et al. NCCN guidelines insights: Non-small cell lung cancer, version 1. 2020. *J Natl Compr Canc Netw.* 2019;17(12):1464–1472. doi: 10.6004/jnccn.2019.0059

5. Planchard D, Popat S, Kerr K, et al. Metastatic non-small cell lung cancer: ESMO clin-ical practice guidelines for diagnosis, treatment and follow-up [published correction appears in Ann Oncol. 2019;30(5):863–870. doi: 10.1093/annonc/mdy474]. *Ann Oncol.* 2018;29(Suppl 4):iv192–iv237. doi: 10.1093/annonc/mdy275

6. Heleno B, Siersma V, Brodersen J. Estimation of overdiagnosis of lung cancer in low-dose computed tomography screening: A secondary

analysis of the danish lung cancer screening trial. *JAMA Intern Med.* 2018;178(10):1420–1422. doi: 10.1001/jamainternmed.2018.3056

7. Lopes Pegna A, Picozzi G, Falaschi F, et al. Four-year results of low-dose CT screen-ing and nodule management in the ITALUNG trial. *J Thorac Oncol.* 2013;8(7):866–875. doi: 10.1097/JTO.0b013e31828f68d6

8. Infante M, Cavuto S, Lutman FR, et al. Long-term follow-up results of the DANTE trial, a randomized study of lung cancer screening with spiral computed tomography. *Am J Respir Crit Care Med.* 2015;191(10):1166–1175. doi: 10.1164/rccm.201408-1475OC

9. De Koning H, van der Aalst C, de Jong P. Reduced lung-cancer mortality with vol-ume CT screening in a randomized trial. *N Engl J Med.* 2020;382(6):503–513. doi: 10.1056/NEJMoa1911793

10. Pastorino U, Silva M, Sestini S, et al. Prolonged lung cancer screening reduced 10-year mortality in the MILD trial: new confirmation of lung cancer screening efficacy. *Ann Oncol.* 2019;30(10):1672. doi: 10.1093/annonc/mdz169

11. Baldwin DR, Duffy SW, Wald NJ, et al. UK Lung Screen (UKLS) nodule manage-ment protocol: modelling of a single screen randomised controlled trial of low-dose CT screening for lung cancer. *Thorax.* 2011;66(4):308–313. doi: 10.1136/thx.2010.152066

12. Detterbeck FC, Boffa DJ, Kim AW, Tanoue LT. The eighth edition lung cancer stage classification. *Chest.* 2017;151(1):193–203. doi: 10.1016/j.chest.2016.10.010

13. Nakajima T, Yasufuku K, Yoshino I. Current status and perspective of EBUS-TBNA. *Gen Thorac Cardiovasc Surg.* 2013;61(7):390–396. doi: 10.1007/s11748-013-0224-6

14. Hartert M, Tripsky J, Huertgen M. Video-assisted mediastinoscopic lymphadenecto-my (VAMLA) for staging & treatment of non-small cell lung cancer (NSCLC). *Mediastinum.* 2020;4:3. doi: 10.21037/med.2019.09.06

15. Ettinger DS, Wood DE, Aisner DL, et al. Non-small cell lung cancer, version 5.2017, NCCN clinical practice guidelines in oncology. *J Natl Compr Canc Netw.* 2017;15(4):504–535. doi: 10.6004/jnccn.2017.0050

16. Roberts PF, Follette DM, von Haag D, et al. Factors associated with false-positive staging of lung cancer by positron emission tomography. *Ann Thorac Surg.* 2000;70(4):1154–1160. doi: 10.1016/s0003-4975(00)01769-0

17. Kanzaki R, Higashiyama M, Fujiwara A, et al. Occult mediastinal lymph node metas-tasis in NSCLC patients diagnosed as clinical N0-1 by preoperative integrated FDG-PET/CT and CT: risk factors, pattern, and histopathological study. *Lung Cancer.* 2011;71(3):333–337. doi: 10.1016/j.lungcan.2010.06.008

18. Verduzco-Aguirre HC, Lopes G, Soto-Perez-De-Celis E. Implementation of diagnostic resources for cancer in developing countries: a focus on PET/CT. *Ecancermedical science.* 2019;13:ed87. doi: 10.3332/ecancer.2019.ed87

19. LeCun Y, Bengio Y, Hinton G. Deep learning. *Nature.* 2015;521(7553):436–444. doi: 10.1038/nature14539

20. Guo D, Ye X, Ge J, et al. Deepstationing: thoracic lymph node station parsing in CT scans using anatomical context encoding and key organ auto-search. In: *International Conference on Medical Image Computing and Computer-Assisted Intervention;* 2021 September 27–October 1; Strasbourg. Available from: https://miccai2021.org/openaccess/paperlinks/2021/09/01/140-Paper0015.html

21. Iuga AI, Carolus H, Höink AJ, et al. Automated detection and segmentation of thorac-ic lymph nodes from CT using 3D foveal fully convolutional neural networks. *BMC Med Imaging.* 2021;21(1):69. doi: 10.1186/s12880-021-00599-z

22. Iuga AI, Lossau T, Caldeira LL, et al. Automated mapping and N-staging of thoracic lymph nodes in contrast-enhanced CT scans of the chest using a fully convolutional neural network. *Eur J Radiol.* 2021;139:109718. doi: 10.1016/j.ejrad.2021.109718

23. Zhong Y, Yuan M, Zhang T, et al. Radiomics approach to prediction of occult medi-astinal lymph node metastasis of lung adenocarcinoma. *AJR Am J Roentgenol.* 2018;211(1):109–113. doi: 10.2214/AJR.17.19074

24. Liu Y, Kim J, Balagurunathan Y, et al. Prediction of pathological nodal involvement by CT-based Radiomic features of the primary tumor in patients with clinically node-negative pe-ripheral lung adenocarcinomas. *Med Phys.* 2018;45(6):2518–2526. doi: 10.1002/mp.12901

25. Cong M, Yao H, Liu H, et al. Development and evaluation of a venous computed to-mography radiomics model to predict lymph node metastasis from non-small cell lung cancer. *Medicine (Baltimore).* 2020;99(18):e20074. doi: 10.1097/MD.0000000000020074

26. Gu P, Zhao YZ, Jiang LY, et al. Endobronchial ultrasound-guided transbronchial nee-dle aspiration for staging of lung cancer: a systematic review and meta-analysis. *Eur J Cancer.* 2009;45(8):1389–1396. doi: 10.1016/j.ejca.2008.11.043

27. Brown G, Richards CJ, Bourne MW, et al. Morphologic predictors of lymph node sta-tus in rectal cancer with use of high-spatial-resolution MR imaging with histopathologic comparison. *Radiology.* 2003;227(2):371–377. doi: 10.1148/radiol.2272011747

28. Som PM. Lymph nodes of the neck. Radiology. 1987;165(3):593–600. doi: 10.1148/radiology.165.3.3317494

29. Curtin HD, Ishwaran H, Mancuso AA, et al. Comparison of CT and MR imaging in staging of neck metastases. *Radiology.* 1998;207(1):123–130. doi: 10.1148/radiology.207.1.9530307

30. Loch FN, Asbach P, Haas M, et al. Accuracy of various criteria for lymph node stag-ing in ductal adenocarcinoma of the pancreatic head by computed tomography and magnetic reso-nance imaging. *World J Surg Oncol. 2*020;18(1):213. doi: 10.1186/s12957-020-01951-3

31. Elsholtz FH, Asbach P, Haas M, et al. Introducing the node reporting and data system 1.0 (Node-RADS): a concept for standardized assessment of lymph nodes in cancer Eur Radiol. 2021;31(8):7217. *Eur Radiol.* 2021;31(9):6116–6124. doi: 10.1007/s00330-020-07572-4 Corrected and republished from: Eur Radiol. 2021;31(9): 7217. doi: 10.1007/s00330-021-07795-z

32. Ceylan N, Doğan S, Kocaçelebi K, et al. Contrast enhanced CT versus integrated PET-CT in pre-operative nodal staging of non-small cell lung cancer. *Diagn Interv Radiol.* 2012;18(5):435–440. doi: 10.4261/1305-3825.DIR.5100-11.2

33. Kamnitsas K, Ledig C, Newcombe VF, et al. Efficient multi-scale 3D CNN with fully connected CRF for accurate brain lesion segmentation. *Med Image Anal.* 2017;36:61–78. doi: 10.1016/j.media.2016.10.004

34. Çiçek Ö, Abdulkadir A, Lienkamp SS, et al. 3D U-net: learning dense volumetric segmentation from sparse annotation. In: *Medical Image Computing and Computer-Assisted Inter-vention (MICCAI 2016), Part II: 19th International Conference;* 2016 October 17–21; Athens. P. 424–432.

35. Milletari F, Navab N, Ahmadi SA. V-net: fully convolutional neural networks for volumetric medical image segmentation. In: *2016 Fourth international conference on 3D vision (3DV): proceedings article.* 2016 October 25–28; California. P. 565–571. doi: 10.1109/3DV.2016.79

36. Van Ginneken B, Armato SG, de Hoop B, et al. Comparing and combining algorithms for computer-aided detection of pulmonary nodules in computed tomography scans: the ANODE09 study. *Med Image Anal.* 2010;14(6):707–722. doi: 10.1016/j.media.2010.05.005

37. Bakas S, Reyes M, Jakab A, et al. Identifying the best machine learning algorithms for brain tumor segmentation, progression assessment, and overall survival prediction in the BRATS challenge. *The international multimodal brain tumor segmentation (BraTS) challenge.* 2018. doi: 10.48550/arXiv.1811.02629

38. Silva F, Pereira T, Frade J, et al. Pre-training autoencoder for lung nodule malignancy assessment using CT images. *Applied Sciences.* 2020;10(21):7837. doi: 10.3390/app10217837

39. Dubost F, Adams H, Yilmaz P, et al. Weakly supervised object detection with 2D and 3D regression neural networks. *Med Image Anal.* 2020;65:101767. doi: 10.1016/j.media.2020.101767

40. Rusch VW, Asamura H, Watanabe H, et al. The IASLC lung cancer staging project: a proposal for a new international lymph node map in the forthcoming seventh edition of the TNM classification for lung cancer. *J Thorac Oncol.* 2009;4(5):568–577. doi: 10.1097/JTO.0b013e3181a0d82e

41. Ronneberger O, Fischer P, Brox T. U-net: convolutional networks for biomedical im-age segmentation. In: *Medical Image Computing and Computer-Assisted Intervention (MICCAI 2015): 18th International Conference;* 2015 May; Munich; P. 234–241. doi: 10.48550/arXiv.1505.04597

42. He K, Zhang X, Ren S, Sun J. Deep residual learning for image recognition. In: *Proceedings of the IEEE conference on computer vision and pattern recognition;* 2016 June 27–30; Las Vegas. P. 770–778. doi: 10.48550/arXiv.1512.03385

43. Ioffe S, Szegedy Ch. Batch normalization: accelerating deep network training by re-ducing internal covariate shift. *ArXiv.* 2015;1. doi: 10.48550/arXiv.1502.03167

44. Nair V, Hinton GE. Rectified linear units improve restricted boltzmann machines. In: *Conference: proceedings of the 27th International Conference on Machine Learning (ICML-10);* 2010 June 21–24; Haifa. Available from: https://icml.cc/Conferences/2010/papers/432.pdf

45. Nair V, Hinton GE. Rectified linear units improve restricted boltzmann machines. In: *Conference: proceedings of the 27th International Conference on Machine Learning (ICML-10), June 21–24, 2010.* Haifa, Israel; 2010. P. 807–814.

46. Roth HR, Lu L, Seff A, et al. A new 2.5D representation for lymph node detection using random sets of deep convolutional neural network observations. *Med Image Comput Comput Assist Interv.* 2014;17(1):520–527. doi: 10.1007/978-3-319-10404-1_65

47. Goncharov M, Pisov M, Shevtsov A, et al. CT-based COVID-19 triage: deep multi-task learning improves joint identification and severity quantification. *Med Image Anal.* 2021;71:102054. doi: 10.1016/j.media.2021.102054

СПИСОК ЛИТЕРАТУРЫ

1. Thandra K.Ch., Barsouk A., Saginala K., et al. Epidemiology of lung cancer // Con-temporary Oncology. 2021. Vol. 25, N 1. P. 45–52. doi: 10.5114/wo.2021.103829

2. Goldstraw P., Chansky K., Crowley J., et al. The IASLC lung cancer staging project: Proposals for revision of the TNM stage groupings in the forthcoming (Eighth) edition of the TNM classification for lung cancer // J Thorac Oncol. 2016. Vol. 11, N 1. P. 39–51. doi: 10.1016/j.jtho.2015.09.009

3. Tanoue L.T., Tanner N.T., Gould M.K., Silvestri G.A. Lung cancer screening // Am J Respir Crit Care Med. 2015. Vol. 191, N 1. P. 19–33. doi: 10.1164/rccm.201410-1777CI

4. Ettinger D.S., Wood D.E., Aggarwal C., et al. NCCN guidelines insights: Non-small cell lung cancer, version 1. 2020 // J Natl Compr Canc Netw. 2019. Vol. 17, N 12. P. 1464–1472. doi: 10.6004/jnccn.2019.0059

5. Planchard D., Popat S., Kerr K., et al. Metastatic non-small cell lung cancer: ESMO clinical practice guidelines for diagnosis, treatment and follow-up [published correction appears in Ann Oncol. 2019;30(5):863–870. doi: 10.1093/annonc/mdy474] // Ann Oncol. 2018. Vol. 29, Suppl 4. P. iv192–iv237. doi: 10.1093/annonc/mdy275

6. Heleno B., Siersma V., Brodersen J. Estimation of overdiagnosis of lung cancer in low-dose computed tomography screening: A secondary analysis of the danish lung cancer screening trial // JAMA Intern Med. 2018. Vol. 178, N 10. P. 1420–1422. doi: 10.1001/jamainternmed.2018.3056

7. Lopes Pegna A., Picozzi G., Falaschi F., et al. Four-year results of low-dose CT screening and nodule management in the ITALUNG trial // J Thorac Oncol. 2013. Vol. 8, N 7. P. 866–875. doi: 10.1097/JTO.0b013e31828f68d6

8. Infante M., Cavuto S., Lutman F.R., et al. Long-term follow-up results of the DANTE trial, a randomized study of lung cancer screening with spiral computed tomography // Am J Respir Crit Care Med. 2015. Vol. 191, N 10. P. 1166–1175. doi: 10.1164/rccm.201408-1475OC

9. De Koning H., van der Aalst C., de Jong P. Reduced lung-cancer mortality with vol-ume CT screening in a randomized trial // N Engl J Med. 2020. Vol. 382, N 6. P. 503–513. doi: 10.1056/NEJMoa1911793

10. Pastorino U., Silva M., Sestini S., et al. Prolonged lung cancer screening reduced 10-year mortality in the MILD trial: new confirmation of lung cancer screening efficacy // Ann Oncol. 2019. Vol. 30, N 10. P. 1672. doi: 10.1093/annonc/mdz169

11. Baldwin D.R., Duffy S.W., Wald N.J., et al. UK Lung Screen (UKLS) nodule man-agement protocol: modelling of a single screen randomised controlled trial of low-dose CT screening for lung cancer // Thorax. 2011. Vol. 66, N 4. P. 308–313. doi: 10.1136/thx.2010.152066

12. Detterbeck F.C., Boffa D.J., Kim A.W., Tanoue L.T. The eighth edition lung cancer stage classification // Chest. 2017. Vol. 151, N 1. P. 193–203. doi: 10.1016/j.chest.2016.10.010

13. Nakajima T., Yasufuku K., Yoshino I. Current status and perspective of EBUS-TBNA // Gen Thorac Cardiovasc Surg. 2013. Vol. 61, N 7. P. 390–396. doi: 10.1007/s11748-013-0224-6

14. Hartert M., Tripsky J., Huertgen M. Video-assisted mediastinoscopic lymphadenec-tomy (VAMLA) for staging & treatment of non-small cell lung cancer (NSCLC) // Mediastinum. 2020. Vol. 4. P. 3. doi: 10.21037/med.2019.09.06

15. Ettinger D.S., Wood D.E., Aisner D.L., et al. Non-small cell lung cancer, version 5.2017, NCCN clinical practice guidelines in oncology // J Natl Compr Canc Netw. 2017. Vol. 15, N 4. P. 504–535. doi: 10.6004/jnccn.2017.0050

16. Roberts P.F., Follette D.M., von Haag D., et al. Factors associated with false-positive staging of lung cancer by positron emission tomography // Ann Thorac Surg. 2000. Vol. 70, N 4. P. 1154–1160. doi: 10.1016/s0003-4975(00)01769-0

17. Kanzaki R., Higashiyama M., Fujiwara A., et al. Occult mediastinal lymph node me-tastasis in NSCLC patients diagnosed as clinical N0-1 by preoperative integrated FDG-PET/CT and CT: risk factors, pattern, and histopathological study // Lung Cancer. 2011. Vol. 71, N 3. P. 333–337. doi: 10.1016/j.lungcan.2010.06.008

18. Verduzco-Aguirre H.C., Lopes G., Soto-Perez-De-Celis E. Implementation of diag-nostic resources for cancer in developing countries: a focus on PET/CT // Ecancermedicalscience. 2019. Vol. 13. P. ed87. doi: 10.3332/ecancer.2019.ed87

19. LeCun Y., Bengio Y., Hinton G. Deep learning // Nature. 2015. Vol. 521, N 7553. P. 436–444. doi: 10.1038/nature14539

20. Guo D., Ye X., Ge J., et al. Deepstationing: thoracic lymph node station parsing in CT scans using anatomical context encoding and key organ auto-search. In: International Conference on Medical Image Computing and Computer-Assisted Intervention (MICCAI 2021): 24th International Conference; 2021 September 27–October 1; Strasbourg. Available from: https://miccai2021.org/openaccess/paperlinks/2021/09/01/140-Paper0015.html

21. Iuga A.I., Carolus H., Höink A.J., et al. Automated detection and segmentation of thoracic lymph nodes from CT using 3D foveal fully convolutional neural networks // BMC Med Imaging. 2021. Vol. 21, N 1. P. 69. doi: 10.1186/s12880-021-00599-z

22. Iuga A.I., Lossau T., Caldeira L.L., et al. Automated mapping and N-staging of tho-racic lymph nodes in contrast-enhanced CT scans of the chest using a fully convolutional neural network // Eur J Radiol. 2021. Vol. 139. P. 109718. doi: 10.1016/j.ejrad.2021.109718

23. Zhong Y., Yuan M., Zhang T., et al. Radiomics approach to prediction of occult me-diastinal lymph node metastasis of lung adenocarcinoma // AJR Am J Roentgenol. 2018. Vol. 211, N 1. P. 109–113. doi: 10.2214/AJR.17.19074

24. Liu Y., Kim J., Balagurunathan Y., et al. Prediction of pathological nodal involve-ment by CT-based Radiomic features of the primary tumor in patients with clinically node-negative peripheral lung adenocarcinomas // Med Phys. 2018. Vol. 45, N 6. P. 2518–2526. doi: 10.1002/mp.12901

25. Cong M., Yao H., Liu H., et al. Development and evaluation of a venous computed tomography radiomics model to predict lymph node metastasis from non-small cell lung cancer // Medicine (Baltimore). 2020. Vol. 99, N 18. P. e20074. doi: 10.1097/MD.0000000000020074

26. Gu P., Zhao Y.Z., Jiang L.Y., et al. Endobronchial ultrasound-guided transbronchial needle aspiration for staging of lung cancer: a systematic review and meta-analysis // Eur J Cancer. 2009. Vol. 45, N 8. P. 1389–1396. doi: 10.1016/j.ejca.2008.11.043

27. Brown G., Richards C.J., Bourne M.W., et al. Morphologic predictors of lymph node status in rectal cancer with use of high-spatial-resolution MR imaging with histopathologic compari-son // Radiology. 2003. Vol. 227, N 2. P. 371–377. doi: 10.1148/radiol.2272011747

28. Som P.M. Lymph nodes of the neck // Radiology. 1987. Vol. 165, N 3. P. 593–600. doi: 10.1148/radiology.165.3.3317494

29. Curtin H.D., Ishwaran H., Mancuso A.A., et al. Comparison of CT and MR imaging in staging of neck metastases // Radiology. 1998. Vol. 207, N 1. P. 123–130. doi: 10.1148/radiology.207.1.9530307

30. Loch F.N., Asbach P., Haas M., et al. Accuracy of various criteria for lymph node staging in ductal adenocarcinoma of the pancreatic head by computed tomography and magnetic res-onance imaging // World J Surg Oncol. 2020. Vol. 18, N 1. P. 213. doi: 10.1186/s12957-020-01951-3

31. Elsholtz F.H., Asbach P, Haas M, et al. Introducing the node reporting and data system 1.0 (Node-RADS): a concept for standardized assessment of lymph nodes in cancer. // Eur Radiol. 2021. Vol. 31, N 8. P. 6116–6124. doi: 10.1007/s00330-020-07572-4 Corrected

and republished from: Eur Radiol. 2021. Vol. 31, N 9. P. 7217. doi: 10.1007/s00330-021-07795-z

32. Ceylan N., Doğan S., Kocaçelebi K., et al. Contrast enhanced CT versus integrated PET-CT in pre-operative nodal staging of non-small cell lung cancer // Diagn Interv Radiol. 2012. Vol. 18, N 5. P. 435–440. doi: 10.4261/1305-3825.DIR.5100-11.2

33. Kamnitsas K., Ledig C., Newcombe V.F., et al. Efficient multi-scale 3D CNN with fully connected CRF for accurate brain lesion segmentation // Med Image Anal. 2017. Vol. 36. P. 61–78. doi: 10.1016/j.media.2016.10.004

34. Çiçek Ö., Abdulkadir A., Lienkamp S.S., et al. 3D U-net: learning dense volumetric segmentation from sparse annotation. In: Medical Image Computing and Computer-Assisted Inter-vention (MICCAI 2016), Part II: 19th International Conference; 2016 October 17–21; Athens. P. 424–432.

35. Milletari F., Navab N., Ahmadi S.A. V-net: fully convolutional neural networks for volumetric medical image segmentation. In: 2016 Fourth international conference on 3D vision (3DV): proceedings article. 2016 October 25–28; California. P. 565–571. doi: 10.1109/3DV.2016.79

36. Van Ginneken B., Armato S.G., de Hoop B., et al. Comparing and combining algo-rithms for computer-aided detection of pulmonary nodules in computed tomography scans: the AN-ODE09 study // Med Image Anal. 2010. Vol. 14, N 6. P. 707–722. doi: 10.1016/j.media.2010.05.005

37. Bakas S., Reyes M., Jakab A., et al. Identifying the best machine learning algorithms for brain tumor segmentation, progression assessment, and overall survival prediction in the BRATS challenge // The international multimodal brain tumor segmentation (BraTS) challenge. 2018. doi: 10.48550/arXiv.1811.02629

38. Silva F., Pereira T., Frade J., et al. Pre-training autoencoder for lung nodule malignan-cy assessment using CT images // Applied Sciences. 2020. Vol. 10, N 21. P. 7837. doi: 10.3390/app10217837

39. Dubost F., Adams H., Yilmaz P., et al. Weakly supervised object detection with 2D and 3D regression neural networks // Med Image Anal. 2020. Vol. 65. P. 101767. doi: 10.1016/j.media.2020.101767

40. Rusch V.W., Asamura H., Watanabe H., et al. The IASLC lung cancer staging project: a proposal for a new international lymph node map in the forthcoming seventh edition of the TNM classification for lung cancer // J Thorac Oncol. 2009. Vol. 4, N 5. P. 568–577. doi: 10.1097/JTO.0b013e3181a0d82e

41. Ronneberger O., Fischer P., Brox T. U-net: convolutional networks for biomedical image segmentation. In: Medical Image Computing and Computer-Assisted Intervention (MICCAI 2015): 18th International Conference; 2015 May; Munich; P. 234–241. doi: 10.48550/arXiv.1505.04597

42. He K., Zhang X., Ren S., Sun J. Deep residual learning for image recognition. In: Pro-ceedings of the IEEE conference on computer vision and pattern recognition; 2016 June 27–30; Las Vegas. P. 770–778. doi: 10.48550/arXiv.1512.03385

43. Ioffe S., Szegedy Ch. Batch normalization: accelerating deep network training by re-ducing internal covariate shift. ArXiv, 2015. doi: 10.48550/arXiv.1502.03167

44. Nair V., Hinton G.E. Rectified linear units improve restricted boltzmann machines. In: Conference: proceedings of the 27th

International Conference on Machine Learning (ICML-10); 2010 June 21–24; Haifa. Available from: https://icml.cc/Conferences/2010/papers/432.pdf

45. Nair V, Hinton GE. Rectified linear units improve restricted boltzmann machines. In: Conference: proceedings of the 27th International Conference on Machine Learning (ICML-10), June 21–24, 2010. Haifa, Israel; 2010. P. 807–814.

46. Roth H.R., Lu L., Seff A., et al. A new 2.5D representation for lymph node detection using random sets of deep convolutional neural network observations // Med Image Comput Comput Assist Interv. 2014. Vol. 17, N 1. P. 520–527. doi: 10.1007/978-3-319-10404-1_65

47. Goncharov M., Pisov M., Shevtsov A., et al. CT-based COVID-19 triage: deep multi-task learning improves joint identification and severity quantification // Med Image Anal. 2021. Vol. 71. P. 102054. doi: 10.1016/j.media.2021.102054

AUTHORS' INFO

* Victor A. Gombolevskiy, MD, Cand. Sci. (Medicine);
address: 30 Bolshoy Boulevard, 121205, Moscow;
ORCID: 0000-0003-1816-1315;
eLibrary SPIN: 6810-3279;
e-mail: v.gombolevskiy@ira-labs.com

Alexey E. Shevtsov;
ORCID: 0000-0003-3085-4325;
e-mail: a.shevtsov@ira-labs.com

Iaroslav D. Tominin;
ORCID: 0000-0002-7210-7208;
e-mail: ia.tominin@ira-labs.com

Vladislav D. Tominin;
ORCID: 0000-0001-5678-3452;
e-mail: v.tominin@ira-labs.com

Vsevolod M. Malevannyi;
ORCID: 0009-0005-8804-2102;
e-mail: v.malevanniy@ira-labs.com

Yury S. Esakov, MD, Cand. Sci. (Medicine);
ORCID: 0000-0002-5933-924X;
eLibrary SPIN: 8424-0756;
e-mail: lungsurgery@mail.ru

Zurab G. Tukvadze, MD;
ORCID: 0000-0002-4550-6107;
e-mail: tukvadze.z.med@gmail.com

Andrei O. Nefedov, MD, Cand. Sci. (Medicine);
ORCID: 0000-0001-6228-182X;
eLibrary SPIN: 2365-9458;
e-mail: herurg78@mail.ru

Petr K. Yablonskiy, MD, Dr. Sci. (Medicine), Professor;
ORCID: 0000-0003-4385-9643;
eLibrary SPIN: 3433-2624;
e-mail: glhirurgb2@mail.ru

Pavel Vl. Gavrilov, MD, Cand. Sci. (Medicine);
ORCID: 0000-0003-3251-4084;
eLibrary SPIN: 7824-5374;
e-mail: pbniifrentgen@mail.ru

Vadim V. Kozlov, MD, Cand. Sci. (Medicine);
ORCID: 0000-0003-3211-5139;
eLibrary SPIN: 8045-4286;
e-mail: vadimkozlov80@mail.ru

Maria E. Blokhina, MD;
ORCID: 0009-0002-9008-9485;
e-mail: mariya.blokhina@astrazeneca.com

ОБ АВТОРАХ

* Гомболевский Виктор Александрович, канд. мед. наук;
адрес: Россия, 121205, Москва, Большой б-р, 30 стр. 1;
ORCID: 0000-0003-1816-1315;
eLibrary SPIN: 6810-3279;
e-mail: v.gombolevskiy@ira-labs.com

Шевцов Алексей Евгеньевич;
ORCID: 0000-0003-3085-4325;
e-mail: a.shevtsov@ira-labs.com

Томинин Ярослав Дмитриевич;
ORCID: 0000-0002-7210-7208;
e-mail: ia.tominin@ira-labs.com

Томинин Владислав Дмитриевич;
ORCID: 0000-0001-5678-3452;
e-mail: v.tominin@ira-labs.com

Малеванный Всеволод Михайлович;
ORCID: 0009-0005-8804-2102;
e-mail: v.malevanniy@ira-labs.com

Есаков Юрий Сергеевич, канд. мед. наук;
ORCID: 0000-0002-5933-924X;
eLibrary SPIN: 8424-0756;
e-mail: lungsurgery@mail.ru

Туквадзе Зураб Георгиевич;
ORCID: 0000-0002-4550-6107;
e-mail: tukvadze.z.med@gmail.com

Нефёдов Андрей Олегович, канд. мед. наук;
ORCID: 0000-0001-6228-182X;
eLibrary SPIN: 2365-9458;
e-mail: herurg78@mail.ru

Яблонский Петр Казимирович, д-р мед. наук, профессор;
ORCID: 0000-0003-4385-9643;
eLibrary SPIN: 3433-2624;
e-mail: glhirurgb2@mail.ru

Гаврилов Павел Владимирович, канд. мед. наук;
ORCID: 0000-0003-3251-4084;
eLibrary SPIN: 7824-5374;
e-mail: pbniifrentgen@mail.ru

Козлов Вадим Викторович, канд. мед. наук;
ORCID: 0000-0003-3211-5139;
eLibrary SPIN: 8045-4286;
e-mail: vadimkozlov80@mail.ru

Блохина Мария Евгеньевна;
ORCID: 0009-0002-9008-9485;
e-mail: mariya.blokhina@astrazeneca.com

Elena A. Nalivkina;
ORCID: 0009-0003-5412-9643;
e-mail: elena.nalivkina@astrazeneca.com

Yuryi A. Vasilev, MD, Dr. Sci. (Medicine);
ORCID: 0000-0002-5283-5961;
eLibrary SPIN: 4458-5608;
e-mail: VasilevYA1@zdrav.mos.ru

Mariya N. Dugova, MD;
ORCID: 0009-0004-5586-8015;
e-mail: m.dugova@ira-labs.com

Valeria Yu. Chernina, MD;
ORCID: 0000-0002-0302-293X;
eLibrary SPIN: 8896-8051;
e-mail: v.chernina@ira-labs.com

Olga V. Omelyanskaya;
ORCID: 0000-0002-0245-4431;
eLibrary SPIN: 8948-6152;
e-mail: OmelyanskayaOV@zdrav.mos.ru

Roman Vl. Reshetnikov, Cand. Sci. (Physics and Mathematics);
ORCID: 0000-0002-9661-0254;
eLibrary SPIN: 8592-0558;
e-mail: reshetnikov@fbb.msu.ru

Ivan A. Blokhin, MD, Cand. Sci. (Medicine);
ORCID: 0000-0002-2681-9378;
eLibrary SPIN: 3306-1387;
e-mail: BlokhinIA@zdrav.mos.ru

Mikhail G. Belyaev, Cand. Sci. (Physics and Mathematics);
ORCID: 0000-0001-9906-6453;
eLibrary SPIN: 2406-1772;
e-mail: belyaevmichel@gmail.com

Наливкина Елена Александровна;
ORCID: 0009-0003-5412-9643;
e-mail: elena.nalivkina@astrazeneca.com

Васильев Юрий Александрович, д-р мед. наук;
ORCID: 0000-0002-5283-5961;
eLibrary SPIN: 4458-5608;
e-mail: VasilevYA1@zdrav.mos.ru

Дугова Мария Николаевна;
ORCID: 0009-0004-5586-8015;
e-mail: m.dugova@ira-labs.com

Чернина Валерия Юрьевна;
ORCID: 0000-0002-0302-293X;
eLibrary SPIN: 8896-8051;
e-mail: v.chernina@ira-labs.com

Омелянская Ольга Васильевна;
ORCID: 0000-0002-0245-4431;
eLibrary SPIN: 8948-6152;
e-mail: OmelyanskayaOV@zdrav.mos.ru

Решетников Роман Вламидимирович, канд. физ.-мат. наук;
ORCID: 0000-0002-9661-0254;
eLibrary SPIN: 8592-0558;
e-mail: reshetnikov@fbb.msu.ru

Блохин Иван Андреевич, канд. мед. наук;
ORCID: 0000-0002-2681-9378;
eLibrary SPIN: 3306-1387;
e-mail: BlokhinIA@zdrav.mos.ru

Беляев Михаил Геннадьевич, канд. физ.-мат. наук;
ORCID: 0000-0001-9906-6453;
eLibrary SPIN: 2406-1772;
e-mail: belyaevmichel@gmail.com

_____

* Corresponding author / Автор, ответственный за переписку

Challenges and benefits of using texture analysis of computed tomography and magnetic resonance imaging scans in diagnosis of bladder cancer

Anastasia A. Kovalenko[1], Valentin E. Sinitsyn[2,3], Victor S. Petrovichev[4]

[1] Central Clinical Hospital of the Management Affair, Moscow, Russia;
[2] Research and Practical Clinical Center for Diagnostics and Telemedicine Technologies, Moscow, Russia;
[3] Lomonosov Moscow State University, Moscow, Russia;
[4] National Medical Research Centre "Treatment and Rehabilitation Centre", Moscow, Russia

ABSTRACT

Radiomics and texture analysis is a new step in the evaluation of digital medical images using specialized software and quantitative assessment of signs invisible to the eye. The textural parameters obtained through mathematical transformations correlate with morphological, molecular, and genotypic characteristics of the examined area.

This article reviews scientific studies on challenges and benefits of using texture analysis in diagnosis of bladder cancer. The authors describe the practical value of this approach, and consider the challenges and potential of using it. Forty publications published between 2016 and 2024 were selected using keywords from PubMed and Google Scholar.

Multiple studies demonstrate high accuracy of radiomics in local staging of bladder cancer, morphologic assessment of the tumor, and prediction of long-term clinical outcomes.

Therefore, texture analysis of medical images can provide additional information to diagnose bladder cancer in uncertain cases. Standardization of the method is currently one of the key issues to accelerate implementation of radiomics analysis in clinical practice.

Keywords: radiomics; texture analysis; bladder cancer; magnetic resonance imaging; computed tomography.

Трудности и перспективы применения текстурного анализа компьютерно-томографических и магнитно-резонансных изображений в диагностике рака мочевого пузыря

А.А. Коваленко[1], В.Е. Синицын[2,3], В.С. Петровичев[4]

[1] Центральная клиническая больница с поликлиникой, Москва, Россия;

[2] Научно-практический клинический центр диагностики и телемедицинских технологий, Москва, Россия;

[3] Московский государственный университет имени М.В. Ломоносова, Москва, Россия;

[4] Национальный медицинский исследовательский центр «Лечебно-реабилитационный центр», Москва, Россия

АННОТАЦИЯ

Радиомика и текстурный анализ — новый шаг в изучении цифровых медицинских изображений, основанный на использовании специализированного программного обеспечения и количественной оценки невидимых глазу показателей. Извлекаемые путём математических преобразований текстурные показатели коррелируют с морфологическими, молекулярными и генотипическими характеристиками исследуемой области.

В настоящей статье проведён обзор научных исследований, посвящённых возможностям и трудностям применения текстурного анализа в диагностике рака мочевого пузыря. Авторами описана практическая значимость данного метода, рассмотрены сложности и перспективы его использования. С помощью поисковых систем PubMed и Google Scholar по ключевым словам отобраны 40 публикаций, изданных за период с 2016 по 2024 гг.

Результаты многочисленных исследований демонстрируют высокую точность радиомики в местном стадировании рака мочевого пузыря, оценке морфологической картины опухоли и прогнозировании отдалённых клинических исходов.

Таким образом, текстурный анализ медицинских изображений способен предоставить дополнительную информацию в диагностике рака мочевого пузыря в неоднозначных клинических случаях. Сегодня стандартизация метода является одной из ключевых задач для ускорения внедрения радиомического анализа в клиническую практику.

Ключевые слова: радиомика; текстурный анализ; рак мочевого пузыря; магнитно-резонансная томография; компьютерная томография.

计算机断层扫描和磁共振图像纹理分析在膀胱癌诊断中的应用困难与前景

Anastasia A. Kovalenko[1], Valentin E. Sinitsyn[2,3], Victor S. Petrovichev[4]

[1] Central Clinical Hospital of the Management Affair, Moscow, Russia;

[2] Research and Practical Clinical Center for Diagnostics and Telemedicine Technologies, Moscow, Russia;

[3] Lomonosov Moscow State University, Moscow, Russia;

[4] National Medical Research Centre "Treatment and Rehabilitation Centre", Moscow, Russia

摘要

放射组学和纹理分析是基于专用软件和对肉眼不可见指标定量评估的数字医学图像研究的一个新阶段。通过数学变换提取的纹理指数与所研究区域的形态、分子和基因型特征相关。

本文对纹理分析在膀胱癌诊断中的可能性和困难的科学研究进行了概述。作者描述了该方法的实际意义，分析了其使用的困难和前景。利用PubMed和Google Scholar搜索引擎，使用关键词筛选出从2016年至2024年期间发表的40篇文章。

大量研究结果显示，放射组学在膀胱癌的局部分期、肿瘤形态学图像评估和远期临床结果预测方面具有很高的准确性。

由此可见，医学图像的纹理分析能在不明确的临床病例中为膀胱癌的诊断提供额外的信息。如今，方法的标准化是放射组学分析加速推广到临床实践中的关键任务之一。

关键词：放射组学；纹理分析；膀胱癌；磁共振成像；计算机断层扫描。

DIFFICULTIES IN DIAGNOSING BLADDER CANCER WITH CONVENTIONAL IMAGING AND THE ROLE OF RADIOMICS

Accurately *predicting muscle invasion* is essential for determining an appropriate treatment approach. Magnetic resonance imaging (MRI) with intravenous contrast serves a critical role in the noninvasive diagnosis and staging of bladder cancer. The Vesical Imaging-Reporting and Data System (VI-RADS) is a standardized framework widely applied for interpreting MRI findings during local staging of bladder cancer [1].

Despite advances in multiparameter imaging and enhanced imaging techniques, assessing the extent of local disease remains difficult. Staging tumors based on MRI findings is particularly challenging when the lesion is located in the bladder trigone, urethral neck, or urethral orifice due to the complex anatomy of these regions. Patients classified as VI-RADS 3 present the greatest uncertainty regarding tumor grade. For instance, morphological assessments in this group revealed absence of muscle invasion in 53% of cases and presence of muscle invasion in 47% [2].

The reliability of morphological evaluations obtained through invasive diagnostic procedures heavily depends on the quality of transurethral resection (TUR) of the tumor. Incomplete resection and coagulation-related tissue damage during TUR contribute to the risk of understanding. A systematic review reported that up to 32% of patients experienced disease upstaging and were subsequently diagnosed with muscle invasion following repeat [3]. Furthermore, up to 50% of specimens collected after an initial TUR lacked a muscle layer [2].

The tumor risk category, which partially relies on tumor grade, guides the selection of adjuvant chemotherapy regimens for non-muscle-invasive bladder cancer.

Texture analysis (TA) has emerged as a promising method to enhance the accuracy of bladder cancer staging and address limitations associated with conventional invasive and noninvasive diagnostic approaches.

PROCEDURE AND PRACTICAL ASPECTS OF TEXTURE ANALYSIS

TA is a technique for postprocessing digital medical images that utilizes specialized software to extract texture features (TFs). Several TA software programs have been developed, including *PyRadiomics*, *MaZda*, *MATLAB*, *3D Slicer*, and *LIFEx*.

TA involves a sequence of stages:
- Stage 1: acquisition of medical images and storage in the Digital Imaging and Communications in Medicine format
- Stage 2: selection of the region of interest (ROI) and image segmentation
- Stage 3: extraction of TFs
- Stage 4: statistical analysis using predictive models followed by model testing [4]

Segmentation may be performed manually, semi-automatically, or automatically and can involve either a single slice (2D ROI) or the entire region of interest (3D ROI). The extracted TFs and study outcomes are closely influenced by image quality and segmentation accuracy. The presence of artifacts or specific morphological features (such as calcifications, hemorrhages, or coagulation areas) within the ROI, or analysis extending beyond the ROI, can affect the results [5].

Image preprocessing is an intermediate step between segmentation and TF extraction. This optional process is intended to homogenize images, which is particularly important when dealing with heterogeneous datasets resulting from the use of different imaging equipment and parameters. A wide range of image preprocessing techniques is available. The most commonly used methods include the following [5]:
- Interpolation to achieve isotropic voxels
- Intensity level filtering
- Sampling of cell (bin) number and width
- Application of various filters (such as Laplace–Gaussian and wavelet filters)

Image preprocessing plays a crucial role in standardizing and enhancing the reproducibility of TFs [6–8].

The extracted TFs are generally categorized into several groups. *First-order features* refer to histogram-based characteristics that describe the distribution of voxel intensities within an image. These include kurtosis, entropy, skewness, intensity, skewness ratio, and uniformity. *Second-order features* are derived from the relationships between voxels within the ROI and describe the spatial distribution of gray-level intensities, using matrices such as the Gray-Level Run Length Matrix, Gray-Level Zone Length Matrix, Gray-Level Co-Occurrence Matrix, and Neighborhood Gray-Level Difference Matrix. *Higher-order features* are based on specific mathematical transformations, such as wavelet filtering and Fourier transforms [4].

In clinical practice, TA is applied across various imaging modalities, including computed tomography (CT), PET/CT, X-ray, MRI, and ultrasound. Most studies have investigated the role of radiomics in cancer management for the following objectives [5]:
- Identifying the type of neoplasm (benign or malignant)
- Evaluating the tumor's morphological and biological characteristics (grade, invasiveness)
- Comparing the tumor's texture profile with its genetic profile (radiogenomics)
- Monitoring the response to treatment

Most researchers agree that TA can enhance the effectiveness of localization diagnosis in cancer. Combined predictive models that incorporate TFs along with clinical, laboratory, genetic, and histological data can support personalized patient assessments [9, 10].

TA, similar to a virtual biopsy, is used to assess tissue heterogeneity [11, 12]. However, traditional biopsy assesses heterogeneity in a specific anatomical site, which may offer limited diagnostic value due to the low number of sampled cells. In contrast, radiomics enables noninvasive analysis of the entire tumor. Additionally, radiomics can help predict overall survival and treatment response [13–16].

TEXTURE ANALYSIS OF MRI IMAGES FOR BLADDER CANCER DIAGNOSIS

In recent years, radiomics has been increasingly applied to the interpretation of MRI findings and the identification of new characteristics and clinically relevant data in bladder cancer. Most published studies on radiomics in bladder cancer focus on identifying TFs that can predict muscle invasion and tumor grade. A three-dimensional ROI (3D ROI) is the preferred segmentation approach among most researchers. The findings of key studies on the TA of MRI images in bladder cancer are summarized in Appendix 1.

Radiomics shows greater effectiveness in bladder cancer diagnosis when combined models incorporating TFs, clinical (morphological) variables, and data from multiple MRI sequences are used [17–19]. For instance, Xu et al. conducted TA on three MRI sequences: T2-weighted imaging (T2WI), diffusion-weighted imaging (DWI), and apparent diffusion coefficient (ADC) maps. Their analysis demonstrated that a model integrating T2WI and DWI TFs was the most effective in distinguishing muscle-invasive from non-muscle-invasive bladder cancer, achieving an area under the curve (AUC) of 0.98, accuracy of 96.3%, sensitivity of 92.6%, and specificity of 100% [18]. Subsequently, Xu et al. reported that combining TUR results with TFs further increased the sensitivity for predicting muscle invasion to 0.96 [17].

Published data indicate that final predictive models capable of differentiating muscle invasion and tumor grade generally incorporate both first- and second-order TFs [20, 21]. However, some studies have concentrated exclusively on histogram features as key TFs [22–24].

Razik et al. reported that only two first-order features— the mean value of positive pixels and kurtosis—extracted from non-preprocessed images were effective in distinguishing high-grade from low-grade tumors. Contrary to expectations, no predictive features were identified when using Laplace–Gaussian filters. Additionally, the study did not identify any TFs capable of differentiating muscle-invasive from non-muscle-invasive bladder cancer. Possible explanations include the use of two-dimensional (2D) segmentation, analysis limited to ADC images, a small sample size (40 observations), standardized machine learning classifiers, and variability in MRI scanners and study protocols [24].

Segmentation can be performed using various methods. Zheng et al. were the first to segment both the tumor and its base. A 3D analysis of T2WI identified 23 discriminative features distinguishing muscle-invasive

from non-muscle-invasive bladder cancer, with 10 (43%) of these features in the tumor base. The AUC for the training and test samples was 0.913 and 0.874, respectively. When tumor size (a morphological parameter) was added to the TFs, the AUC slightly improved to 0.922 and 0.876, respectively [21].

Lim et al. assessed data from 36 patients to compare the effectiveness of T2WI and ADC TA for local disease staging. Notably, the study employed two 2D segmentation approaches: the tumor and the adjacent paravesical fat [23]. Multivariate regression analysis showed that entropy was the only feature with significant differences between ≤T2 and ≥T3 tumors, as well as between T1 and ≥T2 tumors. Unlike the findings of Razik et al., the agreement rates for TFs in this study were not influenced by the use of Laplace–Gaussian filters. The authors concluded that entropy correlates directly with tumor heterogeneity and aggressiveness and that TA can be applied for local staging of bladder cancer. Limitations of the study included MRI scans performed on all patients after TUR, as well as variations in magnetic field strength between the scanners (1.5 and 3 T) [23].

TEXTURE ANALYSIS OF CT IMAGES FOR BLADDER CANCER DIAGNOSIS

The role of CT in assessing the extent of tumor spread beyond the bladder is limited. CT scans remain primarily used for detecting distant metastases. However, some recent large studies have explored the application of TA in diagnosing bladder cancer.

Cui et al. used TFs from the venous phase as prognostic markers for muscle-invasive bladder cancer. The study included data from 188 patients, divided into training and test samples. The accuracy of the model was 0.98 [25].

Similarly, Zhang et al. assessed 196 CT scans during the nephrographic phase. The authors used axial scans for 3D segmentation, selecting the largest tumor for analysis when multiple tumors were present. A total of 851 TFs were extracted for each tumor. Ultimately, 12 first-order (*original_shape_Sphe-ricity, original_shape_Elongation, original_shape_Least-AxisLength*) and second-order TFs were chosen for the models. The authors concluded that the risk of muscle invasion was higher in spherical tumors. Three models were developed: clinical, radiomics, and combined. The combined model was the most accurate for predicting muscle invasion, with an AUC of 0.89, whereas the radiomics model also performed well, with an AUC of 0.85. The combined model incorporated radiomic attributes (RadScore) and tumor grade (high-grade/low-grade) [26].

In contrast to previous studies, Ren et al. investigated the potential of radiomics analysis of CT urograms, alongside excretory phase evaluation. The authors analyzed 296 images after preprocessing with a fixed voxel size ($1 \times 1 \times 1$ mm^3) and pixel size scaling to 0.1. The artificial neutral network-based model showed a sensitivity of 0.89 and specificity of 0.93 in diagnosing muscle-invasive bladder cancer [27].

Jing et al. conducted multiphase TA of 204 thick-slice CT scans. The authors used 54 features from the native, corticomedullary, and nephrographic phases (8 first-order features, 3 shape features, and 43 second-order features) to differentiate between low-grade and high-grade bladder cancer, achieving an AUC of 0.79, accuracy of 0.71, sensitivity of 0.68, and specificity of 0.73. Additionally, three models were developed based on the analysis of each phase individually, with the following results: AUCs of 0.70, 0.74, and 0.75 for the native, corticomedullary, and nephrographic phases, respectively. To enhance efficacy, the authors created a combined clinical and radiomics model, which outperformed the radiomics-only model (AUC 0.90, accuracy 0.79, sensitivity 0.81, specificity 0.77). Based on logistic regression, the combined model included two independent predictors of bladder cancer grade: the patient's age and RadScore. Limitations of the study included the use of thick CT slices (5–6 mm) and the absence of image preprocessing, which could have led to lower AUC values in models based solely on TFs [28].

TEXTURE ANALYSIS FOR PREDICTING RESPONSE TO TREATMENT AND LONG-TERM OUTCOMES IN PATIENTS WITH BLADDER CANCER

Despite advancements in endoscopic imaging (such as photodynamic diagnosis and narrow-band imaging) and improved surgical methods, the prognosis for patients following cystectomy remains poor, with an overall 5-year survival rate of about 60% [29].

Two models are commonly used to assess the risk of relapse and progression in non-muscle-invasive bladder cancer after a macroscopically complete TUR. These are the European Organization for Research and Treatment of Cancer and Club Urologico Español de Tratamiento Oncologico (CUETO) [30, 31] classifications. However, these models, which rely on clinical and histological parameters, have limitations, such as low discriminative ability for predicting relapses and a tendency to overestimate risk.

Currently, there is no reliable method for predicting the response to neoadjuvant chemotherapy (NACT) before or during treatment.

These issues highlight the need for research into radiomics as a novel approach for assessing clinical outcomes in bladder cancer. Identifying up-to-date prognostic markers is crucial for more accurately selecting patients likely to respond to NACT, particularly due to the high toxicity of *cisplatin*, a chemotherapy drug recommended for treatment.

Several studies have explored the potential of TA in monitoring therapy [32, 33]. Cha et al. were the first to investigate the use of radiomics to predict the response to NACT in bladder cancer. The authors analyzed CT scans from 82 patients before and after three chemotherapy cycles, with the model achieving an accuracy of 0.7. Although the analysis was based on follow-up CT scans after three chemotherapy cycles, the authors suggest that trained models could be applied at any clinically significant time point to facilitate timely treatment adjustments or discontinuation, before toxic effects occur [34].

Cai et al. developed a nomogram to predict relapse-free survival in patients after partial or complete cystectomy. The study included data from 80 MRI scans, analyzing four MRI sequences (T2WI, DWI, ADC, and post-contrast images) [35].

LIMITATIONS, CHALLENGES, AND PROSPECTS FOR RADIOMICS

The absence of a standardized and unified workflow hinders the broader clinical application of TA [34, 36]. A study assessing the reproducibility of MRI TFs found that the preprocessing settings needed for reliable feature extraction may vary depending on the MRI sequence [37].

Segmentation is a crucial and debated aspect of radiomics. Semi-automatic segmentation is generally preferred over manual segmentation due to its better reproducibility of TFs and faster analysis time. The reproducibility of segmentation is mainly influenced by the tumor type and location [38].

The reproducibility of specific TFs or groups of TFs can differ based on the image standardization method used [39].

TF agreement rates can vary by software, which limits the interchangeability of software tools. Specialized software packages may be designed to analyze specific pixel ranges or tissue types; therefore, images outside the defined analysis framework may not accurately reflect the tissue texture [40].

CONCLUSION

Radiomics is an emerging noninvasive diagnostic tool. In urologic oncology, it shows promise for local disease staging, tumor grade assessment, and long-term prognosis. However, before routine clinical implementation, multicenter randomized studies are necessary.

ADDITIONAL INFORMATION

REFERENCES

1. Panebianco V, Narumi Y, Altun E, et al. Multiparametric Magnetic Resonance Imaging for Bladder Cancer: Development of VI-RADS (Vesical Imaging-Reporting And Data System). *European Urology.* 2018;74(3):294–306. doi: 10.1016/j.eururo.2018.04.029

2. Wang Z, Shang Y, Luan T, et al. Evaluation of the value of the VI-RADS scoring system in assessing muscle infiltration by bladder cancer. *Cancer Imaging.* 2020;20(1):26. doi: 10.1186/s40644-020-00304-3

3. Cumberbatch MGK, Foerster B, Catto JWF, et al. Repeat Transurethral Resection in Non-muscle-invasive Bladder Cancer: A Systematic Review. *European Urology.* 2018;73(6):925–933. doi: 10.1016/j.eururo.2018.02.014

4. Parekh V, Jacobs MA. Radiomics: a new application from established techniques. *Expert Review of Precision Medicine and Drug Development.* 2016;1(2):207–226. doi: 10.1080/23808993.2016.1164013

5. van Timmeren JE, Cester D, Tanadini-Lang S, et al. Radiomics in medical imaging-»how-to» guide and critical reflection. *Insights Imaging.* 2020;11:91. doi: 10.1186/s13244-020-00887-2

6. Bologna M, Corino V, Mainardi L. Technical Note: Virtual phantom analyses for preprocessing evaluation and detection of a robust feature set for MRI-radiomics of the brain. *Medical Physics.* 2019;46(11):5116–5123. doi: 10.1002/mp.13834

7. Moradmand H, Aghamiri SMR, Ghaderi R. Impact of image preprocessing methods on reproducibility of radiomic features in multimodal magnetic resonance imaging in glioblastoma. *Journal of Applied Clinical Medical Physics.* 2020;21(1):179–190. doi: 10.1002/acm2.12795

8. Shafiq-ul-Hassan M, Zhang GG, Latifi K, et al. Intrinsic dependencies of CT radiomic features on voxel size and number of gray levels. *Medical Physics.* 2017;44(3):1050–1062. doi: 10.1002/mp.12123

9. Li X, Ma Q, Tao C, et al. A CT-based radiomics nomogram for differentiation of small masses (< 4 cm) of renal oncocytoma from clear cell renal cell carcinoma. *Abdom Radiol.* 2021;46(11):5240–5249. doi: 10.1007/s00261-021-03213-6

10. Chu LC, Park S, Soleimani S, et al. Classification of pancreatic cystic neoplasms using radiomic feature analysis is equivalent to an experienced academic radiologist: a step toward computer-augmented diagnostics for radiologists. *Abdom Radiol.* 2022;47(12):4139–4150. doi: 10.1007/s00261-022-03663-6

11. Marusyk A, Janiszewska M, Polyak K. Intratumor Heterogeneity: The Rosetta Stone of Therapy Resistance. *Cancer Cell.* 2020;37(4):471–484. doi: 10.1016/j.ccell.2020.03.007

12. Mayerhoefer ME, Materka A, Langs G, et al. Introduction to Radiomics. *Journal of Nuclear Medicine.* 2020;61(4):488–495. doi: 10.2967/jnumed.118.222893

13. Yip SSF, Aerts HJWL. Applications and limitations of radiomics. *Phys. Med. Biol.* 2016;61(13):R150. doi: 10.1088/0031-9155/61/13/R150

14. Wang J, Shen L, Zhong H, et al. Radiomics features on radiotherapy treatment planning CT can predict patient survival in locally advanced rectal cancer patients. *Scientific Reports.* 2019;9:15346. doi: 10.1038/s41598-019-51629-4

15. Oikonomou A, Khalvati F, Tyrrell PN, et al. Radiomics analysis at PET/CT contributes to prognosis of recurrence and survival in lung cancer treated with stereotactic body radiotherapy. *Scientific Reports.* 2018;8:4003. doi: 10.1038/s41598-018-22357-y

16. Horvat N, Veeraraghavan H, Khan M, et al. MR Imaging of Rectal Cancer: Radiomics Analysis to Assess Treatment Response after Neoadjuvant Therapy. *Radiology.* 2018;287(3):833–843. doi: 10.1148/radiol.2018172300

17. Xu S, Yao Q, Liu G, et al. Combining DWI radiomics features with transurethral resection promotes the differentiation between muscle-invasive bladder cancer and non-muscle-invasive bladder cancer. *European Radiology.* 2020;30:1804–1812. doi: 10.1007/s00330-019-06484-2

18. Xu X, Zhang X, Tian Q, et al. Quantitative Identification of Nonmuscle-Invasive and Muscle-Invasive Bladder Carcinomas: A Multiparametric MRI Radiomics Analysis. *J. Magn. Reson. Imaging.* 2019;49(5):1489–1498. doi: 10.1002/jmri.26327

19. Wang H, Hu D, Yao H, et al. Radiomics analysis of multiparametric MRI for the preoperative evaluation of pathological grade in bladder cancer tumors. *European Radiology.* 2019;29(11):6182–6190. doi: 10.1007/s00330-019-06222-8

20. Zhang X, Xu X, Tian Q, et al. Radiomics assessment of bladder cancer grade using texture features from diffusion-weighted imaging. *J. Magn. Reson. Imaging.* 2017;46(5):1281–1288. doi: 10.1002/jmri.25669

21. Zheng J, Kong J, Wu S, et al. Development of a noninvasive tool to preoperatively evaluate the muscular invasiveness of bladder cancer using a radiomics approach. *Cancer.* 2019;125(24):4388–4398. doi: 10.1002/cncr.32490

22. Xu X, Liu Y, Zhang X, et al. Preoperative prediction of muscular invasiveness of bladder cancer with radiomic features on conventional MRI and its high-order derivative maps. *Abdominal Radiology.* 2017;42(7):1896–1905. doi: 10.1007/s00261-017-1079-6

23. Lim CS, Tirumani S, van der Pol CB, et al. Use of Quantitative T2-Weighted and Apparent Diffusion Coefficient Texture Features of Bladder Cancer and Extravesical Fat for Local Tumor Staging After Transurethral Resection. *American Journal of Roentgenology.* 2019;212(5):1060–1069. doi: 10.2214/AJR.18.20718

24. Razik A, Das CJ, Sharma R, et al. Utility of first order MRI-Texture analysis parameters in the prediction of histologic grade and muscle invasion in urinary bladder cancer: a preliminary study. *British Journal of Radiology.* 2021;94(1122). doi: 10.1259/bjr.20201114

25. Cui Y, Sun Z, Liu X, et al. CT-based radiomics for the preoperative prediction of the muscle-invasive status of bladder cancer and comparison to radiologists' assessment. *Clinical Radiology.* 2022;77(6):e473–e482. doi: 10.1016/j.crad.2022.02.019

26. Zhang R, Jia S, Zhai L, et al. Predicting preoperative muscle invasion status for bladder cancer using computed tomography-based radiomics nomogram. *BMC Medical Imaging.* 2024;24:98. doi: 10.1186/s12880-024-01276-7

27. Ren J, Gu H, Zhang N, et al. Preoperative CT-based radiomics for diagnosing muscle invasion of bladder cancer. *Egyptian Journal of Radiology and Nuclear Medicine.* 2023;54(131). doi: 10.1186/s43055-023-01044-7

28. Jing Q, Yang L, Hu S, et al. Radiomics prediction of the pathological grade of bladder cancer based on multi-phase CT images. *Research Square.* 2022. doi: 10.21203/rs.3.rs-2385545/v1

29. Woźnicki P, Laqua FC, Messmer K, et al. Radiomics for the Prediction of Overall Survival in Patients with Bladder Cancer Prior to Radical Cystectomy. *Cancers.* 2022;14(18):4449. doi: 10.3390/cancers14184449

30. Sylvester RJ, van der Meijden AP, Oosterlinck W, et al. Predicting Recurrence and Progression in Individual Patients with Stage Ta T1 Bladder Cancer Using EORTC Risk Tables: A Combined Analysis of 2596 Patients from Seven EORTC Trials. *European Urology.* 2006;49(3):466–477. doi: 10.1016/j.eururo.2005.12.031

31. Fernandez-Gomez J, Madero R, Solsona E, et al. Predicting Nonmuscle Invasive Bladder Cancer Recurrence and Progression in Patients Treated With Bacillus Calmette-Guerin: The CUETO Scoring Model. *Journal of Urology.* 2009;182(5):2195–2203. doi: 10.1016/j.juro.2009.07.016

32. Zhang X, Wang Y, Zhang J, et al. Development of a MRI-Based Radiomics Nomogram for Prediction of Response of Patients With Muscle-Invasive Bladder Cancer to Neoadjuvant Chemotherapy. *Front. Oncol.* 2022;12. doi: 10.3389/fonc.2022.878499

33. Kimura K, Yoshida S, Tsuchiya J, et al. Usefulness of texture features of apparent diffusion coefficient maps in predicting chemoradiotherapy response in muscle-invasive bladder cancer. *European Radiology.* 2022;32:671–679. doi: 10.1007/s00330-021-08110-6

34. Cha KH, Hadjiiski L, Chan HP, et al. Bladder Cancer Treatment Response Assessment in CT using Radiomics with Deep-Learning. *Scientific Reports.* 2017;7:8738. doi: 10.1038/s41598-017-09315-w

35. Cai Q, Huang Y, Ling J, et al. Radiomics nomogram for predicting disease-free survival after partial resection or radical cystectomy in patients with bladder cancer. *British Journal of Radiology.* 2024;97(1153):201–209. doi: 10.1093/bjr/tqad010

36. Ibrahim A, Primakov S, Beuque M, et al. Radiomics for precision medicine: Current challenges, future prospects, and the proposal of a new framework. *Methods.* 2021;188:20–29. doi: 10.1016/j.ymeth.2020.05.022

37. Wichtmann BD, Harder FN, Weiss K, et al. Influence of Image Processing on Radiomic Features From Magnetic Resonance Imaging. *Investigative Radiology.* 2023;58(3):199–208. doi: 10.1097/RLI.0000000000000921

38. Park JE, Park SY, Kim HJ, et al. Reproducibility and Generalizability in Radiomics Modeling: Possible Strategies in Radiologic and Statistical Perspectives. *Korean J Radiol.* 2019;20(7):1124–1137. doi: 10.3348/kjr.2018.0070

39. Li Q, Bai H, Chen Y, et al. A Fully-Automatic Multiparametric Radiomics Model: Towards Reproducible and Prognostic Imaging Signature for Prediction of Overall Survival in Glioblastoma Multiforme. *Scientific Reports.* 2017;7:14331. doi: 10.1038/s41598-017-14753-7

40. Foy JJ, Armato SG, Al-Hallaq HA. Effects of variability in radiomics software packages on classifying patients with radiation pneumonitis. *Journal of Medical Imaging.* 2020;7(1):014504. doi: 10.1117/1.JMI.7.1.014504

СПИСОК ЛИТЕРАТУРЫ

1. Panebianco V., Narumi Y., Altun E., et al. Multiparametric Magnetic Resonance Imaging for Bladder Cancer: Development of VI-RADS (Vesical Imaging-Reporting And Data System) // European Urology. 2018. Vol. 74, N 3. P. 294–306. doi: 10.1016/j.eururo.2018.04.029

2. Wang Z., Shang Y., Luan T., et al. Evaluation of the value of the VI-RADS scoring system in assessing muscle infiltration by bladder cancer // Cancer Imaging. 2020. Vol. 20, N 1. P. 26. doi: 10.1186/s40644-020-00304-3

3. Cumberbatch M.G.K., Foerster B., Catto J.W.F., et al. Repeat Transurethral Resection in Non-muscle-invasive Bladder Cancer: A Systematic Review // European Urology. 2018. Vol. 73, N 6. P. 925–933. doi: 10.1016/j.eururo.2018.02.014

4. Parekh V., Jacobs M.A. Radiomics: a new application from established techniques // Expert Review of Precision Medicine and Drug Development. 2016. Vol. 1, N 2. P. 207–226. doi: 10.1080/23808993.2016.1164013

5. van Timmeren J.E., Cester D., Tanadini-Lang S., et al. Radiomics in medical imaging-"how-to" guide and critical reflection // Insights Imaging. 2020. Vol. 11. P 91. doi: 10.1186/s13244-020-00887-2

6. Bologna M., Corino V., Mainardi L. Technical Note: Virtual phantom analyses for preprocessing evaluation and detection of a robust feature set for MRI-radiomics of the brain // Medical Physics. 2019. Vol. 46, N 11. P. 5116–5123. doi: 10.1002/mp.13834

7. Moradmand H., Aghamiri S.M.R., Ghaderi R. Impact of image preprocessing methods on reproducibility of radiomic features in multimodal magnetic resonance imaging in glioblastoma // Journal of Applied Clinical Medical Physics. 2020. Vol. 21, N 1. P. 179–190. doi: 10.1002/acm2.12795

8. Shafiq-ul-Hassan M., Zhang G.G., Latifi K., et al. Intrinsic dependencies of CT radiomic features on voxel size and number of gray levels // Medical Physics. 2017. Vol. 44, N 3. P. 1050–1062. doi: 10.1002/mp.12123

9. Li X., Ma Q., Tao C., et al. A CT-based radiomics nomogram for differentiation of small masses (< 4 cm) of renal oncocytoma from clear cell renal cell carcinoma // Abdom Radiol. 2021. Vol. 46, N 11. P. 5240–5249. doi: 10.1007/s00261-021-03213-6

10. Chu L.C., Park S., Soleimani S., et al. Classification of pancreatic cystic neoplasms using radiomic feature analysis is equivalent to an experienced academic radiologist: a step toward computer-augmented diagnostics for radiologists // Abdom Radiol. 2022. Vol. 47, N 12. P. 4139–4150. doi: 10.1007/s00261-022-03663-6

11. Marusyk A., Janiszewska M., Polyak K. Intratumor Heterogeneity: The Rosetta Stone of Therapy Resistance // Cancer Cell. 2020. Vol. 37, N 4. P. 471–484. doi: 10.1016/j.ccell.2020.03.007

12. Mayerhoefer M.E., Materka A., Langs G., et al. Introduction to Radiomics // Journal of Nuclear Medicine. 2020. Vol. 61, N 4. P. 488–495. doi: 10.2967/jnumed.118.222893

13. Yip S.S.F., Aerts H.J.W.L. Applications and limitations of radiomics // Phys. Med. Biol. 2016. Vol. 61, N 13. P. R150. doi: 10.1088/0031-9155/61/13/R150

14. Wang J., Shen L., Zhong H., et al. Radiomics features on radiotherapy treatment planning CT can predict patient survival in locally advanced rectal cancer patients // Scientific Reports. 2019. Vol. 9. P. 15346. doi: 10.1038/s41598-019-51629-4

15. Oikonomou A., Khalvati F., Tyrrell P.N., et al. Radiomics analysis at PET/CT contributes to prognosis of recurrence and survival in lung

cancer treated with stereotactic body radiotherapy // Scientific Reports. 2018. Vol. 8. P. 4003. doi: 10.1038/s41598-018-22357-y

16. Horvat N., Veeraraghavan H., Khan M., et al. MR Imaging of Rectal Cancer: Radiomics Analysis to Assess Treatment Response after Neoadjuvant Therapy // Radiology. 2018. Vol. 287, N 3. P. 833–843. doi: 10.1148/radiol.2018172300

17. Xu S., Yao Q., Liu G., et al. Combining DWI radiomics features with transurethral resection promotes the differentiation between muscle-invasive bladder cancer and non-muscle-invasive bladder cancer // European Radiology. 2020. Vol. 30. P. 1804–1812. doi: 10.1007/s00330-019-06484-2

18. Xu X., Zhang X., Tian Q., et al. Quantitative Identification of Nonmuscle-Invasive and Muscle-Invasive Bladder Carcinomas: A Multiparametric MRI Radiomics Analysis // Magn. Reson. Imaging. 2019. Vol. 49, N 5. P. 1489–1498. doi: 10.1002/jmri.26327

19. Wang H., Hu D., Yao H., et al. Radiomics analysis of multiparametric MRI for the preoperative evaluation of pathological grade in bladder cancer tumors // European Radiology. 2019. Vol. 29, N 11. P. 6182–6190. doi: 10.1007/s00330-019-06222-8

20. Zhang X., Xu X., Tian Q., et al. Radiomics assessment of bladder cancer grade using texture features from diffusion-weighted imaging // J. Magn. Reson. Imaging. 2017. Vol. 46, N 5. P. 1281–1288. doi: 10.1002/jmri.25669

21. Zheng J., Kong J., Wu S., et al. Development of a noninvasive tool to preoperatively evaluate the muscular invasiveness of bladder cancer using a radiomics approach // Cancer. 2019. Vol. 125, N 24. P. 4388–4398. doi: 10.1002/cncr.32490

22. Xu X., Liu Y., Zhang X., et al. Preoperative prediction of muscular invasiveness of bladder cancer with radiomic features on conventional MRI and its high-order derivative maps // Abdominal Radiology. 2017. Vol. 42, N 7. P. 1896–1905. doi: 10.1007/s00261-017-1079-6

23. Lim C.S, Tirumani S., van der Pol C.B., et al. Use of Quantitative T2-Weighted and Apparent Diffusion Coefficient Texture Features of Bladder Cancer and Extravesical Fat for Local Tumor Staging After Transurethral Resection // American Journal of Roentgenology. 2019. Vol. 212, N 5. P. 1060–1069. doi: 10.2214/AJR.18.20718

24. Razik A., Das C.J., Sharma R., et al. Utility of first order MRI-Texture analysis parameters in the prediction of histologic grade and muscle invasion in urinary bladder cancer: a preliminary study // British Journal of Radiology. 2021. Vol. 94, N 1122. doi: 10.1259/bjr.20201114

25. Cui Y., Sun Z., Liu X., et al. CT-based radiomics for the preoperative prediction of the muscle-invasive status of bladder cancer and comparison to radiologists' assessment // Clinical Radiology. 2022. Vol. 77, N 6. P. e473–e482. doi: 10.1016/j.crad.2022.02.019

26. Zhang R., Jia S., Zhai L., et al. Predicting preoperative muscle invasion status for bladder cancer using computed tomography-based radiomics nomogram // BMC Medical Imaging. 2024. Vol. 24. P. 98. doi: 10.1186/s12880-024-01276-7

27. Ren J., Gu H., Zhang N., et al. Preoperative CT-based radiomics for diagnosing muscle invasion of bladder cancer // Egyptian Journal of Radiology and Nuclear Medicine. 2023. Vol. 54. P. 131. doi: 10.1186/s43055-023-01044-7

28. Jing Q., Yang L., Hu S., et al. Radiomics prediction of the pathological grade of bladder cancer based on multi-phase CT images // Research Square. 2022. doi: 10.21203/rs.3.rs-2385545/v1

29. Woźnicki P., Laqua F.C., Messmer K., et al. Radiomics for the Prediction of Overall Survival in Patients with Bladder Cancer Prior to Radical Cystectomy // Cancers. 2022. Vol. 14, N 18. P. 4449. doi: 10.3390/cancers14184449

30. Sylvester R.J., van der Meijden A.P., Oosterlinck W., et al. Predicting Recurrence and Progression in Individual Patients with Stage Ta T1 Bladder Cancer Using EORTC Risk Tables: A Combined Analysis of 2596 Patients from Seven EORTC Trials // European Urology. 2006. Vol. 49, N 3. P. 466–477. doi: 10.1016/j.eururo.2005.12.031

31. Fernandez-Gomez J., Madero R., Solsona E., et al. Predicting Nonmuscle Invasive Bladder Cancer Recurrence and Progression in Patients Treated With Bacillus Calmette-Guerin: The CUETO Scoring Model // Journal of Urology. 2009. Vol. 182, N 5. P. 2195–2203. doi: 10.1016/j.juro.2009.07.016

32. Zhang X., Wang Y., Zhang J., et al. Development of a MRI-Based Radiomics Nomogram for Prediction of Response of Patients With Muscle-Invasive Bladder Cancer to Neoadjuvant Chemotherapy // Front. Oncol. 2022. Vol. 12. doi: 10.3389/fonc.2022.878499

33. Kimura K., Yoshida S., Tsuchiya J., et al. Usefulness of texture features of apparent diffusion coefficient maps in predicting chemoradiotherapy response in muscle-invasive bladder cancer // European Radiology. 2022. Vol. 32. P. 671–679. doi: 10.1007/s00330-021-08110-6

34. Cha K.H., Hadjiiski L., Chan H.P., et al. Bladder Cancer Treatment Response Assessment in CT using Radiomics with Deep-Learning // Scientific Reports. 2017. Vol. 7. P. 8738 doi: 10.1038/s41598-017-09315-w

35. Cai Q., Huang Y., Ling J., et al. Radiomics nomogram for predicting disease-free survival after partial resection or radical cystectomy in patients with bladder cancer // British Journal of Radiology. 2024. Vol. 97, N 1153. P. 201–209. doi: 10.1093/bjr/tqad010

36. Ibrahim A., Primakov S., Beuque M., et al. Radiomics for precision medicine: Current challenges, future prospects, and the proposal of a new framework // Methods. 2021. Vol. 188. P. 20–29. doi: 10.1016/j.ymeth.2020.05.022

37. Wichtmann B.D., Harder F.N., Weiss K., et al. Influence of Image Processing on Radiomic Features From Magnetic Resonance Imaging // Investigative Radiology. 2023. Vol. 58, N 3. P. 199–208. doi: 10.1097/RLI.0000000000000921

38. Park J.E., Park S.Y., Kim H.J., et al. Reproducibility and Generalizability in Radiomics Modeling: Possible Strategies in Radiologic and Statistical Perspectives // Korean J Radiol. 2019. Vol. 20, N 7. P. 1124–1137. doi: 10.3348/kjr.2018.0070

39. Li Q., Bai H., Chen Y., et al. A Fully-Automatic Multiparametric Radiomics Model: Towards Reproducible and Prognostic Imaging Signature for Prediction of Overall Survival in Glioblastoma Multiforme // Scientific Reports. 2017. Vol. 7. P. 14331. doi: 10.1038/s41598-017-14753-7

40. Foy J.J., Armato S.G., Al-Hallaq H.A. Effects of variability in radiomics software packages on classifying patients with radiation pneumonitis // Journal of Medical Imaging. 2020. Vol. 7, N 1. P. 014504. doi: 10.1117/1.JMI.7.1.014504

AUTHORS' INFO

* Anastasia A. Kovalenko, MD;
address: 15 Marshala Timoshenko str., 121359, Moscow, Russia;
ORCID: 0000-0001-8276-3594;
eLibrary SPIN: 6158-0090;
e-mail: nastua_kovalenko@mail.ru

Valentin E. Sinitsyn, MD, Dr. Sci. (Medicine), Professor;
ORCID: 0000-0002-5649-2193;
eLibrary SPIN: 8449-6590;
e-mail: vsini@mail.ru

Victor S. Petrovichev, MD, Cand. Sci. (Medicine);
ORCID: 0000-0002-8391-2771;
eLibrary SPIN: 7730-7420;
e-mail: petrovi4ev@gmail.com

_____

* Corresponding author / Автор, ответственный за переписку

ОБ АВТОРАХ

* Коваленко Анастасия Андреевна;
адрес: Россия, 121359, Москва, ул. Маршала Тимошенко, д. 15;
ORCID: 0000-0001-8276-3594;
eLibrary SPIN: 6158-0090;
e-mail: nastua_kovalenko@mail.ru

Синицын Валентин Евгеньевич, д-р мед. наук, профессор;
ORCID: 0000-0002-5649-2193;
eLibrary SPIN: 8449-6590;
e-mail: vsini@mail.ru

Петровичев Виктор Сергеевич, канд. мед. наук;
ORCID: 0000-0002-8391-2771;
eLibrary SPIN: 7730-7420;
e-mail: petrovi4ev@gmail.com

Remote monitoring of patients with chronic heart failure: a non-invasive approach

Aleksei V. Emelianov, Maria V. Kozhevnikova, Elena A. Zheleznykh, Anastasia L. Panova, Elena V. Privalova, Yuri N. Belenkov

Sechenov First Moscow State Medical University, Moscow, Russia

ABSTRACT

Remote monitoring of patients, including those with chronic heart failure, has been actively used in recent years. Unlike invasive methods, non-invasive methods are not associated with surgical risks and offer a wide range of patient management options such as telemonitoring, virtual visits, emergency department pre-triage, in-hospital telemedicine, telemedicine rehabilitation, psychological support, etc. Previously, remote monitoring required a multidisciplinary medical team to ensure high efficiency, and attempts to use advanced technology to reduce human involvement were often unsuccessful. However, all electronic and telemedicine technologies in healthcare have been dramatically transformed by the COVID-19 pandemic. There is currently a wide variety of remote monitoring methods and technologies. But it is still impossible to clearly assess their effectiveness due to a lack of common standards, inadequate legislation, and regional, social, and economic differences in the availability of these technologies. However, in 2021, remote monitoring was included in the European Society of Cardiology clinical guidelines for the diagnosis and management of acute and chronic heart failure (IIb). This review describes the history of modern remote monitoring methods and the problems they are designed to solve in order to improve outpatient health monitoring for patients with chronic heart failure.

Keywords: chronic heart failure; remote monitoring; telemedicine; e-health.

Дистанционное наблюдение за состоянием пациентов с хронической сердечной недостаточностью: неинвазивный подход

А.В. Емельянов, М.В. Кожевникова, Е.А. Железных, А.Л. Панова, Е.В. Привалова, Ю.Н. Беленков

Первый Московский государственный медицинский университет имени И.М. Сеченова, Москва, Россия

АННОТАЦИЯ

Дистанционное наблюдение за состоянием здоровья пациентов активно используют в последние годы, в том числе у пациентов с хронической сердечной недостаточностью. В отличие от инвазивных методов, неинвазивные не сопряжены с операционными рисками и предоставляют широкие возможности для ведения пациентов: телемониторинг, виртуальные визиты, предварительная сортировка на пути в приёмное отделение, внутригоспитальная телемедицина, телемедицинская реабилитация, психологическая поддержка и многое другое. Ранее дистанционое наблюдение осуществляли с привлечением мультидисциплинарной команды из медработников разных специальностей, что обеспечивало высокую эффективность, а попытки внедрения современных технологий для снижения участия людей часто оказывались безуспешными. Однако пандемия COVID-19 подтолкнула к радикальному изменению всех электронных и телемедицинских технологий в здравоохранении. На сегодняшний день существует огромное разнообразие методов и технологий дистанционного наблюдения, но из-за отсутствия единых стандартов, несовершенства законодательства, региональных, социальных и экономических различий в доступности этих технологий всё ещё нельзя однозначно судить об их эффективности. Тем не менее в 2021 году дистанционное наблюдение включили в клинические рекомендации Европейского общества кардиологов по диагностике и лечению острой и хронической сердечной недостаточности (IIb). Данный обзор посвящён истории развития современных методов дистанционного наблюдения, а также проблемам, которые они призваны решить с целью повышения эффективности амбулаторного наблюдения за состоянием здоровья пациентов с хронической сердечной недостаточностью.

Ключевые слова: хроническая сердечная недостаточность; дистанционное наблюдение; телемедицина; электронное здравоохранение.

远距离观测慢性心力衰竭患者：一种无创方法

Aleksei V. Emelianov, Maria V. Kozhevnikova, Elena A. Zheleznykh, Anastasia L. Panova,
Elena V. Privalova, Yuri N. Belenkov

Sechenov First Moscow State Medical University, Moscow, Russia

摘要

近年来，对患者健康状况的远距离观测得到了积极应用，包括慢性心力衰竭患者。与侵入性方法不同，非侵入性方法不存在操作风险，并为患者就医提供可能：远程监护、虚拟就诊、前往急诊室途中的预分诊、院内远程医疗、远程医疗康复、心理支持等等。此前，远距离观测是由来自不同专业的医护人员组成的多学科团队进行的，这确保了高效率，但试图引入现代技术以减少人工参与的努力往往并不成功。然而，COVID-19大流行推动了医疗保健领域所有电子和远程医疗技术的彻底变革。目前远距离观测的方法和技术种类繁多，但由于缺乏统一标准、立法不完善，以及这些技术的可用性存在地区、社会和经济差异，仍然无法明确判断其有效性。然而，2021年远距离观测被纳入欧洲心脏病学会诊断和治疗急慢性心力衰竭（IIb）的临床指南。本综述介绍了现代远距离观测方法的发展历史，以及它们旨在解决的问题，以提高慢性心力衰竭患者健康状况的门诊监测效率。

关键词：慢性心力衰竭；远距离观测；远程医疗；电子健康。

INTRODUCTION

Globally, chronic heart failure (CHF) affects approximately 60 million individuals and continues to be a major healthcare concern [1]. In Russia, the overall prevalence of CHF is 8.2%. The most frequent causes of CHF include hypertension, coronary artery disease, or their combination, which occurs in half of the patients [2]. Research indicates that the 5-year survival rate in CHF is 50%; however, it declines further in decompensated heart failure patients. The outpatient or inpatient treatment is associated with a significant economic burden [1].

Only sodium-glucose cotransporter-2 (SGLT2) inhibitors have been demonstrated to be effective in heart failure with preserved or moderately reduced ejection fraction (EF). Quadruple therapy, including angiotensin-converting enzyme inhibitors, β-blockers, mineralocorticoid receptor antagonists, and SGLT-2 inhibitors, is indicated in heart failure patients with reduced EF. This therapy lowers the readmission rate for decompensated CHF and the cardiovascular (CV) mortality rate by 72% [3].

Given the challenges of ongoing monitoring and the concern about adverse effects, including hypotension and hyperkalemia, only 16.2% of patients in Russia receive optimal drug therapy [4]. However, the revised dose titration guidelines may result in a decrease in the incidence of these adverse effects [1, 5].

Another crucial element is compliance, which depends on individual patient characteristics and comorbidities. Poor compliance is typically linked to an unfavorable prognosis and decreased physical activity and quality of life [6, 7]. Studies show that the compliance rates vary from 10% to 98%, depending on the assessment technique. Negative factors impacting compliance include inadequate medical assistance, lack of funding, asymptomatic disease, cognitive impairment, adverse reactions, depression, low awareness, polypharmacy, and inconveniences associated with diuretic therapy [8].

Other crucial elements of effective treatment include the doctor–patient relationship, training, rehabilitation, and outpatient follow-up. These issues require complex, modern strategies that consider the current challenges and trends. One of these approaches is remote monitoring.

POTENTIAL SOLUTION

Technological advancements have enabled patients to transmit data regarding their condition that was collected using invasive or noninvasive devices and receive specialist consultations at any time and from any location.

Invasive approaches assess various parameters with remarkable accuracy and respond even to any minor alterations in patients with CHF . There are devices that evaluate pulmonary artery pressure (CardioMEMS), right ventricular pressure (Chronicle IHM), left atrial pressure

(The HeartPOD), cardiac rhythm and conduction, lung tissue bioimpedance, and other deterioration markers [9, 10]. However, the study findings and meta-analysis data demonstrate that these devices are ineffective in patients with CHF. This is due to a lack of standard remote monitoring protocols and the inconsistency of the assessment techniques and parameters. The benefits of devices that measure hemodynamic parameters—particularly pulmonary artery pressure, a well-established marker of clinical deterioration are evident [11]. Invasive techniques demonstrate drawbacks, including the need for surgical intervention, risk of infections, having a limited power supply, and being expensive. These devices are primarily employed in high-risk patients requiring close monitoring and are not suitable for routine practice [12].

Conversely, there are diverse noninvasive devices and techniques for patient monitoring and management. The simplest solutions include devices that evaluate multiple parameters (scales, tonometers, pulse oximeters, smart watches, fitness trackers, etc.). More complicated monitoring techniques include phone interviews and various software. These strategies enable one to collect and process subjective and objective patient data, exchange information with other devices, maintain feedback, provide training and rehabilitation, and facilitate lifestyle adjustments. The spectrum of alternative monitoring methods is expanding, increasing availability and lowering costs, and the cumulative experience demonstrates the efficacy of this approach [12].

DEVELOPMENT OF NON-INVASIVE REMOTE MONITORING

Rich et al. [13] discovered that multidisciplinary management (MDM) of patients aged ≥70 years was effective. MDM includes training, consultations with social services and geriatric cardiologists, additional interactions, and phone interviews. This strategy lowers the overall readmission rate, including for decompensated CHF patients, enhances the quality of life, and saves $460 per patient.

Fonarow et al. [14] validated the advantages of MDM in a study involving transplant-eligible patients with the New York Heart Association (NYHA) Class III–IV CHF. Training patients and family members as well as conducting additional visits and phone interviews improved functional status, lowered readmission rates, and saved $9,800 per patient. Cline et al. [15] demonstrated that while there were no differences in survival rates, training and remote nurse monitoring lengthened the time to readmission.

In 1999, patients with EF < 45% participated in the Pharmacist in Heart Failure Assessment Recommendation and Monitoring Study, the first study to be conducted without face-to-face visits. The treatment group was followed up by a clinical pharmacologist via telephone interviews. The study included status assessment, information, training, discussions with an attending physician, and therapy modifications. The treatment group had considerably lower all-cause

mortality and CHF-associated events, and the patients were more likely to attain the target dose with the same prescription rate [16].

Over time, the inclusion requirements expanded, and the number of publications increased. In 2004, McAlister et al. [17] published a large systematic review of 29 studies in 5,039 patients. The review revealed that MDM was the only approach that lowered the overall readmission rates (including for decompensated CHF patients) and mortality rates. Self-care improvement programs had no impact on mortality. Phone interviews and recommendations to contact a physician in the event of worsening condition improved the readmission rate for decompensated CHF, but all-cause hospitalization and mortality rates were unaffected. The Trans-European Network–Home-Care Management System (TENS-HMS), a landmark randomized clinical study conducted in 2005, demonstrated the potential of telemonitoring (TM). Diuretic-treated patients with an EF < 40% following a decompensation episode were divided into three groups based on the monitoring technique. In Group 1, TM was performed employing specialized devices that collected data on patient status, including body weight, blood pressure (BP) parameters, heart rate (HR), and cardiac rhythm, and transmitted them to a server. In Group 2, patients were followed up by trained nurses via phone interviews. In Group 3, conventional monitoring was conducted. Although the study demonstrated no differences in mortality rates or intensive care admission rates, the one-year mortality in patients belonging to Groups 1 and 2 was lower than in those from Group 3 [18]. The outcomes of the CHANCE study, the first Russian multicenter study to assess training with subsequent follow-up (scheduled phone interviews and three face-to-face visits) for 12 months, were published in 2007. The study revealed reduced all-cause mortality and readmission rates for patients with decompensated CHF, increased six-minute walk distance (6MWD), lowered use of diuretics, and enhanced quality of life. Application of this approach mitigated the relative risk of death by 37% [19].

Available data indicates that MDM is the primary contributor to the enhanced efficacy of remote monitoring in patients with CHF. However, this strategy requires skilled professionals and is linked to an increased workload as well as significant training and labor expenditures. Physicians invest a significant amount of their professional and leisure time in data analysis, and the scarcity of healthcare workers is a global issue [20]. Working after hours has been shown to significantly raise the risk of professional burnout [21]. Patient monitoring in remote areas and low-income countries is another issue [22]. Given the increased workload, novel approaches aimed at identifying effective patient management strategies that reduce the personal engagement of healthcare professionals and financial expenses are garnering substantial attention.

However, studies frequently yield inconsistent results. A meta-analysis of 20 randomized clinical trials (6,258 patients) and 12 cohort studies (2,354 patients) conducted between 2000 and 2008 verified that remote monitoring is effective in lowering mortality and readmission rates [23]. However, it also included studies that used MDM [17]. The subsequent research findings were not promising. For example, Chaudhry et al. [24] assessed the efficacy of remote monitoring using phone interviews to gather data on complaints and body weight, as well as for follow-up physician consultations. This approach had no influence on readmission rates, including for patients with decompensated CHF, duration of hospitalization, and all-cause mortality. The Telemedical Interventional Monitoring in Heart Failure (TIM-HF) study used devices for at home ECG, BP, and body weight monitoring. The devices were connected via Bluetooth to a digital assistant, which provided data to the telemedicine centers. All-cause mortality, cardiovascular mortality, and hospitalization rates for decompensated CHF patients were unaffected by this strategy [25]. Lyngå et al. [26] assessed the efficacy of TM based on body weight changes in two groups of patients. In Group 1, electronic scales were used to transmit data to a clinic; in Group 2, patients kept track of their own body weight. The mortality and readmission rates did not differ between the groups, according to the study. The multicenter, randomized, controlled study Telemonitoring in Heart Failure used a device with a display and four buttons. Data on BP and HR were collected, and interviews with preset questions were conducted. The buttons were used to submit responses, which were subsequently transmitted to a server, and displayed on the nurse's desktop. If any anomalies were found, a consultation was offered. There were no differences in hospitalization and mortality rates, which is due to the small sample size and carefully selected groups. However, there was a reduction in the number of events requiring interaction with a nurse [27].

Additionally, some encouraging outcomes were observed. The Telemonitoring in the Management of Heart Failure (TEMA-HF) study assessed the effectiveness of BP, HR, and body weight monitoring using electronic devices that were connected via Bluetooth to a telephone for data transfer. If there were any abnormalities, a physician was notified to determine the further treatment strategy. For decompensated CHF, the readmission rate, days lost from hospitalization, dialysis, or death, and all-cause mortality all decreased ($p = 0.06$) [28]. In 2015, Inglis et al. [29] published a systematic review of 41 studies, comprising structured phone interviews ($n = 25$) and non-invasive TM ($n = 18$). The review found that remote monitoring can lower all-cause mortality and readmission rates for decompensated CHF, as well as enhance the quality of life, self-care, and awareness of the disease. Most patients, including older adults, mastered the technologies easily and expressed high satisfaction levels. The review revealed the absence of a uniform structure, heterogeneity of studies, and impact on all-cause mortality and readmission rates for patients with decompensated CHF. The European Society of Cardiology's position was reflected in a document published

in 2016 as remote monitoring gained popularity, more research was conducted, and its efficacy was established [30]. This seminal document underscored the significance and efficacy of remote monitoring, considered current issues and potential solutions, and outlined the future development strategy. The issues included a lack of awareness and trust in eHealth solutions, insufficient evidence of cost-effectiveness, absence of clear legal regulations for healthcare mobile applications and transparency regarding data use, including those stored abroad, as well as regional, social, and economic disparities in technology availability [30]. However, the results of the Better Effectiveness After Transition–Heart Failure (BEAT-HF) study were unsatisfactory. Post-training phone interviews and TM were utilized for monitoring. TM employed equipment that tracked BP, HR, symptoms, and body weight, and trained nurses performed monitoring and phone interviews and recorded the actions. There were no intergroup differences in the readmission and all-cause mortality rates; however, there were differences in the quality of life [31].

In 2017, Grebennikova et al. [32] assessed the potential of enhancing self-care via mobile application-based remote monitoring. The study showed a significant improvement in self-care, as evidenced by a decrease in the mean score on the Russian version of the European Heart Failure Self-care Behavior Scale.

The Telemedical Interventional Management in Heart Failure II (TIM-HF2) study evaluated remote monitoring in patients with NYHA Class II–III CHF and EF ⩽ 45% (or >45% in combination with oral diuretic therapy) who were hospitalized for decompensated CHF in the previous 12 months. While there were no intergroup differences in CV death rates, remote monitoring lowered the number of days lost due to hospitalization for decompensated CHF and all-cause mortality [33]. Mareev et al. [34] reviewed clinical studies on telemetry in CHF. The outcomes were inconsistent due to inadequate compliance without direct interactions with healthcare professionals, parameters with insufficient sensitivity, and participants with a stable disease that did not require TM in multiple studies.

Zhu et al. [35] performed a meta-analysis of controlled studies in 10,981 patients conducted between 1999 and 2018. The analysis revealed that remote monitoring mitigated all-cause readmission rates, including for decompensated CHF, all-cause and CV mortality, and length of hospitalization; however, it had no effect on CHF-related mortality. The meta-analysis revealed the heterogeneity of the included studies. The publications that examined the need for MDM corroborated its effectiveness; however, the meta-analysis did not include the TIM-HF2 study results. More comprehensive information is presented in Appendix 1.

The model remains mostly unchanged, despite numerous studies. It includes phone interviews, video calls, and/or home-use devices that automatically transmit data on the patient's condition. The COVID-19 pandemic, during which remote monitoring technology evolved rapidly, had a significant impact. It was found that many tasks and areas can be effectively and safely supplemented, as well as partially or totally replaced. Along with TM advancements, strategies such as virtual visits, preliminary triage on the way to the emergency room, inpatient telemedicine, telerehabilitation, and psychological support have been implemented [36]. Nasonova et al. [37] performed a systematic review of invasive and noninvasive TM for 2010–2020. The review revealed that the heterogeneity of the studies made it impossible to make direct comparisons of remote monitoring systems and to determine an unambiguous efficacy assessment, highlighting the need for standardization. However, noninvasive TM was included in the guidelines of the European Society of Cardiology in 2021 (recommendation class IIb, evidence level B) [1]. Furthermore, novel examination techniques and results continue to be published.

A MODERN NON-INVASIVE TELEMONITORING MODEL

Contemporary non-invasive TM comprises data collection and feedback, server-side data storage and processing, and a healthcare professional interface for data analysis to evaluate the patient's status (Fig. 1) [10].

Interactions with patients are also important, as evidenced by the last mile problem. This problem is common in various sectors and describes how the success of the whole system depends on this particular stage, which includes interactions, data collection method, data type, and user convenience for patients. If the service is costly, the solution is complicated, and the use is challenging and too intrusive, patients will be reluctant to use the system regardless of its worth and complexity. Thus, the quest for an effective, convenient, secure, and inexpensive solution remains relevant.

One option is an application that enables a wide range of possibilities, restricted only by the intended use and the creators' imagination. Web applications and mobile applications serving as digital assistants are already available to patients for teleconsultation, feedback, and data collection via surveys and devices at home, including Russian software[1], training, rehabilitation, and other services. Available publications exhibit strong compliance and high satisfaction levels, improved self-care, and decreased readmission rates for decompensated CHF and all-cause mortality [38–40].

---

[1] Zingerman B.V., Demkina A.E., Fistul I.A., Borodin R.A. [software No. 2021613872] Medsenger. Cardio: A Customizable Script-Based Remote Monitoring System for Patients with Cardiovascular Diseases, 2021
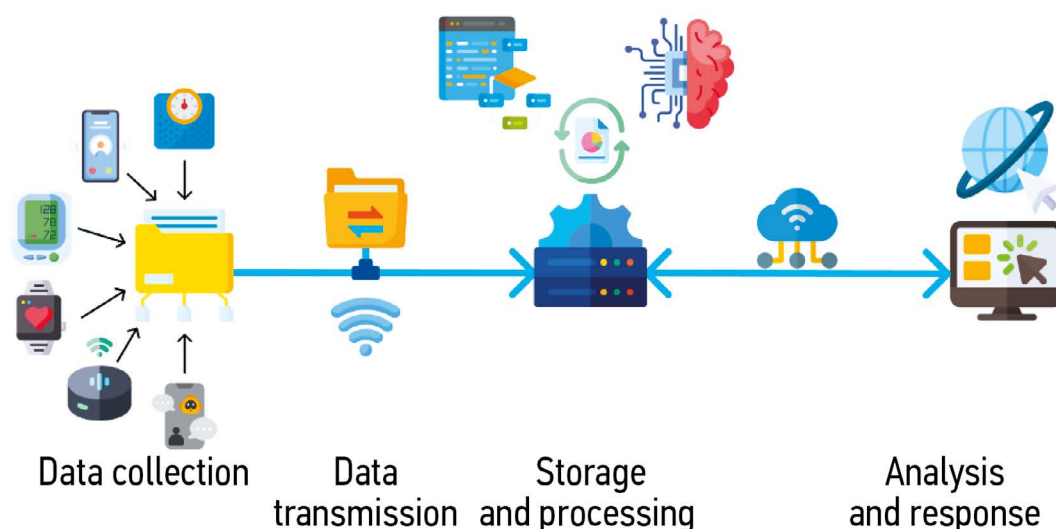
Fig. 1. A modern noninvasive telemonitoring model.

Game models require particular consideration. They are being actively tested as a tool for patient training, behavior modification, and enhanced quality of life, motivation, and self-care. Individual preferences, availability concerns, and computer proficiency are among the limitations. The model must represent real-world challenges that patients encounter during self-care. Moreover, reward-based strategies must be carefully planned to avoid unforeseen consequences [41, 42].

Questionnaires and noninvasive devices linked to an application or telemedicine hub are still convenient. The Heart failure Events reduction with Remote Monitoring and eHealth Support study, one of the landmark studies, demonstrated that an application with video feedback, BP and body weight monitoring, and questionnaire functions mitigates CV mortality rates and the incidence of decompensated CHF by 50% and 64%, respectively. Moreover, it lowers all-cause readmission rates, healthcare resource consumption, all-cause mortality, and CHF mortality. This is especially relevant for patients hospitalized for decompensated CHF during the "vulnerable phase," which lasts for six months following discharge [43].

Voice assistants are also gaining popularity. Moreover, research is exploring alternatives to applications that can be problematic for older patients, as well as the use of questionnaires to gather subjective and objective information. High satisfaction levels have been demonstrated; however, significant variability of responses and the lack of correlation between the severity of symptoms and the risk of readmission necessitate a patient-specific approach to ensure the reliability of acquired data and fully unlock the potential of this technique [44].

Chatbots, which are messenger-based applications controlled by question/answer text commands that are suitable for surveys, are another popular option. These approaches have been shown to boost the quality of life and lower healthcare resource utilization. The disadvantages include the high heterogeneity of the questionnaires, small sample sizes, and brief follow-up periods [45].

Due to the substantial economic and social disparities, tried-and-true, low-cost methods are still applicable. For example, SMS reminders, both monthly and unscheduled, have been proven to augment quality of life, self-care questionnaire scores, and compliance [46]. The Kansas City Cardiomyopathy Questionnaire, completed online or sent by e-mail, assisted researchers in identifying CHF symptoms following myocardial infarction and determining high-risk groups. The most crucial factors included impaired gait, pedal edema, and the progression of symptoms [47].

In addition, numerous gadgets are being actively researched and extensively used. For example, an ECG sensor with accelerometry, impedancemetry, and skin thermometry capabilities allowed for the prompt detection of deteriorating conditions, as well as their prediction with a high sensitivity (comparable to that of implantable devices) [48]. Remote monitoring of CHF patients in rural areas using a tonometer and the Russian ECG recorder CaRe 1.0 decreased the rate of emergency room visits and readmissions [49]. The INME-01 tonometer lowered the hospital admission and CV mortality rates [50]. Lung water measurement is considered a promising method. Impedance and dielectric meters have demonstrated high efficacy, comparable or superior to that of other indicators such as N-terminal prohormone of brain natriuretic peptide (NT-proBNP), body weight, X-ray findings, NYHA class, auscultation findings, edema, and jugular venous pressure. There was a documented decrease in the duration of hospitalization, readmission rate, all-cause mortality, and decompensated CHF mortality [51–53]. Although these devices are still undergoing testing, their relative ease of use and safety are considered additional benefits, and they will eventually be made available to patients.

Decompensated CHF can also be predicted based on fluid accumulation in the lungs, larynx, and vocal cords, as well as voice and breathing changes. A pilot study revealed that

euvolemia is marked by a clearer voice, better articulation, and more fluent speech with longer sentences compared with decompensated CHF. The rate of silent pauses was 14.9% higher in patients with acute heart failure, regardless of sex, age, and EF. This phenomenon persisted in patients with mild edema and dyspnea, which can be interpreted as a marker of deteriorating condition, especially in the absence of typical clinical signs. Moreover, a direct correlation with NT-proBNP levels has also been demonstrated [54, 55].

Applications of telemedicine for rehabilitation are emerging rapidly. Their functionality includes multimedia content, TM activity, patient status assessment with home-use devices and smart watches, motivational messages, and progress reports. These methods are highly valued by patients for their ease, acceptance, and enjoyment, all of which boost physical activity. One disadvantage is the lack of a patient-specific approach that considers individual goals, physical activity, and environmental factors. Patients with lower functional capacity and less experience at baseline were more likely to think favorably of the intervention [56, 57]. However, the Telerehabilitation in Heart Failure Patients (TELEREH-HF) study revealed no differences in mortality and readmission rates when employing invasive TM [58]. Efficacy studies of remote monitoring using various techniques are ongoing [59].

Inpatient TM is a recent area of research. Currently available data indicates that it has no effect on treatment quality. Only one in nine patients receives optimal drug therapy recommendations at discharge. This necessitates further improvements in notifications and physician incentives [60]. Appendix 2 contains more detailed information.

Although there are diverse TM techniques, only 20% of them comply with regulatory requirements and are tested in clinical studies [61]. However, active development in this area is beyond doubt; it is becoming a vital component of patient management, as evidenced by the current guidelines.

CONCLUSION

Non-invasive remote monitoring is a rapidly emerging, promising field that stems from MDM and seeks to minimize the involvement of healthcare professionals. Automated data collection and software-based interactions were initially ineffective due to the existing limitations. However, a unified model is progressively being developed, and efforts to find practical, secure, and efficient methods are still ongoing. Standard remote monitoring protocols for CHF patients and patient-specific approaches, which consider all available options based on patient characteristics and preferences, would substantially boost efficacy.

ADDITIONAL INFORMATION

REFERENCES

1. McDonagh TA, Metra M, Adamo M, et al.; ESC Scientific Document Group. 2021 ESC Guidelines for the diagnosis and treatment of acute and chronic heart failure. *Eur Heart J.* 2021;42(36):3599–3726. doi: 10.1093/eurheartj/ehab368

2. Polyakov DS, Fomin IV, Belenkov YuN, et al. Chronic heart failure in the Russian Federation: what has changed over 20 years of follow-up? Results of the EPOCH-CHF study. *Kardiologiia.* 2021;61(4):4–14. EDN: WSZNFS doi: 10.18087/cardio.2021.4.n1628

3. Tromp J, Ouwerkerk W, van Veldhuisen DJ, et al. A Systematic review and network meta-analysis of pharmacological treatment of heart failure with reduced ejection fraction // *JACC Heart Fail.* 2022;10(2):73–84. doi: 10.1016/j.jchf.2021.09.004

4. Shlyakhto EV, Belenkov YuN, Boytsov SA, et al. Prospective observational multicenter registry study of patients with heart failure in the Russian Federation (PRIORITET-CHF): rationale, objectives and design of the. *Russian Journal of Cardiology.* 2023;28(6):7–14. EDN: LKSHVP doi: 10.15829/1560-4071-2023-5456

5. Maddox TM, Januzzi JL, Jr, Allen LA, et al. 2024 ACC Expert consensus decision pathway for treatment of heart failure with reduced ejection fraction: a report of the American College of Cardiology solution set oversight committee. *J. Am. Coll. Cardiol.* 2024;83(15):1444–1488. doi: 10.1016/j.jacc.2023.12.024

6. Ruppar TM, Cooper PS, Mehr DR, et al. Medication adherence interventions improve heart failure mortality and readmission rates: systematic review and meta-analysis of controlled trials. *J. Am. Heart Assoc.* 2016;5(6):e002606. doi: 10.1161/JAHA.115.002606

7. Wu JR, Moser DK. Medication adherence mediates the relationship between heart failure symptoms and cardiac event-free survival in patients with heart failure. *J. Cardiovasc. Nurs.* 2018;33(1):40–46. doi: 10.1097/JCN.0000000000000427

8. Shah D, Simms K, Barksdale D, Wu J. Improving medication adherence of patients with chronic heart failure: challenges and solutions. *Res. Rep. Clin. Cardiol.* 2015;6:87–95. doi: 10.2147/RRCC.S50658

9. Adamson PB. Pathophysiology of the transition from chronic compensated and acute decompensated heart failure: new insights from continuous monitoring devices. *Curr. Heart Fail. Rep.* 2009;6(4):287–292. doi: 10.1007/s11897-009-0039-z

10. Stevenson LW, Ross HJ, Rathman LD, Boehmer JP. Remote monitoring for heart failure management at home. *J. Am. Coll. Cardiol.* 2023;81(23):2272–2291. doi: 10.1016/j.jacc.2023.04.010

11. Lindenfeld J, Costanzo MR, Zile MR, et al.; GUIDE-HF, CHAMPION, LAPTOP-HF Investigators. Implantable hemodynamic monitors improve survival in patients with heart failure and reduced ejection fraction. *J. Am. Coll. Cardiol.* 2024;83(6):682–694. doi: 10.1016/j.jacc.2023.11.030

12. Scholte NTB, Gürgöze MT, Aydin D, et al. Telemonitoring for heart failure: a meta-analysis. *Eur. Heart J.* 2023;44(31):2911–2926. doi: 10.1093/eurheartj/ehad280

13. Rich MW, Beckham V, Wittenberg C, et al. A multidisciplinary intervention to prevent the readmission of elderly patients with congestive heart failure. *N. Engl. J. Med.* 1995;333(18):1190–1195. doi: 10.1056/NEJM199511023331806

14. Fonarow GC, Stevenson LW, Walden JA, et al. Impact of a comprehensive heart failure management program on hospital readmission and functional status of patients with advanced heart failure. *J. Am. Coll. Cardiol.* 1997;30(3):725–732. doi: 10.1016/s0735-1097(97)00208 8

15. Cline CM, Israelsson BY, Willenheimer RB, et al. Cost effective management programme for heart failure reduces hospitalization. *Heart.* 1998;80(5):442–446. doi: 10.1136/hrt.80.5.442

16. Gattis WA, Hasselblad V, Whellan DJ, O'Connor CM. Reduction in heart failure events by the addition of a clinical pharmacist to the heart failure management team: results of the pharmacist in heart failure assessment recommendation and monitoring (PHARM) Study. *Arch. Intern. Med.* 1999;159(16):1939–1945. doi: 10.1001/archinte.159.16.1939

17. McAlister FA, Stewart S, Ferrua S, McMurray JJ. Multidisciplinary strategies for the management of heart failure patients at high risk for admission. *J. Am. Coll. Cardiol.* 2004;44(4):810–819. doi: 10.1016/j.jacc.2004.05.055

18. Cleland JG, Louis AA, Rigby AS, et al.; TEN-HMS Investigators. Noninvasive home telemonitoring for patients with heart failure at high risk of recurrent admission and death. *J. Am. Coll. Cardiol.* 2005;45(10):1654–1664. doi: 10.1016/j.jacc.2005.01.050

19. Belenkov YuN. Effect of specialized forms of active outpatient management on the functional status, quality of life and hemodynamic parameters in patients with advanced heart failure. Results of the Russian Program «CHANCE». *Russ Heart Fail J.* 2007;8(3):112–116. EDN: ODSNQP

20. Rotenstein LS, Holmgren AJ, Downing N L, Bates DW. Differences in total and after-hours electronic health record time across ambulatory specialties. *JAMA Intern. Med.* 2021;181(6):863–865. doi: 10.1001/jamainternmed.2021.0256

21. Adler-Milstein J, Zhao W, Willard-Grace R, et al. Electronic health records and burnout: time spent on the electronic health record after hours and message volume associated with exhaustion but not with cynicism among primary care clinicians. *J. Am. Med. Inform. Assoc.* 2020;27(4):531–538. doi: 10.1093/jamia/ocz220

22. Azizi Z, Broadwin C, Islam S, et al. Digital health interventions for heart failure management in underserved rural areas of the united states: a systematic review of randomized trials. *J. Am. Heart Assoc.* 2024;13(2):e030956. doi: 10.1161/JAHA.123.030956

23. Klersy C, De Silvestri A, Gabutti G, et al. A meta-analysis of remote monitoring of heart failure patients. *J. Am. Coll. Cardiol.* 2009;54(18):1683–1694. doi: 10.1016/j.jacc.2009.08.017

24. Chaudhry SI, Mattera JA, Curtis JP, et al. Telemonitoring in Patients with Heart Failure. *N. Engl. J. Med.* 2010;363(24):2301–2309. doi: 10.1056/NEJMoa1010029

25. Koehler F, Winkler S, Schieber M, et al.; TIM-HF Investigators. Impact of remote telemedical management on mortality and hospitalizations in ambulatory patients with chronic heart failure: the telemedical interventional monitoring in heart failure study. *Circulation.* 2011;123(17):1873–1880. doi: 10.1161/CIRCULATIONAHA.111.018473

26. Lyngå P, Persson H, Hägg-Martinell A, et al. Weight monitoring in patients with severe heart failure (WISH). A randomized controlled trial. *Eur. J. Heart Fail.* 2012;14(4):438–444. doi: 10.1093/eurjhf/hfs023

27. Boyne JJ, Vrijhoef HJ, Crijns HJ, et al.; TEHAF investigators. Tailored telemonitoring in patients with heart failure: results of a multicentre randomized controlled trial. *Eur. J. Heart Fail.* 2012;14(7):791–801. doi: 10.1093/eurjhf/hfs058

28. Dendal P, De Keulenaer G, Troisfontaines P, et al. Effect of a telemonitoring-facilitated collaboration between general practitioner and heart failure clinic on mortality and rehospitalization rates in severe heart failure: the TEMA-HF 1 (TElemonitoring in the MAnagement of Heart Failure) study. *Eur. J. Heart Fail.* 2012;14(3):333–340. doi: 10.1093/eurjhf/hfr144

29. Inglis SC, Clark RA, Dierckx R, et al. Structured telephone support or non-invasive telemonitoring for patients with heart failure. *Cochrane Database Syst. Rev.* 2015;2015(10):CD007228. doi: 10.1002/14651858.CD007228.pub3

30. Cowie MR, Bax J, Bruining N, et al. e-Health: a position statement of the European Society of Cardiology. *Eur. Heart J.* 2016;37(1):63–66. doi: 10.1093/eurheartj/ehv416

31. Ong MK, Romano PS, Edgington S, et al. Effectiveness of remote patient monitoring after discharge of hospitalized patients with heart failure: the better effectiveness after transition–heart Failure (BEAT-HF) Randomized Clinical Trial. *JAMA Intern. Med.* 2016;176(3):310–318. doi: 10.1001/jamainternmed.2015.7712

32. Grebennikova AA, Stoliarov AU, Lopatin YuM. The use of platform for remote monitoring on the base of mobile app for improving self-care in patients with chronic heart failure. *Kardiologiia.* 2017;57(4S):11–18. EDN: YKUOWF doi: 10.18087/cardio.2413

33. Koehler F, Koehler K, Deckwart O, et al. Efficacy of telemedical interventional management in patients with heart failure (TIM-HF2): a randomised, controlled, parallel-group, unmasked trial. *The Lancet.* 2018;392(10152):1047–1057. doi: 10.1016/S0140-6736(18)31880-4

34. Mareev YuV, Zinchenko AO, Myasnikov RP, et al. Telemonitoring in patients with chronic heart failure. *Kardiologiia.* 2019;59(9S):4–15. EDN: ISWIAY doi: 10.18087/cardio.n530

35. Zhu Y, Gu X, Xu C Effectiveness of telemedicine systems for adults with heart failure: a meta-analysis of randomized controlled trials. *Heart Fail. Rev.* 2020;25(2):231–243. doi: 10.1007/s10741-019-09801-5

36. Tersalvi G, Winterton D, Cioffi GM, et al. Telemedicine in heart failure during COVID-19: a step into the future. *Front. Cardiovasc. Med.* 2020;7:612818. doi: 10.3389/fcvm.2020.612818

37. Nasonova SN, Lapteva AE, Zhirov IV, et al. Remote monitoring of patients with heart failure in real clinical practice. *Kardiologiia.* 2021;61(8):76–86. (In Russ.) EDN: GRIBYY doi: 10.18087/cardio.2021.8.n1683

38. Yokota T, Fukushima A, Tsuchihashi-Makaya M, et al. The AppCare-HF randomized clinical trial: a feasibility study of a novel self-care support mobile app for individuals with chronic heart failure. *Eur. Heart J. - Digit. Health.* 2023;4(4):325–336. doi: 10.1093/ehjdh/ztad032

39. Rao VN, Kaltenbach LA, Granger BB, et al. The Association of Digital Health Application use with heart failure care and outcomes: insights from CONNECT-HF. *J. Card. Fail.* 2022;28(10):1487–1496. doi: 10.1016/j.cardfail.2022.07.050

40. Agapov VV, Kudryashov YuY, Graifer IV, Samitin VV. Development and implementation of a heart failure telemonitoring system: the single centre experience. *Kardiologiia.* 2022;62(5):45–52. EDN: BHAITY doi: 10.18087/cardio.2022.5.n1825

41. Radhakrishnan K, Julien C, O'Hair M, et al. Sensor-controlled digital game for heart failure self-management: protocol for a randomized controlled trial. *JMIR Res. Protoc.* 2023;12:e45801. doi: 10.2196/45801

42. Lukey A, Mackay M, Hasan K, Rush KL. Clinical perspectives on the development of a gamified heart failure patient education web site. *CIN Comput. Inform. Nurs.* 2023;41(8):615–620. doi: 10.1097/CIN.0000000000000983

43. Yun S, Enjuanes C, Cobo M, et al. Effect on cardiovascular mortality and worsening heart failure of mHealth solutions combining telemonitoring and teleintervention: results of the HERMeS multicentre, randomised, controlled trial. In: *Heart Failure*; 2023 May 20–23; Prague. Unpublished.

44. Shara N, Bjarnadottir MV, Falah N, et al. Voice activated remote monitoring technology for heart failure patients: Study design, feasibility and observations from a pilot randomized control trial. *PLOS ONE.* 2022;17(5):e0267794. doi: 10.1371/journal.pone.0267794

45. Emelianov AV, Zheleznykh EA, Kozhevnikova MV, et al. Quality of life and adherence to therapy in patients with chronic heart failure who were remotely monitored by chatbot compared to the standard follow-up group for 3 months. *Digital Diagnostics.* 2023;4(1S):53–56. EDN: PPGJTP doi: 10.17816/DD430343

46. Pyrikova NV, Mozgunov NA, Osipova IV. Results of pilot remote monitoring of heart failure patients. *Cardiovascular Therapy and Prevention.* 2022;21(6):42–51. EDN: ROTHHY doi: 10.15829/1728-8800-2022-3151

47. Wohlfahrt P, Jenča D, Melenovský V, et al. Remote heart failure symptoms assessment after myocardial infarction identifies patients at risk for death. *J. Am. Heart Assoc.* 2024;13(2):e032505. doi: 10.1161/JAHA.123.032505

48. Stehlik J, Schmalfuss C, Bozkurt B, et al. Continuous wearable monitoring analytics predict heart failure hospitalization: the LINK-HF multicenter study. *Circ. Heart Fail.* 2020;13(3):e006513. doi: 10.1161/CIRCHEARTFAILURE.119.006513

49. Potapov AP, Yartsev SE, Lagutova EA. Remote monitoring of patients with chronic heart failure using blood pressure telemonitoring and

ECG. *Russian Journal of Telemedicine and E-Health.* 2021;7(3):42–51. EDN: OFOTQN doi: 10.29188/2712-9217-2021-7-3-42-51

50. Garanin AA, Mullova IS, Shkaeva OV, et al. Remote monitoring of outpatients discharged from the emergency cardiac care department. *Russian Journal of Cardiology.* 2022;27(3S):8–15. EDN: BIRQPJ doi: 10.15829/1560-4071-2022-5072

51. Kleiner Shochat M, Fudim M, Shotan A, et al. Prediction of readmissions and mortality in patients with heart failure: lessons from the IMPEDANCE-HF extended trial. *ESC Heart Fail.* 2018;5(5):788–799. doi: 10.1002/ehf2.12330

52. Abraham WT, Anker S, Burkhoff D, et al. Primary results of the sensible medical innovations lung fluid status monitor allows reducing readmission rate of heart failure patients (smile) trial. *J. Card. Fail.* 2019;25(11):938. doi: 10.1016/j.cardfail.2019.11.007

53. Bensimhon D, Alali SA, Curran L, et al. The use of the reds noninvasive lung fluid monitoring system to assess readiness for discharge in patients hospitalized with acute heart failure: A pilot study. *Heart Lung.* 2021;50(1):59–64. doi: 10.1016/j.hrtlng.2020.07.003

54. Murton OM, Dec GW, Hillman RE, et al. Acoustic voice and speech biomarkers of treatment status during hospitalization for acute decompensated heart failure. *Appl. Sci.* 2023;13(3):1827. doi: 10.3390/app13031827

55. Schöbi D, Zhang YP, Kehl J, et al. Evaluation of speech and pause alterations in patients with acute and chronic heart failure. *J. Am. Heart Assoc.* 2022;11(21):e027023. doi: 10.1161/JAHA.122.027023

56. Atluri N, Mishra SR, Anderson T, et al. Acceptability of a text message-based mobile health intervention to promote physical activity in cardiac rehabilitation enrollees: a qualitative substudy of participant perspectives. *J. Am. Heart Assoc.* 2024;13(2):e030807. doi: 10.1161/JAHA.123.030807

57. Rossetto F, Borgnis F, Isernia S, et al. System integrated digital empowering and telerehabilitation to promote patient activation and well-being in chronic disabilities: a usability and acceptability study. *Front. Public Health.* 2023;11:1154481. doi: 10.3389/fpubh.2023.1154481

58. Piotrowicz E, Pencina MJ, Opolski G, et al. Effects of a 9-week hybrid comprehensive telerehabilitation program on long-term outcomes in patients with heart failure: the telerehabilitation in heart failure patients (TELEREH-HF) randomized clinical trial. *JAMA Cardiol.* 2020;5(3):300–308. doi: 10.1001/jamacardio.2019.5006

59. Dinesen B, Hansen ET, Refsgaard J, et al. «Future patient II» telerehabilitation for patients with heart failure: protocl for a randomized controlled trial. *Int. J. Cardiol. Cardiovasc. Risk Prev.* 2024;20:200239. doi: 10.1016/j.ijcrp.2024.200239

60. Ghazi L, Yamamoto Y, Fuery M, et al. Electronic health record alerts for management of heart failure with reduced ejection fraction in hospitalized patients: the PROMPT-AHF trial. *Eur. Heart J.* 2023;44(40):4233–4242. doi: 10.1093/eurheartj/ehad512

61. Day S, Shah V, Kaganoff S, et al. Assessing the clinical robustness of digital health startups: cross-sectional observational analysis. *J. Med. Internet Res.* 2022;24(6):e37677. doi: 10.2196/37677

СПИСОК ЛИТЕРАТУРЫ

1. McDonagh T.A., Metra M., Adamo M., et al.; ESC Scientific Document Group. 2021 ESC Guidelines for the diagnosis and treatment of acute and chronic heart failure // Eur Heart J. 2021. Vol. 42, N 36. P. 3599–3726. doi: 10.1093/eurheartj/ehab368

2. Поляков Д.С., Фомин И.В., Беленков Ю.Н., и др. Хроническая сердечная недостаточность в Российской Федерации: что изменилось за 20 лет наблюдения? Результаты исследования ЭПОХА-ХСН // Кардиология. 2021. Т. 61, № 4. С. 4–14. EDN: WSZNFS doi: 10.18087/cardio.2021.4.n1628

3. Tromp J., Ouwerkerk W., van Veldhuisen D.J., et al. A Systematic review and network meta-analysis of pharmacological treatment of heart failure with reduced ejection fraction // JACC Heart Fail. 2022. Vol. 10, N 2. P. 73–84. doi: 10.1016/j.jchf.2021.09.004

4. Шляхто Е.В., Беленков Ю.Н., Бойцов С.А., и др. Проспективное наблюдательное многоцентровое регистровое исследование пациентов с хронической сердечной недостаточностью в Российской Федерации (ПРИОРИТЕТ-ХСН): обоснование, цели и дизайн исследования // Российский кардиологический журнал. 2023. Т. 28. № 6. С. 7–14. EDN: LKSHVP doi: 10.15829/1560-4071-2023-5456

5. Maddox T.M., Januzzi J.L., Jr, Allen L.A., et al. 2024 ACC Expert consensus decision pathway for treatment of heart failure with reduced ejection fraction: a report of the American College of Cardiology solution set oversight committee // J. Am. Coll. Cardiol. 2024. Vol. 83, N 15. P. 1444–1488. doi: 10.1016/j.jacc.2023.12.024

6. Ruppar T.M., Cooper P.S., Mehr D.R., et al. Medication adherence interventions improve heart failure mortality and readmission rates: systematic review and meta-analysis of controlled trials // J. Am. Heart Assoc. 2016. Vol. 5, N 6. P. e002606. doi: 10.1161/JAHA.115.002606

7. Wu J.R., Moser D.K. Medication adherence mediates the relationship between heart failure symptoms and cardiac event-free survival in patients with heart failure // J. Cardiovasc. Nurs. 2018. Vol. 33, N 1. P. 40–46. doi: 10.1097/JCN.0000000000000427

8. Shah D., Simms K., Barksdale D., Wu J. Improving medication adherence of patients with chronic heart failure: challenges and solutions // Res. Rep. Clin. Cardiol. 2015. Vol. 6. P. 87–95. doi: 10.2147/RRCC.S50658

9. Adamson P.B. Pathophysiology of the transition from chronic compensated and acute decompensated heart failure: new insights from continuous monitoring devices // Curr. Heart Fail. Rep. 2009. Vol. 6, N 4. P. 287–292. doi: 10.1007/s11897-009-0039-z

10. Stevenson L.W., Ross H.J., Rathman L.D., Boehmer J.P. Remote Monitoring for Heart Failure Management at Home // J. Am. Coll. Cardiol. 2023. Vol. 81, N 23. P. 2272–2291. doi: 10.1016/j.jacc.2023.04.010

11. Lindenfeld J., Costanzo M.R., Zile M.R., et al.; GUIDE-HF, CHAMPION, LAPTOP-HF Investigators. Implantable hemodynamic monitors improve survival in patients with heart failure and reduced ejection fraction // J. Am. Coll. Cardiol. 2024. Vol. 83, N 6. P. 682–694. doi: 10.1016/j.jacc.2023.11.030

12. Scholte N.T.B., Gürgöze M.T., Aydin D., et al. Telemonitoring for heart failure: a meta-analysis // Eur. Heart J. 2023. Vol. 44, N 31. P. 2911–2926. doi: 10.1093/eurheartj/ehad280

13. Rich M.W., Beckham V., Wittenberg C., et al. A multidisciplinary intervention to prevent the readmission of elderly patients with congestive heart failure // N. Engl. J. Med. 1995. Vol. 333, N 18. P. 1190–1195. doi: 10.1056/NEJM199511023331806

14. Fonarow G.C., Stevenson L.W., Walden J.A., et al. Impact of a comprehensive heart failure management program on hospital readmission and functional status of patients with advanced heart failure // J. Am. Coll. Cardiol. 1997. Vol. 30, N 3. P. 725–732. doi: 10.1016/s0735-1097(97)00208 8

15. Cline C.M., Israelsson B.Y., Willenheimer R.B., et al. Cost effective management programme for heart failure reduces hospitalisation // Heart. 1998. Vol. 80, N 5. P. 442–446. doi: 10.1136/hrt.80.5.442

16. Gattis W.A., Hasselblad V., Whellan D.J., O'Connor C.M. Reduction in heart failure events by the addition of a clinical pharmacist to the heart failure management team: results of the pharmacist in heart failure assessment recommendation and monitoring (PHARM) Study // Arch. Intern. Med. 1999. Vol. 159, N 16. P. 1939–1945. doi: 10.1001/archinte.159.16.1939

17. McAlister F.A., Stewart S., Ferrua S., McMurray J.J. Multidisciplinary strategies for the management of heart failure patients at high risk for admission // J. Am. Coll. Cardiol. 2004. Vol. 44, N 4. P. 810–819. doi: 10.1016/j.jacc.2004.05.055

18. Cleland J.G., Louis A.A., Rigby A.S., et al.; TEN-HMS Investigators. Noninvasive home telemonitoring for patients with heart failure at high risk of recurrent admission and death // J. Am. Coll. Cardiol. 2005. Vol. 45, N 10. P. 1654–1664. doi: 10.1016/j.jacc.2005.01.050

19. Беленков Ю.Н. Влияние специализированных форм активного амбулаторного ведения на функциональный статус, качество жизни и показатели гемодинамики больных с выраженной сердечной недостаточностью. Результаты Российской программы «ШАНС» // Журнал сердечная недостаточность. 2007. Т. 8, № 3. С. 112–116. EDN: ODSNQP

20. Rotenstein L.S., Holmgren A.J., Downing N. L., Bates D.W. Differences in total and after-hours electronic health record time across ambulatory specialties // JAMA Intern. Med. 2021. Vol. 181, N 6. P. 863–865. doi: 10.1001/jamainternmed.2021.0256

21. Adler-Milstein J., Zhao W., Willard-Grace R., et al. Electronic health records and burnout: time spent on the electronic health record after hours and message volume associated with exhaustion but not with cynicism among primary care clinicians // J. Am. Med. Inform. Assoc. 2020. Vol. 27, N 4. P. 531–538. doi: 10.1093/jamia/ocz220

22. Azizi Z., Broadwin C., Islam S., et al. Digital health interventions for heart failure management in underserved rural areas of the united states: a systematic review of randomized trials // J. Am. Heart Assoc. 2024. Vol. 13, N 2. P. e030956. doi: 10.1161/JAHA.123.030956

23. Klersy C., De Silvestri A., Gabutti G., et al. A meta-analysis of remote monitoring of heart failure patients // J. Am. Coll. Cardiol. 2009. Vol. 54, N 18. P. 1683–1694. doi: 10.1016/j.jacc.2009.08.017

24. Chaudhry S.I., Mattera J.A., Curtis J.P., et al. Telemonitoring in Patients with Heart Failure // N. Engl. J. Med. 2010. Vol. 363, N 24. P. 2301–2309. doi: 10.1056/NEJMoa1010029

25. Koehler F., Winkler S., Schieber M., et al.; TIM-HF Investigators. Impact of remote telemedical management on mortality and hospitalizations in ambulatory patients with chronic heart failure: the telemedical interventional monitoring in heart failure study // Circulation. 2011. Vol. 123, N 17. P. 1873–1880. doi: 10.1161/CIRCULATIONAHA.111.018473

26. Lyngå P., Persson H., Hägg-Martinell A., et al. Weight monitoring in patients with severe heart failure (WISH). A randomized controlled trial // Eur. J. Heart Fail. 2012. Vol. 14, N 4. P. 438–444. doi: 10.1093/eurjhf/hfs023

27. Boyne J.J., Vrijhoef H.J., Crijns H.J., et al.; TEHAF investigators. Tailored telemonitoring in patients with heart failure: results of a multicentre randomized controlled trial // Eur. J. Heart Fail. 2012. Vol. 14, N 7. P. 791–801. doi: 10.1093/eurjhf/hfs058

28. Dendal P., De Keulenaer G., Troisfontaines P., et al. Effect of a telemonitoring-facilitated collaboration between general practitioner and heart failure clinic on mortality and rehospitalization rates in severe heart failure: the TEMA-HF 1 (TElemonitoring in the MAnagement of Heart Failure) study // Eur. J. Heart Fail. 2012. Vol. 14, N 3. P. 333–340. doi: 10.1093/eurjhf/hfr144

29. Inglis S.C., Clark R.A., Dierckx R., et al. Structured telephone support or non-invasive telemonitoring for patients with heart failure // Cochrane Database Syst. Rev. 2015. Vol. 2015, N 10. P. CD007228. doi: 10.1002/14651858.CD007228.pub3

30. Cowie M.R., Bax J., Bruining N., et al. e-Health: a position statement of the European Society of Cardiology // Eur. Heart J. 2016. Vol. 37, N 1. P. 63–66. doi: 10.1093/eurheartj/ehv416

31. Ong M.K., Romano P.S., Edgington S., et al. Effectiveness of remote patient monitoring after discharge of hospitalized patients with heart failure: the better effectiveness after transition–heart Failure (BEAT-HF) Randomized Clinical Trial // JAMA Intern. Med. 2016. Vol. 176, N 3. P. 310–318. doi: 10.1001/jamainternmed.2015.7712

32. Гребенникова А.А., Столяров А.Ю., Лопатин Ю.М. Применение платформы удалённого мониторинга на базе мобильного приложения для повышения приверженности к самопомощи пациентов с хронической сердечной недостаточностью // Кардиология. 2017. Т. 57, № 4S. С. 11–18. EDN: YKUOWF doi: 10.18087/cardio.2413

33. Koehler F., Koehler K., Deckwart O., et al. Efficacy of telemedical interventional management in patients with heart failure (TIM-HF2): a randomised, controlled, parallel-group, unmasked trial // The Lancet. 2018. Vol. 392, N 10152. P. 1047–1057. doi: 10.1016/S0140-6736(18)31880-4

34. Мареев Ю.В., Зинченко А.О., Мясников Р.П., и др. Применение телеметрии у больных с хронической сердечной недостаточностью // Кардиология. 2019. Т. 59, № 9S. С. 4–15. EDN: ISWIAY doi: 10.18087/cardio.n530

35. Zhu Y., Gu X., Xu C. Effectiveness of telemedicine systems for adults with heart failure: a meta-analysis of randomized controlled trials // Heart Fail. Rev. 2020. Vol. 25, N 2. P. 231–243. doi: 10.1007/s10741-019-09801-5

36. Tersalvi G., Winterton D., Cioffi G.M., et al. Telemedicine in heart failure during COVID-19: a step into the future // Front. Cardiovasc. Med. 2020. Vol. 7. P. 612818. doi: 10.3389/fcvm.2020.612818

37. Насонова С.Н., Лаптева А.Е., Жиров И.В., и др. Дистанционный мониторинг пациентов с сердечной недостаточностью в реальной клинической практике // Кардиология. 2021. Т. 61, № 8. С. 76–86. EDN: GRIBYY doi: 10.18087/cardio.2021.8.n1683

38. Yokota T., Fukushima A., Tsuchihashi-Makaya M., et al. The AppCare-HF randomized clinical trial: a feasibility study of a novel self-care support mobile app for individuals with chronic heart failure // Eur. Heart J. - Digit. Health. 2023. Vol. 4, N 4. P. 325–336. doi: 10.1093/ehjdh/ztad032

39. Rao V.N., Kaltenbach L.A., Granger B.B., et al. The Association of Digital Health Application use with heart failure care and outcomes: insights from CONNECT-HF // J. Card. Fail. 2022. Vol. 28, N 10. P. 1487–1496. doi: 10.1016/j.cardfail.2022.07.050

40. Агапов В.В., Кудряшов Ю.Ю., Грайфер И.В., Самитин В.В. Разработка и внедрение системы телемониторинга хронической сердечной недостаточности: опыт одного центра // Кардиология. 2022. Т. 62, № 5. С. 45–52. EDN: BHAITY doi: 10.18087/cardio.2022.5.n1825

41. Radhakrishnan K., Julien C., O'Hair M., et al. Sensor-controlled digital game for heart failure self-management: protocol for a randomized controlled trial // JMIR Res. Protoc. 2023. Vol. 12. P. e45801. doi: 10.2196/45801

42. Lukey A., Mackay M., Hasan K., Rush K.L. Clinical perspectives on the development of a gamified heart failure patient education web site // CIN Comput. Inform. Nurs. 2023. Vol. 41, N 8. P. 615–620. doi: 10.1097/CIN.0000000000000983

43. Yun S., Enjuanes C., Cobo M. et al. Effect on cardiovascular mortality and worsening heart failure of mHealth solutions combining telemonitoring and teleintervention: results of the HERMeS multicentre, randomised, controlled trial. In: Heart Failure; 2023 May 20–23; Prague. Unpublished.

44. Shara N., Bjarnadottir M.V., Falah N., et al. Voice activated remote monitoring technology for heart failure patients: Study design, feasibility and observations from a pilot randomized control trial // PLOS ONE. 2022. Vol. 17, N 5. P. e0267794. doi: 10.1371/journal.pone.0267794

45. Емельянов А.В., Железных Е.А., Кожевникова М.В., и др. Качество жизни и приверженность лечению у пациентов с хронической сердечной недостаточностью, находящихся на удалённом наблюдении с помощью чат-бота, по сравнению с группой стандартного наблюдения в течение 3 месяцев // Digital Diagnostics. 2023. Т. 4, № 1S. С. 53–56. EDN: PPGJTP doi: 10.17816/DD430343

46. Пырикова Н.В., Мозгунов Н.А., Осипова И.В. Результаты пилотного дистанционного мониторинга пациентов с хронической сердечной недостаточностью // Кардиоваскулярная терапия и профилактика. 2022. Т. 21, № 6. С. 42–51. EDN: ROTHHY doi: 10.15829/1728-8800-2022-3151

47. Wohlfahrt P., Jenča D., Melenovský V., et al. Remote heart failure symptoms assessment after myocardial infarction identifies patients at risk for death // J. Am. Heart Assoc. 2024. Vol. 13, N 2. P. e032505. doi: 10.1161/JAHA.123.032505

48. Stehlik J., Schmalfuss C., Bozkurt B., et al. Continuous wearable monitoring analytics predict heart failure hospitalization: the LINK-HF multicenter study // Circ. Heart Fail. 2020. Vol. 13, N 3. P. e006513. doi: 10.1161/CIRCHEARTFAILURE.119.006513

49. Потапов А.П., Ярцев С.Е., Лагутова Е.А. Дистанционное наблюдение за пациентами с хронической сердечной недостаточностью с применением телемониторинга АД и ЭКГ // Российский журнал телемедицины и электронного здравоохранения. 2021. Т. 7, № 3. С. 42–51. EDN: OFOTQN doi: 10.29188/2712-9217-2021-7-3-42-51

50. Гаранин А.А., Муллова И.С., Шкаева О.В., и др. Амбулаторный дистанционный мониторинг пациентов, выписанных из отделения неотложной кардиологии // Российский кардиологический журнал. 2022. Т. 27, № 3S. С. 8–15. EDN: BIRQPJ doi: 10.15829/1560-4071-2022-5072

51. Kleiner Shochat M., Fudim M., Shotan A., et al. Prediction of readmissions and mortality in patients with heart failure: lessons from the IMPEDANCE-HF extended trial // ESC Heart Fail. 2018. Vol. 5, N 5. P. 788–799. doi: 10.1002/ehf2.12330

52. Abraham W.T., Anker S., Burkhoff D., et al. Primary results of the sensible medical innovations lung fluid status monitor allows reducing readmission rate of heart failure patients (smile) trial // J. Card. Fail. 2019. Vol. 25, N 11. P. 938. doi: 10.1016/j.cardfail.2019.11.007

53. Bensimhon D., Alali S.A., Curran L., et al. The use of the reds noninvasive lung fluid monitoring system to assess readiness for discharge in patients hospitalized with acute heart failure: A pilot study // Heart Lung. 2021. Vol. 50, N 1. P. 59–64. doi: 10.1016/j.hrtlng.2020.07.003

54. Murton O.M., Dec G.W., Hillman R.E., et al. Acoustic voice and speech biomarkers of treatment status during hospitalization for acute decompensated heart failure // Appl. Sci. 2023. Vol. 13, N 3. P. 1827. doi: 10.3390/app13031827

55. Schöbi D., Zhang Y.P., Kehl J., et al. Evaluation of speech and pause alterations in patients with acute and chronic heart failure // J. Am. Heart Assoc. 2022. Vol. 11, N 21. P. e027023. doi: 10.1161/JAHA.122.027023

56. Atluri N., Mishra S.R., Anderson T., et al. Acceptability of a text message-based mobile health intervention to promote physical activity in cardiac rehabilitation enrollees: a qualitative substudy of participant perspectives // J. Am. Heart Assoc. 2024. Vol. 13, N 2. P. e030807. doi: 10.1161/JAHA.123.030807

57. Rossetto F., Borgnis F., Isernia S., et al. System integrated digital empowering and telerehabilitation to promote patient activation and well-being in chronic disabilities: a usability and acceptability study // Front. Public Health. 2023. Vol. 11. P. 1154481. doi: 10.3389/fpubh.2023.1154481

58. Piotrowicz E., Pencina M.J., Opolski G., et al. Effects of a 9-week hybrid comprehensive telerehabilitation program on long-term outcomes in patients with heart failure: the telerehabilitation in heart failure patients (TELEREH-HF) randomized clinical trial // JAMA Cardiol. 2020. Vol. 5, N 3. P. 300–308. doi: 10.1001/jamacardio.2019.5006

59. Dinesen B., Hansen E.T., Refsgaard J., et al. «Future patient II» telerehabilitation for patients with heart failure: protocl for a randomized controlled trial // Int. J. Cardiol. Cardiovasc. Risk Prev. 2024. Vol. 20. P. 200239. doi: 10.1016/j.ijcrp.2024.200239

60. Ghazi L., Yamamoto Y., Fuery M., et al. Electronic health record alerts for management of heart failure with reduced ejection fraction in hospitalized patients: the PROMPT-AHF trial // Eur. Heart J. 2023. Vol. 44, N 40. P. 4233–4242. doi: 10.1093/eurheartj/ehad512

61. Day S., Shah V., Kaganoff S., et al. Assessing the clinical robustness of digital health startups: cross-sectional observational analysis // J. Med. Internet Res. 2022. Vol. 24, N 6. P. e37677. doi: 10.2196/37677

AUTHORS' INFO

* Aleksei V. Emelianov, MD;
address: 6 bldg. 1 Bolshaya Pirogovskaya str., 119435, Moscow, Russia;
ORCID: 0000-0002-4748-8029;
eLibrary SPIN: 4346-1475;
e-mail: emelyanow.alexei@yandex.ru

Maria V. Kozhevnikova, MD, Cand. Sci. (Medicine);
ORCID: 0000-0003-4778-7755;
eLibrary SPIN: 8501-9812;
e-mail: kozhevnikova-m@inbox.ru

Elena A. Zheleznykh, MD, Cand. Sci. (Medicine);
ORCID: 0000-0002-2596-192X;
eLibrary SPIN: 2941-4875;
e-mail: elenavlvp@gmail.com

Anastasia L. Panova, MD;
ORCID: 0009-0000-9543-5282;
e-mail: lanaer@rambler.ru

Elena V. Privalova, MD, Dr. Sci. (Medicine), Professor;
ORCID: 0000-0001-6675-7557;
e-mail: ev_privalova@mail.ru

Yuri N. Belenkov, MD, Dr. Sci. (Medicine),
Academician of the Russian Academy of Sciences;
ORCID: 0000-0002-3014-6129;
eLibrary SPIN: 5661-4691;
e-mail: ynbelenkov@gmail.com

ОБ АВТОРАХ

* Емельянов Алексей Владимирович;
адрес: Россия, 119435, Москва, ул. Большая Пироговская, д. 6, стр. 1;
ORCID: 0000-0002-4748-8029;
eLibrary SPIN: 4346-1475;
e-mail: emelyanow.alexei@yandex.ru

Кожевникова Мария Владимировна, канд. мед. наук;
ORCID: 0000-0003-4778-7755;
eLibrary SPIN: 8501-9812;
e-mail: kozhevnikova-m@inbox.ru

Железных Елена Анатольевна, канд. мед. наук;
ORCID: 0000-0002-2596-192X;
eLibrary SPIN: 2941-4875;
e-mail: elenavlvp@gmail.com

Панова Анастасия Леонидовна;
ORCID: 0009-0000-9543-5282;
e-mail: lanaer@rambler.ru

Привалова Елена Витальевна, д-р мед. наук, профессор;
ORCID: 0000-0001-6675-7557;
e-mail: ev_privalova@mail.ru

Беленков Юрий Никитич, д-р мед. наук,
академик РАН;
ORCID: 0000-0002-3014-6129;
eLibrary SPIN: 5661-4691;
e-mail: ynbelenkov@gmail.com

* Corresponding author / Автор, ответственный за переписку

Digital stethoscope: a new era of auscultation

Andrey A. Garanin, Olesya Yu. Aydumova, Anatoly O. Rubanenko, Elena G. Bibikova

Samara State Medical University, Samara, Russia

ABSTRACT

The article reviews modern electronic and digital stethoscopes. The publications of the last 10 years were analyzed using eLIBRARY.ru, PubMed, Google Scholar with "аускультация" ("auscultation"), "электронный стетоскоп" ("electronic stethoscope"), "цифровой стетоскоп" ("digital stethoscope"), and "телемедицина" ("telemedicine") keywords. New ways to auscultate using digital stethoscopes were considered. Products from the most popular manufacturers were briefly characterized. Improved functionality and versatility of a digital stethoscope (ability to evaluate heart, lung, bowel, and other organ sounds), noise reduction and sound filtering make digital stethoscopes an even more attractive tool. If these challenges are met, a digital stethoscope will undoubtedly become an indispensable tool in the diagnosis, monitoring and treatment of diseases and in patient self-monitoring. Telemonitoring of patients with cardiovascular and respiratory diseases is a promising area of application for modern models of digital stethoscopes. Auscultation is especially important to evaluate changes during long-term follow-up, for early detection of complications and decompensated chronic non-infectious diseases such as chronic obstructive pulmonary disease, asthma, myocardial infarction, etc.

Keywords: auscultation; electronic stethoscope; digital stethoscope; telemedicine.

Цифровой стетоскоп — новая эра аускультации

А.А. Гаранин, О.Ю. Айдумова, А.О. Рубаненко, Е.Г. Бибикова

Самарский государственный медицинский университет, Самара, Россия

АННОТАЦИЯ

В статье представлен обзор современных электронных и цифровых стетоскопов. Проведён анализ публикаций за последние 10 лет с использованием поисковых систем eLIBRARY.ru, PubMed, Google Scholar по ключевым словам: «аускультация», «электронный стетоскоп», «цифровой стетоскоп», «телемедицина». Рассмотрены новые возможности аускультации при использовании цифровых стетоскопов. Даны краткие характеристики изделий наиболее востребованных на рынке производителей. Повышение функционала и универсальности цифрового стетоскопа (возможность анализировать звуки сердца, лёгких, кишечника и других органов), а также улучшение шумоподавления и фильтрации полученного звука позволят сделать цифровые стетоскопы ещё более привлекательными для использования. По мере решения этих задач цифровой стетоскоп определённо станет незаменимым инструментом в диагностике, мониторинге и лечении заболеваний, а также самоконтроле пациентов. Перспективным направлением использования современных моделей цифровых стетоскопов является телемониторинг пациентов с заболеваниями сердечно-сосудистой и дыхательной систем. Особенно важна оценка аускультативной картины пациентов в динамике, при длительном наблюдении, что может способствовать раннему выявлению осложнений и декомпенсаций различных хронических неинфекционных заболеваний, например хронической обструктивной болезни лёгких, бронхиальной астмы, инфаркта миокарда и т.д.

Ключевые слова: аускультация; электронный стетоскоп; цифровой стетоскоп; телемедицина.

数字听诊器 — 听诊新时代

Andrey A. Garanin, Olesya Yu. Aydumova, Anatoly O. Rubanenko, Elena G. Bibikova

Samara State Medical University, Samara, Russia

摘要

本文对现代电子和数字听诊器进行了概述。文章通过eLIBRARY.ru、PubMed、Google Scholar 等搜索引擎，以 "听诊"、"电子听诊器"、"数字听诊器"、"远程医疗" 为关键词，对过去10年的发表文章进行了分析。 研究了使用数字听诊器进行听诊的新的可能性。给出了市场上最受欢迎的制造商的产品简介。数字听诊器功能的增强和多功能性（能够分析心脏、肺、肠和其他器官的声音），以及改进降噪和对接收声音的过滤，将使数字听诊器更具使用吸引力。随着这些挑战的解决，数字听诊器必将成为疾病诊断、监测、治疗，以及患者自我监控不可替代的工具。对心血管和呼吸系统疾病患者进行远程监控是使用现代数字听诊器的一个很有前景的发展方向。尤其重要的是，在长期随访过程中对患者的听诊情况进行动态评估，这有助于及早发现各种慢性非传染性疾病的并发症和失代偿，如慢性阻塞性肺病、支气管哮喘、心肌梗死等等。

关键词：听诊；电子听诊器；数字听诊器；远程医疗。

INTRODUCTION

auscultation of sound phenomena accompanying the functioning of internal organs is one of the most important stages of the objective examination of a patient. Indirect auscultation has been used for almost 200 years, since the invention of the first stethoscope by Laennec in 1816. The funnel with a membrane he introduced made it possible to amplify the volume of sound signals. In 1940, Rappaport and Sprague improved the design of the stethoscope by proposing a dual-head configuration combining a bell and a diaphragm [1]. For a long time, the stethoscope remained unchanged in form.

The simplicity of use, cost-effectiveness, and wide availability make the classical stethoscope a popular tool among healthcare professionals [2]. It should be noted that, despite the simplicity and reliability of the classical auscultation method, it has a number of limitations. First and foremost are the distortions of transmitted sound signals caused by the acoustic properties of the stethoscope head, the flexibility of the tubing walls, and individual patient characteristics (chest wall thickness). In addition, sound perception is subjective and depends on the age and experience of the examiner [3, 4]. Finally, classical auscultation does not allow other specialists to analyze the detected sounds without direct patient presence, and the resulting data cannot be stored or reviewed [5]. This creates challenges in consulting patients using telemedicine technologies, as well as in remote monitoring and interpretation of physical examination findings in controversial clinical situations or legal proceedings [6].

The COVID-19 pandemic also highlighted the need to develop a new approach to auscultation using stethoscopes that can provide remote monitoring and minimize the risk of infection for healthcare workers during patient examination [7].

Electronic Stethoscope

New opportunities for auscultation emerged with the development of the electronic stethoscope. An electronic stethoscope consists of three modules providing for data acquisition, preprocessing, and signal transformation. The data acquisition module performs filtering, buffering, and amplification of the auscultated sounds, and converts the acoustic signal into a digital one. The preprocessing module filters the signal and removes artifacts. The signal transformation module then clusters the data for clinical decision-making [8].

Several types of electronic stethoscope sensors are distinguished based on the mechanism used to convert sound into an analog electrical signal.

Dual-diaphragm sensor: sound vibrations are captured by the stethoscope diaphragm and transmitted to a diaphragm within the microphone. However, the two diaphragms, separated by an air channel, may lead to excessive amplification of ambient noise and inaccurate transmission of the sound signal.

Piezoelectric sensor: sounds captured by the diaphragm alter the structure of a crystalline substance, converting the sound signal into an electrical signal.

Microelectromechanical system. The diaphragm of the stethoscope is located in a nominal capacitance field, which changes in accordance with the pressure of the sound wave. This change in capacitance converts the sound signal into an electrical one [9, 10].

Environmental noise suppression is also a critical function of the electronic stethoscope. Cain et al. [11] tested electronic stethoscopes in simulated helicopter noise conditions at 70–100 dB to determine the noise threshold for auscultation of heart and lung sounds. The noise threshold was 85 dB for heart tones and 75–80 dB for breath sounds. This implies the need for a signal-to-noise ratio improvement of at least 30 dB, which can be achieved by enhanced noise suppression. This would allow electronic stethoscopes to be used during natural disasters and patient transportation. This problem has been addressed using a digital filter capable of isolating the desired frequency range from the signal [1, 2]. The sound phenomena of internal organ function span different frequency ranges. Existing digital stethoscopes offer adjustable frequency modes for optimal auscultation of specific sounds, such as breath or heart sounds. For instance, the Welch Allyn Elite™ electronic stethoscope (Welch Allyn, USA) uses a 20–420 Hz frequency mode for heart auscultation and a 350–1900 Hz mode for lung auscultation. Thus, electronic stethoscopes enhance both sound quality and volume. The 3M™ Littmann® CORE stethoscope (3M, USA) with a piezoelectric sensor amplifies sound up to 40 times, whereas the Thinklabs One™ stethoscope (Thinklabs, USA) with a MEMS sensor amplifies sound up to 100 times [12, 13].

Undoubtedly, the electronic stethoscope increases the diagnostic value of auscultation [14]. In 2016, Azimpour et al. [15] investigated the potential of using an electronic stethoscope for acoustic diagnosis of hemodynamically significant (>50%) coronary artery stenosis by detecting intracoronary murmurs caused by turbulent blood flow within the artery in the presence of such stenosis. The coronary anatomy, as well as the presence and severity of atherosclerotic lesions, were verified using coronary angiography. The sensitivity and specificity of coronary artery stenosis detection by auscultation using an electronic stethoscope were 70% and 80%, respectively ($p < 0.001$). Several electronic auscultation test systems have been proposed for detection of obstructive coronary artery disease: CSA SonoMedica model 3.0™ (SonoMedica, USA), CADence Ironman™ (AUM Cardiovascular, USA), and CADScor System™ (Acarix AB, Sweden). In experimental studies, these test systems showed statistically significant detection of obstructive coronary artery lesions with a sensitivity of 81%–89.5% and specificity of 53%–83% [16].

In general, electronic stethoscope use expands auscultation capabilities by enhancing sound amplification and suppressing background noise.

Digital Stethoscope

The vast majority of modern electronic stethoscopes are equipped with a function to record and transmit sound to a computer or smartphone. By instructing the patient on how to position the stethoscope head, the physician can remotely auscultate and analyze the sounds. This enables remote monitoring of patients under quarantine (e.g., due to COVID-19) or in hard-to-reach areas, as well as the simultaneous interpretation of auscultatory sounds by multiple specialists to improve the quality of telemedicine consultations [17].

Another advantage of the digitalization of auscultation is the improved quality of medical student training. Auscultation simulators reproduce pre-recorded sounds from patients with various heart and lung diseases, allowing an entire audience to listen to the same recording [18]. The ability to display signals graphically as a spectrogram makes auscultation training more visual and facilitates the identification of spectrographic "patterns" associated with specific diseases [19].

The digitization of data has also enabled the use of artificial intelligence (AI) algorithms for sound analysis, opening new possibilities for auscultation. The most common method for sound processing is the Fourier transform, which analyzes the frequency components of the signal. A machine learning algorithm based on an artificial neural network can further process obtained information and correlate different frequencies with specific auscultatory findings. Gurung et al. [20] conducted a meta-analysis of studies to assess the predictive potential of combining digital lung auscultation with computational data analysis algorithms. The sensitivity and specificity of detecting pathological lung sounds using computational algorithms were 85% and 80%, respectively.

The next step in the development of digital auscultation was the ability not only to detect pathological sounds produced by internal organs, but also to diagnose diseases using computational algorithms. For example, Kaddoura et al. [21] analyzed the potential for diagnosing pulmonary hypertension based on heart and lung auscultation. Auscultatory findings obtained with a digital stethoscope were compared between healthy individuals and patients with pulmonary hypertension. The computer algorithm diagnosed pulmonary hypertension based on auscultation data in 74% of cases.

Thus, the modern digital stethoscope offers the following advantages [22]:

High-quality sound signals. Amplification of sounds produced by internal organs and ambient noise suppression facilitate auscultation in high-noise environments, such as in the field, in emergency zones, overcrowded hospital wards, and during patient transportation.

Remote patient examination. The absence of direct contact is essential when patients are geographically remote or when clinicians must use personal protective equipment under radiation, biological, or chemical hazard conditions.

Monitoring of acoustic phenomena in outpatient settings. Continuous auscultation during rest and daily activities, including physical exertion, as well as data collection from multiple sensors placed on different body regions, enable over-time patient assessment.

Auscultation data storage. The ability to reassess recorded data improves the effectiveness of telemedicine consultations and supports resolution of disputes in forensic practice. A database of auscultatory recordings typical of various diseases can be used in the training of medical students.

Disease diagnosis using AI algorithms.

A comparison between traditional and electronic stethoscopes is presented in Table 1.

All digital stethoscope models currently available on the market are equipped with sound amplification and noise reduction functions, as well as the ability to record and transmit acquired data to a personal computer or smartphone via Bluetooth. The 3M™ Littmann® 3200 stethoscope (3M Littmann, USA) is one of the most widely used tools for digital auscultation (Fig. 1a). This device amplifies the sound signal 24-fold and features two auscultation modes (for low- and high-frequency sounds). A backlit liquid crystal display shows heart rate (HR), auscultation mode, volume level, and battery status. The device records data in 30-second tracks, which are saved as audio files. The recorded sounds can be visualized as phonocardiograms using StethAssist™ software [23]. Digital stethoscopes manufactured by 3M™ are the most commonly used tools for evaluating the advantages of digital

Table 1. Comparative characteristics of traditional and electronic stethoscopes

Feature	Traditional stethoscope	Electronic stethoscope
Sound amplification	No	Yes
Noise reduction	No	Yes
Versatility for auscultation of internal organs	Yes	Not all models
Data recording and transmission	No	Yes
Use of AI algorithms	No	Yes
Dependence on power supply	No	Yes
Cost of the device and replaceable parts	Low	High

Note. AI, artificial intelligence.
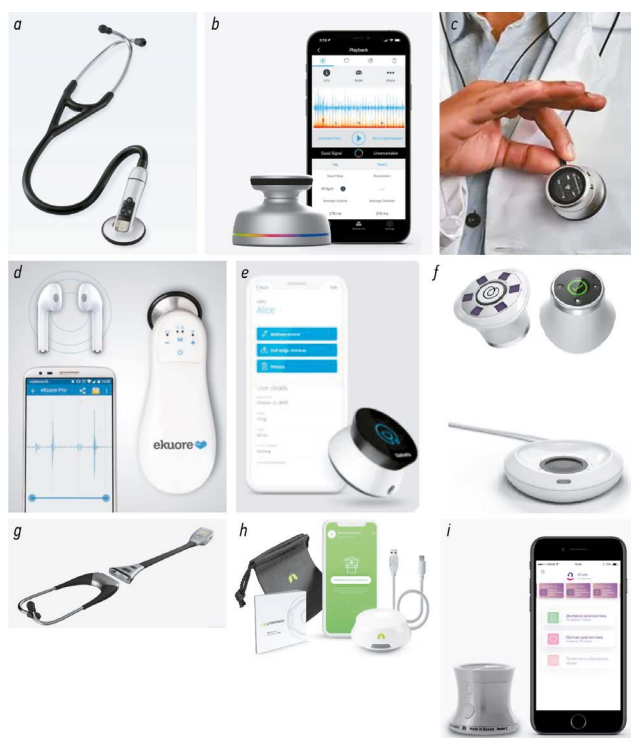
Fig. 1. Appearance of the most popular electronic stethoscopes currently on the market: *a*, 3M™ Littmann 3200 stethoscope (USA), http://stetoskopy.ru/shop/3m-littmann/3200_BK_27.html; *b*, M3DICINE Stethee Pro™ stethoscope (Australia), https://m3dicine.com/#deeper_level; *c*, Thinklabs One™ stethoscope (USA), https://www.thinklabs.com/stethoscopes; *d*, eKuore Pro™ cardiology stethoscope (Spain), https://www.deal-med.ru/stetoskop_elektronniy_ekuore_pro.html; *e*, StethoMe™ stethoscope (Poland), https://www.stethome.com/en-gb/; *f*, Sensors of the CADence™ system for cardiac disease diagnostics (USA), https://evercare.ru/cadence; *g*, Ekoscope™ stethoscope with ECG recording capability (USA), https://ekoscope.com/ekoscope; *h*, Healthy Networks Lung Passport™ stethoscope (Belarus), https://cetez.ru/lungpass/; *i*, Laeneco™ stethoscope (Russia), https://laenecocom.tmweb.ru/.

auscultation [24]. The Stethee Pro™ stethoscope (M3DICINE, Australia) amplifies sound 24-fold during direct auscultation and 96-fold when used with the Stethee Pro™ application. It captures and analyzes sounds in the frequency range from 20 Hz to 2 kHz, followed by AI-based interpretation using the AIDA™ algorithm (Fig. 1*b*). Like the previous device, it features the ability to visualize sound as a phonocardiogram on the screen of the receiving device. It is also equipped with a lithium battery with fast USB charging. Another advantage is the compact size of the model [25].

The most compact and lightweight digital stethoscope on the market with the highest sound amplification (up to 100-fold) is the Thinklabs One™ (Thinklabs, USA) (Fig. 1*c*). It supports multiple auscultation modes and features customizable noise filtering with the option to disable it entirely. This stethoscope allows clinicians to examine patients using personal protective equipment, such as in infectious disease units treating COVID-19 patients, and integrates with most videoconferencing and telemedicine

systems [12]. The eKuore Pro™ stethoscope (eKuore, Spain) is another device suitable for both in-person and remote auscultation (Fig. 1*d*). The device analyzes data using AI and easily integrates with any computer or smartphone software. Its distinctive features include the ability to replace the part that contacts the patient's body and data transmission via Wi-Fi [26]. The StethoMe™ stethoscope (StethoMe, Poland) is designed for home care services and patient self-monitoring in cases of cardiac and respiratory diseases, such as bronchial asthma (Fig. 1*e*). This stethoscope detects pathological breath sounds using the StethoMe AI™ system and automatically transmits the data to a physician, enabling remote monitoring of disease changes in the patient. A unique feature of this stethoscope is its capability to measure body temperature [27]. The CADence™ diagnostic system (AUM Cardiovascular, USA) combines a stethoscope and an electrocardiograph, with built-in sensors for recording electrocardiogram data (Fig. 1*f*). This system operates with the CADence Software™ application for clinical decision support, which assists clinicians in analyzing auscultatory findings in combination with ECG results. Data collection takes approximately 8 minutes, after which a report is automatically sent via email within 12 minutes [28]. The Ekoscope™ device (Ekoscope, USA) is another multifunctional medical tool that enables simultaneous cardiac auscultation and six-lead ECG recording (Fig. 1*g*). It is equipped with a microUSB port for battery charging and data transfer [29]. The Lung Passport™ stethoscope (Healthy Networks, Republic of Belarus) is intended for home-based diagnosis of respiratory diseases (Fig. 1*h*). The device is equipped with a mobile application that uses AI algorithms to analyze the recorded sounds, compares them with those characteristic of pneumonia, chronic obstructive pulmonary disease, bronchial asthma, and several types of bronchitis, and then generates a preliminary diagnosis. To improve diagnostic accuracy, the application also includes a patient questionnaire [30]. The Russian Laeneco™ stethoscope (Laeneco, Russia) is designed for both self-diagnosis and remote physician assessment based on audio recordings (Fig. 1*i*). AI-based data analysis takes 2 minutes, after which the device provides a conclusion regarding the presence or absence of pathological sounds, without issuing a diagnosis [31]. A comparative overview of various digital stethoscope models is presented in Table 2.

Thus, the devices described above offer varying functionalities. Some are suitable for patient self-diagnosis, whereas others are intended exclusively for physician use. Additional features of these stethoscopes—such as ECG recording, sound visualization, and body temperature measurement—are particularly noteworthy. Undoubtedly, a significant limitation of several digital stethoscope models is their specialization in auscultation of either the lungs or the heart only. Another obstacle to the widespread adoption of digital stethoscopes is the relatively high cost of the devices and their replaceable components, as well

Table 2. Comparative characteristics of the most popular digital stethoscope models on the market

Stethoscope model (manufacturer, country)	Advantages	Disadvantages
3M™ Littmann 3200 (Littmann, USA)	• Heart rate (HR) recording • Phonocardiogram visualization • Auscultation of the heart and lungs	• No AI-based data analysis • Not suitable for patient self-diagnosis • Not compatible with PPE use • No rechargeable battery (powered by AA batteries)
Stethee Pro™ (M3DICINE, Australia)	• Respiratory rate, heart rate, systole and diastole duration monitoring • Phonocardiogram visualization • Auscultation of the heart and lungs • Use of AI-based data analysis • Compatible with PPE use • Lithium battery	• Not suitable for patient self-diagnosis
Thinklabs One™ (Thinklabs, USA)	• Auscultation of the heart and lungs • Compatible with PPE use • Lithium battery	• No AI-based data analysis • Not suitable for patient self-diagnosis
eKuore Pro™ (eKuore, Spain)	• Auscultation of the heart and lungs • Compatible with PPE use • Wi-Fi connectivity • Remote monitoring capability • Lithium battery	• No AI-based data analysis • Not suitable for patient self-diagnosis
StethoMe™ (StethoMe, Poland)	• Auscultation of the heart and lungs • Use of AI-based data analysis • Compatible with PPE use • Remote monitoring capability • Suitable for patient self-diagnosis • Body temperature measurement • Lithium battery	• No headphones
CADence™ (CADence, USA)	• ECG recording • Lithium battery	• No lung auscultation • Not suitable for patient self-diagnosis
Ekoscope™ (Ekoscope, USA)	• ECG recording • Use of AI-based data analysis • Lithium battery	• No lung auscultation • Not suitable for patient self-diagnosis • Not compatible with PPE use
Lung Passport™ (Healthy Networks, Belarus)	• Use of AI-based data analysis • Suitable for patient self-diagnosis • Lithium battery	• No heart auscultation
Laeneco™ (Laeneco, Russia)	• Use of AI-based data analysis • Suitable for patient self-diagnosis • Lithium battery	• No heart auscultation

Note. HR, heart rate; AI, artificial intelligence; PPE, personal protective equipment; RR, respiratory rate; ECG, electrocardiogram.

as the complexity and expense of repairs due to the low geographic density of service centers. Nevertheless, the rapid development of clinical decision support systems and AI algorithms, along with the growing need for technologies that enable remote monitoring and telemedicine, position these devices as a promising segment in the medical device industry and market.

Over the past few decades, the development of AI has profoundly transformed key areas of everyday life, including healthcare. It has been shown that healthcare digitalization improves the quality of medical care, enhances treatment adherence, and enables early detection of diseases or their exacerbations [32]. The use of a digital stethoscope allows

auscultation findings to be recorded and stored, thereby eliminating subjectivity in data interpretation. Market analysis indicates that an increasing number of medical devices are patient-centered, enabling self-diagnosis at home. Digital stethoscopes are no exception: home-use digital stethoscopes equipped with AI-based diagnostic algorithms represent a distinct market niche. Furthermore, the use of such devices by patients in outpatient settings may help reduce the burden on primary healthcare services. For instance, preliminary assessments suggest that the use of the Lung Passport device may reduce the number of doctor visits by 35% [7]. Remote patient monitoring and examination using personal protective equipment contributes to reducing

contact between the patient and the healthcare professional, making the examination process as comfortable as possible for both parties. The use of fast-charging, high-capacity batteries and additional functions (ECG and thermometry) may further enhance the competitive advantages of these devices.

CONCLUSION

Enhancing the functionality and versatility of digital stethoscopes (including the ability to analyze sounds from the heart, lungs, intestines, and other organs) as well as improving noise reduction and signal filtering, make these devices increasingly attractive for clinical use. As these challenges are addressed, the digital stethoscope is set to become an indispensable tool for the diagnosis, monitoring, and treatment of diseases, as well as for patient self-monitoring. A particularly promising area of application for modern digital stethoscope models is telemonitoring of patients with cardiovascular and respiratory diseases. Of particular importance is the changes assessment of auscultatory findings over time, which may enable the early

detection of complications and decompensation in various chronic non-infectious diseases, such as chronic obstructive pulmonary disease, bronchial asthma, myocardial infarction, and others.

ADDITIONAL INFORMATION

REFERENCES

1. Swarup S, Mararyus AN. Digital stethoscope: technology update. *Med Devices (Auckl).* 2018;11:29–36. doi: 10.2147/MDER.S135882

2. Landge K, Kidambi BR, Singal A, Basha A. Electronic stethoscopes: brief review of clinical utility, evidence, and future implications. *Journal of the Practice of Cardiovascular Sciences.* 2018;4(2):65–68. doi: 10.4103/jpcs.jpcs_47_18

3. Grenier M-C, Gagnon K, Genest J, et al. Clinical comparison of acoustic and electronic stethoscopes and design of a new electronic stethoscope. *Am J Cardiol.* 1998;81(5):653–656. doi: 10.1016/s0002-9149(97)00977-6

4. Nussbaumer M, Agarwal A. Stethscope acoustics. *J Sound Vib.* 2022;539:1171–1194. doi: 10.1016/j.jsv.2022.117194

5. Tavel ME. Cardiac auscultation: a glorious past — and it does have a future! *Circulation.* 2006;113(9):1255–1259. doi: 10.1161/CIRCULATIONAHA.105.591149.

6. Nowak LJ, Nowak KM. Sound differences between electronic and acoustic stethoscopes. *Biomed Eng Online.* 2018;17(1):104. doi: 10.1186/s12938-018-0540-2

7. Kudryavtseva ES, Akhmetzyanova NM. Electronic stethoscope: new gadget for dianostics and self-diagnostics. *Arkhitektura zdorov'ya.* 2020(1):44–49. (In Russ.) EDN: GUSAON

8. Leng S, Tan RS, Chai KT, et al. The electronic stethoscope. *Biomed Eng Online.* 2015;14(1):66. doi: 10.1186/s12938-015-0056-y

9. Grundlehner B, Buxi D. Methods to characterize sensors for capturing body sounds. In: *International Conference on Body Sensor Networks (BSN)*; 2011 May 23–25; Dallas, TX, USA. doi: 10.1109/BSN.2011.22

10. Kevin TCC, Han D, Ravinder PS, et al. 118-db dynamic range, continuous-time, opened-loop capacitance to voltage converter readout for capacitive MEMS accelerometer. In: *IEEE Asian Solid-State Circuits Conference*; 2010 Nov 08–10; Beijing, China. doi: 10.1109/ASSCC.2010.5716626

11. Cain PA, Ahroon WA, Greenburg D. An Assessment of acoustic and electronic stethoscope performance in the UH-60 noise environment. U.S. Army Aeromedical Research Laboratory, Aircrew Protection Division; 2002 Aug. Report No.: 2002–20. Program element No.: 622787, project No.: 878.

12. Thinklabs One [Internet]. [cited 20 May 2024]. Available from: https://www.thinklabs.com/stethoscopes

13. The 3M Littmann CORE Digital Stethoscope [Internet]. [cited 20 May 2024]. Available from: https://www.littmann.com/3M/en_US/littmann-stethoscopes/advantages/core-digital-stethoscope/

14. Silverman B, Balk M. Digital stethoscope — improved auscultation at the bedside. *Am J Cardiol.* 2019;123(6):984–985. doi: 10.1016/j.amjcard.2018.12.022

15. Azimpour F, Caldwell E, Tawfik P, et al. Audible coronary artery stenosis. *Am J Med.* 2016;129(5):515–521. doi: 10.1016/j.amjmed.2016.01.015

16. Thomas JL, Winther S, Wilson RF, Bøttcher M. A novel approach to diagnosing coronary artery disease: acoustic detection of coronary turbulence. *Int J Cardiovasc Imaging.* 2017;33(1):129–136. doi: 10.1007/s10554-016-0970-5

17. Jain A, Sahu R, Gaumnitz T, et al. Development and validation of a low-cost electronic stethoscope: DIY digital stethoscope. *BMJ Innovations.* 2021;7:609–613. doi: 10.1136/bmjinnov-2021-000715

18. Takashina T, Shimizu M, Muratake T, Mayuzumi S. New stethoscope with extensible diaphragm. *Circ J.* 2016;80(9):2047–2049. doi: 10.1253/circj.CJ-16-0193

19. Legget ME, Toh M, Meintjes A, et al. Digital devices for teaching cardiac auscultation — A randomized pilot study. *Med Educ Online.* 2018;23(1):1524688. doi: 10.1080/10872981.2018.1524688

20. Gurung A, Scafford CG, Tielsch JM, et al. Computerized lung sound analysis as diagnostic aid for the detection of abnormal

lung sounds: a systematic review and meta-analysis. *Respir Med.* 2011;105(9):1396–1403. doi: 10.1016/j.rmed.2011.05.007

21. Kaddoura T, Vadlamudi K, Kumar S, et al. Acoustic diagnosis of pulmonary hypertension: automated speed-recognition-inspired classification algorithm outperforms physicians. *Sci Rep.* 2016;6:331382. doi: 10.1038/srep33182

22. Seah JJ, Zhao J, Wang DY, Lee HP. Review on the advancements of stethoscope types in chest auscultation. *Diagnostics.* 2023;13(9):1545. doi: 10.3390/diagnostics13091545

23. Stetoskopy.ru [Internet]. [cited 14 April 2024]. Available from: http://stetoskopy.ru/shop/3m-littmann/3200_BK_27.html/

24. Mamorita N, Arisaka N, Isonaka R, et al. Development of Smartphone App for visualizing heart sounds and murmurs. *Cardiology.* 2017;137(3):193–200. doi: 10.1159/000466683

25. Stethee Pro [Internet]. [cited 20 May 2024]. Available from: https://m3dicine.com/#deeper_level

26. Dealmed [Internet]. [cited 20 May 2024]. Available from: https://www.deal-med.ru/stetoskop_elektronniy_ekuore_pro.html

27. StethoMe [Internet]. [cited 20 May 2024]. Available from: https://www.stethome.com/en-gb/

28. EverCare [Internet]. [cited 20 May 2024]. Available from: https://evercare.ru/cadence

29. Ekoscope [Internet]. [cited 20 May 2024]. Available from: https://ekoscope.com/ekoscope

30. LungPass [Internet]. [cited 20 May 2024]. Available from: https://cetez.ru/lungpass/

31. Laeneco - Smart stethoscope [Internet]. [cited 20 May 2024]. Available from: https://laenecocom.tmweb.ru/

32. Honkoop P, Usmani O, Bonini M. The current and future role of technology in respiratory care. *PulmTher.* 2022;8(2):167–179. doi: 10.1007/s41030-022-00191-y

СПИСОК ЛИТЕРАТУРЫ

1. Swarup S., Mararyus A.N. Digital stethoscope: technology update // Med Devices (Auckl). 2018. Vol. 11. P. 29–36. doi: 10.2147/MDER.S135882

2. Landge K., Kidambi B.R., Singal A., Basha A. Electronic stethoscopes: brief review of clinical utility, evidence, and future implications // Journal of the Practice of Cardiovascular Sciences. 2018. Vol. 4, N 2. P. 65–68. doi: 10.4103/jpcs.jpcs_47_18

3. Grenier M.-C., Gagnon K., Genest J., et al. Clinical comparison of acoustic and electronic stethoscopes and design of a new electronic stethoscope // Am J Cardiol. 1998. Vol. 81, N 5. P. 653–656. doi: 10.1016/s0002-9149(97)00977-6

4. Nussbaumer M., Agarwal A. Stethscope acoustics // J Sound Vib. 2022. Vol. 539. P. 1171–1194. doi: 10.1016/j.jsv.2022.117194

5. Tavel M.E. Cardiac auscultation: a glorious past — and it does have a future! // Circulation. 2006. Vol. 113, N 9. P. 1255–1259. doi: 10.1161/CIRCULATIONAHA.105.591149

6. Nowak L.J., Nowak K.M. Sound differences between electronic and acoustic stethoscopes // Biomed Eng Online. 2018. Vol. 17, N 1. ID 104. doi: 10.1186/s12938-018-0540-2

7. Кудрявцева Е.С., Ахметзянова Н.М. Электронный стетоскоп: новый гаджет для диагностики и самодиагностики // Архитектура здоровья. 2020. № 1. С. 44–49. EDN: GUSAON

8. Leng S., Tan R.S., Chai K.T., et al. The electronic stethoscope // Biomed Eng Online. 2015. Vol. 14, N 1. ID 66. doi: 10.1186/s12938-015-0056-y

9. Grundlehner B., Buxi D. Methods to characterize sensors for capturing body sounds. In: International conference on body sensor networks (BSN); 2011 May 23–25; Dallas, TX, USA. doi: 10.1109/BSN.2011.22

10. Kevin T.C.C., Han D., Ravinder P.S., et al. 118-db dynamic range, continuous-time, opened-loop capacitance to voltage converter readout for capacitive MEMS accelerometer. In: IEEE Asian Solid-State Circuits Conference; 2010 Nov 08–10; Beijing, China. doi: 10.1109/ASSCC.2010.5716626

11. Cain P.A., Ahroon W.A., Greenburg D. An Assessment of acoustic and electronic stethoscope performance in the UH-60 noise environment. U.S. Army Aeromedical Research Laboratory, Aircrew Protection Division; 2002 Aug. Report No.: 2002–20. Program element No.: 622787, project No.: 878.

12. Thinklabs One [Internet]. [дата обращения: 20.05.2024]. Доступ по ссылке: https://www.thinklabs.com/stethoscopes

13. The 3M Littmann CORE Digital Stethoscope [Internet]. [дата обращения 20.05.2024]. Доступ по ссылке: https://www.littmann.com/3M/en_US/littmann-stethoscopes/advantages/core-digital-stethoscope/

14. Silverman B., Balk M. Digital stethoscope — improved auscultation at the bedside // Am J Cardiol. 2019. Vol. 123, N 6. P. 984–985. doi: 10.1016/j.amjcard.2018.12.022

15. Azimpour F., Caldwell E., Tawfik P., et al. Audible coronary artery stenosis // Am J Med. 2016. Vol. 129, N 5. P. 515–521. doi: 10.1016/j.amjmed.2016.01.015

16. Thomas J.L., Winther S., Wilson R.F., Bøttcher M. A novel approach to diagnosing coronary artery disease: acoustic detection of coronary turbulence // Int J Cardiovasc Imaging. 2017. Vol. 33, N 1. P. 129–136. doi: 10.1007/s10554-016-0970-5

17. Jain A., Sahu R., Gaumnitz T., et al. Development and validation of a low-cost electronic stethoscope: DIY digital stethoscope // BMJ Innovations. 2021. Vol. 7. P. 609–613. doi: 10.1136/bmjinnov-2021-000715

18. Takashina T., Shimizu M., Muratake T., Mayuzumi S. New stethoscope with extensible diaphragm // Circ J. 2016. Vol. 80, N 9. P. 2047–2049. doi: 10.1253/circj.CJ-16-0193

19. Legget M.E., Toh M., Meintjes A., et al. Digital devices for teaching cardiac auscultation — A randomized pilot study // Med Educ Online. 2018. Vol. 23, N 1. ID 1524688. doi: 10.1080/10872981.2018.1524688

20. Gurung A., Scafford C.G., Tielsch J.M., et al. Computerized lung sound analysis as diagnostic aid for the detection of abnormal lung sounds: a systematic review and meta-analysis // Respir Med. 2011. Vol. 105, N 9. P. 1396–1403. doi: 10.1016/j.rmed.2011.05.007

21. Kaddoura T., Vadlamudi K., Kumar S., et al. Acoustic diagnosis of pulmonary hypertension: automated speed-recognition-inspired classification algorithm outperforms physicians // Sci Rep. 2016. Vol. 6. ID 33182. doi: 10.1038/srep33182

22. Seah J.J., Zhao J. Wang D.Y., Lee H.P. Review on the advancements of stethoscope types in chest auscultation // Diagnostics. 2023. Vol. 13, N 9. ID 1545. doi: 10.3390/diagnostics13091545

23. Stetoskopy.ru [Internet]. [дата обращения 14.04.2024]. Режим доступа: http://stetoskopy.ru/shop/3m-littmann/3200_BK_27.html/

24. Mamorita N., Arisaka N., Isonaka R., et al. Development of Smartphone App for visualizing heart sounds and murmurs // Cardiology. 2017. Vol. 137, N 3. P. 193–200. doi: 10.1159/000466683

25. Stethee Pro [Internet]. [дата обращения: 20.05.2024]. Режим доступа: https://m3dicine.com/#deeper_level

26. Деалмед [Internet]. [дата обращения: 20.05.2024]. Режим доступа: https://www.deal-med.ru/stetoskop_elektronniy_ekuore_pro.html

27. StethoMe [Internet]. [дата обращения: 20.05.2024]. Режим доступа: https://www.stethome.com/en-gb/

28. EverCare [Internet]. [дата обращения: 20.05.2024]. Режим доступа: https://evercare.ru/cadence

29. Ekoscope [Internet]. [дата обращения: 20.05.2024]. Режим доступа: https://ekoscope.com/ekoscope

30. LungPass [Internet]. [дата обращения: 20.05.2024]. Режим доступа: https://cetez.ru/lungpass/

31. Laeneco - Smart stethoscope [Internet]. [дата обращения: 20.05.2024]. Режим доступа: https://laenecocom.tmweb.ru/

32. Honkoop P., Usmani O., Bonini M. The current and future role of technology in respiratory care // Pulm Ther. 2022. Vol. 8, N 2. P. 167–179. doi: 10.1007/s41030-022-00191-y

AUTHORS' INFO

* Andrey A. Garanin, MD, Cand. Sci. (Medicine);
address: 165b Karl-Marx avenue, 443079, Samara, Russia;
ORCID: 0000-0001-6665-1533;
eLibrary SPIN: 9976-3085;
e-mail: a.a.garanin@samsmu.ru

Olesya Yu. Aydumova, MD;
ORCID: 0000-0001-5673-7958;
eLibrary SPIN: 6330-2186;
e-mail: o.yu.ajdumova@samsmu.ru

Anatoly O. Rubanenko;
ORCID: 0000-0002-3996-4689;
eLibrary SPIN: 6947-1028;
e-mail: a.o.rubanenko@samsmu.ru

Elena G. Bibikova;
ORCID: 0009-0005-9392-1101;
eLibrary SPIN: 1578-1620;
e-mail: e.g.bibikova@samsmu.ru

ОБ АВТОРАХ

* Гаранин Андрей Александрович, канд. мед. наук;
адрес: Россия, 443079, Самара, пр. Карла-Маркса, д. 165б;
ORCID: 0000-0001-6665-1533;
eLibrary SPIN: 9976-3085;
e-mail: a.a.garanin@samsmu.ru

Айдумова Олеся Юрьевна;
ORCID: 0000-0001-5673-7958;
eLibrary SPIN: 6330-2186;
e-mail: o.yu.ajdumova@samsmu.ru

Рубаненко Анатолий Олегович;
ORCID: 0000-0002-3996-4689;
eLibrary SPIN: 6947-1028
e-mail: a.o.rubanenko@samsmu.ru

Бибикова Елена Григорьевна;
ORCID: 0009-0005-9392-1101;
eLibrary SPIN: 1578-1620;
e-mail: e.g.bibikova@samsmu.ru

* Corresponding author / Автор, ответственный за переписку

Potential use of virtual and augmented reality technologies in modern cardiology and cardiac surgery

Seda S. Rashidova[1], Emma A. Bdoyan[2], Madina M. Timurzieva[3], Sofya A. Lobanovskaya[3], Valeria V. Naumenko[2], Angelina V. Rakhmanova[2], Valeriya D. Timofeeva[4], Alexey S. Gutsulyak[5], Artem A. Zainullin[5], Karina R. Uzbekova[5], Valeriya A. Kharitonova[5], Narina F. Akhmetova[5]

[1] Khasavyurt Perinatal Center, Khasavyurt, Russia;
[2] Rostov State Medical University, Rostov-on-Don, Russia;
[3] Pirogov Russian National Research Medical University, Russia;
[4] Academician I.P. Pavlov First St. Petersburg State Medical University, Saint Petersburg, Russia;
[5] Bashkir State Medical University, Ufa, Russia

ABSTRACT

Innovative technologies have dramatically changed medical practice, particularly in cardiac surgery, which requires precision and caution due to the challenging nature of procedures. The use of virtual reality (VR) and augmented reality (AR) in this area has great potential to improve surgical planning, medical education and patient outcomes.

This review analyzes the literature on the role of VR and AR in modern cardiology and discusses possible directions for their development.

The search retrieved 3,858 publications from PubMed/MEDLINE, 69 publications from eLibrary, and 1,115 publications from Google Scholar. Searches included the following keywords and combinations thereof: virtual reality; augmented reality; cardiology; cardiac surgery. Publications were searched from the time the relevant databases were created to May 2024.

Cardiac care today involves increasingly sophisticated procedures that require a high level of expertise. VR becomes a powerful tool for both surgical planning and education. It opens new opportunities for educating and training cardiologists. It can be used to create realistic simulations of situations healthcare professionals may encounter in their practice. Students are able to gain hands-on experience with no risk to real patients. Integrating virtual reality into cardiology practice has great potential, but several issues need to be addressed. Standards for safety and efficacy of the medical use of virtual reality should be developed. Further research is also needed to assess the long-term health effects of VR use on patients.

Keywords: artificial intelligence; virtual reality; augmented reality; cardiology; imaging; training.

Возможности применения технологий виртуальной и дополненной реальности в современной кардиологии и кардиохирургии

С.С. Рашидова[1], Э.А. Бдоян[2], М.М. Тимурзиева[3], С.А. Лобановская[3], В.В. Науменко[2], А.В. Рахманова[2], В.Д. Тимофеева[4], А.С. Гуцуляк[5], А.А. Зайнуллин[5], К.Р. Узбекова[5], В.А. Харитонова[5], Н.Ф. Ахметова[5]

[1] Перинатальный центр г. Хасавюрта, Хасавюрт, Россия;
[2] Ростовский государственный медицинский университет, Ростов-на-Дону, Россия;
[3] Российский национальный исследовательский медицинский университет имени Н.И. Пирогова, Москва, Россия;
[4] Первый Санкт-Петербургский государственный медицинский университет имени академика И.П. Павлова, Санкт-Петербург, Россия;
[5] Башкирский государственный медицинский университет, Уфа, Россия

АННОТАЦИЯ

Технологические инновации произвели революцию в медицинской практике, особенно в области кардиохирургии, где сложный характер вмешательств требует точности и предусмотрительности. Использование виртуальной и дополненной реальности в этой области открывает огромные перспективы для улучшения предоперационного планирования, повышения качества медицинского образования и, в конечном счёте, улучшения результатов лечения пациентов.

В данном обзоре проанализирована литература, посвящённая роли виртуальной и дополненной реальности в современной кардиологии, а также обсуждаются возможные направления развития данной области.

В результате поиска извлечено 3858 публикаций из PubMed/MEDLINE, 69 публикаций из eLibrary и 1115 публикаций, найденных с помощью Google Scholar. Поисковые запросы включали следующие ключевые слова и их сочетания: виртуальная реальность; дополненная реальность; кардиология; кардиохирургия; virtual reality; augmented reality; cardiology; cardiac surgery. Временной интервал поиска: с момента основания соответствующих баз данных по май 2024 года.

Современная кардиологическая помощь включает в себя всё более сложные процедуры, требующие высокого уровня квалификации. Виртуальная реальность становится мощным инструментом как для предпроцедурного планирования, так и для образовательных мероприятий. Она открывает новые возможности для обучения и подготовки специалистов в области кардиологии. С её помощью можно создавать реалистичные симуляции различных ситуаций, с которыми врачи могут столкнуться в своей работе. Это позволяет обучающимся получить практический опыт без риска для реальных пациентов. Интеграция виртуальной реальности в кардиологическую практику имеет большой потенциал, однако для этого необходимо решить ряд проблем. Следует разработать стандарты безопасности и эффективности использования виртуальной реальности в медицинских целях. Также необходимо провести дополнительные исследования, чтобы оценить долгосрочные последствия её использования для здоровья пациентов.

Ключевые слова: искусственный интеллект; виртуальная реальность; дополненная реальность; кардиология; визуализация; обучение.

在现代心脏病学和心脏外科中应用虚拟现实和增强现实技术的可能性

Seda S. Rashidova[1], Emma A. Bdoyan[2], Madina M. Timurzieva[3], Sofya A. Lobanovskaya[3], Valeria V. Naumenko[2], Angelina V. Rakhmanova[2], Valeriya D. Timofeeva[4], Alexey S. Gutsulyak[5], Artem A. Zainullin[5], Karina R. Uzbekova[5], Valeriya A. Kharitonova[5], Narina F. Akhmetova[5]

[1] Khasavyurt Perinatal Center, Khasavyurt, Russia;
[2] Rostov State Medical University, Rostov-on-Don, Russia;
[3] Pirogov Russian National Research Medical University, Russia;
[4] Academician I.P. Pavlov First St. Petersburg State Medical University, Saint Petersburg, Russia;
[5] Bashkir State Medical University, Ufa, Russia

摘要

技术创新彻底改变了医疗实践，特别是在心脏外科领域，干预的复杂性需要精确性和预见性。虚拟现实和增强现实在该领域的应用，对于改善术前规划、提高医学教育质量，并最终改善患者治疗效果，具有巨大的前景。

本综述分析了虚拟现实和增强现实在现代心脏病学中的作用的文献，并讨论了该领域可能的发展方向。

最终从PubMed/MEDLINE检索到3858篇发表文章，从　　eLibrary检索到69篇发表文章，并使用Google　Scholar检索到1115篇发表文章。搜索查询包括以下关键词及其词组：虚拟现实；增强现实；心脏病学；心脏外科；virtual reality；augmented reality；cardiology；cardiac surgery。检索时间间隔：自各数据库建库至2024年5月。

现代心脏护理，包括日益复杂的程序，需要高水平的专业知识。虚拟现实正在成为程序前规划和教育活动的强大工具。它为心脏病学的教育和培训提供了新的可能性。它可对医生在工作中可能遇到的各种情况进行真实的模拟。这使得学员能够获得实践经验，而真正的患者无需承担风险。将虚拟现实融入心脏病学实践具有巨大潜力，但为此必须解决许多问题。应制定将虚拟现实技术用于医疗目的的虚拟现实的安全性和有效性的标准。还需要进一步的研究来评估其使用对患者健康的长期影响。

关键词：人工智能；虚拟现实；增强现实；心脏病学；可视化；学习。

INTRODUCTION

Modern healthcare is seeing a global trend toward the utilization of virtual, augmented, and mixed reality [1]. *Virtual reality* (VR) systems use computerized three-dimensional digital information visualization to simulate real or virtual objects. VR technology was invented in the 1950s [2]. It had undergone substantial change by the 1980s and was the subject of in-depth preclinical research [3]. Notably, the introduction of head-mounted displays with a frontal screen (also known as VR headsets) in the 1980s marked a shift in medical imaging [4]. During the process, VR headset components continuously travel back and forth to create 3D images [5].

Augmented reality (AR) is characterized by the seamless integration of virtual elements and reality. Unlike VR, which fully immerses the user in a simulated digital reality, AR incorporates virtual information into the user environment. AR functions are implemented via gadgets like smartphones, tablets, and head-mounted devices outfitted with transparent glasses or projectors that project virtual images directly into the real world [6–8]. This difference serves as the foundation for investigating the unique properties of both virtual and augmented reality in the context of the advancement of cardiac surgery.

Innovative technologies have significantly altered medical practice, particularly cardiac surgery, which requires precision and caution due to the challenging nature of the procedures. The application of VR and AR in this field has great potential for improving surgical planning, medical education, and patient outcomes.

DATA SEARCH METHODOLOGY

Publications were assessed in accordance with the *PRISMA* guidelines. The selection algorithm is presented in Fig. 1.

The search yielded 3,858 publications from *PubMed/MEDLINE*, 69 publications from *eLIBRARY. RU*, and 1,115 publications from *Google Scholar* databases. The search terms included the following keywords and their combinations: *виртуальная реальность (virtual reality), дополненная реальность (augmented reality), кардиология (cardiology),* and *кардиохирургия (cardiac surgery).* Publications from the creation of pertinent databases to May 2024 were searched. All authors independently screened the titles and abstracts of the identified publications. When relevant studies were found, the full text of the respective publications was retrieved. Duplicates and non-full-text publications were excluded. Full-text publications were assessed for compliance with the following inclusion criteria:
- Publications in either English or Russian;
- Publications in peer-reviewed journals;
- Reviews, experimental studies, and clinical studies containing the specified keywords.

After screening, 55 publications were included in the review.

ROLE OF VIRTUAL REALITY IN INTERVENTIONAL CARDIOLOGY

Peri-procedural VR and AR technologies are modern technologies that generate 3D images of anatomical structures for facilitating pre- and postoperative planning. VR enables radiologists to examine complex anatomy in a virtual world [9, 10], whereas AR assists in applying digital data to patients both before and after surgery. Rymuza et al. described the preoperative use of *CarnaLife Holo* in a patient with bicuspid aortic valve stenosis [11]. Radiologists could visualize a 3D hologram of the heart during a successful *transcatheter aortic valve replacement* (TAVR). Both VR and AR technologies enable the modeling of congenital

Identification
Identified studies (*n* = 5,431):
PubMed/MEDLINE (*n* = 3858)
eLIBRARY.RU (*n* = 69)
Google Scholar (*n* = 1115)

Duplicates excluded prior to screening (*n* = 735)

Screening
Studies with screened abstracts and titles (*n* = 4696)

Studies excluded based on the abstract and title (*n* = 4274)

Eligibility
Full-text articles (*n* = 422)

Do not fulfill the inclusion criteria (*n* = 367)

Included
Articles included in the review (*n* = 55)

Fig. 1. Publication search algorithm.

heart diseases as well as various phases of structural heart interventions such as TAVR and other valvular interventions [12–14]. Endovascular occlusion of the *left atrial appendage* (LAA), electrophysiological ablation, and TAVR are complex interventions that require a thorough understanding of the cardiac anatomy [15]. TAVR can be modeled by developing individual models and identifying the optimal site for prosthetic aortic valve placement. Several factors can be considered when determining this site, including valve morphology and calcification, presumed distances to relevant structures in cardiac conduction disorders, and coronary ostia, which are useful in other interventions such as LAA occlusion or transaortic reconstruction of the posterior mitral leaflet. In these cases, mitral valve interventions can be planned after determining the precise transseptal puncture site [16]. VR simulators assist in selecting the optimal surgical approach, thereby mitigating the risk of fatal complications such as aortic perforation, mitral valve apparatus destruction, left ventricular outflow tract obstruction, or coronary artery damage. Additionally, radiologists employ real-time X-ray imaging to assess the patient's anatomy. Furthermore, they can use alternative imaging modalities such as preoperative *computed tomography* (CT), cardiac *magnetic resonance imaging* (MRI), and *echocardiography* (ECG). These techniques can also be useful for pericardiocentesis and electrophysiological procedures [17].

In addition to the benefits of VR for physicians, it can also be used to improve patient comfort during treatment. For example, immersive VR promotes positive emotions and improves mood by synchronizing and stabilizing electric pulses in the prefrontal cortex, thereby reducing pain and discomfort [18]. Several studies have assessed the impact of VR on interventional cardiology procedures using different applications and multimedia content.

Based on the *State-Trait Anxiety Inventory* score, Keshvari et al. demonstrated that undergoing a 5-min VR session featuring natural scenarios and sounds, such as quiet music and sounds of birds and waterfalls, prior to *coronary angiography* (CAG) reduced anxiety levels [19]. There were significant differences in outcomes between the treatment group and the control group participants who received the conventional treatment. Moreover, the authors found that a 5-min VR session stabilized the heart rate and blood pressure [19].

Aardoom et al. reported that the VR-based training content administered one or two weeks before undergoing CAG reduced the procedure-related anxiety. Patients used a VR headset at home or in a clinic to virtually review all surgical stages, from admission to the postoperative period. The training addressed diverse medical care-related topics, including behavior in a hospital ward, clothing for patients, persons who can accompany them, and drugs prescribed after surgery. Patients could interact with healthcare personnel avatars to obtain essential information about each stage. The VR session lasted approximately 20 minutes; however, the time spent in each module likely affected how long it lasted [20].

Morgan et al. found a considerably greater decline in anxiety in patients who received a 10-min VR training session prior to CAG, which explained the pre-procedure phase and the procedure, compared with the control group. Moreover, compared to the control group, the treatment group understood the procedure better and expressed greater satisfaction with the outcomes. In a clinical study by Gökçe and Arslan, VR-based training for patients undergoing CAG was more effective in lowering pain and anxiety, as well as improving patient comfort, systolic blood pressure, respiratory rate, and heart rate, compared to conventional treatment in the control group [22].

VR has also been employed in patients who received conscious sedation[1] during TAVR. Patients in the treatment group received a 30-min VR session in a relaxing environment of their choice. Overall, 91.3% of the patients used VR prior to undergoing the procedure, while 37.5% used it during the procedure. A significant decrease in anxiety was noted on the *visual analog scale* (VAS) [23] compared to the control group participants who received conventional TAVR. However, these findings should be interpreted with caution due to the small sample size (32 patients) [23].

VR can be used prior to administering catheter-based ablation for *atrial fibrillation* (AF). The procedure boosted patient awareness, self-efficacy, and satisfaction while mitigating the anxiety associated with surgery [24–26]. Moreover, the use of VR prior to ablation effectively reduced anxiety and pain during the surgery [26]. Brewer et al. used VR in 40 patients who underwent unilateral radiofrequency ablation of the great saphenous vein. All procedures were successful, with no variations in the overall surgery time, and every patient was largely satisfied with the treatment. VR significantly reduced surgery-related anxiety compared to the control group that received standard care. Moreover, during surgery, anxiety increased in the control group but decreased in the VR group. Finally, 85% of the VR group participants indicated that they would recommend VR to others undergoing this surgery [27].

ROLE OF VIRTUAL REALITY IN HEART FAILURE TREATMENT

In addition to its use in interventional procedures, VR can assist with the anatomical planning of *mechanical circulatory support*. In the treatment of *heart failure* (HF), it is essential to understand the interactions between hemodynamics and the anatomy and function of the myocardium and valves. One example is the use of *ventricular assist devices* (VADs)

---

[1] Conscious intravenous sedation is a technique that uses sedative drugs to induce light sleep.

in patients with different ventricular shapes, sizes, and functional characteristics. Modern VADs can be used in children as a foundation for therapy prescription. VAD implantation using VR simulation can assist in determining both the design and the best position of the device in a specific patient, considering anatomical features [28]. Specifically, virtual models enable the real-time testing of VAD implantation and the determination of the appropriate orientation of the cannula. The proper position of the cannula (parallel to the *septum*, in line with the atrioventricular valve) is crucial for achieving optimal outcomes. Improper positioning can impede blood flow, resulting in thrombosis. Preoperative assessment can be useful for preventing complications, especially in children, who can develop complications associated with left ventricular failure following surgery. Patient-specific models can also provide critical insights on the spatial relationship between a VAD and major structures such as the interventricular septum and coronary arteries, the orientation of cardiac valves, and the interactions between extracardiac devices and the chest wall and diaphragm.

Stepanenko et al. described their experience with 3D printing and VR in 53 adult patients with progressive HF [29]. 3D modeling facilitated optimal clinical decisions on the type of mechanical circulatory support to be administered. Similarly, Davies et al. [30] and Ramaswamy et al. [31] described the use of VR to assess the placement of the *HeartWare VAD* (HVAD; Medtronic, Dublin, Ireland) and *HeartMate 3* (Abbott, Chicago, Illinois) intrapericardial devices in children.

Furthermore, these models can be used for surgeon training because they enable physical manipulation and implant testing, boosting surgeons' confidence during interventions. Thus, VR reconstructions and specialized 3D models can facilitate precise surgical planning, identify potential risks, and assist in patient-specific medical emergency planning.

ROLE OF VIRTUAL REALITY IN PREPROCEDURAL PLANNING

The advancement of digital technology continuously modifies knowledge and opportunities in cardiac care [32]. It is now possible to use *artificial intelligence* (AI) for performing automated ECGs and robot-assisted surgery in minimally invasive mitral valve procedures. Complex structural cardiovascular interventions require adequate technical competence and preparedness for any unexpected life-threatening complications. Progress in this area is based on advancements in multimodal visualization, optimizing measurements, calibration, and preprocedural planning. VR technologies can play a significant role in this field as a useful tool for both patients and physicians.

Interactive 3D images and VR simulators can facilitate the imaging of complex heart anatomy for determining the best treatment strategy (percutaneous or surgical intervention).

In cases where neighboring structures or severe calcification can prevent the use of modern imaging tools, VR in combination with other imaging techniques, such as ECG and cardiac CT, allows for precise surgical planning and the determination of appropriate implantation sites for TAVR or MitraClip-based techniques [15, 16]. Similar to flight simulators, modern VR systems can ensure patient safety by predicting and preventing fatal complications, such as implant displacement, aortic perforation, and acute coronary syndrome [16].

INTRA-PROCEDURAL APPLICATION OF VIRTUAL REALITY

VR is used in many complex cases, such as mitral valve interventions with varied and complex mitral valve anatomy, which typically require multimodal visualization for optimal outcomes [26]. VR augments accuracy and lowers the procedure time compared to conventional transesophageal ECG. Moreover, VR can enhance paravalvular regurgitation imaging following TAVR and assist in VAD selection [33, 34].

In congenital heart diseases, such as *atrial septal defects* with abnormal pulmonary venous drainage, VR prevented errors in transseptal puncture in combination with CT and biplanar X-ray imaging [33, 35, 36]. Furthermore, VR can facilitate the comprehensive assessment of the LAA and adjacent structures, such as the pulmonary artery and circumflex artery, in LAA occlusion associated with AF and high-risk bleeding [33]. A holographic model of the heart can be made utilizing a holographic environment made with 3D pictures from an ECG or CT scan, allowing for interactive device control using voice commands and movements. This makes the platform convenient for performing cardiac surgery [37].

ROLE OF VIRTUAL REALITY IN CONGENITAL HEART DISEASE

Procedure planning in *congenital heart diseases* (CHDs) can be challenging due to their wide spectrum and diverse clinical manifestations. In cardiology, VR is utilized for training and procedure planning. Its use began during the preclinical stage of implantable device development. Moreover, it has been used for creating and testing prototypes prior to animal studies and subsequent strictly regulated tests for implanting these devices in humans.

Because of their ease of cropping, surface mesh models based on the manual segmentation of CT, angiography, or cardiac MRI scans assist cardiac surgeons in surgical planning [38]. However, their development can be challenging. Raimondi et al. described the use of a novel VR technology for cardiac MRI data processing without intermediate segmentation stages. The average post-processing duration for the VR models using this software was five minutes [39].

Full-immersion VR significantly improved the diagnostic accuracy in heart diseases compared to a 2D display and VR software (by 54.49% and 146.82%, respectively). There were no significant differences between the diagnostic data provided to each study participant (t = −1.01, p = 0.31) [40]. Another study compared the efficacy of stereoscopic VR and a monoscopic PC. The evaluation of the anatomy in CHDs was not enhanced by stereoscopic VR (p = 0.11). The group of patients receiving monoscopic PC reported that its interface was more user-friendly than that of the stereoscopic VR (p = 0.01) [41].

Recent studies comparing VR and 3D-printed heart models in CHDs revealed that VR was more useful in medical training and preoperative planning than 3D-printed models; however, the differences were not statistically significant [42]. Similar findings were noted during a VR session while assessing anatomical features in patients with CHDs. Healthcare professionals with diverse expertise and experience (cardiac surgeons, cardiologists, cardiac anesthesiologists, pediatricians, and pathologists) and medical students participated in the session. In total, 72% of the participants rated the VR interaction methods (e.g., grasping objects, using cutting tools) as "extremely intuitive," and 94% were willing to implement the VR system in their institutions, awarding it four or five points on a 5-point scale [43].

A medical facility must make significant investments in the necessary infrastructure, software, screens, and VR headsets before implementing VR. However, compared to 3D printing, the cost of the equipment and materials for 3D printing, as well as the operating expenses, remain constant. VR enables the editing and updating of visualized 3D models and meshes as necessary, saving them in a digital format, and linking them to medical records for future use [44].

VR is particularly beneficial in planning complex intra- and extracardiac interventions. For example, a research group of pediatric cardiac surgeons reported increased confidence when planning and performing surgeries in two-thirds of cases and improvements in the surgical strategy in 60% of cases [38]. Davies et al. reported the use of VR to plan adult VAD placement in a child (17 kg, 0.67 m^2). This approach preserved the atrioventricular valve function and reduced the distortion of the cardiac structures [30]. The use of VR is currently limited to a few centers; however, it is gaining acceptance in academic and therapeutic organizations.

VIRTUAL REALITY EXPANSION USING ARTIFICIAL INTELLIGENCE

AI is essential for complicated and multidomain data processing in VR and AR, facilitating the adoption of novel technologies. More specifically, AI contributes to VR functionality in three areas:

Segmentation: AI facilitates accurate and rapid data labeling. Deep learning algorithms enable structure tracking, which can be totally automated or supervised.

The pre-processing time is reduced from several days to several minutes, making this step crucial for implementing VR in clinical practice [38, 45].

Reconstruction: AI enables human model reconstructions in VR for specific applications, such as coronary artery modeling with automatic calculation of atherosclerotic plaque volume or echocardiogram conversion into a VR model with 3D anatomy and blood flow visualization for surgical planning [38]. This step allows the user to focus on the work in the virtual environment rather than the application settings [46]. Franson et al. developed a system that converts 2D MRI images into interactive 4D structures that users can view in real time, with the rendering speed exceeding the data collection speed [47]. Similarly, the solution proposed by Bindschadler et al. was further refined, making it possible to manipulate cardiac models in AR. These models can be viewed on mobile devices using simple gestures, a function optimized for patient counseling [48].

Man–machine interaction: User interactions with VR can generate vast volumes of multidomain data, which must be integrated with reduced dimensions, upgraded machine learning, and user–VR interactions. This function is primarily employed in medical training [49, 50]. Moreover, this technology can mitigate VR sickness, which many users find to be a limitation. This is achieved by using a system with six degrees of freedom, which boosts oculomotor responses and reduces the spatial disorientation that induces nausea and dizziness [51].

These features allowed systems like *Immersive* and *Elucis* to create VR platforms. These platforms can be used for a single examination with cardiac imaging, procedure planning, remote communication between experts, and patient counseling. Moreover, they allow preservation of models for training, thus enabling delivery of high-quality medical care.

PROSPECTS

The use of VR can immensely impact modern cardiology. Integration of CT, MRI, and ECG findings is still a developing area, with the possibility of real-time data fusion and generating high-resolution 3D anatomical structures [52, 53]. Modern cardiac surgery procedures are becoming increasingly complex and demand excellent skills [53, 54]. VR can be used as a training tool for acquiring the skills required for clinical practice. Moreover, VR eliminates geographic barriers, providing easy access to training programs and conferences and offering practical experience. Patients can also benefit from these educational opportunities, enhancing their comprehension of human anatomy and surgical procedures. VR-based technologies are ready to be incorporated into standard treatment plans and be implemented in medical institutions [53, 55].

However, several issues must be addressed before VR is extensively used in clinical practice. Most published studies

are small-scale, including a small number of cases, and are performed in individual centers. Reliable VR efficacy assessment in clinical practice requires large-scale studies and randomized clinical trials. Moreover, the methods must be standardized to ensure consistency and facilitate widespread use. The integration of multimodal images is ongoing, although it has not yet reached its full potential. Furthermore, the use of diverse VR platforms, each requiring developing special skills, can present users with additional challenges. The introduction of VR in clinical practice can add to the existing heavy workload. Despite the promising future of VR in medicine, it is extremely important to conduct randomized clinical trials to validate its utility.

Although difficulties exist, the value of VR in clinical practice has become increasingly obvious. VR use in healthcare requires ongoing technological advancements and standardized applications to reach its full potential.

CONCLUSION

cardiac care today entails performing increasingly sophisticated procedures that require a high level of expertise. In this context, VR becomes a powerful tool for both preprocedural planning and training. It opens new opportunities for training cardiologists. It can be used to create realistic simulations of various situations that healthcare professionals may encounter in their practice. Students can obtain practical experience without endangering actual patients. Moreover, VR can be used for preprocedural planning of complex cardiac surgeries. It allows for the comprehensive assessment of patient anatomy, surgical planning, and predicting potential complications. This can significantly improve surgical accuracy and safety.

However, several issues must be addressed before VR becomes widely used in clinical practice. It is necessary to create guidelines for the effectiveness and safety of VR in medical contexts. Moreover, further research is needed to determine the long-term health effects of VR use. Overall, VR integration in cardiology exhibits great potential. It can significantly improve medical care quality, reduce risks, and facilitate training. To fully maximize this potential, additional research and relevant standards are required.

ADDITIONAL INFORMATION

REFERENCES

1. Nikolaev VA, Nikolaev AA. Virtual, augmented and mixed reality technologies in the context of digitalization of healthcare system. Medical Technologies. *Assessment and Choice.* 2020;(2):35–42. EDN: AWZZTL doi: 10.17116/medtech20204002135

2. Jiang Z, Guo Y, Wang Z. Digital twin to improve the virtual-real integration of industrial IoT. *J Ind Inf Integr.* 2021;22(11):100196. doi: 10.1016/j.jii.2020.100196

3. Nikitin AI, Abramov MK. The use of VR in medicine. In: Aktual'nye problemy aviacii i kosmonavtiki. *Sbornik materialov V Mezhdunarodnoj nauchno-prakticheskoj konferencii, posvyashchennoj Dnyu kosmonavtiki.* 2019;2:193–194. (In Russ.) EDN: RLBTYQ

4. Haleem A, Javaid M. Industry 5.0 and its applications in orthopaedics. *J Clin Orthop Trauma.* 2019;10(4):807–808. doi: 10.1016/j.jcot.2018.12.010

5. Cho KH, Hong MR, Song WK. Upper-Limb Robot-Assisted Therapy Based on Visual Error Augmentation in Virtual Reality for Motor Recovery and Kinematics after Chronic Hemiparetic Stroke: A Feasibility Study. *Healthcare (Basel).* 2022;10(7):1186. doi: 10.3390/healthcare10071186

6. Namiot ED. Augmented reality in medicine. *International Journal of Open Information Technologies.* 2019;7(11):94–99. EDN: ULRJCX

7. Sutherland J, Belec J, Sheikh A, et al. Applying Modern Virtual and Augmented Reality Technologies to Medical Images and Models. *J Digit Imaging.* 2019;32(1):38–53. doi: 10.1007/s10278-018-0122-7

8. Taghian A, Abo-Zahhad M, Sayed MS, Abd El-Malek AH. Virtual and augmented reality in biomedical engineering. *Biomed Eng Online.* 2023;22(1):76. doi: 10.1186/s12938-023-01138-3

9. Buytaert JA, Dirckx JJ. Design and quantitative resolution measurements of an optical virtual sectioning three-dimensional imaging technique for biomedical specimens, featuring two-micrometer slicing resolution. *J Biomed Opt.* 2007;12(1):014039. doi: 10.1117/1.2671712

10. Silva JNA, Southworth M, Raptis C, Silva J. Emerging Applications of Virtual Reality in Cardiovascular Medicine. *JACC Basic Transl Sci.* 2018;3(3):420–430. doi: 10.1016/j.jacbts.2017.11.009

11. Rymuza B, Grodecki K, Kamiński J, et al. Holographic imaging during transcatheter aortic valve implantation procedure in bicuspid aortic valve stenosis. *Kardiol Pol.* 2017;75(10):1056. doi: 10.5603/KP.2017.0195

12. Aslani N, Behmanesh A, Garavand A, et al. The Virtual Reality Technology Effects and Features in Cardiology Interventions Training: A Scoping Review. *Med J Islam Repub Iran.* 2022;36:77. doi: 10.47176/mjiri.36.77

13. Southworth MK, Silva JR, Silva JNA. Use of extended realities in cardiology. *Trends Cardiovasc Med.* 2020;30(3):143–148. doi: 10.1016/j.tcm.2019.04.005

14. Culbertson C, Nicolas S, Zaharovits I, et al. Methamphetamine craving induced in an online virtual reality environment. *Pharmacol Biochem Behav.* 2010;96(4):454–460. doi: 10.1016/j.pbb.2010.07.005

15. Arslan F, Gerckens U. Virtual support for remote proctoring in TAVR during COVID-19. *Catheter Cardiovasc Interv.* 2021;98(5):E733–E736. doi: 10.1002/ccd.29504

16. Liu J, Al'Aref SJ, Singh G, et al. An augmented reality system for image guidance of transcatheter procedures for structural heart disease. *PLoS One.* 2019;14(7):e0219174. doi: 10.1371/journal.pone.0219174

17. de Jesus Catalã CA, Pan R, Rossetto Kron-Rodrigues M, de Oliveira Freitas N. Virtual Reality Therapy to Control Burn Pain: Systematic Review of Randomized Controlled Trials. *J Burn Care Res.* 2022;43(4):880–888. doi: 10.1093/jbcr/irab213

18. Salisbury JP. Using Medical Device Standards for Design and Risk Management of Immersive Virtual Reality for At-Home Therapy and Remote Patient Monitoring. *JMIR Biomed Eng.* 2021;6(2):e26942. doi: 10.2196/26942

19. Keshvari M, Yeganeh MR, Paryad E, et al. The effect of virtual reality distraction on reducing patients' anxiety before coronary angiography: a randomized clinical trial study. *Egypt Heart J.* 2021;73(1):98. doi: 10.1186/s43044-021-00224-y

20. Aardoom JJ, Hilt AD, Woudenberg T, et al. A Preoperative Virtual Reality App for Patients Scheduled for Cardiac Catheterization: Pre-Post Questionnaire Study Examining Feasibility, Usability, and Acceptability. *JMIR Cardio.* 2022;6(1):e29473. doi: 10.2196/29473

21. Morgan H, Nana M, Phillips D, Gallagher S. The Effect of a Virtual Reality Immersive Experience Upon Anxiety Levels, Procedural Understanding, and Satisfaction in Patients Undergoing Cardiac Catheterization: The Virtual Cath Trial. *J Invasive Cardiol.* 2021;33(9):E681–E686. doi: 10.25270/jic/20.00664

22. Gökçe E, Arslan S. Effects of virtual reality and acupressure interventions on pain, anxiety, vital signs and comfort in catheter extraction processes for patients undergoing coronary angiography: A randomized controlled trial. *Int J Nurs Pract.* 2023;29(6):e13176. doi: 10.1111/ijn.13176

23. Bruno RR, Lin Y, Wolff G, et al. Virtual reality-assisted conscious sedation during transcatheter aortic valve implantation: a randomised pilot study. *EuroIntervention.* 2020;16(12):e1014–e1020. doi: 10.4244/EIJ-D-20-00269

24. Hermans ANL, Betz K, Verhaert DVM, et al. 360° Virtual reality to improve patient education and reduce anxiety towards atrial fibrillation ablation. *Europace.* 2023;25(3):855–862. doi: 10.1093/europace/euac246

25. Chang SL, Kuo MJ, Lin YJ, et al. Virtual reality informative aids increase residents' atrial fibrillation ablation procedures-related knowledge and patients' satisfaction. *J Chin Med Assoc.* 2021;84(1):25–32. doi: 10.1097/JCMA.0000000000000464

26. Chang SL, Kuo MJ, Lin YJ, et al. Virtual reality-based preprocedural education increases preparedness and satisfaction of patients about the catheter ablation of atrial fibrillation. *J Chin Med Assoc.* 2021;84(7):690–697. doi: 10.1097/JCMA.0000000000000555

27. Brewer MB, Lau DL, Chu EA, et al. Virtual reality can reduce anxiety during office-based great saphenous vein radiofrequency ablation. *J Vasc Surg Venous Lymphat Disord.* 2021;9(5):1222–1225. doi: 10.1016/j.jvsv.2020.12.081

28. Goo HW, Park SJ, Yoo SJ. Advanced Medical Use of Three-Dimensional Imaging in Congenital Heart Disease: Augmented

Reality, Mixed Reality, Virtual Reality, and Three-Dimensional Printing. *Korean J Radiol.* 2020;21(2):133–145. doi: 10.3348/kjr.2019.0625

29. Stepanenko A, Perez LM, Ferre JC, et al. 3D Virtual modelling, 3D printing and extended reality for planning of implant procedure of short-term and long-term mechanical circulatory support devices and heart transplantation. *Front Cardiovasc Med.* 2023;10:1191705. doi: 10.3389/fcvm.2023.1191705

30. Davies RR, Hussain T, Tandon A. Using virtual reality simulated implantation for fit-testing pediatric patients for adult ventricular assist devices. *JTCVS Tech.* 2020;6:134–137. doi: 10.1016/j.xjtc.2020.10.017

31. Ramaswamy RK, Marimuthu SK, Ramarathnam KK, et al. Virtual reality-guided left ventricular assist device implantation in pediatric patient: Valuable presurgical tool. *Ann Pediatr Cardiol.* 2021;14(3):388–392. doi: 10.4103/apc.apc_81_21

32. Tautz L, Walczak L, Georgii J, et al. Combining position-based dynamics and gradient vector flow for 4D mitral valve segmentation in TEE sequences. *Int J Comput Assist Radiol Surg.* 2020;15(1):119–128. doi: 10.1007/s11548-019-02071-4

33. Bruckheimer E, Rotschild C. Holography for imaging in structural heart disease. *EuroIntervention.* 2016;12 Suppl X:81–84. doi: 10.4244/EIJV12SXA15

34. Currie ME, McLeod AJ, Moore JT, et al. Augmented Reality System for Ultrasound Guidance of Transcatheter Aortic Valve Implantation. *Innovations (Phila).* 2016;11(1):31–39. doi: 10.1097/IMI.0000000000000235

35. Butera G, Sturla F, Pluchinotta FR, et al. Holographic Augmented Reality and 3D Printing for Advanced Planning of Sinus Venosus ASD/Partial Anomalous Pulmonary Venous Return Percutaneous Management. *JACC Cardiovasc Interv.* 2019;12(14):1389–1391. doi: 10.1016/j.jcin.2019.03.020

36. Zbroński K, Rymuza B, Scisło P, et al. Augmented reality in left atrial appendage occlusion. *Kardiol Pol.* 2018;76(1):212. doi: 10.5603/KP.2018.0017

37. Iannotta M, d'Aiello FA, Van De Bruaene A, et al. Modern tools in congenital heart disease imaging and procedure planning: a European survey. *J Cardiovasc Med (Hagerstown).* 2024;25(1):76–87. doi: 10.2459/JCM.0000000000001569

38. Deng S, Wheeler G, Toussaint N, et al. A Virtual Reality System for Improved Image-Based Planning of Complex Cardiac Procedures. *J Imaging.* 2021;7(8):151. doi: 10.3390/jimaging7080151

39. Raimondi F, Vida V, Godard C, et al. Fast-track virtual reality for cardiac imaging in congenital heart disease. *J Card Surg.* 2021;36(7):2598–2602. doi: 10.1111/jocs.15508

40. Kim B, Loke YH, Mass P, et al. A Novel Virtual Reality Medical Image Display System for Group Discussions of Congenital Heart Disease: Development and Usability Testing. *JMIR Cardio.* 2020;4(1):e20633. doi: 10.2196/20633

41. Patel N, Costa A, Sanders SP, Ezon D. Stereoscopic virtual reality does not improve knowledge acquisition of congenital heart disease. *Int J Cardiovasc Imaging.* 2021;37(7):2283–2290. doi: 10.1007/s10554-021-02191-6

42. Lau I, Gupta A, Sun Z. Clinical Value of Virtual Reality versus 3D Printing in Congenital Heart Disease. *Biomolecules.* 2021;11(6):884. doi: 10.3390/biom11060884

43. Milano EG, Pajaziti E, Schievano S, et al. P369 Patient specific virtual reality for education in con- genital heart disease. *Eur Heart J Cardiovasc Imaging.* 2020;21(suppl 1). doi: 10.1093/ehjci/jez319.218

44. Ong CS, Krishnan A, Huang CY, et al. Role of virtual reality in congenital heart disease. *Congenit Heart Dis.* 2018;13(3):357–361. doi: 10.1111/chd.12587

45. Sadeghi AH, Maat APWM, Taverne YJHJ, et al. Virtual reality and artificial intelligence for 3-dimensional planning of lung segmentectomies. *JTCVS Tech.* 2021;7:309–321. doi: 10.1016/j.xjtc.2021.03.016

46. van de Woestijne PC, Bakhuis W, Sadeghi AH, et al. 3D Virtual Reality Imaging of Major Aortopulmonary Collateral Arteries: A Novel Diagnostic Modality. *World J Pediatr Congenit Heart Surg.* 2021;12(6):765–772. doi: 10.1177/21501351211045064

47. Franson D, Dupuis A, Gulani V, et al. A System for Real-Time, Online Mixed-Reality Visualization of Cardiac Magnetic Resonance Images. *J Imaging.* 2021;7(12):274. doi: 10.3390/jimaging7120274

48. Bindschadler M, Buddhe S, Ferguson MR, et al. HEARTBEAT4D: An Open-source Toolbox for Turning 4D Cardiac CT into VR/AR. *J Digit Imaging.* 2022;35(6):1759–1767. doi: 10.1007/s10278-022-00659-y

49. Aeckersberg G, Gkremoutis A, Schmitz-Rixen T, Kaiser E. The relevance of low-fidelity virtual reality simulators compared with other learning methods in basic endovascular skills training. *J Vasc Surg.* 2019;69(1):227–235. doi: 10.1016/j.jvs.2018.10.047

50. Andersen NL, Jensen RO, Posth S, et al. Teaching ultrasound-guided peripheral venous catheter placement through immersive virtual reality: An explorative pilot study. *Medicine (Baltimore).* 2021;100(27):e26394. doi: 10.1097/MD.0000000000026394

51. Arshad I, De Mello P, Ender M, et al. Reducing Cybersickness in 360-Degree Virtual Reality. *Multisens Res.* 2021:1–17. doi: 10.1163/22134808-bja10066

52. Jung C, Wolff G, Wernly B, et al. Virtual and Augmented Reality in Cardiovascular Care: State-of-the-Art and Future Perspectives. *JACC Cardiovasc Imaging.* 2022;15(3):519–532. doi: 10.1016/j.jcmg.2021.08.017

53. Mahtab EAF, Egorova AD. Current and future applications of virtual reality technology for cardiac interventions. *Nat Rev Cardiol.* 2022;19(12):779–780. doi: 10.1038/s41569-022-00789-4

54. Pezel T, Coisne A, Bonnet G, et al. Simulation-based training in cardiology: State-of-the-art review from the French Commission of Simulation Teaching (Commission d'enseignement par simulation-COMSI) of the French Society of Cardiology. *Arch Cardiovasc Dis.* 2021;114(1):73–84. doi: 10.1016/j.acvd.2020.10.004

55. Spiegel B, Fuller G, Lopez M, et al. Virtual reality for management of pain in hospitalized patients: A randomized comparative effectiveness trial. *PLoS One.* 2019;14(8):e0219115. doi: 10.1371/journal.pone.0219115

СПИСОК ЛИТЕРАТУРЫ

1. Николаев В.А., Николаев А.А. Опыт и перспективы использования технологий виртуальной, дополненной и смешанной реальности в условиях цифровой трансформации системы здравоохранения // Медицинские технологии. Оценка и выбор. 2020. № 2. С. 35–42. EDN: AWZZTL doi: 10.17116/medtech20204002135

2. Jiang Z., Guo Y., Wang Z. Digital twin to improve the virtual-real integration of industrial IoT // J Ind Inf Integr. 2021. Vol. 22, N 11. P. 100196. doi: 10.1016/j.jiii.2020.100196

3. Никитин А.И., Абрамов М.К. Применение VR в медицине. В кн.: Актуальные проблемы авиации и космонавтики. Сборник материалов V Международной научно-практической конференции, посвященной Дню космонавтики. 2019. Т. 2. С. 193–194. EDN: RLBTYQ

4. Haleem A., Javaid M. Industry 5.0 and its applications in orthopaedics // J Clin Orthop Trauma. 2019. Vol. 10, N 4. P. 807–808. doi: 10.1016/j.jcot.2018.12.010

5. Cho K.H., Hong M.R., Song W.K. Upper-Limb Robot-Assisted Therapy Based on Visual Error Augmentation in Virtual Reality for Motor Recovery and Kinematics after Chronic Hemiparetic Stroke: A Feasibility Study // Healthcare (Basel). 2022. Vol. 10, N 7. P. 1186. doi: 10.3390/healthcare10071186

6. Намиот Е.Д. Дополненная реальность в медицине // International Journal of Open Information Technologies. 2019. Т. 7, № 11. С. 94–99. EDN: ULRJCX

7. Sutherland J., Belec J., Sheikh A., et al. Applying Modern Virtual and Augmented Reality Technologies to Medical Images and Models // J Digit Imaging. 2019. Vol. 32, N 1. P. 38–53. doi: 10.1007/s10278-018-0122-7

8. Taghian A., Abo-Zahhad M., Sayed M.S., Abd El-Malek A.H. Virtual and augmented reality in biomedical engineering // Biomed Eng Online. 2023. Vol. 22, N 1. P. 76. doi: 10.1186/s12938-023-01138-3

9. Buytaert J.A., Dirckx J.J. Design and quantitative resolution measurements of an optical virtual sectioning three-dimensional imaging technique for biomedical specimens, featuring two-micrometer slicing resolution // J Biomed Opt. 2007. Vol. 12, N 1. P. 014039. doi: 10.1117/1.2671712

10. Silva J.N.A., Southworth M., Raptis C., Silva J. Emerging Applications of Virtual Reality in Cardiovascular Medicine // JACC Basic Transl Sci. 2018. Vol. 3, N 3. P. 420–430. doi: 10.1016/j.jacbts.2017.11.009

11. Rymuza B., Grodecki K., Kamiński J., et al. Holographic imaging during transcatheter aortic valve implantation procedure in bicuspid aortic valve stenosis // Kardiol Pol. 2017. Vol. 75, N 10. P. 1056. doi: 10.5603/KP.2017.0195

12. Aslani N., Behmanesh A., Garavand A., et al. The Virtual Reality Technology Effects and Features in Cardiology Interventions Training: A Scoping Review // Med J Islam Repub Iran. 2022. Vol. 36. P. 77. doi: 10.47176/mjiri.36.77

13. Southworth M.K., Silva J.R., Silva J.N.A. Use of extended realities in cardiology // Trends Cardiovasc Med. 2020. Vol. 30, N 3. P. 143–148. doi: 10.1016/j.tcm.2019.04.005

14. Culbertson C., Nicolas S., Zaharovits I., et al. Methamphetamine craving induced in an online virtual reality environment // Pharmacol Biochem Behav. 2010. Vol. 96, N 4. P. 454–460. doi: 10.1016/j.pbb.2010.07.005

15. Arslan F., Gerckens U. Virtual support for remote proctoring in TAVR during COVID-19 // Catheter Cardiovasc Interv. 2021. Vol. 98, N 5. P. E733–E736. doi: 10.1002/ccd.29504

16. Liu J., Al'Aref S.J., Singh G., et al. An augmented reality system for image guidance of transcatheter procedures for structural heart disease // PLoS One. 2019. Vol. 14, N 7. P. e0219174. doi: 10.1371/journal.pone.0219174

17. de Jesus Catalã C.A., Pan R., Rossetto Kron-Rodrigues M., de Oliveira Freitas N. Virtual Reality Therapy to Control Burn Pain: Systematic Review of Randomized Controlled Trials // J Burn Care Res. 2022. Vol. 43, N 4. P. 880–888. doi: 10.1093/jbcr/irab213

18. Salisbury J.P. Using Medical Device Standards for Design and Risk Management of Immersive Virtual Reality for At-Home Therapy and Remote Patient Monitoring // JMIR Biomed Eng. 2021. Vol. 6, N 2. P. e26942. doi: 10.2196/26942

19. Keshvari M., Yeganeh M.R., Paryad E., et al. The effect of virtual reality distraction on reducing patients' anxiety before coronary angiography: a randomized clinical trial study // Egypt Heart J. 2021. Vol. 73, N 1. P. 98. doi: 10.1186/s43044-021-00224-y

20. Aardoom J.J., Hilt A.D., Woudenberg T., et al. A Preoperative Virtual Reality App for Patients Scheduled for Cardiac Catheterization: Pre-Post Questionnaire Study Examining Feasibility, Usability,

and Acceptability // JMIR Cardio. 2022. Vol. 6, N 1. P. e29473. doi: 10.2196/29473

21. Morgan H., Nana M., Phillips D., Gallagher S. The Effect of a Virtual Reality Immersive Experience Upon Anxiety Levels, Procedural Understanding, and Satisfaction in Patients Undergoing Cardiac Catheterization: The Virtual Cath Trial // J Invasive Cardiol. 2021. Vol. 33, N 9. P. E681–E686. doi: 10.25270/jic/20.00664

22. Gökçe E., Arslan S. Effects of virtual reality and acupressure interventions on pain, anxiety, vital signs and comfort in catheter extraction processes for patients undergoing coronary angiography: A randomized controlled trial // Int J Nurs Pract. 2023. Vol. 29, N 6. P. e13176. doi: 10.1111/ijn.13176

23. Bruno R.R., Lin Y., Wolff G., et al. Virtual reality-assisted conscious sedation during transcatheter aortic valve implantation: a randomised pilot study // EuroIntervention. 2020. Vol. 16, N 12. P. e1014–e1020. doi: 10.4244/EIJ-D-20-00269

24. Hermans A.N.L., Betz K., Verhaert D.V.M., et al. 360° Virtual reality to improve patient education and reduce anxiety towards atrial fibrillation ablation // Europace. 2023. Vol. 25, N 3. P. 855–862. doi: 10.1093/europace/euac246

25. Chang S.L., Kuo M.J., Lin Y.J., et al. Virtual reality informative aids increase residents' atrial fibrillation ablation procedures-related knowledge and patients' satisfaction // J Chin Med Assoc. 2021. Vol. 84, N 1. P. 25–32. doi: 10.1097/JCMA.0000000000000464

26. Chang S.L., Kuo M.J., Lin Y.J., et al. Virtual reality-based preprocedural education increases preparedness and satisfaction of patients about the catheter ablation of atrial fibrillation // J Chin Med Assoc. 2021. Vol. 84, N 7. P. 690–697. doi: 10.1097/JCMA.0000000000000555

27. Brewer M.B., Lau D.L., Chu E.A., et al. Virtual reality can reduce anxiety during office-based great saphenous vein radiofrequency ablation // J Vasc Surg Venous Lymphat Disord. 2021. Vol. 9, N 5. P. 1222–1225. doi: 10.1016/j.jvsv.2020.12.081

28. Goo H.W., Park S.J., Yoo S.J. Advanced Medical Use of Three-Dimensional Imaging in Congenital Heart Disease: Augmented Reality, Mixed Reality, Virtual Reality, and Three-Dimensional Printing // Korean J Radiol. 2020. Vol. 21, N 2. P. 133–145. doi: 10.3348/kjr.2019.0625

29. Stepanenko A., Perez L.M., Ferre J.C., et al. 3D Virtual modelling, 3D printing and extended reality for planning of implant procedure of short-term and long-term mechanical circulatory support devices and heart transplantation // Front Cardiovasc Med. 2023. Vol. 10. P. 1191705. doi: 10.3389/fcvm.2023.1191705

30. Davies R.R., Hussain T., Tandon A. Using virtual reality simulated implantation for fit-testing pediatric patients for adult ventricular assist devices // JTCVS Tech. 2020. Vol. 6. P. 134–137. doi: 10.1016/j.xjtc.2020.10.017

31. Ramaswamy R.K., Marimuthu S.K., Ramarathnam K.K., et al. Virtual reality-guided left ventricular assist device implantation in pediatric patient: Valuable presurgical tool // Ann Pediatr Cardiol. 2021. Vol. 14, N 3. P. 388–392. doi: 10.4103/apc.apc_81_21

32. Tautz L., Walczak L., Georgii J., et al. Combining position-based dynamics and gradient vector flow for 4D mitral valve segmentation in TEE sequences // Int J Comput Assist Radiol Surg. 2020. Vol. 15, N 1. P. 119–128. doi: 10.1007/s11548-019-02071-4

33. Bruckheimer E., Rotschild C. Holography for imaging in structural heart disease // EuroIntervention. 2016. Vol. 12 Suppl X. P. 81–84. doi: 10.4244/EIJV12SXA15

34. Currie M.E., McLeod A.J., Moore J.T., et al. Augmented Reality System for Ultrasound Guidance of Transcatheter Aortic Valve Implantation // Innovations (Phila). 2016. Vol. 11, N 1. P. 31–39. doi: 10.1097/IMI.0000000000000235

35. Butera G., Sturla F., Pluchinotta F.R., et al. Holographic Augmented Reality and 3D Printing for Advanced Planning of Sinus Venosus ASD/Partial Anomalous Pulmonary Venous Return Percutaneous Management // JACC Cardiovasc Interv. 2019. Vol. 12, N 14. P. 1389–1391. doi: 10.1016/j.jcin.2019.03.020

36. Zброński K., Rymuza B., Scisło P., et al. Augmented reality in left atrial appendage occlusion // Kardiol Pol. 2018. Vol. 76, N 1. P. 212. doi: 10.5603/KP.2018.0017

37. Iannotta M., d'Aiello F.A., Van De Bruaene A., et al. Modern tools in congenital heart disease imaging and procedure planning: a European survey // J Cardiovasc Med (Hagerstown). 2024. Vol. 25, N. 1. P. 76–87. doi: 10.2459/JCM.0000000000001569

38. Deng S., Wheeler G., Toussaint N., et al. A Virtual Reality System for Improved Image-Based Planning of Complex Cardiac Procedures // J Imaging. 2021. Vol. 7, N 8. P. 151. doi: 10.3390/jimaging7080151

39. Raimondi F., Vida V., Godard C., et al. Fast-track virtual reality for cardiac imaging in congenital heart disease // J Card Surg. 2021. Vol. 36, N 7. P. 2598–2602. doi: 10.1111/jocs.15508

40. Kim B., Loke Y.H., Mass P., et al. A Novel Virtual Reality Medical Image Display System for Group Discussions of Congenital Heart Disease: Development and Usability Testing // JMIR Cardio. 2020. Vol. 4, N 1. P. e20633. doi: 10.2196/20633

41. Patel N., Costa A., Sanders S.P., Ezon D. Stereoscopic virtual reality does not improve knowledge acquisition of congenital heart disease // Int J Cardiovasc Imaging. 2021. Vol. 37, N 7. P. 2283–2290. doi: 10.1007/s10554-021-02191-6

42. Lau I., Gupta A., Sun Z. Clinical Value of Virtual Reality versus 3D Printing in Congenital Heart Disease // Biomolecules. 2021. Vol. 11, N 6. P. 884. doi: 10.3390/biom11060884

43. Milano E.G., Pajaziti E., Schievano S., et al. P369 Patient specific virtual reality for education in con- genital heart disease // Eur Heart J Cardiovasc Imaging. 2020. Vol. 21, Suppl. 1. doi: 10.1093/ehjci/jez319.218

44. Ong C.S., Krishnan A., Huang C.Y., et al. Role of virtual reality in congenital heart disease // Congenit Heart Dis. 2018. Vol. 13, N 3. P. 357–361. doi: 10.1111/chd.12587

45. Sadeghi A.H., Maat A.P.W.M., Taverne Y.J.H.J., et al. Virtual reality and artificial intelligence for 3-dimensional planning of lung segmentectomies // JTCVS Tech. 2021. Vol. 7. P. 309–321. doi: 10.1016/j.xjtc.2021.03.016

46. van de Woestijne P.C., Bakhuis W., Sadeghi A.H., et al. 3D Virtual Reality Imaging of Major Aortopulmonary Collateral Arteries: A Novel Diagnostic Modality // World J Pediatr Congenit Heart Surg. 2021. Vol. 12, N 6. P. 765–772. doi: 10.1177/21501351211045064

47. Franson D., Dupuis A., Gulani V., et al. A System for Real-Time, Online Mixed-Reality Visualization of Cardiac Magnetic Resonance Images // J Imaging. 2021. Vol. 7, N 12. P. 274. doi: 10.3390/jimaging7120274

48. Bindschadler M., Buddhe S., Ferguson M.R., et al. HEARTBEAT4D: An Open-source Toolbox for Turning 4D Cardiac CT into VR/AR // J Digit Imaging. 2022. Vol. 35, N 6. P. 1759–1767. doi: 10.1007/s10278-022-00659-y

49. Aeckersberg G., Gkremoutis A., Schmitz-Rixen T., Kaiser E. The relevance of low-fidelity virtual reality simulators compared with other learning methods in basic endovascular skills training // J Vasc Surg. 2019. Vol. 69, N 1. P. 227–235. doi: 10.1016/j.jvs.2018.10.047

50. Andersen N.L., Jensen R.O., Posth S., et al. Teaching ultrasound-guided peripheral venous catheter placement through immersive virtual reality: An explorative pilot study // Medicine (Baltimore). 2021. Vol. 100, N 27. P. e26394. doi: 10.1097/MD.0000000000026394

51. Arshad I., De Mello P., Ender M., et al. Reducing Cybersickness in 360-Degree Virtual Reality // Multisens Res. 2021. P. 1–17. doi: 10.1163/22134808-bja10066

52. Jung C., Wolff G., Wernly B., et al. Virtual and Augmented Reality in Cardiovascular Care: State-of-the-Art and Future Perspectives // JACC Cardiovasc Imaging. 2022. Vol. 15, N 3. P. 519–532. doi: 10.1016/j.jcmg.2021.08.017

53. Mahtab E.A.F., Egorova A.D. Current and future applications of virtual reality technology for cardiac interventions // Nat Rev Cardiol. 2022. Vol. 19, N 12. P. 779–780. doi: 10.1038/s41569-022-00789-4

54. Pezel T., Coisne A., Bonnet G., et al. Simulation-based training in cardiology: State-of-the-art review from the

French Commission of Simulation Teaching (Commission d'enseignement par simulation-COMSI) of the French Society of Cardiology // Arch Cardiovasc Dis. 2021. Vol. 114, N 1. P. 73–84. doi: 10.1016/j.acvd.2020.10.004

55. Spiegel B., Fuller G., Lopez M., et al. Virtual reality for management of pain in hospitalized patients: A randomized comparative effectiveness trial // PLoS One. 2019. Vol. 14, N 8. P. e0219115. doi: 10.1371/journal.pone.0219115

AUTHORS' INFO

* Seda S. Rashidova, MD;
address: 21 Aliev str., 368000, Khasavyurt, Russia;
ORCID: 0009-0002-9090-0688;
eLibrary SPIN: 5824-7314;
e-mail: rrstr1990@mail.ru

Emma A. Bdoyan;
ORCID: 0009-0002-4343-1049;
e-mail: emma.bdoyan@mail.ru

Madina M. Timurzieva;
ORCID: 0009-0002-6048-7108;
e-mail: timurziyeva.madina@bk.ru

Sofya A. Lobanovskaya;
ORCID: 0009-0009-7486-0672;
e-mail: sonyalobanovsk11@yandex.ru

Valeria V. Naumenko;
ORCID: 0009-0000-3836-9231;
e-mail: valerianaumenko555@gmail.com

Angelina V. Rakhmanova;
ORCID: 0009-0002-2209-8988;
e-mail: alyarakhmanova@mail.ru

Valeriya D. Timofeeva;
ORCID: 0009-0000-0040-6447;
e-mail: timofeeva-valera@mail.ru

Alexey S. Gutsulyak, MD;
ORCID: 0009-0002-3242-9859;
e-mail: alex.guculyak@gmail.com

Artem A. Zainullin;
ORCID: 0000-0003-1581-7120;
e-mail: artem.z011@mail.ru

Karina R. Uzbekova;
ORCID: 0009-0009-7099-2635;
eLibrary SPIN: 7263-6262;
e-mail: uzkarina@mail.ru

Valeriya A. Kharitonova;
ORCID: 0009-0009-0978-2997;
e-mail: valeriya0901@bk.ru

Narina F. Akhmetova;
ORCID: 0000-0003-0073-4672;
eLibrary SPIN: 7830-7828;
e-mail: junehiltoncamp@gmail.com

ОБ АВТОРАХ

* Рашидова Седа Сулеймановна;
адрес: Россия, 368000, Хасавюрт, ул. Алиева, д. 21
ORCID: 0009-0002-9090-0688;
eLibrary SPIN: 5824-7314;
e-mail: rrstr1990@mail.ru

Бдоян Эмма Альбертовна;
ORCID: 0009-0002-4343-1049;
e-mail: emma.bdoyan@mail.ru

Тимурзиева Мадина Мухарбековна;
ORCID: 0009-0002-6048-7108;
e-mail: timurziyeva.madina@bk.ru

Лобановская Софья Александровна;
ORCID: 0009-0009-7486-0672;
e-mail: sonyalobanovsk11@yandex.ru

Науменко Валерия Викторовна;
ORCID: 0009-0000-3836-9231;
e-mail: valerianaumenko555@gmail.com

Рахманова Ангелина Вадимовна;
ORCID: 0009-0002-2209-8988;
e-mail: alyarakhmanova@mail.ru

Тимофеева Валерия Дмитриевна;
ORCID: 0009-0000-0040-6447;
e-mail: timofeeva-valera@mail.ru

Гуцуляк Алексей Сергеевич;
ORCID: 0009-0002-3242-9859;
e-mail: alex.guculyak@gmail.com

Зайнуллин Артем Артурович;
ORCID: 0000-0003-1581-7120;
e-mail: artem.z011@mail.ru

Узбекова Карина Рустамовна;
ORCID: 0009-0009-7099-2635;
eLibrary SPIN: 7263-6262;
e-mail: uzkarina@mail.ru

Харитонова Валерия Артуровна;
ORCID: 0009-0009-0978-2997;
e-mail: valeriya0901@bk.ru

Ахметова Нарина Фаритовна;
ORCID: 0000-0003-0073-4672;
eLibrary SPIN: 7830-7828;
e-mail: junehiltoncamp@gmail.com

* Corresponding author / Автор, ответственный за переписку

Comparative analysis of modifications of U–Net neuronal network architectures in medical image segmentation

Anastasia M. Dostovalova[1,2], Andrey K. Gorshenin[1,2], Julia V. Starichkova[1], Kirill M. Arzamasov[1,3]

[1] MIREA — Russian Technological University, Moscow, Russia;
[2] Federal Research Center Computer Science and Control of the Russian Academy of Sciences, Moscow, Russia;
[3] Research and Practical Clinical Center for Diagnostics and Telemedicine Technologies, Moscow, Russia

ABSTRACT

Data processing methods based on neural networks are becoming increasingly popular in medical diagnostics. They are most commonly used to evaluate medical images of human organs using computed tomography, magnetic resonance imaging, ultrasound, and other non–invasive diagnostic methods. Disease diagnosis involves solving the problem of medical image segmentation, i.e. finding groups (regions) of pixels that characterize specific objects in the image. The U–Net neural network architecture developed in 2015 is one of the most successful tools to solve this issue. This review evaluated various modifications of the classic U–net architecture. The papers considered were divided into several key categories, such as modifications of the encoder and decoder; use of attention blocks; combination with elements of other architectures; methods for introducing additional attributes; transfer learning; and approaches for processing small sets of real–world data. Different training sets with the best parameters found in the literature were evaluated (Dice similarity score; Intersection over Union; overall accuracy, etc.). A summary table was developed showing types of images evaluated and abnormalities detected. Promising directions for further modifications to improve the quality of the segmentation are identified. The results can be used to detect diseases, especially cancer. Intelligent medical assistants can implement the presented algorithms.

Keywords: U–Net architecture; segmentation; computed tomography; magnetic resonance imaging; medical diagnostics; oncology diseases.

Сравнительный анализ модификаций нейросетевых архитектур U-Net в задаче сегментации медицинских изображений

А.М. Достовалова[1,2], А.К. Горшенин[1,2], Ю.В. Старичкова[1], К.М. Арзамасов[1,3]

[1] МИРЭА — Российский технологический университет, Москва, Россия;
[2] Федеральный исследовательский центр «Информатика и управление» Российской академии наук, Москва, Россия;
[3] Научно-практический клинический центр диагностики и телемедицинских технологий, Москва, Россия

АННОТАЦИЯ

Методы обработки данных с использованием нейронных сетей завоёвывают всё большую популярность в области медицинской диагностики. Наиболее часто их применяют при исследовании медицинских изображений органов человека с использованием компьютерной и магнитно-резонансной томографии, ультразвуковых и иных средств неинвазивных исследований. Диагностирование патологии в таком случае сводится к решению задачи сегментации медицинского изображения, то есть поиска групп (областей) пикселов, характеризующих некоторые объекты на снимке. Один из наиболее успешных методов решения данной задачи — разработанная в 2015 году нейросетевая архитектура U-Net. В настоящем обзоре авторы проанализировали разнообразные модификации классической архитектуры U-Net. Рассмотренные работы разделены на несколько ключевых направлений: модификации кодировщика и декодировщика; использование блоков внимания; комбинирование с элементами других архитектур; методы внедрения дополнительных признаков; трансферное обучение и подходы для обработки малых наборов реальных данных. Изучены различные обучающие наборы, для которых приведены лучшие достигнутые в литературе значения метрик (показатель сходства Dice; пересечение над объединением Intersection over Union; общая точность и др.). Также создана сводная таблица с указанием типов анализируемых изображений и выявляемых патологий на них. Обозначены перспективные направления дальнейших модификаций для повышения качества решения задач сегментации. Результаты могут быть полезны в области выявления заболеваний, прежде всего, онкологических. Представленные алгоритмы могут стать частью профессиональных медицинских интеллектуальных ассистентов.

Ключевые слова: архитектура U-Net; сегментация; компьютерная томография; магнитно-резонансная томография; медицинская диагностика; онкологические заболевания.

U-Net神经网络架构在医学图像分割任务中的改型比较分析

Anastasia M. Dostovalova[1,2], Andrey K. Gorshenin[1,2], Julia V. Starichkova[1], Kirill M. Arzamasov[1,3]

[1] MIREA-Russian Technological University, Moscow, Russia;
[2] Federal Research Center Computer Science and Control of the Russian Academy of Sciences, Moscow, Russia;
[3] "Research and Practical Clinical Center for Diagnostics and Telemedicine Technologies of the Moscow Health Care Department", Moscow, Russia

摘要

在医学诊断领域，使用神经网络的数据处理方法越来越受欢迎。它们最常用于使用计算机断层扫描和磁共振成像、超声波和其他非侵入性研究工具来研究人体器官的医学图像。在这种情况下，病理诊断归结为解决医学图像分割的问题，即搜索表征图像中某些对象的像素组（区域）。2015年开发的U-Net神经网络架构是解决这一问题的最成功方法之一。在本文中，作者分析了典型的　　U-Net架构的各种改型。研究工作分为几个关键领域：编码器和解码器的改型；注意力模块的使用；与其他架构元素的结合；引入附加特征的方法；迁移学习和处理小型现实数据集的方法。研究了各种训练集，列出了文献中实现的最佳度量值（Dice相似度指标；交集大于联合Intersection　over　Union；总体准确性等等）。还创建了一份汇总表，说明所分析的图像类型和在这些图像上检测到的病理情况。概述了进一步改型以提高分割任务质量的有前景的方向。这些结果可能有助于疾病检测，主要是肿瘤检测。　　所提出的算法可以成为专业医疗智能助手的一部分。

关键词：U-Net架构；分割；计算机断层扫描；磁共振成像；医学诊断；肿瘤病。

INTRODUCTION

Image processing using artificial-intelligence (AI)-based software plays a central role in modern medical diagnosis. Advancements in computational technology and machine learning algorithms have considerably expanded the capabilities of image analysis in recent decades. Comprehensive clinical decision support systems, including autonomous models, have replaced the previous generation of simple classification frameworks.

Medical image processing initially relied on basic imaging modalities such as radiography and mammography. These modalities have since evolved, and computed tomography (CT) and magnetic resonance imaging (MRI) data are now processed with high efficiency. In the context of diagnostic radiology, AI-based software is applied to a range of tasks, including data visualization, segmentation, recording, classification, and interpretation.

Among these, medical image segmentation remains among the most challenging tasks, as it involves identifying clusters of pixels that correspond to specific image objects, particularly in CT and MRI scans. Deep learning algorithms have demonstrated promising performance in segmenting abnormal regions (selecting target regions) and subsequently classifying them. These algorithms notably outperform conventional approaches in both processing accuracy and speed [1].

Various neural network architectures have been employed for segmentation tasks. These models differ in structural characteristics, including the number of layers, neurons per layer, activation functions, and optimization algorithms. Among these architectures, frameworks such as U-Net, V-Net, DenseNet, and Mask R-CNN have demonstrated strong performance in segmentation tasks [2–6].

Since its introduction in 2015, the U-Net segmentation network has become a standard tool in biomedical image processing. Nevertheless, the basic U-Net architecture continues to demonstrate strong performance in analyzing medical images for detecting organ abnormalities, such as those seen in kidney CT scans and lung changes associated with COVID-19 or obstructive pulmonary disease [7–9]. The U-Net3D architecture extends the conventional U-Net by replacing two-dimensional (2D) convolutions with 3D convolutions [10]. It is employed for the segmentation of 3D medical images. For instance, Pantovic et al. used U-Net3D to analyze CT scans of a brain containing neural implants to identify surgical sites for epileptogenic zone removal [11]. Han et al. used the same architecture to segment liver MRI scans and delineate both the contours and internal structures of the liver [12].

The standard architecture of the U-Net neural network consists of two primary components: the encoder and decoder. The encoder compresses the input data and extracts the most relevant features for subsequent recognition.
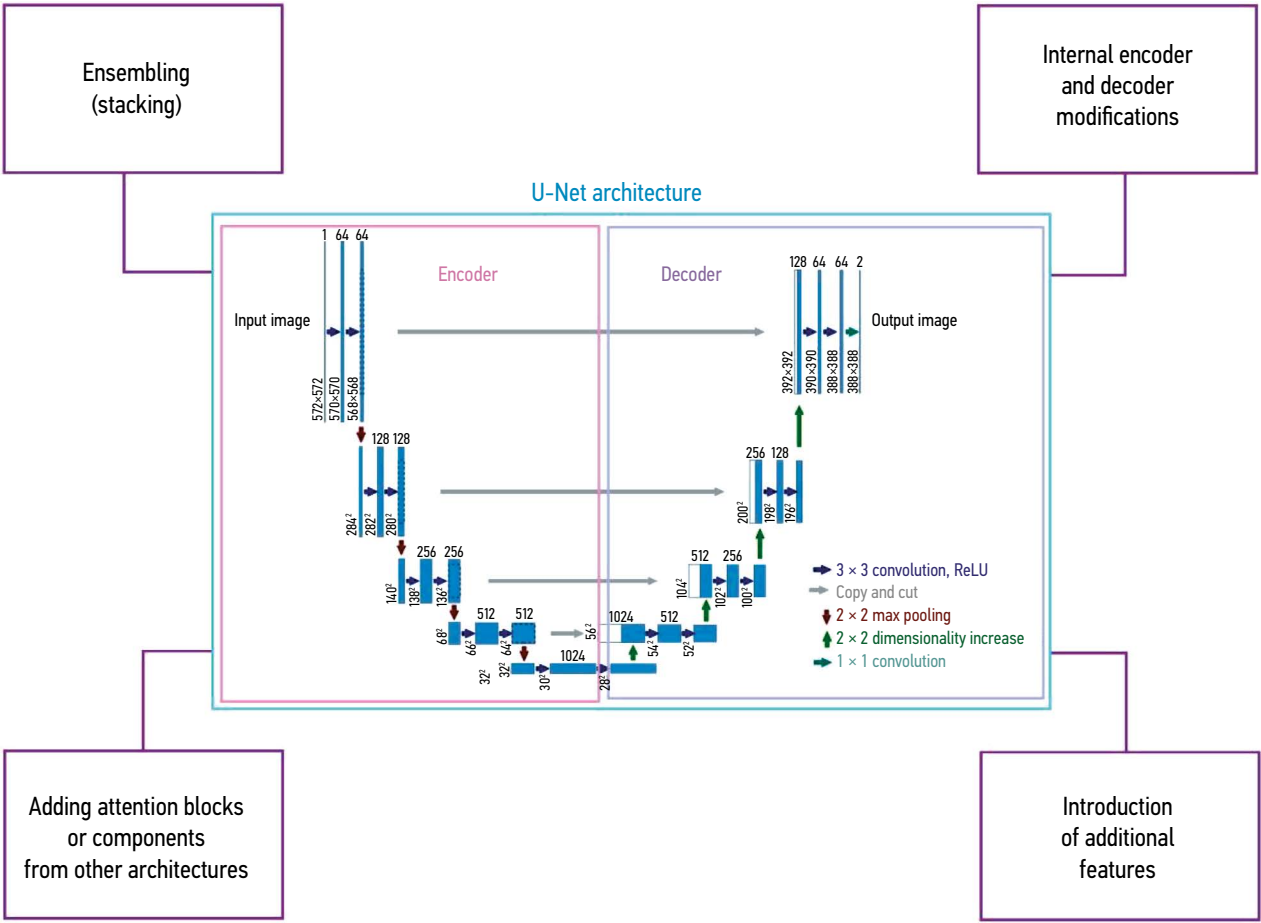

Fig. 1. Classic U-Net architecture proposed in 2015 and the main categories of its modification methods.
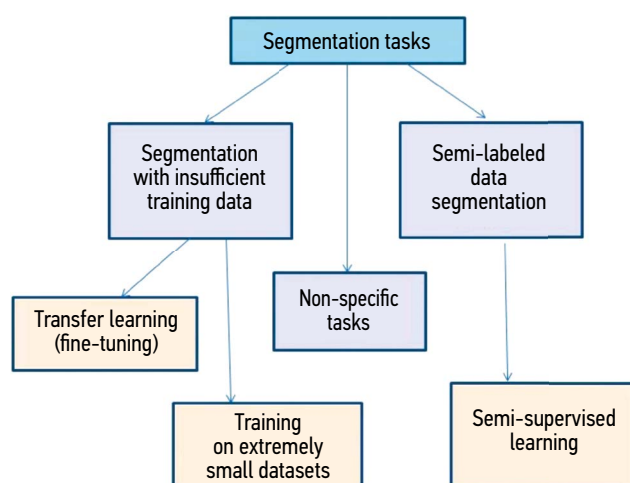
Fig. 2. Segmentation tasks categorized by the availability and type of training data.

Meanwhile, the decoder reconstructs a segmented image from the compressed data generated by the encoder. Since 2015, numerous modifications to the standard U-Net architecture (referred to as the U-architecture) (Fig. 1) have been developed to enhance its accuracy, speed, and robustness. These modifications can be grouped into four main categories: (1) modifying the encoder and decoder while preserving the overall network structure; (2) combining multiple U-architecture models through ensembling; (3) integrating additional architectural components, such as attention blocks; and (4) incorporating supplementary features into the model.

These modifications have also been applied to address image segmentation challenges arising during semi-supervised learning or when training data are limited (Fig. 2). The limited-training-data scenario can be further categorized into cases involving small and extremely small datasets. Specifically, when training on small datasets, transfer learning and fine-tuning are typically applied to networks pretrained on more diverse datasets.

Meanwhile, when training on extremely small datasets (few-shot learning), pretraining is inadequate; such cases generally require original architectures and data models.

This review explores the application of U-Net architecture modifications in medical image processing. Section 1 outlines the main modification strategies for the U-architecture, including (1) changing the encoder and decoder internally, (2) integrating additional architectural components such as attention blocks, and (3) altering the network's learning process. Section 2 explores how these modifications can be applied to address specific challenges in medical image segmentation. The conclusion in Section 3 summarizes the key findings of the review.

DATA SEARCH METHODOLOGY

The authors conducted a literature search using the Web of Science, Scopus, and PubMed databases, covering publications from 2018 to 2024. The search results were comparable across databases and reflected the primary trends in U-Net architecture modification methods. The search keywords included U-Net, medical images, and modification. The initial search returned approximately 5,000 sources. This was subsequently refined using additional terms, including attention, few-shot, unsupervised, semi-supervised, ensemble, stack, additional features, metadata, and DICOM data.

The selected publications were reviewed with a focus on the use of specific architectures for medical image processing. The inclusion criteria were as follows:
- Quality of result validation (e.g., comparison with other architectures, use of established evaluation metrics, and study completeness);
- Originality of the architectural modification in relation to its intended application;
- Specificity of the task (e.g., type of abnormality detected or organ segmented);
- Use of open datasets.

The U-Net architecture has substantially impacted medical image segmentation owing to its effectiveness. Originally proposed by Ronneberger et al. [2], U-Net has since evolved into several notable variants, including U-Net++ [13], Attention U-Net [5], 3D U-Net [10], EU-Net [14], NAS-U-Net [15], U-Net 3+ [16], and SwinAttU-Net [17]. Appendix 1 provides an overview of key studies on U-Net modification methods and segmentation accuracy evaluations, as well as datasets used for testing. It also includes studies wherein U-Net was applied to address specific segmentation challenges. The following abbreviations are used for performance metrics: DC, Dice coefficient; IoU, intersection over union; OA, overall accuracy [18, 19].

U-NET ARCHITECTURE MODIFICATIONS

Internal encoder and decoder modifications

This section discusses structural elements that are altered by internal modifications to the encoder and decoder of the U-architecture.

Encoder and decoder convolution blocks. To process spinal cord images (Verse2019 and Verse2020 datasets), Xu et al. replaced convolution layers with linear layers in the encoder and with octave convolutions in the decoder. Octave convolutions combine standard convolution blocks with pooling operations to extract frequency-based data [57]. Ayalew et al. reduced the number of convolution channels and incorporated batch normalization into the original U-architecture to detect liver tumors in CT scans [58]. This modification improved network accuracy on datasets with considerable class imbalance. Guan et al. proposed an architecture with modified convolution blocks wherein the outputs of each layer were concatenated and jointly processed to minimize distortion in photoacoustic images, such as brain scans [59].

Connections between encoder and decoder blocks. Özcan et al. used a U-Net variant to identify tumor regions in liver CT scans. In this variant, connections between encoder and decoder blocks passed through an inception block composed of convolutions with different kernel sizes, whose outputs were concatenated. In other studies, these connections passed through a pyramid of pooling layers (consisting of multiple pooling layers with different kernel sizes applied to the same data) [61]. This approach was used to accelerate the segmentation of liver ultrasound images.

Encoder or decoder regularization blocks. Omarov et al. applied a modified U-Net architecture to detect brain regions affected by ischemic stroke on CT scans. In this architecture, dropout and L2 regularization layers were incorporated into the decoder [62].

Ensembling U-Net architectures. A concatenated ensemble of U-Net networks trained on ImageNet images converted to sinograms was used to reconstruct CT images from projection data obtained by rotating an object [63]. In another example, an ensemble of two U-Net3D networks pretrained on the LiTS dataset was applied for detecting liver tumors in 3D CT scans [24, 64]. The first network processed low-resolution images (reduced source images), and its segmentation output was passed to the second network. A combined loss function incorporating the DC and cross-entropy was used. In another study, a two-stage U-Net ensemble was developed for liver tumor detection. Here, one network functioned as a post-processing and refinement stage [65].

Koirala et al. used an ensemble of U-Net3D, ONet3D, and SphereNet3D networks to locate brain tumors. Ensembling was achieved by weighing (summing and multiplying by a number reflecting the network's contribution to the overall result, i.e., its weight) the outputs of all models to determine the most probable class.

Li et al. used an unmodified U-Net architecture to select the optimal model for their application [67].

Overall, existing studies suggest that even minor architectural changes to U-Net can improve its effectiveness in medical imaging tasks.

Modifications using attention mechanisms

This section outlines how previous studies modified the standard U-Net architecture by integrating spatial and channel attention blocks [68]. In one study, a U-Net3D-based variant incorporating efficient channel attention in the encoder blocks was applied to detect COVID-19-related abnormalities in chest CT scans [69]. In another study, a pyramid fusion module was implemented at the lower layer of the U-architecture. In this module, features extracted using neural networks with varying window sizes were concatenated, and the resulting data were processed using a pooling layer with a global mean value. The Tversky loss function was used for optimization [70].
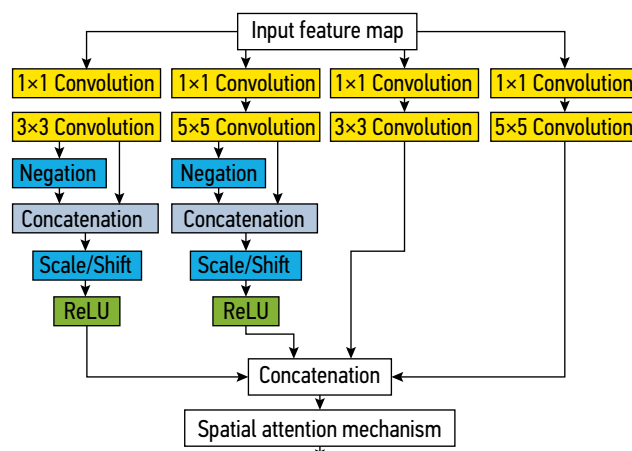
Fig. 3. Spatial attention block positioned between encoder elements [75].

Another study focused on the simultaneous segmentation of multiple organs using CT scans [71]. The proposed U-Net architecture included an attention block that took the outputs of both the encoder and decoder as input. These outputs were concatenated and processed using a 1D convolution operation with ReLU activation sigmoid functions [72].

One study [73] employed a U-Net architecture with spatial multi-scale attention blocks to segment liver tumors in CT scans. These attention blocks were placed at multiple points in the architecture, including within the encoder and decoder, as well as along the connections between them.

Zhang et al. applied pyramid pooling in the lower part of the U-architecture (corresponding to the point of maximum data reduction) and used efficient channel attention blocks on the connections between the encoder and decoder blocks [74]. Another study proposed a U-Net architecture with spatial attention between encoder blocks, incorporating convolutions with multiple receptive fields (Fig. 3). This architecture was trained using the Tversky loss function for breast cancer detection [75].

Subhan Akbar et al. introduced attention blocks into the connections between the encoder and decoder blocks of the U-architecture. For feature extraction, they also added a positional attention block and a self-attention block to each layer of the decoder [76, 77].

Thus, in U-Net, various attention blocks have been used to capture spatial relationships between image elements at different scales. Notably, these relationships cannot be detected using the basic architecture.

Modifications through the integration of elements from other architectures

A common approach to modifying the U-Net architecture involves incorporating elements from other networks, such as ResNet or transformers. Several variations of this approach have been proposed.

Full modification of the encoder and/or decoder. Xingfei et al. modified the U-Net architecture by replacing

the encoder with ResNet50 for segmenting COVID-19-related abnormalities in the lungs [78, 79]. A channel attention block combined with a pyramid pooling module was applied following the encoder. Alternatively, a transformer encoder can be integrated, with its output upsampled via deconvolution for use in different parts of the U-architecture [80].

Modification of encoder and decoder blocks while maintaining the general U-Net architecture. Eskandari et al. focused on segmenting liver structures in CT scans [81]. To account for the considerable variability in liver shape, size, and position, they used a position-determining classifier network in combination with a modified U-Net architecture. This modification replaced standard convolution blocks with ConvLSTM blocks, which were also incorporated into the connections between encoder and decoder blocks [82].

In another study, a hybrid architecture combining efficient transformer blocks with the U-Net architecture was proposed for identifying skin abnormalities in medical images (Fig. 4) [83]. This architecture outperformed the classic U-Net, Attention U-Net, TransU-Net, FAT-Net, and Swin U-Net in terms of DC, sensitivity, specificity, and accuracy on the ISIC 2018 skin lesion dataset.

Ghofrani et al. applied a combination of an unmodified U-Net and transformer blocks to segment polyp images, achieving higher accuracy than U-Net, ResU-Net++, and DoubleU-Net [36, 37, 84–86].

For 3D liver image segmentation, U-Net was combined with Swin Transformer, BTSwin Transformer, and DenseNet components [87–89].

In summary, similar to attention-based modifications, integrating elements from other architectures enhances image processing quality by identifying subtle relationships between image regions. Transformer blocks that employ self-attention mechanisms to extract latent features are frequently used in this context.

Introducing additional features into u-net

Researchers often use metadata from DICOM files as supplementary features in medical image analysis. These data are typically tabulated and include both continuous and categorical variables. The metadata are often input into a separate network, which may be trained either jointly with or independently from the main segmentation model. This supplementary information is generally incorporated into the base network using attention mechanisms. For instance, in a previous study on spinal tumor segmentation, metadata were integrated into a U-Net-based segmentation model. Each block included a linear transformation block applied to the output of the preceding convolutional layer [90]. The U-Net-based generator computed transformation parameters (shift and scale) after receiving metadata related to the segmented image. In another study, Du et al. proposed a channel attention mechanism wherein metadata were used to train the 3D-RADNet network to detect image slices containing the target organ (liver) [91]. Slices selected using metadata were processed by a U-Net-based segmentation model. In kidney tumor segmentation, channel attention has been used to incorporate metadata into the network,
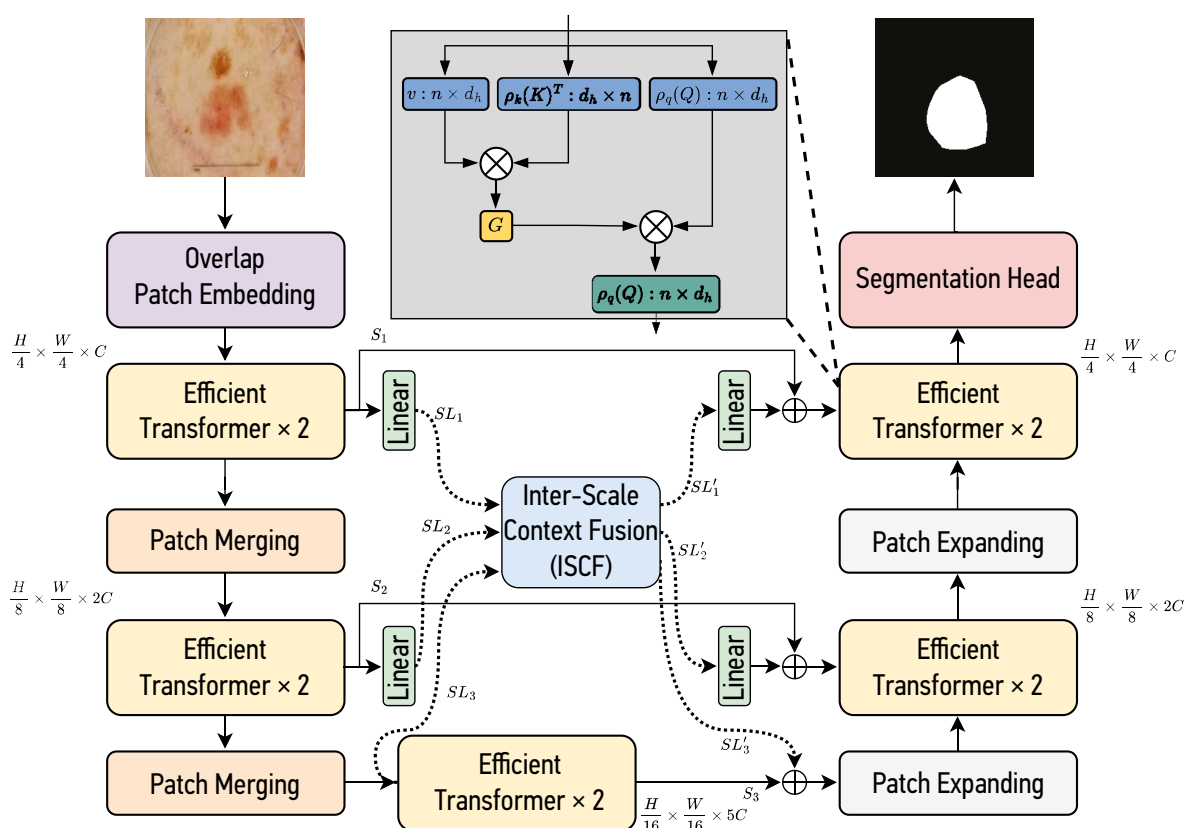
Fig. 4. Architecture integrating transformer blocks into the U-Net framework [81].
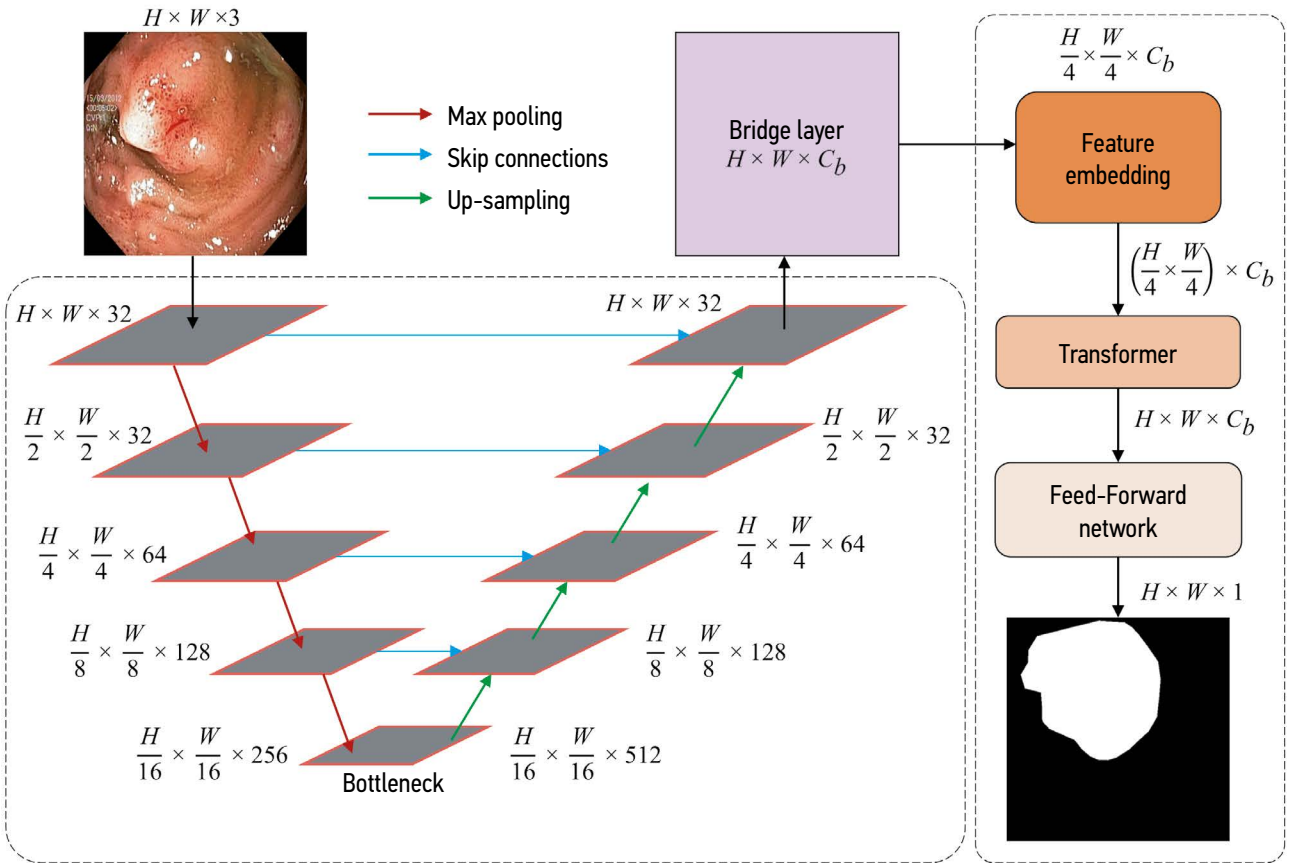
Fig. 5. Combined U-Net and transformer-based architecture [83].

allowing the data to serve as the outputs of U-Net blocks [92]. After the final convolutional layer of each block, both image data and metadata are passed to a layer where the metadata are input into a multi-layer perceptron (MLP) with a sigmoid activation function. The MLP outputs are then multiplied, on a per-channel basis, with the image data from the preceding convolutional layer.

In addition to metadata, other sources of auxiliary information have been used to enhance U-Net models:
- A two-branch architecture based on a convolutional network [93];
- CNNFormer for liver segmentation, which accounts for both intra-slice spatial relationships and inter-slice hierarchical structures [94];
- Additional features, such as spine, lung, and skin segmentation results obtained using the Python library Body Navigation [95].

These data have been concatenated with the input images to enhance the localization of the target organ. This approach has been applied to liver CT segmentation using both U-Net and U-Net3D architectures, depending on whether individual slices or entire scans were processed.

Many modifications to U-Net training involve the iterative reuse of features. For example, Ernst et al. focused on reconstructing CT images from sinograms [96]. They employed a combination of U-Net3D and Primal-Dual networks with iterative learning, where the output at each

step was combined with the results of the previous iteration. Another study proposed a method to improve segmentation accuracy by reusing features extracted during learning [97]. RecycleNet, an architecture derived from U-Net, comprises three main blocks:
- I: input data block;
- R: latent feature reuse block;
- O: outcome block (Fig. 6).
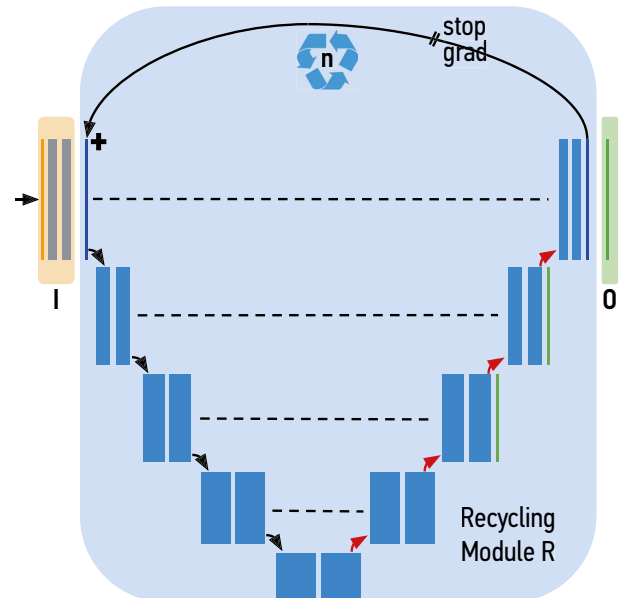
Fig. 6. Structural blocks of the U-Net architecture [97].

The feature reuse algorithm is illustrated in Fig. 6. First, the number of iterations to be used for decision-making is randomly selected from a predefined range. The features extracted in the previous iteration are normalized and added to those from the current iteration, incorporating spatial embedding. After completing the selected number of iterations, the network generates the final output. In a previous study, RecycleNet was experimentally evaluated on the KiTS 2019 (kidney cancer), LiTS, BTCV, AMOS (multi-organ segmentation), and CHAOS (MRI) datasets [23, 24, 33, 40]. The proposed architecture was compared with a DC-optimized variant of nnU-Net and the DRU network [98]. RecycleNet outperformed the compared architectures on all evaluated datasets.

Thus, incorporating additional features can improve the accuracy of image processing using U-Net. Such supplementary data often reveal patterns that are not present or are only weakly expressed in the image itself.

ADDRESSING SPECIFIC SEGMENTATION CHALLENGES USING THE U-NET ARCHITECTURE

Transfer learning and fine-tuning of U-Net

In medical image processing, available training datasets are often small and structurally complex. This limitation arises from the difficulties encountered during data labeling and restrictions imposed by privacy agreements. A common approach in such cases is to employ pretrained models and fine-tune them on the available datasets.

Heker et al. investigated liver tumor segmentation using a small dataset of CT scans [99]. To this end, they first trained the U-Net architecture on the LiTS dataset and applied a hierarchical freezing strategy to its encoder weights. Initially, the encoder weights were frozen, meaning they were not updated during training. The rest of the network was trained

for a set number of iterations. Afterward, the frozen encoder weights were gradually unfrozen and fine-tuned one by one.

Several researchers employed a U-Net architecture with a ResNet32-based encoder, initially pretrained on ImageNet and subsequently fine-tuned using optical coherence tomography images [100]. Meanwhile, others have explored fine-tuning techniques for U-Net and U-Net3D in the segmentation of various organs and diseases, including approaches involving a variable number of trainable layers [101, 102].

Moreover, transfer learning with U-Net and EfficientNet architectures—both originally developed for 2D image segmentation—has been applied to facilitate data transfer during 3D image processing [103, 104]. The authors of the aforementioned paper proposed two approaches: 1) increasing the sampling rate of 2D weights in the corresponding blocks of 3D architectures and 2) obtaining plane projections of 3D data and subsequently processing them using a network trained on 2D data (Fig. 7).

Another approach to training involves using U-Net for post-processing image segmentation results. Hong et al. applied this strategy for liver segmentation in CT scans. In their proposed modification, U-Net's segmentation output underwent post-processing through the optimization of an energy functional. This functional included two components: one for contour delineation in an image and another for optimizing voxel class labels within the evaluated region.

The effectiveness of fine-tuning and transfer learning strategies strongly depends on the datasets used during pretraining. The closer the training and target datasets are in terms of the types of objects assessed, the more effective fine-tuning and transfer learning become. However, achieving this similarity is not always feasible, particularly for specialized tasks. Large datasets are often unavailable—especially for 3D data. A promising alternative is to fine-tune using simpler, lower-dimensional data, which are generally easier to collect in sufficient quantities.
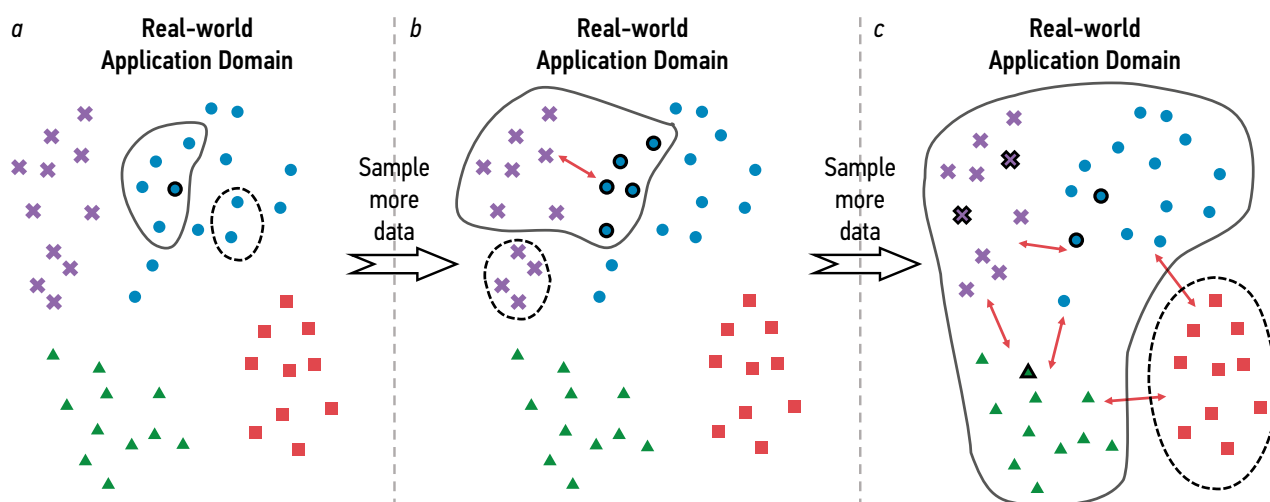
Fig. 7. Ratios of labeled and unlabeled data in network training and testing: (*a*) semi-supervised learning (SSL), (*b*) unsupervised domain adaptation (UDA), and (*c*) semi-supervised domain generalization (SemiDG) [106].

Semi-supervised learning methods

The shortage of sufficient training data for complex architectures is often due to the lack of expert annotation of raw data—a task that requires substantial domain-specific knowledge and expertise. To address this limitation, various training strategies based on the U-Net architecture have been developed to leverage unlabeled data and semi-supervised learning approaches.

Wang et al. explored the training of segmentation networks for 3D organ models using semi-supervised learning techniques [106]. They developed a framework capable of handling different proportions of labeled and unlabeled data during both training and testing phases (See Fig. 7):

- Fig. 7(a): labeled and unlabeled data, as well as testing data, are of the same type (testing data indicated with a dotted line);
- Fig. 7(b): labeled and unlabeled data are of different types;
- Fig. 7(c): the training set contains labeled and unlabeled data of different types, while the testing data are entirely distinct from both.

The resulting framework consists of two main components (Fig. 8): an aggregation block and a decoupling block. The aggregation block includes the encoder of the proposed Diffusion VNet, which performs image segmentation for type 1 relationships. The decoupling block contains three VNet decoders, each responsible for generating class labels of a specific type. The first decoder produces labels that are unbiased with respect to the type of labeled data, using a loss function that combines cross-entropy and DC. These labels are then used to generate re-weighted class labels, where the weights are applied in a loss function consisting of the sum of DCs across all labeled data classes. This weighting strategy enhances the training effectiveness for classes that perform poorly. The second decoder generates class pseudo-labels for unlabeled data, which are subsequently used to train the third decoder in an unsupervised manner.

In a previous study, the above framework was trained using the LASeg (brain MRI), Synapse (various organs), MMWHS, and M&Ms (heart) datasets [47–50]. Its performance was evaluated against that of UA-MT, LMISA-3D, vMFNet, SS-Net, and other architectures using metrics such as DC, Jaccard index, and HD95. In several cases, the framework demonstrated performance that was either superior to or comparable with that of specialized architectures.

Wang et al. investigated trained network adaptation for segmenting a small target dataset focused on polyp detection [107]. The study evaluated a scenario wherein the target dataset consisted of images similar to those used for network training but lacked labels. Two techniques were applied for training: contrastive learning and pseudo-labeling with calibration.

In the contrastive learning phase, unlabeled images were labeled as either positive (consistent with a given image) or negative. Images obtained through augmentation were treated as positive, while others were treated as negative. A network trained on a different dataset generated pseudo-masks for the target dataset. These predicted masks were then used to calculate entropy and determine class centers within the target scans.

To improve the reliability of the generated pseudo-masks, a per-pixel calibration block was introduced. This block incorporated previous predictions to refine the mask quality. To evaluate the effectiveness of the proposed method in polyp segmentation, experiments were conducted using the ClinicDB, ETIS-LARIB, and Kvasir-SEG datasets. The proposed
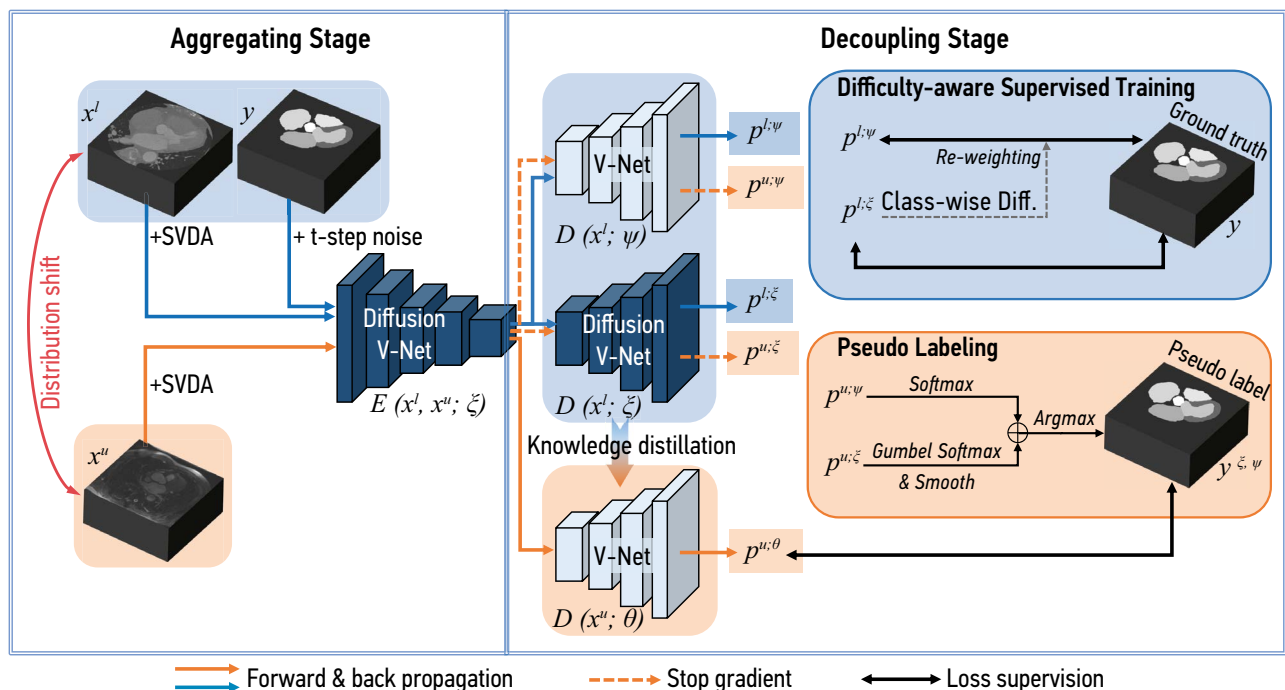
Fig. 8. A&D framework [106].

architecture was compared with other networks employing techniques such as bidirectional learning (BDL), Fourier domain adaptation, historical contrastive learning, and denoised pseudo-labeling. The proposed architecture outperformed these alternatives in terms of DC and IoU variations.

Wang et al. also proposed a method for segmenting human organ images, including those captured during surgery, using semi-labeled datasets.

For unlabeled data processing, a dual-network configuration was used (Fig. 9), in which two networks with identical architectures received the same image input. Although the networks were initialized differently, aggregating their outputs enabled more accurate predictions than either network could achieve independently. To avoid distortion when assigning pseudo-labels to unlabeled data in cases where the training dataset exhibited heterogeneous class representations, individual class distributions were reconstructed rather than relying on the overall data distribution.

To align individual class densities, an exponential moving average transformation was applied to class alignment matrices of both labeled and unlabeled data. The effectiveness of the proposed method was evaluated using the CaDIS (surgical images), LGE-MRI, and ACDC (heart disease) datasets. Its performance was compared with that of the URPC, UAMT, CLD, and CPS architectures using the DC, Jaccard index, and additional metrics. The proposed method outperformed all of these architectures across the evaluated parameters.

Thus, a properly selected architecture enables the effective use of unlabeled data in training U-Net-based models, even in the presence of class imbalance.

U-Net training using extremely small sets of real-world data

Developing AI-based software for specific medical tasks is hindered by the challenge of assembling a sufficiently large training dataset [109]. In many cases, dedicated tools are required to process and structure text-based protocols [110–112]. Combined with the high cost of data annotation, these challenges frequently force developers to work with limited amounts of labeled data for machine learning. Consequently, few-shot learning has become a widely adopted approach in medical image processing.

A study investigated the use of CT and positron emission tomography scans for lung cancer detection [113]. A standard U-Net architecture without modifications was trained using data augmentation, with additional data introduced during both training and testing phases based on feedback from an expert evaluating the model's performance. A similar approach was later applied to COVID-19 data [114]. In another study, the encoder of the U-Net architecture was modified using a Siamese-Net-type structure to enhance segmentation quality. A second encoder branch was introduced; it received the image multiplied by its corresponding mask (segment). The weights from this branch were then combined with those of the primary encoder branch, which processed the original, unmodified image [115].
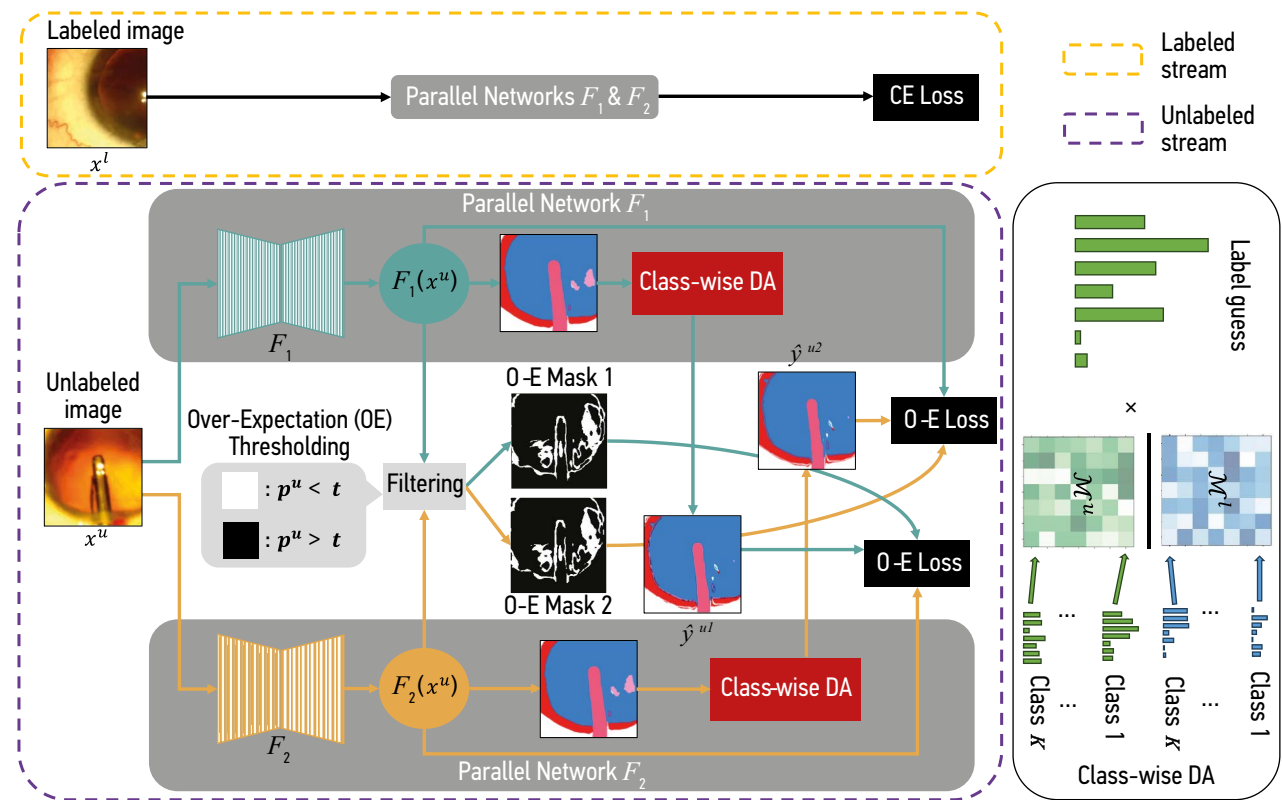
Fig. 9. Dual-network architecture trained on datasets with heterogeneous class representation [108].

In the context of medical imaging, this approach is more frequently applied to architectures other than U-Net, which may be due to the network's size and the number of neurons it contains.

CONCLUSION

The classic U-Net architecture has proven highly effective for medical image segmentation, which explains its widespread use and the ongoing development of various performance-enhancing modifications. These modifications are designed to improve the interpretation of available data and to pool features obtained during pretraining on diverse datasets, including those that are unlabeled. U-Net modifications can also be categorized according to their intended tasks—such as segmentation or the detection of affected tissues—as well as by the types of datasets used, particularly those representing specific diseases. Additionally, the diagnostic accuracy of U-Net-based solutions can be further enhanced by incorporating supplementary training features derived from text, tabular data, or mathematical models.

U-Net architectures are applied across a wide range of medical image segmentation tasks, which vary in both problem formulation and data type (various types of images and diseases). Each task presents its own unique challenges, making it difficult to define a single, universally effective architecture or even a universally applicable class of models. However, among the approaches assessed, U-Net modifications incorporating elements from other architectures demonstrate the strongest performance. These hybrid models are effective for standard image segmentation tasks—particularly when integrating transformer blocks—as well as for situations where training data are limited, such as through pretraining with networks of lower dimensionality than the target data. The integration of additional features into neural network architectures also shows promise. Similarly, the application of physics-informed neural networks, which incorporate information on object models or image structure, is another promising direction [116–119].

ADDITIONAL INFORMATION

REFERENCES

1. Shen D, Wu G, Suk HI. Deep Learning in Medical Image Analysis. *Annual Review of Biomedical Engineering.* 2017;19:221–248. doi: 10.1146/annurev-bioeng-071516-044442

2. Ronneberger O, Fischer P, Brox T. U-Net: Convolutional Networks for Biomedical Image Segmentation. *Medical Image Computing and Computer-Assisted Intervention (MICCAI) 2015.* 2015;9351. doi: 10.1007/978-3-319-24574-4_28

3. Milletari F, Navab N, Ahmadi SA. V-Net: Fully Convolutional Neural Networks for Volumetric Medical Image Segmentation. *Fourth International Conference on 3D Vision (3DV).* 2016:565–571. doi: 10.48550/arXiv.1606.04797

4. Chen LC, Papandreou G, Kokkinos I, Murphy K, Yuille A. DeepLab: Semantic Image Segmentation with Deep Convolutional Nets, Atrous Convolution, and Fully Connected CRFs. *IEEE Transactions on Pattern Analysis and Machine Intelligence.* 2017;40(4):834–848. doi: 10.1109/TPAMI.2017.2699184

5. Huang G, Liu Z, Van Der Maaten L, Weinberger KQ. Densely Connected Convolutional Networks. *IEEE Conference on Computer Vision and Pattern Recognition (CVPR).* 2017:2261–2269. doi: 10.1109/CVPR.2017.243

6. He K, Gkioxari G, Dollár P, Girshick R. Mask R-CNN. *IEEE International Conference on Computer Vision (ICCV).* 2017:2980–2988. doi: 10.1109/ICCV.2017.322

7. Khalal DM., Azizi H, Maalej N. Automatic segmentation of kidneys in computed tomography images using U-Net. *Cancer/Radiothérapie.* 2023;27(2):109–114. doi: 10.1016/j.canrad.2022.08.004

8. Bernardo Gois FN, Lobo Marques JA. Segmentation of CT-Scan Images Using UNet Network for Patients Diagnosed with COVID-19. *Computerized Systems for Diagnosis and Treatment of COVID-192023.* 2023:29–44. doi: 10.1007/978-3-031-30788-1_3

9. Sarsembayeva T, Shomanov A, Sarsembayev M, et al. UNet Model for Segmentation of COPD Lung Lesions on Computed Tomography Images. *Proceedings of the 7th International Conference*

on *Digital Technologies in Education, Science and Industry (DTESI 2022).* 2022. Available at: https://ceur-ws.org/Vol-3382/Short5.pdf. Accessed: November 9, 2024.

10. Çiçek Ö, Abdulkadir A, Lienkamp S, Brox T, Ronneberger O. 3D U-Net: Learning Dense Volumetric Segmentation from Sparse Annotation. *Medical Image Computing and Computer-Assisted Intervention — MICCAI 2016.* 2016:424–432. doi: 10.1007/978-3-319-46723-8_4

11. Pantovic A, Ollivier I, Essert C. 2D and 3D-UNet for segmentation of SEEG electrode contacts on post-operative CT scans. *Medical Imaging 2022: Image-Guided Procedures, Robotic Interventions, and Modeling.* 2022. doi: 10.1117/12.2606538

12. Han X, Wu X, Wang S, et al. Automated segmentation of liver segment on portal venous phase MR images using a 3D convolutional neural network. *Insights Imaging.* 2022;13(26). doi: 10.1186/s13244-022-01163-1

13. Zhou Z, Rahman Siddiquee MM, Tajbakhsh N, Liang J. UNet++: A Nested U-Net Architecture for Medical Image Segmentation. *Deep Learning in Medical Image Analysis and Multimodal Learning for Clinical Decision Support.* 2018:3–11. doi: 10.1007/978-3-030-00889-5_1

14. Yu C, Wang Y, Tang C, Feng W, Lv J. EU-Net: Automatic U-Net neural architecture search with differential evolutionary algorithm for medical image segmentation. *Computers in Biology and Medicine.* 2023;167:107579. doi: 10.1016/j.compbiomed.2023.107579

15. Weng Y, Zhou T, Li Y, Qiu X. NAS-Unet: Neural Architecture Search for Medical Image Segmentation. *IEEE Access.* 2019;7:44247–44257. doi: 10.1109/ACCESS.2019.2908991

16. Huang H, Lin L, Tong R, et al. UNet 3+: A Full-Scale Connected UNet for Medical Image Segmentation. *ICASSP 2020–2020 IEEE International Conference on Acoustics, Speech and Signal Processing (ICASSP).* 2020:1055–1059. doi: 10.1109/ICASSP40776.2020.9053405

17. Li C, Bagher-Ebadian H, Sultan RI, et al. A new architecture combining convolutional and transformer-based networks for automatic 3D multi-organ segmentation on CT images. *Med Phys.* 2023;50(11):6990–7002. doi: 10.1002/mp.16750

18. Müller D, Soto-Rey I, Kramer F. Towards a guideline for evaluation metrics in medical image segmentation. *BMC Research Notes.* 2022;15(210). doi: 10.1186/s13104-022-06096-y

19. Alberg AJ, Park JW, Hager BW, Brock MV, Diener-West M. The use of «overall accuracy» to evaluate the validity of screening or diagnostic tests. *Journal of General Internal Medicine.* 2004;19:460–465. doi: 10.1111/j.1525-1497.2004.30091.x

20. Soler L, Hostettler A, Agnus V, et al. 3D image reconstruction for comparison of algorithm database: A patient specific anatomical and medical image database. *IRCAD.* 2010. Available at: https://www-sop.inria.fr/geometrica/events/wam/abstract-ircad.pdf. Accessed: November 9, 2024.

21. Löffler M, Sekuboyina A, Jakob A, et al. A Vertebral Segmentation Dataset with Fracture Grading. *Radiology: Artificial Intelligence.* 2020;2(4). doi: 10.1148/ryai.2020190138

22. Wang Z, Bovik AC, Sheikh HR, Simoncelli EP. Image quality assessment: from error visibility to structural similarity. *IEEE Transactions on Image Processing.* 2004;13(4):600–612. doi: 10.1109/TIP.2003.819861

23. Kavur AE, Gezer NS, Barış M, et al. CHAOS Challenge – combined (CT-MR) healthy abdominal organ segmentation. *Medical Image Analysis.* 2021;69:101950. doi: 10.1016/j.media.2020.101950

24. Bilic P, Christ P, Li HB, et al. The Liver Tumor Segmentation Benchmark (LiTS). *Medical Image Analysis.* 2023;84:102680. doi: 10.1016/j.media.2022.102680

25. Petrusca L, Cattin P, De Luca V, et al. Hybrid ultrasound/ magnetic resonance simultaneous acquisition and image fusion for motion monitoring in the upper abdomen. *Investigative Radiology.* 2013;48(5):333–340. doi: 10.1097/RLI.0b013e31828236c3

26. Jun M, Cheng G, Yixin W, et al. Covid-19 CT lung and infection segmentation dataset. *Zenodo.* 2020. Available at: https://zenodo.org/records/3757476#.YLov8vkzaUk. Accessed: November 9, 2024.

27. Morozov SP, Andreychenko AE, Blokhin IA, et al. MosMedData: data set of 1110 chest CT scans performed during the COVID-19 epidemic. *Digital Diagnostics.* 2020;1(1):49–59. doi: 10.17816/DD46826

28. Roth HR, Oda H, Hayashi Y, et al. Hierarchical 3D fully convolutional networks for multi-organ segmentation. *ArXiv.* 2017. Available at: https://arxiv.org/abs/1704.06382v1. Accessed: November 9, 2024.

29. Roth H, Farag A, Turkbey EB, et al. Data from Pancreas-CT. Data From Pancreas-CT (Version 2) [Data set]. *The Cancer Imaging Archive.* 2016. doi: 10.7937/K9/TCIA.2016.tNB1kqBU

30. Heimann T, Styner M, van Ginneken B. 3D Segmentation in the Clinic: A Grand Challenge. *MICCAI 2007, the 10th Intel Conf. on Medical Image Computing and Computer Assisted Intervention.* 2007:7–15. Available at: https://www.diagnijmegen.nl/publications/ginn07/. Accessed: November 9, 2024.

31. Suckling J. The Mammographic Image Analysis Society Digital Mammogram Database. *International Congress Series.* 1994:375–378. Available at: http://peipa.essex.ac.uk/info/mias.html. Accessed: November 9, 2024.

32. WHO Director-General's opening remarks at the media briefing on COVID-19 — 11 March 2020 [Internet]. 2020. Available at: https://www.who.int/director-general/speeches/detail/who-director-general-s-opening-remarks-at-the-media-briefing-on-covid-19---11-march-2020. Accessed: November 9, 2024.

33. Landman B, Xu Z, Igelsias J, et al. Miccai multi-atlas labeling beyond the cranial vault–workshop and challenge. *Proceedings of the MICCAI Multi-Atlas Labeling Beyond Cranial Vault — Workshop Challenge.* 2015;5:12.

34. Simpson AL, Antonelli M, Bakas S, et al. A large annotated medical image dataset for the development and evaluation of segmentation algorithms. *ArXiv.* 2019. doi: 10.48550/arXiv.1902.09063

35. Gutman D, Codella NCF, Celebi E, et al. Skin Lesion Analysis toward Melanoma Detection: A Challenge at the International Symposium on Biomedical Imaging (ISBI) 2016, hosted by the International Skin Imaging Collaboration (ISIC). *ArXiv.* 2016. doi: 10.48550/arXiv.1605.01397

36. Jha D, Smedsrud PH, Riegler MA, et al. Kvasir-SEG: A Segmented Polyp Dataset. *MultiMedia Modeling.* 2020;11962:451–462. doi: 10.1007/978-3-030-37734-2_37

37. Bernal J, Sánchez FJ, Fernández-Esparrach G, et al. WM-DOVA maps for accurate polyp highlighting in colonoscopy: Validation vs. saliency maps from physicians. *Computerized Medical Imaging and Graphics.* 2015;43:99–111. doi: 10.1016/j.compmedimag.2015.02.007

38. Grove O, Berglund AE, Schabath MB, et al. Quantitative Computed Tomographic Descriptors Associate Tumor Shape Complexity and Intratumor Heterogeneity with Prognosis in Lung Adenocarcinoma. *PLOS ONE.* 2015;10(3):e0118261. doi: 10.1371/journal.pone.0118261

39. Heller N, Sathianathen N, Kalapara A, et al. The KiTS19 Challenge Data: 300 Kidney Tumor Cases with Clinical Context, CT Semantic Segmentations, and Surgical Outcomes. *ArXiv.* 2019:13. doi: 10.48550/arXiv.1904.00445

40. Ji Y, Bai H, Yang J, et al. AMOS: A Large-Scale Abdominal Multi-Organ Benchmark for Versatile Medical Image Segmentation. *ArXiv.* 2022. doi: 10.48550/arXiv.2206.08023

41. Lemay A, Gros C, Zhuo Z, et al. Multiclass Spinal Cord Tumor Segmentation on MRI with Deep Learning. *ArXiv.* 2021. doi: 10.48550/arXiv.2012.12820

42. Ali MAS, Misko O, Salumaa SO, et al. Evaluating Very Deep Convolutional Neural Networks for Nucleus Segmentation from Brightfield Cell Microscopy Images. *SLAS Discovery.* 2021;26(9):1125–1137. doi: 10.1177/24725552211023214

43. Gibson E, Giganti F, Hu Y, et al. Automatic Multi-Organ Segmentation on Abdominal CT With Dense V-Networks. *IEEE Transactions on Medical Imaging.* 2018;37(8):1822–1834. doi: 10.1109/TMI.2018.2806309

44. Jimenez-del Toro O, Müller H, Krenn M, et al. Cloud-Based Evaluation of Anatomical Structure Segmentation and Landmark Detection Algorithms: VISCERAL Anatomy Benchmarks. *IEEE Transactions on Medical Imaging.* 2016;35(11):2459–2475. doi: 10.1109/TMI.2016.2578680

45. Regan EA, Hokanson JE., Murphy JR, et al. Genetic Epidemiology of COPD (COPDGene) Study Design. *COPD: Journal of Chronic Obstructive Pulmonary Disease.* 2010;7(1):32–43. doi: 10.3109/15412550903499522

46. Litjens G, Toth R, van de Ven W, et al. Evaluation of prostate segmentation algorithms for MRI: The PROMISE12 challenge. *Medical Image Analysis.* 2014;18(2):359–373. doi: 10.1016/j.media.2013.12.002

47. Xiong Z, Xia Q, Hu Z, et al. A global benchmark of algorithms for segmenting the left atrium from late gadolinium-enhanced cardiac magnetic resonance imaging. *Medical Image Analysis.* 2021;67:101832. doi: 10.1016/j.media.2020.101832

48. Landman B, Xu Z, Igelsias J, et al. 2015 MICCAI multi-atlas labeling beyond the cranial vault–workshop and challenge. *MICCAI Multi-Atlas Labeling Beyond Cranial Vault — Workshop Challenge.* 2015;5:12.

49. Zhuang X, Shen J. Multi-scale patch and multi-modality atlases for whole heart segmentation of MRI. *Medical Image Analysis.* 2016;31:77–87. doi: 10.1016/j.media.2016.02.006

50. Campello VM, Gkontra P, Izquierdo C, et al. Multi-Centre, Multi-Vendor and Multi-Disease Cardiac Segmentation: The M&Ms Challenge. *IEEE Transactions on Medical Imaging.* 2021;40(12):3543–3554. doi: 10.1109/TMI.2021.3090082

51. Silva J, Histace A, Romain O, Dray X, Granado B. Toward embedded detection of polyps in WCE images for early diagnosis of colorectal cancer. *International Journal of Computer Assisted Radiology and Surgery.* 2014;9:283–293. doi: 10.1007/s11548-013-0926-3

52. Trikha S, Turnbull A, Morris R, Anderson D, Hossain P. The journey to femtosecond laser-assisted cataract surgery: New beginnings or a false dawn? *Eye.* 2013;27(4):461–473. doi: 10.1038/eye.2012.293

53. Xiong Z, Xia Q, Hu Z, et al. A global benchmark of algorithms for segmenting the left atrium from late gadolinium-enhanced cardiac magnetic resonance imaging. *Medical Image Analisys.* 2021;67:101832. doi: 10.1016/j.media.2020.101832

54. Bernard O, Lalande A, Zotti C, et al. Deep Learning Techniques for Automatic MRI Cardiac Multi-Structures Segmentation and Diagnosis: Is the Problem Solved? *IEEE Transactions on Medical Imaging.* 2018;37(11):2514–2525. doi: 10.1109/TMI.2018.2837502

55. Li P, Wang S, Li T, et al. A Large-Scale CT and PET/CT Dataset for Lung Cancer Diagnosis (Lung-PET-CT-Dx) [Data set]. *The Cancer Imaging Archive.* 2020. doi: 10.7937/TCIA.2020.NNC2-0461

56. Clark K, Vendt B, Smith K, et al. The Cancer Imaging Archive (TCIA): Maintaining and Operating a Public Information Repository. *Journal of Digital Imaging.* 2013;26:1045–1057. doi: 10.1007/s10278-013-9622-7

57. Xu Z, Jia Z, Sun J, Dong W, Li Z. DO-U-Net: Improved U-Net Model for CT Image Segmentation using DBB and Octave Convolution. *Proceedings of the 2023 International Conference on Computer, Vision and Intelligent Technology (ICCVIT '23).* 2023:1–8. doi: 10.1145/3627341.3630403

58. Ayalew Y, Fante K, Aliy M. Modified U-Net for liver cancer segmentation from computed tomography images with a new class balancing method. *BMC Biomedical Engineering.* 2021;3(4). doi: 10.1186/s42490-021-00050-y

59. Guan S, Khan AA, Sikdar S, Chitnis PV. Fully Dense UNet for 2-D Sparse Photoacoustic Tomography Artifact Removal. *IEEE Journal of Biomedical and Health Informatics.* 2020;24(2):568–576. doi: 10.1109/JBHI.2019.2912935

60. Özcan F, Uçan ON, Karaçam S, Tunçman D. Fully Automatic Liver and Tumor Segmentation from CT Image Using an AIM-UNet. *Bioengineering.* 2023;10(2). doi: 10.3390/bioengineering10020215

61. Ansari MY, Yang Y, Meher PK, Dakua SP. Dense-PSP-UNet: A neural network for fast inference liver ultrasound segmentation. *Computers in Biology and Medicine.* 2023;153:106478. doi: 10.1016/j.compbiomed.2022.106478

62. Omarov B, Tursynova A, Postolache O, et al. Modified UNet Model for Brain Stroke Lesion Segmentation on Computed Tomography Images. *Computers, Materials and Continua.* 2022;71(3):4701–4717. doi: 10.32604/cmc.2022.020998

63. Mizusawa S, Sei Y, Orihara R, Ohsuga A. Computed tomography image reconstruction using stacked U-Net. *Computerized Medical Imaging and Graphics.* 2021;90:101920. doi: 10.1016/j.compmedimag.2021.101920

64. Golts A, Khapun D, Shats D, Shoshan Y, Gilboa-Solomon F. An Ensemble of 3D U-Net Based Models for Segmentation of Kidney and Masses in CT Scans. *Kidney and Kidney Tumor Segmentation (KiTS 2021).* 2022;13168:103–115. doi: 10.1007/978-3-030-98385-7_14

65. Araújo JDL, da Cruz LB, Diniz JOB, et al. Liver segmentation from computed tomography images using cascade deep learning. *Computers in Biology and Medicine.* 2022;140:105095. doi: 10.1016/j.compbiomed.2021.105095

66. Koirala CP, Mohapatra S, Gosai A, Schlaug G. Automated Ensemble-Based Segmentation of Adult Brain Tumors: A Novel Approach Using the BraTS AFRICA Challenge Data. *ArXiv.* 2023. doi: 10.48550/arXiv.2308.07214

67. Li Z, Zhu Q, Zhang L, et al. A deep learning-based self-adapting ensemble method for segmentation in gynecological brachytherapy. *Radiation Oncology.* 2022;17(152). doi: 10.1186/s13014-022-02121-3

68. Woo S, Park J, Lee J-Y, Kweon IS. CBAM: Convolutional Block Attention Module. *Proceedings of the European conference on computer vision (ECCV).* 2018:3–19. doi: 10.48550/arXiv.1807.06521

69. Nazir S, Zheng R, Zheng Y, Dong-Ye C. Improved 3D U-Net for COVID-19 Chest CT Image Segmentation. *Scientific Programming.* 2021;2021(9999368):9. doi: 10.1155/2021/9999368

70. Salehi SSM, Erdogmus D, Gholipour A. Tversky Loss Function for Image Segmentation Using 3D Fully Convolutional Deep Networks. *Machine Learning in Medical Imaging.* 2017;10541:379–387. doi: 10.1007/978-3-319-67389-9_44

71. Oktay O, Schlemper J, Folgoc LL, et al. Attention U-Net: Learning Where to Look for the Pancreas. *ArXiv.* 2018. doi: 10.48550/arXiv.1804.03999

72. Agarap AF. Deep Learning using Rectified Linear Units (ReLU). *ArXiv.* 2018:7. doi: 10.48550/arXiv.1803.08375

73. Wu J, Zhou S, Zuo S, et al. U-Net combined with multi-scale attention mechanism for liver segmentation in CT images. *BMC Medical Informatics and Decision Making.* 2021;21(283). doi: 10.1186/s12911-021-01649-w

74. Zhang L, Liu Y, Li Z, Li D. Epa-unet:automatic Segmentation of Liver and Tumor in Ct Images Based on Residual U-net and Efficient Multiscale Attention Methods. *Research Square.* 2023. doi: 10.21203/rs.3.rs-3273964/v1

75. Zarbakhsh P. Spatial Attention Mechanism and Cascade Feature Extraction in a U-Net Model for Enhancing Breast Tumor Segmentation. *Applied Sciences.* 2023;13(15):8758. doi: 10.3390/app13158758

76. Subhan Akbar A, Fatichah C, Suciati N. UNet3D with Multiple Atrous Convolutions Attention Block for Brain Tumor Segmentation. *Brainlesion: Glioma, Multiple Sclerosis, Stroke and Traumatic Brain Injuries.* 2022:182–193. doi: 10.1007/978-3-031-08999-2_14

77. Yu Z, Han S, Song Z. 3D Medical Image Segmentation based on multi-scale MPU-Net. *ArXiv.* 2023. doi: 10.48550/arXiv.2307.05799

78. Xingfei F, Chaobing H. CAE-UNet: An Effective Automatic Segmentation Model for CT Images of COVID-19. *2022 6th International Conference on Communication and Information Systems (ICCIS).* 2022:113–117. doi: 10.1109/ICCIS56375.2022.9998131

79. He K, Zhang X, Ren S, Sun J. Deep Residual Learning for Image Recognition. *2016 IEEE Conference on Computer Vision and Pattern Recognition (CVPR).* 2016:770–778. doi: 10.1109/cvpr.2016.90

80. Hatamizadeh A, Tang Y, Nathet V, et al. U-NETR: Transformers for 3D Medical Image Segmentation. *2022 IEEE/CVF Winter Conference on Applications of Computer Vision (WACV).* 2022:1748–1758. doi: 10.1109/WACV51458.2022.00181

81. Eskandari S, Lumpp J. Inter-Scale Dependency Modeling for Skin Lesion Segmentation with Transformer-based Networks. *ArXiv.* 2023. doi: 10.48550/arXiv.2310.13727

82. Shi X, Chen Z, Wang H, et al. Convolutional LSTM Network: A Machine Learning Approach for Precipitation Nowcasting. *Neural Information Processing Systems.* 2015. doi: 10.48550/arXiv.1506.04214

83. Pham TH, Li X, Nguyen KD. SeU-Net-Trans: A Simple yet Effective UNet-Transformer Model for Medical Image Segmentation. *ArXiv.* 2023. doi: 10.48550/arXiv.2310.09998

84. Ghofrani F, Behnam H, Motlagh HDK. Liver Segmentation in CT Images Using Deep Neural Networks. *2020 28th Iranian Conference on Electrical Engineering (ICEE).* 2020:1–6. doi: 10.1109/ICEE50131.2020.9260809

85. Diakogiannis FI, Waldner F, Caccetta P, Wuet C, et al. ResUNet-a: A deep learning framework for semantic segmentation of remotely sensed data. *ISPRS Journal of Photogrammetry and Remote Sensing.* 2020;16(2):94–114. doi: 10.1016/j.isprsjprs.2020.01.013

86. Jha D, Riegler MA, Johansen D, Halvorsen P, Johansen HD. Doubleu-net: DoubleU-Net: A Deep Convolutional Neural Network for Medical Image Segmentation. *IEEE 33rd International symposium on computer-based medical systems (CBMS).* 2020:558–564. doi: 10.1109/CBMS49503.2020.00111

87. Lee HH, Bao S, Huo Y, Landman BA. 3D UX-Net: A Large Kernel Volumetric ConvNet Modernizing Hierarchical Transformer for Medical Image Segmentation. *International Conference on Learning Representations.* 2023. doi: 10.48550/arXiv.2209.15076

88. Liang J, Yang C, Zhong J, Ye X. BTSwin-U-Net: 3D U-shaped Symmetrical Swin Transformer-based Network for Brain Tumor Segmentation with Self-supervised Pre-training. *Neural Processing Letters.* 2022;55:3695–3713. doi: 10.1007/s11063-022-10919-1

89. Alalwan N, Abozeid A, ElHabshy AA, Alzahrani A. Efficient 3D Deep Learning Model for Medical Image Semantic Segmentation. *Alexandria Engineering Journal.* 2021;60(1):1231–1239. doi: 10.1016/j.aej.2020.10.046

90. Lemay A, Gros C, Vincent O, et al. Benefits of Linear Conditioning with Metadata for Image Segmentation. *ArXiv.* 2021. doi: 10.48550/arXiv.2102.09582

91. Du R, Vardhanabhuti V. 3D-RADNet: Extracting labels from DICOM metadata for training general medical domain deep 3D convolution neural networks. *International Conference on Medical Imaging with Deep Learning.* 2020;121:174–192. Available at: https://proceedings.mlr.press/v121/du20a/du20a.pdf. Accessed: November 9, 2024.

92. Plutenko I, Papkov M, Palo K, Parts L, Fishman D. Metadata Improves Segmentation Through Multitasking Elicitation. *Domain Adaptation and Representation Transfer.* 2023:147–155. doi: 10.1007/978-3-031-45857-6_15

93. Jiang J, Peng Y, Hou Q, Wang J. MDCF_Net: A Multi-dimensional hybrid network for liver and tumor segmentation from CT. *Biocybernetics and Biomedical Engineering.* 2023;43(2):494–506. doi: 10.1016/j.bbe.2023.04.004

94. Fu T, Yu Q, Lao H, Liu P, Wan S. Traffic Safety Oriented Multi-Intersection Flow Prediction Based on Transformer and CNN. *Security and Communication Networks.* 2023:1–13. doi: 10.1155/2023/1363639

95. Chen X, Wei X, Tang M, et al. Liver segmentation in CT imaging with enhanced mask region-based convolutional neural networks. *Annals of Translational Medicine.* 2021;9(24):1768. doi: 10.21037/atm-21-5822

96. Ernst P, Chatterjee S, Rose G, Nürnberger A. Primal-Dual U-Net for Sparse View Cone Beam Computed Tomography Volume Reconstruction. *ArXiv.* 2022. doi: 10.48550/arXiv.2205.07866

97. Koehler G, Wald T, Ulrichet C, et al. RecycleNet: Latent Feature Recycling Leads to Iterative Decision Refinement. *ArXiv.* 2023. doi: 10.48550/arXiv.2309.07513

98. Jafari M, Auer D, Francis S, Garibaldi J, Chen X. DRU-net: An Efficient Deep Convolutional Neural Network for Medical Image Segmentation. *2020 IEEE 17th International Symposium on Biomedical Imaging (ISBI).* 2020:1144–1148. doi: 10.48550/arXiv.2004.13453

99. Heker M, Ben-Cohen A, Greenspan H. Hierarchical Fine-Tuning for joint Liver Lesion Segmentation and Lesion Classification in CT. *2019 41st Annual International Conference of the IEEE Engineering in Medicine and Biology Society (EMBC).* 2019:895–898. doi: 10.1109/EMBC.2019.8857127

100. Matovinovic IZ, Loncaric S, Lo J, Heisler M, Sarunic M. Transfer Learning with U-Net type model for Automatic Segmentation of Three Retinal Layers In Optical Coherence Tomography Images. *2019 11th International Symposium on Image and Signal Processing and Analysis (ISPA).* 2019:49–53. doi: 10.1109/ISPA.2019.8868639

101. Kora P, Ooi CP, Faust O, et al. Transfer learning techniques for medical image analysis: A review. *Biocybernetics and Biomedical Engineering.* 2022;42(1):79–107. doi: 10.1016/j.bbe.2021.11.004

102. Humpire-Mamani GE, Jacobs C, Prokop M, van Ginneken B, Lessmann N. Transfer learning from a sparsely annotated dataset of 3D medical images. *ArXiv.* 2023. doi: 10.48550/arXiv.2311.05032

103. Messaoudi H, Belaid A, Salem DB, Conze P-H. Cross-dimensional transfer learning in medical image segmentation with deep learning. *Medical Image Analysis.* 2023;88:102868. doi: 10.1016/j.media.2023.102868

104. Tan M, Le Q. EfficientNet: Rethinking Model Scaling for Convolutional Neural Networks. *International conference on machine learning (PMLR).* 2019:6105–6114. doi: 10.48550/arXiv.1905.11946

105. Hong Y, Mao X, Hui Q. et al. Automatic liver and tumor segmentation based on deep learning and globally optimized refinement. *Applied Mathematics-A Journal of Chinese Universities.* 2021;36:304–316. doi: 10.1007/s11766-021-4376-3

106. Wang H, Li X. Towards Generic Semi-Supervised Framework for Volumetric Medical Image Segmentation. *ArXiv.* 2023. doi: 10.48550/arXiv.2310.11320

107. Wang J, Chen C. Unsupervised Adaptation of Polyp Segmentation Models via Coarse-to-Fine Self-Supervision. *Information Processing in Medical Imaging.* 2023:250–262. doi: 10.1007/978-3-031-34048-2_20

108. Wang T, Huang Z, Wu J, Cai Y, Li Z. Semi-Supervised Medical Image Segmentation with Co-Distribution Alignment. *Bioengineering.* 2023;10(7):869. doi: 10.3390/bioengineering10070869

109. Vasilev YA, Bobrovskaya TM, Arzamasov KM, et al. Medical datasets for machine learning: fundamental principles of standartization and systematization. *Manager Zdravoochranenia.* 2023(4):28–41. doi: 10.21045/1811-0185-2023-4-28-41

110. Kokina DYu, Gombolevskiy VA. Arzamasov KM, Andreychenko AE, Morozov SP Possibilities and limitations of using machine text-processing tools in Russian radiology reports. *Digital Diagnostics.* 2022;3(4):374–383. doi: 10.17816/DD101099

111. Ronzhin LV, Astanin PA, Kokina DYu, et al Semantic analysis methods in the system for authomated marking of the unstructured radiological chest examination protocols. *Social'nye aspekty zdorov'a naselenia.* 2023;69(1):12. doi: 10.21045/2071-5021-2023-69-1-12

112. Tomashevskaya VS, Yakovlev DA. Research of unstructured data interpretation problems. *Russian Technological Journal.* 2021;9(1):7–17. doi: 10.32362/2500-316X-2021-9-1-7-17

113. Protonotarios N, Katsamenis I, Sykiotis S, et al. A few-shot U-Net deep learning model for lung cancer lesion segmentation via PET/CT imaging. *Biomedical Physics and Engineering Express.* 2022;8:025019. doi: 10.1088/2057-1976/ac53bd

114. Voulodimos A, Protopapadakis E, Katsamenis I, Doulamis A, Doulamis N. A Few-Shot U-Net Deep Learning Model for COVID-19 Infected Area Segmentation in CT Images. *Sensors.* 2021;21(6):2215. doi: 10.3390/s21062215

115. Zhao G, Zhao H. One-Shot Image Segmentation with U-Net. *Journal of Physics: Conference Series.* 2021;1848(1):012113. doi: 10.1088/1742-6596/1848/1/012113

СПИСОК ЛИТЕРАТУРЫ

1. Shen D., Wu G., Suk H.I. Deep Learning in Medical Image Analysis // Annual Review of Biomedical Engineering. 2017. Vol. 19. P. 221–248. doi: 10.1146/annurev-bioeng-071516-044442

2. Ronneberger O., Fischer P., Brox T. U-Net: Convolutional Networks for Biomedical Image Segmentation // Medical Image Computing and Computer-Assisted Intervention (MICCAI) 2015. 2015. Vol. 9351. doi: 10.1007/978-3-319-24574-4_28

3. Milletari F., Navab N., Ahmadi S.A. V-Net: Fully Convolutional Neural Networks for Volumetric Medical Image Segmentation // Fourth International Conference on 3D Vision (3DV). 2016. P. 565–571. doi: 10.48550/arXiv.1606.04797

4. Chen L.C., Papandreou G., Kokkinos I., Murphy K., Yuille A. DeepLab: Semantic Image Segmentation with Deep Convolutional Nets, Atrous Convolution, and Fully Connected CRFs // IEEE Transactions on Pattern Analysis and Machine Intelligence. 2017. Vol. 40, N 4. P. 834–848. doi: 10.1109/TPAMI.2017.2699184

5. Huang G., Liu Z., Van Der Maaten L., Weinberger K.Q. Densely Connected Convolutional Networks // IEEE Conference on Computer Vision and Pattern Recognition (CVPR). 2017. P. 2261–2269. doi: 10.1109/CVPR.2017.243

6. He K., Gkioxari G., Dollár P., Girshick R. Mask R-CNN // IEEE International Conference on Computer Vision (ICCV). 2017. P. 2980–2988. doi: 10.1109/ICCV.2017.322

7. Khalal D.M., Azizi H., Maalej N. Automatic segmentation of kidneys in computed tomography images using U-Net // Cancer/Radiothérapie. 2023. Vol. 27, N 2. P. 109–114. doi: 10.1016/j.canrad.2022.08.004

8. Bernardo Gois F.N., Lobo Marques J.A. Segmentation of CT-Scan Images Using UNet Network for Patients Diagnosed with COVID-19 // Computerized Systems for Diagnosis and Treatment of COVID-192023. 2023. P. 29–44. doi: 10.1007/978-3-031-30788-1_3

9. Sarsembayeva T., Shomanov A., Sarsembayev M., et al. UNet Model for Segmentation of COPD Lung Lesions on Computed Tomography Images // Proceedings of the 7th International Conference on Digital Technologies in Education, Science and Industry (DTESI 2022). 2022. Available at: https://ceur-ws.org/Vol-3382/Short5.pdf. Accessed: November 9, 2024.

10. Çiçek Ö., Abdulkadir A., Lienkamp S., Brox T., Ronneberger O. 3D U-Net: Learning Dense Volumetric Segmentation from Sparse Annotation // Medical Image Computing and Computer-Assisted Intervention — MICCAI 2016. 2016. P. 424–432. doi: 10.1007/978-3-319-46723-8_4

11. Pantovic A., Ollivier I., Essert C. 2D and 3D-UNet for segmentation of SEEG electrode contacts on post-operative CT scans // Medical Imaging 2022: Image-Guided Procedures, Robotic Interventions, and Modeling. 2022. doi: 10.1117/12.2606538

12. Han X., Wu X., Wang S., et al. Automated segmentation of liver segment on portal venous phase MR images using a 3D convolutional neural network // Insights Imaging. 2022. Vol. 13, N 26. doi: 10.1186/s13244-022-01163-1

13. Zhou Z., Rahman Siddiquee M.M., Tajbakhsh N., Liang J. UNet++: A Nested U-Net Architecture for Medical Image Segmentation // Deep Learning in Medical Image Analysis and Multimodal Learning for Clinical Decision Support. 2018. P. 3–11. doi: 10.1007/978-3-030-00889-5_1

14. Yu C., Wang Y., Tang C., Feng W., Lv J. EU-Net: Automatic U-Net neural architecture search with differential evolutionary algorithm for medical image segmentation // Computers in Biology and Medicine. 2023. Vol. 167. P. 107579. doi: 10.1016/j.compbiomed.2023.107579

15. Weng Y., Zhou T., Li Y., Qiu X. NAS-Unet: Neural Architecture Search for Medical Image Segmentation // IEEE Access. 2019. Vol. 7. P. 44247–44257. doi: 10.1109/ACCESS.2019.2908991

16. Huang H., Lin L., Tong R., et al. UNet 3+: A Full-Scale Connected UNet for Medical Image Segmentation // ICASSP 2020–2020 IEEE International Conference on Acoustics, Speech and Signal Processing (ICASSP). 2020. P. 1055–1059. doi: 10.1109/ICASSP40776.2020.9053405

17. Li C., Bagher-Ebadian H., Sultan R.I., et al. A new architecture combining convolutional and transformer-based networks for

automatic 3D multi-organ segmentation on CT images // Med Phys. 2023. Vol. 50, N 11. P. 6990–7002. doi: 10.1002/mp.16750

18. Müller D., Soto-Rey I., Kramer F. Towards a guideline for evaluation metrics in medical image segmentation // BMC Research Notes. 2022. Vol. 15, N 210. doi: 10.1186/s13104-022-06096-y

19. Alberg A.J., Park J.W., Hager B.W., Brock M.V., Diener-West M. The use of «overall accuracy» to evaluate the validity of screening or diagnostic tests // Journal of General Internal Medicine. 2004. Vol. 19. P. 460–465. doi: 10.1111/j.1525-1497.2004.30091.x

20. Soler L., Hostettler A., Agnus V., et al. 3D image reconstruction for comparison of algorithm database: A patient specific anatomical and medical image database // IRCAD. 2010. Available at: https://www-sop.inria.fr/geometrica/events/wam/abstract-ircad.pdf. Accessed: November 9, 2024.

21. Löffler M., Sekuboyina A., Jakob A., et al. A Vertebral Segmentation Dataset with Fracture Grading // Radiology: Artificial Intelligence. 2020. Vol. 2, N 4. doi: 10.1148/ryai.2020190138

22. Wang Z., Bovik A.C., Sheikh H.R., Simoncelli E.P. Image quality assessment: from error visibility to structural similarity // IEEE Transactions on Image Processing. 2004. Vol. 13, N 4. P. 600–612. doi: 10.1109/TIP.2003.819861

23. Kavur A.E., Gezer N.S., Barış M., et al. CHAOS Challenge – combined (CT-MR) healthy abdominal organ segmentation // Medical Image Analysis. 2021. Vol. 69. P. 101950. doi: 10.1016/j.media.2020.101950

24. Bilic P., Christ P., Li H.B., et al. The Liver Tumor Segmentation Benchmark (LiTS) // Medical Image Analysis. 2023. Vol. 84. P. 102680. doi: 10.1016/j.media.2022.102680

25. Petrusca L., Cattin P., De Luca V., et al. Hybrid ultrasound/ magnetic resonance simultaneous acquisition and image fusion for motion monitoring in the upper abdomen // Investigative Radiology. 2013. Vol. 48, N 5. P. 333–340. doi: 10.1097/RLI.0b013e31828236c3

26. Jun M., Cheng G., Yixin W., et al. Covid-19 CT lung and infection segmentation dataset // Zenodo. 2020. Available at: https://zenodo.org/records/3757476#.YLov8vkzaUk. Accessed: November 9, 2024.

27. Morozov S.P., Andreychenko A.E., Blokhin I.A., et al. MosMedData: data set of 1110 chest CT scans performed during the COVID-19 epidemic // Digital Diagnostics. 2020. Vol. 1, N 1. P. 49–59. doi: 10.17816/DD46826

28. Roth H.R., Oda H., Hayashi Y., et al. Hierarchical 3D fully convolutional networks for multi-organ segmentation // ArXiv. 2017. Available at: https://arxiv.org/abs/1704.06382v1. Accessed: November 9, 2024.

29. Roth H., Farag A., Turkbey E.B., et al. Data from Pancreas-CT // The Cancer Imaging Archive. 2016. doi: 10.7937/K9/TCIA.2016.tNB1kqBU

30. Heimann T., Styner M., van Ginneken B. 3D Segmentation in the Clinic: A Grand Challenge // MICCAI 2007, the 10th Intel Conf. on Medical Image Computing and Computer Assisted Intervention. 2007. P. 7–15. Available at: https://www.diagnijmegen.nl/publications/ginn07/. Accessed: November 9, 2024.

31. Suckling J. The Mammographic Image Analysis Society Digital Mammogram Database // International Congress Series. 1994. P. 375–378. Available at: http://peipa.essex.ac.uk/info/mias.html. Accessed: November 9, 2024.

32. WHO Director-General's opening remarks at the media briefing on COVID-19 - 11 March 2020 [Internet]. 2020. Доступ по ссылке: https://www.who.int/director-general/speeches/detail/who-director-general-s-opening-remarks-at-the-media-briefing-on-covid-19---11-march-2020 [Дата обращения: 9.11.2024].

33. Landman B., Xu Z., Igelsias J., et al. Miccai multi-atlas labeling beyond the cranial vault–workshop and challenge // Proceedings of the MICCAI Multi-Atlas Labeling Beyond Cranial Vault — Workshop Challenge. 2015. Vol. 5. P. 12.

34. Simpson A.L., Antonelli M., Bakas S., et al. A large annotated medical image dataset for the development and evaluation of segmentation algorithms // ArXiv. 2019. doi: 10.48550/arXiv.1902.09063

35. Gutman D., Codella N.C.F., Celebi E., et al. Skin Lesion Analysis toward Melanoma Detection: A Challenge at the International Symposium on Biomedical Imaging (ISBI) 2016, hosted by the International Skin Imaging Collaboration (ISIC) // ArXiv. 2016. doi: 10.48550/arXiv.1605.01397

36. Jha D., Smedsrud P.H., Riegler M.A., et al. Kvasir-SEG: A Segmented Polyp Dataset // MultiMedia Modeling. 2020. Vol. 11962. P. 451–462. doi: 10.1007/978-3-030-37734-2_37

37. Bernal J., Sánchez F.J., Fernández-Esparrach G., et al. WM-DOVA maps for accurate polyp highlighting in colonoscopy: Validation vs. saliency maps from physicians // Computerized Medical Imaging and Graphics. 2015. Vol. 43. P. 99–111. doi: 10.1016/j.compmedimag.2015.02.007

38. Grove O., Berglund A.E., Schabath M.B., et al. Quantitative Computed Tomographic Descriptors Associate Tumor Shape Complexity and Intratumor Heterogeneity with Prognosis in Lung Adenocarcinoma // PLOS ONE. 2015. Vol. 10, N 3. P. e0118261. doi: 10.1371/journal.pone.0118261

39. Heller N., Sathianathen N., Kalapara A., et al. The KiTS19 Challenge Data: 300 Kidney Tumor Cases with Clinical Context, CT Semantic Segmentations, and Surgical Outcomes // ArXiv. 2019. P. 13. doi: 10.48550/arXiv.1904.00445

40. Ji Y., Bai H., Yang J., et al. AMOS: A Large-Scale Abdominal Multi-Organ Benchmark for Versatile Medical Image Segmentation // ArXiv. 2022. doi: 10.48550/arXiv.2206.08023

41. Lemay A., Gros C., Zhuo Z., et al. Multiclass Spinal Cord Tumor Segmentation on MRI with Deep Learning // ArXiv. 2021. doi: 10.48550/arXiv.2012.12820

42. Ali M.A.S., Misko O., Salumaa S.O., et al. Evaluating Very Deep Convolutional Neural Networks for Nucleus Segmentation from Brightfield Cell Microscopy Images // SLAS Discovery. 2021. Vol. 26, N 9. P. 1125–1137. doi: 10.1177/24725552211023214

43. Gibson E., Giganti F., Hu Y., et al. Automatic Multi-Organ Segmentation on Abdominal CT With Dense V-Networks // IEEE Transactions on Medical Imaging. 2018. Vol. 37, N 8. P. 1822–1834. doi: 10.1109/TMI.2018.2806309

44. Jimenez-del Toro O., Müller H., Krenn M., et al. Cloud-Based Evaluation of Anatomical Structure Segmentation and Landmark Detection Algorithms: VISCERAL Anatomy Benchmarks // IEEE Transactions on Medical Imaging. 2016. Vol. 35, N 11. P. 2459–2475. doi: 10.1109/TMI.2016.2578680

45. Regan E.A., Hokanson J.E., Murphy J.R., et al. Genetic Epidemiology of COPD (COPDGene) Study Design // COPD: Journal of Chronic Obstructive Pulmonary Disease. 2010. Vol. 7, N 1. P. 32–43. doi: 10.3109/15412550903499522

46. Litjens G., Toth R., van de Ven W., et al. Evaluation of prostate segmentation algorithms for MRI: The PROMISE12 challenge // Medical Image Analysis. 2014. Vol. 18, N 2. P. 359–373. doi: 10.1016/j.media.2013.12.002

47. Xiong Z., Xia Q., Hu Z., et al. A global benchmark of algorithms for segmenting the left atrium from late gadolinium-enhanced cardiac magnetic resonance imaging // Medical Image Analysis. 2021. Vol. 67. P. 101832. doi: 10.1016/j.media.2020.101832

48. Landman B., Xu Z., Igelsias J., et al. 2015 MICCAI multi-atlas labeling beyond the cranial vault–workshop and challenge // MICCAI Multi-Atlas Labeling Beyond Cranial Vault — Workshop Challenge. 2015. Vol. 5. P. 12.

49. Zhuang X., Shen J. Multi-scale patch and multi-modality atlases for whole heart segmentation of MRI // Medical Image Analysis. 2016. Vol. 31. P. 77–87. doi: 10.1016/j.media.2016.02.006

50. Campello V.M., Gkontra P., Izquierdo C., et al. Multi-Centre, Multi-Vendor and Multi-Disease Cardiac Segmentation: The M&Ms Challenge // IEEE Transactions on Medical Imaging. 2021. Vol. 40, N 12. P. 3543–3554. doi: 10.1109/TMI.2021.3090082

51. Silva J., Histace A., Romain O., Dray X., Granado B. Toward embedded detection of polyps in WCE images for early diagnosis of colorectal cancer // International Journal of Computer Assisted Radiology and Surgery. 2014. Vol. 9. P. 283–293. doi: 10.1007/s11548-013-0926-3

52. Trikha S., Turnbull A., Morris R., Anderson D., Hossain P. The journey to femtosecond laser-assisted cataract surgery: New beginnings or a false dawn? // Eye. 2013. Vol. 27, N 4. P. 461–473. doi: 10.1038/eye.2012.293

53. Xiong Z., Xia Q., Hu Z., et al. A global benchmark of algorithms for segmenting the left atrium from late gadolinium-enhanced cardiac magnetic resonance imaging // Medical Image Analisys. 2021. Vol. 67. P. 101832. doi: 10.1016/j.media.2020.101832

54. Bernard O., Lalande A., Zotti C., et al. Deep Learning Techniques for Automatic MRI Cardiac Multi-Structures Segmentation and Diagnosis: Is the Problem Solved? // IEEE Transactions on Medical Imaging. 2018. Vol. 37, N 11. P. 2514–2525. doi: 10.1109/TMI.2018.2837502

55. Li P., Wang S., Li T., et al. A Large-Scale CT and PET/CT Dataset for Lung Cancer Diagnosis (Lung-PET-CT-Dx) [Data set] // The Cancer Imaging Archive. 2020. doi: 10.7937/TCIA.2020.NNC2-0461

56. Clark K., Vendt B., Smith K., et al. The Cancer Imaging Archive (TCIA): Maintaining and Operating a Public Information Repository // Journal of Digital Imaging. 2013. Vol. 26. P. 1045–1057. doi: 10.1007/s10278-013-9622-7

57. Xu Z., Jia Z., Sun J., Dong W., Li Z. DO-U-Net: Improved U-Net Model for CT Image Segmentation using DBB and Octave Convolution // Proceedings of the 2023 International Conference on Computer, Vision and Intelligent Technology (ICCVIT '23). 2023. P. 1–8. doi: 10.1145/3627341.3630403

58. Ayalew Y., Fante K., Aliy M. Modified U-Net for liver cancer segmentation from computed tomography images with a new class balancing method // BMC Biomedical Engineering. 2021. Vol. 3, N 4. doi: 10.1186/s42490-021-00050-y

59. Guan S., Khan A.A., Sikdar S., Chitnis P.V. Fully Dense UNet for 2-D Sparse Photoacoustic Tomography Artifact Removal // IEEE Journal of Biomedical and Health Informatics. 2020. Vol. 24, N 2. P. 568–576. doi: 10.1109/JBHI.2019.2912935

60. Özcan F., Uçan O.N., Karaçam S., Tunçman D. Fully Automatic Liver and Tumor Segmentation from CT Image Using an AIM-UNet // Bioengineering. 2023. Vol. 10, N 2. doi: 10.3390/bioengineering10020215

61. Ansari M.Y., Yang Y., Meher P.K., Dakua S.P. Dense-PSP-UNet: A neural network for fast inference liver ultrasound segmentation // Computers in Biology and Medicine. 2023. Vol. 153. P. 106478. doi: 10.1016/j.compbiomed.2022.106478

62. Omarov B., Tursynova A., Postolache O., et al. Modified UNet Model for Brain Stroke Lesion Segmentation on Computed Tomography Images // Computers, Materials and Continua. 2022. Vol. 71, N 3. P. 4701–4717. doi: 10.32604/cmc.2022.020998

63. Mizusawa S., Sei Y., Orihara R., Ohsuga A. Computed tomography image reconstruction using stacked U-Net // Computerized Medical Imaging and Graphics. 2021. Vol. 90. P. 101920. doi: 10.1016/j.compmedimag.2021.101920

64. Golts A., Khapun D., Shats D., Shoshan Y., Gilboa-Solomon F. An Ensemble of 3D U-Net Based Models for Segmentation of Kidney and Masses in CT Scans // Kidney and Kidney Tumor Segmentation (KiTS 2021). 2022. Vol. 13168. P. 103–115. doi: 10.1007/978-3-030-98385-7_14

65. Araújo J.D.L., da Cruz L.B., Diniz J.O.B., et al. Liver segmentation from computed tomography images using cascade deep learning // Computers in Biology and Medicine. 2022. Vol. 140. P. 105095. doi: 10.1016/j.compbiomed.2021.105095

66. Koirala C.P., Mohapatra S., Gosai A., Schlaug G. Automated Ensemble-Based Segmentation of Adult Brain Tumors: A Novel Approach Using the BraTS AFRICA Challenge Data // ArXiv. 2023. doi: 10.48550/arXiv.2308.07214

67. Li Z., Zhu Q., Zhang L., et al. A deep learning-based self-adapting ensemble method for segmentation in gynecological brachytherapy // Radiation Oncology. 2022. Vol. 17, N 152. doi: 10.1186/s13014-022-02121-3

68. Woo S., Park J., Lee J.-Y., Kweon I.S. CBAM: Convolutional Block Attention Module // Proceedings of the European conference on computer vision (ECCV). 2018. P. 3–19. doi: 10.48550/arXiv.1807.06521

69. Nazir S., Zheng R., Zheng Y., Dong-Ye C. Improved 3D U-Net for COVID-19 Chest CT Image Segmentation // Scientific Programming. 2021. Vol. 2021, N 9999368. P. 9. doi: 10.1155/2021/9999368

70. Salehi S.S.M., Erdogmus D., Gholipour A. Tversky Loss Function for Image Segmentation Using 3D Fully Convolutional Deep Networks // Machine Learning in Medical Imaging. 2017. Vol. 10541. P. 379–387. doi: 10.1007/978-3-319-67389-9_44

71. Oktay O., Schlemper J., Folgoc L.L., et al. Attention U-Net: Learning Where to Look for the Pancreas // ArXiv. 2018. doi: 10.48550/arXiv.1804.03999

72. Agarap A.F. Deep Learning using Rectified Linear Units (ReLU) // ArXiv. 2018. P. 7. doi: 10.48550/arXiv.1803.08375

73. Wu J., Zhou S., Zuo S., et al. U-Net combined with multi-scale attention mechanism for liver segmentation in CT images // BMC Medical Informatics and Decision Making. 2021. Vol. 21, N 283. doi: 10.1186/s12911-021-01649-w

74. Zhang L., Liu Y., Li Z., Li D. Epa-unet:automatic Segmentation of Liver and Tumor in Ct Images Based on Residual U-net and Efficient Multiscale Attention Methods // Research Square. 2023. doi: 10.21203/rs.3.rs-3273964/v1

75. Zarbakhsh P. Spatial Attention Mechanism and Cascade Feature Extraction in a U-Net Model for Enhancing Breast Tumor Segmentation // Applied Sciences. 2023. Vol. 13, N 15. P. 8758. doi: 10.3390/app13158758

76. Subhan Akbar A., Fatichah C., Suciati N. UNet3D with Multiple Atrous Convolutions Attention Block for Brain Tumor Segmentation // Brainlesion: Glioma, Multiple Sclerosis, Stroke and Traumatic Brain Injuries. 2022. P. 182–193. doi: 10.1007/978-3-031-08999-2_14

77. Yu Z., Han S., Song Z. 3D Medical Image Segmentation based on multi-scale MPU-Net // ArXiv. 2023. doi: 10.48550/arXiv.2307.05799

78. Xingfei F., Chaobing H. CAE-UNet: An Effective Automatic Segmentation Model for CT Images of COVID-19 // 2022 6th

International Conference on Communication and Information Systems (ICCIS). 2022. P. 113–117. doi: 10.1109/ICCIS56375.2022.9998131

79. He K., Zhang X., Ren S., Sun J. Deep Residual Learning for Image Recognition // 2016 IEEE Conference on Computer Vision and Pattern Recognition (CVPR). 2016. P. 770–778. doi: 10.1109/cvpr.2016.90

80. Hatamizadeh A., Tang Y., Nathet V., et al. U-NETR: Transformers for 3D Medical Image Segmentation // 2022 IEEE/CVF Winter Conference on Applications of Computer Vision (WACV). 2022. P. 1748–1758. doi: 10.1109/WACV51458.2022.00181

81. Eskandari S., Lumpp J. Inter-Scale Dependency Modeling for Skin Lesion Segmentation with Transformer-based Networks // ArXiv. 2023. doi: 10.48550/arXiv.2310.13727

82. Shi X., Chen Z., Wang H., et al. Convolutional LSTM Network: A Machine Learning Approach for Precipitation Nowcasting // Neural Information Processing Systems. 2015. doi: 10.48550/arXiv.1506.04214

83. Pham T.H., Li X., Nguyen K.D. SeU-Net-Trans: A Simple yet Effective UNet-Transformer Model for Medical Image Segmentation // ArXiv. 2023. doi: 10.48550/arXiv.2310.09998

84. Ghofrani F., Behnam H., Motlagh H.D.K. Liver Segmentation in CT Images Using Deep Neural Networks // 2020 28th Iranian Conference on Electrical Engineering (ICEE). 2020. P. 1–6. doi: 10.1109/ICEE50131.2020.9260809

85. Diakogiannis F.I., Waldner F., Caccetta P., Wuet C., et al. ResUNet-a: A deep learning framework for semantic segmentation of remotely sensed data // ISPRS Journal of Photogrammetry and Remote Sensing. 2020. Vol. 16, N 2. P. 94–114. doi: 10.1016/j.isprsjprs.2020.01.013

86. Jha D., Riegler M.A., Johansen D., Halvorsen P., Johansen H.D. Doubleu-net: DoubleU-Net: A Deep Convolutional Neural Network for Medical Image Segmentation // IEEE 33rd International symposium on computer-based medical systems (CBMS). 2020. P. 558–564. doi: 10.1109/CBMS49503.2020.00111

87. Lee H.H., Bao S., Huo Y., Landman B.A. 3D UX-Net: A Large Kernel Volumetric ConvNet Modernizing Hierarchical Transformer for Medical Image Segmentation // International Conference on Learning Representations. 2023. doi: 10.48550/arXiv.2209.15076

88. Liang J., Yang C., Zhong J., Ye X. BTSwin-U-Net: 3D U-shaped Symmetrical Swin Transformer-based Network for Brain Tumor Segmentation with Self-supervised Pre-training // Neural Processing Letters. 2022. Vol. 55. P. 3695–3713. doi: 10.1007/s11063-022-10919-1

89. Alalwan N., Abozeid A., ElHabshy A.A., Alzahrani A. Efficient 3D Deep Learning Model for Medical Image Semantic Segmentation // Alexandria Engineering Journal. 2021. Vol. 60, N 1. P. 1231–1239. doi: 10.1016/j.aej.2020.10.046

90. Lemay A., Gros C., Vincent O., et al. Benefits of Linear Conditioning with Metadata for Image Segmentation // ArXiv. 2021. doi: 10.48550/arXiv.2102.09582

91. Du R., Vardhanabhuti V. 3D-RADNet: Extracting labels from DICOM metadata for training general medical domain deep 3D convolution neural networks // International Conference on Medical Imaging with Deep Learning. 2020. Vol. 121. P. 174–192. Available at: https://proceedings.mlr.press/v121/du20a/du20a.pdf. Accessed: November 9, 2024.

92. Plutenko I., Papkov M., Palo K., Parts L., Fishman D. Metadata Improves Segmentation Through Multitasking Elicitation // Domain Adaptation and Representation Transfer. 2023. P. 147–155. doi: 10.1007/978-3-031-45857-6_15

93. Jiang J., Peng Y., Hou Q., Wang J. MDCF_Net: A Multi-dimensional hybrid network for liver and tumor segmentation from CT //

Biocybernetics and Biomedical Engineering. 2023. Vol. 43, N 2. P. 494–506. doi: 10.1016/j.bbe.2023.04.004

94. Fu T., Yu Q., Lao H., Liu P., Wan S. Traffic Safety Oriented Multi-Intersection Flow Prediction Based on Transformer and CNN // Security and Communication Networks. 2023. P. 1–13. doi: 10.1155/2023/1363639

95. Chen X., Wei X., Tang M., et al. Liver segmentation in CT imaging with enhanced mask region-based convolutional neural networks // Annals of Translational Medicine. 2021. Vol. 9, N 24. P. 1768. doi: 10.21037/atm-21-5822

96. Ernst P., Chatterjee S., Rose G., Nürnberger A. Primal-Dual U-Net for Sparse View Cone Beam Computed Tomography Volume Reconstruction // ArXiv. 2022. doi: 10.48550/arXiv.2205.07866

97. Koehler G., Wald T., Ulrichet C., et al. RecycleNet: Latent Feature Recycling Leads to Iterative Decision Refinement // ArXiv. 2023. doi: 10.48550/arXiv.2309.07513

98. Jafari M., Auer D., Francis S., Garibaldi J., Chen X. DRU-net: An Efficient Deep Convolutional Neural Network for Medical Image Segmentation // 2020 IEEE 17th International Symposium on Biomedical Imaging (ISBI). 2020. P. 1144–1148. doi: 10.48550/arXiv.2004.13453

99. Heker M., Ben-Cohen A., Greenspan H. Hierarchical Fine-Tuning for joint Liver Lesion Segmentation and Lesion Classification in CT // 2019 41st Annual International Conference of the IEEE Engineering in Medicine and Biology Society (EMBC). 2019. P. 895–898. doi: 10.1109/EMBC.2019.8857127

100. Matovinovic I.Z., Loncaric S., Lo J., Heisler M., Sarunic M. Transfer Learning with U-Net type model for Automatic Segmentation of Three Retinal Layers In Optical Coherence Tomography Images // 2019 11th International Symposium on Image and Signal Processing and Analysis (ISPA). 2019. P. 49–53. doi: 10.1109/ISPA.2019.8868639

101. Kora P., Ooi C.P., Faust O., et al. Transfer learning techniques for medical image analysis: A review // Biocybernetics and Biomedical Engineering. 2022. Vol. 42, N 1. P. 79–107. doi: 10.1016/j.bbe.2021.11.004

102. Humpire-Mamani G.E., Jacobs C., Prokop M., van Ginneken B., Lessmann N. Transfer learning from a sparsely annotated dataset of 3D medical images // ArXiv. 2023. doi: 10.48550/arXiv.2311.05032

103. Messaoudi H., Belaid A., Salem D.B., Conze P.-H. Cross-dimensional transfer learning in medical image segmentation with deep learning // Medical Image Analysis. 2023. Vol. 88. P. 102868. doi: 10.1016/j.media.2023.102868

104. Tan M., Le Q. EfficientNet: Rethinking Model Scaling for Convolutional Neural Networks // International conference on machine learning (PMLR). 2019. P. 6105–6114. doi: 10.48550/arXiv.1905.11946

105. Hong Y., Mao X., Hui Q. et al. Automatic liver and tumor segmentation based on deep learning and globally optimized refinement // Applied Mathematics-A Journal of Chinese Universities. 2021. Vol. 36. P. 304–316. doi: 10.1007/s11766-021-4376-3

106. Wang H., Li X. Towards Generic Semi-Supervised Framework for Volumetric Medical Image Segmentation // ArXiv. 2023. doi: 10.48550/arXiv.2310.11320

107. Wang J., Chen C. Unsupervised Adaptation of Polyp Segmentation Models via Coarse-to-Fine Self-Supervision // Information Processing in Medical Imaging. 2023. P. 250–262. doi: 10.1007/978-3-031-34048-2_20

108. Wang T., Huang Z., Wu J., Cai Y., Li Z. Semi-Supervised Medical Image Segmentation with Co-Distribution Alignment // Bioengineering. 2023. Vol. 10, N 7. P. 869. doi: 10.3390/bioengineering10070869

109. Васильев Ю.А., Бобровская Т.М., Арзамасов К.М., и др. Основополагающие принципы стандартизации и систематизации информации о наборах данных для машинного обучения в медицинской диагностике // Менеджер здравоохранения. 2023. № 4. С. 28–41. doi: 10.21045/1811-0185-2023-4-28-41

110. Кокина Д.Ю., Гомболевский В.А., Арзамасов К.М., Андрейченко А.Е., Морозов С.П. Возможности и ограничения использования инструментов машинной обработки текстов в лучевой диагностике // Digital Diagnostics. 2022. Т. 3, № 4. С. 374–383. doi: 10.17816/DD101099

111. Ронжин Л.В., Астанин П.А., Кокина Д.Ю., и др. Система автоматической разметки неструктурированных протоколов рентгенологических исследований грудной клетки с использованием методов семантического анализа // Социальные аспекты здоровья населения. 2023. Т. 69, № 1. С. 12. doi: 10.21045/2071-5021-2023-69-1-12

112. Томашевская В.С., Яковлев Д.А. Способы обработки неструктурированных данных // Российский технологический журнал. 2021. Т. 9, № 1. С. 7–17. doi: 10.32362/2500-316X-2021-9-1-7-17

113. Protonotarios N., Katsamenis I., Sykiotis S., et al. A few-shot U-Net deep learning model for lung cancer lesion segmentation via PET/CT imaging // Biomedical Physics and Engineering Express. 2022. Vol. 8. P. 025019. doi: 10.1088/2057-1976/ac53bd

114. Voulodimos A., Protopapadakis E., Katsamenis I., Doulamis A., Doulamis N. A Few-Shot U-Net Deep Learning Model for COVID-19 Infected Area Segmentation in CT Images // Sensors. 2021. Vol. 21, N 6. P. 2215. doi: 10.3390/s21062215

115. Zhao G., Zhao H. One-Shot Image Segmentation with U-Net // Journal of Physics: Conference Series. 2021. Vol. 1848, N 1. P. 012113. doi: 10.1088/1742-6596/1848/1/012113

AUTHORS' INFO

* Kirill M. Arzamasov, MD, Cand. Sci. (Medicine);
address: 24 bldg. 1 Petrovka str., 127051, Moscow, Russia;
ORCID: 0000-0001-7786-0349;
eLibrary SPIN: 3160-8062;
e-mail: ArzamasovKM@zdrav.mos.ru

Anastasia M. Dostovalova;
ORCID: 0009-0004-9420-4182;
eLibrary SPIN: 3784-0791;
e-mail: ADostovalova@frccscs.ru

Andrey K. Gorshenin, Dr. Sci. (Physics and Mathematics), Assistant Professor;
ORCID: 0000-0001-8129-8985;
eLibrary SPIN: 1512-3425;
e-mail: AGorshenin@frccsc.ru

Jullia V. Starichkova, Cand. Sci. (Engineering), Assistant Professor;
ORCID: 0000-0003-1804-9761;
eLibrary SPIN: 3001-6791;
e-mail: starichkova@mirea.ru

_____
* Corresponding author / Автор, ответственный за переписку

ОБ АВТОРАХ

* Арзамасов Кирилл Михайлович, канд. мед. наук;
адрес: Россия, 127051, Москва, ул. Петровка, д. 24, стр. 1;
ORCID: 0000-0001-7786-0349;
eLibrary SPIN: 3160-8062;
e-mail: ArzamasovKM@zdrav.mos.ru

Достовалова Анастасия Михайловна;
ORCID: 0009-0004-9420-4182;
eLibrary SPIN: 3784-0791;
e-mail: ADostovalova@frccscs.ru

Горшенин Андрей Константинович, д-р. физ.-мат. наук, доцент;
ORCID: 0000-0001-8129-8985;
eLibrary SPIN: 1512-3425;
e-mail: AGorshenin@frccsc.ru

Старичкова Юлия Викторовна, канд. техн. наук, доцент;
ORCID: 0000-0003-1804-9761;
eLibrary SPIN: 3001-6791;
e-mail: starichkova@mirea.ru

Potential use of radiation methods for diagnosing bone metastases of castration-resistant prostate cancer: a literature review

Anastasia A. Karpova[1], Nikolay I. Sergeev[2], Olga A. Borisova[2], Pavel A. Nikitin[1], Dmitriy K. Fomin[2], Vladimir A. Solodkiy[2]

[1] Pulmonology Scientific Research Institute, Moscow, Russia;
[2] Russian Scientific Center of Roentgenoradiology, Moscow, Russia

ABSTRACT

Metastatic castration-resistant prostate cancer (mCRPC) is the tumor progression with the development of resistance to androgen deprivation therapy. The incidence of bone metastases in these patients reaches 90%. Radiology is widely used to diagnose mCRPC. Computed tomography (CT) and magnetic resonance imaging (MRI) are beneficial in anatomic imaging, but have some limitations in evaluating effectiveness of disease treatment. Scintigraphy is used to screen for bone metastases, but is poorly suited for assessing disease progression. Positron emission tomography (PET) combined with CT and single-photon emission CT are used for early detection of local or systemic spread of prostate cancer. PET of prostate-specific membrane antigen is used to predict the effectiveness of anti-tumor therapy based on the absorbed dose of a radiopharmaceutical (RP). The introduction of RPs (^{177}Lu-PSMA) opens up new perspectives for radionuclide therapy with simultaneous evaluation of its efficacy using hybrid visualization. The potential use of radiology in the diagnosis of bone metastases is of particular interest for the analysis and systematization of the data obtained and for the development of indications for radioligand therapy and the evaluation of its efficacy.

Published data indicate that radiologic modalities for the diagnosis of mCRPC vary in sensitivity and specificity and have their own advantages and limitations, so these modalities should be combined.

The development and improvement of methods to quantitatively assess treatment efficacy and identify prognostic markers will enable more informed selection of treatment strategies and radiopharmaceuticals, leading to improved overall survival.

Keywords: prostate cancer; bone metastases; single-photon emission computed tomography; positron emission tomography; magnetic resonance imaging; multislice computed tomography; radiomics.

Возможности лучевых методов диагностики метастазов в кости кастрационно-резистентного рака предстательной железы (обзор литературы)

А.А. Карпова[1], Н.И. Сергеев[2], О.А. Борисова[2], П.А. Никитин[1], Д.К. Фомин[2], В.А. Солодкий[2]

[1] Научно-исследовательский институт пульмонологии Федерального медико-биологического агентства России, Москва, Россия;
[2] Российский научный центр рентгенорадиологии Минздрава России, Москва, Россия

АННОТАЦИЯ

Метастатический кастрационно-резистентный рак предстательной железы (мКРРПЖ) — это прогрессирование опухолевого процесса при формировании невосприимчивости к андроген-депривационной терапии. Частота появления метастазов в костях у таких пациентов достигает 90%. В диагностике мКРРПЖ широко используют лучевые методы исследований. Компьютерная томография и магнитно-резонансная томография обладают преимуществами в анатомической визуализации, однако имеют ограничения в оценке эффективности лечения заболевания. Сцинтиграфию применяют для скрининга метастатического поражения костей скелета, но при этом затруднён анализ прогрессирования заболевания. Позитронно-эмиссионную томографию (ПЭТ), совмещённую с компьютерной томографией, и однофотонную эмиссионную компьютерную томографию используют для раннего выявления местного или системного распространения рака предстательной железы. Информация о количестве поглощённого радиофармпрепарата (РФП) с помощью ПЭТ-визуализации простатоспецифичного мембранного антигена используют для прогнозирования эффективности противоопухолевой терапии. С внедрением в практическую деятельность РФП (^{177}Lu-PSMA) открылась перспектива проведения радионуклидной терапии с одновременным определением её эффективности методами гибридной визуализации. Возможности методов лучевой диагностики метастазов в кости представляют особый интерес для изучения и систематизации получаемых данных и разработки показаний для проведения радиолигандной терапии и анализа её эффективности.

Опубликованные данные свидетельствуют о том, что лучевые методы диагностики мКРРПЖ обладают различной чувствительностью и специфичностью, имеют свои преимущества и недостатки, что говорит о необходимости комплексного подхода в их использовании.

Разработка и развитие методик количественной оценки эффективности лечения, выявление прогностических маркёров позволит грамотно выбрать необходимую тактику лечения и облегчит подбор РФП, что приведёт к увеличению общей выживаемости.

Ключевые слова: рак предстательной железы; костные метастазы; однофотонная эмиссионная компьютерная томография; позитронно-эмиссионная томография; магнитно-резонансная томография; мультиспиральная компьютерная томография; радиомика.

放射方法诊断去势抵抗性前列腺癌骨转移的可能性（文献综述）

Anastasia A. Karpova[1], Nikolay I. Sergeev[2], Olga A. Borisova[2], Pavel A. Nikitin[1], Dmitriy K. Fomin[2], Vladimir A. Solodkiy[2]

[1] Pulmonology Scientific Research Institute, Moscow, Russia;
[2] Russian Scientific Center of Roentgenoradiology, Moscow, Russia

摘要

转移性去势抵抗性前列腺癌（mCRPC）是一种对雄激素剥夺疗法形成耐药性的肿瘤发展阶段。此类患者骨转移的发生率达90%。放射方法广泛用于mCRPC的检查。计算机断层扫描和磁共振成像在解剖成像方面具有优势，但在疾病疗效评估方面存在局限性。闪烁扫描法用于筛查转移性骨骼病变，但很难分析疾病的进展情况。正电子发射计算机断层扫描（PET）结合计算机断层扫描和单光子发射计算机断层扫描可用于早期检测前列腺癌的局部或全身扩散。前列腺特异性膜抗原PET成像中放射性药物吸收量的信息，可用于预测抗癌治疗的效果。随着放射性药物（177Lu-PSMA）在实践活动中的推广，开辟了混合成像方法同时确定其疗效的放射性核素疗法的前景。骨转移放射诊断方法的可能性对于研究和系统化所获得的数据、研究放射配体治疗的适应症和分析其疗效具有特别重要的意义。

已发表的数据证明，用于诊断mCRPC的放射方法具有不同的敏感性和特异性，并且各有优缺点，这表明在使用这些方法时需要采取综合方法。

定量评估治疗方法、预后标志物判定的研究和发展，可以正确的选择必要的治疗策略，并简化放射性药物的选择，从而提高总体存活率。

关键词：前列腺癌；骨转移；单光子发射计算机断层扫描；正电子发射计算机断层扫描；磁共振成像；多螺旋计算机断层扫描；放射组学。

INTRODUCTION

Prostate cancer (PC), one of the most prevalent cancers in men, originates in the glandular epithelium of the prostate [1]. From 2011 to 2021, the incidence of PC in Russia rose by 41.69% [2], making it a socially and economically significant concern. The development of metastatic castration-resistant PC (mCRPC), which is caused by a proliferation of androgen-insensitive cells, makes resistance to androgen deprivation therapy particularly significant [3]. The mean time to hormone therapy resistance is 1.5–2 years, which limits future therapeutic choices. This is complicated by significant variability in tumor morphology, serum prostate-specific antigen (PSA) levels, disease stage, and the risk of relapse [4].

The prognosis worsens with metastatic disease, with only 30% of patients surviving for five years [5]. The incidence of bone metastases in patients with mCRPC can reach 90% [6]. Visceral metastases are most frequently observed when secondary bone lesions are already present, which suggests a poor prognosis [7].

The initial development of bone metastases is determined by an imbalance between bone-resorbing cells (osteoclasts) and bone-forming cells (osteoblasts) resulting from interactions between cancer cells and elements of the internal bone milieu [8, 9].

Diagnostic imaging techniques are essential for the initial assessment of the tumor grade and the number and size of metastases, as well as for monitoring patients with mCRPC during treatment. Each diagnostic radiology technique has its own advantages and limitations. Multislice computed tomography (MSCT) and magnetic resonance imaging (MRI) effectively detect advanced tumors owing to anatomical imaging; however, their application in assessing PC treatment efficacy is restricted. Scintigraphy performs well in screening for bone metastases because of its high sensitivity, but is less effective in evaluating disease progression [10].

For the early detection of local or systemic tumors in PC, hybrid diagnostic techniques like positron emission tomography with computed tomography (PET/CT) and single-photon emission computed tomography with computed tomography (SPECT/CT) with diagnostic radiopharmaceuticals are utilized, taking into account the functional and morphological components of the obtained data [11].

Prostate-specific membrane antigen (PSMA) ligand PET has significantly augmented diagnostic algorithms for patients with PC owing to quantitative data on radiopharmaceutical uptake in the targeted areas. Though there are some unresolved concerns, PSMA PET/CT has demonstrated promising results in predicting the efficacy of cancer treatment [12].

Radionuclide therapy in mCRPC targets PSMA, with subsequent imaging examinations to confirm radionuclide binding [13]. Early relapses, high serum PSMA levels, Gleason scores, and a more aggressive illness are all correlated with PSMA expression [14, 15].

Physiologically, PSMA is also expressed in the lacrimal and salivary glands, proximal renal tubules, liver, spleen, and proximal small intestine [14]. The presence of PSMA activity has been documented in the peripheral ganglia and central nervous system [16].

The most promising and frequently used isotopes for radioligand therapy are ^{177}Lu and ^{225}Ac. ^{177}Lu has unique diagnostic and therapeutic benefits, including the binding of PSMA molecules by β– and γ-emitters ^{177}Lu-PSMA. ^{225}Ac exerts a powerful therapeutic effect via binding of PSMA by the α-emitter ^{225}Ac-PSMA [3]. Prostate tumor cells accumulate ^{225}Ac- or ^{177}Lu-labeled PSMA ligands, which damages DNA and eventually results in tumor cell death [17, 18].

Clinicians treating PC should focus on defining objective patient selection parameters for radioligand therapy, as well as on the early detection and imaging assessment of relapses following various PC therapies.

This review examines the potential of various diagnostic radiological modalities in mCRPC patients.

DIAGNOSTIC RADIOLOGY TECHNIQUES

Radiography is an imaging technique that generates consolidated images of organs, bone structures, and tissues employing the penetrative properties of X-rays. It is a reliable and accessible method for evaluating the structure and location of bone metastases [19]. Kitagawa et al. [20] revealed that radiography exhibits high specificity (80.9%), low sensitivity (45.8%) [due to limited contrast uptake by bone marrow lesions], and an accuracy of 74.8% [20]. If the bone matrix loss is less than 25%–30%, it is difficult to detect bone metastases early by radiography; also, there is limited ability to evaluate medulla alterations [21]. Thus, conventional radiography techniques are more effective for the urgent detection of fractures and postoperative monitoring of surgical hardware and implants [21].

Multislice CT (MSCT) is a modern diagnostic radiology technique that uses X-rays to generate cross-sectional images. Because of its high resolution, MSCT produces detailed organ and tissue images. In a meta-analysis examining the diagnostic utility of diagnostic radiology modalities in patients with spinal metastases, the sensitivity and specificity of MSCT were 79.2% and 92.3%, respectively [22–24].

One of the primary benefits of MSCT is the short scan time, which is especially essential in emergency circumstances where patients suddenly develop pain. This technique identifies fractures caused by existing secondary bone lesions and spinal nerve compression [21, 23]. However, due to the limited contrast uptake by soft tissues, MSCT is seldom used as a primary diagnostic tool in PC. It is more typically employed for the detection of distant metastases and for biopsy guidance [19]. This technique determines

the structure of the bone metastases and the extent of bone destruction. Additionally, it enables the use of extra image processing techniques for metal artifact reduction in the imaging-based evaluation of surgical hardware [23]. The formation of reactive sclerosis during treatment and the progression of osteoblastic metastases appear to be similar on MSCT scans (by increased lesion density). Because of this characteristic of bone metastases, the RECIST 1.1 criteria categorize these lesions as non-measurable (Fig. 1) [24]. Radiomics facilitate the quantitative assessment of lesions [25].

Magnetic resonance imaging is a diagnostic radiological modality that generates images using electromagnetic waves in a constant magnetic field. The advantages of MRI include the lack of ionizing radiation and superior soft tissue imaging. It is one of the most effective techniques for noninvasive bone marrow evaluation (Fig. 2). In addition to anatomical diagnosis, MRI is useful in determining the degree of spinal stenosis and compression, the size and location of lesions, and the extent of vascular supply [23]. The disadvantages include a lengthy scan time and a variety of contraindications, such as the presence of pacemakers and metal implants [26, 27].

A multiparametric approach to the diagnosis of mCRPC involves the evaluation of anatomical T1-weighted images (T1WIs) (scar tissue identification for evidence of replacement fibrosis) and T2WIs (for edema detection) for a detailed examination of the anatomical zones of the prostate and surrounding soft tissues. Short tau inversion recovery sequences, which eliminate the influence of fluid in the resulting images, can be used to differentiate between fat and fluid inclusions in the lesions. Functional diffusion-weighted imaging (DWI) sequences with apparent diffusion coefficient maps may be employed to determine tumor location and aggressiveness. Dynamic contrast-enhanced MRI is utilized for differentiating between inflammatory and benign changes, as well as for ascertaining tumor location and grade [28].

In a prospective study by Perez-Lopez et al. (TOPARP-A) [29], a whole-body DWI MRI was performed in 21 patients with bone metastases at baseline and 12 weeks following treatment. Out of all the bone metastases, five lesions were selected and evaluated. The volume and diameter of the lesions declined 12 weeks after olaparib therapy; the outcomes were inversely proportional to the treatment response. The authors concluded that DWI can play a critical role in assessing the response of bone metastases to mCRPC treatment.

The published results of studies comparing bone scintigraphy and whole-body MRI varies, most likely because different MR scanners are used and there are no established protocols. A meta-analysis revealed that whole-body MRI exhibits a higher sensitivity and specificity (94% and 99%, respectively) than bone scintigraphy (80% and 95%, respectively), indicating that whole-body MRI can be used to verify or rule out bone metastases [30, 31].

Padhani et al. [32] developed and presented guidelines (MET-RADS-P) for whole-body MRI efficacy criteria to assess
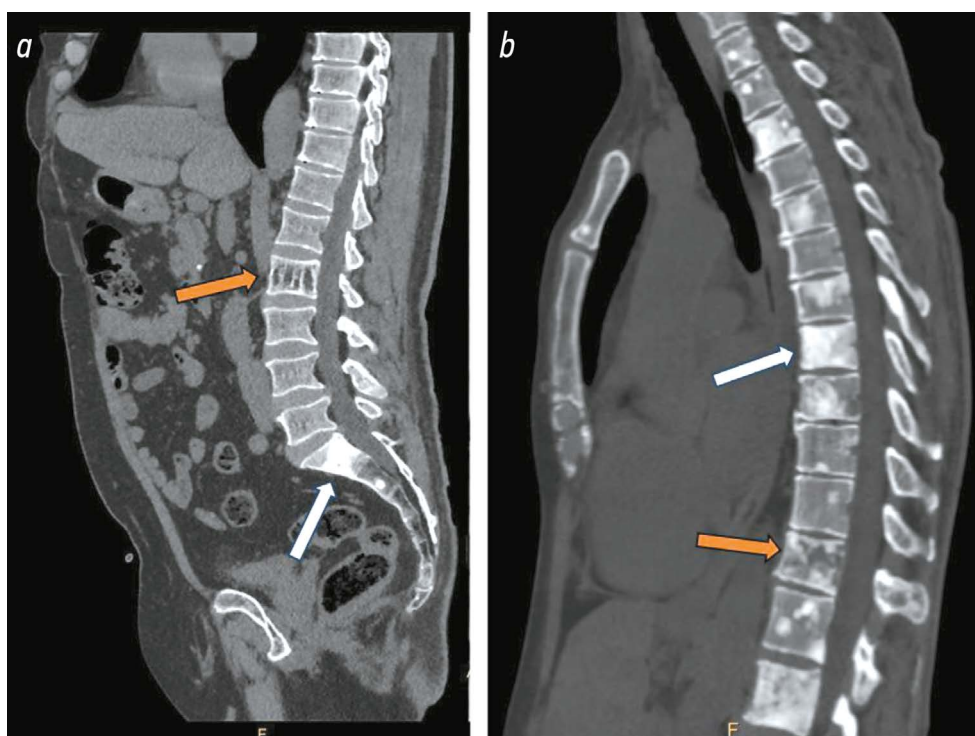

Fig. 1. *a*, Lumbar spine MSCT, sagittal plane: osteoblastic lesions observed in the S1 and S2 vertebral bodies (white arrow), hemangioma in the L2 vertebral body (orange arrow); *b*, thoracic spine MSCT, sagittal plane: osteoblastic lesions in thoracic vertebral bodies (white arrow), mixed lesion noted in the Th12 vertebral body (orange arrow).
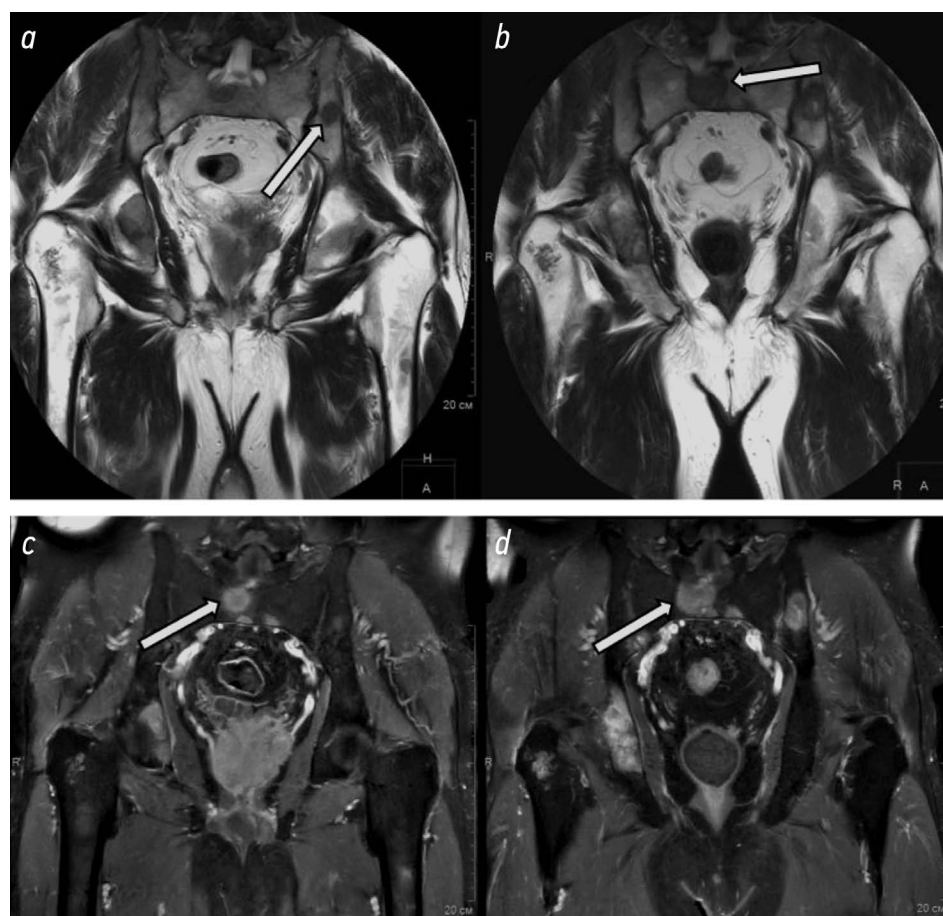
Fig. 2. *a, b*, Pelvic MRI, coronal plane, T2WI; *c, d*, pelvic MRI, coronal plane, T1WI; case follow-up *a, c* of February 2023 and *b, d* July 2023: osteoblastic lesions in pelvic bones, increase in lesion size during follow-up (white arrows).

lesions in patients with advanced PC. According to the authors, accurate assessment of the response to treatment will facilitate the future development of targeted therapy [27].

Due to radiopharmaceutical absorption, hybrid diagnosis techniques are more successful in determining the functional state of lesions than anatomical imaging and bone metastasis follow-up using MSCT and MRI [26].

Bone scintigraphy is a radionuclide imaging technique that utilizes diphosphonate complexes to examine bone lesions. The technique entails assessing the radiopharmaceutical uptake involved in bone metabolism at active bone formation sites, which are linked to benign and malignant abnormalities, as well as physiological processes [24]. In posttraumatic, neoplastic, and infectious alterations, radiopharmaceutical uptake is correlated with local blood flow and osteoblast/osteoclast activity [33].

When activity is identified in the scintigrams of patients with bone metastases, the 2 + 2 rule is used to account for the flare phenomenon detected during osteoblast activation and sclerotic transformation of lesions in the early treatment period [34]. The emergence of two new lesions at a follow-up imaging test six weeks or more after the initial diagnosis is considered progression. An increase in the size of the lesions detected on bone scintigraphy is not regarded as a sign of disease progression [35]. Since this phenomenon

is identified within the first three months following chemotherapy and hormone therapy, it may resemble disease progression [36].

Of significance are the scintigram quantitative assessment parameters, such as the bone scan index (BSI) and bone scan lesion area (BSLA).

BSI is the sum of individual bone areas multiplied by the percentage of each bone's involvement in metastasis. Processing BSI values manually or semiautomatically is time-consuming and subjective. Therefore, scintigram assessment techniques using aBSI automated computer analysis were developed [37, 38], which significantly increase the reproducibility of quantitative assessment to 10 s as opposed to 5–30 minutes with manual assessment [39]. When combined with the diagnostic evaluation of anatomical images, aBSI parameters can be utilized as prognostic biomarkers.

Dennis et al. [40, 41] assessed preliminary data and discovered that BSI changes during treatment were closely correlated with overall survival in patients receiving chemotherapy. The evaluation was carried out three to six months following treatment. The authors concluded that a twofold increase in BSI during treatment results in a 1.9-fold increased risk of death.

Bone scintigraphy enables the detection of early metabolic changes, frequently several weeks or months

before they are detected by radiography. Given that the sensitivity and specificity of this technique for detecting bone metastases in PC are 74.5%–83% [42–44] and 62%–82%, respectively, the use of complementary anatomical imaging approaches, such as radiography, MSCT, MRI, or hybrid methods (SPECT/CT and PET/CT) is required [34].

After comparing bone scintigraphy and MRI findings [44], the authors concluded that bone scintigraphy is a rapid and cost-effective technique for the early detection of bone metastases. However, there are several limitations, including the accumulation of radiopharmaceutical agents in inflammatory lesions and regions of intensive bone formation. Lytic bone lesion imaging is challenging due to the lack of bone remodeling and the presence of a soft tissue component where radiopharmaceutical uptake is not feasible [12].

This method can be supplemented by SPECT/CT findings. An additional benefit is the use of BSI as a prognostic marker. The limitations of bone scintigraphy include reduced potential for imaging of lytic lesions (only lesions with radiopharmaceutical uptake can be assessed), lengthy scan time, lower sensitivity compared to CT and MRI, and the flare phenomenon in response to treatment [27, 33].

An additional SPECT/CT can help avoid these limitations.

Single-photon emission computed tomography with computed tomography is a hybrid diagnostic radiology technique that generates 3D images using a gamma chamber and a multislice CT scanner. After computer processing, maps with functional information on metabolic processes in various organs and tissues were matched with anatomical CT images [45]. This approach reduces the disadvantages of each method and improves the diagnostic value.

SPECT/CT results are used to semi-quantitatively assess lesions using the standardized uptake value body weight (SUVbw), a parameter based on body weight. The following formula is used for differentiating between degenerative changes and metastatic lesions:

$$SUVbw = \frac{A \times B}{C},$$

where A = local activity concentration, B = body weight, and C = administered activity. SUV_{bw} values in bone metastases are significantly higher than in degenerative changes; the sensitivity and specificity in differential diagnosis are 73.8% and 85.4%, respectively [46, 47].

The diagnostic utility of scintigraphy with ^{177}Lu-PSMA was assessed in patients with PC with elevated PSA levels and negative findings on conventional imaging examinations (MSCT, MRI) [48]. The analysis included 26 patients with PSA failure after curative therapy; ^{177}Lu-PSMA was administered, and SPECT/CT and whole-body planar scintigraphy were then performed. According to SPECT/CT findings, the total metastasis detection rate was 38.5%, with secondary lesions being most frequently detected in the lungs, abdominal lymph nodes, and mediastinum. When PET/CT with ^{68}Ga-PSMA

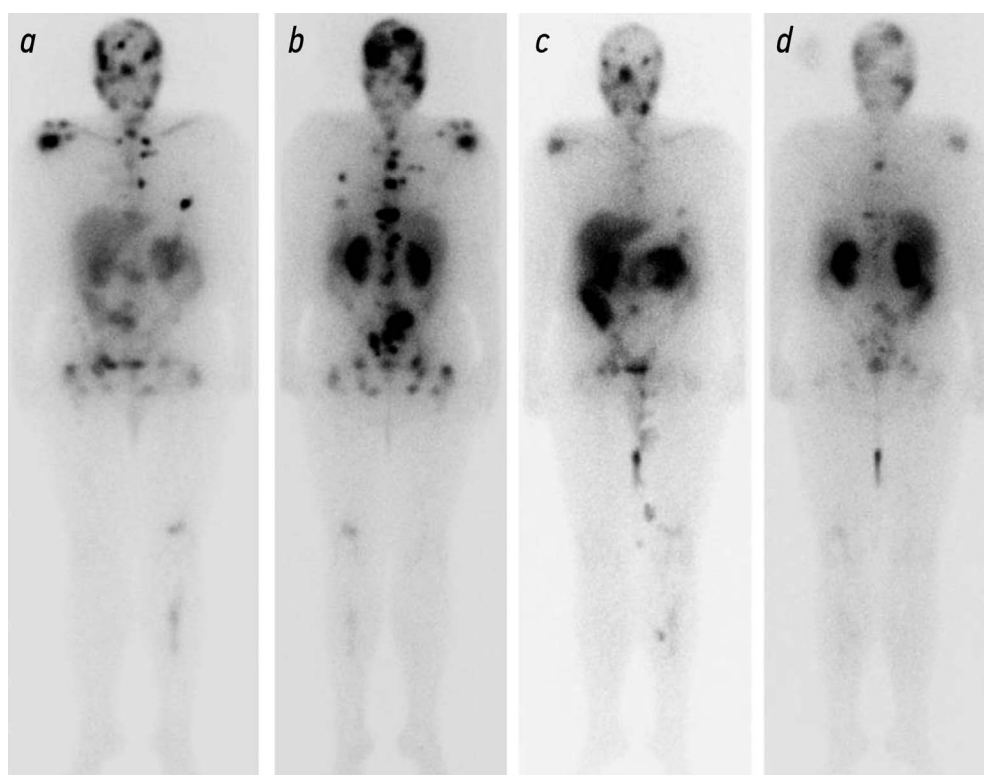**Fig. 3.** *a*, Whole-body scintigraphy with ^{177}Lu-PSMA, anterior view; *b*, posterior view of December 2021: diffuse-plus-focal radiopharmaceutical hyper uptake of differing intensity, multiple PSMA-positive bone lesions; *c*: whole-body scintigraphy with ^{177}Lu-PSMA, anterior view; *d*, posterior view of April 2022: reduced radiopharmaceutical uptake in the lesions, absence of new areas of radiopharmaceutical hyper uptake.

861

is unavailable, SPECT/CT with ^{177}Lu-PSMA can detect secondary lesions in more than one-third of patients, making it a valuable diagnostic tool in mCRPC patients (Fig. 3).

Several authors have conducted comparative studies of SPECT/CT and MRI. When assessing the potential of SPECT/CT and whole-body MRI in patients with bone metastases, the sensitivity, specificity, and precision of both methods were found to be 94.4%, 75%, and 92.3%, respectively, indicating that these modalities are complementary (Table 1) [23, 49, 50].

Positron emission tomography with CT is a hybrid radionuclide diagnostic method that makes use of a three-dimensional distribution of radio-emitting indicators labeled with positron (β+) emitters. This enables the noninvasive assessment of the body's biochemical and functional processes [45]. PET/CT uses radiopharmaceuticals such as ^{18}F-FDG (fluorodeoxyglucose) and amino acid-based agents to detect diverse molecular and cellular mechanisms of tumor metabolism [45].

Semiquantitative measurements and the standardized uptake value (SUV) allow for the differentiation of malignant and benign lesions [51].

The use of ^{18}F-FDG PET/CT in the initial assessment and PC staging is restricted. This approach is not recommended for detecting bone metastases in patients with PC. Low bone tissue glucose consumption and inadequate ^{18}F-FDG uptake make it difficult to identify osteoblastic lesions. Moreover, this approach does not distinguish between primary and secondary lesions, particularly for small lesions [45].

[18]F-NaF (sodium fluoride) is a positron emitter that binds to osteoblasts during osteogenesis, producing positive findings in both benign and malignant lesions [51].

In PC, proliferating tumor cell membranes contain ^{18}F-CH (fluorocholine) [52]. ^{18}F-CH exhibits a longer half-life than ^{11}C-choline (up to 109.8 minutes vs. 20.4 minutes), making it appropriate for PET centers without a cyclotron and increasing its availability. Compared to ^{18}F-FDG, this agent was reported to be more successful in detecting metastases in PC because of greater radiopharmaceutical uptake in bone lesions [53].

When analyzing the PET/CT findings in patients with bone metastases, ^{18}F-CH and ^{18}F-NaF demonstrated comparable sensitivity of 91%. However, the specificity of PET/CT with ^{18}F-CH and [8]F-NaF was 89% and 83%, respectively [54].

PET/CT identifies metabolic changes before the detection of morphological changes by MSCT. ^{18}F-CH PET/CT is comparable to whole-body MRI and superior to bone scintigraphy and MSCT. However, it is linked to disadvantages such as the flare phenomenon, inadequate liver and urinary tract imaging, and inconsistent detection of small lesions at low serum PSA levels [27].

The effectiveness of antineoplastic treatment can be predicted using quantitative data on radiopharmaceutical uptake provided by PSMA PET.

The FDA approved ^{68}Ga-PSMA and ^{18}F-PSMA in 2020 and 2021, respectively, as the first and second PSMA PET indicators for patients with PSA failure [55].

According to the working group guidelines (PCWG3, 2016), the evaluation of baseline data and follow-up in patients with PC must be based on diagnostic radiological findings [43]. The RECIST 1.1 criteria for anatomical imaging must be used to solid tumors identified by MSCT and MRI [56], whereas the response criteria (PERCIST) must be used to evaluate PET/CT results [57].

Anatomical imaging methods along with serum PSA measurement are used to evaluate therapy response for solid tumors in PC patients based on the RECIST criteria [58].

According to the PERCIST criteria, the response to treatment is assessed qualitatively (e.g., based on the presence/absence of lesion activity) and quantitatively, where the initial and follow-up imaging parameters must be identical. The standardized uptake value normalized by lean body mass (SUL) is used for measurements. The results are presented as a percentage of the peak SUL for the lesion exhibiting the highest activity [59].

Table 1. Comparison of the diagnostic criteria for bone lesion detection employing diagnostic radiological techniques

Diagnostic method	Study (publication)	Patients/studies, n	Sensitivity, %	Specificity, %
Radiography	Kitagawa et al., 2018 [20]	129	45.8	80.9
MSCT	Liu et al., 2017 [22]	183 (3)	79.2	92.3
MRI	Liu et al., 2017 [22]	381 (7)	94.1	94.2
	Sun et al., 2020 [31]	1939 (15)	94	99
SPECT/CT	Sun et al., 2020 [31]	1939 (15)	80	95
	Sheikhbahaei et al., 2019 [42]	507 (14)	79	62
	Shen et al., 2014 [43]	901 (12)	83	82
ОФЭКТ/КТ	Liu et al., 2017 [22]	343 (4)	90.3	86
	Mohd Rohani et al., 2020 [46]	34	73.8	85.4
ПЭТ/КТ	Liu et al., 2017 [22]	403 (5)	89.8	63.3

Maffey-Steffan et al. [58] compared the findings of ^{68}Ga-PSMA PET/CT (interpreted using modified PERCIST criteria, with a semiquantitative SUVmax analysis) and whole-body ^{177}Lu-PSMA scintigraphy performed 24 hours after treatment, using the tumor-to-background ratio. Progression was defined as the emergence of new lesions and/or increased radiopharmaceutical uptake, partial remission as the elimination of one or more lesions and/or decreased radiopharmaceutical uptake, and stable disease as no changes in the number of lesions and radiopharmaceutical uptake. A mixed response was characterized by the elimination of some lesions and/or their decreased radiopharmaceutical uptake, with the emergence of new lesions. The results matched the visual perception of various imaging methods. The interpretation of 24-hour SPECT/CT findings is sufficiently accurate, and the technique is simple and cost-effective. Follow-up PET/CT is time-consuming, making examinations in patients with pain syndrome challenging. For monitoring patients, the PSA level must be measured and 24-hour SPECT/CT findings must be analyzed, whereas PET/CT should be utilized for patient selection and treatment efficacy assessment [59].

The LifeX software was used for assessing ^{68}Ga-PSMA PET/CT images, including the analysis of PSMA levels and their expression in the tumor, with a prespecified SUV threshold of 3.0 (based on software settings) and 45% (based on published findings of previous studies). The resulting data were manually updated. A decline in tumor volume and PSMA expression after treatment was reported in 63% and 74% of patients, respectively; moreover, there were significant differences in SUV_{max} values before and after treatment. The authors concluded that a quantitative analysis of the molecular volume and PSMA expression in the tumor can be employed to assess the response to ^{177}Lu-PSMA therapy [57, 60].

Another study used ^{18}F-NaF PET/CT and ^{99m}Tc SPECT/CT to assess SUV_{max}, SUV_{peak}, SUV_{mean}, metabolic bone volume, and total bone uptake. The formula $SUV_{mean} \times MBV$ was applied for each lesion with radiopharmaceutical uptake. The preliminary conclusion was that SUV parameters with SPECT/CT were substantially lower than those with PET/CT. However, compared to PET/CT, the radiopharmaceutical uptake with SPECT/CT was significantly higher. The values of metrics calculated for metastatic lesions were significantly higher than those for benign lesions [61].

Vlachostergios et al. [62] compared ^{68}Ga-PSMA PET/CT with a quantitative assessment and SPECT/CT with a semiquantitative assessment in ^{177}Lu-PSMA therapy. Three lesions with the highest radiopharmaceutical uptake in comparison to the liver were evaluated using SPECT/CT results. A five-point scale was used, with 0 denoting no changes, 1 denoting low tumor activity, 2 denoting strong tumor activity but below that of the liver, 3 denoting tumor activity equal to that of the liver, and 4 denoting tumor activity

greater than that of the liver. The PET/CT findings were then used to evaluate the average SUV_{max} for the five lesions with the greatest radiopharmaceutical uptake compared to the SUV_{mean} of the liver. The following scale was used: 0 = no changes, 1 = SUV_{max} < SUV_{mean} of the liver, 2 = SUV_{max} = 1–2.5 × SUV_{mean} of the liver, 3 = SUV_{max} = 2.5–5 × SUV_{mean} of the liver, and 4 = SUV_{max} >5 × SUV_{mean} of the liver. The authors found that semiquantitative PSMA measurements using SPECT/CT and PET/CT can serve as prognostic indicators of overall survival in patients with mCRPC because this parameter represents the metastatic load.

A study [63] assessed the efficacy of radioligand therapy with ^{177}Lu-PSMA in patients with mCRPC. A technique developed in Germany has shown a significant increase in the overall survival and quality of life. In a multicenter study, 145 patients received one to four rounds of ^{177}Lu-PSMA treatment, with an overall biochemical response of 45%. For patients with PSA failure, PSMA-based hybrid imaging greatly increases the diagnostic efficacy. PSMA PET/CT can be valuable in radiotherapy planning because it can identify affected lymph nodes and rule out distant metastases, resulting in treatment adjustments in up to 30% of patients. Radionuclide therapy with labeled PSMA analogs enhances the diagnosis and treatment of mCRPC, which needs to be validated in prospective studies.

A multicenter, retrospective study was conducted by a group of researchers [64] to establish a RECIP 1.0-based approach (PSA + RECIP) to standardize the criteria of response to ^{177}Lu-PSMA therapy based on PET/CT findings for treatment efficacy assessment in mCRPC. This study aimed to formulate an integrated response classification combining laboratory PSA levels and response criteria based on PET/CT findings. This approach incorporated the analysis of the PSMA-positive tumor volume (PSMA VOL) and the detection of new metastases, employing a standardized system to determine the response criteria.

This method yielded four response categories: RECIP-CR for complete response, RECIP-PR for partial response, RECIP-PD for disease progression, and RECIP-SD for stable disease.

The results achieved using the RECIP 1.0 approach (PSA + RECIP) included the following:
- Reduction in PSA levels by ≥50% or RECIP-CR/RECIP-PR;
- Rise in PSA levels by ≥25% or RECIP-PD.

The study assessed the predictive value of RECIP 1.0 in terms of increases in overall survival. However, these findings must be corroborated in prospective studies [64].

Like all diagnostic radiology techniques, PET/CT has limitations, including motion artifacts, which result in incorrect image matching, and truncation artifacts due to differences in the field of view of CT and PET scanners (50 cm vs. 70 cm), especially in patients with excess body weight. Another disadvantage is that when PET shows radiopharmaceutical uptake, no changes are observed on CT. The results of these examinations must be interpreted with caution [45].

Table 2. Comparison of the diagnostic radiological techniques

Diagnostic radiological technique	Bone tissue morphology	Bone tissue metabolism	Bone marrow lesions	Diffusion	Radiopharmaceutical metabolism
Radiography	■				
MSCT	■				
MRI			■	■	
Bone scintigraphy		■			
SPECT/CT		■			
PET/CT	■	■			■

Note. Highlighted: the parameter is present; not highlighted: the parameter is absent.

Table 2 presents a comparison of diagnostic radiological procedures based on the parameters that indicate the presence of bone metastases in PC (adapted from Isaac et al. [65]).

Thus, available evidence demonstrates the heterogeneity of data regarding the diagnostic utility and potential of diagnostic radiological techniques, which are essential for the noninvasive assessment of mCRPC.

CONCLUSION

There are multiple diagnostic radiological techniques and associated approaches for the quantitative assessment of mCRPC. These techniques are widely employed in mCRPC diagnosis and staging, as well as in treatment strategy selection and efficacy assessment. The advantages and disadvantages of imaging examinations in this patient population are considered complementary because of their differing sensitivity and specificity; thus, an integrated use of these techniques is recommended.

A review of published evidence suggests that radionuclide diagnosis and therapy with ^{177}Lu-PSMA and [225]Ac-PSMA can be a promising strategy. These radiopharmaceuticals offer unique opportunities for targeted therapy and quantitative assessment of ^{177}Lu-PSMA therapy efficacy through diagnostic radiological techniques.

Further development of quantitative efficacy assessment tools for mCRPC therapy and the identification of prognostic biomarkers using radionuclide imaging techniques will help select the optimal treatment strategy, thereby improving overall survival.

ADDITIONAL INFORMATION

REFERENCES

1. Kaprin AD, Alekseev BYa, Matveev VB, et al. Rak predstatel'noi zhelezy. Klinicheskie rekomendatsii // Obshcherossiiskii natsional'nyi soyuz «Assotsiatsiya onkologov Rossii». 2021. (In Russ.) EDN: RLCXWE

2. Gevorkyan AR, Molodtsov MS, Aleksandrov EV. Prostate cancer diagnosis as part of high-tech advanced outpatient medical care. *Urology Herald.* 2023;11(1):26–33. doi: 10.21886/2308-6424-2023-11-1-26-33

3. Ling SW, de Blois E, Hooijman E, et al. Advances in ^{177}Lu-PSMA and [225]Ac-PSMA Radionuclide Therapy for Metastatic Castration-Resistant Prostate Cancer. *Pharmaceutics.* 2022;14(10):2166. doi: 10.3390/pharmaceutics14102166

4. Sekhoacha M, Riet K, Motloung P, et al. Prostate Cancer Review: Genetics, Diagnosis, Treatment Options, and Alternative Approaches. *Molecules.* 2022;27(17):5730. doi: 10.3390/molecules27175730

5. Solodky VA, Pavlov AYu, Fomin DK, et al. Determination of the role of lutetium-PSMA in prostate cancer. *Vestnik RNTsRR.* 2022;22(2):27–36. EDN: UNNDSN

6. Medvedeva AA, Chernov VI, Usynin EA, et al. Use of ^{177}Lu-PSMA for radionuclide therapy in patients with castrate-resistant prostate cancer. *Siberian Journal of Oncology.* 2021;20(3):115–123. EDN: DIJSIE doi: 10.21294/1814-4861-2021-20-3-115-123

7. Pezaro CJ, Omlin A, Lorente D, et al. Visceral Disease in Castration-resistant Prostate Cancer. *Eur Urol.* 2014;65(2):270–273. doi: 10.1016/j.eururo.2013.10.055

8. Clezardin P, Coleman R, Puppo M, et al. Bone metastasis: mechanisms, therapies, and biomarkers. *Physiol Rev.* 2021;101(3):797–855. doi: 10.1152/physrev.00012.2019

9. Zhang X. Interactions between cancer cells and bone microenvironment promote bone metastasis in prostate cancer. *Cancer Commun.* 2019;39(1):76. doi: 10.1186/s40880-019-0425-1

10. Hofman MS, Lawrentschuk N, Francis RJ, et al. Prostate-specific membrane antigen PET-CT in patients with high-risk prostate cancer before curative-intent surgery or radiotherapy (proPSMA): a prospective, randomised, multicentre study. *Lancet.* 2020;395(10231):1208–1216. doi: 10.1016/S0140-6736(20)30314-7

11. Awenat S, Piccardo A, Carvoeiras P, et al. Diagnostic Role of 18F-PSMA-1007 PET/CT in Prostate Cancer Staging: A Systematic Review. *Diagnostics.* 2021;11(3):552. doi: 10.3390/diagnostics11030552

12. Alberts I, Sachpekidis C, Fech V, et al. PSMA-negative prostate cancer and the continued value of choline-PET/CT. *Nuklearmedizin.* 2020;59(1):33–34. doi: 10.1055/a-1044-1855

13. Sartor O, Baghian A. Prostate specific membrane antigen binding radiopharmaceuticals: Current data and new concepts. *Front Med (Lausanne).* 2022;9(1060922). doi: 10.3389/fmed.2022.1060922

14. Plichta KA, Graves SA, Buatti JM. Prostate-Specific Membrane Antigen (PSMA) Theranostics for Treatment of Oligometastatic Prostate Cancer. *Int J Mol Sci.* 2021;22(22):12095. doi: 10.3390/ijms222212095

15. Sun M, Niaz MJ, Niaz MO, et al. Prostate-Specific Membrane Antigen (PSMA)-Targeted Radionuclide Therapies for Prostate Cancer. *Curr Oncol Rep.* 2021; 23(5):59. doi: 10.1007/s11912-021-01042-w

16. Alberts I, Sachpekidis C, Dijkstra L, et al. The role of additional late PSMA-ligand PET/CT in the differentiation between lymph node metastases and ganglia. *Eur J Nucl Med Mol Imaging.* 2020;47(3):642–651. doi: 10.1007/s00259-019-04552-9

17. Khreish F, Ebert N, Ries M, et al. ^{225}Ac-PSMA-617/^{177}Lu-PSMA-617 tandem therapy of metastatic castration-resistant prostate cancer: pilot experience. *Eur J Nucl Med Mol Imaging.* 2020;47(3):721–728. doi: 10.1007/s00259-019-04612-0

18. Kendrick J, Francis R, Hassan GM, et al. Radiomics for Identification and Prediction in Metastatic Prostate Cancer: A Review of Studies. *Front Oncol.* 2021;11:771–787. doi: 10.3389/fonc.2021.771787

19. Macedo F, Ladeira K, Pinho F, et al. Bone metastases: an overview. *Oncol Rev.* 2017;11(1):321. doi: 10.4081/oncol.2017.321

20. Kitagawa Y, Yamaoka T, Yokouchi M, et al. Diagnostic Value of Plain Radiography for Symptomatic Bone Metastasis at the First Visit. *J Nippon Med Sch.* 2018;85(6):315–321. doi: 10.1272/jnms.JNMS.2018_85-51

21. Cornford P, van den Bergh RCN, Briers E, et al. EAU-EANM-ESTRO-ESUR-SIOG Guidelines on Prostate Cancer. Part II–2020 Update: Treatment of Relapsing and Metastatic Prostate Cancer. *Eur Urol.* 2021;79(2):263–282. doi: 10.1016/j.eururo.2020.09.046

22. Liu T, Wang S, Liu H, et al. Detection of vertebral metastases: a meta-analysis comparing MRI, CT, PET, BS and BS with SPECT. *J Cancer Res Clin Oncol.* 2017;143(3):457–465. doi: 10.1007/s00432-016-2288-z

23. Sergeev NI, Kotlyarov PM, Teplyakov VV, et al. Features of the application of diagnostic imaging methods in evaluating the results of treatment of bone metastases. *Russian Electronic Journal of Radiology.* 2021;11(4):84–93. EDN: YQNNKI doi: 10.21294/1814-4861-2018-17-1-5-10

24. Chen Z, Chen X, Wang R. Application of SPECT and PET / CT with computer-aided diagnosis in bone metastasis of prostate cancer: a review. *Cancer Imaging.* 2022;22(1):18. doi: 10.1186/s40644-022-00456-4

25. Steinhauer V, Sergeev NI. Radiomics in Breast Cancer: In-Depth Machine Analysis of MR Images of Metastatic Spine Lesion. *Sovremennye tehnologii v medicine.* 2022;14(2):16. doi: 10.17691/stm2022.14.2.02

26. Vilanova JC, Garcia-Figueiras R, Luna A, et al. Update on Whole-body MRI in Musculoskeletal Applications. *Semin Musculoskelet Radiol.* 2019;23(3):312–323. doi: 10.1055/s-0039-1685540

27. Padhani AR, Lecouvet FE, Tunariu N, et al. Rationale for Modernising Imaging in Advanced Prostate Cancer. *Eur Urol Focus.* 2017;3(2–3):223–239. doi: 10.1016/j.euf.2016.06.018

28. Karman AV, Abakumova EA, Shimanets SV, et al. Multiparametric MRI prostate cancer detection and staging. *Oncological journal.* 2019;1(49):136–147. EDN: VTNFYB

29. Perez-Lopez R, Mateo J, Mossop H, et al. Diffusion-weighted Imaging as a Treatment Response Biomarker for Evaluating Bone Metastases in Prostate Cancer: A Pilot Study. *Radiology.* 2017;283(1):168–177. doi: 10.1148/radiol.2016160646

30. Nakanishi K, Tanaka J, Nakaya Y, et al. Whole-body MRI: detecting bone metastases from prostate cancer. *Jpn J Radiol.* 2022;40(3):229–244. doi: 10.1007/s11604-021-01205-6

31. Sun G, Zhang Y.X., Liu F., et al. Whole-body magnetic resonance imaging is superior to skeletal scintigraphy for the detection of bone metastatic tumors: a meta-analysis. *Eur Rev Med Pharmacol Sci.* 2020;24(13):7240–7252. doi: 10.26355/eurrev_202007_21879

32. Padhani AR, Lecouvet FE, Tunariu N, et al. METastasis Reporting and Data System for Prostate Cancer: Practical Guidelines for Acquisition, Interpretation, and Reporting of Whole-body Magnetic Resonance Imaging-based Evaluations of Multiorgan Involvement in Advanced Prostate Cancer. *Eur Urol.* 2017;71(1):81–92. doi: 10.1016/j.eururo.2016.05.033

33. Van den Wyngaert T, Strobel K, Kampen WU, et al. The EANM practice guidelines for bone scintigraphy. *Eur J Nucl Med Mol Imaging.* 2016;43(9):1723–1738. doi: 10.1007/s00259-016-3415-4

34. Scher HI, Morris MJ, Stadler WM, et al. Trial Design and Objectives for Castration-Resistant Prostate Cancer: Updated Recommendations From the Prostate Cancer Clinical Trials Working Group 3. *J Clin Oncol.* 2016;34(12):1402–1418. doi: 10.1200/JCO.2015.64.2702

35. Anand A, Heller G, Fox J, et al. Automated Bone Scan Index to Optimize Prostate Cancer Working Group Radiographic Progression Criteria for Men With Metastatic Castration-Resistant Prostate Cancer. *Clin Genitourin Cancer.* 2022;20(3):270–277. doi: 10.1016/j.clgc.2022.02.002

36. Chao HS, Chang CP, Chiu CH, et al. Bone Scan Flare Phenomenon in Non-Small-Cell Lung Cancer Patients Treated With Gefitinib. *Clin Nucl Med.* 2009;34(6):346–349. doi: 10.1097/RLU.0b013e3181a344df

37. van der Zande K, Oyen WJG, Zwart W, et al. Radium-223 Treatment of Patients with Metastatic Castration Resistant Prostate Cancer: Biomarkers for Stratification and Response Evaluation. *Cancers (Basel).* 2021;13(17):4346. doi: 10.3390/cancers13174346

38. Nakajima K, Edenbrandt L, Mizokami A. Bone scan index: A new biomarker of bone metastasis in patients with prostate cancer. *Int J Urol.* 2017;24(9):668–673. doi: 10.1111/iju.13386

39. Ruchalski K, Dewan R, Sai V, et al. Imaging response assessment for oncology: An algorithmic approach. *Eur J Radiol Open.* 2022;9:100426. doi: 10.1016/j.ejro.2022.100426

40. Eremenko AV, Kosyh NE, Razuvaev VA, et al. Investigation of computer automated analysis capabilities for the effective diagnosis of disseminated prostate cancer. *Diagnostic radiology and radiotherapy.* 2019;1:74–85. EDN: NQOKHZ doi: 10.22328/2079-5343-2019-10-1-74-85

41. Dennis ER, Jia X, Mezheritskiy IS, et al. Bone Scan Index: A Quantitative Treatment Response Biomarker for Castration-Resistant Metastatic Prostate Cancer. *J Clin Oncol.* 2012;30(5):519–524. doi: 10.1200/JCO.2011.36.5791

42. Sheikhbahaei S., Jones K.M., Werner R.A., et al. ^{18}F-NaF-PET/CT for the detection of bone metastasis in prostate cancer: a meta-analysis of diagnostic accuracy studies. *Ann Nucl Med.* 2019;33(5): 351–361. doi: 10.1007/s12149-019-01343-y

43. Shen G, Deng H, Hu S, et al. Comparison of choline-PET/CT, MRI, SPECT, and bone scintigraphy in the diagnosis of bone metastases in patients with prostate cancer: a meta-analysis. *Skeletal Radiol.* 2014;43(11):1503–1513. doi: 10.1007/s00256-014-1903-9

44. Sergeev NI, Fomin DK, Kotlyarov PM, et al. Comparative Study of the Possibilities of Bone Scintigraphy and Magnetic Resonance Imaging of the Whole Body in the Diagnosis of Bone Metastases. *Medical Visualization.* 2014;4:107–113. EDN: SNIDQB

45. Blackwell W. Radiology-Nuclear Medicine Diagnostic Imaging: A Correlative Approach. First. Edited by Gholamrezanezhad A, Assadi M, Jadvar H USA. 2023.

46. Mohd Rohani MF, Mat Nawi N, Shamim SE, et al. Maximum standardized uptake value from quantitative bone single-photon emission computed tomography/computed tomography in differentiating metastatic and degenerative joint disease of the spine in prostate cancer patients. *Ann Nucl Med.* 2020;34(1):39–48. doi: 10.1007/s12149-019-01410-4

47. Okamoto S, Thieme A, Allmann J, et al. Radiation Dosimetry for 177Lu-PSMA I&T in Metastatic Castration-Resistant Prostate Cancer: Absorbed Dose in Normal Organs and Tumor Lesions. *J Nucl Med.* 2017;58(3):445–450. doi: 10.2967/jnumed.116.178483

48. Ghodsirad MA, Pirayesh E, Akbarian R, et al. Diagnostic Utility of Lutetium-177 (Lu 177) Prostate-Specific Membrane Antigen (PSMA) Scintigraphy In Prostate Cancer Patients With PSA Rise And Negative Conventional Imaging. *Urol J.* 2020; 23;17(4):374–378. doi: 10.22037/uj.v0i0.5451

49. Venkatachalapathy VSS, Rajeshkannan R, Sarma M, et al. Comparison of whole-body bone scintigraphy with axial skeleton magnetic resonance imaging in the skeletal evaluation of carcinoma prostate. *Indian J Urol.* 2021;37(1):72–78. doi: 10.4103/iju.IJU_238_20

50. Sergeev NI, Fomin DK, Kotlyarov PM, Solodkiy VA. Comparative study of the possibilities of SPECT/CT and whole body MRI in the diagnosis of bone metastases. *Bulletin of the Russian Scientific Center of Roentgenoradiology.* 2015;15(3):8. EDN: UXMAVX

51. Li R, Ravizzini GC, Gorin MA, et al. The use of PET/CT in prostate cancer. *Prostate Cancer Prostatic Dis.* 2018;21(1):4–21. doi: 10.1038/s41391-017-0007-8

52. Azad GK, Cook GJ. Multi-technique imaging of bone metastases: spotlight on PET-CT. *Clin Radiol.* 2016;71(7):620–631. doi: 10.1016/j.crad.2016.01.026

53. Kannivelu A, Loke K, Kok T, et al. The Role of PET/CT in the Evaluation of Skeletal Metastases. *Semin Musculoskelet Radiol.* 2014;18(2):149–165. doi: 10.1055/s-0034-1371017

54. Jadvar H. Molecular Imaging of Prostate Cancer: PET Radiotracers. *AJR Am J Roentgenol.* 2012;199(2):278–291. doi: 10.2214/AJR.12.8816

55. Alam MR, Singh SB, Thapaliya S, et al. A Review of [177]Lutetium-PSMA and [225]Actinium-PSMA as Emerging Theranostic Agents in Prostate Cancer. *Cureus.* 2022; 14(9):29369. doi: 10.7759/cureus.29369

56. Eisenhauer EA, Therasse P, Bogaerts J, et al. New response evaluation criteria in solid tumours: Revised RECIST guideline (version 1.1). *Eur J Cancer.* 2009;45(2):228–247. doi: 10.1016/j.ejca.2008.10.026

57. Acar E, Özdoğan Ö, Aksu A, et al. The use of molecular volumetric parameters for the evaluation of Lu-177 PSMA I&T therapy response and survival. *Ann Nucl Med.* 2019;33(9):681–688. doi: 10.1007/s12149-019-01376-3

58. Maffey-Steffan J, Scarpa L, Svirydenka A, et al. The ^{68}Ga/^{177}Lu-theragnostic concept in PSMA-targeting of metastatic castration-resistant prostate cancer: impact of post-therapeutic whole-body scintigraphy in the follow-up. *Eur J Nucl Med Mol Imaging.* 2020;47(3):695–712. doi: 10.1007/s00259-019-04583-2

59. O J, Lodge M, Wahl R. Practical PERCIST: A Simplified Guide to PET Response Criteria in Solid Tumors 1.0. *Radiology.* 2016;280(2):576–584. doi: 10.1148/radiol.2016142043

60. Schmuck S, von Klot CA, Henkenberens C, et al. Initial Experience with Volumetric 68 Ga-PSMA I&T PET/CT for Assessment of Whole-Body Tumor Burden as a Quantitative Imaging Biomarker in Patients with Prostate Cancer. *J Nucl Med.* 2017;58(12):1962–1968. doi: 10.2967/jnumed.117.193581

61. Tanaka K, Norikane T, Mitamura K, et al. Quantitative [99mTc]Tc-MDP SPECT/CT correlated with [18F]NaF PET/CT for bone metastases in patients with prostate cancer. *EJNMMI Phys.* 2022;9(1):83. doi: 10.1186/s40658-022-00513-8

62. Vlachostergios PJ, Niaz MJ, Sun M, et al. Prostate-Specific Membrane Antigen Uptake and Survival in Metastatic Castration-Resistant Prostate Cancer. *Front Oncol.* 2021;11:630589. doi: 10.3389/fonc.2021.630589

63. Beyersdorff D, Rahbar K, Essler M, et al. Interdisziplinärer Expertenkonsensus zu Innovationen der bildgebenden Diagnostik und radionuklidbasierten Therapien des fortgeschrittenen Prostatakarzinoms. *Urologe A.* 2021;60:1579–1585. doi: 10.1007/s00120-021-01598-2

64. Gafit A, Rauscher I, Weber M, et al. Novel Framework for Treatment Response Evaluation Using PSMA PET/CT in Patients with Metastatic Castration-Resistant Prostate Cancer (RECIP 1.0): An International Multicenter Study. *J Nucl Med.* 2022;63(11):1651–1658. doi: 10.2967/jnumed.121.263072

65. Isaac A, Dalili D, Dalili D, et al. State-of-the-art imaging for diagnosis of metastatic bone disease. *Radiologe.* 2020;60(1):1–16. doi: 10.1007/s00117-020-00666-6

СПИСОК ЛИТЕРАТУРЫ

1. Каприн А.Д., Алексеев Б.Я., Матвеев В.Б., и др. Рак предстательной железы. Клинические рекомендации // Общероссийский национальный союз «Ассоциация онкологов России». 2021. https://oncology-association.ru/wp-content/uploads/2021/02/rpzh.pdf. Дата обращения: 24.03.2024. EDN: RLCXWE

2. Gevorkyan A.R., Molodtsov M.S., Aleksandrov E.V. Prostate cancer diagnosis as part of high-tech advanced outpatient medical care // Urology Herald. 2023. Vol. 11, N 1. P. 26–33. doi: 10.21886/2308-6424-2023-11-1-26-33

3. Ling S.W., de Blois E., Hooijman E., et al. Advances in ^{177}Lu-PSMA and [225]Ac-PSMA Radionuclide Therapy for Metastatic Castration-Resistant Prostate Cancer // Pharmaceutics. 2022. Vol. 14, N 10. P. 2166. doi: 10.3390/pharmaceutics14102166

4. Sekhoacha M., Riet K., Motloung P., et al. Prostate Cancer Review: Genetics, Diagnosis, Treatment Options, and Alternative Approaches // Molecules. 2022. Vol. 27, N 17. P. 5730. doi: 10.3390/molecules27175730

5. Солодкий В.А., Павлов А.Ю., Фомин Д.К., и др. Определение роли Лютеция-ПСМА и других препаратов, нацеленных на ПСМА, при раке предстательной железы // Вестник РНЦРР. 2022. Т. 22, № 2. С. 27–36. EDN: UNNDSN

6. Медведева А.А., Чернов В.И., Усынин Е.А., и др. Использование ^{177}Lu-ПСМА для радионуклидной терапии у пациентов с кастрационно-резистентным раком предстательной железы // Сибирский онкологический журнал. 2021. Т. 20, № 3. С. 115–123. EDN: DIJSIE doi: 10.21294/1814-4861-2021-20-3-115-123

7. Pezaro C., Omlin A., Lorente D., et al. Visceral Disease in Castration-resistant Prostate Cancer // Eur Urol. 2014. Vol. 65, N 2. P. 270–273. doi: 10.1016/j.eururo.2013.10.055

8. Clezardin P., Coleman R., Puppo M., et al. Bone metastasis: mechanisms, therapies, and biomarkers // Physiol Rev. 2021. Vol. 101, N 3. P. 797–855. doi: 10.1152/physrev.00012.2019

9. Zhang X. Interactions between cancer cells and bone microenvironment promote bone metastasis in prostate cancer // Cancer Commun. 2019. Vol. 39, N 1. P. 76. doi: 10.1186/s40880-019-0425-1

10. Hofman M., Lawrentschuk N., Francis R., et al. Prostate-specific membrane antigen PET-CT in patients with high-risk prostate cancer before curative-intent surgery or radiotherapy (proPSMA): a prospective, randomised, multicentre study // Lancet. 2020. Vol. 395, N 10231. P. 1208–1216. doi: 10.1016/S0140-6736(20)30314-7

11. Awenat S., Piccardo A., Carvoeiras P., et al. Diagnostic Role of ^{18}F-PSMA-1007 PET/CT in Prostate Cancer Staging: A Systematic Review // Diagnostics. 2021. Vol. 11, N 3. P. 552. doi: 10.3390/diagnostics11030552

12. Alberts I., Sachpekidis C., Fech V., et al. PSMA-negative prostate cancer and the continued value of choline-PET/CT // Nuklearmedizin. 2020. Vol. 59, N 1. P. 33–34. doi: 10.1055/a-1044-1855

13. Sartor O., Baghian A. Prostate specific membrane antigen binding radiopharmaceuticals: Current data and new concepts // Front Med (Lausanne). 2022. Vol. 9, 1060922. doi: 10.3389/fmed.2022.1060922

14. Plichta K., Graves S., Buatti J. Prostate-Specific Membrane Antigen (PSMA) Theranostics for Treatment of Oligometastatic Prostate Cancer // Int J Mol Sci. 2021. Vol. 22, N 22. P. 12095. doi: 10.3390/ijms222212095

15. Sun M., Niaz M., Niaz M., et al. Prostate-Specific Membrane Antigen (PSMA)-Targeted Radionuclide Therapies for Prostate Cancer // Curr Oncol Rep. 2021. Vol. 23, N 5. P. 59. doi: 10.1007/s11912-021-01042-w

16. Alberts I., Sachpekidis C., Dijkstra L., et al. The role of additional late PSMA-ligand PET/CT in the differentiation between lymph node metastases and ganglia // Eur J Nucl Med Mol Imaging. 2020. Vol. 47, N 3. P. 642–651. doi: 10.1007/s00259-019-04552-9

17. Khreish F., Ebert N., Ries M., et al. ^{225}Ac-PSMA-617/^{177}Lu-PSMA-617 tandem therapy of metastatic castration-resistant prostate cancer: pilot experience // Eur J Nucl Med Mol Imaging. 2020. Vol. 47, N 3. P. 721–728. doi: 10.1007/s00259-019-04612-0

18. Kendrick J., Francis R., Hassan G.M., et al. Radiomics for Identification and Prediction in Metastatic Prostate Cancer: A Review of Studies // Front Oncol. 2021. Vol. 11, P. 771–787. doi: 10.3389/fonc.2021.771787

19. Macedo F., Ladeira K., Pinho F., et al. Bone metastases: an overview // Oncol Rev. 2017. Vol. 11, N 1. P. 321. doi: 10.4081/oncol.2017.321

20. Kitagawa Y., Yamaoka T., Yokouchi M., et al. Diagnostic Value of Plain Radiography for Symptomatic Bone Metastasis at the First Visit // J Nippon Med Sch. 2018. Vol. 85, N 6. P. 315–321. doi: 10.1272/jnms.JNMS.2018_85-51

21. Cornford P., van den Bergh R.C.N., Briers E., et al. EAU-EANM-ESTRO-ESUR-SIOG Guidelines on Prostate Cancer. Part II–2020 Update: Treatment of Relapsing and Metastatic Prostate Cancer // Eur Urol. 2021. Vol. 79, N 2. P. 263–282. doi: 10.1016/j.eururo.2020.09.046

22. Liu T., Wang S., Liu H., et al. Detection of vertebral metastases: a meta-analysis comparing MRI, CT, PET, BS and BS with SPECT // J Cancer Res Clin Oncol. 2017. Vol. 143, N 3. P. 457–465. doi: 10.1007/s00432-016-2288-z

23. Сергеев Н.И., Котляров П.М., Солодкий В.А. Стандарты анализа метастатического поражения костных структур по данным современных методов лучевой диагностики // Сибирский онкологический журнал. 2018. Т. 17. № 1. С. 5–10. EDN: YQNNKI doi: 10.21294/1814-4861-2018-17-1-5-10

24. Chen Z., Chen X., Wang R. Application of SPECT and PET / CT with computer-aided diagnosis in bone metastasis of prostate cancer: a review // Cancer Imaging. 2022. Vol. 22, N 1. P. 18. doi: 10.1186/s40644-022-00456-4

25. Steinhauer V., Sergeev N.I. Radiomics in Breast Cancer: In-Depth Machine Analysis of MR Images of Metastatic Spine Lesion // Sovrem Tekhnologii Med. 2022. Vol. 14, N 2. P. 16–24. doi: 10.17691/stm2022.14.2.02

26. Vilanova J., Garcia-Figueiras R., Luna A., et al. Update on Whole-body MRI in Musculoskeletal Applications // Semin Musculoskelet Radiol. 2019. Vol. 23, N 3. P. 312–323. doi: 10.1055/s-0039-1685540

27. Padhani A.R., Lecouvet F.E., Tunariu N., et al. Rationale for Modernising Imaging in Advanced Prostate Cancer // Eur Urol Focus. 2017. Vol. 3, N 2–3. P. 223–239. doi: 10.1016/j.euf.2016.06.018

28. Карман А.В. Абакумова Е.А., Шиманец С.В., и др. Мультипараметрическая МРТ в диагностике и стадировании рака предстательной железы // Онкологический журнал. 2019. Т. 1, № 49. С. 136–147. EDN: VTNFYB

29. Perez-Lopez R., Mateo J., Mossop H., et al. Diffusion-weighted Imaging as a Treatment Response Biomarker for Evaluating Bone Metastases in Prostate Cancer: A Pilot Study // Radiology. 2017. Vol. 283, N 1. P. 168–177. doi: 10.1148/radiol.2016160646

30. Nakanishi K., Tanaka J., Nakaya Y., et al. Whole-body MRI: detecting bone metastases from prostate cancer // Jpn J Radiol. 2022. Vol. 40, N 3. P. 229–244. doi: 10.1007/s11604-021-01205-6

31. Sun G., Zhang Y., Liu F., et al. Whole-body magnetic resonance imaging is superior to skeletal scintigraphy for the detection of bone metastatic tumors: a meta-analysis // Eur Rev Med Pharmacol Sci. 2020. Vol. 24, N 13. P. 7240–7252. doi: 10.26355/eurrev_202007_21879

32. Padhani A., Lecouvet F., Tunariu N., et al. METastasis Reporting and Data System for Prostate Cancer: Practical Guidelines for Acquisition, Interpretation, and Reporting of Whole-body Magnetic Resonance Imaging-based Evaluations of Multiorgan Involvement in Advanced Prostate Cancer // Eur Urol. 2017. Vol. 71, N 1. P. 81–92. doi: 10.1016/j.eururo.2016.05.033

33. Van den Wyngaert T., Strobel K., Kampen W., et al. The EANM practice guidelines for bone scintigraphy // Eur J Nucl Med Mol Imaging. 2016. Vol. 43, N 9. P. 1723–1738. doi: 10.1007/s00259-016-3415-4

34. Scher H., Morris M., Stadler W., et al. Trial Design and Objectives for Castration-Resistant Prostate Cancer: Updated Recommendations From the Prostate Cancer Clinical Trials Working Group 3 // J Clin Oncol. 2016. Vol. 34, N 12. P. 1402–1418. doi: 10.1200/JCO.2015.64.2702

35. Anand A., Heller G., Fox J., et al. Automated Bone Scan Index to Optimize Prostate Cancer Working Group Radiographic Progression Criteria for Men With Metastatic Castration-Resistant Prostate Cancer // Clin Genitourin Cancer. 2022. Vol. 20, N 3. P. 270–277. doi: 10.1016/j.clgc.2022.02.002

36. Chao H., Chang C., Chiu C., et al. Bone Scan Flare Phenomenon in Non–Small–Cell Lung Cancer Patients Treated With Gefitinib // Clin Nucl Med. 2009. Vol. 34, N 6. P. 346–349. doi: 10.1097/RLU.0b013e3181a344df

37. van der Zande K., Oyen W.J.G., Zwart W., et al. Radium-223 Treatment of Patients with Metastatic Castration Resistant Prostate Cancer: Biomarkers for Stratification and Response Evaluation // Cancers (Basel). 2021. Vol. 13, N 17. P. 4346. doi: 10.3390/cancers13174346

38. Nakajima K., Edenbrandt L., Mizokami A. Bone scan index: A new biomarker of bone metastasis in patients with prostate cancer // Int J Urol. 2017. Vol. 24, N 9. P. 668–673. doi: 10.1111/iju.13386

39. Ruchalski K., Dewan R., Sai V., et al. Imaging response assessment for oncology: An algorithmic approach // Eur J Radiol Open. 2022. Vol. 9, P. 100426. doi: 10.1016/j.ejro.2022.100426

40. Еременко А.В., Косых Н.Э., Разуваев В.А., Савин С.З. Исследование возможностей компьютерного автоматизированного анализа для задач эффективной диагностики диссеминированного рака предстательной железы // Лучевая диагностика и терапия. 2019. № 1. С. 74–85. EDN: NQOKHZ doi: 10.22328/2079-5343-2019-10-1-74-85

41. Dennis E., Jia X., Mezheritskiy I., et al. Bone Scan Index: A Quantitative Treatment Response Biomarker for Castration-Resistant Metastatic Prostate Cancer // J Clin Oncol. 2012. Vol. 30, N 5. P. 519–524. doi: 10.1200/JCO.2011.36.5791

42. Sheikhbahaei S., Jones K., Werner R., et al. ^{18}F-NaF-PET/CT for the detection of bone metastasis in prostate cancer: a meta-analysis of diagnostic accuracy studies // Ann Nucl Med. 2019 Vol. 33, N 5. P. 351–361. doi: 10.1007/s12149-019-01343-y

43. Shen G., Deng H., Hu S., et al. Comparison of choline-PET/CT, MRI, SPECT, and bone scintigraphy in the diagnosis of bone metastases in patients with prostate cancer: a meta-analysis // Skeletal Radiol. 2014. Vol. 43, N 11. P. 1503–1513. doi: 10.1007/s00256-014-1903-9

44. Сергеев Н.И., Фомин Д.К., Котляров П.М., и др. Сравнительное исследование возможностей остеосцинтиграфии и магнитно-резонансной томографии всего тела в диагностике костных метастазов // Медицинская Визуализация. 2014. Т. 4. С. 107–113. EDN: SNIDQB

45. Blackwell W. Radiology-Nuclear Medicine Diagnostic Imaging: A Correlative Approach. First. ed. Gholamrezanezhad A., Assadi M., Jadvar H., editors. USA. 2023.

46. Mohd Rohani M., Mat Nawi N., Shamim S., et al. Maximum standardized uptake value from quantitative bone single-photon emission computed tomography/computed tomography in differentiating metastatic and degenerative joint disease of the spine in prostate cancer patients // Ann Nucl Med. 2020. Vol. 34, N 1. P. 39–48. doi: 10.1007/s12149-019-01410-4

47. Okamoto S., Thieme A., Allmann J., et al. Radiation Dosimetry for 177Lu-PSMA I&T in Metastatic Castration-Resistant Prostate Cancer: Absorbed Dose in Normal Organs and Tumor Lesions // J Nucl Med. 2017. Vol. 58, N 3. P. 445–450. doi: 10.2967/jnumed.116.178483

48. Ghodsirad M., Pirayesh E., Akbarian R., et al. Diagnostic Utility of Lutetium-177 (Lu 177) Prostate-Specific Membrane Antigen (PSMA) Scintigraphy In Prostate Cancer Patients With PSA Rise And Negative Conventional Imaging // Urol J. 2020. Vol. 17, N 4. P. 374–378. doi: 10.22037/uj.v0i0.5451

49. Venkatachalapathy V., Rajeshkannan R., Sarma M., et al. Comparison of whole-body bone scintigraphy with axial skeleton magnetic resonance imaging in the skeletal evaluation of carcinoma prostate // Indian J Urol. 2021. Vol. 37, N 1. P. 72–78. doi: 10.4103/iju.IJU_238_20

50. Сергеев Н.И., Фомин Д.К., Котляров П.М., Солодкий В.А.. Сравнительное исследование возможностей ОФЭКТ/КТ и магнитно-резонансной томографии всего тела в диагности-

ке костных метастазов // Вестник российского научного центра рентгенорадиологии. 2015. Т. 15, № 3. С. 8. EDN: UXMAVX

51. Li R., Ravizzini G., Gorin M., et al. The use of PET/CT in prostate cancer // Prostate Cancer Prostatic Dis. 2018. Vol. 21, N 1. P. 4–21. doi: 10.1038/s41391-017-0007-8

52. Azad G., Cook G. Multi-technique imaging of bone metastases: spotlight on PET-CT // Clin Radiol. 2016. Vol. 71, N 7. P. 620–631. doi: 10.1016/j.crad.2016.01.026

53. Kannivelu A., Loke K., Kok T., et al. The Role of PET/CT in the Evaluation of Skeletal Metastases // Semin Musculoskelet Radiol. 2014. Vol. 18, N 2. P. 149–165. doi: 10.1055/s-0034-1371017

54. Jadvar H. Molecular Imaging of Prostate Cancer: PET Radiotracers // AJR Am J Roentgenol. 2012. Vol. 199, N 2. P. 278–291. doi: 10.2214/AJR.12.8816

55. Alam M., Singh S., Thapaliya S., et al. A Review of ^{177}Lutetium-PSMA and ^{225}Actinium-PSMA as Emerging Theranostic Agents in Prostate Cancer // Cureus. 2022. Vol. 14, N 9. P. 29369. doi: 10.7759/cureus.29369

56. Eisenhauer E., Therasse P., Bogaerts J., et al. New response evaluation criteria in solid tumours: Revised RECIST guideline (version 1.1) // Eur J Cancer. 2009. Vol. 45, N 2. P. 228–247. doi: 10.1016/j.ejca.2008.10.026

57. Acar E., Özdoğan Ö., Aksu A., et al. The use of molecular volumetric parameters for the evaluation of Lu-177 PSMA I&T therapy response and survival // Ann Nucl Med. 2019. Vol. 33, N 9. P. 681–688. doi: 10.1007/s12149-019-01376-3

58. Maffey-Steffan J., Scarpa L., Svirydenka A., et al. The ^{68}Ga/^{177}Lu-theragnostic concept in PSMA-targeting of metastatic castration-resistant prostate cancer: impact of post-therapeutic whole-body scintigraphy in the follow-up // Eur J Nucl Med Mol Imaging. 2020. Vol. 47, N 3. P. 695–712. doi: 10.1007/s00259-019-04583-2

59. O J., Lodge M., Wahl R. Practical PERCIST: A Simplified Guide to PET Response Criteria in Solid Tumors 1.0 // Radiology. 2016. Vol. 280, N 2. P. 576–584. doi: 10.1148/radiol.2016142043

60. Schmuck S., von Klot C., Henkenberens C., et al. Initial Experience with Volumetric 68 Ga-PSMA I&T PET/CT for Assessment of Whole-Body Tumor Burden as a Quantitative Imaging Biomarker in Patients with Prostate Cancer // Journal of Nuclear Medicine. 2017. Vol. 58, N 12. P. 1962–1968. doi: 10.2967/jnumed.117.193581

61. Tanaka K., Norikane T., Mitamura K., et al. Quantitative [^{99m}Tc] Tc-MDP SPECT/CT correlated with [18F]NaF PET/CT for bone metastases in patients with prostate cancer // EJNMMI Phys. 2022. Vol. 9, N 1. P. 83. doi: 10.1186/s40658-022-00513-8

62. Vlachostergios P., Niaz M., Sun M., et al. Prostate-Specific Membrane Antigen Uptake and Survival in Metastatic Castration-Resistant Prostate Cancer // Front Oncol. 2021. Vol. 11, P. 630589. doi: 10.3389/fonc.2021.630589

63. Beyersdorff D., Rahbar K., Essler M., et al. Interdisziplinärer Expertenkonsensus zu Innovationen der bildgebenden Diagnostik und radionuklidbasierten Therapien des fortgeschrittenen Prostatakarzinoms // Urologe. 2021. Vol. 60, P. 1579–1585. doi: 10.1007/s00120-021-01598-2

64. Gafita A., Rauscher I., Weber M., et al. Novel Framework for Treatment Response Evaluation Using PSMA PET/CT in Patients with Metastatic Castration-Resistant Prostate Cancer (RECIP 1.0): An International Multicenter Study // J Nucl Med. 2022. Vol. 63, N 11. P. 1651–1658. doi: 10.2967/jnumed.121.263072

65. Isaac A., Dalili D., Dalili D., Weber M. State-of-the-art imaging for diagnosis of metastatic bone disease // Radiologe. 2020. Vol. 60, N 1. P. 1–16. doi: 10.1007/s00117-020-00666-6

AUTHORS' INFO

* Anastasia A. Karpova, MD;
address: 28 Orekchovy blvd., 115682, Moscow, Russia;
ORCID: 0000-0002-0251-254X;
eLibrary SPIN: 9993-5553;
e-mail: karpovaaadoc@yandex.ru

Nikolay I. Sergeev, MD, Dr. Sci. (Medicine);
ORCID: 0000-0003-4147-1928;
eLibrary SPIN: 2408-6502;
e-mail: sergeevnickolay@yandex.ru

Olga A. Borisova, MD, Cand. Sci. (Medicine);
ORCID: 0009-0003-7809-0130;
eLibrary SPIN: 2416-1885;
e-mail: Mihanikborisov@gmail.com

Pavel A. Nikitin, MD, Cand. Sci. (Medicine);
ORCID: 0000-0003-1809-6330;
eLibrary SPIN: 6257-2399;
e-mail: paul2003@mail.ru

Dmitriy K. Fomin, MD, Dr. Sci. (Medicine), Professor of the Russian
Academy of Sciences;
ORCID: 0000-0002-7316-3519;
eLibrary SPIN: 4593-1292;
e-mail: dkfomin@yandex.ru

Vladimir A. Solodkiy, MD, Dr. Sci. (Medicine), Professor,
Academician of the Russian Academy of Sciences;
ORCID: 0000-0002-1641-6452;
eLibrary SPIN: 9556-6556;
e-mail: director@rncrr.ru

_____

* Corresponding author / Автор, ответственный за переписку

ОБ АВТОРАХ

* Карпова Анастасия Анатольевна;
адрес: Россия, 115682, Москва, Ореховый бульвар, д. 28;
ORCID: 0000-0002-0251-254X;
eLibrary SPIN: 9993-5553;
e-mail: karpovaaadoc@yandex.ru

Сергеев Николай Иванович, д-р мед. наук;
ORCID: 0000-0003-4147-1928;
eLibrary SPIN: 2408-6502;
e-mail: sergeevnickolay@yandex.ru

Борисова Ольга Анатольевна, канд. мед. наук;
ORCID: 0009-0003-7809-0130;
eLibrary SPIN: 2416-1885;
e-mail: Mihanikborisov@gmail.com

Никитин Павел Алексеевич, канд. мед. наук;
ORCID: 0000-0003-1809-6330;
eLibrary SPIN: 6257-2399;
e-mail: paul2003@mail.ru

Фомин Дмитрий Кириллович, д-р мед. наук,
профессор РАН;
ORCID: 0000-0002-7316-3519;
eLibrary SPIN: 4593-1292;
e-mail: dkfomin@yandex.ru

Солодкий Владимир Алексеевич, д-р мед. наук, профессор,
академик РАН;
ORCID: 0000-0002-1641-6452;
eLibrary SPIN: 9556-6556;
e-mail: director@rncrr.ru

Ultrasound in *in vitro* fertilization programs

Evgeniya V. Kirakosyan

City Clinical Hospital № 31, Moscow, Russia

ABSTRACT

Currently, increasing attention is being paid to the value of ultrasound as an integral part of *in vitro* fertilization programs, which determines the relevance of the topic of this review. This review analyzes the main studies published in recent years and attempts to identify the leading method for assessing ovarian reserve and predicting in vitro fertilization outcome, which remains controversial. The paper evaluates advantages and limitations of two-dimensional and three-dimensional transvaginal ultrasound methods for counting ovarian follicles. Ultrasound characteristics of the endometrium and blood flow parameters in the uterine arteries are presented as possible predictors of the outcome of in vitro fertilization programs. The current options for transabdominal oocyte aspiration for in vitro fertilization programs are presented. The analysis of literature data concluded the high informational value of ultrasound for in vitro fertilization programs.

Keywords: ovarian reserve; number of ovarian follicles; transvaginal ultrasound; in vitro fertilization; assisted reproductive technologies.

Ультразвуковое исследование в программах экстракорпорального оплодотворения

Е.В. Киракосян

Городская клиническая больница № 31 имени академика Г.М. Савельевой, Москва, Россия

АННОТАЦИЯ

В настоящее время всё больше внимания уделяют ценности ультразвукового исследования как неотъемлемой части программ экстракорпорального оплодотворения, чем обусловлена актуальность темы данного обзора. В представленном обзоре научной литературы, основанном на самых значимых исследованиях последних лет, сделана попытка ответить на дискуссионный вопрос о выборе ведущего метода оценки овариального резерва и прогнозирования результатов программ экстракорпорального оплодотворения. В работе проведён анализ преимуществ и недостатков методов двухмерного и трёхмерного трансвагинального ультразвукового исследования при подсчёте количества фолликулов яичников. Приведены ультразвуковые характеристики эндометрия и показатели кровотока в маточных артериях, являющиеся возможными предикторами результатов программ экстракорпорального оплодотворения. Представлены современные возможности трансабдоминальной аспирации ооцитов в программах экстракорпорального оплодотворения. В результате анализа данных литературы сделан вывод о высокой информативности ультразвукового исследования в программах экстракорпорального оплодотворения.

Ключевые слова: овариальный резерв; количество фолликулов яичников; трансвагинальное ультразвуковое исследование; экстракорпоральное оплодотворение; вспомогательные репродуктивные технологии.

体外受精项目中的超声检查

Evgeniya V. Kirakosyan

City Clinical Hospital № 31, Moscow, Russia

摘要

目前，超声检查作为体外受精项目不可分割的部分，其价值越来越受到人们的关注，这正是本综述主题的现实意义。在这篇科学文献综述中，以近年来最重要的研究为基础，试图回答一个有争议的问题，那就是如何选择主要的方法来评估卵巢储备和预测体外受精计划的结果。本文对二维和三维经阴道超声检查在计算卵泡数量时的优缺点进行了分析。列出了子宫内膜的超声特征和子宫动脉血流指标，它们是体外受精计划结果的可能预测因素。介绍了在体外受精项目中经腹卵母细胞抽吸的现代可能性。通过对文献数据的分析，可以做出如下结论，超声在体外受精项目中可提供的信息量巨大。

关键词：卵巢储备；卵泡数量；经阴道超声波检查；体外受精；辅助生殖技术。

OVARIAN RESERVE MARKER: ANTRAL FOLLICLE COUNT OR ANTI-MÜLLERIAN HORMONE LEVEL?

In vitro fertilization (IVF) programs rely on assessing ovarian reserve, tailoring ovarian stimulation protocols, and predicting the ovarian response. These steps are crucial for obtaining mature oocytes, ensuring effective aspiration, generating high-quality embryos, and ultimately improving clinical pregnancy rates [1]. The follicular apparatus—comprising follicles at various stages of development within the ovarian cortex—serves as an ultrasound (US)-based indicator of ovarian reserve [2]. In 2018, an international consensus endorsed the use of the antral follicle count (AFC) via transvaginal US for this purpose [3]. The examination is conducted with the patient in the lithotomy position and the bladder emptied. The ovaries are evaluated using the following protocol:

- Each ovary is scanned in both longitudinal and coronal views to identify the best imaging plane.
- The ovary is positioned to fill at least 50% of the US screen along its longest axis.
- US settings are adjusted to maximize contrast between the follicular fluid and ovarian stroma.
- Measurements are taken along the inner diameter of all non-echogenic follicular areas, spanning from the upper to the lower pole of the ovary. For round follicles, the diameter is measured directly; for oval follicles, both the long and short axes are measured, and the mean is calculated.
- Only follicles measuring 2–10 mm in diameter are counted; those smaller than 2 mm or larger than 10 mm are excluded.
- The presence or absence of a dominant follicle, ovarian cysts, or tumors is noted.
- If uncertainty arises, the scan is repeated from an alternative imaging plane.
- The total follicle count from both ovaries is recorded [3].

Discrepancies between AFC and blood anti-Müllerian hormone (AMH) levels are frequently encountered in clinical settings. In 2019, the Peking University Clinic conducted a study involving 1,121 women with infertility who underwent IVF. AFC and AMH levels were assessed on Days 2–3 of the menstrual cycle. Transvaginal US was performed using the Aloka™ SSD-1000 scanner (Hitachi Aloka Medical, Japan) equipped with a 5 MHz vaginal probe. Based on the results, patients were categorized into four groups: group A ($n = 611$) included those with both normal AFC (≥ 7) and AMH (≥ 1.1 ng/mL); group B ($n = 85$) had normal AFC (≥ 7) but low AMH (<1.1 ng/mL); group C ($n = 118$) had low AFC (<7) with normal AMH (≥ 1.1 ng/mL); and group D ($n = 307$) had both low AFC (<7) and low AMH (<1.1 ng/mL). A total of 203 patients (18.11%, Groups B and C) exhibited discordance between AFC and AMH values. Among these, patients in group B had significantly higher numbers of aspirated oocytes and high-grade embryos, along with a higher clinical pregnancy rate, and a lower incidence of poor ovarian response compared to group C [4]. The study revealed that approximately one in five patients undergoing IVF showed discrepancies between AFC and AMH levels in routine clinical practice. AFC was identified as the more reliable marker for assessing ovarian reserve and predicting ovarian response and IVF outcomes.

A multicenter retrospective study was conducted using data from 5 reproductive medicine centers in China, comprising 89,002 patients and 327,059 IVF cycles, to compare the diagnostic value of various ovarian reserve markers. The markers assessed included AFC, AMH level, follicle-stimulating hormone (FSH) level, and patient age. Both AMH and AFC individually demonstrated high diagnostic performance, with AUC[1] values of 0.862 and 0.842, respectively. However, the highest diagnostic accuracy was achieved when combining AMH level, AFC, FSH level, and age (AUC 0.873). The authors noted that AMH levels can be reliably evaluated using an automated electrochemiluminescence assay. They also recommended assessing AFC in conjunction with patient age (AUC 0.846) [5].

Another study analyzed data from 15,283 patients and 25,854 ovarian stimulation cycles conducted across 12 assisted reproductive technology (ART) centers in France. Among 25-year-old patients, the mean AFC was 16.3 (95% CI[2], 14.5–18.4), showing a linear decline of 3.9% per year ($p < 0.001$). The mean AMH level was 3.9 ng/mL (95% CI, 3.6–4.2 ng/mL), decreasing by 5% annually. The study found only a weak correlation between AMH levels and AFC, with half of the patients who had low AMH levels still exhibiting normal AFC values. According to the authors, two main factors limit the reliability of AMH level assessment: the absence of international standardization in automated laboratory methods—which tend to report AMH values 16%–20% lower than manual methods—and the high cost of testing. In France, AMH is typically measured once per year, whereas transvaginal US with AFC evaluation is routinely included in all ART protocols [6].

A 2023 systematic review and meta-analysis of 42 studies involving 7,190 patients demonstrated that both AFC and AMH levels are strong predictors of ovarian response, whether favorable or poor. The review concluded that AFC is slightly more accurate than AMH in identifying poor ovarian response [7].

Currently, there is no consensus on whether AFC or AMH should be the primary marker for guiding ovarian

---

[1] AUC ROC, area under the ROC curve (the sensitivity and specificity parameter characterizing the validity of diagnostic tests).

[2] Confidence interval.

stimulation. However, most researchers agree that AFC is at least as diagnostically valuable as AMH, and in some cases preferable due to its greater technical accessibility and lower cost.

DOES THE NUMBER OF FOLLICLES VARY BY MENSTRUAL CYCLE DAY?

Ovarian reserve depends on the number of primordial follicles present in the ovaries. As there are currently no methods to directly measure the number of primordial follicles, ovarian reserve is assessed indirectly using patient age, AFC, and serum AMH levels. AMH levels can be measured on any day of the menstrual cycle [8]. Over the past decade, it has been recommended to perform AFC assessment during the early follicular phase of the cycle, likely to standardize evaluation. However, this timing for transvaginal US is often inconvenient for both patients and clinicians [9].

A study published in 2022 included 410 patients aged 20–42 years with regular menstrual cycles who underwent a single IVF cycle. AFC was measured twice using transvaginal US with the Voluson™ S8, E8, or E10 systems (GE Healthcare, USA), equipped with a high-frequency 3D vaginal probe (>7 MHz). Follicles measuring 2–10 mm in diameter were counted in each ovary, and the total AFC was calculated as the sum. The first AFC measurement was taken during the initial consultation on a random day of the menstrual cycle: 150 patients (36.8%) in the early follicular phase (Days 1–6), 177 patients (43.2%) in the midfollicular phase (Days 7–12), and 83 patients (20%) in the luteal phase (Day 13 or later). The second AFC was measured on the day ovarian stimulation began. AMH levels were measured during the early follicular phase. A positive correlation was found between the random-day AFC and AMH levels ($r = 0.69$, $p < 0.001$), the AFC on the day of stimulation ($r = 0.75$, $p < 0.001$), and the number of aspirated oocytes ($r = 0.49$, $p < 0.001$) [9]. These findings indicate AFC has strong diagnostic value for assessing ovarian reserve and is a reliable predictor of ovarian response, regardless of the menstrual cycle day.

A retrospective study involving 3,117 women with infertility demonstrated that AFC is a reliable predictor of poor ovarian response (defined as fewer than four aspirated oocytes), regardless of the menstrual cycle day [10]. In a separate analysis of 72 women with malignant neoplasms who underwent IVF for fertility preservation, AFC measured on any day of the cycle was found to be a strong predictor of the number of mature oocytes retrieved [11]. Importantly, the ability to assess AFC on any day of the menstrual cycle avoids scheduling difficulties during menstruation for both patients and physicians and reduces the need for repeat examinations, thereby lowering the logistical burden. Performing transvaginal US with AFC assessment during the midfollicular or late follicular phase also offers reliable information on ovarian reserve and allows simultaneous assessment of ovarian and uterine anatomy [9].

COUNTING OVARIAN FOLLICLES AND PREDICTING THE NUMBER OF MATURE OOCYTES: 2D OR 3D TRANSVAGINAL ULTRASOUND EXAMINATION?

Recent improvements in US technology have significantly enhanced image resolution and quality. In ART programs, high-frequency vaginal probes have replaced abdominal transducers, leading to better visualization of the uterus and ovaries. 2D transvaginal US is a well-established diagnostic method in reproductive medicine. 3D transvaginal US is a newer technique, and ongoing research is evaluating its potential benefits and limitations. The quality of ovarian imaging by transvaginal US largely depends on the US system used. In 2D US, the accuracy of follicle identification and measurement depends heavily on the operator's experience. In contrast, 3D US requires only one high-quality image per ovary to automatically calculate ovarian volume, follicle diameter, and AFC [12, 13]. The oblique coronal plane view available in 3D US allows for more precise volume measurement, improving the consistency and reliability of the results—particularly important when evaluating irregularly shaped structures like follicles during ovarian stimulation [14]. The ability to store and later review data, including images in any plane, helps reduce diagnostic uncertainty during treatment planning. A prospective study involving 89 women undergoing IVF found no significant differences in the number or size of follicles when comparing manual assessment to 3D transvaginal US. However, 3D transvaginal US significantly reduced total examination time compared to 2D US (1 min vs. 2 min, $p < 0.01$), even though it required additional time for operator setup. Additionally, 3D US demonstrated significantly better data reproducibility than 2D, indicating lower interoperator variability [15].

Another study assessed 50 women aged 18–37 years undergoing IVF. Both 2D and 3D transvaginal US were performed using the Voluson™ S8 system with a 5–10 MHz RIC5-9-RS vaginal probe (GE Healthcare, USA). To evaluate interoperator variability, two operators performed scans 1 h apart. 2D US followed standard procedures. Subsequently, each patient underwent 3D US with the following steps:
- Identification of the maximum ovarian diameter
- Image stabilization
- Full ovary 3D scanning
- Ovary volume measurement using Virtual Organ Computer-Aided Analysis (VOCAL™, GE Healthcare), with 30° rotational steps in the coronal and longitudinal planes, and reconstruction of transverse and coronal images

• Definition of the region of interest through computerized mechanical slow scanning, followed by saving of the 3D dataset

The SonoAVC™ automated volume count software (GE Medical Systems, Austria) was used to identify and measure the number and diameter of fluid-filled areas (follicles). The time for each 2D and 3D transvaginal US procedure was recorded with a precision of 1 s. The mean time for automated AFC and ovary volume assessment using 3D transvaginal US was significantly shorter than with 2D US, although the diagnostic value of both methods was similar [16].

Assessing follicle maturation and determining the appropriate timing for oocyte aspiration are critical for obtaining mature oocytes without complications [17]. Previous studies have suggested that final follicular maturation should be triggered when the dominant follicle reaches a diameter of 16–22 mm according to 2D transvaginal US [18]. A recent study found that aspirating follicles with diameter of 19–24.5 mm result in high-quality embryos [19]. Manually counting follicles with an average diameter of ⩾10 mm using 2D transvaginal US remains a reliable predictor of mature oocyte numbers, although some studies indicate this parameter does not always correlate with mature oocyte counts [20]. In a study involving 515 women undergoing IVF, 3D transvaginal US was used on the day of final follicular maturation trigger to assess the dominant follicle volume as a predictor of mature oocyte count, using artificial intelligence. The threshold dominant follicle volume was found to be 0.5 см3, and this new marker significantly outperformed the conventional marker ($p <$ 0.001) [21].

Both 2D and 3D transvaginal US offer comparable diagnostic value for assessing the AFC and determining ovarian reserve. 3D transvaginal US allows for automated AFC and ovary volume measurement with high accuracy and efficacy, and its ability to measure follicle volume helps predict the number of mature oocytes. Additionally, 3D transvaginal US has the advantage of a shorter examination time compared to 2D US. In high-volume ART clinics, using 3D transvaginal US can reduce exam time and increase the number of IVF procedures. Conversely, 2D transvaginal US can still be effectively used in clinics with lower patient volumes or in resource-limited settings with fewer healthcare resources [16].

ULTRASOUND EXAMINATION OF THE ENDOMETRIUM FOR PREDICTING CLINICAL PREGNANCY RATES

Transvaginal US is a noninvasive, reproducible, and accessible method commonly used in IVF programs to assess the endometrium [22]. A 2014 systematic review and meta-analysis of 22 studies involving 10,724 patients found that endometrial thickness measured by transvaginal US does not significantly predict IVF outcomes. The analysis showed that an endometrial thickness of <7 mm was associated with a decreased likelihood of pregnancy; however, such thin endometrium are rare. Notably, none of the studies included in the review examined the endometrial histology in patients with thin endometrium to explore the potential underlying pathophysiological mechanisms [23].

In 2016, a study conducted in China evaluated 3D transvaginal US parameters as potential predictors of implantation and pregnancy rates in IVF programs. The study included 435 first-time IVF patients who underwent a long ovarian stimulation protocol. On the day of human chorionic gonadotropin injection, 3D transvaginal US was used to assess endometrial thickness, structure, volume, and hemodynamic parameters, including peak systolic velocity, end-diastolic velocity, pulsatility index (PI), resistance index (RI), systolic/diastolic ratio (S/D), vascularization index (VI), flow index (FI), and endometrial and subendometrial vascularization flow index (VFI). Two or more high-grade embryos were obtained in all cases, and they were transferred on Day 3. The procedure led to clinical pregnancy in 253 patients (58.2%) and miscarriage in 49 patients (11.3%), while 133 patients (30.5%) did not conceive. No significant differences were found in endometrial thickness, volume, and structure, or in the hemodynamic parameters (PI, RI, S/D, VI, FI, and VFI) among the three groups. Patients with relatively low endometrial thickness (⩽8.5 mm; 10%) experienced both successful and unsuccessful pregnancies, and these patients had similar endometrial volume and structure and hemodynamic parameters (PI, RI, S/D, VI, FI, and VFI) [24].

A recent meta-analysis that included 14 studies involving 4,842 women of similar age who underwent IVF found that women who became pregnant had significantly higher endometrial thickness and volume, as well as higher uterine artery vascularization indices (VI, FI, and VFI), compared to those who did not become pregnant. In contrast, the S/D was lower in women who achieved pregnancy. There were no significant differences in the RI and PI. The authors concluded that endometrial receptivity plays a significant role in implantation rates and that endometrial thickness and volume, in combination with uterine artery S/D, VI, FI, and VFI assessed via transvaginal US, can serve as predictors of IVF outcomes [25].

Thus, the role of US evaluation of the endometrium and uterine blood flow in predicting clinical pregnancy rates in IVF remains a subject of debate.

TRANSABDOMINAL OOCYTE ASPIRATION IN THE IN VITRO FERTILIZATION PROGRAM

Transvaginal oocyte aspiration is preferred over the transabdominal approach due to its quicker and less invasive nature [26]. In a 2015 comparative study conducted

in the USA, 278 patients underwent transvaginal oocyte aspiration, while 95 patients underwent transabdominal oocyte aspiration (15 had only transabdominal oocyte aspiration, and 80 had both transabdominal and transvaginal approaches). The average age of the patients was 37.60 ± 5.15 years. The average procedure time was 20.2 min for transvaginal oocyte aspiration and 28.2 min for transabdominal oocyte aspiration, with the latter usually performed after an attempted transvaginal oocyte aspiration. Hemostatic suturing was required in two patients in the transvaginal group and one in the transabdominal group. No hospitalizations or infections requiring antibiotics were reported in either group. After transabdominal oocyte aspiration, 39.4% of patients experienced mild pain, and 51.1% experienced moderate to severe pain. In the transvaginal oocyte aspiration group, 20.4% of patients reported mild pain, while 42.5% reported moderate to severe pain. There were no significant differences in the incidence of complications or pregnancy rates between the study. The authors created a scoring system to determine the need for transabdominal oocyte aspiration based on the following factors: low-quality ovarian imaging with transvaginal US (4 points), a history of pelvic surgery (3 points), and a body mass index $\geqslant 30$ kg/m^2 (2 points). For a total score of $\geqslant 4$ points, the system showed a sensitivity of 75%, specificity of 80%, positive predictive value of 57%, and negative predictive value of 90%. In this study, only 57% of patients with a score of $\geqslant 4$ points required transabdominal oocyte aspiration after transvaginal oocyte aspiration. Therefore, a positive score indicates a higher risk of needing transabdominal oocyte aspiration but is not an absolute indication for it. The authors concluded that transabdominal oocyte aspiration is a useful supplementary approach to transvaginal oocyte aspiration, yielding more oocytes in certain cases when the scoring system is applied [27].

A 2020 study involved 64 women who underwent transabdominal oocyte aspiration for various reasons, including fertility preservation in virgins with diminished ovarian reserve, malignant and benign neoplasms, ovarian transposition due to intestinal surgery, and Mayer–Rokitansky–Küster–Hauser syndrome. The procedure was performed using a 17G double-lumen aspiration needle (Cook Medical, USA) and a 150–180 mm Hg aspiration pump (Labotec, Germany), under US guidance with the Logiq™ P5 scanner and a 4–8 MHz vaginal US sensor (Shimadzu, Japan). The vaginal US sensor was chosen for its pointed tip and smaller surface area, which allowed for precise pressure application in the target area during oocyte aspiration. The sensor was positioned to view the ovary, and all patients emptied their bladder before the procedure to ensure the ovaries were close to the sensor. The average AFC was 6.14 ± 1.30, with a total of 315 aspirated oocytes and an average of 4.92 ± 1.70 per patient. The mean procedure time was 12.4 ± 1.2 min, similar to the transvaginal approach. The number and percentage of mature oocytes were 272

and 86.3%, respectively, which was a favorable outcome. A total of 14 frozen embryos were obtained for 4 patients, and transferring one embryo resulted in a live birth [28].

In 2023, the same authors conducted a study on transabdominal oocyte aspiration using a vaginal US sensor for fertility preservation in 116 virgins with diminished ovarian reserve (80.1%) and malignant or benign neoplasms (19.9%). The control group consisted of 33 women of similar age, clinical characteristics, hormone levels, and ovarian reserve who underwent transvaginal oocyte aspiration for the same indications (84.8% and 15.2%, respectively). No significant differences were observed between the groups in terms of the mean duration of ovarian stimulation (8.05 ± 1.91 days vs. 8.35 ± 1.72 days), mean total gonadotropin dose per stimulation cycle ($1,507.9 \pm 475.3$ IU vs. $1,571.74 \pm 404.60$ IU), average procedure time (12.4 ± 1.2 min vs. 13.4 ± 1.6 min), mean AFC (4.62 ± 4.54 vs. 5.44 ± 4.52), mean number of aspirated oocytes (4.44 ± 4.14 vs. 5.33 ± 4.52), mean number of frozen mature oocytes (4.01 ± 3.67 vs. 4.53 ± 4.13), percentage of mature oocytes ($78 \pm 24\%$ vs. $82 \pm 26\%$), and percentage of follicles ($86 \pm 63\%$ vs. $84 \pm 19\%$). Two patients in the treatment group experienced a superficial epigastric artery injury, which resolved on its own[29].

In 2006, a clinical case of transabdominal oocyte aspiration was reported in Israel involving a 29-year-old patient with Mayer–Rokitansky–Küster–Hauser syndrome and an unusually high ovarian position in the hypochondrium. A 3–5 MHz abdominal US sensor (Philips Medical Systems, USA) was used. A single puncture was made on each side with a 17-G double-lumen aspiration needle. All accessible follicles were aspirated along the shortest path from the anterior abdominal wall to the ovaries, with simultaneous imaging of the right kidney, gallbladder, intestine, liver, and spleen. A total of 4 IVF cycles were performed, resulting in the aspiration of 19 oocytes, retrieval of 13 zygotes, and transfer of 11 embryos to a surrogate mother; however, pregnancy did not occur [30].

In 2011, a comparative retrospective study was conducted in the USA with 69 patients who underwent transvaginal oocyte aspiration and 69 patients who underwent transabdominal oocyte aspiration (of which 57 patients had transabdominal oocyte aspiration alone, and 12 patients had both transabdominal and transvaginal oocyte aspiration). Transabdominal oocyte aspiration was performed when one or both ovaries were inaccessible for transvaginal aspiration due to conditions such as adenomyosis, uterine fibroids, obesity, congenital reproductive tract disorders, surgical ovarian transposition, or pelvic adhesions. A 17G double-lumen aspiration needle (Cook Medical, USA) and a 1–4 MHz abdominal US sensor (Acuson Sequoia™, Siemens Healthineers AG, Germany) were used, positioned in the ovary view. The number of retrieved oocytes in the transabdominal oocyte aspiration group (including both transabdominal and transvaginal) was significantly lower

than in the transvaginal oocyte aspiration group (11.9 ± 0.8 vs. 14.1 ± 1.0, respectively; *p* = 0.008). However, there were no significant differences between the groups in the number of mature oocytes (9.2 ± 0.9 vs. 7.3 ± 0.9, respectively; *p* = 0.14), damaged oocytes (0.09 ± 0.05 vs. 0.07 ± 0.04, respectively; *p* = 0.94), fertilization rate (63.4 ± 3.1% vs. 67.1 ± 2.7%, respectively; p = 0.35), high-grade embryos (6.4 ± 0.6 vs. 7.7 ± 0.7, respectively; *p* = 0.08), or pregnancy rates (27.5% and 36.2%, respectively; *p* = 0.36). The authors concluded that US-guided transabdominal oocyte aspiration is a safe and effective method that can be used when ovaries are inaccessible for transvaginal aspiration [31].

Available studies suggest that US-guided transabdominal oocyte aspiration is a feasible, effective, and safe option for oocyte retrieval in IVF programs, particularly for fertility preservation and in cases where ovaries are inaccessible for transvaginal oocyte aspiration.

CONCLUSION

US examinations play a crucial role in IVF programs, providing diagnostic value comparable to other diagnostic methods. Assessing ovarian reserve and predicting ovarian response and IVF outcomes requires determining the number of ovarian follicles. Some studies suggest that the AFC can be measured at any point during the menstrual cycle without compromising diagnostic accuracy, offering convenience for both patients and clinicians. 3D transvaginal

US enables automated, highly accurate, and efficient AFC assessment, and it is quicker than 2D transvaginal US. The use of 3D transvaginal US with artificial intelligence-based data processing has been employed to establish the threshold dominant follicle volume (0.5 cm3) as a predictor of mature oocyte count in IVF programs. While the role of US in evaluating the endometrium and uterine blood flow for predicting clinical pregnancy rates in IVF is still debated, available research indicates that factors such as endometrial thickness and volume, along with VI, FI, VFI, and S/D ratio in the uterine artery, measured via transvaginal US, may help predict IVF outcomes. Transabdominal oocyte aspiration, using different US sensors, is a feasible, effective, and safe method for oocyte retrieval in IVF programs, particularly for patients with ovaries inaccessible for transvaginal aspiration.

ADDITIONAL INFORMATION

REFERENCES

1. Li YW, Liang XW, Fang JH, Chen ZY. Application of ultrasound markers measured at different time points of COH cycle in the prediction of ovarian response for individualised ovulation induction. *J Obstet Gynaecol.* 2022;42(5):1467–1473. doi: 10.1080/01443615.2021.2004101

2. Ozerskaya IA. *Manual on ultrasound diagnostics in obstetrics and gynecology: textbook.* Moscow: MEDpress-Inform; 2021. (In Russ.). EDN: RNUAOE doi: 10.24421/978-5-00030-860-8

3. Coelho Neto MA, Ludwin A, Borrell A, et al. Counting ovarian antral follicles by ultrasound: a practical guide. *Ultrasound Obstet Gynecol.* 2018;51(1):10–20. doi: 10.1002/uog.18945

4. Zhang Y, Xu Y, Xue Q, et al. Discordance between antral follicle counts and anti-Müllerian hormone levels in women undergoing in vitro fertilization. *Reprod Biol Endocrinol.* 2019;17(1):51. doi: 10.1186/s12958-019-0497-4

5. Wang X, Jin L, Mao YD, et al. Evaluation of Ovarian Reserve Tests and Age in the Prediction of Poor Ovarian Response to Controlled Ovarian Stimulation-A Real-World Data Analysis of 89,002 Patients. *Front Endocrinol (Lausanne).* 2021;12:702061. doi: 10.3389/fendo.2021.702061

6. Arvis P, Rongières C, Pirrello O, Lehert P. Reliability of AMH and AFC measurements and their correlation: a large multicenter study. *J Assist Reprod Genet.* 2022;39(5):1045–1053. doi: 10.1007/s10815-022-02449-5

7. Liu Y, Pan Z, Wu Y, et al. Comparison of anti-Müllerian hormone and antral follicle count in the prediction of ovarian response: a systematic review and meta-analysis. *J Ovarian Res.* 2023;16(1):117. doi: 10.1186/s13048-023-01202-5

8. Jacobs MH, Reuter LM, Baker VL, et al. A multicentre evaluation of the Elecsys anti-Müllerian hormone immunoassay for prediction of antral follicle count. *Reprod Biomed Online.* 2019;38(5):845–852. doi: 10.1016/j.rbmo.2018.12.041

9. Razafintsalama-Bourdet M, Bah M, Amand G, et al. Random antral follicle count performed on any day of the menstrual cycle has the same predictive value as AMH for good ovarian response in IVF cycles. *J Gynecol Obstet Hum Reprod.* 2022;51(1):102233. doi: 10.1016/j.jogoh.2021.102233

10. Rombauts L, Onwude JL, Chew HW, Vollenhoven BJ. The predictive value of antral follicle count remains unchanged across the menstrual cycle. *Fertil Steril.* 2011;96(6):1514–1518. doi: 10.1016/j.fertnstert.2011.09.005

11. Filippi F, Martinelli F, Paffoni A, et al. Fertility preservation in women with malignancies: the accuracy of antral follicle count collected randomly during the menstrual cycle in predicting the number of oocytes retrieved. *J Assist Reprod Genet.* 2019;36(3):569–578. doi: 10.1007/s10815-018-1377-0

12. Chen Q, Sun L, Huang J, et al. Three-dimensional transvaginal ultrasonography in the evaluation of diminished ovarian reserve and premature ovarian failure. *Pak J Med Sci.* 2023;39(3):747–751. doi: 10.12669/pjms.39.3.7372

13. Mathur P, Kakwani K, Diplav, et al. Deep Learning based Quantification of Ovary and Follicles using 3D Transvaginal Ultrasound in Assisted Reproduction. *Annu Int Conf IEEE Eng Med Biol Soc.* 2020;2020:2109–2112. doi: 10.1109/EMBC44109.2020.9176703

14. Srivastava D, Gupta S, Kudavelly S, et al. Unsupervised Deep Learning based Longitudinal Follicular Growth Tracking during IVF Cycle using 3D Transvaginal Ultrasound in Assisted Reproduction. *Annu Int Conf IEEE Eng Med Biol Soc.* 2021;2021:3209–3212. doi: 10.1109/EMBC46164.2021.9630495

15. Raine-Fenning N, Jayaprakasan K, Deb S, et al. Automated follicle tracking improves measurement reliability in patients undergoing ovarian stimulation. *Reprod Biomed Online.* 2009;18(5):658–663. doi: 10.1016/s1472-6483(10)60010-7

16. Re C, Mignini Renzini M, Rodriguez A, et al. From a circle to a sphere: the ultrasound imaging of ovarian follicle with 2D and 3D technology. *Gynecol Endocrinol.* 2019;35(3):184–189. doi: 10.1080/09513590.2018.1522297

17. Yang J, Gao J, Wang Y, et al. Impact of follicular size categories on oocyte quality at trigger day in young and advanced-age patients undergoing GnRH-ant therapy. *Front Endocrinol (Lausanne).* 2023;14:1167395. doi: 10.3389/fendo.2023.1167395

18. Abbara A, Patel A, Hunjan T, et al. FSH Requirements for Follicle Growth During Controlled Ovarian Stimulation. *Front Endocrinol (Lausanne).* 2019;10:579. doi: 10.3389/fendo.2019.00579

19. Shapiro BS, Rasouli MA, Verma K, et al. The effect of ovarian follicle size on oocyte and embryology outcomes. *Fertil Steril.* 2022;117(6):1170–1176. doi: 10.1016/j.fertnstert.2022.02.017

20. Liang X, Zeng F, Li H, et al. Deep Learning Based Two-Dimensional Ultrasound for Follicle Monitoring in Infertility Patients. *BIOI.* 2023;4(3):125–131. doi: 10.15212/bioi-2022-0024

21. Liang X, Liang J, Zeng F, et al. Evaluation of oocyte maturity using artificial intelligence quantification of follicle volume biomarker by three-dimensional ultrasound. *Reprod Biomed Online.* 2022;45(6):1197–1206. doi: 10.1016/j.rbmo.2022.07.012

22. Devine K, Dolitsky S, Ludwin I, Ludwin A. Modern assessment of the uterine cavity and fallopian tubes in the era of high-efficacy assisted reproductive technology. *Fertil Steril.* 2022;118(1):19–28. doi: 10.1016/j.fertnstert.2022.05.020

23. Kasius A, Smit JG, Torrance HL, et al. Endometrial thickness and pregnancy rates after IVF: a systematic review and meta-analysis. *Hum Reprod Update.* 2014;20(4):530–541. doi: 10.1093/humupd/dmu011

24. Zhang T, He Y, Wang Y, et al. The role of three-dimensional power Doppler ultrasound parameters measured on hCG day in the prediction of pregnancy during in vitro fertilization treatment. *Eur J Obstet Gynecol Reprod Biol.* 2016;203:66–71. doi: 10.1016/j.ejogrb.2016.05.016

25. Wu J, Sheng J, Wu X, Wu Q. Ultrasound-assessed endometrial receptivity measures for the prediction of in vitro fertilization-embryo transfer clinical pregnancy outcomes: A meta-analysis and systematic review. *Exp Ther Med.* 2023;26(3):453. doi: 10.3892/etm.2023.12152

26. ESHRE Working Group on Ultrasound in ART; D'Angelo A, Panayotidis C, Amso N, et al. Recommendations for good practice in ultrasound: oocyte pick up. *Hum Reprod Open.* 2019;2019(4):hoz025. doi: 10.1093/hropen/hoz025

27. Roman-Rodriguez CF, Weissbrot E, Hsu CD, et al. Comparing transabdominal and transvaginal ultrasound-guided follicular aspiration: A risk assessment formula. *Taiwan J Obstet Gynecol.* 2015;54(6):693–699. doi: 10.1016/j.tjog.2015.02.004

28. Sönmezer M, Gülümser Ç, Sönmezer M, et al. Transabdominal ultrasound guided oocyte retrieval using vaginal ultrasound probe: Definition of the technique. *J Obstet Gynaecol Res.* 2021;47(2):800–806. doi: 10.1111/jog.14618

29. Sönmezer M, Saçıntı KG, Gülümser Ç, et al. Transabdominal ultrasound-guided oocyte retrieval for oocyte cryopreservation using a vaginal probe: a comparison of applicability, effectiveness, and safety with conventional transvaginal approach. *J Assist Reprod Genet.* 2023;40(2):399–405. doi: 10.1007/s10815-022-02705-8

30. Raziel A, Vaknin Z, Schachter M, et al. Ultrasonographic-guided percutaneous transabdominal puncture for oocyte retrieval in a rare patient with Rokitansky syndrome in an in vitro fertilization surrogacy program. *Fertil Steril.* 2006;86(6):1760–1763. doi: 10.1016/j.fertnstert.2006.05.039

31. Barton SE, Politch JA, Benson CB, et al. Transabdominal follicular aspiration for oocyte retrieval in patients with ovaries inaccessible by transvaginal ultrasound. *Fertil Steril.* 2011;95(5):1773–1776. doi: 10.1016/j.fertnstert.2011.01.006

СПИСОК ЛИТЕРАТУРЫ

1. Li Y.W., Liang X.W., Fang J.H., Chen Z.Y. Application of ultrasound markers measured at different time points of COH cycle in the prediction of ovarian response for individualised ovulation induction // J Obstet Gynaecol. 2022. Vol. 42, N 5. P. 1467–1473. doi: 10.1080/01443615.2021.2004101

2. Озерская И.А. Руководство по ультразвуковой диагностике в акушерстве и гинекологии: учебно-методическое пособие. Москва: МЕДпресс-информ, 2021. EDN: RNUAOE doi: 10.24421/978-5-00030-860-8

3. Coelho Neto M.A., Ludwin A., Borrell A., et al. Counting ovarian antral follicles by ultrasound: a practical guide // Ultrasound Obstet Gynecol. 2018. Vol. 51, N 1. P. 10–20. doi: 10.1002/uog.18945

4. Zhang Y., Xu Y., Xue Q., et al. Discordance between antral follicle counts and anti-Müllerian hormone levels in women undergoing in vitro fertilization // Reprod Biol Endocrinol. 2019. Vol. 17, N 1. ID 51. doi: 10.1186/s12958-019-0497-4

5. Wang X., Jin L., Mao Y.D., et al. Evaluation of Ovarian Reserve Tests and Age in the Prediction of Poor Ovarian Response to Controlled Ovarian Stimulation-A Real-World Data Analysis of 89,002 Patients // Front Endocrinol (Lausanne). 2021. Vol. 12. ID 702061. doi: 10.3389/fendo.2021.702061

6. Arvis P., Rongières C., Pirrello O., Lehert P. Reliability of AMH and AFC measurements and their correlation: a large multicenter study // J Assist Reprod Genet. 2022. Vol. 39, N 5. P. 1045–1053. doi: 10.1007/s10815-022-02449-5

7. Liu Y., Pan Z., Wu Y., et al. Comparison of anti-Müllerian hormone and antral follicle count in the prediction of ovarian response: a systematic review and meta-analysis // J Ovarian Res. 2023. Vol. 16, N 1. ID 117. doi: 10.1186/s13048-023-01202-5

8. Jacobs M.H., Reuter L.M., Baker V.L., et al. A multicentre evaluation of the Elecsys anti-Müllerian hormone immunoassay for prediction of antral follicle count // Reprod Biomed Online. 2019. Vol. 38, N 5. P. 845–852. doi: 10.1016/j.rbmo.2018.12.041

9. Razafintsalama-Bourdet M., Bah M., Amand G., et al. Random antral follicle count performed on any day of the menstrual cycle has the same predictive value as AMH for good ovarian response in IVF cycles // J Gynecol Obstet Hum Reprod. 2022. Vol. 51, N 1. ID 102233. doi: 10.1016/j.jogoh.2021.102233

10. Rombauts L., Onwude J.L., Chew H.W., Vollenhoven B.J. The predictive value of antral follicle count remains unchanged across the menstrual cycle // Fertil Steril. 2011. Vol. 96, N 6. P. 1514–1518. doi: 10.1016/j.fertnstert.2011.09.005

11. Filippi F., Martinelli F., Paffoni A., et al. Fertility preservation in women with malignancies: the accuracy of antral follicle count collected randomly during the menstrual cycle in predicting the number of oocytes retrieved // J Assist Reprod Genet. 2019. Vol. 36, N 3. P. 569–578. doi: 10.1007/s10815-018-1377-0

12. Chen Q., Sun L., Huang J., et al. Three-dimensional transvaginal ultrasonography in the evaluation of diminished ovarian reserve and premature ovarian failure // Pak J Med Sci. 2023. Vol. 39, N 3. P. 747–751. doi: 10.12669/pjms.39.3.7372

13. Mathur P., Kakwani K., Diplav, et al. Deep Learning based Quantification of Ovary and Follicles using 3D Transvaginal Ultrasound in Assisted Reproduction // Annu Int Conf IEEE Eng Med Biol Soc. 2020. Vol. 2020. P. 2109–2112. doi: 10.1109/EMBC44109.2020.9176703

14. Srivastava D., Gupta S., Kudavelly S., et al. Unsupervised Deep Learning based Longitudinal Follicular Growth Tracking during IVF Cycle using 3D Transvaginal Ultrasound in Assisted Reproduction // Annu Int Conf IEEE Eng Med Biol Soc. 2021. Vol. 2021. P. 3209–3212. doi: 10.1109/EMBC46164.2021.9630495

15. Raine-Fenning N., Jayaprakasan K., Deb S., et al. Automated follicle tracking improves measurement reliability in patients undergoing ovarian stimulation // Reprod Biomed Online. 2009. Vol. 18, N 5. P. 658–663. doi: 10.1016/s1472-6483(10)60010-7

16. Re C., Mignini Renzini M., Rodriguez A., et al. From a circle to a sphere: the ultrasound imaging of ovarian follicle with 2D and 3D technology // Gynecol Endocrinol. 2019. Vol. 35, N 3. P. 184–189. doi: 10.1080/09513590.2018.1522297

17. Yang J., Gao J., Wang Y., et al. Impact of follicular size categories on oocyte quality at trigger day in young and advanced-age patients undergoing GnRH-ant therapy // Front Endocrinol (Lausanne). 2023. Vol. 14. ID 1167395. doi: 10.3389/fendo.2023.1167395

18. Abbara A., Patel A., Hunjan T., et al. FSH Requirements for Follicle Growth During Controlled Ovarian Stimulation // Front Endocrinol (Lausanne). 2019. Vol. 10. ID 579. doi: 10.3389/fendo.2019.00579

19. Shapiro B.S., Rasouli M.A., Verma K., et al. The effect of ovarian follicle size on oocyte and embryology outcomes // Fertil Steril. 2022. Vol. 117, N 6. P. 1170–1176. doi: 10.1016/j.fertnstert.2022.02.017

20. Liang X., Zeng F., Li H., et al. Deep Learning Based Two-Dimensional Ultrasound for Follicle Monitoring in Infertility Patients // BIOI. 2023. Vol. 4, N 3. P. 125–131. doi: 10.15212/bioi-2022-0024

21. Liang X., Liang J., Zeng F., et al. Evaluation of oocyte maturity using artificial intelligence quantification of follicle volume biomarker by three-dimensional ultrasound // Reprod Biomed Online. 2022. Vol. 45, N 6. P. 1197–1206. doi: 10.1016/j.rbmo.2022.07.012

22. Devine K., Dolitsky S., Ludwin I., Ludwin A. Modern assessment of the uterine cavity and fallopian tubes in the era of high-efficacy assisted reproductive technology // Fertil Steril. 2022. Vol. 118, N 1. P. 19–28. doi: 10.1016/j.fertnstert.2022.05.020

23. Kasius A., Smit J.G., Torrance H.L., et al. Endometrial thickness and pregnancy rates after IVF: a systematic review and meta-analysis // Hum Reprod Update. 2014. Vol. 20, N 4. P. 530–541. doi: 10.1093/humupd/dmu011

24. Zhang T., He Y., Wang Y., et al. The role of three-dimensional power Doppler ultrasound parameters measured on hCG day in the prediction of pregnancy during in vitro fertilization treatment // Eur J Obstet Gynecol Reprod Biol. 2016. Vol. 203. P. 66–71. doi: 10.1016/j.ejogrb.2016.05.016

25. Wu J., Sheng J., Wu X., Wu Q. Ultrasound-assessed endometrial receptivity measures for the prediction of in vitro fertilization-embryo transfer clinical pregnancy outcomes: A meta-analysis and systematic review // Exp Ther Med. 2023. Vol. 26, N 3. ID 453. doi: 10.3892/etm.2023.12152

26. ESHRE Working Group on Ultrasound in ART; D'Angelo A., Panayotidis C., Amso N., et al. Recommendations for good practice in ultrasound: oocyte pick up // Hum Reprod Open. 2019. Vol. 2019, N 4. ID hoz025. doi: 10.1093/hropen/hoz025

27. Roman-Rodriguez C.F., Weissbrot E., Hsu C.D., et al. Comparing transabdominal and transvaginal ultrasound-guided follicular aspiration: A risk assessment formula // Taiwan J Obstet Gynecol. 2015. Vol. 54, N 6. P. 693–699. doi: 10.1016/j.tjog.2015.02.004

28. Sönmezer M., Gülümser Ç., Sönmezer M., et al. Transabdominal ultrasound guided oocyte retrieval using vaginal ultrasound probe: Definition of the technique // J Obstet Gynaecol Res. 2021. Vol. 47, N 2. P. 800–806. doi: 10.1111/jog.14618

29. Sönmezer M., Saçıntı K.G., Gülümser Ç., et al. Transabdominal ultrasound-guided oocyte retrieval for oocyte cryopreservation using a vaginal probe: a comparison of applicability, effectiveness, and safety with conventional transvaginal approach // J Assist Reprod Genet. 2023. Vol. 40, N 2. P. 399–405. doi: 10.1007/s10815-022-02705-8

30. Raziel A., Vaknin Z., Schachter M., et al. Ultrasonographic-guided percutaneous transabdominal puncture for oocyte retrieval in a rare patient with Rokitansky syndrome in an in vitro fertilization surrogacy program // Fertil Steril. 2006. Vol. 86, N 6. P. 1760–1763. doi: 10.1016/j.fertnstert.2006.05.039

31. Barton S.E., Politch J.A., Benson C.B., et al. Transabdominal follicular aspiration for oocyte retrieval in patients with ovaries inaccessible by transvaginal ultrasound // Fertil Steril. 2011. Vol. 95, N 5. P. 1773–1776. doi: 10.1016/j.fertnstert.2011.01.006

AUTHOR'S INFO

* Evgeniya V. Kirakosyan, MD, Cand. Sci. (Medicine);
address: 42 Lobachevsky str., 119415, Moscow, Russia;
ORCID: 0000-0002-6021-2449;
eLibrary SPIN: 4813-5625;
e-mail: evgeniya.kirakosyan@gmail.com

ОБ АВТОРЕ

* Киракосян Евгения Валериковна, канд. мед. наук;
адрес: Россия, 119415, Москва, ул. Лобачевского, д. 42;
ORCID: 0000-0002-6021-2449;
eLibrary SPIN: 4813-5625;
e-mail: evgeniya.kirakosyan@gmail.com

Magnetic resonance imaging in diagnosis of serous adenocarcinoma of fallopian tubes: a case report

Oleg I. Mynko[1,2], Anna P. Gonchar[1,3], Valentin A. Nechaev[3], Evgeniya A. Kulikova[3],
Andrey L. Yudin[2,3], Elena A. Yumatova[2,3]

[1] Research and Practical Clinical Center for Diagnostics and Telemedicine Technologies, Russia;
[2] Pirogov Russian National Research Medical University, Russia;
[3] City Clinical Oncological Hospital 1, Russia

ABSTRACT

Serous adenocarcinoma of fallopian tubes is an extremely rare and difficult-to-diagnose type of cancer of the female reproductive system. This condition is often asymptomatic or has a non-specific clinical presentation including serosanguineous vaginal discharge and colic-like pain in the lower abdomen and pelvis. These symptoms are reported in the literature as the Latzko's triad and are considered pathognomonic for tubal cancer, but their combination is observed in less than 15% of patients. The low incidence and lack of the pathognomonic clinical presentation lead to many diagnostic errors or detection of advanced disease, which significantly worsens the patient's prognosis. An accurate surgical diagnosis is made in only 4% of cases. This case report describes serous adenocarcinoma of fallopian tubes with all signs of the Latzko's triad and MRI suggestive of serous adenocarcinoma of fallopian tubes at a preoperative stage.

Keywords: fallopian tube cancer; serous adenocarcinoma of fallopian tubes; magnetic resonance imaging; case report.

Магнитно-резонансная томография в диагностике серозной аденокарциномы фаллопиевых труб: клинический случай

О.И. Мынко[1,2], А.П. Гончар[1,3], В.А. Нечаев[3], Е.А. Куликова[3], А.Л. Юдин[2,3], Е.А. Юматова[2,3]

[1] Научно-практический клинический центр диагностики и телемедицинских технологий, Москва, Россия;

[2] Российский национальный исследовательский медицинский университет им. Н.И. Пирогова, Москва, Россия;

[3] Городская клиническая онкологическая больница №1, Москва, Россия

АННОТАЦИЯ

Серозная аденокарцинома фаллопиевых труб — крайне редкая и сложная для диагностики форма злокачественных новообразований женской репродуктивной системы. Данная патология часто протекает бессимптомно или сопровождается неспецифической клинической картиной, включающей серозно-кровянистые выделения из влагалища, коликообразную боль в нижней части живота и таза. Эти симптомы известны в литературе как триада Лацко и считаются патогномоничными для рака маточной трубы, однако их сочетание наблюдается менее чем у 15% больных. Низкая частота встречаемости и отсутствие патогномоничной клинической картины приводят к высокому числу диагностических ошибок либо к выявлению заболевания уже в запущенной стадии, что существенно ухудшает прогноз для пациента. Точный диагноз на предоперационном этапе устанавливается всего лишь в 4% случаев. В данном клиническом наблюдении приводится описание случая серозной аденокарциномы фаллопиевых труб со всеми проявлениями триады Лацко и МР-картины, позволившей заподозрить наличие у пациентки серозной аденокарциномы фаллопиевых труб на предоперационном этапе.

Ключевые слова: рак фаллопиевых труб; серозная аденокарцинома фаллопиевых труб; магнитно-резонансная томография; описание клинического случая.

磁共振成像在输卵管浆液性腺癌诊断中的应用：临床病例

Oleg I. Mynko[1,2], Anna P. Gonchar[1,3], Valentin A. Nechaev[3], Evgeniya A. Kulikova[3],
Andrey L. Yudin[2,3], Elena A. Yumatova[2,3]

[1] Research and Practical Clinical Center for Diagnostics and Telemedicine Technologies, Russia;
[2] Pirogov Russian National Research Medical University, Russia;
[3] City Clinical Oncological Hospital 1, Russia

摘要

输卵管浆液性腺癌是一种极其罕见且难以诊断的女性生殖系统恶性肿瘤。这种病理通常无症状或伴有非特异性临床表现，包括浆液性血性阴道分泌物、下腹部和骨盆绞痛。这些症状在文献中被称为 "Latzko三联征"，被认为是输卵管癌的标志性症状，但只有不到15%的患者会同时出现这些症状。因其发病率低，临床症状不明显，导致大量诊断错误，或发现时疾病已处于晚期，从而大大恶化了患者的预后。只有4%的病例可在术前得到准确诊断。本临床观察描述了一例输卵管浆液性腺癌病例，该病例具有"Latzko三联征"的所有表现和磁共振成像，因此在术前阶段就被怀疑为输卵管浆液性腺癌。

关键词：输卵管癌；输卵管浆液性腺癌；磁共振成像；临床病例描述。

INTRODUCTION

Serous adenocarcinoma of the fallopian tube (SAFT) is a histological subtype of primary fallopian tube cancer. At present, primary malignancies of the fallopian tube, ovary, and peritoneum are classified together as epithelial ovarian cancer [1], due to their similar clinical presentations and treatment approaches. These cancers are thought to originate from the same precursor cells, as suggested by the shared histological tumor types across all three sites. However, research in this area is still ongoing [1].

Some researchers propose that many cases of ovarian cancer and peritoneal carcinomatosis may originate from undiagnosed fallopian tube cancer. The absence of specific clinical symptoms and imaging characteristics often leads to delayed diagnosis, particularly when the disease has already spread to nearby organs and tissues, making it difficult to pinpoint the primary origin. Detecting fallopian tube cancer in its subclinical phase remains a significant challenge, with most cases diagnosed at an advanced stage, negatively affecting the prognosis [2].

We believe this issue warrants closer attention. This article presents a clinical case of pathologically confirmed SAFT, initially suspected at an early stage based on magnetic resonance imaging (MRI) findings.

CASE DESCRIPTION

Patient information

A 38-year-old female patient was referred to the radiology department at City Clinical Oncology Hospital No. 1 for a contrast-enhanced pelvic MRI to further evaluate bilateral adnexal lesions previously identified through ultrasound (US) and contrast-enhanced computed tomography (CT).

Anamnesis morbi

The patient reported feeling unwell for 2 weeks, presenting with abnormal abdominal pain and heavy menstrual bleeding. These symptoms persisted for 14 days from the onset of her menstrual cycle, leading to her admission to the emergency hospital's gynecology department via ambulance. At the time of admission, her symptoms continued; however, the gynecological examination revealed no abnormalities.

Approximately 10 years earlier, the patient had undergone hysteroscopy for uterine fibroids and had one operative delivery at 38 weeks via lower segment cesarean section.

Upon admission, pelvic US showed a solid mass with irregular margins located in the right ovary. The lesion, measuring about 100 × 60 × 80 mm, demonstrated active vascularity on color flow Doppler (Ovarian-Adnexal Reporting and Data System [O-RADS] 4) and occupied the rectouterine pouch and the entire right adnexal region. The left ovary was not clearly visualized. Additionally, up to 1,000 mL of free fluid (ascites) was detected in the pelvic cavity.

The following morning, a contrast-enhanced CT scan of the abdomen and pelvis revealed ascites and partially calcified cystic and solid formations in the right adnexal area (Fig. 1).

Laboratory tests showed no evidence of inflammation. However, tumor marker levels were elevated: CA-125 was 682.9 IU/mL (reference range, 0.0–35.0 IU/mL) and HE-4 was 106.1 pmol/L (reference range, 0.0–60.5 pmol/L).

The patient was treated with symptomatic medications, including tranexamic acid 500 mg twice daily intravenously and ketorolac 60 mg twice daily intramuscularly.

After symptom resolution and clinical improvement, she was discharged from the gynecology department for outpatient follow-up by a local oncologist to continue diagnostic evaluation and determine an appropriate treatment plan.
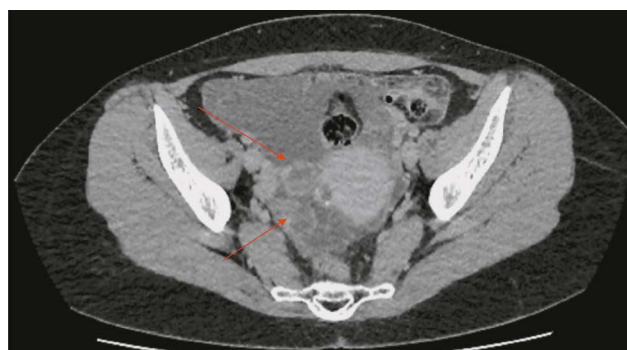

Fig. 1. Pelvic computed tomography (axial view). Rounded cystic and solid lesions (indicated by red arrows) and free fluid (ascites) are visible in the right ovarian area.

Findings of physical, laboratory, and imaging examinations

Five days later, the patient presented to the radiology department of City Clinical Oncology Hospital No. 1 for a contrast-enhanced pelvic MRI. The exam was conducted following a standard protocol, utilizing T1, T2, STIR, and DWI/ADC sequences, both with and without contrast (Gadovist).

MRI results showed that the ovaries were not enlarged and contained follicles; a hemorrhagic cyst was identified in the right ovary (Figs. 2 and 3).

A tubular structure with high fluid signal intensity and an irregular lumen, measuring up to 17 mm, was located adjacent to the anterior and outer contours of the right ovary. This structure had multiple hypervascular solid nodules on the walls and showed signs of restricted diffusion in the DWI sequence (Fig. 4). A smaller structure with similar MRI characteristics was observed on the left (Fig. 5).

The remaining pelvic organs appeared normal, with a small amount of free fluid present in the pelvic cavity. No signs of peritoneal carcinomatosis were detected on MRI.

The final conclusions from the MRI findings were as follows: a fallopian tube lesion (O-RADS 5), right ovarian

endometrioma, simple cyst of the left ovary, and a small amount of fluid in the pelvic cavity.

Differential diagnosis

Diagnosing primary fallopian tube tumors before surgery is difficult due to the nonspecific nature of both clinical symptoms and imaging findings. The differential diagnosis typically includes the following conditions:

- Primary ovarian cancer with involvement of the fallopian tube
- Tubal ectopic pregnancy
- Adnexitis, including tubo-ovarian abscess

Treatment

After the examination, the patient was admitted to the gynecologic oncology department. An elective surgery was performed, which included radical hysterectomy,
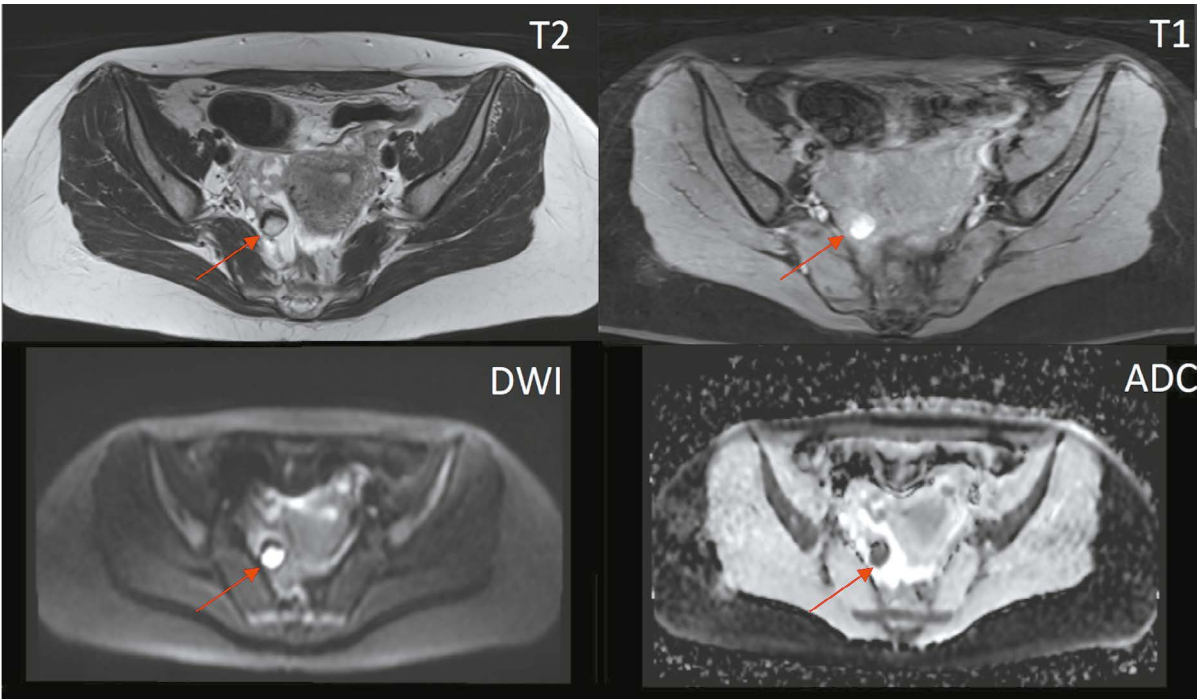
Fig. 2. Pelvic magnetic resonance imaging (axial view). A single hemorrhagic cyst is observed in the stroma of the right ovary (O-RADS 1, red arrow).
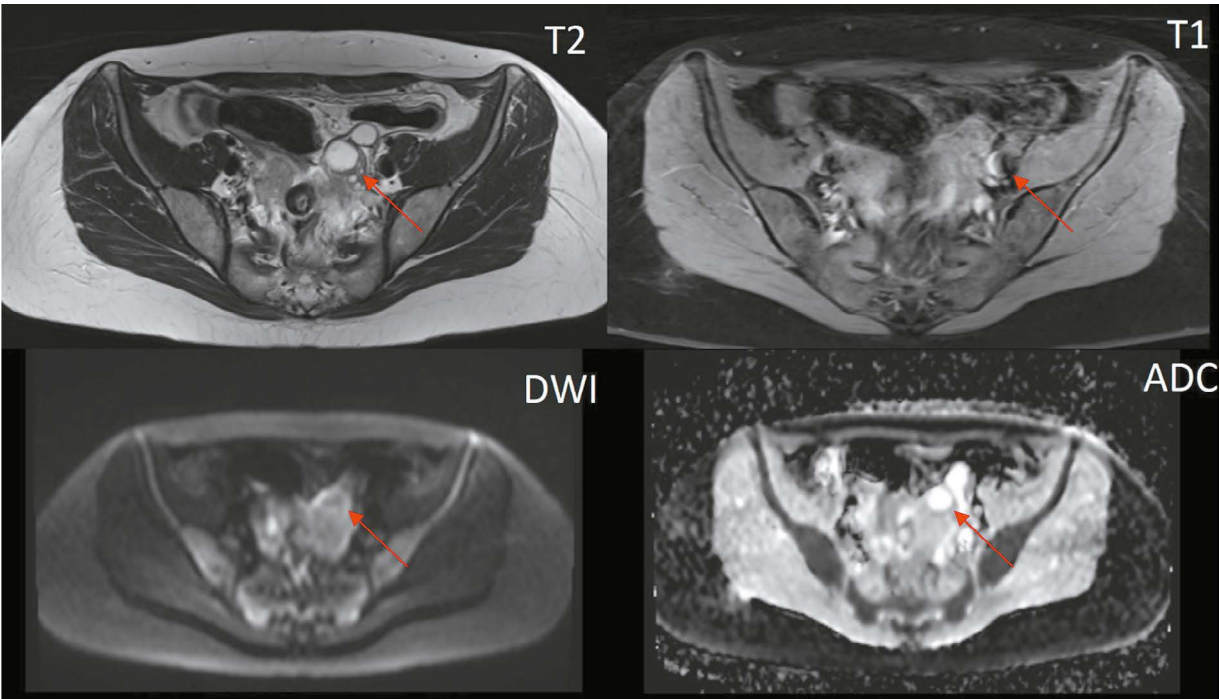
Fig. 3. Pelvic magnetic resonance imaging (axial view). The left ovary shows follicles and a simple cyst (O-RADS 1, red arrow).
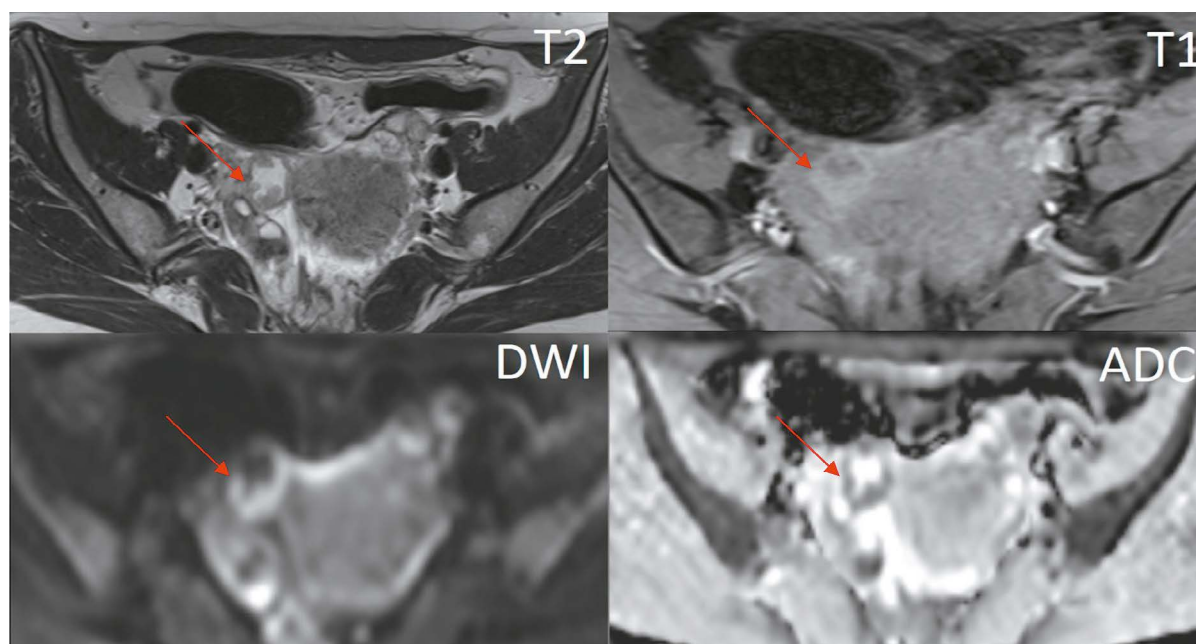
Fig. 4. Pelvic magnetic resonance imaging (axial view). The right fallopian tube contains fluid and solid nodules, with signs of restricted diffusion on DWI mode (red arrow).
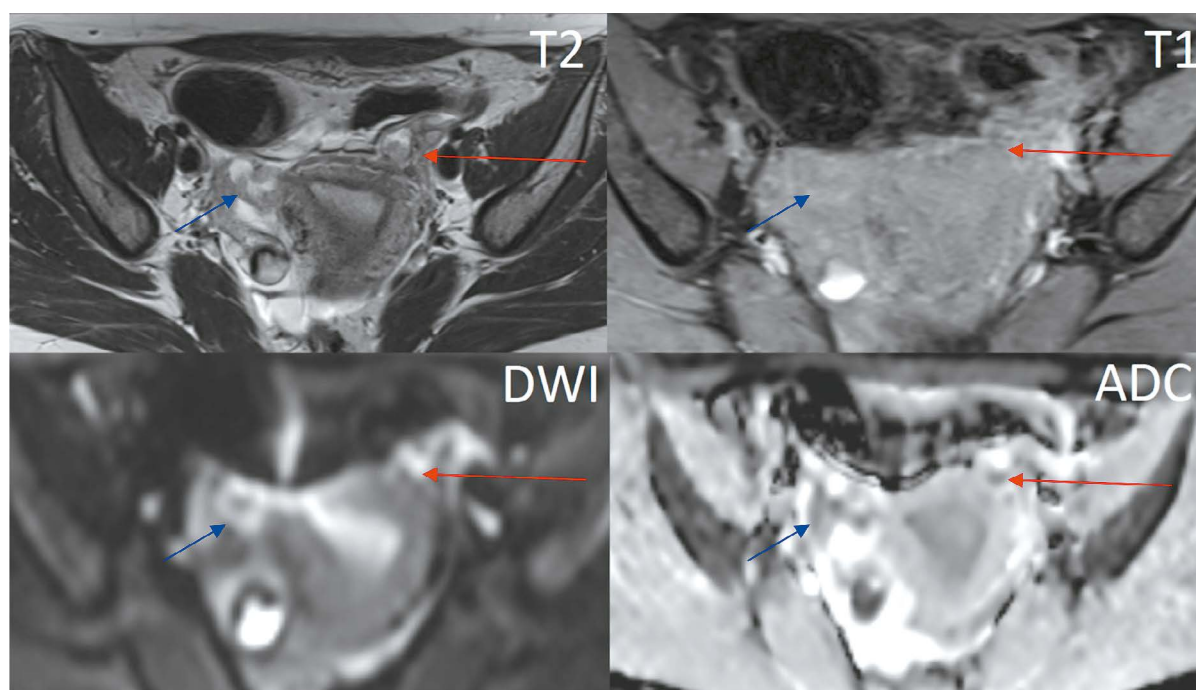
Fig. 5. Pelvic magnetic resonance imaging (axial view). Similar solid nodules are present in the left fallopian tube (red arrow). The right fallopian tube appears convoluted in this slice (blue arrow).

omentectomy, and adhesiolysis. Intraoperative and urgent histological examinations showed no evidence of peritoneal carcinomatosis.

The histology and immunohistochemistry results indicated the tumor was a high-grade SAFT.

Based on the disease stage, the surgical treatment performed, and the findings from histology and physical examinations, the oncology team decided to proceed with six cycles of adjuvant chemotherapy and genetic testing for *BRCA1* and *BRCA2* mutations.

Follow-up and outcomes

At the time of writing, the patient had completed a chemotherapy course with paclitaxel and carboplatin, which was well tolerated. No mutations in *BRCA1* or *BRCA2* were found.

DISCUSSION

Published data shows that the incidence of primary fallopian tube cancer ranges from 0.36 to 0.41 cases per 100,000 women

annually, or approximately 300–400 cases per year [3, 4]. Ulrich et al. reported 69 morphologically confirmed cases of SAFT between 1980 and 2005 at the pathology laboratory of the N.N. Petrov National Medical Research Center of Oncology and the Leningrad Region Cancer Center. As a result, Russian experts estimate that SAFT represents 0.14%–1.8% of all female genital cancers [5].

However, the actual incidence may be higher, as SAFT is often misdiagnosed as ovarian cancer. It is generally believed that primary fallopian tube cancer accounts for about 1% (0.2%–1.1%) of all gynecologic cancers, making it one of the rarest conditions in gynecologic oncology [6].

Statistically, this condition is more common in postmenopausal women aged 50–60 years. Primary fallopian tube cancer is 14% more prevalent in Caucasian women compared to other racial groups [7].

The main risk factors for fallopian tube cancer are similar to those for ovarian cancer and include the following [8]:
- Family history
- *BRCA1* or *BRCA2* mutations
- Other hereditary conditions, such as hereditary nonpolyposis colorectal cancer (Lynch syndrome)
- Endometriosis
- Hormone replacement therapy (including postmenopausal use)
- Obesity

In this clinical case, the patient was in premenopause at the time of disease onset and had no history of the risk factors mentioned earlier.

The disease is usually asymptomatic or presents with nonspecific symptoms. Latzko's triad, which includes serosanguineous vaginal discharge, colic-like lower abdominal pain, and a palpable or visualized pelvic mass, is seen in fewer than 15% of cases [9]. In this case, the patient exhibited all three components of Latzko's triad, highlighting its clinical importance.

Due to the nonspecific nature of symptoms, radiological findings are essential for detecting fallopian tube neoplasms. US remains the primary diagnostic tool for identifying adnexal lesions, though differentiating between ovarian and fallopian tube neoplasms is often difficult due to its limitations. CT imaging is particularly useful for cancer staging and detecting distant metastases, especially when combined with positron emission tomography [10]. However, among all imaging techniques, MRI provides the highest sensitivity and specificity in diagnosing fallopian tube neoplasms, as it most effectively distinguishes between the soft tissue structures of the pelvic organs [11, 12]. MRI findings are key in making the diagnosis, staging the tumor, planning treatment, and preparing for any necessary surgeries.

In current clinical practice, MRI examinations of the uterine adnexa are typically performed using the O-RADS. The approach provided by the O-RADS authors takes into account various factors, including MRI signal, tumor size and structure, as well as signs of restricted diffusion and/or abnormal contrast uptake. These criteria can be applied to ovarian lesions, fallopian tube lesions (as in our case), and adjacent ligament lesions (round, broad, or utero-ovarian ligament) [13, 14]. The most common MRI findings that raise suspicions for fallopian tube cancer include the following [15]:
- Oblong or tubular lesions in the adnexal area, often with relatively uniform fluid signal intensity (low on T1WI and high on T2WI). In our case, the lesion contained several solid foci on the walls, clearly visible against the backdrop of the distended fallopian tube. These solid foci showed restricted diffusion on DWI/ADC and early contrast uptake in the dynamic contrast-enhanced sequence.
- Fluid in the fallopian tubes (hydrosalpinx): This condition results from tumor secretions that block the fallopian tube, causing colic-like pelvic pain due to stretching. The contents of the hydrosalpinx can vary, leading to different MRI signals. In our case, the fallopian tubes were distended with serous fluid, although a hemorrhagic component due to recurrent bleeding is also possible.
- If the fallopian tube is unobstructed, there may be fluid or serosanguineous contents in the uterine cavity or free fluid in the pelvic cavity.

Primary fallopian tube cancer is generally not considered a separate disease due to its rarity and nonspecific symptoms. For instance, the World Health Organization classifies primary cancers of the peritoneum, ovaries, and fallopian tubes as a single group because of their similar pathogenesis and treatment options [1]. The International Federation of Gynecology and Obstetrics follows a similar classification, including stromal and germ cell tumors in this group as well [16, 17]. According to the current guidelines from the Ministry of Health of Russia, ovarian cancer, fallopian tube cancer, and primary peritoneal cancer are also grouped together as malignant tumors because they originate from the epithelium of these organs and share similar clinical course and treatment strategies [18].

However, despite these classifications, several international and Russian studies suggest that many cases of ovarian cancer may actually be caused by fallopian tube lesions [18–21]. Although the two cancers share similar histological features, the 5-year survival rate for fallopian tube cancer is lower than that for ovarian cancer (50% vs. 77%) [22].

As mentioned earlier, the treatment approaches for ovarian and fallopian tube cancers are similar, regardless of histological type. These typically include surgical treatment, which is based on the tumor stage (usually radical hysterectomy), and adjuvant chemotherapy with carboplatin and paclitaxel [18, 23, 25].

The 5-year survival rate for fallopian tube cancer depends on the stage at diagnosis. According to the American Cancer Society and the Surveillance, Epidemiology, and End Results program, if fallopian tube cancer is diagnosed early, before it spreads beyond the ovaries and fallopian tubes, the 5-year survival rate can reach 93%. However, if surrounding tissues or organs are affected, the survival rate drops to 74%, and with distant metastases, it further decreases to 31% [24, 26].

Given these statistics, we urge the medical community to focus on providing additional educational materials and programs for medical imaging professionals to improve awareness of the diagnostic tools and clinical signs of SAFT [27, 28].

CONCLUSION

This paper presents a rare clinical case. While the clinical presentation was typical, it was the MRI findings that raised the suspicion of primary fallopian tube cancer before surgery. We believe primary fallopian tube cancer should be more routinely considered in the differential diagnosis of patients with suspected adnexal malignancies. Some studies suggest that this cancer could lead to other malignant tumors that are currently regarded as separate disease entities.

ADDITIONAL INFORMATION

REFERENCES

1. Meinhold-Heerlein I, Fotopoulou C, Harter P, et al. The new WHO classification of ovarian, fallopian tube, and primary peritoneal cancer and its clinical implications. *Arch Gynecol Obstet.* 2016;293(4):695–700. doi: 10.1007/s00404-016-4035-8

2. Burghardt E, Girardi F, Lahousen M, et al. Patterns of pelvic and paraaortic lymph node involvement in ovarian cancer. *Gynecol Oncol.* 1991;40(2):103–106. doi: 10.1016/0090-8258(91)90099-q

3. Stasenko M, Fillipova O, Tew W. Fallopian Tube Carcinoma. *J Oncol Pract.* 2019;15(7):375–382. doi: 10.1200/JOP.18.00662

4. Reid B, Permuth J, Sellers T. Epidemiology of ovarian cancer: a review. *Cancer Biol Med.* 2017;14(1):9–32. doi: 10.20892/j.issn.2095-3941.2016.0084

5. Ulrikh EA, Papunidi MD, Urmancheeva AF, Matsko DE. Fallopian tube carcinoma: clinical and morphological features, analysis of 69 cases. *Voprosy onkologii.* 2014;60(3):375–378. EDN: SJTCOH

6. Kim MY, Rha SE, Oh SN, et al. MR Imaging findings of hydrosalpinx: a comprehensive review. *Radiographics.* 2009;29(2):495–507. doi: 10.1148/rg.292085070

7. Riska A, Leminen A. Updating on primary fallopian tube carcinoma. *Acta Obstet Gynecol Scand.* 2007;86:1419–1426. doi: 10.1080/00016340701771034

8. PDQ Adult Treatment Editorial Board. Ovarian Epithelial, Fallopian Tube, and Primary Peritoneal Cancer Treatment (PDQ®): Health Professional Version. 2023. In: PDQ Cancer Information Summaries [Internet]. Bethesda (MD): National Cancer Institute (US), 2002. Available from: https://www.ncbi.nlm.nih.gov/books/NBK66007/

9. Kalampokas E, Kalampokas T, Tourountous I. Primary fallopian tube carcinoma. *Eur J Obstet Gynecol Reprod Biol.* 2013;169(2):155–161. doi: 10.1016/j.ejogrb.2013.03.023

10. Carvalho J, Moretti-Marques R, Filho A. Adnexal mass: diagnosis and management. *Rev Bras Ginecol Obstet.* 2020;42(7):438–443. doi: 10.1055/s-0040-1715547

11. Anthoulakis C, Nikoloudis N. Pelvic MRI as the "gold standard" in the subsequent evaluation of ultrasound-indeterminate adnexal lesions: a systematic review. *Gynecol Oncol.* 2014;132(3):661–668. doi: 10.1016/j.ygyno.2013.10.022

12. Nishino M, Hayakawa K, Minami M, et al. Primary retroperitoneal neoplasms: CT and MR imaging findings with anatomic and pathologic diagnostic clues. *Radiographics.* 2003;23(1):45–57. doi: 10.1148/rg.231025037

13. Sadowski E, Thomassin-Naggara I, Rockall A, et al. O-RADS MRI Risk Stratification System: Guide for Assessing Adnexal Lesions from the ACR O-RADS Committee. *Radiology.* 2022;303(1):35–47. doi: 10.1148/radiol.204371

14. Bulanov MN, Chekalova MA, Mazurkevich MN, Vetsheva NN. Primenenie sistemy O-RADS pri ultrazvukovom issledovanii pridatkov matki. Moscow: Research and Practical Clinical Center for Diagnostics and Telemedicine Technologies of the Moscow Health Care Department, 2022. 27 p. (In Russ.) EDN: BUBNGP

15. Veloso G, Dias F, Lucas R, Cunha T. Primary fallopian tube carcinoma: review of MR imaging findings. *Insights Imaging.* 2015;6(4):431–439. doi: 10.1007/s13244-015-0416-y

16. Duska LR, Kohn EC. The new classifications of ovarian, fallopian tube, and primary peritoneal cancer and their clinical implications. *Ann Oncol.* 2017;28(suppl_8):viii8-viii12. doi: 10.1093/annonc/mdx445

17. Nudnov NV, Ivashina SV, Aksenova SP. Radiation methods in the diagnosis of primary and recurrent malignant ovarian struma: A case report. *Digital Diagnostics.* 2023;4(2):214–225. EDN: YNASOM doi: 10.17816/DD322846

18. Klinicheskie rekomendatsii MZ RF "Rak yaichnikov / rak matochnoi truby / pervichnyi rak bryushiny". 2022. Ministerstvo zdravookhraneniya RF. Available from: https://oncology.ru/specialist/treatment/references/actual/547.pdf

19. Singh N, Gilks C, Wilkinson N, et al. Assignment of primary site in high-grade serous tubal, ovarian and peritoneal carcinoma: a proposal. *Histopathology.* 2014;65(2):149–154. doi: 10.1111/his.12419

20. Zhordania KI, Payanidi YuG, Kalinicheva EV. Two ways of the development of serous epithelial "Ovarian" cancer. *Oncogynecology.* 2014;(3):42–48. EDN: TAOOQL

21. Zhordania KI, Payanidi YuG, Kalinicheva EV. Novaya paradigma v etiologii seroznogo raka yaichnikov. *Rossiiskii bioterapevticheskii zhurnal.* (In Russ.) 2014;13(2):95–102. EDN: SNANEL

22. Zhordania KI. Serous ovarian carcinoma or serous carcinoma of uterine (fallopian) tube? *Oncogynecology.* 2012;(3):4–9. EDN: SZRFTZ

23. SEER*Explorer: An interactive website for SEER cancer statistics [Internet]. Surveillance Research Program, National Cancer Institute; 2023. Available from: https://seer.cancer.gov/statistics-network/explorer/

24. Tokunaga H, Mikami M, Nagase S, et al. The 2020 Japan Society of Gynecologic Oncology guidelines for the treatment of ovarian cancer, fallopian tube cancer, and primary peritoneal cancer. *J Gynecol Oncol.* 2021;32(2):e49. doi: 10.3802/jgo.2021.32.e49

25. Kuroki L, Guntupalli SR. Treatment of epithelial ovarian cancer. *BMJ.* 2020;371:m3773. doi: 10.1136/bmj.m3773

26. Trabert B, Coburn SB, Mariani A, et al. Reported Incidence and Survival of Fallopian Tube Carcinomas: A Population-Based Analysis From the North American Association of Central Cancer Registries. *J Natl Cancer Inst.* 2018;110(7):750–757. doi: 10.1093/jnci/djx263

27. Morozov SP, Lindenbraten LD, Gabai PG, et al. Osnovy menedzhmenta meditsinskoi vizualizatsii. Moscow: GEOTAR-Media, 2020. 432 p. EDN: ZRGBGE doi: 10.33029/9704-5247-9-MEN-2020-1-424

28. Svidetelstvo o gosudarstvennoi registratsii programmy dlya EVM № 2024618494. Rossiiskaya Federatsiya. *Platforma testirovaniya i obucheniya vrachei: № 2024617367.* Vasilev YuA, Shulkin IM, Arzamasov KM, et al. Nauchno-prakticheskii klinicheskii tsentr diagnostiki i telemeditsinskikh tekhnologii. (In Russ.) EDN: POELJA

СПИСОК ЛИТЕРАТУРЫ

1. Meinhold-Heerlein I., Fotopoulou C., Harter P., et al. The new WHO classification of ovarian, fallopian tube, and primary peritoneal cancer and its clinical implications // Arch Gynecol Obstet. 2016. Vol. 293. N 4. P. 695–700. doi: 10.1007/s00404-016-4035-8

2. Burghardt E., Girardi F., Lahousen M., et al. Patterns of pelvic and paraaortic lymph node involvement in ovarian cancer // Gynecol Oncol. 1991. Vol. 40. N 2. P. 103–106. doi: 10.1016/0090-8258(91)90099-q

3. Stasenko M., Fillipova O., Tew W. Fallopian Tube Carcinoma // J Oncol Pract. 2019. V. 15. N 7. P. 375–382. doi: 10.1200/JOP.18.00662

4. Reid B., Permuth J., Sellers T. Epidemiology of ovarian cancer: a review // Cancer Biol Med. 2017. Vol. 14. N. 1. P. 9–32. doi: 10.20892/j.issn.2095-3941.2016.0084

5. Ульрих Е.А., Папуниди М.Д., Урманчеева А.Ф., Мацко Д.Е. Рак маточный трубы: клинико-морфологические особенности, анализ 69 случаев // Вопросы онкологии. 2014. Т. 60. № 3. С. 375–378. EDN: SJTCOH

6. Kim M.Y., Rha S.E., Oh S.N., et al. MR Imaging findings of hydrosalpinx: a comprehensive review // Radiographics. 2009. Vol. 29. N 2. P. 495–507. doi: 10.1148/rg.292085070

7. Riska A., Leminen A. Updating on primary fallopian tube carcinoma // Acta Obstet Gynecol Scand. 2007. Vol. 86. N 12. P. 1419–1426. doi: 10.1080/00016340701771034

8. PDQ Adult Treatment Editorial Board. Ovarian Epithelial, Fallopian Tube, and Primary Peritoneal Cancer Treatment (PDQ®): Health Professional Version. 2023 // PDQ Cancer Information Summaries [Internet]. Available from: https://www.ncbi.nlm.nih.gov/books/NBK66007/

9. Kalampokas E., Kalampokas T., Tourountous I. Primary fallopian tube carcinoma // Eur J Obstet Gynecol Reprod Biol. 2013. Vol. 169. N 2. P. 155–161. doi: 10.1016/j.ejogrb.2013.03.023

10. Carvalho JP, Moretti-Marques R, Filho A. Adnexal mass: diagnosis and management // Rev Bras Ginecol Obstet. 2020. Vol. 42. N 7. P. 438–443. doi: 10.1055/s-0040-1715547

11. Anthoulakis C., Nikoloudis N. Pelvic MRI as the "gold standard" in the subsequent evaluation of ultrasound-indeterminate adnexal lesions: a systematic review // Gynecol Oncol. 2014. Vol. 132. N 3. P. 661–668. doi: 10.1016/j.ygyno.2013.10.022

12. Nishino M., Hayakawa K., Minami M., et al. Primary retroperitoneal neoplasms: CT and MR imaging findings with anatomic and pathologic diagnostic clues // Radiographics. 2003. Vol. 23. N 1. P. 45–57. doi: 10.1148/rg.231025037

13. Sadowski E., Thomassin-Naggara I., Rockall A., et al. O-RADS MRI Risk Stratification System: Guide for Assessing Adnexal Lesions from the ACR O-RADS Committee // Radiology. 2022. Vol. 303. N 1. P. 35–47. doi: 10.1148/radiol.204371

14. Буланов М.Н., Чекалова М.А., Мазуркевич М.Н., Ветшева Н.Н. Применение системы O-RADS при ультразвуковом исследовании придатков матки. М.: Научно-практический клинический центр диагностики и телемедицинских технологий Департамента здравоохранения города Москвы. 2022. 27 с. EDN: BUBNGP

15. Veloso G., Dias F., Lucas R., Cunha T. Primary fallopian tube carcinoma: review of MR imaging findings // Insights Imaging. 2015. Vol. 6. N 4. P. 431–439. doi: 10.1007/s13244-015-0416-y

16. Duska L., Kohn E. The new classifications of ovarian, fallopian tube, and primary peritoneal cancer and their clinical implications // Ann Oncol. 2017. Vol. 28. Suppl. 8. P. viii8-viii12. doi: 10.1093/annonc/mdx445

17. Нуднов Н.В., Ивашина С.В., Аксенова С.П. Лучевые методы в диагностике первичной и рецидивной злокачественной струмы яичников: клинический случай // Digital Diagnostics. 2023. Т. 4, № 2. С. 214–225. EDN: YNASOM doi: 10.17816/DD322846

18. Клинические рекомендации МЗ РФ «Рак яичников / рак маточной трубы / первичный рак брюшины». 2022 г. Министерство здравоохранения РФ. Режим доступа: https://oncology.ru/specialist/treatment/references/actual/547.pdf

19. Singh N., Gilks C., Wilkinson N., et al. Assignment of primary site in high-grade serous tubal, ovarian and peritoneal carcinoma: a proposal // Histopathology. 2014. Vol. 65. N 2. P. 149–154. doi: 10.1111/his.12419

20. Жордания К.И., Паяниди Ю.Г., Калиничева Е.В. Два пути развития серозного рака яичников // Онкогинекология. 2014. № 3. С. 42–48. EDN: TAOOQL

21. Жордания К.И., Паяниди Ю.Г., Калиничева Е.В. Новая парадигма в этиологии серозного рака яичников // Российский биотерапевтический журнал. 2014. Т. 13, № 2. С. 95–102. EDN: SNANEL

22. Жорданиа К.И. Серозный рак яичников или серозный рак маточной трубы? // Онкогинекология. 2012. № 3. С. 4–9. EDN: SZRFTZ

23. Tokunaga H., Mikami M., Nagase S., et al. The 2020 Japan Society of Gynecologic Oncology guidelines for the treatment of ovarian cancer, fallopian tube cancer, and primary peritoneal cancer // J Gynecol Oncol. 2021. Vol. 32. N 2. P. e49. doi: 10.3802/jgo.2021.32.e49

24. SEER*Explorer: An interactive website for SEER cancer statistics [Internet]. Surveillance Research Program, National Cancer Institute. 2023. Available from: https://seer.cancer.gov/statistics-network/explorer/

25. Kuroki L., Guntupalli S. Treatment of epithelial ovarian cancer // BMJ. 2020. Vol. 371. P. m3773. doi: 10.1136/bmj.m3773

26. Trabert B., Coburn S., Mariani A., et al. Reported Incidence and Survival of Fallopian Tube Carcinomas: A Population-Based Analysis From the North American Association of Central Cancer Registries // J Natl Cancer Inst. 2018. Vol. 110. N 7. P. 750–757. doi: 10.1093/jnci/djx263

27. Морозов С.П., Линденбратен Л.Д., Габай П.Г., и др. Основы менеджмента медицинской визуализации. М.: ГЭОТАР-Медиа, 2020. 432 с. EDN: ZRGBGE doi: 10.33029/9704-5247-9-MEN-2020-1-424

28. Свидетельство о государственной регистрации программы для ЭВМ № 2024618494 Российская Федерация. Платформа тестирования и обучения врачей: № 2024617367: заявл. 08.04.2024: опубл. 12.04.2024 / Ю.А. Васильев, И.М. Шулькин, К.М. Арзамасов, и др. ГБУЗ г. Москвы «Научно-практический клинический центр диагностики и телемедицинских технологий Департамента здравоохранения города Москвы». EDN: POELJA

AUTHORS' INFO

* Oleg I. Mynko, MD;
address: 24 bldg. 1 Petrovka str., 127051, Moscow, Russia;
ORCID: 0009-0005-3984-4045;
eLibrary SPIN: 3556-3510;
e-mail: o.mynko@icloud.com

Anna P. Gonchar, MD;
ORCID: 0000-0001-5161-6540;
eLibrary SPIN: 3513-9531;
e-mail: a.gonchar@npcmr.ru

Valentin A. Nechaev, MD, Cand. Sci. (Medicine);
ORCID: 0000-0002-6716-5593;
eLibrary SPIN: 2527-0130;
e-mail: dfkz2005@gmail.com

Evgeniya A. Kulikova, MD;
ORCID: 0000-0002-0319-4934;
eLibrary SPIN: 2884-4803;
e-mail: kulikovaEA14@zdrav.mos.ru

Andrey L. Yudin, MD, Dr. Sci. (Medicine), Professor;
ORCID: 0000-0002-0310-0889;
eLibrary SPIN: 6184-8284;
e-mail: rsmu@rsmu.ru

Elena A. Yumatova, MD, Cand. Sci. (Medicine);
ORCID: 0000-0002-6020-9434;
eLibrary SPIN: 8447-8748;
e-mail: yumatova_ea@mail.ru

ОБ АВТОРАХ

* Мынко Олег Игоревич,
адрес: Россия, 127051, Москва, ул. Петровка, д. 24, стр. 1;
ORCID: 0009-0005-3984-4045;
eLibrary SPIN: 3556-3510;
e-mail: o.mynko@icloud.com

Гончар Анна Павловна;
ORCID: 0000-0001-5161-6540;
eLibrary SPIN: 3513-9531;
e-mail: a.gonchar@npcmr.ru

Нечаев Валентин Александрович, канд. мед. наук;
ORCID: 0000-0002-6716-5593;
eLibrary SPIN: 2527-0130;
e-mail: dfkz2005@gmail.com

Куликова Евгения Александровна;
ORCID: 0000-0002-0319-4934;
eLibrary SPIN: 2884-4803;
e-mail: kulikovaEA14@zdrav.mos.ru

Юдин Андрей Леонидович, д-р мед. наук, профессор;
ORCID: 0000-0002-0310-0889;
eLibrary SPIN: 6184-8284;
e-mail: rsmu@rsmu.ru

Юматова Елена Анатольевна, канд. мед. наук;
ORCID: 0000-0002-6020-9434;
eLibrary SPIN: 8447-8748;
e-mail: yumatova_ea@mail.ru

* Corresponding author / Автор, ответственный за переписку

The role of computed tomography in the differential diagnosis of an intracardiac mass of the mitral valve: a case series

Maria V. Onoyko[1], Elena A. Mershina[1], Amalia A. Arakelyants[1,2], Valentin E. Sinitsyn[1]

[1] Lomonosov Moscow State University, Moscow, Russia;
[2] Sechenov First Moscow State Medical University, Moscow, Russia

ABSTRACT

The differential diagnosis of an echocardiographically detected intracardiac mass in the mitral annulus can be challenging and usually requires a multimodal approach. This type of lesion is very often associated with subvalvular calcification of the mitral valve. The rare, caseous, variant is the most difficult to diagnose. This case series highlights the clinical significance of computed tomography in detecting and characterizing subvalvular mitral annular calcification when other modalities, particularly echocardiography, are inconclusive. The aim of this article was to raise awareness among specialists of the classic signs of caseous subvalvular calcification of the mitral annulus when visualized with different modalities. Special attention is also given to providing a differential diagnostic series that identifies features that differentiate subvalvular calcification of the mitral annulus from other conditions at this site. Healthcare professionals need to be aware of these mitral valve lesions in order to predict possible associated complications and plan a treatment strategy that may help avoid unnecessary surgical procedures in some cases.

Keywords: caseous calcification of the mitral annulus; intracardiac mass; echocardiography; computed tomography; magnetic resonance imaging; case report.

Роль компьютерной томографии в дифференциальной диагностике интракардиального объёмного образования в области митрального клапана: серия клинических случаев

М.В. Онойко[1], Е.А. Мершина[1], А.А. Аракелянц[1,2], В.Е. Синицын[1]

[1] Московский государственный университета имени М.В. Ломоносова, Москва, Россия;
[2] Первый Московский государственный медицинский университет имени И.М. Сеченова, Москва, Россия

АННОТАЦИЯ

Дифференциальная диагностика интракардиального объёмного образования в области кольца митрального клапана, выявленного при проведении эхокардиографии, может быть непростой задачей. Её решение обычно требует мультимодального подхода. Очень часто природа такого образования связана с подклапанным кальцинозом митрального клапана. Наибольшую трудность в диагностике представляет достаточно редкий его вариант — казеозная форма. На примере представленной серии клинических случаев подчёркивается важность и клиническая значимость компьютерной томографии для выявления и характеристики подклапанного кальциноза кольца митрального клапана при неоднозначных результатах других методов диагностики, в частности эхокардиографии. Данная работа нацелена на повышение информированности специалистов о классических признаках казеозной формы подклапанного кальциноза кольца митрального клапана при визуализации в различных модальностях. Особое внимание уделяется построению дифференциально-диагностического ряда, выделению характеристик, позволяющих отличить подклапанный кальциноз кольца митрального клапана от других патологических состояний в данной локализации. Осведомлённость врачей о существовании такого рода изменений в области митрального клапана необходима для прогнозирования возможных осложнений, связанных с ней, и планирования тактики лечения, что поможет в некоторых случаях избежать неоправданных хирургических вмешательств.

Ключевые слова: казеозный кальциноз кольца митрального клапана; интракардиальное объёмное образование; эхокардиография; компьютерная томография; магнитно-резонансная томография; клинический случай.

计算机断层扫描在二尖瓣区心内占位性病变鉴别诊断中的作用：临床病例系列

Maria V. Onoyko[1], Elena A. Mershina[1], Amalia A. Arakelyants[1,2], Valentin E. Sinitsyn[1]

[1] Lomonosov Moscow State University, Moscow, Russia;
[2] Sechenov First Moscow State Medical University, Moscow, Russia

摘要

通过超声心动图识别的二尖瓣环区心内占位性病变的鉴别诊断可能具有挑战性。其解决方案通常需要采用多模式方法。通常这种形成的性质与二尖瓣的瓣膜下钙化有关。诊断的最大困难是其相当罕见的变体 — 干酪样形式。在其他诊断方法，特别是超声心动图结果不明确的情况下，本系列病例突出了计算机断层扫描在二尖瓣环瓣下钙化的检测和定性方面的重要性和临床意义。本文旨在提高专家对二尖瓣瓣下环干酪样钙化在不同成像模式下的典型体征的认识。同时，还特别关注鉴别诊断系列的构建，确定能够区分二尖瓣瓣下环干酪样钙化与该定位中的其他病理状况的特征。医生有必要了解二尖瓣区域存在的这种变化，以便预测可能出现的相关并发症，并制定治疗策略，这在某些情况下有助于避免不必要的手术干预。

关键词：二尖瓣环干酪样钙化；心内占位性病变；超声心动图；计算机断层扫描；磁共振成像；临床病例。

INTRODUCTION

Intracardiac masses are often incidentally identified during transthoracic echocardiography, which is a primary imaging modality in cardiology. Masses located near the mitral annulus may suggest caseous subvalvular calcification.

Subvalvular calcification of the mitral valve (SCMV) is relatively common, particularly in individuals over 50 years of age. It occurs twice as frequently in women compared to men [1, 2]. In SCMV, calcifications typically appear in the fibrous tissue of the posterior mitral leaflet, the area between its base and the left ventricular wall, and within the left ventricular myocardium. SCMV has been linked to conditions such as atherosclerosis, hypertension, coronary artery disease, heart failure, atrial fibrillation, and chronic kidney disease. Additionally, SCMV is associated with an increased risk of adverse cardiovascular events and mortality [3]. The diagnosis of SCMV is generally straightforward.

Caseous pseudoneoplastic SCMV is an uncommon variant marked by the transformation of dense calcified tissue into a paste-like consistency due to colliquative necrosis. Histologically, these lesions consist of amorphous material with infiltration by lymphocytes and macrophages, as well as cholesterol and calcium deposits [4, 5]. Deluca et al. reported that this variant is detected in approximately 0.64% of patients with SCMV and 0.068% of all echocardiographic examinations [6]. However, autopsy studies suggest a prevalence of up to 2.7%, indicating it is likely underdiagnosed due to limited clinician awareness or the inherent limitations of echocardiography [7]. Caseous SCMV can be mistaken for abscesses, tumors, or thrombotic lesions when assessed using transthoracic echocardiography or magnetic resonance imaging (MRI).

The following clinical cases illustrate the diagnostic utility of computed tomography (CT) in differentiating intracardiac masses in the mitral valve region that are incidentally detected on transthoracic echocardiography or MRI.

CASES DESCRIPTION

Clinical case 1

A 60-year-old male patient with a history of long-standing hypertension, myocardial infarction, multiple coronary stent placements, and implantation of a bifocal cardioverter-defibrillator was admitted to the cardiology department in November 2023. He reported symptoms of fatigue, shortness of breath, swelling of the feet and lower legs, and chest pain triggered by minimal exertion (such as climbing two flights of stairs), which subsided with rest.

Transthoracic echocardiography revealed a left ventricular apical aneurysm, moderate hypertrophy of the remaining viable myocardium, dilation of all cardiac chambers, and moderately reduced global contractility. Atherosclerotic changes were observed in the aorta, aortic valve,

and mitral valve. Additionally, grade II–III mitral and tricuspid regurgitation and grade I pulmonary hypertension were noted. A fixed, hyperechoic mass measuring 28 × 26 × 37 mm was identified near the posterior mitral leaflet. The mass lacked acoustic shadowing and showed no evidence of blood flow. It appeared to be adjacent to or arising from the posterior basal segment of the left ventricle, the posterior mitral leaflet, or the mitral annulus (Fig. 1). Retrospective evaluation of echocardiograms from May 2017 and October 2018 showed a large calcification at the site of the lesion.

To further assess the nature of the lesion, electrocardiogram (ECG)-gated cardiac CT angiography was performed. It revealed an irregularly shaped lesion measuring 25 × 23 × 43 mm located at the base of the posterior mitral leaflet and within the left ventricular myocardium. The lesion exhibited peripheral calcifications with densities ranging from 1,335 to 1,350 HU and a central area of lower density (540–560 HU), with no contrast enhancement during either the arterial or venous phases. These findings were consistent with caseous subvalvular calcification beneath the posterior mitral leaflet (Fig. 2).

CT also showed advanced coronary atherosclerosis, signs of scarring in the apical segments of the left ventricle, and left atrial enlargement. Medical therapy led to improvement the the patient's coronary artery disease, and he was discharged with instructions for ongoing cardiology follow-up.

Clinical case 2

A 72-year-old female patient underwent routine transthoracic echocardiography, which revealed a fixed, hyperechoic mass located in the inferior wall of the left atrium, near the mitral valve. The lesion measured 21 × 15 mm and had a well-defined, smooth margins. A left atrial myxoma was initially suspected.

To further evaluate the lesion, ECG-gated cardiac CT angiography was performed. The scan identified a rounded calcified lesion measuring 35 × 12 mm at the level of the mitral annulus in the subvalvular region of the left ventricle. The lesion appeared heterogeneous, with calcified areas showing densities of 1,300–1,350 HU and a central region of lower density (330–340 HU), with no contrast enhancement observed during either the arterial or venous phases. These characteristics were consistent with caseous subvalvular calcification of the mitral annulus (Fig. 3).

Additional imaging using the bone window demonstrated a heterogeneous calcified area near the base of the posterior mitral leaflet, also measuring approximately 35 × 12 mm, with a density reaching up to 1,680 HU.

Clinical case 3

A 66-year-old male underwent cardiac MRI to assess the extent of scarring in the inferior wall of the left ventricle following a myocardial infarction that had occurred 20 years earlier. The scan revealed a 10 × 12 mm mass near the posterior mitral leaflet, characterized by low
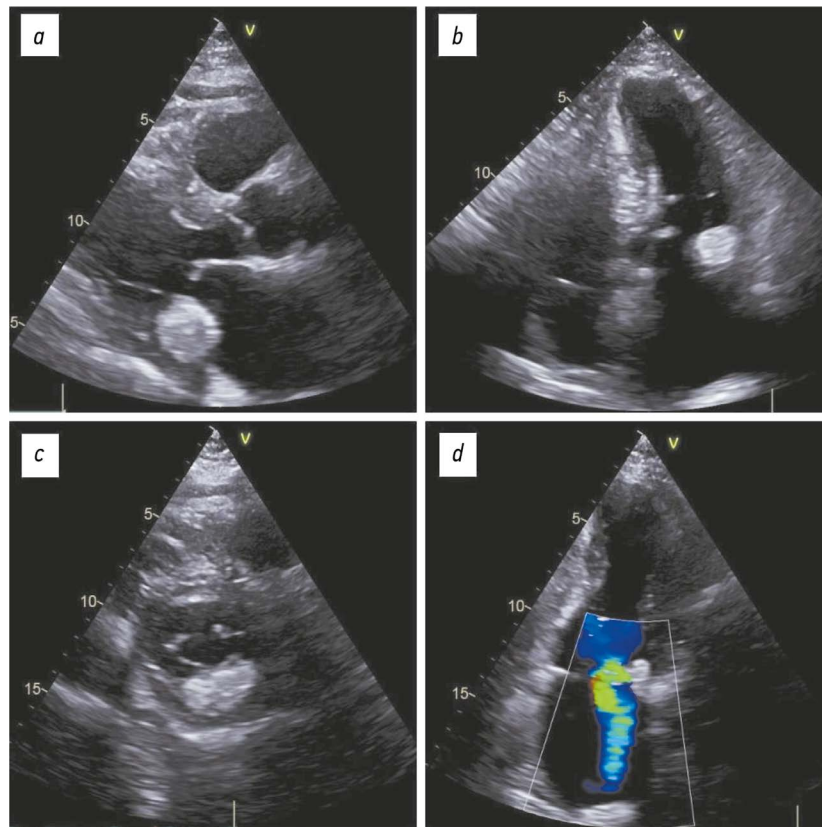
Fig. 1. Transthoracic echocardiography, B-mode, clinical case 1: *a–c*, mass located near the posterior mitral leaflet; *d*, evidence of mitral regurgitation on Doppler ultrasonography; *a*, parasternal long-axis view; *b*, apical four-chamber view; *c*, parasternal short-axis view at the mitral valve level; *d*, apical two-chamber view.
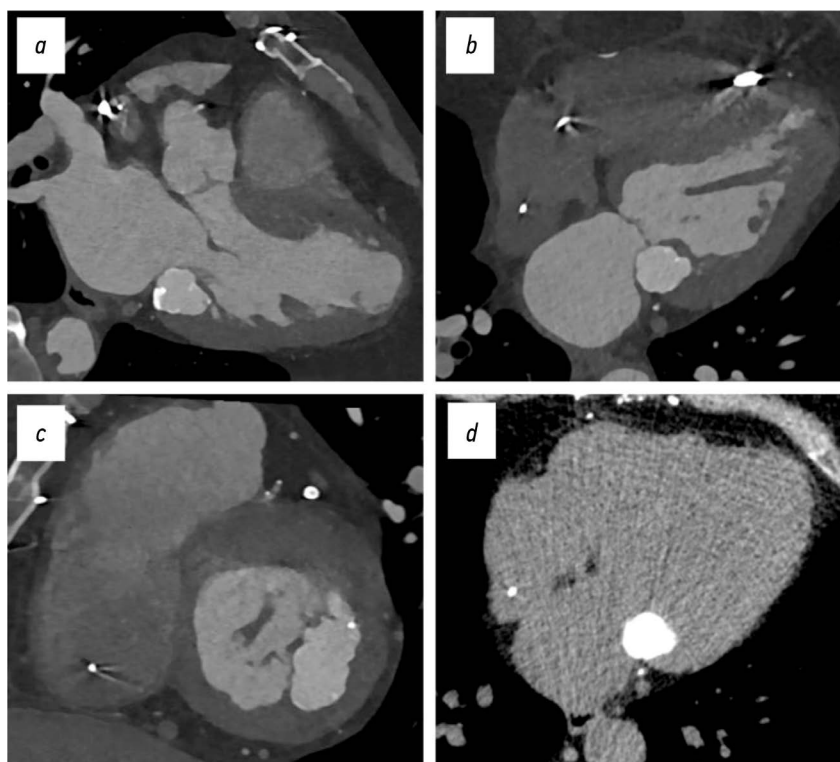

Fig. 2. ECG-gated cardiac computed tomography, clinical case 1: *a–c*, contrast-enhanced images, bone window; *d*, non-contrast image, soft tissue window; findings consistent with caseous subvalvular calcification beneath the posterior mitral leaflet: *a*, three-chamber view; *b*, four-chamber view; *c*, short-axis view at the mitral valve level; *d*, axial view.

MR signal intensity and peripheral contrast enhancement with delayed uptake. Subsequently, ECG-gated cardiac CT angiography was conducted. A comparison of the MRI and CT findings confirmed that the lesion was consistent with caseous SCMV (Fig. 4).

DISCUSSION

Echocardiography is the most widely used noninvasive method for assessing cardiac structure and function. It is typically effective in identifying echogenic subvalvular lesions of the mitral valve, including SCMV. The brightness mode (B-mode) is most effective for detecting SCMV on echocardiography. In this mode, SCMV appears as a hyperechoic lesion with a characteristic location, well-defined borders, and an acoustic shadow. However, when SCMV undergoes transformation into its caseous form, the ultrasound characteristics change notably. Caseous SCMV appears as a heterogeneous, ovoid lesion with a hypoechoic center, lacking both an acoustic shadow and Doppler-detectable blood flow [7]. Since caseous SCMV can resemble a mass lesion on echocardiography, distinguishing it from cardiac tumors, abscesses, or thrombotic formations is essential.

Cardiac CT is a fast and reliable imaging method for detecting SCMV and serves as a valuable adjunct in preoperative planning for mitral valve surgery. CT provides both qualitative and quantitative information about calcific lesions. It also enables calculation of the coronary artery calcium score, which is relevant because SCMV is often associated with coronary artery disease [8]. On noncontrast CT, SCMV typically appears as an ovoid, high-density lesion consistent with calcification. In the bone window setting, the internal heterogeneity of the lesion becomes more apparent, with either a dense homogeneous or heterogeneous central area and prominent peripheral calcifications [9]. The absence of contrast enhancement in SCMV lesions is a key feature aiding in differential diagnosis.

On MRI, SCMV usually presents as a hypointense mass on both T1- and T2-weighted images. However, these MRI characteristics are nonspecific and primarily suggest the possibility of mitral valve calcifications. In contrast, CT provides more definitive characterization, as it is not limited by this ambiguity.

The most typical MRI features of caseous SCMV include:
- An isointense or hyperintense signal in the central region with a hypointense peripheral signal on T1-weighted images
- A hypointense signal on short tau inversion recovery (STIR) sequences
- A signal that is either less intense or isointense compared to the myocardium on steady-state free precession (SSFP) sequences
- Delayed peripheral contrast enhancement within the fibrous capsule [9, 10].

The ultrasound, MRI, and CT findings in the clinical cases presented here are consistent with previously reported imaging characteristics of caseous subvalvular calcification in the posterior mitral leaflet region [9, 11–13].

Transthoracic echocardiography of the mitral valve is useful in considering a range of differential diagnoses for mass-like lesions, including tumors such as papillary fibroelastoma and mixoma, thrombotic formations, and abscesses. However, establishing a definitive diagnosis often requires additional imaging, particularly CT.
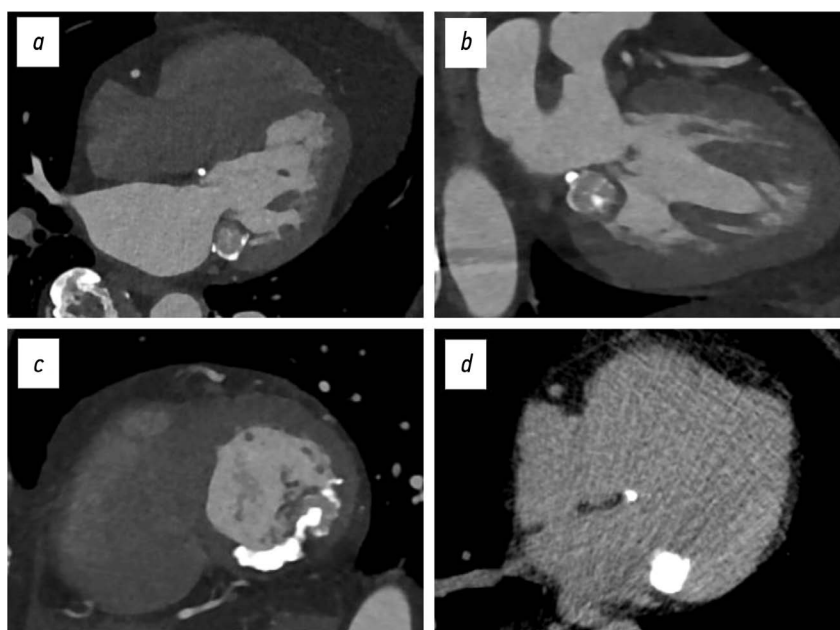

Fig. 3. ECG-gated cardiac computed tomography, clinical case 2: *a–c*, contrast-enhanced images, bone window; *d*, noncontrast image, soft tissue window; findings consistent with caseous subvalvular calcification of the posterior mitral leaflet: *a*, four-chamber view; *b*, two-chamber long-axis view; *c*, short-axis view at the mitral valve level; d, axial view.
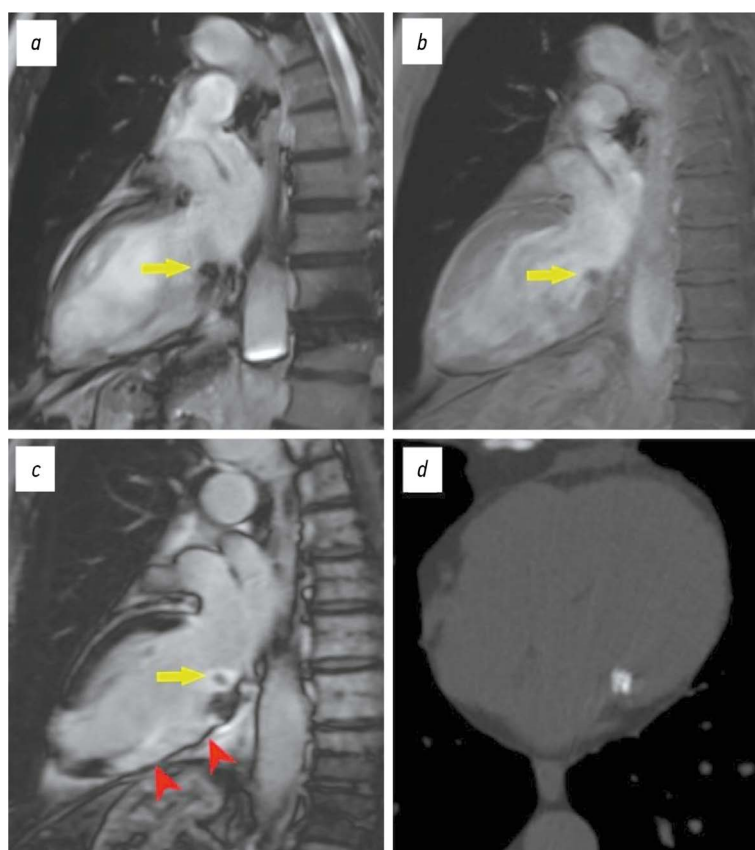
Fig. 4. Clinical case 3: *a–c*, cardiac magnetic resonance imaging; *d*, ECG-gated cardiac computed tomography; green arrows indicate a mass adjacent to the posterior mitral leaflet; red arrows show postinfarction transmural fibrotic changes in the inferior wall of the left ventricle at the middle and basal segments; *a–b*, steady-state free precession (SSFP) sequence, two-chamber long-axis view, without contrast; *c*, T1-weighted image with myocardium signal suppression and delayed contrast enhancement, two-chamber long-axis view; *d*, axial view, bone window.

CT and/or MRI can help differentiate caseous SCMV from mixoma or papillary fibroelastoma by assessing features such as contrast enhancement (which is absent in SCMV), tumor mobility, presence of a pedicle, MR signal characteristics of tumor tissue, and tumor density on CT.

Since infective endocarditis is the most common cause of valvular abscesses, correlating imaging findings with clinical and laboratory data is critical. On CT, abscesses typically appear as encapsulated masses with contrast enhancement and a central hypodense necrotic area.

On contrast-enhanced CT, thrombotic masses typically appear as hypodense, avascular lesions. On MRI, the signal intensity of thrombi varies depending on their age. Organized thrombi with a high content of fibrous tissue may demonstrate mild peripheral contrast enhancement—a feature also seen in caseous SCMV. Since conventional calcifications, caseous SCMV, and thrombi may exhibit similar MRI characteristics, it is essential to interpret MRI findings alongside CT results.

CONCLUSION

Interpreting echocardiographic findings and performing differential diagnosis of intracardiac masses can be difficult, highlighting the importance of incorporating additional imaging modalities such as CT and MRI. Caseous SCMV is a rare and usually asymptomatic condition, contributing to its under recognition among clinicians. It is important to note that, although uncommon, SCMV can lead to complications such as stroke, arrhythmias, mitral regurgitation, or stenosis. SCMV is also associated with established cardiovascular risk factors. Accurate identification of an incidentally discovered intracardiac mass and selection of the most appropriate treatment approach require a comprehensive, multimodal diagnostic strategy.

ADDITIONAL INFORMATION

REFERENCES

1. Savage DD, Garrison RJ, Castelli WP, et al. Prevalence of submitral (anular) calcium and its correlates in a general population-based sample (the Framingham Study). *Am J Cardiol.* 1983;51(8):1375–1378. doi: 10.1016/0002-9149(83)90315-6

2. Abramowitz Y, Jilaihawi H, Chakravarty T, et al. Mitral Annulus Calcification. *J Am Coll Cardiol.* 2015;66(17):1934–1941. doi: 10.1016/j.jacc.2015.08.872

3. Kanjanauthai S, Nasir K, Katz R, et al. Relationships of mitral annular calcification to cardiovascular risk factors: the Multi-Ethnic Study of Atherosclerosis (MESA). *Atherosclerosis.* 201;213(2):558–562. doi: 10.1016/j.atherosclerosis.2010.08.072

4. Harpaz D, Auerbach I, Vered Z, et al. Caseous calcification of the mitral annulus: a neglected, unrecognized diagnosis. *J Am Soc Echocardiogr.* 2001;14(8):825–831. doi: 10.1067/mje.2001.111877

5. Silbiger JJ. Anatomy, mechanics, and pathophysiology of the mitral annulus. *Am Heart J.* 2012;164(2):163–176. doi: 10.1016/j.ahj.2012.05.014

6. Deluca G, Correale M, Ieva R, et al. The incidence and clinical course of caseous calcification of the mitral annulus: a prospective echocardiographic study. *J Am Soc Echocardiogr.* 2008;21(7):828–833. doi: 10.1016/j.echo.2007.12.004

7. Akram M, Hasanin AM. Caseous mitral annular calcification: Is it a benign condition? *J Saudi Hear Assoc.* 2012;24(3):205–208. doi: 10.1016/j.jsha.2012.02.003

8. Hamirani YS, Nasir K, Blumenthal RS, et al. Relation of mitral annular calcium and coronary calcium (from the Multi-Ethnic Study of Atherosclerosis [MESA]). *Am J Cardiol.* 2011;107(9):1291–1294. doi: 10.1016/j.amjcard.2011.01.005

9. Shriki J, Rongey C, Ghosh B, et al. Caseous mitral annular calcifications: Multimodality imaging characteristics. *World J Radiol.* 2010;2(4):143-147. doi: 10.4329/wjr.v2.i4.143

10. Gravina M, Casavecchia G, Manuppelli V, et al. Mitral annular calcification: Can CMR be useful in identifying caseous necrosis? *Interv Med Appl Sci.* 2019;11(1):71-73. doi: 10.1556/1646.10.2018.47

11. Mayr A, Müller S, Feuchtner G. The Spectrum of Caseous Mitral Annulus Calcifications. *JACC Case Rep.* 2021;3(1):104–108. doi: 10.1016/j.jaccas.2020.09.039

12. Belkind MB, Butorova EA, Stukalova OV, et al. Caseous calcification of the mitral annulus. *Eurasian heart journal.* 2023;(4):90–93. doi: 10.38109/2225-1685-2023-4-90-93

13. Saidova MA, Atabaeva LS, Stukalova OV. Caseous calcification of the mitral annulus. *Russian Cardiology Bulletin.* 2019;14(3):62–67. doi: 10.36396/MS.2019.14.03.010

СПИСОК ЛИТЕРАТУРЫ

1. Savage D.D., Garrison R.J., Castelli W.P., et al. Prevalence of submitral (anular) calcium and its correlates in a general population-based sample (the Framingham Study) // Am J Cardiol. 1983. Vol. 51, N 8. P. 1375–1378. doi: 10.1016/0002-9149(83)90315-6

2. Abramowitz Y., Jilaihawi H., Chakravarty T., et al. Mitral Annulus Calcification // J Am Coll Cardiol. 2015. Vol. 66, N 17. P. 1934–1941. doi: 10.1016/j.jacc.2015.08.872

3. Kanjanauthai S., Nasir K., Katz R., et al. Relationships of mitral annular calcification to cardiovascular risk factors: the Multi-Ethnic Study of Atherosclerosis (MESA) // Atherosclerosis. 2010. Vol. 213, N 2. P. 558–562. doi: 10.1016/j.atherosclerosis.2010.08.072

4. Harpaz D., Auerbach I., Vered Z., et al. Caseous calcification of the mitral annulus: a neglected, unrecognized diagnosis // J Am Soc Echocardiogr. 2001. Vol. 14, N 8. P. 825–831. doi: 10.1067/mje.2001.111877

5. Silbiger J.J. Anatomy, mechanics, and pathophysiology of the mitral annulus // Am Heart J. 2012. Vol. 164, N 2. P. 163–176. doi: 10.1016/j.ahj.2012.05.014

6. Deluca G., Correale M., Ieva R., et al. The incidence and clinical course of caseous calcification of the mitral annulus: a prospective echocardiographic study // J Am Soc Echocardiogr. 2008. Vol. 21, N 7. P. 828–33. doi: 10.1016/j.echo.2007.12.004

7. Akram M., Hasanin A.M. Caseous mitral annular calcification: Is it a benign condition? // J Saudi Heart Assoc. 2012. Vol. 24, N 3. P. 205–208. doi: 10.1016/j.jsha.2012.02.003

8. Hamirani Y.S., Nasir K., Blumenthal R.S., et al. Relation of mitral annular calcium and coronary calcium (from the Multi-Ethnic Study of Atherosclerosis [MESA]) // Am J Cardiol. 2011. Vol. 107, N 9. P. 1291–1294. doi: 10.1016/j.amjcard.2011.01.005

9. Shriki J., Rongey C., Ghosh B., et al. Caseous mitral annular calcifications: Multimodality imaging characteristics // World J Radiol. 2010. Vol. 2, N 4. P. 143–147. doi: 10.4329/wjr.v2.i4.143

10. Gravina M., Casavecchia G., Manuppelli V., et al. Mitral annular calcification: Can CMR be useful in identifying caseous necrosis? // Interv Med Appl Sci. 2019. Vol. 11, N 1. P. 71–73. doi: 10.1556/1646.10.2018.47

11. Mayr A., Müller S., Feuchtner G. The Spectrum of Caseous Mitral Annulus Calcifications // JACC Case Rep. 2021. Vol. 3, N 1. P. 104–108. doi: 10.1016/j.jaccas.2020.09.039

12. Белькинд М.Б., Буторова Е.А., Стукалова О.В., Гаман С.А., Смирнов С.М. Казеозный кальциноз кольца митрального клапана // Евразийский Кардиологический Журнал. 2023. № 4. С. 90–93. doi: 10.38109/2225-1685-2023-4-90-93

13. Саидова М.А., Атабаева Л.С., Стукалова О.В. Казеозный кальциноз митрального клапана // Кардиологический вестник. 2019. Т. 14, № 3. С. 62–67. doi: 10.36396/MS.2019.14.03.010

AUTHORS' INFO

* Maria V. Onoyko, MD;
address: 1 block B Leninskie Gory, 119234, Moscow, Russia;
ORCID: 0000-0002-7727-3360;
eLibrary SPIN: 6380-7495;
e-mail: onoykomary@gmail.com

ОБ АВТОРАХ

* Онойко Мария Викторовна;
адрес: Россия, 119234, Москва, Ленинские горы, д. 1, корп. В;
ORCID: 0000-0002-7727-3360;
eLibrary SPIN: 6380-7495;
e-mail: onoykomary@gmail.com

Elena A. Mershina, MD, Cand. Sci. (Medicine), Assistant Professor;
ORCID: 0000-0002-1266-4926;
eLibrary SPIN: 6897-9641;
e-mail: elena_mershina@mail.ru
Amalia A. Arakelyants, MD, Cand. Sci. (Medicine);
ORCID: 0000-0002-1243-2471;
eLibrary SPIN: 4990-6008;
e-mail: nxrrimma@mail.ru
Valentin E. Sinitsyn, MD, Dr. Sci. (Medicine), Professor;
ORCID: 0000-0002-5649-2193;
eLibrary SPIN: 8449-6590;
e-mail: vsini@mail.ru

Мершина Елена Александровна, канд. мед. наук, доцент;
ORCID: 0000-0002-1266-4926;
eLibrary SPIN: 6897-9641;
e-mail: elena_mershina@mail.ru
Аракелянц Амалия Ашотовна, канд. мед. наук;
ORCID: 0000-0002-1243-2471;
eLibrary SPIN: 4990-6008;
e-mail: nxrrimma@mail.ru
Синицын Валентин Евгеньевич, д-р мед. наук, профессор;
ORCID: 0000-0002-5649-2193;
eLibrary SPIN: 8449-6590;
e-mail: vsini@mail.ru

_____
* Corresponding author / Автор, ответственный за переписку

Hypoplasia of the inferior vena cava with hypertrophic *azygos/hemiazygos* and collateral venous circles of the abdomen: a case report

Manuela Montatore[1], Gianmichele Muscatella[1], Federica Masino[1], Giovanni Ricatti[2],
Marina Balbino[1], Rossella Gifuni[1], Giuseppe Guglielmi[1,2,3]

[1] Foggia University School of Medicine, Foggia, Italy;
[2] «Monsignor Raffaele Dimiccoli» Hospital, Barletta, Italy;
[3] IRCCS Casa Sollievo della Sofferenza Hospital, Giovanni Rotondo, Italy

ABSTRACT

Hypoplasia of the *inferior vena cava* is a rare congenital vascular defect with various forms; thus, identifying a specific anatomical variant in the literature is challenging. In some cases, the *inferior vena cava* may also be interrupted. Herein, we present a unique case of of an unknown subrenal hypoplasia of the *inferior vena cava* with *azygos* and *hemiazygos* hypertrophy and the creation of several collateral circles, particularly in the anterior wall of the abdomen, in an asymptomatic 75-year-old man. This report not only describes this unusual instance but also quickly demonstrates the variations of the venous system in the abdomen, particularly on the right side, and the *inferior vena cava* and the *azygos* system, and explains the significance of imaging in recognizing vascular anomalies. The case was explored using a multiphase computed tomography technique, which correctly identified this complex vascular anomaly. The patient had never experienced symptoms associated with the same vascular defect previously. Moreover, his symptoms did not appear to be related; therefore, a periodic follow-up was recommended.

Keywords: hypertrophic azygos; inferior vena cava; inferior vena cava hypoplasia; collateral venous circles; venous system.

Гипоплазия нижней полой вены, сопровождающаяся гипертрофией непарной и полунепарной вен и образованием сети коллатеральных вен в брюшной полости: клинический случай

M. Montatore[1], G. Muscatella[1], F. Masino[1], G. Ricatti[2], M. Balbino[1], R. Gifuni[1], G. Guglielmi[1,2,3]

[1] Foggia University School of Medicine, Фоджа, Италия;
[2] «Monsignor Raffaele Dimiccoli» Hospital, Барелетта, Италия;
[3] IRCCS Casa Sollievo della Sofferenza Hospital, Сан Джованни Ротондо, Италия

АННОТАЦИЯ

Гипоплазия нижней полой вены — это редкая врождённая сосудистая аномалия, которая отличается разнообразием форм. В некоторых случаях нижняя полая вена прерывается. Именно поэтому поиск описания определённых анатомических вариантов данной аномалии в литературе — это достаточно трудная задача. В настоящей статье представлен уникальный случай бессимптомной гипоплазии инфраренального сегмента нижней полой вены, сопровождающейся гипертрофией непарной и полунепарной вен, а также формированием сети коллатеральных вен на передней брюшной стенке. Сосудистая аномалия выявлена случайно у мужчины 75 лет. Помимо описания клинического случая, в статье кратко охарактеризованы сопутствующие изменения венозной системы брюшной полости, особенно выраженные с правой стороны, а также изменения нижней полой вены и системы непарной вены. В работе также приведено обоснование важности проведения визуализационных исследований для выявления сосудистых аномалий. В представленном клиническом случае визуализация выполнена с помощью компьютерной томографии с многофазным контрастированием, что позволило точно определить наличие сложной сосудистой аномалии. У пациента ранее никогда не возникало симптомов, указывающих на наличие данной аномалии, а проявлявшиеся симптомы, по-видимому, не были с ней связаны, поэтому пациенту рекомендовано периодическое наблюдение.

Ключевые слова: гипертрофия парной вены; нижняя полая вена; гипоплазия нижней полой вены; коллатеральные вены; венозная система.

下腔静脉发育不全伴奇静脉和半奇静脉肥大及腹腔侧支静脉网络形成：临床病例

Manuela Montatore[1], Gianmichele Muscatella[1], Federica Masino[1], Giovanni Ricatti[2],
Marina Balbino[1], Rossella Gifuni[1], Giuseppe Guglielmi[1,2,3]

[1] Foggia University School of Medicine, Foggia, Italy;
[2] «Monsignor Raffaele Dimiccoli» Hospital, Barletta, Italy;
[3] IRCCS Casa Sollievo della Sofferenza Hospital, Giovanni Rotondo, Italy

摘要

下腔静脉发育不全是一种罕见的先天性血管异常，其解剖变异形式多种多样，有时甚至导致下腔静脉的中断。文献中对这些具体解剖变异的描述较少，因此该领域的研究仍面临挑战。本文报道了一例 75岁男性患者 的独特病例，其 无症状性下腔静脉肾下段发育不全 伴有奇静脉和半奇静脉肥大，以及 腹前壁侧支静脉网络 的形成。发现方式：该血管异常是在患者无相关症状的情况下，通过 多期对比增强计算机断层扫描（CT） 偶然发现的。影像学表现：患者 右侧腹腔静脉系统 显著异常；下腔静脉中断及奇静脉系统代偿性肥大；腹前壁形成了明显的 侧支静脉网络，提示血液回流路径的重组。临床观察：患者没有既往相关症状，观察到的解剖异常未与临床症状相关。本文强调 影像学检查，特别是 多期对比增强CT，在检测血管异常中的关键作用。在该病例中，影像学技术成功识别了复杂的血管异常，提供了清晰的解剖学细节。鉴于患者既往无症状，建议定期影像学随访，以监测异常血管结构的潜在进展及可能引发的并发症。

关键词：奇静脉肥大；下腔静脉；下腔静脉发育不全；侧支静脉；静脉系统。

INTRODUCTION

Hypoplasia or the absence of the *inferior vena cava* (IVC) is a rare congenital condition that causes venous return from the lower body through the *azygos* or *hemiazygos* venous system [1,2]. The IVC may be hypoplastic or absent and is termed "interrupted" in this case: this term refers to total agenesis.

In most cases, this vascular anomaly is due to some embryologic mechanisms, and a failed anastomosis exists between the right subcardinal vein and the vitelline vein, resulting in hypoplasia or, in some cases, agenesis of the infrarenal/subrenal IVC and an interruption at the suprarenal venous segment [3].

In some cases, the newborn suprahepatic IVC could be missing or hypoplastic, resulting in direct outflow into the right atrium [4]. In this case, the small suprarenal IVC in the hepatic hilum drains through the *azygos* vein, while the hepatic IVC exclusively receives the hepatic veins. These anatomical variants are asymptomatic if the *azygos/hemiazygos* continuation is well-developed and the venous collateral loop is intact [5]. However, recurrent deep vein thrombosis of the lower limbs, leg swelling, leg pain, varices of the lower extremities, abdominal pain, and hematochezia

in rare cases may present in the future [6,7]. Asymptomatic conditions are frequently discovered in the early to middle years of life, as in this case.

DESCRIPTION OF THE CASE

Anamnesis

A 75-year-old Caucasian man presented to the emergency department after a referred fall and underwent his first contrast-enhanced computed tomography (CT). A multiphase examination was performed using a 64-detector scanner, beginning with an unenhanced scan and progressing to postcontrast scans of the arterial and portal venous phases.

Diagnostic assessment and differential diagnosis

CT did not detect fractures, and no consequences visible under a radiological examination were observed. However, during imaging, the radiologist detected an unknown venous anomaly in the chest and abdomen.

The patient was not aware of this variant in the vascular anatomy and had never had symptoms related to it (Fig. 1).
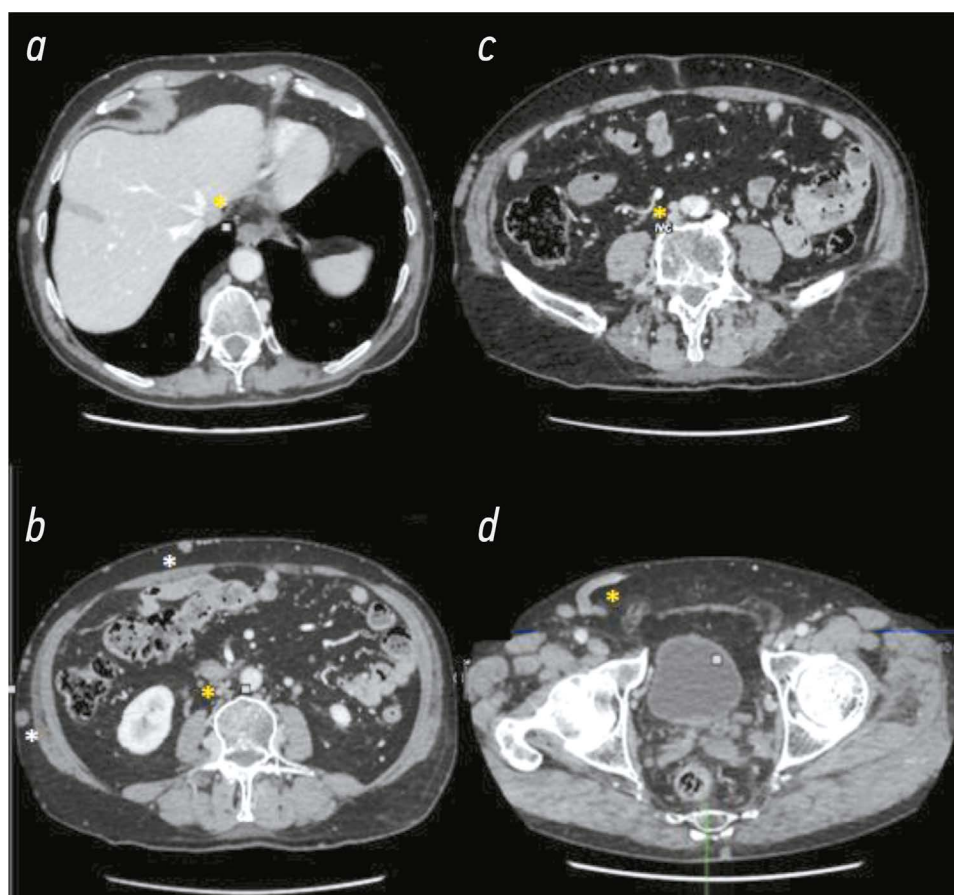

Fig. 1. Computed tomography images of the axial section of the abdomen (portal phase): *a*) The small suprarenal IVC is indicated by a yellow asterisk. *b*) Lower in the abdomen, the yellow asterisk indicates the hypoplastic IVC, and the hypertrophic collateral venous circles in the anterior abdomen wall on the right are indicated by a white asterisk. *c*) Another lower axial section showing the small IVC (yellow asterisk). *d*) The drainage on the right side is accomplished by a constant iliac vessel (yellow asterisk).

Interventions

To adequately study this vascular anomaly, postprocessing reconstruction was conducted on all planes (axial, coronal, and sagittal) using the MIP program, and 3D images were generated.

At first glance, the most evident imaging finding of the vascular anomaly was the presence of multiple collateral venous circles on the anterior wall of the abdomen, particularly on the right side, and the IVC under the kidneys was hypoplastic (Fig. 2).

Certain distended azygos and hemiazygos veins received blood from the abdomen. The *azygos* vein connected with the *superior vena cava* (SVC) through its arch; however, its dimensions were abnormal. It began from D7 and extended to D10–11, from the confluence of the right renal vein, transhepatic vein, and an aberrant vein (Fig. 3 and Fig. 4).

Follow-up and outcomes

The patient had previously never experienced symptoms that could be correlated with the same vascular abnormality, and the symptoms he experienced did not appear to be related. Therefore, periodic follow-up was recommended.
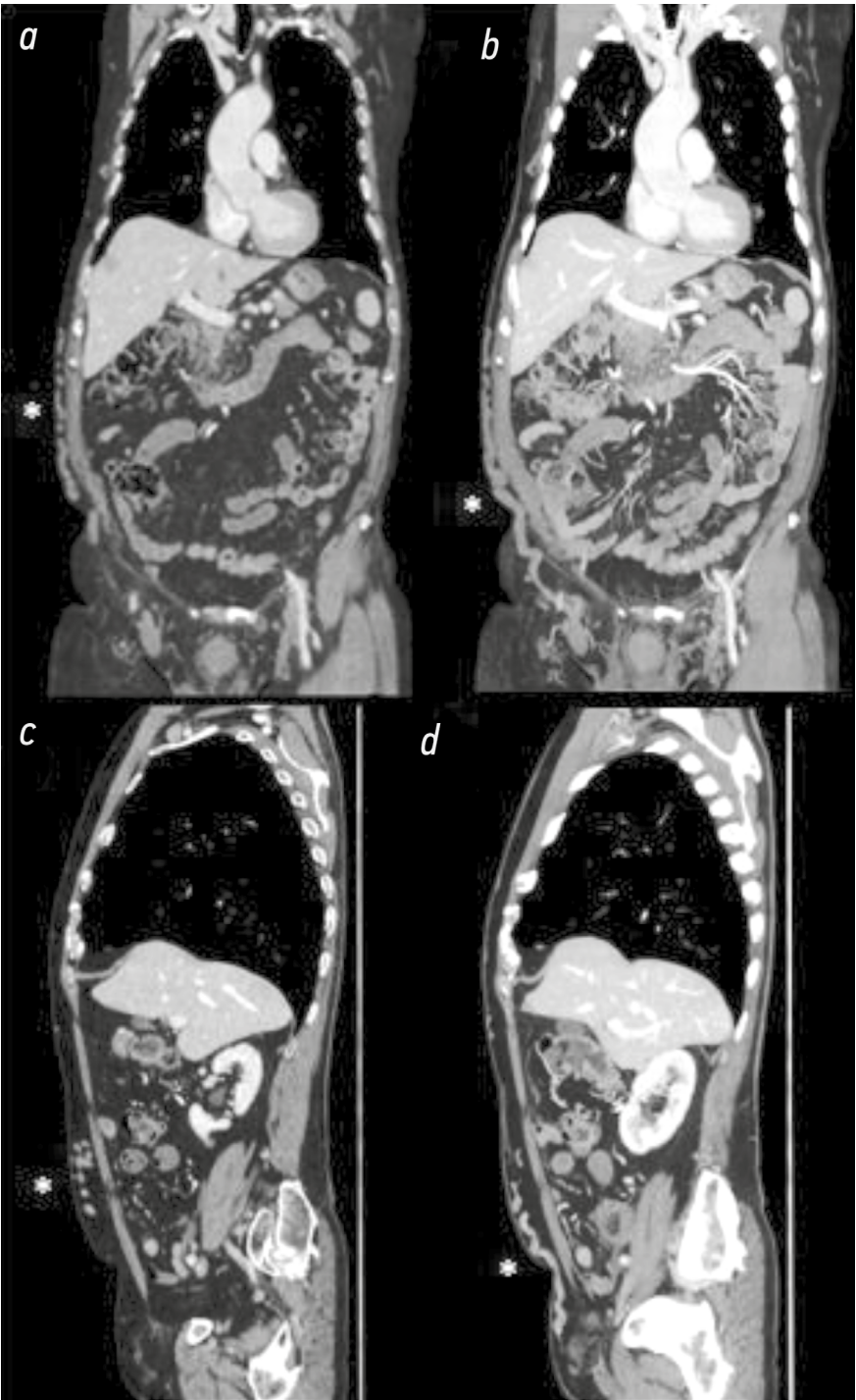

Fig. 2. Computed tomography images of the coronal (up) and sagittal (down) sections in the portal phase of the chest and abdomen: *a*) Right abdominal wall: consistent venous collateral circles are visible (white asterisk). *b*) The same image with a rising MIP value indicates venous collateral rings, particularly on the patient's right side. *c*) and *d*) Hypertrophic venous collateral circles in the sagittal section at different levels.
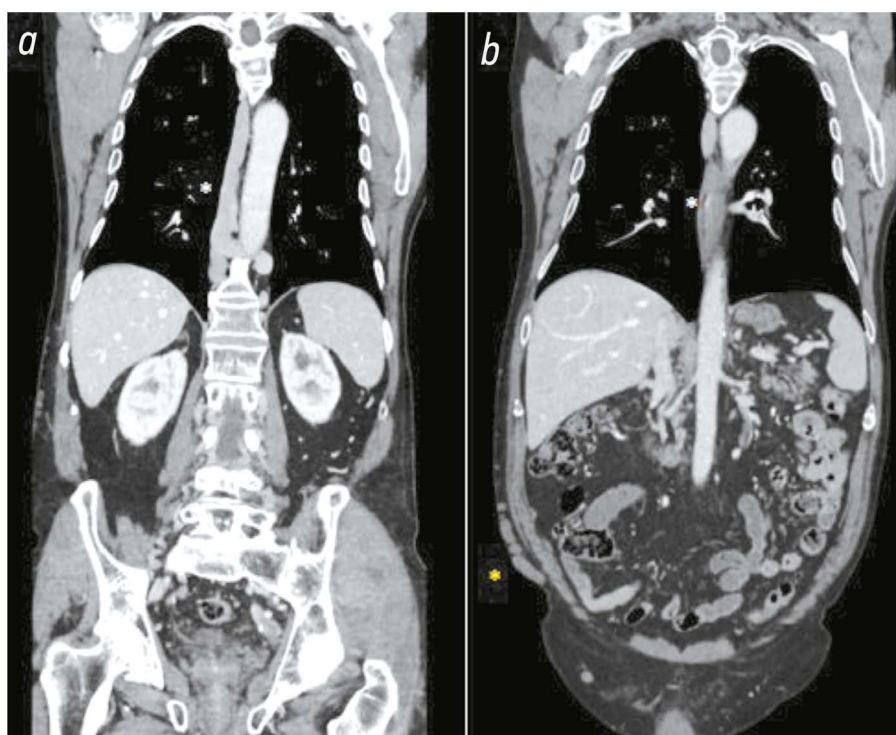
Fig. 3. Computed tomography images of the coronal section and portal phase of the chest and abdomen: *a)* The white asterisk indicates the confluence of the giant azygos, hemiazygos, and an aberrant vein. *b)* Same image at different sections. The yellow asterisk on the right side at the level of the anterior abdominal wall indicates marked collateral vein circles.
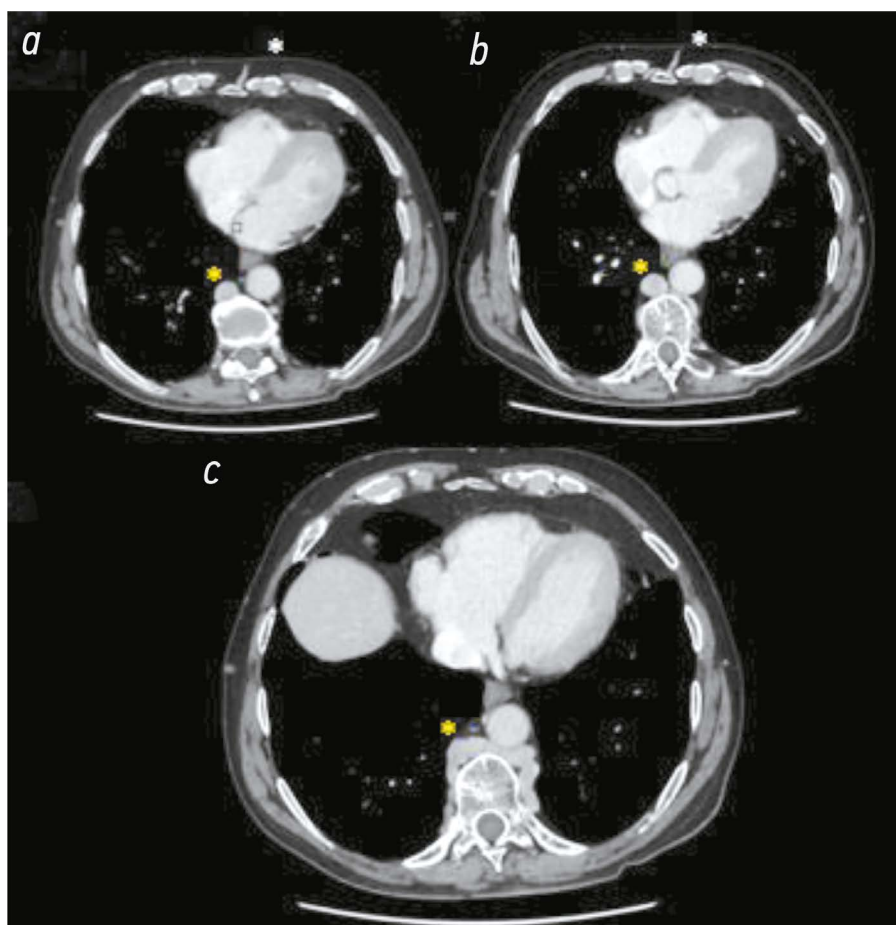

Fig. 4. Computed tomography images of the axial section of the chest: the confluence with the hypertrophic azygos and hemiazygos veins is seen in all images at different levels (from upper to lower). In *a)* and *b)*, the white asterisk marks the confluence of the collateral circles of the abdomen and chest.

DISCUSSION

The IVC is a large retroperitoneal vein that transports deoxygenated blood from the lower extremities, pelvis, and abdomen to the right atrium. The *azygos* venous system is a paravertebral connection in the posterior thorax that connects the SVC to the IVC. The *azygos*, *hemiazygos*, accessory *hemiazygos*, and left superior intercostal veins form a H-shaped pattern, indicating the *azygos* venous system [2,3]. IVC hypoplasia, characterized by an *azygos/hemiazygos* system and collateral circle compensation, is an uncommon vascular defect with numerous variations [4-8]. The anomaly is primarily caused by the abnormal regression or persistence of embryological veins (anterocardinal, postcardinal, subcardinal, supracardinal, and vitelline) that form the five embryological segments of the final structure of the IVC, namely, iliac, subrenal, renal, suprarenal, and hepatic, including suprahepatic and retrohepatic [9]. In this case, the patient had a very small IVC in the right iliac fossa, with larger *azygos/hemiazygos* veins, indicating an expanded *hemiazygos* system as the primary drainage system.

Imaging plays a critical role in the detection of this type of vascular abnormality. Herein, CT helped differentiate all vessels, discover variants, and increase the *azygos* system. The imaging options for studying the vascular abnormality include echocardiographic techniques and color Doppler.

Imaging, CT angiography, and IVC angiography can detect hypoplastic/interrupted IVC, identify abnormal vessels, and assess *azygos* system dilatation due to increased flow. Angiography is useful for determining the precise anatomy of vessel drainage for surgical purposes. Detecting venous abnormalities is crucial because they can interfere with right heart catheterization, cardiopulmonary bypass surgery, and pacemaker insertion. IVC hypoplasia, or interrupted IVC in extreme cases, also known as *azygos–hemiazygos* continuation, is a benign disorder that does not require treatment owing to adequate vascularization [10-11].

However, patient knowledge is critical in the event of surgical intervention [9-14]. A misdiagnosis mayoccurr because of possible mediastinal shadow enlargement on chest X-ray images or dilated azygos or hemiazygos vein adjacent to the descending aorta on transesophageal echocardiography mimicking aortic pathology [5,10,12].

Interrupted IVC is often linked to other congenital defects, particularly in the cardiac region, prompting a search for related conditions. The presence of other pathologies must be evaluated. Excluding portosystemic shunting is crucial for management because chronic congenital portosystemic shunts can lead to serious complications. The presented case did not correlate with other congenital defects or the patient's malignancy. Both situations can be regarded as independent.

CONCLUSION

This report presents an uncommon venous abnormality in the chest and abdomen of an asymptomatic adult with hypoplastic IVC accompanied by *azygos/hemiazygos* hypertropia and the presence of numerous collateral venous circles. This case highlights the importance of imaging in the detection of complex vascular abnormalities. Physicians should carefully examine this unique vascular abnormality to prevent misdiagnosis and improve surgical outcomes.

ADDITIONAL INFORMATION

REFERENCES

1. Koudounas G, Giannopoulos S, Volteas P, Virvilis D. A unique case of hypoplastic inferior vena cava leading to bilateral iliofemoral venous outflow obstruction and review of literature. *J Vasc Surg Cases Innov Tech.* 2022;8(4):842–849. doi: 10.1016/j.jvscit.2022.10.010

2. Ghandour A, Partovi S, Karuppasamy K, Rajiah P. Congenital anomalies of the IVC–embryological perspective and clinical relevance. *Cardiovasc Diagn Ther.* 2016;6(6):482–492. doi: 10.21037/cdt.2016.11.18

3. Li SJ, Lee J, Hall J, Sutherland TR. The inferior vena cava: anatomical variants and acquired pathologies. *Insights Imaging.* 2021;12(1):123. doi: 10.1186/s13244-021-01066-7

4. Masino F, Muscatella G, Montatore M, et al. A remarkable case report of an interrupted inferior vena cava with hemiazygos and transhepatic continuation. *Acta Biomed.* 2023;94(5):e2023238. doi: 10.23750/abm.v94i5.15085

5. Vignesh S, Bhat TA. Unique Medley of Cardinal Veins: Duplicated Superior and Inferior Venae Cavae With Left Renal Agenesis and Hemiazygos Continuation of Left Inferior Vena Cava With Draiage Into Left Atrium. *Vasc Endovascular Surg.* 2022;56(3):330–334. doi: 10.1177/15385744211051493

6. Liu Y, Guo D, Li J, et al. Radiological features of azygos and hemiazygos continuation of inferior vena cava: A case report. *Medicine (Baltimore)*. 2018;97(17):e0546. doi: 10.1097/MD.0000000000010546
7. Chen S-J, Wu M-H, Wang J-K. Clinical implications of congenital interruption of inferior vena cava. *J Formos Med Assoc.* 2022;121(10):1938–1944. doi: 10.1016/j.jfma.2022.01.021
8. Morosetti D, Picchi E, Calcagni A, et al. Anomalous development of the inferior vena cava: Case reports of agenesis and hypoplasia. *Radiol Case Rep.* 2018;13(4):895–903. doi: 10.1016/j.radcr.2018.04.018
9. Sneed D, Hamdallah I, Sardi A. Absence of the Retrohepatic Inferior Vena Cava: What the Surgeon Should Know. *Am Surg.* 2005;71(6):502–504. doi: 10.1177/00031348050710061
10. Sahin H, Pekcevik Y, Aslaner R. Double Inferior Vena Cava (IVC) With Intrahepatic Interruption, Hemiazygos Vein Continuation,

and Ivenous Shunt. *Vasc Endovascular Surg.* 2017;51(1):38–42. doi: 10.1177/1538574416687734
11. Demos TC, Posniak HV, Pierce KL, et al. Venous anomalies of the thorax. *AJR Am J Roentgenol.* 2004;182(5):1139–1150. doi: 10.2214/ajr.182.5.1821139
12. Koc Z, Oguzkurt L. Interruption or congenital stenosis of the inferior vena cava: prevalence, imaging, and clinical findings. *Eur J Radiol.* 2007;62(2):257–266. doi: 10.1016/j.ejrad.2006.11.028
13. Mandato Y, Pecoraro C, Gagliardi G, Tecame M. Azygos and hemiazygos continuation: An occasional finding in emergency department. *Radiol Case Rep.* 2019;14(9):1063–1068. doi: 10.1016/j.radcr.2019.06.003
14. Holemans JA. Azygos, not azygous. *AJR Am J Roentgenol.* 2001;176(6):1602–1602. doi: 10.2214/ajr.176.6.1761602b

СПИСОК ЛИТЕРАТУРЫ

1. Koudounas G., Giannopoulos S., Volteas P., Virvilis D. A unique case of hypoplastic inferior vena cava leading to bilateral iliofemoral venous outflow obstruction and review of literature // J Vasc Surg Cases Innov Tech. 2022. Vol 8, N 4. P. 842–849. doi: 10.1016/j.jvscit.2022.10.010
2. Ghandour A., Partovi S., Karuppasamy K., Rajiah P. Congenital anomalies of the IVC—embryological perspective and clinical relevance // Cardiovasc Diagn Ther. 2016. Vol 6, N 6. P. 482–492. doi: 10.21037/cdt.2016.11.18
3. Li S.J., Lee J., Hall J., Sutherland T.R. The inferior vena cava: anatomical variants and acquired pathologies // Insights Imaging. 2021. Vol 12, N 1. ID: 123. doi: 10.1186/s13244-021-01066-7
4. Masino F., Muscatella G., Montatore M., et al. A remarkable case report of an interrupted inferior vena cava with hemiazygos and transhepatic continuation // Acta Biomed. 2023. Vol 94, N 5. ID: e2023238. doi: 10.23750/abm.v94i5.15085
5. Vignesh S., Bhat T.A. Unique Medley of Cardinal Veins: Duplicated Superior and Inferior Venae Cavae With Left Renal Agenesis and Hemiazygos Continuation of Left Inferior Vena Cava With Drainage Into Left Atrium // Vasc Endovascular Surg. 2022. Vol. 56, N 3. P. 330–334. doi: 10.1177/15385744211051493
6. Liu Y., Guo D., Li J., et al. Radiological features of azygos and hemiazygos continuation of inferior vena cava: A case report // Medicine (Baltimore). 2018. Vol. 97, N 17. ID: e0546. doi: 10.1097/MD.0000000000010546

7. Chen S.-J., Wu M.-H., Wang J.-K. Clinical implications of congenital interruption of inferior vena cava // J Formos Med Assoc. 2022. Vol. 121, N 10. P. 1938–1944. doi: 10.1016/j.jfma.2022.01.021
8. Morosetti D., Picchi E., Calcagni A., et al. Anomalous development of the inferior vena cava: Case reports of agenesis and hypoplasia // Radiol Case Rep. 2018. Vol. 13, N 4. P. 895–903. doi: 10.1016/j.radcr.2018.04.018
9. Sneed D., Hamdallah I., Sardi A. Absence of the Retrohepatic Inferior Vena Cava: What the Surgeon Should Know // Am Surg. 2005. Vol. 71, N 6. P. 502-504. doi: 10.1177/00031348050710061
10. Sahin H., Pekcevik Y., Aslaner R. Double Inferior Vena Cava (IVC) With Intrahepatic Interruption, Hemiazygos Vein Continuation, and Intrahepatic Venous Shunt // Vasc Endovascular Surg. 2017. Vol. 51, N 1. P. 38–42. doi: 10.1177/1538574416687734
11. Demos T.C., Posniak H.V., Pierce K.L., et al. Venous anomalies of the thorax // AJR Am J Roentgenol. 2004. Vol. 182, N 5. P. 1139–1150. doi: 10.2214/ajr.182.5.1821139
12. Koc Z., Oguzkurt L. Interruption or congenital stenosis of the inferior vena cava: prevalence, imaging, and clinical findings // Eur J Radiol. 2007. Vol. 62, N 2. P. 257–266. doi: 10.1016/j.ejrad.2006.11.028
13. Mandato Y., Pecoraro C., Gagliardi G., Tecame M. Azygos and hemiazygos continuation: An occasional finding in emergency department // Radiol Case Rep. 2019. Vol. 14, N 9. P. 1063–1068. doi: 10.1016/j.radcr.2019.06.003
14. Holemans J.A. Azygos, not azygous // AJR Am J Roentgenol. 2001. Vol. 176, N 6. P. 1602–1602. doi: 10.2214/ajr.176.6.1761602b

AUTHORS' INFO

* Giuseppe Guglielmi, MD, Professor;
address: 1 Viale L. Pinto, 71121, Foggia, Italy;
ORCID: 0000-0002-4325-8330;
e-mail: giuseppe.guglielmi@unifg.it
Manuela Montatore, MD;
ORCID: 0009-0002-1526-5047;
e-mail: manuela.montatore@unifg.it
Gianmichele Muscatella, MD;
ORCID: 0009-0004-3535-5802;
e-mail: muscatella94@gmail.com

ОБ АВТОРАХ

* Giuseppe Guglielmi, профессор;
адрес: Италия, 71121, Фоджа, Viale L. Pinto, 1;
ORCID: 0000-0002-4325-8330;
e-mail: giuseppe.guglielmi@unifg.it
Manuela Montatore;
ORCID: 0009-0002-1526-5047;
e-mail: manuela.montatore@unifg.it
Gianmichele Muscatella;
ORCID: 0009-0004-3535-5802;
e-mail: muscatella94@gmail.com

Federica Masino, MD;
ORCID: 0009-0004-4289-3289;
e-mail: federicamasino@gmail.com
Giovanni Ricatti, MD;
ORCID: 0009-0006-7620-1011;
e-mail: g.ricatti@live.com
Marina Balbino, MD;
ORCID: 0009-0009-2808-5708;
e-mail: marinabalbino93@gmail.com
Rossella Gifuni, MD;
ORCID: 0009-0009-9679-3861;
e-mail: rossella.gifuni@unifg.it

Federica Masino;
ORCID: 0009-0004-4289-3289;
e-mail: federicamasino@gmail.com
Giovanni Ricatti;
ORCID: 0009-0006-7620-1011;
e-mail: g.ricatti@live.com
Marina Balbino;
ORCID: 0009-0009-2808-5708;
e-mail: marinabalbino93@gmail.com
Rossella Gifuni;
ORCID: 0009-0009-9679-3861;
e-mail: rossella.gifuni@unifg.it

* Corresponding author / Автор, ответственный за переписку

Federica Masino, MD;
ORCID: 0009-0004-4289-3289;
e-mail: federicamasino@gmail.com